AGARD-CP-590

AGARD

ADVISORY GROUP FOR AEROSPACE RESEARCH & DEVELOPMENT
7 RUE ANCELLE, 92200 NEUILLY-SUR-SEINE, FRANCE

AGARD CONFERENCE PROCEEDINGS 590

Bolted/Bonded Joints in Polymeric Composites

(Assemblages boulonnés/collés en matériaux composites polymères)

Papers presented at the 83rd Meeting of the AGARD Structures and Materials Panel, held in Florence, Italy, 2-3 September 1996.

DISTRIBUTION STATEMENT A
Approved for public release
Distribution Unlimited

NORTH ATLANTIC TREATY ORGANIZATION

Published January 1997

Distribution and Availability on Back Cover

DISCLAIMER NOTICE



THIS DOCUMENT IS BEST QUALITY AVAILABLE. THE COPY FURNISHED TO DTIC CONTAINED A SIGNIFICANT NUMBER OF PAGES WHICH DO NOT REPRODUCE LEGIBLY.

AGARD-CP-590

AGARD

ADVISORY GROUP FOR AEROSPACE RESEARCH & DEVELOPMENT
7 RUE ANCELLE, 92200 NEUILLY-SUR-SEINE, FRANCE

AGARD CONFERENCE PROCEEDINGS 590

Bolted/Bonded Joints in Polymeric Composites

(Assemblages boulonnés/collés en matériaux composites polymères)

Papers presented at the 83rd Meeting of the AGARD Structures and Materials Panel, held in Florence, Italy, 2-3 September 1996.

19970214 022



North Atlantic Treaty Organization
Organisation du Traité de l'Atlantique Nord

DTIC QUALITY INSPECTED 1

The Mission of AGARD

According to its Charter, the mission of AGARD is to bring together the leading personalities of the NATO nations in the fields of science and technology relating to aerospace for the following purposes:

- Recommending effective ways for the member nations to use their research and development capabilities for the common benefit of the NATO community;
- Providing scientific and technical advice and assistance to the Military Committee in the field of aerospace research and development (with particular regard to its military application);
- Continuously stimulating advances in the aerospace sciences relevant to strengthening the common defence posture;
- Improving the co-operation among member nations in aerospace research and development;
- Exchange of scientific and technical information;
- Providing assistance to member nations for the purpose of increasing their scientific and technical potential;
- Rendering scientific and technical assistance, as requested, to other NATO bodies and to member nations in connection with research and development problems in the aerospace field.

The highest authority within AGARD is the National Delegates Board consisting of officially appointed senior representatives from each member nation. The mission of AGARD is carried out through the Panels which are composed of experts appointed by the National Delegates, the Consultant and Exchange Programme and the Aerospace Applications Studies Programme. The results of AGARD work are reported to the member nations and the NATO Authorities through the AGARD series of publications of which this is one.

Participation in AGARD activities is by invitation only and is normally limited to citizens of the NATO nations.

The content of this publication has been reproduced
directly from material supplied by AGARD or the authors.

Published January 1997

Copyright © AGARD 1997
All Rights Reserved

ISBN 92-836-1046-6



Printed by Canada Communication Group
45 Sacré-Cœur Blvd., Hull (Québec), Canada K1A 0S7

Bolted/Bonded Joints in Polymeric Composites

(AGARD CP-590)

Executive Summary

In aerospace structures, the selection of the methods for joining individual parts can be critical to reliability, durability, supportability, initial and in-service costs.

Mechanically fastened joints, extensively used in metallic structures, have been widely used in the first generation of composite structures. The fact that they are dismountable allows for easier inspection and replacement of damaged or defective components. However, they exhibit highly localised stresses near the fasteners and so tend to act as damage initiators.

Bonded joints have the advantage that they can usually be designed to be much lighter. Manufacturing costs also tend to be significantly lower. However, in the absence of effective non-destructive methods to verify bond integrity, quality must be ensured through careful process control. In composite structures they have generally been used only in thinner, more lightly-loaded components.

Since the fabrication of composite structures and components generally involves making the material and the component at the same time, a range of novel joining methods, such as weaving and stitching, becomes possible, and these methods are being exploited in attempts to overcome the limitations imposed by the low interlaminar strength of composites.

The Specialists' Meeting held by the Structures and Materials Panel of AGARD showed that there is a range of methods for the design of bolted and bonded joints in polymeric composites, based on a combination of stress analysis, semi-empirical strength criteria, test data and engineering experience. These methods can produce fully-effective joints, but they are probably not sufficiently robust to ensure that the joints are always optimised. The novel joining methods described can exhibit significant structural benefits; and further improvements in the understanding and design of both conventional and novel joining methods should lead to steady improvements in efficiency, durability and cost effectiveness.

Assemblages boulonnés/collés en matériaux composites polymères

(AGARD CP-590)

Synthèse

Dans le domaine des structures aérospatiales, le choix de méthodes pour l'assemblage des pièces peut être déterminant pour la fiabilité, la durabilité, la supportabilité, ainsi que pour les coûts initiaux et d'exploitation.

Les assemblages par fixations mécaniques, qui sont largement utilisés pour les structures métalliques, ont également trouvé de nombreuses applications pour la première génération des structures composites. Ils sont démontables, ce qui facilite le contrôle et le remplacement des composants endommagés ou défectueux. Cependant, ils présentent des contraintes très localisées au droit des fixations et, en conséquence, ils peuvent être à l'origine de dommages.

Les assemblages collés ont l'avantage de la légèreté. Les coûts de fabrication sont également moins onéreux que pour les fixations mécaniques. Cependant, en l'absence de méthodes non-destructives efficaces pour la vérification de l'intégrité de l'assemblage, il est essentiel d'assurer la qualité par le biais de contrôles très rigoureux durant la fabrication. Leur emploi dans les structures composites a généralement été limité aux composants plus fins et moins sollicités.

Puisque la fabrication de structures et composants en composite implique normalement la création du matériau et du composant simultanément, tout un éventail de méthodes d'assemblage originales, telles que la couture et le tissage, sont envisageables. Celles-ci sont actuellement exploitées dans le but de surmonter les limitations imposées par la faible résistance interlaminaire des composites.

La réunion de spécialistes organisée par le Panel des structures et matériaux de l'AGARD a démontré qu'il existe un choix de méthodes pour la conception d'assemblages boulonnés et collés pour les composites polymères, basé sur une combinaison de l'analyse des contraintes, des critères de résistance semi-empiriques, des données d'essais et de l'expérience en ingéniérie. S'il est possible de réaliser des assemblages tout à fait sûrs à l'aide de ces méthodes, elles ne sont probablement pas assez robustes pour garantir que les joints soient systématiquement optimisés. Les nouvelles méthodes d'assemblage décrites peuvent apporter des avantages structurales considérables. Une meilleure compréhension de la conception des méthodes d'assemblage classiques et nouvelles devrait conduire à des améliorations progressives sur le plan de l'efficacité, la durabilité et la rentabilité.

Contents

	Page
Executive Summary	iii
Synthèse	iv
Preface	vii
Structures and Materials Panel	viii
Technical Evaluation Report by J. Bauer and L.J. Hart-Smith	T
	Reference
SESSION I: OVERVIEW	
Bolted Joints in Composite Structures -- An Overview by D.W. Oplinger	1
Bolted Joint Technology in Composite Structures -- Analytical Tools Development by C. Poon and Y. Xiong	2
A Review of Composite Joint Analysis Programs by V.B. Venkayya and V.A. Tischler	3
SESSION II: BOLTED JOINTS — STRESS ANALYSIS AND FAILURE	
Stress Analysis of Open and Fastener Hole Composites Based on Three-Dimensional Spline Variational Technique by E.V. Iarve and J.R. Schaff	4
Development of a Stressing Method for Bolted Joints by J. Bauer and E. Mennle	5
Development of Failure in Bolted Joints in Woven CFRP Laminates by J.L. Oakeshott, M. Gower, S. Perinpanayagam and F.L. Matthews	6
Three-Dimensional Progressive Failure Analysis of Pin/Bolt Loaded Composite Laminates by M.M. Shokrieh, L.B. Lessard and C. Poon	7
Analysis Methods for Bolted Composite Joints Subjected to In-Plane Shear Loads by L.J. Hart-Smith	8
SESSION III: BONDED JOINTS — STRESS ANALYSIS, DURABILITY AND FAILURE	
Stress and Failure Analysis of Bonded Composite-to-Metal Joints by Y. Xiong and D. Raizenne	9
Strength Prediction of Bonded Joints by M.N. Charalambides, A.J. Kinloch and F.L. Matthews	10

Numerical Strength Predictions of Adhesively Bonded Multimaterial Joints 11
by G. Laschet

Structural Efficiency of Different Assembly Methods for Stiffened Composite Panels: Cocuring and Secondary Bonding 11A
by F. Elaldi and S. Lee

Surface Treatment and Bonding of Thermoplastic Composites 12
by S.J. Shaw, J. Comyn and L. Mascia

Hygrothermal Fatigue of Composite Bonded Joints 13
by V. Giavotto, C. Caprile and G. Sala

Cyclic Fatigue and Environmental Effects with Adhesively Bonded Joints 14
by I.A. Ashcroft, R.B. Gilmore and S.J. Shaw

SESSION IV: NOVEL JOINTS

Attachment of Ceramic Matrix Composites to AFR700B Composites for Exhaust Washed Airframe Structures 15
by S. ATMUR, M. COLBY, M. TOMASEK, M. HAGEN, D. SHERRILL, C. FOREMAN and D. DOLVIN

3-D Composites in Primary Aircraft Structure Joints 16
by L. Bersuch, K. Hunten, B. Baron and J. Tuss

Z-Fiber Technology and Products for Enhancing Composite Design 17
by G. Freitas, T. Fusco, T. Campbell, J. Harris and S. Rosenberg

An Investigation on a Bolted-Cold Bonded Joint for Large Diameter Structures 18
by M. Montabone, M. Nebiolo and C. Vigada

SESSION V: DESIGN, VALIDATION AND SERVICE EXPERIENCE

The Assembly of Thermoplastics by Adhesive Bonding: Process and Control 19
by J. Lecomte

Design Loads for Bonded and Bolted Joints 20
by M.J. Broome

Paper 21 withdrawn

Tiltrotor Transport Bonded Wing Design Summary 22
by R.V. Dompka and R.C. Holzwarth

Royal Air Force Experience of Mechanically-Fastened Repairs to Composite Aircraft Structures 23
by S.H. Chicken

Quality Assurance and Certification Procedures for Bonded Joints in On-Aircraft Scenarios 24
by A. Maier and G. Günther

Probabilistic Evaluation of Bolted Joints in Polymer Matrix Composites 25
by C.C. Chamis and L. Minnetyan

Preface

Degradation and failure of aerospace structures are frequently initiated at the joints, so that safety, durability and repairability are strongly influenced by the adequacy of joint design. Current and future military aircraft make extensive use of advanced composite materials in both primary and secondary structure, and both mechanically fastened and bonded joints have been used.

Mechanically fastened joints have generally been used for highly-loaded composite components, although the low bearing stiffness of composites can lead to problems of bolt bending and hole elongation under fatigue loading. Secondary bending can also give rise to significant through-thickness stresses, but effective and reliable joints are usually achieved through a combination of design, testing and re-design.

Bonded joints can usually be designed to be lighter, but as there are no inspection techniques yet available which can guarantee the adequacy of the bond, they have not gained widespread acceptance for highly-loaded joints.

The objective of the Specialists' Meeting is to examine the state-of-the-art in joining of polymeric composites, to consider the relative merits of the various methods and to highlight gaps in the technology which should be addressed.

Prof. R. POTTER
Chairman
Sub-Committee on
Bolted/Bonded Joints in Polymeric Composites

Structures and Materials Panel

Chairman: Prof. O. Sensburg
Chief Engineer
Daimler Benz Aeropace
Militaerflugzeuge LM2
Postfach 80 11 60
81663 Munich
Germany

Deputy Chairman: Prof. S. Paipetis
Prof. of Applied Mechanics
School of Engineering
Dept of Mechanical Engineering
University of Patras
26110 Patras
Greece

SUB-COMMITTEE MEMBERS

Chairman: Prof. R. Potter
Manager Non-Metallic
SMC, R178 Building
Aerospace Division
DRA Farnborough
Farnborough, Hants GU14 6TD
United Kingdom

Members:

P. Armando	—	FR	S. Paipetis	—	GR
D. Chaumette	—	FR	D. Paul	—	US
M. Curbillon	—	FR	C. Perron	—	CA
B. Eksi	—	TU	H. Perrier	—	FR
E.E. Gdoutos	—	GR	E. Sanchiz	—	SP
F.N. Goncalo	—	PO	O. Sensburg	—	GE
A.R. Humble	—	UK	D.L. Simpson	—	CA
R. Kochendörfer	—	GE	A. Yucel	—	TU
H.H. Ottens	—	NE			

PANEL EXECUTIVE

Dr Jose M. CARBALLAL, SP

Mail from Europe:
AGARD-OTAN
7, rue Ancelle
92200 Neuilly-sur-Seine
France

Mail from US and Canada:
From USA and Canada
AGARD-NATO/SMP
PSC 116
APO AE 09777

Tel: 33 (0)1 55 61 22 90 & 92
Telefax: 33 (0)1 55 61 22 99 & 98
Telex: 610176F

TECHNICAL EVALUATION REPORT

83rd Meeting of the Structures and Materials Panel

Bolted / Bonded Joints in Polymeric Composites

J. Bauer
Daimler Benz Aerospace
Military Aircraft Division

and

L. J. Hart-Smith
Douglas Aircraft Company
McDonnell Douglas Corporation

The papers presented at this meeting cover a number of aspects concerning the application of adhesively bonded and mechanically fastened joints in the analysis, design, manufacturing, and repair of fibre-polymer composites. The focus is on aerospace rather than commercial products. The number of papers presented is 25, of which 8 cover the subject of Bolted Joints, 6 address Bonded Joints, 4 pertain to so-called Novel Joints, and 8 papers discuss Design Validation and Service Experience.

The overviews of the history and current status of this work reflect several valuable contributions to design and analysis methods developed many years ago, most of which were funded by various government agencies. Incomplete as they are, these remain the most widely applied methods today, and have been very useful. Most of the more modern research examines the governing phenomena in far greater depth, but requires the establishment of so many more material parameters that these works are usually applied only to specific cases. An exception is the agreement by the four partners involved to agree on common analysis methods for bolted joints in the EFA program. The need remains for more methods, or the extension of existing methods, with which to optimize bolted joint proportions to maximize the design strain levels in composite structures. Likewise, in regard to adhesively bonded and co-cured joints, the influence of joint proportions on strength – particularly by suppressing or minimizing peel stresses – has yet to be fully explained.

New analysis methods would be more credible, and valuable, if they were demonstrated in the predictive mode, on new data or on old data not used in their formulation, rather than being fitted to any one particular set of data. Analyzing tests coupons is really less valuable than designing a truly optimized structural joint. The preceding criticisms (or in the modern vernacular "opportunities for further research") notwithstanding, the meeting included interesting information about a number of real hardware programs and structures.

Regarding the subject of bolted joints in composite structures, all of the analytical tools already developed in the USA were given as computer codes. The subject is still under further consideration, and the current North American research and development activities and targets are discussed. These focus primarily on an improved assessment of the stress distribution around the bolt hole, taking into account secondary effects at, or in the vicinity of, the bolt hole. The contact problem, i.e. the bolt-to-plate interaction, particularly in regard to variation in stresses in the third direction and the interaction between bolt holes in multi-fastener joints are topics of current research presented at the meeting. The question of whether or not this improved understanding of precisely what is happening in the immediate vicinity of the hole will finally lead to more reliable strength predictions is not resolved. These micromechanical effects seem to be quite complex; it can be predicted that another considerable scientific effort will be needed until all such problems are solved. The hope is that this action might decrease the magnitude of the test effort for composite material qualifications related to bolted joints, and save money throughout the industry. However, it should be noted that it has already long been established that the most efficient structural joints in composite laminates fail by tension-through-the hole, at bearing stresses no more than half those needed to cause bearing failures. In contrast to this sophisticated computer-based analysis, the search

for more simple approaches is still ongoing. These methods are more useful for application in aircraft design, as well as for commercial applications, and the development of stressing methods which are easy to use should never stop. One such method is presented, using simple analytical equations and tied directly to overall physical behaviour. This represents an expansion to new in-plane-shear boundary conditions, for which no test data are currently available, of an old well-established and validated method for more straightforward joint geometries.

There is no corresponding overview of the European state of the art in regard to the art of stressing bolted composite joints. That the European contribution to this topic is limited to only two papers may lead to the conclusion that the subject is no longer considered important. Such an attitude cannot be justified and it is still recommended that academics keep the subject in mind and try to improve the physical understanding, improve and validate the predictive techniques, and ensure the dissemination of the knowledge. The understanding of this subject in the composites community has not yet reached a satisfactory level of uniformity, particularly in regard to optimizing the design process to maximize structural efficiency.

The advantages of bonded joints, in terms of higher structural efficiencies by eliminating bolt holes, seem to be well understood, but manufacturing and quality assurance problems continue to require individual solutions. These are dependent on the adherend materials and the required environmental service conditions, which govern the selection of the adhesive and its curing temperature. One key issue is surface preparation; another the presence of pre-bond moisture during the cure of the adhesive. An informal presentation on problems associated with trying to bond directly to the surface left by stripping off a peel ply offered enlightenment on the subject and sparked a lively discussion. The key issue is that after-the-fact inspections are incapable of detecting weak, or "kissing", bonds. Not all process specifications ensure that these cannot happen. Only grit-blasted ,or thoroughly abraded, surfaces on completely dried theromset laminates have been found to be totally immune from degradation of strength in service. The reasons why other treatments sometimes fail prematurely are neither fully understood nor fully accepted. The standard test coupons cannot reveal all of the problems which can lead to failures in service. There is no equivalent for composite structures of the Boeing wedge-crack test coupon which plays such a vital role in ensuring the durability of bonded metallic structures. There is not even universal acceptance that interfacial failure between the adhesive and the resin is an unambiguous indicator of a defective bond. These effects must be properly understood or cures which are worse than the disease will continue to be prescribed. In summary, the bonding technology remains a sophisticated manufacturing process which requires easily applied, but strict, controls of the process parameters – and an appreciation of the consequences of not doing so. Adhesive bonding is actually remarkably tolerant of many process variables, often needing two errors to create a weakness when either could be tolerated alone. For example, pre-bond moisture is a major problem when it cannot escape and is confined to the bonding surfaces during cure, but is often quite harmless if the venting and bond dimensions are such as to permit it to easily escape before the adhesive has gelled.

From the industrial point of view, the (usually unrecognized) incompleteness of the standard set of test coupons, and a blind reliance on costly ultrasonic NDI, which has been notoriously unreliable in detecting global processing errors (which may or may not be a violation of the processing specification), has given bonding of composites such a bad name in some areas that it has lost its appeal. The fact that some manufacturers produce high-quality bonded composite parts consistently and economically should have indicated where the real problems lie – and that they are not inherent in the process – but this has not happened yet. At the meeting, many of these problem areas were discussed. Especially the effects of the peel ply, and the need to grit blast whether the peel ply is "contaminated" by release agent or not, became evident. The texture of the peel-ply surface makes it absolutely critical that there be no pre-bond moisture in the adhesive or the cured laminates. Also, typically small travelling coupons often fail to represent the cure conditions for large bonded components, particularly in regard to escape of volatiles and, sometimes, heat-up rates and hence the flow (wetting) of the adhesive. The quality of the bond is best tested by peel tests and not by the customary shear tests. It is also necessary that the test coupons be made from unidirectional laminates, even if the part is not, to demonstrate the inherent joint strengths of properly cured and processed adhesives. (Woven fabric laminates have there own distinctive modes of delamination which can easily mask weaknesses in bond strength.)

The analysis and design methods used for adhesively bonded joints include both continuum-mechanics and finite-element approaches. It is important to recognize the need for nonlinear analyses of these problems.

One paper suggests that co-bonding seems to be superior to adhesive bonding in regard to cyclic fatigue. However, the mechanism whereby eliminating only one of two secondary bonds could also eliminate any adverse effects from the other bond surface is unclear. Co-curing can eliminate the interface completely, but often at the price of embedded wrinkles in the fibres of more complicated one-shot parts. Even then, interlayers of adhesive film, cured with the panel, are often found to be effective in alleviating stress concentrations.

Under the heading of Design Validation and Service Experience a variety of applications has been presented, providing an insight into manufacturing, stressing, and quality-assurance problems associated with the joining techniques.

The joining of materials for high-temperature applications requires new techniques because of the effects of differential thermal expansion. In this context, a paper is included on the mechanical fastening of a ceramic-matrix composite component to a conventional metallic rear fuselage.

New composite materials are arising and are the subject for investigations and discussions. Fibre reinforcement in the 3rd direction improves the damage tolerance of composite laminates and such techniques are in development to introduce this feature into composite materials. Beside the textile techniques of weaving and braiding, up to now the most popular joining technique of preforms is stitching. At the meeting, an alternative to this was presented, the so-called Z-pinning, which aroused considerable interest. This technique allows the joining of stiffeners and skins and, in addition, can be applied to improve the damage tolerance of the skin itself. It is said to be relatively inexpensive in manufacturing and also to provide improvements in resistance to edge delaminations and lap-shear strength – all without major effects on the in-plane properties. This technique seems to be promising for future aircraft designs and will be the subject of future research and development activities. A potentially crucial application concerns repairs, since it is claimed that the fibres can be ultrasonically inserted in pre-cured laminates. This could overcome the prevailing strain limit set by bolted repairs. On the other hand, given the known difficulties of making epoxy resin adhere to titanium or to carbon fibres, there must be obvious concerns about long-term durability if the pins. Nevertheless, the possibilities are powerful; it might even be possible to actually restore strength to embedded delaminations instead of merely filling them with resin so that they can no longer be detected.

The difficulty of adhesive bonding to either thermoset of thermoplastic materials is addressed. Successful techniques for thermoplastics are described, even though no explanation could be given for why they worked. The fundamentally inert surface of both forms of composites needs to be activated. Grit blasting is effective for thermoset resins, provided that the surface is not poisoned by subsequent application of "cleaning" solvents, but thermoplastics such as PEEK require etching, plasma treatment, corona discharge, flame spraying, or some aggressive treatment. Without appropriate surface treatment, the life of bonded composite structures cannot be assured. For both kinds of composites, it is significant that virtually zero-peel-strength conditions can occur while there is still significant shear-transfer capability.

Certification plans and quality-assurance procedures needed for ensuring that bonded composite joints can be relied upon are provided. However, no alternative is provided to compensate for the great inherent weakness of ultrasonic NDI – that it can only find gaps and is totally unable to detect the globally weak bonds caused by inappropriate processing, much of which is done in accordance with approved specifications. Nevertheless, this limitation emphasizes the importance of properly validated bonding processes, for repair and for initial manufacture, since there is usually no after-the-fact method of restoring the laminate strength even for the flaws which are detected.

A review of the development of an all-bonded wing equivalent to that in the V-22 tilt-rotor aircraft explains how much money (50% of the total) was saved by eliminating the cost of purchasing and installing the many fasteners which would otherwise be needed. Significantly, the cost is minimized by the secondary bonding of large torsionally soft integrally stiffened panels, each of which is simplified by omitting intersecting stiffeners. A 30% weight saving was achieved because the removal of fasteners allowed an increase in gross-section strain to an average of

0.008, per test. However, since the leading-and trailing-edge structures need to be bolted to the main torque box, there may still be further strain limits to be accounted for. (This could be done by bolting simulated or real leading- and trailing-edge structures to the test box.) Damage tolerance is achieved by the use of soft (predominantly ±45°) skins and webs and predominantly 0° stiffeners, in the form of pultruded 0° rods. The skin-to-rib attachment is improved over the earlier mouse-hole concept by bonding sloping flanges of the ribs directly to the side walls of the stiffeners. Proper alignment and positioning of all the details is achieved by using and I..M.L. skin tool.

The difficulties encountered by the customer in maintaining composite aircraft structures are addressed at both the Structural Repair Manual and Design Authority level, the former conventionally covering only small standard repairs. (As a point of reference, it may be noted that the first Lear Fan aircraft had a 150 cm by 225 cm portion of the nose in the pressure cabin replaced during manufacture, with no problems encountered on any of the flights. Since both the skin and the frames were separate pre-cured details, and could have been spared as such, bonding on a replacement skin was no problem. The load intensity in a patch is proportional to its thickness, in this case 1.3 mm, *not* its area.) While the patches described at the meeting worked effectively, the need for more foresight in design for repairs is emphasized, with particular attention to the virtual impossibility of making co-cured or bonded repairs at 180°C rather than 120°C or lower.

The repair examples discussed include what should have been a simple bolt-on panel, with pre-drilled holes. Because the hole pattern on the aircraft does not necessarily match that on a separately made spare panel, the installation can be, and in this case was, quite difficult. This suggests that either the tolerances need to be adhered to or the spare parts be furnished with no holes at all.

While it is true that over-simplified macro-level strength-prediction models can be quite unreliable, history suggests that the use of micro-level analysis will achieve the most response when used to formulate macro-level models rather than as a direct design or analysis tool in their own right. For instance, matrix failures are strongly influenced by intralaminar residual thermal stresses, from high-temperature curing, even more than by interlaminar or in-plane stresses. Yet the former are almost always overlooked and even the latter are not always accounted for scientifically. While the graphical presentation of bolted-joint design charts given here might yet need to account for further variables, at least it is simple enough that it is likely to be used by practicing structural designers.

Suggestions for future work include the following.

- A de-emphasis on after-the-fact inspection of all composite structures as part of a quality-assurance program, with a greater emphasis on pre-bonding and pre-curing inspections and cure monitoring. The former doesn't work reliably and the latter is far less expensive overall.
- Demonstration of any new strength-prediction technique in the predictive mode, preferably including comparisons with test data not used in their formulation.
- Far more attention to consideration of design for repair. (The bolt-on metal patch approach for the AV-8B wing is a good example of this process, but it works best only with near-quasi-isotropic laminates and imposes severe limits on the design operating strains.) The idea of bonding pre-cured details to make spare parts available for repairs at a bond temperature far lower than normal laminate-curing temperature is a *must*. The need to dry laminates for bonding, and the difficulty of doing so with honeycomb structures, should be noted.
- More needs to be done to identify optimum bolted joint geometries rather than merely accepting or rejecting them one at a time. The performance criterion needs to be overall gross-section stress level, and nothing else. The truly optimum solution is *not* simultaneously critical in all possible modes of failure; usually only one or two will be critical – and the others will exhibit large margins. This is not widely known, being as misunderstood for long-fatigue-life metallic strictures as for composites.
- A thorough effort should be made to remove from the list of accepted processes those operations which are known to almost invariably produce premature failures in service – any process (or omission of a process) which results in the weak link in a bond or co-cure process being at the interface between the adhesive and the resin, for example. Also, bonding to Nomex core or to pre-cured composite laminates without both thorough drying first and the provision of reliable venting to allow volatiles to escape during cure should

be outlawed. Tests need to be performed to show the difference. Otherwise, even a mandated change is unlikely to be obeyed. Calling for a water-break test is a particularly useful technique in bonding composite structures. Even when it fails in its nominal purpose, it cleans off any dust more harmlessly than cleaning solvent and causes the laminate to be dried because it is *seen* to be wet, when it otherwise wouldn't have been.

- Consideration should be given to test coupons which do not necessarily replicate the composite structure, but which respond far more convincingly to undesirable effects. For instance, pre-bond moisture may have little short-term effect on an autoclave cured or bonded component, but would be devastating to a bonded joint cured under roughly half an atmosphere – a joint which would be almost as strong as for autoclave cures in the absence of such moisture. (Testing with a full vacuum would be inconclusive because very few polymers will cure without boiling in such a condition.) Lap-shear coupons should be made from unidirectional tape laminates, even if the structure is not, because only then is it possible to stress the adhesive layer to a load sufficient to fail a properly cured bond.
- The Boeing wedge-crack test, on unidirectional laminates, needs to be evaluated and, if successful, mandated as a durability test for bonded composite structures. Today, there is no requirement for such a test, even though the need for it – in terms of in-service failures – is just as great as it was for metal-bonding 20 years ago.
- An aversion on the part of some manufacturers against rivetting composite structures needs to be overcome by highlighting the successes of others, and the relevant specifications widely distributed. Soft rivets are far easier to drill out for repairs than blind fasteners made from tool steel. They are also less expensive and fill the holes better, permitting greater tolerances than with conventional threaded or swaged fasteners. Their reduced shear strength also leads to larger fastener holes and, with it, to stronger mechanical joints in brittle composite structures
- The usual approach to repairs, and the small areas permitted under conventional SRM's needs to be re-assessed, for pre-cured details at least, based on the recognition that the load intensity through the patch is proportional to its thickness, not its area.

BOLTED JOINTS IN COMPOSITE STRUCTURES -- AN OVERVIEW

D. W. Oplinger
FAA William J. Hughes Technical Center
Atlantic City International Airport
New Jersey 08405
USA

1. SUMMARY

Investigations of bolted joints from the introduction of advanced composites in the mid-to-late 1960's to the present are reviewed. Numerous efforts aimed at applying two-dimensional elastic stress analysis in conjunction with appropriate testing have been conducted. Modelling of the pin-plate contact problem by a radial displacement condition rather than a radial pressure distribution is physically more realistic and has been done in a number of efforts, startying with that of Oplinger and Gandhi in the early 1970's. However in the case of the problem of bearing-bypass stress interaction which is in principle controlled by the radial displacement description of the contact problem, a number of efforts have provided useful results, especially in conjunction with adjustments based on test data by superposition of the half-cosine radial pressure distribution for pure bolt bearing load and the open-hole plate solution for bypass load. Approaches to predicting failure using results of 2-D elasticity analysis are discussed. In addition, recent effort addressing bearing failure on the basis of the three dimensional stress state is considered. Currently, the details of the three-dimensional contact problem associated with bending deflections of the fastener as well as the interaction of the fastener head with the surfaces of the joint plate elements are seen to need additional study.

2. INTRODUCTION

Bolted joints in composite structures are among the most challenging problems an engineering mechanics specialist has to deal with. While in bolted joints in general, severe stress concentrations tend to develop around fastener holes, in joints between metallic elements, ductile behavior tends to smooth out stress peaks and designers tend to ignore their effect . In fibrous composite structures, however, the response of the composite elements tends to be nearly linear to failure and smoothing out of stress peaks does not happen to nearly the same extent as in metals, making it essential for a detailed knowledge of the distribution of stresses to be made available. In addition to complexities of geometry, especially in multi-fastener joints, which make even elastic stress analysis of bolted joints challenging, bolted joints are characterized by nonlinear effects of contact corresponding to the bearing of the bolt shaft and head against the surfaces of the bolt hole and lateral surfaces of the joined composite plates. Finally, even when an adequate knowledge of the distribution of stresses is obtained by whatever analysis method is chosen, failure of the composite tends to be progressive, so that nonlinear material response of the composite which is difficult to predict tends to occur.

The objective of this paper is to review the progress that has been made in the analysis and design of bolted joints in composite structures since advanced composite materials were introduced in the mid 60's, in order to identify where this technology stands at the present time.

The discussion which follows will be structured in terms of: (1) two-dimensional stress analysis methods; (2) failure prediction. based on the two dimensional stress analysis; (3) requirements for three-dimensional stress analysis, and; (4) methods for treating bolt load distribution in multi-fastener joints.

3. HISTORICAL OVERVIEW

Much of the material being discussed in this paper is covered in greater detail in an upcoming review of structural joints given in Reference 1. References 2-24 provide a list of representative experimental and analytical efforts which have been carried out on bolted joints since the introduction of advanced composite materials around 1965.

The design of bolted joints in composite structures is considerably more complicated than that of metal structures because of: (1) the lack of ductile response of composites and; (2) the multiplicity of failure modes that have to be taken into account in composite laminates. Because of nearly elastic response to failure, elastic stress analysis plays a more prominent role in composite joint design than in metals.

Prior to the introduction of high tech composites in the mid 60's, the classical literature of elastic response of bolted joints included a number of experimental stress analysis efforts based on the photo elasticity approach [25]. Because of the limited access to automated computing tools up to that time, analytic efforts [26-28] were limited. With the growth of major computing resources in the 1960's there have been numerous stress analysis efforts based on two-dimensional orthotropic elasticity formulations using complex variable boundary collocation approaches, boundary element methods, or finite element analyses. The work of Waszczak and Cruise [2,3] and of Oplinger and Gandhi [4-6] represent perhaps the first instances in which the complications introduced by finite outer

Paper presented at the 83rd Meeting of the AGARD SMP on "Bolted/Bonded Joints in Polymeric Composites", held in Florence, Italy, 2-3 September 1996, and published in CP-590.

boundary geometries and the orthotropic behavior of the joint elements were taken into account. Moreover [4-6], in particular, provided the first approach to dealing with the complications introduced by the nonlinear behavior associated with the displacement statement of the pin-plate contact problem. It is fortunate that although the stresses around fasteners are inherently three dimensional in nature, most of the significant behavior features of fastener-plate interactions can be treated by two-dimensional elasticity analysis, provided appropriate experimentally generated correction factors for failure predictions are introduced. In addition to the work of Waszczak and Cruise (boundary element methods) and of Oplinger and Gandhi (complex variable boundary collocation), this type of effort has been characterized by the work of Air Force sponsored programs in the late 70's to mid 80's by Garbo et al. at McDonnell Douglas [13-15] and by Ramkumar and colleagues at Northrop [16,17], work at NASA by Crews and Naik [18,19] (finite element) in the early to late 80's and recent work by Madenci and Illeri [20] and by Xiong and Poon [21] (orthotropic elasticiy solution with variationl statement of boundary conditions). Similar efforts which have taken place since the early 1970's in India under A. K. Rao and colleagues [29-31] featured, in addition to the use of complex variable collocation approaches, an inverse method for dealing with the contact problem in which the contact angle is assumed while the corresponding bolt load is determined by an iterative process. The finite element approach of Naik and Crews [18,19] represents an adaptation of the inverse method by Eshwar [29-30].

Of special interest is the work of Hart-Smith [7-10] who made judicious use of the classical results for isotropic plates [25-28] in combination with empirical correction factors to account for effects of orthotropy as well as softening effects of local matrix damage at regions of high stress.

The details of the problem of contact between the fastener and the surrounding hole is a major challenge in the analysis of the bolted joint problem. Without a reasonably accurate knowledge of the size of the contact region it is not possible to determine the pressure distribution at the edge of the bolt hole with any degree of confidence, although a number of efforts have used the expedient of representing the pressure distribution by a "half-cosine" function in which 180 degrees of the circumference, assumed to represent the part of the fastener hole in contact with the bolt shank, is subjected to a pressure proportional to the cosine of the polar angle under consideration with the remaining part of the circumference unloaded. In the case of combined bearing and bypass loading it is customary to superpose stresses obtained this way for the bolt load component of the problem with the open hole solution (plate under tension or compression containing an interior hole with no bolt present) to treat the bypass load.

Along with analytical efforts, companion experimental efforts were conducted in the work of Waszczak and Cruise [2,3], Oplinger and colleagues [6], Hart-Smith et al. [7-10], Garbo et al. [13-15], Ramkumar and colleagues [16,17] and by Crews and Naik [18,19]. The most important point to come out of the comparison of experimental and analytical effort was that: (1) two-dimensional elasticity analysis is an effective means of predicting trends in joint behavior with respect to orthotropic response of the joint elements as well as geometric parameters such as lateral spacing of fasteners, the spacing of fastener rows, and the distances between fasteners from nearby free edges; (2) failure modes are also reasonably well predicted through two dimensional elasticity analysis. On the other hand, numerical values of failure loads tend to be under-predicted from point stress values although there has been considerable success in combining two-dimensional elastic stress analysis with the stress averaging approach of Nuismer and Whitney [32] for joint strength prediction. Considerable additional effort has been conducted by Hart-Smith and colleagues which provided simplified methods for dealing with combined bearing and bypass loading. These procedures were used by Hart-Smith et al for joint design in a number of aircraft design programs sponsored by NASA and DoD. The work of Hart-Smith and colleagues has also provided important insight into the effects of fastener deformations, including bending effects as well as the effects of fastener head contact with the outer surfaces of the joint elements [9].

Extensive work in the area of bearing-bypass interaction was also conducted by Crews and Naik [18-19] who developed important test procedures for providing design parameters in joints involving combined bearing and bypass. These and other test procedures have been discussed by Shyprykevich [33] as well as in MIL-HDBK-17-1E[34]. The procedures for pure bearing strength tests described in [33,34] have also been incorporated in ASTM test standard D5961-1M [35].

Only in recent years has much work of any substance been done on the three-dimensional problem. Recent work by Chang and colleagues [23,24], which includes extensive companion experimental effort, has done much to clarify the nature of the bearing failure problem as an out-of-plane shear failure process. In addition, the approach taken by Schaff and Iarve [36] represents a promising new analytic technique for efficient stress analysis in general and for three dimensional problems in particular.

In addition to the problem of determining stresses and failure loads for individual fasteners, prediction of load distribution among fasteners in a complex fastener array is a key step in joint design. Work by Ramkumar et al. [16,17], and by Hart-Smith and

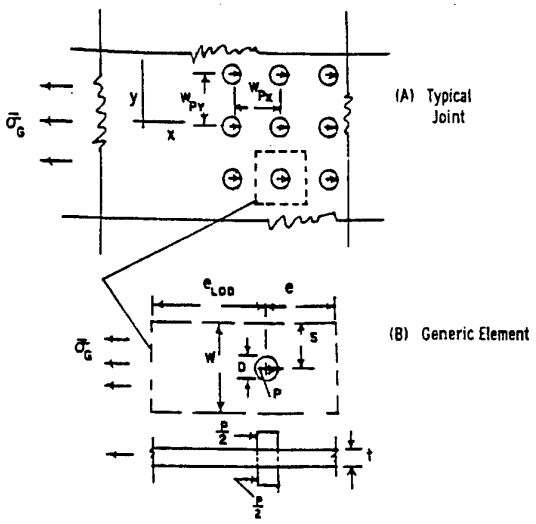


Figure 1 Joint Configuration

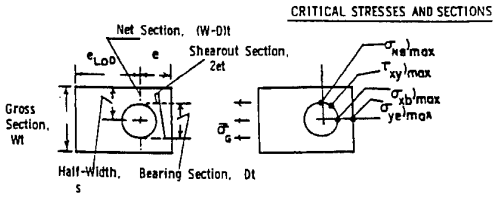


Figure 2 Critical stresses

colleagues [7-9] has been reported extensively. In particular, the Hart-Smith work has been embodied in a series of computer programs under the name "A4Exx" which have been made available for general distribution by the Air Force Aerospace Structures Information and Analysis Center (ASIAC). Other computer programs of this type, including SAMCJ developed by Ramkumar and colleagues under the Northrop Air Force sponsored program [16,17] as well as the more recent work of Madenci and Illeri [20] and of Xiong and Poon [21] have provided bolt load distribution calculations as a basis for joint design systems.

4. SELECTED RESULTS

Figure 1 shows the notation used in the following discussion for various geometric parameters, the most important being W, the lateral fastener spacing, D, the bolt diameter and e, the edge distance (i.e. from the bolt center to the unloaded edge). Figure 2 indicates various sections of the joint that participate in bearing the load and control failure, the"gross section" of area Wt (t being the laminate thickness), the n"net section" of area (W-D)t, the "shearout section" of area 2et and the "bearing section" of area Dt. Corresponding stresses which are of key importance in controlling joint failure are the gross section stress, $\bar{\sigma}_G$ and the peak net section, shearout and bearing stresses, $\sigma_{NS})_{max}$, $\tau_{xy})_{max}$ and $\sigma_{bx})_{max}$, respectively.

4.1 The Contact Problem

Figure 3 taken from Reference 6 compares predictions of stress concentrations in a pin loaded laminate containig 40 percent of 0 degree fibers with 60 percent of ±45 degree fibers, for a W/D of 2. (Although fastener spacings as small of this would not correspond to a realistic joint design, the results are illustrative of the general situation.) The stress concentration factors denoted K_G^{nt}, K_G^{b} and K_G^{s}, tabulated to the left of the figure, are net section, bearing and shearout stress concentration factors relating peak net section tension, bearing and shearout stresses shown in Figure 3 as ratios to the gross section stress ($\bar{\sigma}_G$ in Figure 1B). The differences between the stress concentration values for the half-cosine pressure vs. the displacement solution differ by 30-40%, indicating that the assumed pressure distribution would under- or over- predict the stress peaks depending on which failure mode is controlling failure of the joint. Note that these predictions are for an exact pin fit with no bypass loading, for which References 4 to 6 have shown that the contact angle is close to -90 to +90 degrees as indicated in the figure. Figure 4 shows some other examples of interest. Here radial pressure distributions predicted for a number of geometries are shown. The hexagonal and circular symbols represent predicted results for a pin in an infinite plate vs. a finite width plate with W/D equal to 2, giving fairly similar pressure distributions which, for practical purposes, could be modelled as a half cosine distribution without a great sacrifice of accuracy. On the other hand the triangles, representing a case of a pin clearance as small as .025 per cent, demonstrate that for typical load values the contact angle decreases significantly (to -75 to +75 degrees) and the half-cosine load which implies non-zero radial pressure from -90 to +90 degrees is no longer reasonable. Clearances on the order of 0.2% are fairly routine in accepted design practice, so that this effect has to be of concern. In addition, the square symbols show that the predicted pressure distribution for a small edge distance (e/D of 0.75) which tends to induce beam bending of the part of

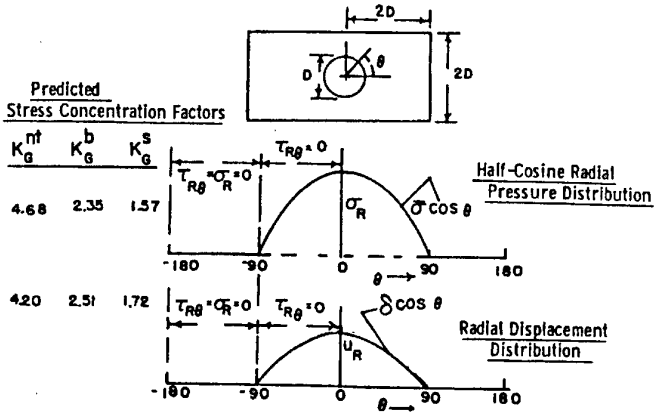


Figure 3 "Half cosine" pressure distribution vs. radial displacement boundary condition [6]

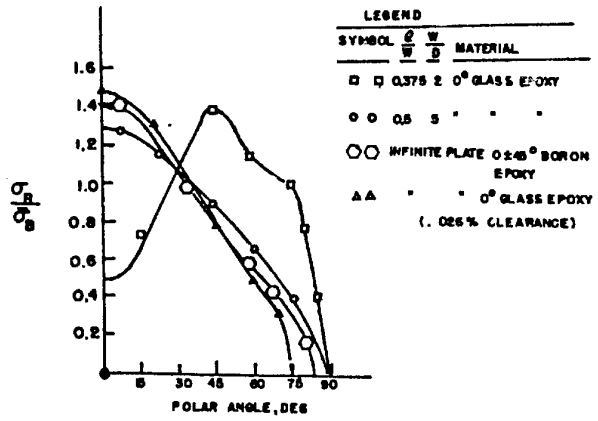


Figure 4 Radial pressure distributions predicted by contact solution [6]

the plate in front of the pin (illustrated in Figure 5) is radically different from the half-cosine distribution, so that investigations of any other than perfect pin fits with sizeable edge distances cannot be carried out with an assumed half-cosine pressure distribution.

The case of combined bearing and bypass stresses is another situation in which solution of the contact problem is important("bypass" stresses referring to the stresses at a given bolt hole in a multi-row joint produced by loads on fasteners other than the one in the hole under consideration). Figure 6 compares the behavior of the joint for pure bypass loading vs. pure bearing loading, for the case of an exact fit. Note that for pure bypass loading in particular a split contact region occurs, again being radically different from the half-cosine distribution. For combinations of bearing and bypass loading treated in [6] the contact situation was generally intermediate between the two cases shown in Figure 6. Although failure data for combined bearing and bypass loading are usually represented by a linear failure envelope, the predicted stresses concentrations presented in [6] were a nonlinear function of the bearing/bypass load ratio. Naik and Crews [18], who as stated earlier, adapted the inverse approach for the contact solution to the finite element method, investigated the validity of the superposition approach for combined bearing and bypass loads and reported that superposition of the open hole solution for bypass loading with the half-cosine solution for bolt bearing load gives unacceptable predictions of bearing stresses although the predicted peak net section tensile (or compression) stress predictions may not be unreasonable.

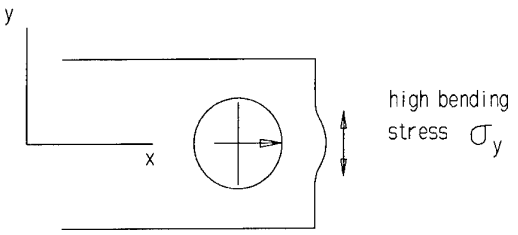


Figure 5 In-plane bending effects with Small e/D

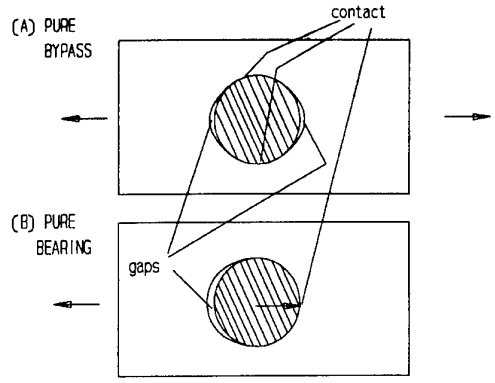


Figure 6 Contact Angles for Pure Bearing Load vs. Pure Bypass Load

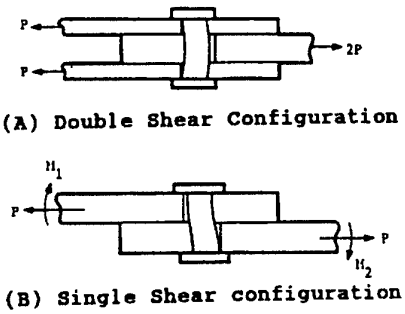


Figure 7 Single shear vs. double Shear configurations

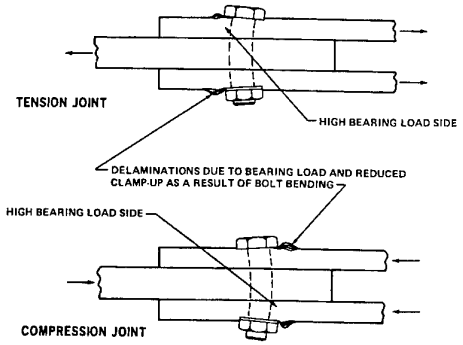


Figure 8 Effects of Fastener Bending on Joint Failure [9]

The two-dimensional solution unavoidably ignores the details of the pressure distribution through the thicknesses of the joint plate elements. As suggested in Figure 7, the contact area may be concentrated in fairly narrow bands near the surfaces of the joint plate elements. This is especially important in evaluating the difference in performance of single and double shear joints. A full three dimensional analysis is needed to develop an accurate assessment of the details of the through-the-thickness pressure distribution, although Harris et and Ojalvo [37] introduced a two-dimensional approximation in which the bolt is treated as a beam on an elastic foundation representing the plate area surrounding the bolt. This type of approach was used by Ramkumar et al [16,17] in developing the single fastener SASCJ code. It appears, incidentally, that the most crucial deformations of the bolt correspond to transverse shear and bending deformations of a beam. On the basis of analytical efforts by Hyer et al [12], distortions of the circular cross section of the bolt appear to be negligible.

Additional contact effects are represented in Figure 8 taken from [9] which illustrates the role of the bolt head and washer periphery in controlling the bolt deformations. Little analytical effort appears to have been devoted to this issue at this point.

It is apparent that full three dimensional stress analyses can throw considerable light on these issues, although it is not clear that much effort has been done in this area as yet.

4.2 Stress concentrations and failure prediction

Typical results obtained from two-dimensional elasticity analysis are represented by those discussed in [4-6] on the effects of fastener spacing and edge distance for single fastener elements (Figures 9 and 10) as well as parallel arrays of fasteners. Single fastener geometries correspond to the behavior of bolt bearing test coupons while parallel arrays reflect the behavior of rows of bolts loaded normally to the

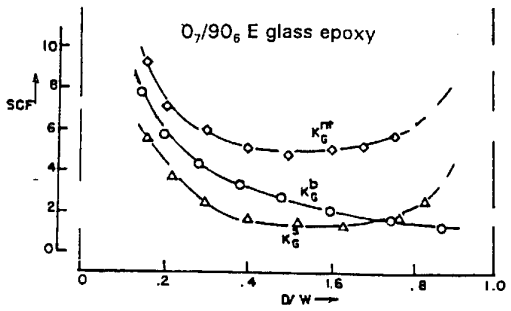
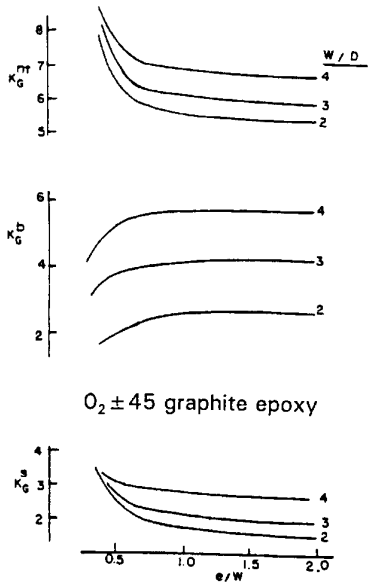


Figure 9 **Stress concentrations vs. D/W**[6]



$0_2 \pm 45$ graphite epoxy

Figure 10 **Stress concentrations vs. edge distance**[6]

center lines of the rows, eg. the vertical rows in Figure 1. Figures 9 and 10 for single fastener geometries give typical behavior of the three stressconcentration factors (peak net section tension, shear and bearing stress) as functions of joint geometry, ie. of the fastener spacing in terms of D/W and the edge distance in terms of e/W. The most significant characteristic of Figure 9 is the tendency for minimum peak stresses to occur at a joint width (or fastener spacing for the parallel array case) of twice the bolt diameter, which is considerably smaller than the four diameter or larger spacings usually considered to be good design practice. The results discussed in [8] by Hart-Smith based on empirically corrected isotropic stress analysis indicated a slightly larger optimum spacing (about 2.5D) for the single fastener case though not radically different from what Figure 9 suggests.

Note that a minimum in the net section and shear stress concentrations can be expected to correspond to maxima in joint strength, provided the joint does not fail by bearing failure, which it is not likely to for such small values of W/D.

The results given in Figure 10 are of similar interest. Although the effects of edge distance, e, are customarily considered in terms of the edge distance-to-diameter ratio e/D, the results of Figure 10 suggest that for laminates which fail in either net tension or shear failure, the controlling peak stresses are not minimized until e is at least equal to W, regardless of the bolt diameter. This is illustrated in Figure 11, which shows an arrangement of three fasteners having the same effective W but with differing diameters. Based on the curves for the stress concentrations shown in Figure 10, the minimum edge distance for full joint strength, denoted e_{min}, is equal to W in all three cases. Edge distances specified in terms of e/D would lead to different e values for each of the bolt diameters in Figure 11. Note that in [8] Hart-Smith gave curve-fitting formulas for the predicted stress concentration factors in isotropic plates which contained e/W rather than e/D to represent edge distance, in agreement with the results discussed in [6] for orthotropic laminates.

Experimental data related to the analytical results in Figures 9 and 10 are given in Figures 12 and 13 [6]. Figure 12 gives bearing strength test results for a number of laminates, verifying the observed effect of W/D suggested by the analytical results of Figure 9, and confirming the expected strength maximum for W/D=2. The materials considered in both Figure 12 and 13 are given at the upper right of Figure 12. Figure 13 gives test results similarly confirming the trends of joint strength vs. e/W suggested in Figure 10. Thus the analytic results based on two-dimensional elasticity analysis from bearing tests.

Prediction of actual strength values from the results of two-dimensional elasticity analyses requires the addition of a laminate strength analysis routine to the stress analysis, since the latter treats the laminate as a homogenous orthotropic body with no consideration of the details of laminate stacking sequence. Attempts to make such strength predictions based on inputting thickness-averaged stress values from the stress analysis into the laminate strength routine were carried out in the early work reported by Waszczak and Cruise [2,3] as well

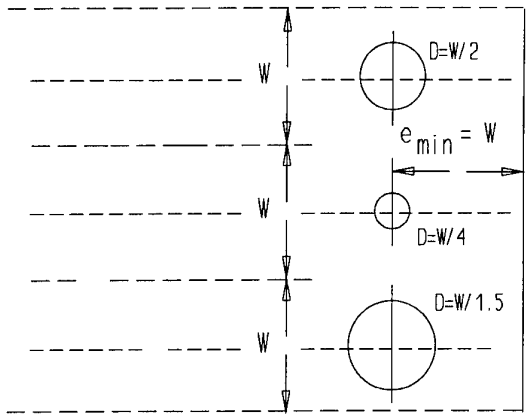


Figure 11 Minimum Edge Distance is Equal to W (independent of D)

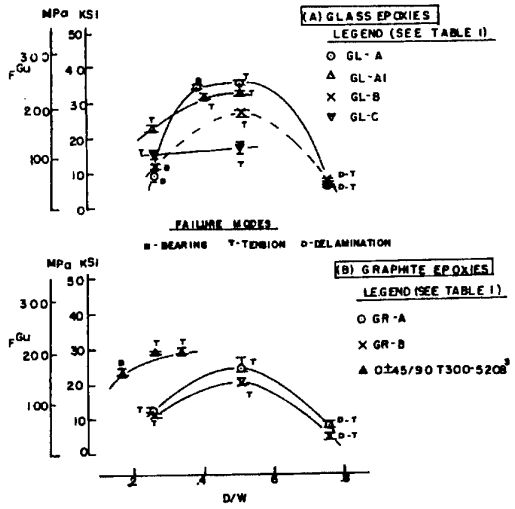


Figure 12 Experimental Results on Strength vs. D/W [6]

as that of Oplinger and Ghandi [4-6]. It was apparent that while these types of predictions could identify trends in strength vs. stacking sequence as well as determining failure modes, strength levels were usually under- predicted by this approach, since while organic matrix composites are relatively brittle compared with metals, there is some relief of peak stresses because of local softening of the matrix in the vicinity of the stress peaks.

Figure 14 [6] compares the strength of metallic [38] and composite bearing test specimens on the basis of the reduction of the average net section strength denoted F^{tnu} to the strength of the virgin material, denoted F^{tu}. Note that the results in Figure 14 are plotted against W/D, so that bolt size decreases and relative fastener spacing increases toward the right of the figure. The dashed curve in the upper portion of the figure for metal joints represents the failure prediction for ideally brittle isotropic materials obtained from the inverse of the net section stress concentration factor given in [25] for bolt loaded lugs. Results lying above the brittle failure curve indicate the presence of a stress relief mechanism, and it is clear that in the case of metals, yielding does have this effect. The results for the composite materials shown in the lower part of the figure likewise lie for the most part above the brittle failure curve, again indicating the presence of a stress relief mechanism. It has become generally accepted[8] on the basis of microscopic examination of failed bolt bearing specimens that localized damage in the form of delamination and fiber splitting around the region of peak net-section stresses is responsible for this stress relief effect. Note that the matrix in fibrous composites has the function of providing lateral transfer of loads through

Notation	%0^0/%45°/%90°	Material
"GL A " --	40/60/0	S glass epoxy
"GL A1" --	"	" " "
"GR A " --	40/60/0	carbon epoxy
"GL B " --	20/60/20	S glass epoxy
"GR B" --	"	carbon epoxy
"GL C" --	54/0/46	E glass epoxy

shear stresses, and if the matrix is depleted or softened locally, removal of this shear transfer mechanism reduces the composite to a system of cables, in which case the stresses will tend to be averaged over the region of localized damage. Nuismer and Whitney[32] conducted studies of plates under tension containing holes of various shapes and sizes, from circular holes to crack-like slits. The results of their study indicated that by assuming a region of local matrix damage to be present and independent of the details of the hole shape or size, failure load could be predicted by determining the load at which the stress at a fixed distance from the hole boundary (presumably related to the damage zone size and commonly denoted a_o) is equal to the strength of the laminate as determined from test coupons without holes. The value of a_o is determined by empirical fits of data on plate strength vs. hole size. Once a_o is determined for a given laminate, the strength of bolted joints as well as plates with open holes can be successfully predicted by comparing the stress predicted at the distance a_o from the boundary of the bolt hole to the strength of the unnotched laminate. The work of Garbo et al. [13-15] made extensive use of this type of prediction. It has

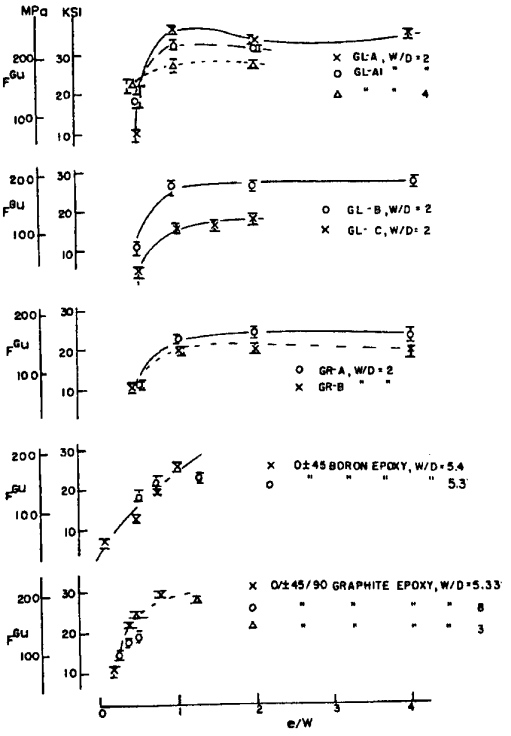


Figure 13 **Experimental results on e/W [6]**

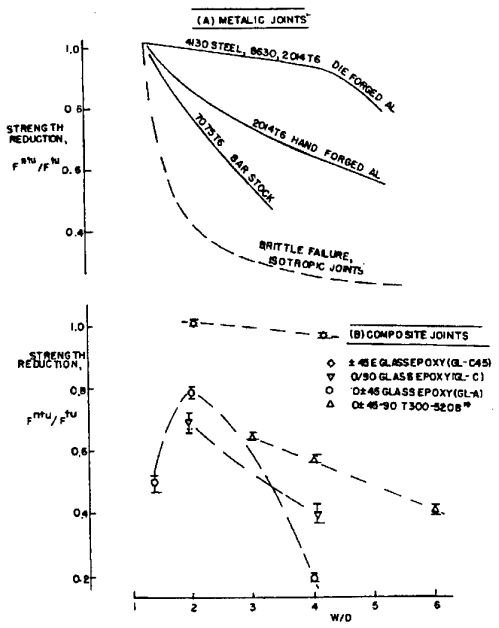


Figure 14 **Comparison of metallic and composite bearing test results[6]**

become common practice to use this approach in conjunction with two-dimensional elasticity analysis in the prediction of bolted joint strength for design purposes. It is generally accepted that the Nuismer Whitney approach is reasonably successful for predicting joint loads for net section tensile and compressive failures as well as for shear failures, although not for bearing failure.

In an alternative approach, Hart-Smith [8] presented a method of predicting strength based on the application of empirical correction factors to stress predictions for isotropic joint materials given in Petersen [25] and elsewhere. Hart-Smith defined an effective stress concentration factor at failure, denoted k_{tc}, which is equivalent to the inverse of the abscissae of Figure 14, ie. to F^{tu}/F^{ntu}, and reported data that implies a linear relationship between k_{te}, the elastic net section stress concentration calculated as a function of W/D and e/W, and k_{tc}, of the form $k_{tc}-1=C(k_{te}-1)$. Data presented in [8] for various joint geometries and including data from open-hole tests reflected a range of k_{te} values from about 2.5 to 7.5, for both quasi-isotropic (25% 0° /50% 45° /25% 90°) and $0_2\pm45$ carbon epoxy laminates tended to confirm this linear relation. The results showed that for geometries with a k_{te} a value of 5, for example, the effective stress concentration factor k_{tc} was 2 for the quasi-isotropic laminates and 2.85 for the $0_2\pm45$ material, verifying the reduction of stress concentration factor from the elastic stress analysis prediction. (In the case of $0_2\pm45$ laminates the k_{tc} value obviously included a correction for orthotropy of elastic response as well as the stress concentration suppression effect.) Hart-Smith's results are interesting in confirming the occurrence of a stress relief mechanism. The Nuismer Whitney approach has the advantage for predictions based on the application of an orthotropic stress analysis in providing a method for directly using the stress results to predict joint strength without the need for extensive testing.

A more direct failure prediction approach based on physical modelling of the laminate which has been developed by Chang et al.[22-24] incorporates a progressive damage model into associated two-dimensional finite element calculations. Results of this approach lead to conclusions similar to those obtained from the Nuismer Whitney correction to 2-D linear elasticity analysis. Recently the progressive failure approach has been applied in conjunction with investigations of bearing failure [23] and an FAA supported effort involving comparison of open and filled hole response [24] of bolted joints. The latter is an issue in development of test data for determining the Nuismer Whitney a_o parameter, since filled hole specimens (equivalent to plates with interior holes with bolts inserted to provide the restraint against radially inward displacement of

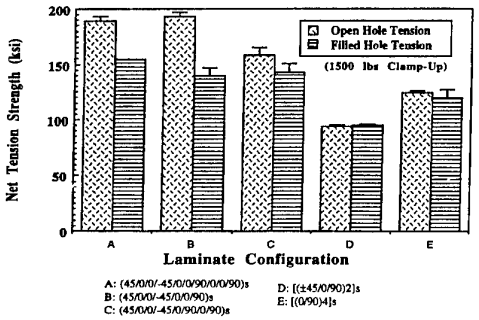


Figure 15 Open hole vs. filled hole joint strength[24]

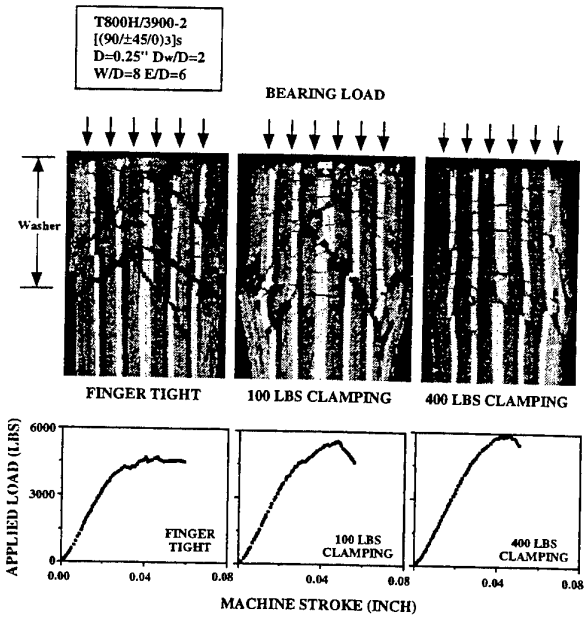


Figure 16 Bearing failure studies [23]

the laminate) are physically more representative of actual joints than are open holes with no restraint at the hole boundaries. Figure 15 gives an example of data which has been obtained in this study. It shows that filled hole specimens are usually weaker than open hole specimens, and it is suggested that this is because edge delamination, which is a factor in the determination of a_o, is suppressed in filled hole specimens. The effect of the presence of clamping pressure has been found to have an additional influence on the results of such tests.

Bearing failure studies reported in [23] led to important observations on the nature of bearing failure. Bearing failures for bolted joints with typical clamping arrangements are illustrated in Figure 16. These results clarify the fact that bearing failure is a form of out-of-plane shear failure occurring along planes oriented at 45 degrees to the mid-plane of the laminate. On the basis of these results it appears that bearing failure may not be associated with the same damage zone feature that controls net section tension and shear failure. In the latter case, the thicknesses of individual plies probably control the damage zone size while in the case of bearing failure it is more likely to be controlled by the total laminate thickness.

4.3 Three dimensional analysis efforts

As discussed earlier, two-dimensional analysis necessarily ignores the details of through-the-thickness contact between the between the bolt and the joint plate elements. As discussed by Shyprykevich [33] issues which are affected by through-thickness variations in contact pressure, eg. differences in performance of single and double shear joints (Figure 7) as well as between protruding head and countersunk fasteners are usually investigated through standard tests giving coupon bolt bearing strength as a function of joint geometry. Fastener deflection characteristics which are needed for prediction of bolt load distribution in multi-row joints have been addressed using the beam-on-elastic foundation [37] representation for the bolt, but three dimensional stress analysis would provide a more accurate assessment of this aspect of the joint design problem.

Until the 1980's extensive use of three dimensional analysis to investigate joint behavior was relatively difficult not only because of the lack of computing power but also because of a lack of efficient methods of creating three dimensional meshes and for presentation of output data. The graphical capabilities which are routinely available at this point for pre- and post-processing of finite element data as well as the computing power that can be applied to the main computational effort have made three-dimensional analysis of bolted joints a relatively straightforward endeavor.

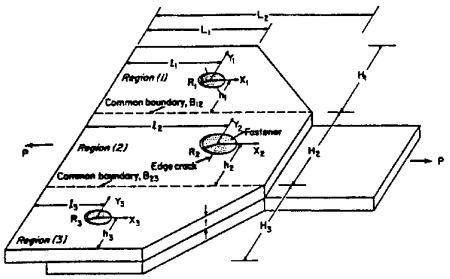


Figure 17 Analysis of multi-fastener joints by modified mapping/collocation [20]

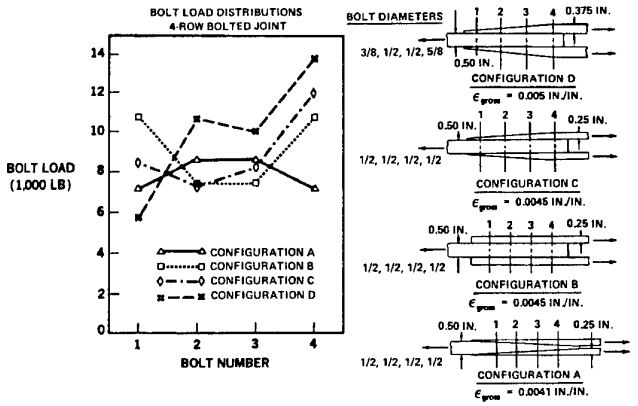


Figure 18 Load distribution in multi-fastener joints [9]

Studies being presented at this workshop [36,39] are examples of what is currently feasible.

Other than standard displacement-based finite element approaches, a new approach [36] based on the use of multi-dimensional spline functions for representing various quantities entering into the analysis is of interest as a more efficient approach to three-dimensional analysis. Three dimensional analysis including effects of progressive damage are reported in [39]. In addition, F. K. chiang [41] reports work at Standford University in which progressive failure models are incorporated into a standard ABAQUS analysis, ABAQUS having the capability for incorporating user-generated elements and modelling features. It is anticipated that considerable progress with the three-dimensional bolted joint problem will be realized in the next few years.

4.4 **Analysis of multi-fastener joints and joint design routines.**

In addition to routines for determining stresses around bolt holes in mechanically fastened joints and procedures for predicting joint failure on the basis of the stresses, joint design systems have to provide a method for the distribution of loads among various fasteners present in the joint.

Various Government-funded design and analysis packages such as A4EK [7-10]and SAMCJ [16,17] have been developed in the US and are available on a limited basis from the U. S. Air Force's Aerospace Structures Information and Analysis Center (ASIAC). Other efforts providing calculations of bolt load distribution include that of Waszczak and Cruise [2,3] as well as recent efforts such as that of Madenci et al [40] which is supported by FAA grant, and the effort of Xiong and Poon [21].

Bolt load distributions are controlled by stretching deformations of the joint plate elements together with effects of fastener rotation, slippage due to fastener hole clearance and beam shear and bending deformations. Plate stretching deformations can be predicted effectively by two dimensional stress analysis of single fastener elements, but the effects related to the fastener-controlled deformations are normally determined from bearing tests. Once the deformation characteristics of the single-fastener element ar determined, the load distribution for the joint as a whole can be obtained from a redundant structural analysis in which the single fastener elements and fasteners are treated as an array of springs. For single shear joints, bending deformations have to be taken into account in these calculations.

A more elaborate approach is incorporated by Madenci [20, 40] as illustrated in Figure 17. Here the joint is divided into regions containing the individual fasteners for which the stresses and deformations can be simultaneously determined using the complex variable-collocation approach with continuity of stresses and displacements imposed at the zone boundaries. The zones thus are analogous to super-elements in a finite element analysis. Examples of bolt load distributions obtained are shown in Figure 18 [9] for several practical joint configurations. Note that joint plate tapering as well as variation of fastener diameters (fastener diameters are listed to the left of the sketch of each joint type) may be used to optimize the joint. Configurations C and D (the upper sketches in the figure) both have tapered outer plate elements, but the strongest joint based on the maximum strains listed at the right of the sketches show that the D configuration which varies the bolt diameters is the strongest.

5. CONCLUSIONS

• Two dimensional elastic stress analysis gives good predictions of joint behavior if the problem of contact between the bolt and plate is addressed with displacement rather than assumed pressure boundary conditions. Effects of high bypass loading, hole clearance and short edge distance will introduce significant solution errors unless the contact problem is treated realistically.

• Two dimensional orthotropic elastic stress analysis in conjunction with laminate strength analysis with corrections such as that of Nuismer-Whitney for stress relief effect give good predictions of joint strength and failure mode as functions of geometric parameters such as W/D and e/D as well as of the laminate material and stacking sequence.
• Three dimensional analysis is needed to give a better understanding of through-the thickness contact pressure distributions associated with bolt bending and other effects. Recent 3D investigations and development of new approaches to 3D analysis promise to give a better understanding of these effects in the near future.
• A number of routines such as A4EK and SAMCJ have been developed for providing bolt load distributions for design purposes. These may be used in conjunction with test methods such as those described in [33] and [34] for determining the effect of joint configuration and fastener type on fastener deflections.

6. REFERENCES

1. D. W. Oplinger "Structural Joints", Lubin's Advanced Composites Handbook 2nd ed. Chapter 28 , to be published (1997)

2. J. P. Wascczak and T. A. Cruise "Failure Mode and Strength Predictions of Anisotropic Strength Predictions of Anisotropic Bolt Bearing Specimens" *J. composite Materials*, v. 421 (1970)

3. J. P. Waszczak and T. A. Cruse, "A Synthesis Procedure for Mechanically Fastened Joints in Advanced Composite Materials", Air Force Materials Laboratory Report AFML-TR-73-145 (Carnegie-Mellon University Doctoral Dissertation, J. Waszczak) (1973)

4. D. W. Oplinger and K. R. Gandhi, "Stresses in Mechanically Fastened Orthotropic Laminates", Proceedings of the First Conference on Fibrous Composites in Flight Vehicle Design, Air Force Flight Dynamics Laboratory Report AFFDL-TR-74-103 (1974)

5. D. W. Oplinger and K. R. Gandhi, "Analytical Studies of Structural Performance in Mechanically Fastened Fiber-Reinforced Plates", Proceedings of the Army Solid Mechanics Conference 1974, Army Materials and Mechanics Research Center Manuscript Report AMMRC MS 74-8 (1974)

6 D. W. Oplinger "On the Structural Behavior of Mechanically Fastened Joints in Composite Structures" in *Fibrous Composites in Structural Design*, Proceedings of the Fourth NASA DoD Conference on Fibrous Composites in Structural Design, Plenum Press, New York pp. 575-602 (1980)

7. L. J. Hart-Smith "Bolted Joints in Graphite -epoxy Composites" NASA Langley Contractor Report NASA CR-144899 (1977)

8. L. J. Hart-Smith, "Mechanically -Fastened Joints for Advanced Composites - Phenomenological Considerations and Simple analyses" in *Fibrous Composites in Structural Design*, Proceedings of the Fourth NASA DoD Conference on Fibrous Composites in Structural Design, pp. 543-574, Plenum Press, New York (1980)

9. W. D. Nelson, B. L. Bunin and L. J. Hart-Smith, "Critical Joints in Large Composite Aircraft Structure", Proceedings of the Sixth Conference on Fibrous Composites in Structural Design, pp II-2 to II-38, Army Materials and Mechanics Research Center Manuscript Report AMMRC MS 83-2 (1983)

10. L. J. Hart-Smith "Design Methodology for Bonded-Bolted Composite Joints " v. 1 Air Force Wright Aeronautical Laboratories Report AFWAL-TR-81-3154 (1982)

11. M. W. Hyer and E. C. Klang, "Contact Stresses in Pin-Loaded Orthotropic Plates", Virginia Tech Center for Composite Materials and Structures Report CCMS-84-02 (1984)

12. M. W. Hyer, E. C. Klang and D. E. Cooper "The effects of pin elasticity, clearance and friction on the stresses in a pin loaded orthotropic plate" , Virginia Tech Center for Composite Materials and Structures Report CCMS-85-04 (1985)

13. S. P. Garbo, J. M. Ogonowski and H. E. Reiling, Jr, "Effect of Variances and Manufacturing Tolerances on the Design Strength and Life of Mechanically Fastened Composite Joints" v. 2 Air Force Wright Aeronautical Laboratories Report AFWAL-TR-81-3041 (1981)

14. S. P. Garbo, "Effects of Bearing/Bypass Load Interaction on Laminate Strength", Air Force Flight Dynamics Laboratory Report AFWAL-TR-81-3114 (1981)

15. S. P. Garbo and J. M. Ogonowski, "Effect of Variances and Manufacturing Tolerances on the Design Strength and Life of Mechanically Fastened Composite Joints" Air Force Flight Dynamics Laboratory Report AFFDL-TR-78-179 (1978)

16. R. L. Ramkumar, E. S. Saether and K. Appa, "Strength Analysis of Laminated and Metallic Plates Bolted Together by Many Fasteners", Air Force Flight Dynamics Laboratory Report AFWAL-TR-86-3034 (1986)

17. R L. Ramkumar, E. Saether and D. Cheng, "Design Guide for Bolted Joint in Composite Structures", Air Force

Wright Aeronautical Laboratories Report AFWAL-TR-88-3035 (1986)

18. R. A. Naik and J. H. Crews "Combined Bearing and Bypass Loading on a Graphite/Epoxy Laminate", *Composite Structures*, v. 6 pp. 21-40 (1986)

19. J. H. Crews and R. A. Naik, "Ply-Level Failure analysis of a Graphite/Epoxy Laminate under Bearing /Bypass Loading" NASA Technical Memorandum 100578 (1988)

20. E. Madenci and L. Illeri, "Analytical Determination od Contact Stresses in Mechanically Fastened Composite Laminates with Finite Boundaries", University of Arizona Department of Aerospace and Mechanical Engineering Report (1993)

21. Y. Xiong and C. Poon "A Design Model for composite joints with multiple fasteners" National Research Council Report NRC 32165, NRC Canada (1994)

22. F. K. Chang "A progressive failure model for laminated composites containing stress concentrations" J. Compos. Materials pp. 834-855 (1987)

23. F. K. Chang and Chang- Li Hung, "Response of Double Shear-Lap Bolted Composite Joints under Multiple Bypass Loads", Standford University Dept. of Aeronautics and Astronautics Report (Doctoral dissertation of Chang-Li Hung) (1993)

24. Y. Yan, H. T. Sun and F. K. Chang "Net Tension Strength of Laminated Composites Containing a Bolt", Grant Report FAA Grant 95-G-012 (1996)

25. R. E. Petersen, "Stress Concentration Factors", p. 135 John Wiley and Sons, New York (1974)

26. W. G. Bickley "The distribution of stress around a circular hole in a plate" Phil Transactions of the Roy. Soc. London Series A v. 227 pp. 383-415 (1928)

27. R. C. Knight "Action of a rivet in a plate of finite breadth" Philosophical Mag. Series 7 v. 19 pp. 517-540 (1935)

28. W. Koiter "An elementary solution of two stress concentration problems" J. applied Math. v. XV pp. 303-308 (1957)

29. V. A. Eshwar, B. Dattaguru and A. K. Rao, "Partial Contact and Friction in Pin Joints", Report No. ARDB-STR-5010, Aeronautics and Research and Development Board, New Delhi India (1977)

30. V. A. Eshwar, "Analysis of Clearance Fit Pin Joints", Int. J. Mech. Sci., v. 20 pp. 477-484 (1978)

31. S. P. Gosh "Analysis of Joints with Elastic Pins" Doctoral Thesis, Indian Institute of Science (1978)

32. J. M. Whitney and R. Nuismer, "Stress Fracture Criteria for Laminated Composites Containing Stress Concentrations", *Journal of Composite Materials*, v. 8 pp. 253-265 (1974)

33. P. Shyprykevich, "Characterization of Bolted Joints Behavior: MIL-HDBK-17 Accomplishments at Standardization" ASTM Journal of Composites Technology and Research, v. 17 No. 3 (1995)

34. American Society for Testing and Materials Standard ASTM D5961-1M, "Standard Test Method for Bearing Response of Composite Laminates" (1995)

35. Military Handbook MIL-HDBK-17-1E *Guidelines for Characterization of Structural Materials* Chapter 7 (1996)

36. J. R. Schaff and E. Iarve "Stress analysis of Open and Fastener Hole Composites Based on the Three Dimensional Spline Variational Technique" Specialists Meeting on Bolted/Bonded Joints in Polymeric Composites 83 AGARD SMP (1996)

37. H. Harris and I. Ojalvo, "Simplified three dimensional analysis of mechanically fastened joints", Proceedings of the Fourth Army Symposium on Solid Mechanics, Army Materials and Mechanics Research Center Report AMMRC MS 74-8 (1974)

38. E. F. Bruhn *Analysis adn Design of Flight Vehicle Structures*, p. D1.7, True State Offset Co. (1973)

39. M. M. Shokrieh, L. B. Lessard and C. Poon, "Three dimensional progressive failure analysis of pin/bolt loaded composite laminates", Specialists Meeting on Bolted/Bonded Joints in Polymeric Composites 83 AGARD SMP (1996)

40. "Contact stresses and stress intensity factors in a mechanical joint with arbitrarily located fasteners" FAA Grant 94-G-0029 (1994)

41. F. K. Chang private communication August 1996

Bolted Joint Technology in Composite Structures -- Analytical Tools Development

C. Poon and Y. Xiong
Structures, Materials and Propulsion Laboratory
Institute for Aerospace Research
National Research Council Canada
Montreal Road, Ottawa, Canada K1A 0R6

1. SUMMARY

Graphite fiber reinforced polymeric composites have been used extensively in the primary and secondary structures of modern military and civilian aircraft. In these structures, bolted joints are important considerations in structural design and repair. Reviews of the literature indicated that most of the current design methods were developed for single fastener joints and, in general, design optimization, three dimensional effects and fatigue behaviour required further research and development. This paper reviews the results of the bolted joint technology development project sponsored by the Institute for Aerospace Research and the Canadian Department of National Defence. The project includes the development of computer-aided design tools for optimizing the design of multi-fastener composite joints and for predicting the fatigue behaviour of pin/bolt loaded composite laminates. Current focus and future direction of the development of analytical tools for repair of composite structures and other applications are presented.

2. INTRODUCTION

Carbon fiber reinforced polymeric composites are used extensively today in many aerospace applications because their superior strength-to-weight and stiffness-to-weight ratios enable light-weight primary structures be manufactured. For example, the primary structure of the Canadian Space Station Remote Manipulator System (SSRMS) consists of four composite arm boom segments. Each segment consists of a thermoplastic composite cylinder mechanically fastened to metallic flanges at both ends. These segments are then connected by bolted joints. Another example is that modern airframes are manufactured from many different parts such as skins, stiffeners, spars, etc. These parts must be assembled to form components and then finally the whole structure. For composite parts, adhesive bonding and mechanical fastening are the prevalent joining methods used in assembly. Although adhesive bonding has many advantages, including higher joint efficiency and lower part counts, mechanically fastened joints are often required for thick laminates and are indispensable when manufacturing breaks are required for disassembly, inspection, repair or replacement. Since bolted joints are a major source of stress concentration, they are perhaps the most prone to failure. The material's anisotropic behaviour, poor yielding capability, and the absence of fiber reinforcement in the through-the-thickness direction make the failure modes very different from those of a metallic joint. As a result, design methods for metallic joints cannot be applied directly in composite bolted joints. This concern had prompted extensive engineering effort in developing appropriate design methods for mechanically fastened composite joints.

An earlier literature review [1] identified that most design and analysis methods were, in general, based on finite element methods, two dimensional theory of elasticity, and boundary collocation methods. The methods were developed for the design of single fastener joints. In general, design optimization was not available. This finding had prompted the initiation of a project at the Institute for Aerospace Research (IAR) which aimed at developing a computer-aided tool capable of optimizing the design of multi-fastener composite joints. As a result of this effort, the authors have developed an analytical method based on a complex variational approach for multi-fastener joint design optimization [2].

In a more recent literature review [3], Shokrieh found that the static behaviour of pin/bolt loaded composite laminates had been studied extensively; however, work was required in predicting the behaviour of pin/bolt loaded composite laminates under fatigue loading. The team from McGill University was awarded a contract from IAR to develop a new modeling method, known as *fatigue damage progressive modeling*, for predicting fatigue behaviour. The development of the fatigue model was completed.

At present, the design optimization module developed at IAR is being modified for implementation into a computer-aided design tool for bolted patch repair. This project has just begun and is expected to be completed in two years. The technical highlight of the work is the biaxial bearing/bypass testing of composites to develop better allowables and failure criteria for joint strength prediction.

In this paper, the results of the projects undertaken at IAR and McGill University are reviewed. In addition, the scope and progress of the development of the computer-aided design tool for bolted patch repair are presented.

3. DESIGN OPTIMIZATION OF JOINTS

The technical aspects of the analytical model developed at IAR for optimizing the design of multiple fastener composite joints are reviewed in this section. The analytical model consists of three parts: (i) stress analysis, (ii) strength prediction, and (iii) design optimization . A flowchart illustrating the major stages in joint design optimization is shown in Fig. 1. The model has been incorporated into a computer code which enables joint design to be optimized on a personal computer.

3.1 Analytical Model

The first stage is to identify whether the type of joint to be used in the structure is single-lap or double-lap. These configurations consist of two plates for the single-lap joint or three plates for the double-lap joint connected by two or more fasteners. The plate material can be composite or metal. The plates are of the same finite width, W, and have, in general, m circular or elliptical holes of various sizes which are arbitrarily located in the plate as shown in Fig. 2. The load, P, applied at the end of a plate is in equilibrium with the m fastener loads, P_i

Paper presented at the 83rd Meeting of the AGARD SMP on "Bolted/Bonded Joints in Polymeric Composites", held in Florence, Italy, 2-3 September 1996, and published in CP-590.

(i = 1, 2,...., m). The model assumes that the load on one plate is transferred by flexible frictionless fasteners over half of the hole edge and the secondary bending of the plate in the single-lap configuration is negligible compared to the in-plane deformation. The fasteners are modeled as elastic beams, as shown in Fig. 2, with both ends fixed for the double-lap joint. For the single-lap joint, the fasteners are fixed at one end and are free to translate in the loading direction at the other end, see Fig. 2. In this way, the rotation of fasteners is simulated.

3.1.1 Stress analysis

The next stage is joint stress analysis which takes into account the flexibility of the plates and fasteners. In order to determine the stress state in the joint, the fastener loads must be known. The model uses an iterative scheme, see Fig. 1, to determine the fastener loads for joint stress analysis. In single-lap joints, the applied load at the end of one plate is transferred by fasteners loaded in shear to the other plate which is fixed at one end. In double-lap joints, the applied load at the end of the middle plate is transferred to two identical side plates which are both fixed at one end. Since the side plates are assumed to be identical, the load is evenly distributed between them and as a result, only one of the side plates is modeled in the analysis for the double-lap configuration. The iterative scheme involves the following steps:

1. Assign an initial value for each fastener load based on the bending stiffness, EI, of the fastener.
2. Perform a two dimensional stress analysis on the first plate. The analysis is based on a displacement-based complex variational formulation which involves only force boundary conditions. The fastener loads, which are obtained from step 1, are simulated by a cosine function. In this step, the hole elongations under the fastener loads and by-pass loads are calculated.
3. Calculate the deflections of the fasteners under the shear loads using the mechanics of materials approach.
4. Calculate the summation of hole elongations and fastener deflections in the first plate and use the combined displacement as the rigid body movement of the contact region of the corresponding fastener holes in the second plate. Perform a two dimensional stress analysis on the second plate. Since the analysis involves both displacement and force boundary conditions, a mixed variational formulation is employed. In this step, the reaction forces at the fastener holes in the second plate under the rigid body displacements and the applied load are calculated.
5. Use the reaction forces on holes of the second plate as new fastener loads and repeat steps 2 to 4 until the solution converges.

In this iterative scheme, the joint stress analysis is performed based on fastener loads which are calculated rather than assumed. A detailed description of the complex variational formulations is presented in Ref. 2.

3.1.2 Failure analysis

Following the stress analysis, joint strengths and failure modes are predicted by applying failure criteria. There are many existing failure criteria as indicated in a critical review by Rowlands [4]. In this model, the point stress criterion and the quadratic tensor polynomial criterion [5, 6] are used to predict laminate failure instead of first-ply failure. In order to ignore the three-dimensional effect and the nonlinear behaviour at the hole edge, a set of characteristic lines arranged in a rectangular pattern around the loaded half of the fastener hole is used [2]. In this model, the joint strength is predicted based on two-dimensional elastic stresses determined along the characteristic lines and the failure modes are identified according to the failure locations on the lines. The present model can predict three failure modes which are net-tension, shear-out and bearing.

3.1.3 Design optimization

The joint strength is influenced by many parameters which can be broadly divided into two categories: (a) laminate construction, and (b) joint geometry. In the category of laminate construction, parameters such as material system and layup have significant effects on joint strength and failure mode. In the category of joint geometry, laminate thickness, hole diameter, pitch distance, edge distance, number of fasteners and hole pattern are important parameters. The optimization of joint strength with respect to these design parameters is carried out in two steps. In the first step, the joint strength is maximized with respect to a set of material systems and layups. The joint geometry is held constant. In the second step, the joint strength is optimized with respect to a set of geometric parameters using the optimized material and layup for the laminate. The optimization algorithm proceeds on a one-by-one basis amongst the candidate configurations until the maximum joint strength is determined.

3.2. Joint Design Test Cases

Results of joint stress analysis, failure prediction and design optimization are presented. These results are compared with numerical results obtained from finite element analysis and data obtained from the literature in order to validate the design model. The material properties [7-9] used in the test cases are shown in Table 1.

3.2.1 Stress distribution around bolt hole

The intent is to verify the accuracy of the complex variational method in determining stress distributions around a bolt hole. The problem, as shown in Fig. 3, consists of a rectangular AS4/3502 $[0/45/-45/90/0]_S$ laminate with an elliptical loaded hole. The problem was studied by Wang, *et al* [7] using a boundary collocation approach to examine the benefit of using elliptical fasteners in composite joints. Both the width, W, and edge distance, e, of the laminate are 1.5 *in.* The major and minor axes of the elliptical hole are 0.3 *in* and 0.25 *in*, respectively. The bearing and hoop stress distributions along the loaded half of the hole determined by using the present method are shown together with the analytical and finite element results from Wang, *et al* [7] in Fig. 3. Good agreements between these results are demonstrated.

3.2.2 Predictions of joint strengths and failure modes

The joint strengths and failure modes were predicted for several composite-to-metal joints with multiple fasteners. These joints were investigated theoretically and experimentally by Ramkumar, *et al* [8,9]. In all the cases studied, one plate is aluminum and the other plate is AS1/3501-6. The percentages of the 0^o, $\pm 45^o$ and 90^o fibers are 50, 40 and 10, respectively. All fasteners are steel with protruding heads. The material properties of AS1/3501-6 are shown in Table 1. The material properties of aluminum and steel are: $E_{al} = 10\times10^6$ *psi*, $\nu_{al} = 0.3$ and $E_{st} = 30\times10^6$ *psi*, and $\nu_{st} = 0.3$, respectively. The failure of the composite plate was predicted using the point

stress criterion and the quadratic tensor polynomial criterion. A least squares curve fit procedure was used to determine the characteristic dimensions from bolted joint test data [8,9].

For the cases considered, the joint strengths at each fastener hole were predicted for tension, shear-out and bearing failure. The results are summarized in Tables 2 to 4. The lowest value identifies the most critical hole and the prevailing failure mode. When two or more predicted strengths are close, the joint may fail in a combination of the corresponding modes. The fastener loads, joint failure loads, failure locations, and failure modes predicted from the present model were compared with the test data and predicted results from SAMCJ (Stress Analysis of Multifastener Composite Joints) finite element computer code [8,9]. Good agreement of joint strengths and failure modes is obtained for the 20-ply, 50/40/10 laminates shown in Tables 2 to 4.

3.2.3 Design optimization

In the design of bolted composite joints, it is important to consider the effects of laminate and geometric parameters on the joint strength and failure mode. A design study was performed to illustrate the application of the model in the selection of parameters for optimizing the joint strength. A composite-to-metal joint, with the configuration shown in Table 2, was used for this study. The composite and metal used in the joint are AS1/3501-6 and aluminum, respectively. In the first stage, the model optimized the layup based on the configuration shown in Table 2. Three layups, $[45/0/-45/0_3/90/0_3]_S$, $[(45/0/-45/0)_2/0/90]_S$ and $[45/0/-45/0/45/90/-45/0/45/-45]_S$, were investigated. The result of the optimization shows that the layup $[(45/0/-45/0)_2/0/90]_S$, which contains 50%, 40% and 10% of 0°, 45° and 90° fibers, respectively, yields the highest strength amongst the three layups.

In the second stage, the model optimized the joint configuration for the $[(45/0/-45/0)_2/0/90]_S$ laminate. Both the hole diameter, *d*, and the edge distance, *e*, vary over a range of values in this study. The distance between the first and second row of fasteners, s_l, is equal to twice the edge distance. The pitch distance, s_w, is constant and is equal to 1.5 *in.* A multivariate constrained optimization scheme was conducted amongst the ranges of *d* and *e*. A three-dimensional plot of the failure strength and the optimum joint design are shown in Fig. 4. It is noted that the failure strength of the joint varies significantly with *d*, while it is relatively stable over the range for *e*.

4. FATIGUE PROGRESSIVE DAMAGE MODELING

A new modeling technique called fatigue progressive damage modeling for predicting the behaviour of composite pinned/bolted joints under cyclic loading was developed under a contract from IAR to McGill University. This technique uses a phenomenological approach to predict the residual stiffness, residual strength, and fatigue life of composite pinned/bolted joints.

The model consists of three major components: stress analysis, failure analysis, and material property degradation rules. The stress analysis of a single pin/bolt loaded fastener hole is performed using a nonlinear, three-dimensional finite element technique. Failure analysis is performed using a set of stress-based failure criteria. The ability to distinguish between different modes of failure is one of the most important requirements of these failure criteria. The model is capable of detecting the following modes: matrix tension, matrix compression, fiber tension, fiber compression, fiber-matrix shear-out, delamination tension, and delamination compression. Material properties are degraded by using sudden and gradual degradation rules. For each mode of failure listed above, there exists an appropriate sudden material degradation rule. In addition, the model has a gradual degradation rule to predict material properties degradation after a fixed number of loading cycles when failure is not detected. A detailed description of fatigue progressive damage modeling technique can be found in Ref. 10.

5. BOLTED PATCH REPAIR APPLICATION

The advent of composite materials in primary load bearing structure of military and civilian aircraft has brought new challenges in structural repair. The principal repair technique is to attach a patch over the damaged area. The patch can be attached using adhesive bonding. This technique requires controlled repair material storage, specialized surface preparation and extended cure times. As a result, adhesive bonding is usually used for depot level repairs. In the case of military aircraft used during combat, battle damage repair is usually performed in the field without sophisticated facilities. In order to minimize downtime of the aircraft, the repair is carried out under a severe time constraint and the repair is temporary. As a result, bonded repair is not desirable. In addition, bonded repair of thick parts requires scarf or stepped-lap joint configurations. These complicated joint configurations cannot be produced under field conditions. Because of these limitations, the adhesive bonding technique is seldom used in aircraft battle damage repair (ABDR).

The preferred ABDR technique involves the attachment of a metallic patch over the damaged area using "blind fasteners" which can be installed from the accessible side of the damaged structure. In the bolted patch repair case of an aircraft wing containing projectile impact damage, for example, single shear aluminum or titanium patches are attached by multiple rows of relatively slender blind fasteners. A schematic illustration of a bolted patch repair of a cleaned impact damage hole is shown in Fig. 5. Since the bolted patch repair scheme is similar to a single-lap bolted joint, the design optimization tool discussed earlier has the potential of being applied in ABDR or other bolted repairs.

However, the existing design optimization tool requires further development before it can be applied. The reason is that the bolted patch repair scenario involves damage which is simulated as an elliptical hole, as shown in Fig. 5, while in the bolted joint design case such a hole is not present. In the present repair example, the patch takes all the skin loads of the cleaned damage hole and so the fasteners on the patch and hole edges take high bearing loads. Multiple external loads are imposed on the wing therefore the loads in the skin under the patch are not simple uniaxial but are significantly biaxial. Under a biaxial loading condition in the presence of a randomly oriented elliptical hole, the fastener loading directions and fastener load distributions at the fastener holes are complex. In order to determine both the fastener load distribution and loading direction, the iterative scheme shown in Fig. 1 must be modified such that the complex variational formulations can handle the deformation characteristics of a repaired plate under biaxial loading.

In addition to improving the iterative scheme, biaxial failure criteria and allowables are required for accurate predictions of joint strength and failure mode. Preliminary experience [11] has

shown that for one axis reacted entirely in bearing with a completely bypass lateral load, the bearing allowable is reduced by as much as 50% from the case where lateral load is absent. Because of the many stress concentration sites resulting from fastener holes in a bolted repair, it is important that the repair be designed with accurate biaxial allowables to ensure that the repair is effective.

5.1 Bolted Patch Repair Project

A literature review has shown that there is a strong need for the development of a personal computer based, user-friendly tool for damage assessment and repair design optimization. It is believed that such a tool would be useful to both normal and aircraft battle damage repair (ABDR) situations. As a result, the current focus of the bolted joint technology project is on the development of a computer-aided design tool for bolted repair based on the existing design optimization module for bolted joints. Earlier discussions have identified the technical issues which must be addressed in the current development. Specific tasks of the present project are:

- Develop finite element models and analytical methods for bolted patch analysis.
- Develop biaxial bearing/bypass test methods to generate allowables.
- Develop the computer-aided design tool equipped with a graphical user interface for the repair design.
- Verify repair designs by performing full-scale structural tests on impact damaged and repaired wing box specimens.

5.1.1 Finite element analysis

Finite element models were developed for the stress analysis of bolted patch repairs. Based on the finite element analysis, the deformation characteristics and the stress distribution of a bolted patch repair subjected to inplane uniaxial and biaxial loads were determined. These finite element results will be used to develop the repair design optimization module.

The finite element model, shown in Fig. 6 for the case of a repair using 36 fasteners, consists of a square composite plate made of AS4/3501-6 with lay-up $[45/0/-45/90]_{6S}$ and a metallic patch mechanically fastened to a composite plate. The center of the composite plate has an inclined elliptical cutout which represents the cleaned damage hole. The repair consists of a 0.16 inch thick titanium patch attached to the composite plate by a number of fasteners. A series of finite element analyses were performed using models which had 28 and 36 fasteners. The baseline model was the composite plate with the elliptical hole without a patch. Both uniaxial tension and biaxial tension-tension (ratio = 1) loading conditions were considered. The finite element models were developed using a commercial code called NISA. The composite plate and the patch were modeled using plane stress elements and therefore the secondary bending deformation was ignored. The fasteners were modeled using beam elements. The contact regions between the fasteners and the hole boundaries were simulated using frictional gap elements. The effects of the patch on the reduction of stress concentrations at the elliptical hole edge and at the fastener hole edge in the composite plate were examined. The results of the analysis are shown in Table 5.

The results of the finite element analysis show that the bolted patch repair is effective in reducing the maximum K_t at the edge of the elliptical cutout in both loading cases. Increasing the number of fasteners from 28 to 36 by having two rows of fasteners on each of the four sides of the square patch does not change the maximum K_t at the edge of the elliptical cutout for the uniaxial loading case but has an improvement of approximately 12% for the biaxial loading case. The maximum K_t at the edges of the fastener holes vary in a narrow range between 3.33 and 3.56 for all cases and these values are significantly higher than those at the edge of the elliptical cutout.

5.1.2 Biaxial bearing/bypass testing

In order to predict the strength of the bolted patch under biaxial loading, accurate biaxial allowables and suitable failure criteria are required. The present work aims at developing an experimental method to generate the biaxial bearing/bypass allowables using a special cruciform bolted joint specimen and reviewing existing failure criteria to determine if new criteria are needed.

A suitable cruciform bolted joint specimen is crucial to the biaxial bearing/bypass testing. A comprehensive review of cruciform specimen designs is given in Ref. 12. A successful specimen design must have a test section which has a uniform distribution of plane stress and is large relative to the fastener diameter. Amongst the designs discussed in Ref. 12, the specimen designed by Lucking [13] is considered to the most appropriate because of the existence of finite element and photoelastic results [12] which confirm that the nonuniformity in stress distribution is less than 5%. Lucking's method in designing the specimen is to truncate all nonaxial plies in the arms of the cruciform specimen and replace them by a film adhesive. In this way, the transverse stiffness of the arms is significantly reduced which leads to less load being attracted from the transverse axis. Finite element results showed that the indirectly induced transverse stress was less than 3.12% of the axial stress [12]. Lucking's specimen design concept has been adopted in the present project and the design of a cruciform specimen is underway.

The bearing/bypass test method will involve application of biaxial loads to the cruciform specimens in tension/tension, tension/compression and compression/compression. A special test fixture is being developed to firmly anchor a bolt in the center of the cruciform specimen for bearing load reaction. The four arms of the cruciform specimen will be gripped by mechanical grips which contain roller bearings to allow transverse displacement in order to eliminate undesirable shear stresses in the test section. An existing MTS biaxial test machine at IAR will be used for the testing. The test results will be used to evaluate existing failure criteria and to develop new criteria if necessary.

5.1.3 Design tool development

The result of this project will be a personal computer based, user-friendly design optimization tool which is capable of assessing damage and optimizing repair designs. The development of the tool will require integration of an existing damage assessment module [14] and other components which are currently under development into a single computer code. These components include the design optimization module, material database and failure criteria. A graphical user interface will be developed for the code to facilitate inputting of damage characteristics and other required information, for example, the location of damage in the structure and the repair materials available. The tool will proceed to assess the damage to determine whether a repair is required. If a repair is required, the tool will determine the optimal repair design for the damage.

5.1.4 Design verification

The development will include, in its final phase, a design verification test program. The test program will involve full-scale structural testing of wing box test articles. A detailed description of these wing box test articles is given in Ref. 15. The box was designed to duplicate the construction and loading of a portion of the outer wing of the CF-18 and so had similar substructure dimensions and skin lay-up. Six wing box test articles were built and they will be impact damaged and then repaired by the bolted patch technique. The repair design will be generated from the design optimization tool developed in this project. For design verification, full-scale structural tests will be performed on these boxes by a three-point cantilever arrangement [15].

6. CONCLUSIONS

1. An analytical model was developed for optimization of multi-fastener composite joint design. Algorithms for stress analysis, strength prediction and optimization were coded in a computer program which could be executed efficiently on a personal computer.
2. Since closed form solutions were used, the burden of mesh regeneration for a new design, as needed in a finite element analysis, was not required.
3. The computer code was successfully validated by comparing results with published test data and SAMCJ joint strength predictions.
4. A new modeling technique called fatigue progressive damage modeling for predicting the residual stiffness, residual strength, and fatigue life of pin/bolt loaded composite laminate was developed. Static and fatigue material properties for AS4/3501-6 were characterized. Fatigue life predictions were validated by experimental results.
5. A new project on bolted patch repair of composite structures was initiated. Work is being performed in modifying the complex variational formulations to account for the deformation characteristics of a notched plate with a bolted patch under biaxial loads and in developing biaxial bearing/bypass test method.

7. ACKNOWLEDGMENTS

This work has been performed under NRC Project 3G3, Aerospace Structures, Structural Dynamics & Acoustics, Sub-Project JGM-02, Bolted Joint Technology in Composite Structures. The partial financial support from the Department of National Defence Financial Encumbrance 220794NRC08 is gratefully acknowledged.

8. REFERENCES

1. Poon, C., "Literature Review on the Design of Mechanically Fastened Composite Joints", *in* "Behaviour and Analysis of Mechanically Fastened Joints in Composite Structures", AGARD CP427, April 1987, Paper 1.
2. Xiong, Y. and Poon, C., "A design model for composite joints with multiple fasteners", Institute for Aerospace Research, IAR-AN-80, Ottawa, August 1994.
3. Shokrieh, M.M., "Failure of Laminated Pinned Connections", M. Eng. Thesis, Department of Mechanical Engineering, McGill University, 1991.
4. Rowlands, R.E., "Strength (failure) theories and their experimental correlation", *in* "Failure mechanics of composites", Elsevier Science Publishers, 1985, pp 71-125.
5. Whitney, R.J. and Nuismer, R.J., "Stress Fracture Criteria for Laminated Composites Containing Stress Concentrations", J. Comp. Mat., 8, July 1974, pp 253-265.
6. Tsai, W. and Wu, E.M., "A general theory of strength of anisotropic materials", J. Comp. Mater., 5, 1971, pp 58-80.
7. Wang, J.T., Lotts, C.G., and Davis, D.D. Jr., "Analysis of Bolt-Loaded Elliptical Holes in Laminated Composite Joints", J. Reinforced Plastics and Comp., 12, 1993, pp 128-138.
8. Ramkumar, R.L., Saether, E.S., and Appa, K., "Strength Analysis of Laminated and Metallic Plates Bolted together by Many Fasteners", AFWAL-TR-86-3034, 1986.
9. Ramkumar, R.L., Saether, E.S., and Cheng, D., "Design Guide for Bolted Joints in Composite Structures", AFWAL-TR-86-3035, 1986.
10. Lessard, L.B. and Shokrieh, M.M., "Fatigue Behaviour of Composite Pinned/Bolted Joints", Final Report, NRC Contract No. 31946-1-0008/01-SR, October 1995.
11. Poon, C., Xiong, Y., and Lucking, W.M., "Bolted Patch Repair of Composite Structures", Proceedings of Third International Conference on Composites Engineering, July 1996, pp 29-31.
12. Hoa, S.V., "Biaxial Bearing/Bypass Testing of Single Bolt Joint Graphite/Epoxy Composite Laminates", DREP CP 93-46, July 1993.
13. Lucking, W.M.,"Analysis of Specimens for Biaxial Testing of Composite Laminate", DREP Report, January 1990.
14. Xiong, Y. and Poon, C., "Prediction of Compression-after-Impact Strength of Quasi-Isotropic T800H/3900-2 Laminates", IAR LTR-ST-1913, January 1993.
15. Ferguson, J.S., Russell, A.J., Moore, R., and Miller, M., "Finite Element Modelling of Bolted Composite Repairs", Proceedings of Second Canadian International Composites Conference and Exhibition, 1993, pp 899-907.

Table 1. Material Properties

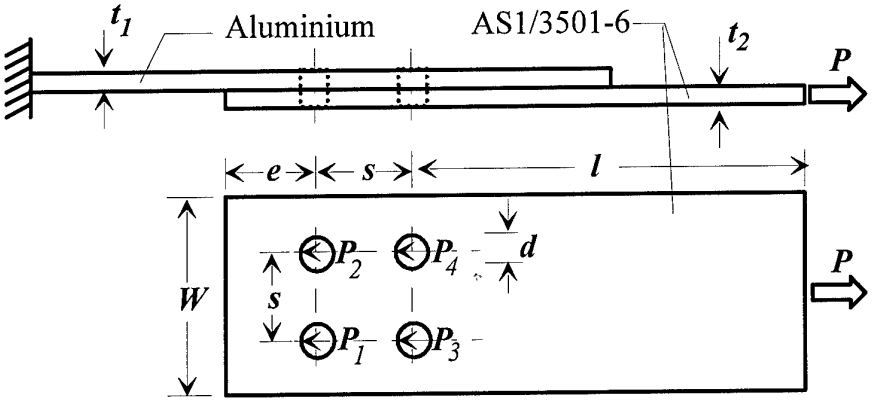
Material Name	AS1/3501-6	AS4/3501-6	AS4/3502
E_L (*Msi*)	18.5	20.3	18.0
E_T (*Msi*)	1.90	1.19	1.41
G_{LT} (*Msi*)	0.85	0.90	0.54
ν_{LT}	0.3	0.3	0.28
X (*Ksi*)	230.0	311.0	258.0
X' (*Ksi*)	321.0	119.5	204.0
Y (*Ksi*)	9.50	6.70	7.76
Y' (*Ksi*)	38.9	25.0	34.6
S (*Ksi*)	17.3	16.0	14.8

Table 2. Results of Test Case on Single Lap Joint (20-ply, 50/40/10 Laminate)

$t_1 = 0.31\ in,\ t_2 = 0.117\ in,\ d = 0.3125\ in$

$W/d = 10,\ s/d = 4,\ e/d = 3,\ l/d = 8.8$

$d_o^t = 0.032\ in,\ d_o^b = 0.032\ in$



(i) Present Prediction of Failure Strength

Hole No.	Failure Strength of Various Modes ($\times 10^3\ Psi$)					
	Point Stress Criterion			Laminate Polynomial Criterion		
	σ_f^t	σ_f^b	σ_f^s	σ_f^t	σ_f^b	σ_f^s
1	90.6	70.5	68.7	93.2	66.2	69.5
2	90.6	70.5	68.7	93.2	66.2	69.5
3	48.4	69.9	46.5	51.4	61.4	45.0
4	48.4	69.9	46.5	51.4	61.4	45.0

(ii) Comparison of Fastener Loads and Failure Load (Location)

	Present Prediction		Results from [8]	
	PSC	LPC	SAMCJ	Testing
P_1/P	0.23	0.23	0.24	0.25
P_2/P	0.23	0.23	0.24	0.25
P_3/P	0.27	0.27	0.26	0.29
P_4/P	0.27	0.27	0.26	0.21
P_f ($\times 10^3\ lb$)	17.0 (17.7)*	16.4 (18.8)*	18.1 (18.9)*	17.1
Location	3, 4	3, 4	4 (3)	3, 4
Mode	shear-out (net-tension)	shear-out (net-tension)	shear-out	shear-out net-tension delamination

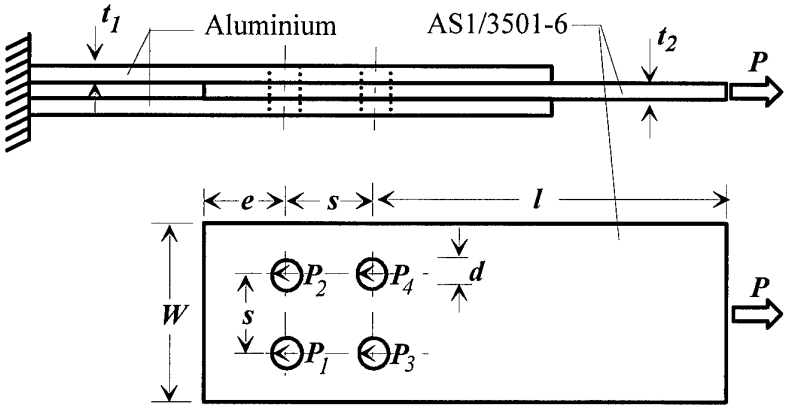
* possible failure mode at a slightly higher load level

Table 3. Results of Test Case on Double Lap Joint (20-ply, 50/40/10 Laminate)

$t_1 = 0.26\ in,\ t_2 = 0.117\ in,\ d = 0.3125\ in$

$W/d = 10,\ s/d = 4,\ e/d = 3,\ l/d = 18.6$

$d_o^t = 0.032\ in,\ d_o^b = 0.032\ in$



(i) Present Prediction of Failure Strength

Hole No.	Failure Strength of Various Modes ($\times 10^3\ Psi$)					
	Point Stress Criterion			Laminate Polynomial Criterion		
	σ_f^t	σ_f^b	σ_f^s	σ_f^t	σ_f^b	σ_f^s
1	104.8	76.8	78.9	105.1	73.2	79.6
2	104.8	76.8	78.9	105.1	73.2	79.6
3	47.6	61.7	45.3	50.4	56.1	43.9
4	47.6	61.7	45.3	50.4	56.1	43.9

(ii) Comparison of Fastener Loads and Failure Load (Location)

	Present Prediction		Results from [8]	
	PSC	LPC	SAMCJ	Testing
P_1/P	0.22	0.22	---	0.23
P_2/P	0.22	0.22	---	0.26
P_3/P	0.29	0.29	---	0.25
P_4/P	0.29	0.29	---	0.27
P_f ($\times 10^3\ lb$)	16.6 (17.4)*	16.1 (18.5)*	---	15.9
Location	3, 4	3, 4	---	3, 4
Mode	shear-out (net-tension)	shear-out (net-tension)	---	net-tension

* possible failure mode at a slightly higher load level

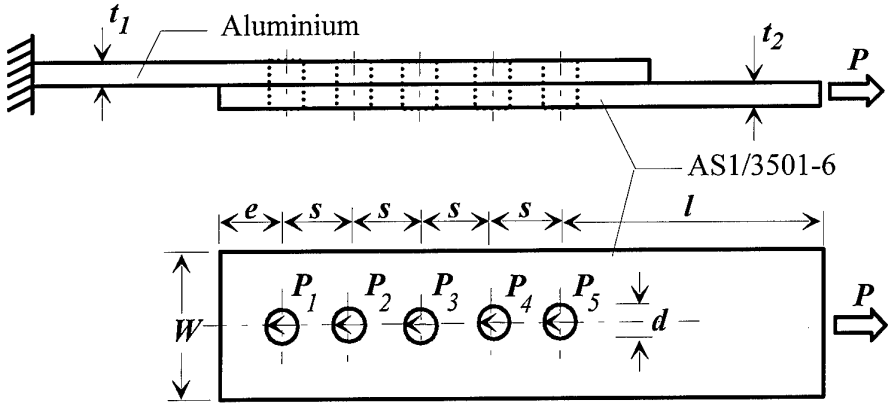
Table 4. Results of Test Case on Single Lap Joint with Multiple Fastener in Tandem

(40-ply, 50/40/10 laminate)

$t_1 = 0.50\ in,\ t_2 = 0.243\ in,\ d = 0.3125\ in$

$W/d = 4.8,\ s/d = 4,\ e/d = 3.2,\ l/d = 4.8$

$d_o^t = 0.020\ in,\ d_o^b = 0.020\ in$



(i) Present Prediction of Failure Strength

Hole No.	Failure Strength of Various Modes ($\times 10^3\ Psi$)					
	Point Stress Criterion			Laminate Polynomial Criterion		
	σ_f^t	σ_f^b	σ_f^s	σ_f^t	σ_f^b	σ_f^s
1	218.5	184.2	195.2	223.2	179.5	196.9
2	166.4	300.2	205.6	169.6	245.6	193.4
3	122.6	287.9	162.5	124.9	207.8	150.0
4	83.4	184.0	107.0	84.7	135.1	100.1
5	46.7	98.8	61.0	49.7	78.2	57.6

(ii) Comparison of Fastener Loads and Failure Load (Location)

	Present Prediction		Results from [8]	
	PSC	LPC	SAMCJ	Testing
P_1/P	0.204	0.204	0.193	0.204
P_2/P	0.141	0.141	0.168	0.177
P_3/P	0.170	0.170	0.170	0.171
P_4/P	0.166	0.166	0.202	0.178
P_5/P	0.319	0.319	0.267	0.270
P_f ($\times 10^3\ lb$)	17.1	18.0	12.4	16.6
Location	5	5	5	5

Mode	net-tension	net-tension	net-tension	net-tension

Table 5. Results of Finite Element Analysis

Case	Cutout Uniaxial Load	Cutout Biaxial Load	28 Fasteners Uniaxial Load	28 Fasteners Biaxial Load	36 Fasteners Uniaxial Load	36 Fasteners Biaxial Load
Maximum K_t @ Cutout	4.39	4.52	1.76	1.98	1.75	1.75
Maximum K_t @ Bolt Hole	-----	-----	3.55	3.51	3.56	3.33

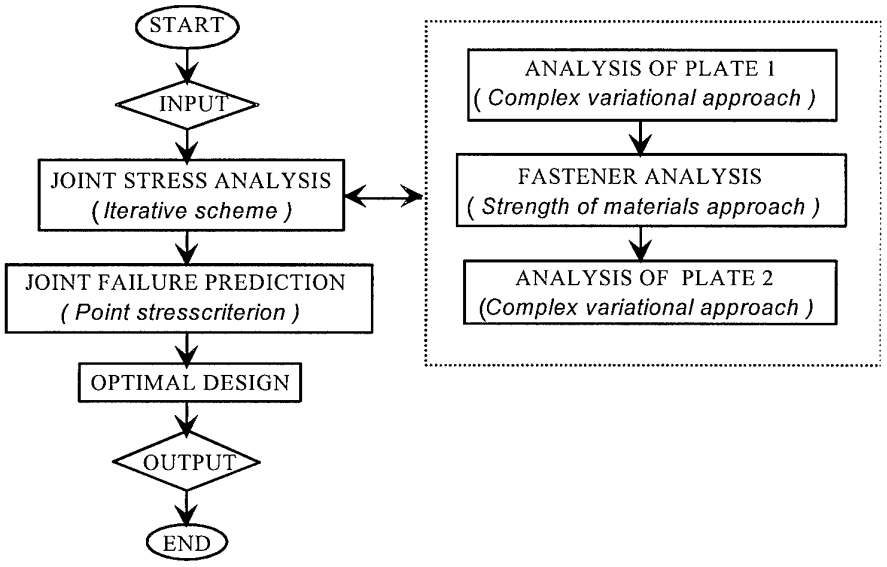


Figure 1. Flowchart of joint design model

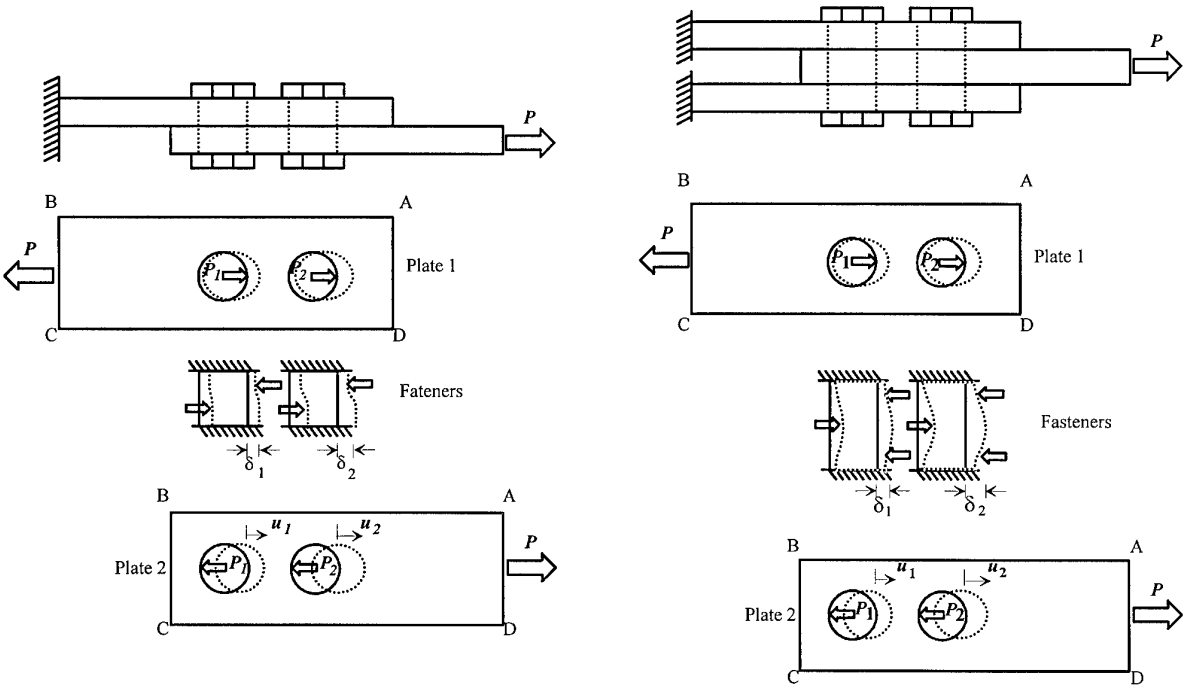


Figure 2. Geometric configurations of single and double lap joints

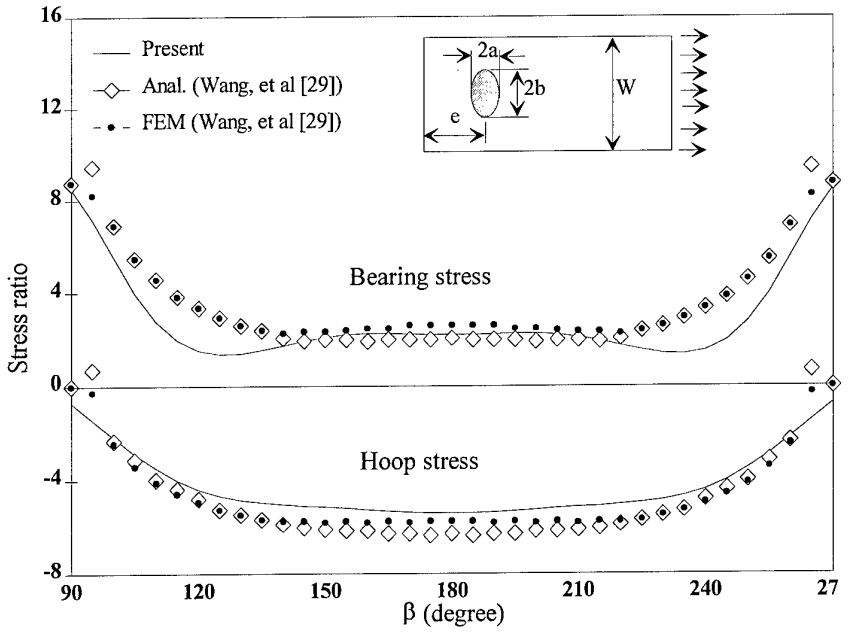


Figure 3. Bearing and hoop stresses around a pin-loaded hole

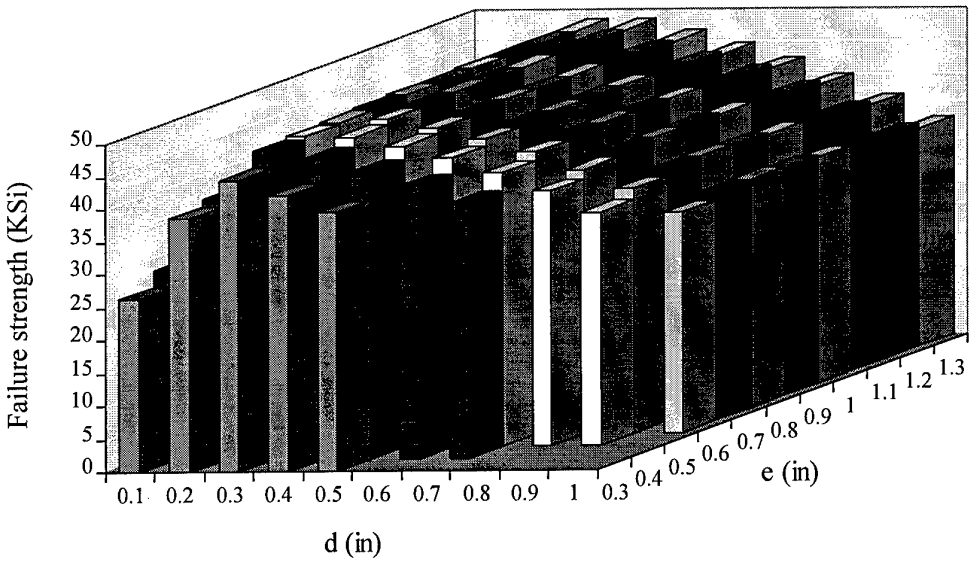


Figure 4. Failure strength versus hole diameter and edge distance

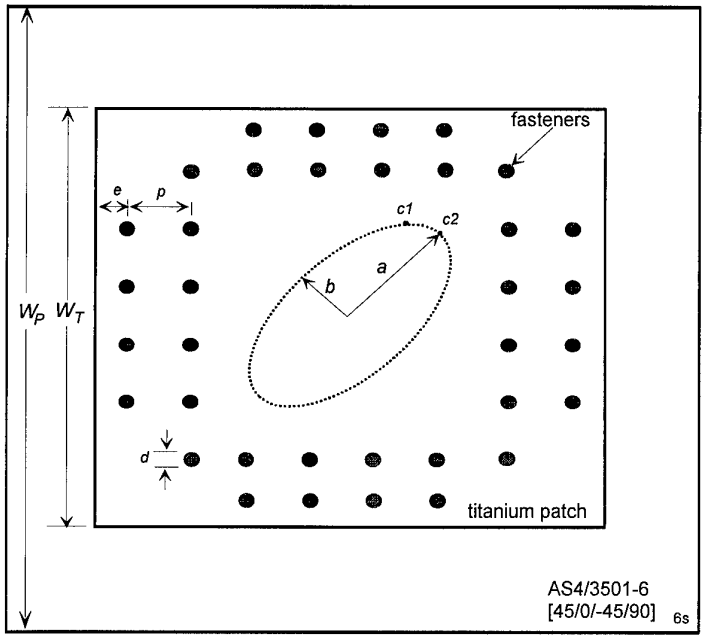


Figure 5. A bolted patch repair with 36 fasteners

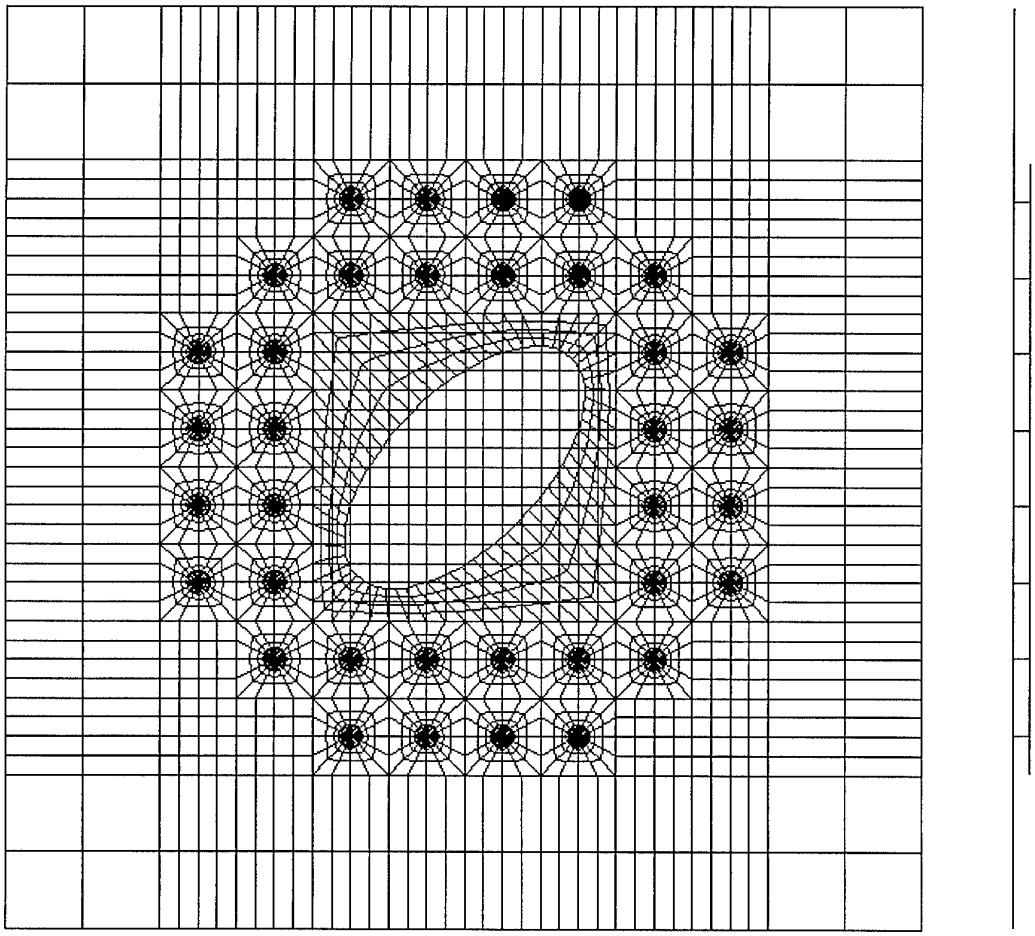


Figure 6. Finite element mesh for a repair with 36 fasteners

A REVIEW OF COMPOSITE JOINT ANALYSIS PROGRAMS

V. B. Venkayya and V. A. Tischler
WL/FIBAD Bldg 45
2130 Eighth St Ste 1
Wright-Patterson AFB OH 45433-7542

SUMMARY

Several joint analysis programs funded by U.S. government agencies during the 1970s, 1980s and 1990s were reviewed. The review covered bolted, bonded, bolted-bonded and repair programs. In a few cases the results obtained from these programs are compared. A number of related references were cited for the purpose of obtaining additional details.

INTRODUCTION

It has been almost ten years since the last AGARD Structures and Materials Panel Specialists Meeting on the Analysis of Mechanically Fastened Joints in Composite Structures[1-3]. The primary interest at that time, and even now, is the service life prediction of composite structures, in general, and determining how much of it is driven by joint failures. Although, the analysis methods discussed in that conference are generally applicable to any anisotropic material system, the emphasis at that time was on organic composites such as graphite epoxy and/or carbon fiber reinforced plastics. The behavior of joints in composites is uncertain under the general operating conditions of an aircraft. They lack the forgiving qualities of metals such as, ductility, low sensitivity to changes in environmental conditions and manufacturing anomalies. In addition delamination, debonding, etc., coupled with uncertain material property data, such as interlaminar shear, matrix cracking present difficulties in developing reliable structural design criteria.

The scope of the specialists meeting in Florence has been expanded to include other joining issues. They include bonded joints, multimaterial joints, repair issues and different material systems such as Thermoplastics and Ceramic Matrix Composites. The technology for optimum joint design for composite structures is still evolving, albeit slowly. The joint design variables are too numerous, and their various combinations can result in many joint configurations which cannot be analyzed with certainty much less validated experimentally. For example, a partial list of the variables may include:

- thickness of the laminate
- composition of the fiber orientations
- stacking sequence of the layers
- three dimensional effects such as interlaminar shear
- finite width effects in an infinite plate analysis
- load sharing in multifastener joints
- non-linear effects
- fastener flexibility
- clamping effect due to bolt torque
- new material systems
- high temperature joints

The purpose of this paper is to review the joint analysis programs available in the United States. The development of these programs was directly or indirectly funded by the Air Force or

Paper presented at the 83rd Meeting of the AGARD SMP on "Bolted/Bonded Joints in Polymeric Composites", held in Florence, Italy, 2-3 September 1996, and published in CP-590.

other U.S. government agencies. Much of the material for this review is derived from references 4 and 5. This review is somewhat cursory, partly because of the twelve page limitation imposed by AGARD-SMP. Additional details can be found in references 4 and 5. The review in reference 4 is limited to bolted joints only. The review in reference 5 is more up-to-date and covers bolted-bonded and repair programs as well.

REVIEW ORGANIZATION

Joint programs can be classified into four categories:

1. Bolted Joints - Single Fastener Analysis
2. Bolted Joints - Multiple Fasteners - Load Sharing
3. Bonded Joints Analysis
4. Bolted/Bonded Joint Repair

The following joint analysis programs are reviewed in this paper.

- JOINT — Analysis of Single and Multi-Fastener Joints Bonded Joints
- A4EJ — Multi-Fastener Bolted Joint Analysis
- SASCJ — Single Fastener Analysis
- BJSFM — Single Fastener Analysis
- SCAN — Single Fastener Analysis
- SAMCJ — Multi-Fastener Analysis
- CREPAIR — Multi-row Bolted Joint Repair
- SVELT — Single Fastener Double Lap Bolted Joint
- A4EI — Bonded Joints Analysis
- PGLUE — Bonded Joint Repair
- JTSDL/JTSTP — Bonded Single, Double and Step-Lap Joints
- BONJO — Bonded Joints Analysis
- MOSAIC — Bonded Joints Analysis
- A4EK — Bonded and Bolted Joint Analysis

Most of the programs reviewed here are empirical or approximations of continuum solutions. More recently, interest in finite element solutions is growing, because of their versatility in modeling non-traditional boundary conditions. They can also accommodate modeling joints as part of large built-up structures when the primary load paths need not be identified a priori. Above all there is the availability of numerous well tested commercial packages.

JOINT ANALYSIS CODE

JOINT is a composite joint analysis code developed by the Douglas Aircraft Company from 1976 to 1978[6]. The code is capable of analyzing both bonded and bolted joints from an interactive graphics terminal. JOINT is based on a simplified theory that relies on empirical test data for its simplicity. JOINT is capable of analyzing the following types of joints: balanced double-lap, supported single-lap, stepped-lap and unsupported single-lap. The code is capable of performing a limited type (brute force, trial and error) of joint optimization on the following types of infinite width bolted joints: double-lap, supported single-lap, and unsupported single-lap. For the optimization, the code determines the number of bolt rows, bolt diameter, bolt spacing and joint thickness for the lightest joint that will carry the applied load. The coupling effects of the bolt rows has been neglected which can cause severe error for some types of joint analysis.

The code assumes a bypass stress equal to

$$\sigma_t = K_{t1}\frac{P_t}{t(w-d)} + K_{t2}\frac{P_b}{t_e(w-d)} \qquad (1)$$

and a bending stress equal to

$$\sigma_b = \frac{6M_0}{t^2} \qquad (2)$$

where P_b = bolt bearing load, P_t = bypass load,

K_{t1} = stress concentration factor for an unloaded hole, K_{t2} = stress concentration factor for a loaded hole, d = the bolt hole diameter, t = the lap thickness, t_e = the effective thickness reacting bolt hole and M_0 = the bending moment at the edge of the overlap. The stress concentration factors K_{t1} and K_{t2} are derived from test data. K_{t1} and K_{t2} are functions of the diameter of the bolt holes and widthwise bolt spacing, w. The constants in the functions are determined for an AS/3501-6 graphite epoxy composite with different percentages of 0^o plies. The code only has the functions calculated for composites with 25% and 37.5%, 0^o plies. The bolt load distribution depends on the bolt and joint flexibility, but bolt torque-up and bolt type aren't accounted for. The code allows four different failure modes: 1) tension at the hole, 2) bolt bearing, 5) bolt shear, and 4) shear tear-out. The bending stress is determined differently for each type of failure. With the bearing stress equal to,,

$$\sigma_b = \frac{6M_0}{t^2} \qquad M_0 = kN_x\frac{t}{2} \qquad (3)$$

and

$$k = \frac{1}{1 + \xi C + \frac{1}{6}\xi^2 C^2} \qquad (4)$$

$$\xi^2 = D_x N_x = \frac{12(1-\nu^2)}{Et^3}N_x \qquad (5)$$

where C = the half-distance between the outer rows of bolts (for single lap joints), E = the modulus of elasticity, ν = Poisson's ratio and the allowable joint load, N_x, depends on the failure mode. For a tensile mode of failure,

$$N_x = \frac{F^t_{tu}(1 - d/w)}{P_t K_{t1} + P_b\frac{t}{t_e}K_{t2} + 3K(1 - d/\mathrm{w})} \qquad (6)$$

where F^t_{tu} = the ultimate tensile stress allowable and K = the bending moment coefficient for a single lap joint M_0. For a bearing failure,

$$N_x = \frac{F_{br}t}{P_b}\ \frac{d}{w} \qquad (7)$$

where F_{br} = the ultimate bearing stress allowable. For a bolt shear failure,

$$N_x = \frac{\pi}{2}\frac{F_{su}(bolt)d}{P_b}\ \frac{d}{w} \qquad (8)$$

where F_{su} = the ultimate joint shear stress allowable. For a bolt tear-out failure,

$$N_x = 2\left(\frac{e}{d} - \frac{1}{2}\right)\frac{F_{su}t}{P_b}\ \frac{d}{w} \qquad (9)$$

where e = the edge distance. The analysis is performed for an infinite width plate with a specified bolt spacing through the width of the plate.

The JOINT analysis code makes several simplifying assumptions in the analysis. Test data must be used to obtain stress concentration relief data for the composite plates. After the empirical data is obtained, the stress concentration factors are found. These functions are used to determine the stresses in the plate. Only uniaxial loadings can be applied to the joint. JOINT is not capable of analyzing compressively loaded joints and the analysis assumes that the fasteners don't fail. For all of the different types of joints the JOINT program can analyze, the following restrictions apply:

$$\frac{e}{d} = 3 \qquad 3 \le \frac{w}{d} \le 12 \qquad t \le d$$

$$\frac{3}{16} \le d \le 1\frac{1}{2} \qquad \text{row pitch} = 6d$$

Other limitations are: 1) a choice of two bolt materials, 2) a choice of two composite layups,

3) a joint load limitation of 40,000.*lbs,* and 4) a limitation on the number of bolt rows

For a double-lap configuration, the thickness of the two outer splice plates must be one-half the thickness of the center plate. A stepped lap joint configuration assumes that the bolts are at the center of the steps. Varying step lengths, bolt diameters, and lengthwise spacing between bolts can be specified. All bolt row coupling effects are neglected and the bolts are assumed to be lined up one behind the other. For an optimization problem, the bolts must be the same size for every bolt row. Bolt row spacing is assumed to be uniform for the whole joint. The code echos all the input data. In summary, the code applies quite a few constraints to problem definitions and has a limited analysis and data output capability. Problems do run very quickly which allows many design iterations to be performed in a short period of time.

A4EJ ANALYSIS CODE

A4EJ is a composite bolted joint analysis code developed by the Douglas Aircraft Company from 1979 to 1981 [7]. A4EJ has the capability to analyze multi-row joints having a nonlinear load-deflection characteristic for the fasteners, and linear or Ramberg-Osgood characterizations of the adherends. A4EJ accounts for nonlinearities in the joint due to: 1) fastener load-deflection characteristics, 2) fastener clearance, 3) elastomechanical deformation of the members between the fasteners, and 4) interaction between bearing and bypass loads. A4EJ is based on continuum mechanics techniques, requiring shorter computer run times than finite element modeling techniques. A4EJ provides a detailed definition of the internal load transfer within a joint and requires a large amount of input data.

The load transfer through the fasteners within a joint is characterized in terms of the relative displacement between the members at each fastener station. A4EJ assumes a bi-linear elastic load deflection curve. The known boundary conditions are at both ends of the joint. The problem is solved iteratively by starting at one end of the joint and assuming a value for an unknown quantity. You can assume the total joint strength or the displacement at the first fastener induced by a specified load. By calculating progressively along the joint and satisfying both equilibrium and compatability requirements, the reactions at the other end of the joint can be determined. The initial assumption can be modified until all the boundary conditions are satisfied at both ends of the joint. The initial assumption must be very close, otherwise the solution will diverge.

Figure 1 shows how the typical equations for each step of the joint are established. The conditions of equilibrium for member 1 between stations k and $k+1$ are

$$T_{1_{(k+1)}} = T_{1_{(k)}} - P_{(k)} + p_1 \iota_{(k)} \qquad (10)$$

where:

T_1 = member 1 internal load (+ for tensile)

P = fastener load (+ for tensile lap shear)

p_1 = member 1 running shear load (+ in direction of tensile load)

ι = step length

Similarly for member 2,

$$T_{2_{(k+1)}} = T_{2_{(k)}} - P_{(k)} - p_2 \iota_{(k)} \qquad (11)$$

Figure 1 shows a joint in single lap shear. In a double shear joint, the two portions of member 1 or 2 would be combined and the fastener load P would be changed from single to double shear values. To make sure the analysis complies with compatability requirements, the mechanical and thermal properties of the members must be used. The user must input the stiffness of each member between each adjacent

pair of fastener stations, allowing variations in width and thickness. Provisions are also made for thermally induced strains. The non-linear load-deflection behavior of materials is accounted for by using the Ramberg-Osgood model for loading beyond the material proportional limit.

The extension of the members between stations k and $k + 1$ is given by:

$$\delta_{1_{k+1}} - \delta_{1_{(k)}} = \alpha_1 \Delta T \iota_{(k)} + \varepsilon_1 \iota_{(k)} \qquad (12)$$

and

$$\delta_{2_{k+1}} - \delta_{2_{(k)}} = \alpha_2 \Delta T \iota_{(k)} + \varepsilon_2 \iota_{(k)} \qquad (13)$$

where:

δ_1, δ_2 = displacement

α_1, α_2 = coefficient of thermal expansion

$\Delta T = T_{operation} - T_{assembly}$

$\varepsilon_1, \varepsilon_2$ = mechanically induced strains

Any running load is applied uniformly along the length of the joint, and in calculating the strains, the deformation is that which would be associated with the average member load in each segment. The average loads causing the stretching of each member between stations k and $k+1$ are

$$T_{1_{(k+1)}} = T_{1_{(k)}} - P_{(k)} + p_1 \iota_{(k)}/2 \qquad (14)$$

and

$$T_{2_{(k+1)}} = T_{2_{(k)}} + P_{(k)} - p_2 \iota_{(k)}/2 \qquad (15)$$

The corresponding stresses are

$$\sigma_{1_{(k)}} = \frac{T_{1_{(k)}}}{[w_{1_{(k)}} t_{1_{(k)}}]} \qquad (16)$$

and

$$\sigma_{2_{(k)}} = \frac{T_{2_{(k)}}}{[w_{2_{(k)}} t_{2_{(k)}}]} \qquad (17)$$

For linear elastic materials, the equivalent strains would be

$$\varepsilon_{1_{(k)}} = \frac{\sigma_{1_{(k)}}}{E_{1_{(k)}}} \qquad (18)$$

and

$$\varepsilon_{2_{(k)}} = \frac{\sigma_{2_{(k)}}}{E_{2_{(k)}}} \qquad (19)$$

For ductile materials, the Ramberg-Osgood model is incorporated and the equivalent strains are calculated to be

$$\varepsilon_i = \frac{\sigma_i}{E_i}\left[1 + \left(\frac{\sigma_1}{F_{0.7}}\right)^{n-1}\right] \quad (i = 1, 2) \qquad (20)$$

where $F_{0.7}$ = the stress value at.7 x E on the stress strain curve. After determining the member strains, the relative displacement between the members at the next station is

$$\delta_{(k+1)} = \delta_{2_{(k+1)}} - \delta_{1_{(k+1)}} \qquad (21)$$

as shown in Figure 1. This allows a new increment of fastener load transfer to be evaluated. After computing the bearing and bypass loads at each station the failure criterion is checked to see if the combination of the two loadings is capable of causing joint failure.

A4EJ requires the user to input a relatively large amount of empirical data for the materials that are being joined. The input of the data is not user friendly, requiring formatted, non-interactive input of the data. Data for composite materials is input on the laminate level. A4EJ does have short turnaround times and outputs

joint failure load, fastener station loads, deflection and strains, however it is an iterative technique and certain values must be checked and adjusted to get the solution to converge. Joints in compression as well as tension can be analyzed. A4EJ accounts for temperature effects, but only with respect to each material's coefficient of linear thermal expansion; A4EJ does not account for material strength degradation with temperature. Although A4EJ analyzes multi-row bolted joints, it is not capable of analyzing single fastener joints or joints with open holes. A4EJ performs the same analysis on single lap and double lap joints and doesn't account for single lap eccentricities. The exact fastener locations cannot be input, but are accounted for by inputting the distances between fastener stations. Fasteners are assumed to be evenly spaced throughout a row. A specific plate loading can be input, and A4EJ can account for running shear loads but biaxial loadings cannot be specified. Boundary conditions can be input but are not required. A4EJ doesn't output the specific mode of failure, but the mode can be determined from the failure location and loads. A4EJ isn't capable of calculating stress distributions around fasteners. A4EJ is effective in analyzing multi-row bolted joints, however users encounter difficulties in obtaining and inputting the required data.

SASCJ ANALYSIS CODE[2,3,8,9]

SASCJ is an acronym for Strength Analysis of Single Fastener Composite Joints. The code was developed by the Northrop Corporation from 1983-1985. As the name implies, the code can only perform an analysis on single or double lap joints connected with one fastener or plates with an open hole. SASCJ has the capability to perform a two-dimensional analysis of a finite bolted composite plate. The two-dimensional stress field in the finite bolted plate is expressed in terms of an Airy stress function, F(x,y), that automatically satisfies the equilibrium equations in the plate. The displacement solution satisfies the compatability equations when:

$$A_{22}\frac{\partial^4 F}{\partial x^4} - 2A_{26}\frac{\partial^4 F}{\partial x^3 \partial y} + (2A_{12} + A_{66})\frac{\partial^4 F}{\partial x^2 \partial y^2}$$

$$- 2A_{16}\frac{\partial^4 F}{\partial x \partial y^3} + A_{11}\frac{\partial^4 F}{\partial y^4} = 0 \qquad (22)$$

is satisfied by the Airy stress function. The laminate compliance coefficients, A_{ij}, for the laminate are given by

$$\underset{\sim}{\varepsilon} = \underset{\sim}{A}\underset{\sim}{N} \qquad (23)$$

where the matrices $\underset{\sim}{\varepsilon}$ and $\underset{\sim}{N}$ are the in-plane strains and stress resultants, respectively, in an anisotropic plate. The complex stress function, F, can be written as

$$F(x, y) = 2Re[F_1(z_1) + F_2(z_2)] \qquad (24)$$

The complex stress functions $F_1(z_1)$ and $F_2(z_2)$ are analytic functions of the complex characteristic coordinates z_1 and z_2 respectively. The coordinates z_1 and z_2 are given by

$$z_1 = x + \mu_1 y \qquad z_2 = x + \mu_2 y \qquad (25)$$

Using the complex stress function the complex functions

$$\phi_1(z_1) = \frac{dF_1}{dz_1} \qquad \phi_2(z_2) = \frac{dF_2}{dz_2} \qquad (26)$$

are introduced. The above equations lead to the following expressions for stresses and displacements in the plate:

$$\sigma_x = 2Re[\mu_1^2\phi_1'(z_1) + \mu_2^2\phi_2'(z_2)] \qquad (27)$$

$$\sigma_y = 2Re[\phi_1'(z_1) + \phi_2'(z_2)] \qquad (28)$$

$$\tau_{xy} = -2Re[\mu_1\phi_1'(z_1) + \mu_2\phi_2'(z_2)] \quad (29)$$

$$u = 2Re[p_1\phi_1(z_1) + p_2\phi_2(z_2)] \quad (30)$$

$$v = 2Re[q_1\phi_1(z_1) + q_2\phi_2(z_2)] \quad (31)$$

where p_1, p_2, q_1 and q_2 are defined as:

$$p_1 = A_{11}\mu_1^2 + A_{12} - A_{16}\mu_1 \quad (32)$$

$$p_2 = A_{11}\mu_2^2 + A_{12} - A_{16}\mu_2 \quad (33)$$

$$q_1 = A_{12}\mu_1 + \frac{A_{22}}{\mu_1} - A_{26} \quad (34)$$

$$q_2 = A_{12}\mu_2 + \frac{A_{22}}{\mu_2} - A_{26} \quad (35)$$

The complex functions ϕ_1 and ϕ_2 automatically satisfy the governing equation. For a finite geometry problem with specified boundary conditions, the complex functions cannot be solved so a Laurent series expansion is used.

$$\phi_1(\xi_1) = \alpha_0 \ln\xi_1 + \sum_{n=1}^{N} (\alpha_{-n}\xi_1^{-n} + \alpha_n\xi_1^n) \quad (36)$$

$$\phi_2(\xi_2) = \beta_0 \ln\xi_2 + \sum_{n=1}^{N} (\beta_{-n}\xi_2^{-n} + \alpha_n\xi_2^n) \quad (37)$$

Mapping functions are incorporated into the expansions to make the series converge faster. The rigid body rotation constraint and single valuedness of the displacement constraint are imposed on the complex functions. The complex coefficients of the series expansions are determined, and the displacements and stresses can be calculated using equations 27 through 31. To get an accurate solution, approximately 100 collocation points are used in the expansion at the hole boundary. These points are sufficient to recover the imposed boundary conditions at the edges of the plate and at the hole boundary. With an open hole the imposed boundary conditions are self-equilibrating. With a loaded hole, a cosine bolt load distribution is assumed for the hole boundary. This bolt load distribution is equilibrated to the imposed externally applied loads. The bolt in a loaded hole plate is modeled as a Timoshenko beam on an elastic foundation. A finite difference approximation of the governing equation is used to determine the loading distribution and displacements on the plate. SASCJ uses a progressive failure procedure that predicts local ply failures and combines them to get the plate strength.

The SASCJ analysis code considers many of the complexities of composite bolted joints. The symmetry of a double-lap shear problem is taken into account in the problem to reduce the amount of input required and computation time. Bilinear elastic ply behavior is assumed. No fastener friction effects are taken into account in the code but an approximation to the fastener and plate contact is incorporated by an assumed radial stress distribution. The user must specify a bypass ratio for the joint. The bypass ratio is the ratio of load carried by the plates to the load carried by the fastener. This quantity is dependent on how much torque is applied to a fastener when it is tightened. An edge distance to bolt diameter ratio must be greater than 3 and the plate width to bolt diameter ratio must be greater than 4. SASCJ allows for protruding and countersunk head fasteners. The only difference the analysis makes between the two types of fasteners is in the determination of the boundary conditions for the bolt. The protruding head fasteners are given fixed boundary conditions at both ends. The countersunk fasteners are given a free boundary condition at the countersunk head and a fixed boundary condition at the bolted end. The analysis assumes that the fasteners don't fail. The failure criteria are checked at locations

specified by the user. The input data for the failure criteria depends on the failure option chosen; point stress, average stress, maximum strain or Hoffman/Tsai-Hill. The same failure prediction procedure is used for all of the plates in the bolted joint. The SASCJ analysis code outputs the following joint properties upon completion of the analysis: failure load, failure mode, joint loads at specified nodal points and an echo of a limited amount of the input data. The SASCJ code at Wright-Patterson AFB has been modified to output the stresses, strains and displacements at the hole boundary at the failure load. The code cannot determine stresses in a joint for a given load but a tensile or compressive loading can be specified. The code allows for the analysis of finite geometry joints with nearby free edges. The analysis accounts for the actual laminate stacking sequence and asymmetric laminates can be input. SASCJ considers fastener bending, torque and shear in the analysis. For most cases, the code runs relatively slowly. SASCJ is a versatile code that can analyze most single fastener joints.

BJSFM ANALYSIS CODE[10, 11]

BJSFM was developed by the McDonnell Aircraft Company from 1978 to 1981. BJSFM is an acronym for Bolted Joint Stress Field Model. BJSFM can predict stress distributions and perform failure analysis of an anisotropic double lap plate with a single loaded or unloaded fastener hole. The analysis is based on 1) anisotropic theory of elasticity, 2) lamination plate theory, and 3) a failure hypothesis. The principle of elastic superposition is used to obtain laminate stress distributions as a result of the combination of bearing and bypass loading. The developed analysis can be used with various failure criteria to predict laminate load carrying capability. The derivation of the equations used in the BJSFM and SASCJ codes are identical up to equation 35. BJSFM uses conformal mapping techniques to obtain exact solutions for an infinite plate with a circular hole and uniform stresses at infinity. A mapping function was used to map the physical circular boundary of radius, b in the z_k. plane (k=1,2) onto a unit circle in the ξ_k plane. The mapping function is given by

$$\xi_k = \frac{z_k \pm \sqrt{z_k^2 - b^2 - \mu_k^2 b^2}}{b(1 - i\mu_k)} \qquad (38)$$

The sign of the square root is chosen such that the hole is mapped to a unit circle. The above equations contain unknown stress functions $\phi_1(z_1)$ and $\phi_2(z_2)$ For an infinite plate these functions will have the general form:

$$\phi_1(z_1) = B_1 z_1 + a_1 \ln \xi_1 + \sum_{m=1}^{\infty} a_{1m} \xi_1^{-m} \qquad (39)$$

$$\phi_2(z_2) = B_2 z_2 + a_2 \ln \xi_2 + \sum_{m=2}^{\infty} a_{2m} \xi_2^{-m} \qquad (40)$$

Linear z_1 and z_2 terms are required for a uniform stress at infinity. Terms with ln ξ_1 and ln ξ_2 are present whenever the resultant of the applied stresses on the circular boundary are nonzero. Boundary conditions on the circular hole are satisfied by the a_{1m} and the a_{2m} series coefficients. Only the linear terms and the first coefficient of the summation are used for the unloaded hole solution. Loaded hole analysis is performed by specifying a radial stress boundary condition varying as a cosine over half the hole. Boundary conditions at infinity, required to satisfy equilibrium, result in stress free conditions since the finite force required to balance the bolt load is applied to an infinite boundary. Thus, the linear terms are not required. Since the specified hole loading is not self-equilibrating on the boundary, single-valued displacement conditions are imposed to determine the log term coefficients. The following set of simultaneous equations are given for the a_1 and a_2 complex coefficients.

$$a_1 - \bar{a}_1 + a_2 - \bar{a}_2 = \frac{p_2}{2}\pi i \qquad (41)$$

$$\mu_1 a_1 - \bar{\mu}_1 \bar{a}_1 + \mu_2 a_2 - \bar{\mu}_2 \bar{a}_2 = -\frac{p_1}{2}\pi i \qquad (42)$$

$$\mu_1^2 a_1 - \bar{\mu}_1^2 \bar{a}_1 + \mu_2^2 a_2 - \bar{\mu}_2^2 \bar{a}_2 =$$

$$\frac{-A_{12}p_2 - A_{16}p_1}{2\pi i A_{22}} \qquad (43)$$

$$\frac{a_1}{\mu_1} - \bar{\mu}_1 \bar{a}_1 + \frac{a_2}{\mu_2} - \frac{\bar{a}_2}{\bar{\mu}_2} = \frac{A_{12}p_1 + A_{26}p_2}{2\pi i A_{22}} \qquad (44)$$

Expressing the radial stress boundary conditions on the hole in terms of a Fourier series and equating the series representation of the solution, the unknown a_{1m} and a_{2m} coefficients are obtained. The coefficients are:

$$a_{12} = \frac{bPi(1 + i\mu_2)}{[16(\mu_2 - \mu_1)]} \qquad (45)$$

$$a_{22} = -\frac{bPi(1 + i\mu_1)}{[16(\mu_2 - \mu_1)]} \quad m = 4, 6, 8.... \qquad (46)$$

$$a_{1m} = a_{2m} = 0 \quad m = 1, 3, 5, ... \qquad (47)$$

$$a_{1m} = -\frac{bPi(-1)^{(m-1)/2}(2 + im\mu_2)}{[\pi m^2(m^2 - 4)(\mu_2 - \mu_1)]} \qquad (48)$$

$$a_{2m} = \frac{bPi(-1)^{(m-1)/2}(2 + im\mu_1)}{[\pi m^2(m^2 - 4)(\mu_2 - \mu_1)]} \qquad (49)$$

These equations give the complete elastic stress distribution in an infinite, two-dimensional, anisotropic material with a circular hole. These solutions are valid only for homogeneous materials, but are assumed to be valid also for midplane symmetric laminates. Laminate strains are calculated using material compliance constitutive relations. Laminate compliance coefficients A_{jk}, are derived using classical lamination plate theory with unidirectional material elastic constants, ply angular orientations, and ply thicknesses. Assuming that laminate strain remains constant through the thickness, strains for individual plies along lamina principal material axes are calculated using coordinate transformations. Stress distributions resulting from an arbitrary set of in-plane loads are obtained using the principle of superposition. To account for inelastic or nonlinear material behavior at the hole boundary, the characteristic dimension' hypothesis of Whitney and Nuismer was adopted[12]. Various material failure criteria can be used with the characteristic dimension failure hypothesis. The failure criteria options are: Tsai-Hill, maximum stress, maximum strain, Hoffman and modified Tsai-Wu. Finite width effects have a significant influence on the circumferential stress distribution around a loaded fastener hole. A superposition of stress distributions from loaded and unloaded hole infinite plate solutions is used to evaluate the effects of finite width. In the loaded hole analysis the bolt load is reacted by tensile and compressive loads of P/2. By superimposing the solution for an unloaded hole under a remote tensile loading of P/2 the desired loading on the bolt and overall equilibrium is attained. The resulting stress distribution gives a good approximation of the state of stress in a plate of finite width but differs from an exact solution in that the superimposed normal and shear stresses at the "edge" of the plate are non-zero.

BJSFM does not require the user to input a large amount of data and the input procedure is user friendly. The data is input interactively, but if a mistake is discovered after a response to a prompt is already entered, the user must start over from the beginning. BJSFM has a very short turnaround time and offers a variety of output options and failure criteria. BJSFM can

account for material anisotropy, general in-plane loadings (tension, compression, biaxiality, shear bearing), and arbitrary hole sizes. BJSFM can also account for composites that are made of more than one type of material. Only mechanical properties for the basic unidirectional ply lamina are required to obtain strength predictions. BJSFM does not account for compression or temperature effects, and has joint geometry restrictions. When inputting the plate properties, BJSFM uses the thickness of each ply orientation normalized by the total plate thickness. BJSFM views a joint as a single plate with an equivalent loading from a second plate. The properties and geometry of the second plate never enter into the analysis. Although BJSFM accounts for the percentages of plies of different orientations for composite materials, it does not account for ply layup sequence. BJSFM can output stresses, strains and displacements at fixed distances and angular locations about the bolt hole. BJSFM is a useful tool that can produce a significant amount of information about a problem.

SCAN ANALYSIS CODE [13,14]

SCAN is an updated version of the BJSFM composite joint analysis code. SCAN is an acronym for: Stress Concentrations ANalysis. The code was developed by the McDonnell Aircraft Company from 1985-1986. The code can only analyze joints connected with one fastener. Improvements have been made to the BJSFM code, which makes the analysis procedure closely match the SASCJ analysis. The analysis is based on anisotropic theory of elasticity, laminated plate theory and a boundary collocation procedure. The SCAN and SASCJ analysis formulations are identical until the point where a Laurent series expansion is assumed for the complex functions ϕ_1 and ϕ_2. SCAN uses the following expansions:

$$\phi_1(z_1) = a_1 1nz_1 + \sum_{n=-\infty}^{\infty} a_{1n} z_1^n \qquad (50)$$

$$\phi_2(z_2) = a_2 1nz_2 + \sum_{n=-\infty}^{\infty} a_{2n} z_2^n \qquad (51)$$

where a_1 and a_2 are determined by solving equations 41 to 44 simultaneously. No mapping function for the z coordinates is used in the SCAN derivation. The constants a_{1n} and a_{2n} are determined by using a least squares boundary collocation technique similar to the one used in SASCJ. Using SCAN, the user can obtain the stresses at any point in a plate, given a set of internal and external boundary conditions.

SCAN is capable of handling joints in a double-lap configuration. The code can analyze a single plate with an unloaded elliptical hole. SCAN can account for any quadrilateral plate shape and bilinear elastic ply behavior is assumed. A limitation on the dimensions of the quadrilateral plate is that the aspect ratio of the plate must be less than 2. The code assumes the bolt bearing load acts in a cosinusoidal distribution over one-half of the bolt hole. No fastener friction effects are considered in the code but their effects on the joint can be approximated. You can specify a bolt load, axial load, transverse load and shear loading. The loads are given in terms of stresses applied to the plate edges and the bolt hole. SCAN, like BJSFM, considers the force of the bolt to be just an input force on the hole. Typically the input loadings, especially the bolt loading, can only be determined experimentally. The user must also know how much load is transferred through the bolt and how much is bypassed around the bolt. The failure criteria are checked at a characteristic distance specified by the user. The failure criteria options are as follows: Maximum Strain, Maximum Stress, Tsai-Hill, Modified Tsai-Wu, Hoffman. The failure criteria is used at the laminate level.

The SCAN analysis code has many different output options. The user can print out laminate

and ply stresses and strains, failure criteria and failure stresses. The analysis doesn't account for the actual laminate stacking sequence and asymmetric laminates cannot be specified. Instead of inputting the stacking sequence, the user inputs the percentage of plies for each different orientation. The code is strictly valid for homogeneous anisotropic flat plates and is assumed to be valid for mid-plane symmetric laminates. The user can input stress or displacement boundary conditions for a plate edge. The boundary conditions can be input as a constant or as a quadratic distribution over the length of the plate edge. To enforce equilibrium on a loaded hole joint, the bearing load, P, must be equal to the edge loading, P_x, divided by the plate width, w. The user can input up to eight different ply angular orientations and can have up to three different materials for hybrid laminates. SCAN is a versatile code for singly fastened composite bolted joints. The code runs relatively fast compared to the SASCJ and SAMCJ codes and has many output options.

SAMCJ ANALYSIS CODE[15]

SAMCJ was also developed by the Northrop Corporation from 1983 to 1985. SAMCJ is an acronym for: Strength Analysis of Multifastener Composite Joints. As the name implies, the code can analyze joints connected by multiple fasteners. In addition to this capability, the code can also effectively model a combination of loaded and unloaded holes and cutouts. SAMCJ also performs a two-dimensional analysis of finite bolted composite plates. SAMCJ is derived from SASCJ, so the basic analysis is the same. Many identical or slightly modified subroutines are used for both analysis codes. The main difference is that SAMCJ uses special finite elements to perform the analysis. The special finite elements include: elements with loaded holes, elements with unloaded holes, regular plate elements and beam elements to model the bolts. The user is required to input the geometry of the bolted joint, the type of elements, the material properties, loading condition, and fastener geometry. SAMCJ applies a 1 kip load to the joint and also applies the constraints. The stiffness matrices for all of the elements are assembled. The code allows the user to take advantage of multiple elements with similar stiffness matrices to reduce run times. The fastener load distribution is determined without the aid of any empirical test data. An average stress failure criteria is used for all joint types in SAMCJ. The failure criteria determines the joint failure load, the location of the failure, and the failure mode.

The SAMCJ analysis code has many of the same options as the SASCJ code. The code is capable of handling multiply fastened joints in a double or single-lap configuration. The symmetry of a double-lap shear problem is taken into account to reduce the amount of input required and computation time. The code can't analyze a single plate with an unloaded hole, but it can analyze joints with only one bolt. A two-dimensional analysis is performed on any finite anisotropic joint. SAMCJ can account for finite geometries which include cutouts, nearby free edges, and tapered or stepped plates. Bilinear elastic ply behavior is assumed. The code assumes the bolt bearing loads act in a cosinusoidal distribution. No fastener friction effects are taken into account and there is no way to specify a bypass ratio in the SAMCJ code. The code internally calculates the bolt load distribution. The edge distance to bolt diameter ratio must be greater than 3. The plate width to bolt diameter ratio must be greater than 4. The user can specify a protruding or countersunk head fastener as in SASCJ. All of the fasteners are assumed to be made of the same material and are identical in type and size. The analysis assumes that the fasteners don't fail. The failure criteria are checked at locations specified by the user. The SAMCJ analysis code outputs the following joint properties upon completion of the analysis: failure load, failure mode, joint loads in the elements, element forces and an

echo of a limited amount of the input data. Like SASCJ, the code cannot determine stresses in a joint for a given load. The analysis accounts for the actual laminate stacking sequence and asymmetric laminates can be specified. SAMCJ accounts for fastener bending, torque and shear. Run times for the analysis can be very long depending on the number of elements that make up the joint.

COMPARISONS AND RECOMMENDED USAGE OF BOLTED JOINTS PROGRAMS

The authors decided to examine and compare the six composite bolted joints analysis codes by performing analysis on various types of joints using as many different codes as possible. We began by selecting various joint test cases for which data from actual experimental strength tests already existed. A test program of joint geometries which had already been experimentally tested in References 5 and 8, were compared to the calculations of each of the bolted joint analysis programs described above. Nine typical joint geometries were chosen to demonstrate some of the capabilities and limitations of each code. The assumptions that were made are: 1) One of the plates being joined (inner plate for the double lap joints) is made of graphite/epoxy with the properties shown in Table 1. 2) The outer plate of each double lap joint and one plate for single lap joints is made of steel with the properties also shown in Table 1. 3) The fasteners used for each joint are steel bolts with protruding heads. Some of the fasteners had bushings, but they were not accounted for in the analyses. 4) The fasteners were assumed to fit exactly and no fastener clearance was considered. 5) No fastener torque-up effects were considered, however it was experimented with in adjusting the bearing/bypass loads for some of the analysis codes. 6) For the experimental tests, the average of the failure loads for each joint geometry is considered to be the actual failure load for that geometry. 7) All joint loadings are uniaxial. SCAN, SASCJ, SAMCJ and BJSFM check for joint failure at a characteristic distance which is away from the edge of the hole. The standard distance which was used for this effort was.02 inches. For all joints with bolts that carry a load, the bypass ratio plays a role in the definition of the problem. SASCJ requires the user to input the bypass ratio; SAMCJ, A4EJ and JOINT internally calculate a bypass ratio. The SCAN and BJSFM codes require that the user know the bolt loading, which in turn implies the bypass ratio for the joint. For the SASCJ code, the bypass ratio was adjusted to get a feel for the correct bypass ratio. For the JOINT analysis code, the percentage of 0^{o} plies was assumed to be 37% instead of the actual 50% because of the limitations of the code. Table 2 gives the laminate ply orientations for the three layups used. The following discussion gives an explanation of the results summarized in Table 3.

Open Hole

BJSFM, SCAN and SASCJ are capable of analyzing open holes. The output from all of the analyses is very close as shown in the graph in Figure 2, even though the composite laminate stacking sequence is not considered in the BJSFM and SCAN codes. The BJSFM and SCAN codes are quicker, require less and more fundamental input data, provide more output data, and are unique in their capability to analyze biaxial loadings. SCAN is also the only code capable of analyzing elliptical holes and quadratic loadings. Both the SCAN and SASCJ codes can perform an analysis for a non-rectangular quadrilateral plate shape. SCAN or BJSFM are the recommended codes to use if you are analyzing plates with open holes.

Single Bolt, Double Lap

All of the codes except A4EJ are capable of analyzing double lap joints with a single fastener. Actually the JOINT analysis code isn't capable of doing an analysis of a single bolt joint either because the code assumes an infinite

width plate with uniform bolt spacing through the width of the plate. The JOINT analysis was included in this section to give you a feel for how the capabilities of the code can be stretched.

If the bolt loading is already known from another analysis or through testing, and stress or strain displacement data is desired, then BJSFM and SCAN are the recommended codes to use. If the bolt loading is not known, the user can look at trend data or case studies to get a feel for how the joint is reacting to varying loading conditions. SASCJ should be used if you simply want the failure load of the joint for a particular bypass ratio. The compressively loaded joint shows that SAMCJ tends to predict an unconservative value for the failure load.

Single Bolt, Single Lap

JOINT, SASCJ and SAMCJ are capable of analyzing single lap joints with a single fastener. Again, the JOINT analysis code performs an infinite width plate analysis so the results should be used with this in mind. The SASCJ and SAMCJ codes run relatively slowly but they are only codes capable of performing an analysis on single lap joints. SASCJ requires the user to input a bypass ratio or to look at a worst case situation. SAMCJ doesn't require the user to input a bypass ratio and it internally calculates this value. Both SASCJ and SAMCJ do well at determining the failure load if the user has a good understanding of the problem and the joint parameters. There is no capability to output stresses, strains or displacements in the SASCJ or SAMCJ codes.

Multiple Bolted Joints

A4EJ, JOINT and SAMCJ are capable of analyzing multiply fastened joints. A4EJ and SAMCJ are capable of accounting for compressive loadings. In all codes, the magnitude of the error tended to increase as the number of fasteners increased. A4EJ has a relatively short run time, but can only analyze joints containing at least two rows of fasteners with at least two fasteners per row. A4EJ is recommended for use in design studies of multiply fastened joints. JOINT has a relatively quick run time and although the code assumes an infinite width plate, the code produced good results for some cases. JOINT is limited in the amount of output it can produce so it is recommended for preliminary design studies. SAMCJ is capable of analyzing many types of multiply fastened joints because of its finite element based formulation.

CREPAIR PROGRAM[16]

The CREPAIR (Composite Bolted Repair) program was developed by McDonnell Douglas Corporation (T. Hinkle and G. Hoehn) on a contract from Wright Laboratory, Flight Dynamics Directorate's Structures Division. The purpose of this program is for the evaluation (strength) of composite skins (damaged or undamaged) with an axisymmetric cutout, and subjected to inplane biaxial and shear loads. The program accounts for thermal loads induced by a material mismatch. It includes a tapered patch analysis as well. CREPAIR predicts strain distributions and fastener loads for a finite-width orthotropic skin having an axisymmetric cutout and a mechanically-attached, tapered, orthotropic patch. The primary loads on the repaired area are assumed to be inplane, biaxial and shear loads accounting for the thermal loads induced by the material mismatch. The CREPAIR program was derived from an earlier program called BREPAIR developed by the Navy[16]. The theoretical approach in BREPAIR was based on the boundary collocation method. The purpose of BREPAIR was to evaluate the strength of repair patches mechanically fastened to repaired (or unrepaired) skin having a circular cutout formed after smoothing-out the damaged area. The CREPAIR extensions include elliptical, slotted, or rectangular cutouts with

tapered patches and thermal mismatch considerations. Also the theoretical basis was modified to the boundary element method.

SVELT[17-19]

SVELT, Spline Variation Elastic Laminate Technology, currently under development at the University of Dayton Research Institute is sponsored by Wright Laboratory, Materials Directorate. The program's objective is to obtain a detailed (three-dimensional) strength analysis of bolted joints by modeling an open elastically filled through-the-thickness opening (loaded or unloaded holes) in laminated plates. It is based on a Ritz analysis procedure based on a mixed variational energy principle. The distribution of displacements and interlaminar stress components in each layer are independently approximated in terms of cubic B-spline functions to assure continuity of displacements and stresses. This is one of the few research efforts addressing accuracy issues in joint strength analysis. The computer program is intended primarily for numerical validation of the method.

A4EI - BONDED JOINTS[7]

This program was developed by Hart-Smith of McDonnell Aircraft Company, and it was sponsored by the U.S. Air Force Wright Laboratory's Structures Division. A4EI, A4EJ and A4EK are three programs developed undr this effort. A4EI is a bonded joints analysis program. It is intended for the nonlinear analysis of adhesively bonded stepped-lap joints and doublers. It is based on a continuum mechanics approach combined with empirical estimates from tests. A4EJ is a multi-row bolted joints (mechanically fastened) analysis program in composite structures. The A4EK program analyzes joints in which both bonding and mechanical fasteners are used.

PGLUE- BONDED JOINT REPAIR[20]

The PGLUE program was developed by Fogarty and Saff of McDonnell Aircraft Company. The purpose of the program was to evaluate the strength characteristics of adhesively bonded repair patches. The program's input are the geometry, material properties and loading conditions. The output consists of stresses and deflections in the skin, the patch and the adhesive. Some of the salient features of PGLUE are: a) performs three-dimensional analysis of bonded repairs, b) accommodates bilinear as well as elastic/perfectly plastic material models for the adhesive, and c) analyses tapered patches with variable thickness. It is a finite element analysis program with solid (eight node hexahedron) elements.

JTSDL/JTSTP[21]

This program was developed in the early 70s by Grimes et. al. for the U.S. Air Force Flight Dynamics Laboratory. Its purpose was the analysis of bonded single, double and step-lap joints. The analysis method is based on a elastic continuum. The material model for the adhesive and the adherend is based on the Ramberg-Osgood three parameter stress-strain curves. The number of simplifying assumptions limits the utility of the program to relatively lightly loaded conservative designs.

BONJO PROGRAM[22]

The programs BONJOIG, BONJOIS and BONJO were developed under Air Force Flight Dynamics Laboratory sponsorship during the early 70s. Although the BONJO series of programs addresses both bolted and bonded joints analysis, only the bonded joints issues are discussed in this review. The BONJOIG program analyzes single-lap and double-lap joint configurations. The adhesive material model is assumed to be linearly elastic. The BONJOIS analysis is limited to single-lap bonded joints

with identical adherends with a linearly elastic adhesive. BONJO is simply an expansion of the BONJOIG program with a bilinear elastic, perfectly plastic material model. For additional details refer to the reference cited above.

MOSIAC[23]

The MOSAIC program is currently under development at ADTECH Corporation under partial funding from the Air Forces' SBIR (Small Business Innovative Research) Phase II program. The purpose of the program is to perform an accurate three-dimensional stress analysis of multi-layered structures having material property variations in all three orthogonal directions. It is an ambitious undertaking under development, and the current status is described in the cited reference.

A4EK PROGRAM[7]

This program is part of a three program series (A4EI, A4EJ and A4EK) discussed earlier. The purpose of its development was to investigate the advantages (if any) in using both bonding and bolting of composite elements. These three programs are extremely popular and have been widely distributed over the years. For more details the reader is referred to the cited references.

CONCLUSIONS

The programs cited in this review were developed primarily under the sponsorship of the Air Force and other U.S. government agencies. There were a number of joints analysis and testing programs funded during the 1970s and 1980s. Fundinghas been relatively scarce during the 1990s, as a result, both industry and research organizations are concentrating on enhancements and innovative use of the existing programs. The current trend is to treat the joint design issue as a integral part of the overall service life prediction of composite structures. This attitude makes sense, because issues such as delamination, debonding, fatigue life, and impact damage affect joints design as well. The reviewer is aware of at least two or more SBIR (Small Business Innovative Research) efforts devoted to the development of a user friendly software environment for joints analysis and their design optimization. Adtech Systems Research, Inc. in Dayton, Ohio is working on an SBIR - Phase II program, funded by the Flight Dynamics Directorate at Wright-Patterson Air Force Base. The primary objectives of this project are as follows:

- Develop a computer infrastructure (both on a PC and a workstation environment) for using any or all of the public domain (government funded) joint analysis programs with common input and output features wherever possible.
- Bench-mark the programs with common/ duplicate features.
- Survey the aerospace industry and identify desirable features beyond those available and enhance the infrastructure to the extent resources allow or seek government and/or industry funding.
- Plan for high-temperature applications with the new metal and ceramic matrix composites.
- Develop a marketing plan for technology transfer in the context of the Integrated Product Development initiatives of DoD (Department of Defense), NASA and other government agencies.

Similar SBIR PHASE II and PHASE III efforts are underway at the American Joining Institute, Oak Ridge, Tennessee. The funding agency for this effort is ARPA (Advanced Research Agency). The thrust of this effort is commercial applications as opposed to the previous effort which is intended for military applications. However, a significant overlap is anticipated in these two programs. Steven Hall of Celaris

However, a significant overlap is anticipated in these two programs. Steven Hall of Celaris Aerospace Corporation has undertaken a similar effort in Canada with partial support or at least moral support from the National Research Council of Canada.

In addition to the reviewed programs industry is using commercial finite element (FE) programs for joint analysis. The following features are necessary for a FE analysis:

- Non-linear material modeling such as a piecewise linear analysis.
- Non-linear springs and/or fastener elements for modeling fasteners and adherends.
- Extensive bench-marking for validating FE analysis.

In conclusion industry appears to be in good shape for joint analysis, but training and modeling guidlines are needed for effective use. Additional research efforts are necessary to address new material systems and high temperature issues.

REFERENCES

1. AGARD Conference Proceedings No.427, "Behaviour and Analysis of Mechanically Fastened Joints in Composite Structures," Structures and Materials Panel Specialists' Meeting, Madrid, Spain, 27-29 April 1987.

2. Venkayya, V. B., Ramkumar, R. L., Tischler, V. A., Snyder, B. D., Burns, J. G., "Recent Studies on Bolted Joints in composite Structures," 65th AGARD SMP Meeting, Madrid, Spain, April 1987.

3. Ramkumar, R. L., Saether, E. S., and Tossavainen, E., "Design, Fabrication Testing and Analysis of Bolted Structural Elements," AFWAL-TR-86-3033, 1986.

4. Snyder, B.D., Burns, J.G., and Venkayya, V.B., "Composite Bolted Joints Analysis Programs,", AIAA/ASME/ASCE/AHS 29th Structures, Structural Dynamics and Materials Conference, Williamsburg, Virginia, 18-20 April 1988, Paper No. 88-2423.

5. Soni, S. R., et. al., "State-of-the-Art in the Stress Analysis and Strength Prediction of Bolted and Bonded Joints in Composite Structures,"WL-TR-XXXX, Interim Report PHASE 2 SBIR Contract, "Fracture Mechanics Based Life Prediction of High Temperature Composite Joints," 1996.

6. Smith, M. K., Hart-Smith, L. J. and Dietz, C. G., "Interactive Composite Joint Design," AFWAL-TR-78-38, Part 1, 2 and 3, April 1978.

7. Hart-Smith, L. J., "Design Methodology for Bonded-Bolted Composite Joints," AFWAL-TR-81-3154, Volume I and II, February 1982.

8. Ramkumar, R. L., et al., "Strength Analysis of Composite and Metallic Plates Bolted Together by a Single Fastener," AFWAL-TR-85-3064, August 1985.

9. Ramkumar, R. L., Saether, E. S. and Cheng, D., "Design Guide for Bolted Joints in Composite Structures," AFWAL-TR-86-3035, March 1986.

10. Garbo, S. P. and Ogonowski, J. M., "Effect of Variances and Manufacturing Tolerances on the Design Strength and Life of Mechanically Fastened Composite Joints," AFFDL-TR-78-179, 1978.

11. Garbo, S. P. and Ogonowski, J. M., "Effect of Variances and Manufacturing Tolerances on the Design Strength and Life of Mechanically Fastened Composite Joints,". Volume I, II, and III, AFWAL-TR-81-3041, April 1981.

12. Whitney, J. M.,and Nuismer, R. J., "Stress Fracture Criteria for Laminated Composites Containing Stress Concentrations," Journal of Composite Materials, Vol. 8, July 1974.

13. Hoehn, G., "Enhanced Analysis/Design Methodology Development for High Load Joints and Attachments for Composite Structures," NADC-87011-60, November 1986.

14. Buchanan, D. L., Ogonowaki, J. M., and Reiling, H. E., Jr., "Development of High Load Joints and Attachments for Composite Wing Structures," NADC-86007-60, November 1985.

15. Ramkumar, R. L., Saether, E. S., and Appa K., "Strength Analysis of Laminated and Metallic

Plates Bolted Together By Many Fasteners," AFWAL-TR-86-3034, 1986.

16. Hinkle, T. and Hoehn, G., "Verification of Analytical Methodology for Designing Repairs to Composite Skin," Vols. 1 and 2, AFWAL-TR-87-3049, Air Force Flight Dynamics Laboratory, Wright-Patterson AFB OH, 1987.

17. Yarve, E. V. and Soni, S. R., "Three-dimensional Analysis in Compression Loaded Laminates, Containing an Open Hole," Composite Materials and Structures, AMD-Vol. 179, 1993, pp. 117-132.

18. Yarve, E. V., "On the Accuracy of Interlaminar Stress Calculation in the Vicinity of an Open Hole in Composite by Use of Spline Variational Technique," Proceedings of the ASC 9th Composite Materials, Mechanics, and Processing Technical Conference, University of Delaware, Newark DE, September 20-22, 1994, pp. 797-806.

19. Yarve, E. V., "Stress Analysis in Laminated Composites with Fastener Holes," Proceedings of the ASC 10th Composite Materials, Mechanics, and Processing Technical Conference, Santa Monica CA, October 18-20, 1995, pp. 408-419.

20. Fogarty, J. H. and Saff, C. R., "PGLUE User's Manual - Rev. A," MDC Report No. B0288, McDonnell Aircraft Company, St Louis MO, August 1987.

21. Bogdanovich, A. E. and Yarve, E. V., "Numerical Analysis of Impact Deformation of Composite Plates," Mechanics of Composite Materials, Vol. 5, 1989, pp. 804-820.

22. Dickson, J. N., Hsu, T. M. and McKinney, J. M., "Development of an Understanding of the Fatigue Phenomena of Bonded and Bolted Joints in Advanced Filamentary Composite Materials," AFFDL-TR-72-64, Vols. I and II, 1972, Air Force Flight Dynamics Laboratory, Wright-Patterson AFB OH.

23. Bogdanovich, A. E. and Rastogi, N., "3-D Variational Analysis of Bonded Composite Plates," Proceedings of ASME Winter Annual Meeting, Atlanta GA, November 1966 (Submitted for presentation).

Table 1: MATERIAL PROPERTIES

Graphite Epoxy	Steel
$E_1^t = 18.9 \times 10^6 psi$	$E = 30.0 \times 10^6 psi$
$E_1^c = 18.2 \times 10^6 psi$	$\nu = 0.3$
$E_2^t = 1.9 \times 10^6 psi$	
$G_{12} = 0.85 \times 10^6 psi$	
$\nu_{12} = 0.3$	

Table 2: SYMMETRIC PLY LAYUPS

44 ply symmetric laminate:

$(45, 0_2, -45, (0, 45)_2, 90, (-45, 0, 0, 45, 0, -45)_2, 0)_S$

44 ply layup has:

- 50.0% - 0° plies
- 22.7% - 45° plies
- 22.7% - -45° plies
- 4.6% - 90° plies

40 ply symmetric laminate:

$(45, 0_2, -45, 90, (0, 45)_2, 90, -45, 0_4, 45, (-45, 0)_2)_S$

20 ply symmetric laminate:

$(45, 0_2, -45, 0_2, 90, -45, 45, 0)_S$

20 and 40 ply layups have:

- 50.0% - 0° plies
- 20.0% - 45° plies
- 20.0% - -45° plies
- 10.0% - 90° plies

Table 3: COMPOSITE BOLTED JOINT PROBLEM RESULTS

Joint Type	Analysis Code	Bypass Ratio 0.-full bearing 1.-open hole	Predicted Failure Load (lbs)	Cross Section Area (in^2)	Predicted Failure Mode	Failure Criteria	Actual Failure Mode	% diff	Actual Failure Load (lbs)
OH[a]	SASCJ	N/A	27800	0.431	N/A	HTH	NS	+10%	25033
OH[a]	SCAN	N/A	30444	0.431	N/A	HTH	NS	+18%	25033
OH[a]	BJSFM	N/A	24138	0.431	N/A	HTH	NS	-4%	25033
DL1[b]	JOINT	0.0	16753	0.9385	B	N/A	SO	-22%	21525
DL1[b]	BJSFM	N/A	17768	0.9385	N/A	MS	SO	-17%	21525
DL1[b]	SCAN	N/A	28800	0.9385	N/A	MS	SO	+25%	21525
DL1[b]	SASCJ	0.6	19375	0.9385	B/SO	AS	SO	-10%	21525
DL1[b]	SAMCJ	N/A	20956	0.9385	B	AS	SO	-3%	21525
DL1C[b]	BJSFM	N/A	22636	0.938	N/A	MS	B	-10%	25183
DL1C[b]	SCAN	N/A	26100	0.938	N/A	MS	B	+4%	25183
DL1C[b]	SASCJ	0.5	25595	0.938	SO/B	AS	B	+2%	25183
DL1C[b]	SAMCJ	N/A	32418	0.938	B	AS	B	+22%	25183
SL1	JOINT	0.0	5072	0.467	TN	N/A	SO/B	-44%	8980
SL1	SASCJ	0.6	9915	0.467	NS/B	AS	SO/B	+9%	8980
SL1	SAMCJ	N/A	10479	0.467	B	AS	SO/B	+14%	8980
DL2	JOINT	0.0	15392	0.626	TN	N/A	SO/B	-28%	21475
DL2	SAMCJ	N/A	13660	0.626	B	AS	SO/B	-36%	21475
DL2C	SAMCJ	N/A	18721	0.312	NS	AS	B	+24%	14165
DL4	JOINT	0.0	15653	0.521	TN	N/A	NS	-39%	25613
DL4	A4EJ	N/A	6786	0.521	N/A	N/A	NS	-74%	25613
DL4	SAMCJ	N/A	14236	0.521	B	AS	NS	-44%	25613
SL2	SAMCJ	N/A	7120	0.313	B	AS	SO/B	-39%	11640
SL2	JOINT	0.0	4141	0.313	TN	N/A	SO/B	-64%	11640
SL4	JOINT	0.0	7415	0.521	TN	N/A	SO/B	-70%	24963
SL4	A4EJ	N/A	6859	0.521	N/A	N/A	SO/B	-73%	24963
SL4	SAMCJ	N/A	14258	0.521	B	AS	SO/B	-43%	24963

Analysis Codes:

1 - JOINT
2 - A4EJ
3 - BJSFM
4 - SCAN
5 - SASCJ
6 - SAMCJ

[a] - 44 ply layup
[b] - 40 ply layup
all others - 20 ply layup

Failure Criteria:

HTH - Hoffman/Tsai-Hill
AS - Average Stress
MS - Maximum Stress

SO - shear out
B - bearing
NS - net section
TN - tension at hole

Joint Types:

OH - open hole
DL1 - double lap 1 bolt
DL1C - double lap 1 bolt, compression
SL1 - single lap 1 bolt
DL2 - double lap 2 bolts
DL2C - double lap 2 bolts, compression
DL4 - double lap 4 bolts
SL2 - single lap 2 bolts
SL4 - single lap 4 bolts

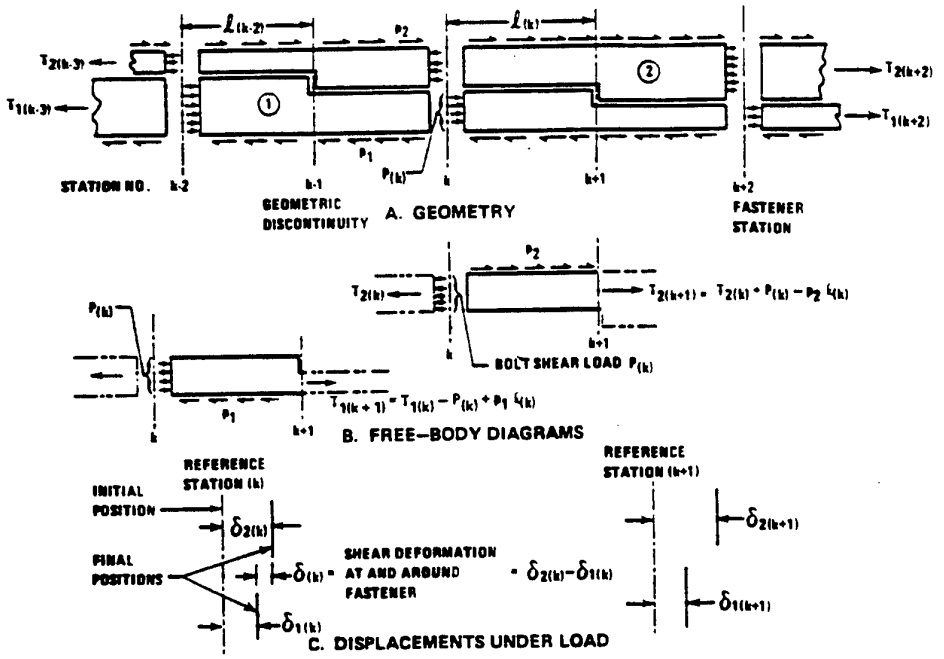


Figure 1: Loads and Deformations on Elements of Bolted Joint

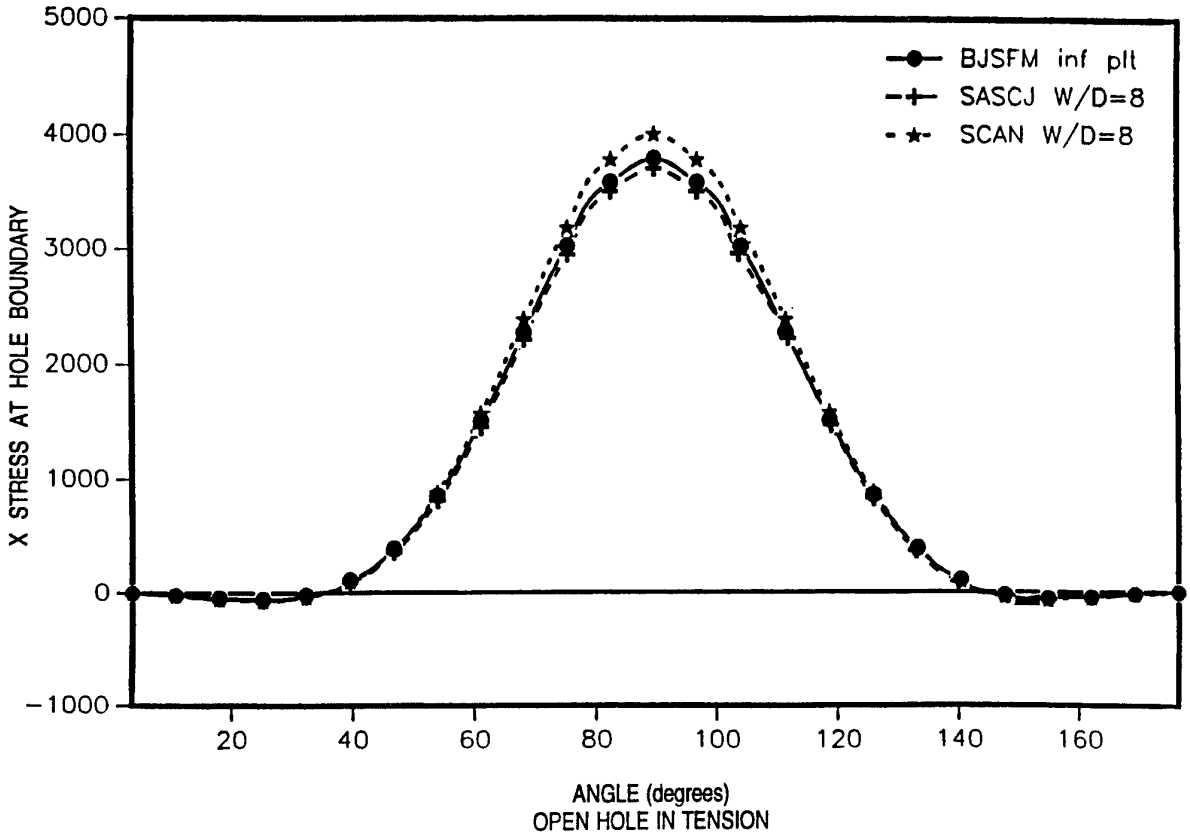


Figure 2: COMPARISON OF ANALYSIS CODES

Stress Analysis of Open and Fastener Hole Composites Based on Three-Dimensional Spline Variational Technique

Endel V. Iarve
University of Dayton Research Institute
300 College Park
Dayton OH 45469-0168

and

Jeffery R. Schaff
Wright Laboratory Materials Directorate
2941 P. Street Bldg 654 Ste 1
Wright-Patterson AFB OH 45433-7750

1. SUMMARY *A three-dimensional stress analysis method has been developed and verified for open and fastener hole laminated composites. This method is based on independent spline approximation of displacement and interlaminar stress components. Spline approximation offers continuity of displacement, strain and stress fields within homogeneous domains, preserving at the same time the advantages of local approximation, such as sparcity of the resulting system of equations. Verification of the spline approximation solution for a fiber dominated 28 ply, IM7/5250-4, laminate with an open hole was performed through comparisons with experimentally obtained surface strain measurements using the moiré interferometry technique. For the filled hole case, the contact problem describing the interaction between a composite plate with a circular hole and an elastic fastener has been solved with three-dimensional spline approximation of displacements and using the Lagrangian multiplier method. Direct comparisons are made with an asymptotic solution of the three body contact problem appearing at the elastic fastener hole edge in a composite laminate. Good agreement between the singular term of the asymptotic solution and spline variational solution for all stress components was observed in the open and filled hole tension problems. The power of singularity at a ±45 ply interface in a $[\pm 45]_s$ AS4/3501-6 laminate with a filled hole was calculated for different stiffnesses of the fastener.*

2. INTRODUCTION

Although, the principal method for assembling composite structures is the use of mechanical fasteners, no method exists capable of accurately predicting the strength of resulting joints. Admittedly, the analysis of composite bolted joints is a complex task in which material, lay-up, hole diameter, loading type, clearance, bolt torque, etc. influence the local response. For this reason, the design of such joints in composite structures is based primarily on experimental test data (Shyprykevich, 1995). Clearly, the first step in the development of an improved design methodology is the accurate determination of stresses in close proximity of the fastener in each ply of a laminate.

Stress analysis of composite laminates with elastic fasteners has evolved starting with the original works of Lehknitskii (1954) who obtained a two-dimensional elasticity solution for an infinite anisotropic plate with an inclusion. More recent developments which utilize complex variable techniques for calculating two-dimensional stress fields in a finite anisotropic plate resulted in several composite bolted joint analysis programs and is described by Snyder, et al. (1990). A limitation of these methods is due to simplifications that were made in order to avoid solving the contact problem between the plate and the bolt, that is, the mechanical response of the fastener is simulated by imposing a contact stress which varies as a cosine function over half the hole circumference.

Advancements in addressing the plate/fastener contact were made by applying the

Paper presented at the 83rd Meeting of the AGARD SMP on "Bolted/Bonded Joints in Polymeric Composites", held in Florence, Italy, 2-3 September 1996, and published in CP-590.

finite element method to solve the plane strain problem for an orthotropic plate with a fastener hole where material properties were averaged through the thickness. Using finite element analysis to determine the contact region and to solve for the contact stresses in a two-dimensional formulation, Crews et al. (1981) showed that the cosine distribution assumption is very accurate for isotropic plates. However it under-predicts the amplitude of the contact stress by about 40% for an orthotropic plate with $E_1/E_2 = 13.5$.

A three-dimensional analysis is required to properly account for stacking sequence effects, non-uniform contact regions, and bolt clamping effects. The critical stage in the development of such capability is thorough verification of stress predictions at ply interfaces in the vicinity of the hole edge. Iarve (1996) concluded that direct comparisons with existing analytical solutions are inadequate due to wide discrepancies of results reported in the literature for interlaminar stresses even at the mid-surface of a symmetric cross-ply laminate.

Relatively few papers are devoted to three-dimensional stress analysis in composite laminates with fastener holes. Chen et al. (1995) utilized the eight-node brick finite element approach for the plate and elastic fastener. All possible factors (friction, clamp-up force, clearance, stacking sequence and fastener stiffness) have been included in the analysis. However, the only verification of the results, consists of a comparison between surface strains measured experimentally away from the hole edge, for a thin CFRP $[45/0/-45/90]_s$ laminate. No verification of interlaminar stress results is presented.

Marshall et al. (1989) calculated interlaminar stresses by utilizing a 20-node isoparametric finite element model for stress analysis of pin loaded and fastener holes in $[0/90]_s$ and $[90/0]_s$ laminates. Inside the contact zone, which was assumed uniform through-the-thickness, the radial displacement of the plate were assumed to be zero to simulate contact with a rigid fastener. Interlaminar normal stresses calculated at the edge of a rigid fastener hole in $[0/90]_s$ and $[90/0]_s$ laminates were compared. According to the authors, however, the finite element mesh was not suitably refined to accurately predict normal and shear interlaminar stresses at the free edge.

Independent spline approximation of interlaminar stress components and displacements proposed by Iarve (1996, 1993) allow for accurate three-dimensional stress prediction in practical composites containing open holes. Spline approximation offers a simple solution to inter-element incompatibility of finite element methods by eliminating artificial field discontinuities within homogeneous domains. Spline approximation shape function can be defined to have an arbitrary number of continuous derivatives at the nodes inside the homogeneous domain, ensuring continuity of both displacement and strain fields. Furthermore, the advantages of local approximation resulting in a sparse rigidity matrix are maintained by utilizing basic spline functions with local supporters. This makes the spline approximation approach ideally suited for boundary value problems for multi-layer domains containing regions of singular stress behavior. This approach was extended for the case of a plate with a rigid fastener and verified for $[\pm 45]_s$ and $[90/0]_s$ laminates (Iarve, 1995).

In this work, the accuracy of surface strain predictions for a 28-ply, IM7/5250-4, laminate with an open hole is evaluated based on a comparison with moiré interferometry measurements in the hole vicinity. An asymptotic solution was developed for analytical verifications of a composite laminate results with an open hole or an elastic fastener. Based on a comparison of all stress components including interlaminar stresses, good agreement was obtained using a common value of the stress intensity factor. Due to a highly non-uniform through the thickness stress-strain field, a rigorous automated algorithm was developed for explicit contact zone definition at all locations through the thickness.

3. PROBLEM STATEMENT

Consider a rectangular orthotropic plate containing a circular hole having a diameter D, as shown in Figure 1. The plate consists of N plies of total thickness H in the z- direction and has a length L in the x-direction and width A in y- direction. A circular isotropic elastic fastener of diameter d is situated at the center of the hole. The length of the fastener in the z direction is equal to the plate thickness H.

A general three-dimensional contact interaction problem between the fastener and the plate is considered. Bypass loading conditions are imposed in the x-direction. At the opposite edges of the plate: x=0,L, constant displacement in x- direction is prescribed, other displacement components at these edges are presumed to be zero:

$$u_x(0,y,z) = u_0,\ u_y(0,y,z) = u_z(0,y,z) = 0$$
$$u_x(L,y,z) = u_L,\ u_y(L,y,z) = u_z(L,y,z) = 0. \quad (1)$$

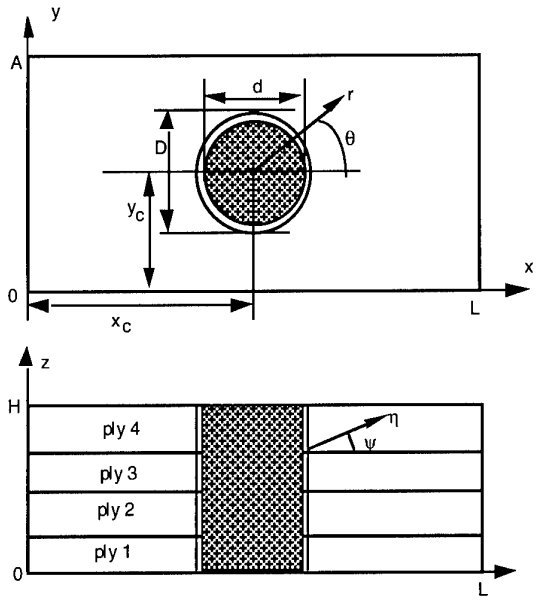


Figure 1. Plate with a fastener hole and the coordinate systems.

An important loading case is the filled hole tension problem when $u_L = -u_0 > 0$. We will distinguish the bearing loading conditions for the plate when the bypass load is equal to zero and the side x=L is free:

$$u_x(L,y,z) = u_L, \quad u_y(L,y,z) = u_z(L,y,z) = 0,$$
$$\sigma_{xx}(0,y,z) = \sigma_{xy}(0,y,z) = \sigma_{xz}(0,y,z) = 0 \qquad (2)$$

A cylindrical coordinate system is defined originating from the center of the hole:

$$x = r\cos\theta + x_c, y = r\sin\theta + y_c, z = z. \qquad (3)$$

where x_c , y_c are the coordinates of the center of the hole. The fastener displacements will be denoted as v_r , v_θ and v_z. The fastener is fixed at two points: at the top and bottom surfaces z=0 and z=H, so that in cylindrical coordinates the boundary conditions are as follows:

$$v_r(0,\theta,0) = v_\theta(0,\theta,0) = v_z(0,\theta,0) = 0,$$
$$v_r(0,\theta,H) = v_\theta(0,\theta,H) = v_z(0,\theta,H) = 0. \qquad (4)$$

For small displacements and deformations the nonpenetration condition can be simplified as

$$u_r(D/2,\theta,z) - v_r(d/2,\theta,z) + \Delta R \geq 0\,, \qquad (5)$$

where $\Delta R = D/2 - d/2$ – is the clearance between the hole and the fastener. Relationship (5) becomes an equality over the contact region $\Omega(\theta,z)$.

Minimum potential energy principle along with the Lagrangian multiplier method was used to solve the problem. Frictionless contact is considered. First variation of the following functional is required to be equal to zero:

$$\delta\Big(\Pi_p + \Pi_b + \iint_{\Omega(\theta,z)} \lambda(\theta,z) \times (u_r(D/2,\theta,z) - v_r(d/2,\theta,z) + \Delta R)dS\Big) = 0 \qquad (6)$$

The potential energy of the plate is denoted as Π_p and the potential energy of the elastic fastener as Π_b. The size and location of the contact zone is unknown initially. Functional (6) suggests a simple interpretation for the Lagrangian multiplier as the value of the contact stress at the contact surface , i.e.

$$\sigma_{rr}^{(p)}(D/2,\theta,z) = \sigma_{rr}^{(b)}(d/2,\theta,z) =$$
$$= \lambda(\theta,z); (\theta,z) \in \Omega(\theta,z).$$

In the following sections the spline approximation of the functions included in functional (6) will be constructed.

4. SPLINE APPROXIMATION OF THE DISPLACEMENT AND INTERLAMINAR STRESS COMPONENTS IN THE PLATE

A detailed description of the spline approximation procedure and the properties of spline functions is given by Iarve (1996). The x,y plane was mapped into a rectangular region ρ, ϕ , where $0 \leq \rho \leq 1$ and $0 \leq \phi \leq 2\pi$. The transformation was defined as follows:

$$x = \frac{D}{2} F_1(\rho)\cos\phi + L \cdot F_2(\rho)\alpha(\phi) + x_c$$
$$y = \frac{D}{2} F_1(\rho)\sin\phi + A \cdot F_2(\rho)\beta(\phi) + y_c \qquad (7)$$

Functions F_1 and F_2 were defined as

$$F_1(\rho) = \begin{cases} 1 + \kappa \cdot \rho, \rho \leq \rho_h \\ \dfrac{(1+\kappa\cdot\rho_h)(1-\rho)}{1-\rho_h}, \rho_h \leq \rho \leq 1 \end{cases}$$

$$F_2(\rho) = \begin{cases} 0, \rho \leq \rho_h \\ \dfrac{\rho - \rho_h}{1-\rho_h}, \rho_h \leq \rho \leq 1 \end{cases}$$

This transformation was defined so that the coordinate line ρ=0 describes the contour of the hole, and the coordinate line ρ=1 describes the rectangular contour of the plate. Inside the near hole region $D/2 \leq r \leq (1+\kappa)D/2$, which

corresponds to $0 \le \rho \le \rho_h$, a simple relationship between the polar coordinates and the curvilinear coordinates ρ, ϕ exists:

$$r - \frac{D}{2} = \frac{D\kappa}{2}\rho \quad \text{and} \quad \theta = \phi.$$

The width of this region is typically two hole radii, i.e. $\kappa\rho_h = 2$. Beyond this region a transition between the circular contour of the opening and the rectangular contour of the plate is performed. Functions $\alpha(\phi)$ and $\beta(\phi)$ describing the rectangular contour of the plate boundary were given in Iarve (1996). These functions are introduced so that parametric equations $x=\alpha(\phi)+x_c$, $y=\beta(\phi)+y_c$ describe the rectangular contour of the plate, and $0 \le \phi < \phi^{(1)}$ corresponds to $0 < x \le L, y=A$, $\phi^{(1)} \le \phi < \phi^{(2)}$ corresponds to $x=0$, $0 < y \le A$, $\phi^{(2)} \le \phi < \phi^{(3)}$ corresponds to $0 \le x < L$, $y=0$ and $\phi^{(3)} \le \phi < 2\pi$ corresponds to $x=L$, $0 \le y < A$.

Spline approximation of displacement and interlaminar stress components in curvilinear coordinates was utilized. Subdivisions were introduced through the thickness of each ply

$$z^{(s-1)} = z_0 < z_1 < z_2 < \ldots < z_{n_s} = z^{(s)}$$

where s=1,...,N-total number of plies. The s-th ply occupies a region $z^{(s)} \le z \le z^{(s-1)}$, and n_s- is the number of sublayers in s-th ply. Nodal points are also introduced in the ρ and ϕ directions as follows:

$0 = \rho_0 < \rho_1 < \ldots < \rho_m = 1,$

$0 = \phi_0 < \phi_1 < \ldots < \phi_k = 2\pi$. The subdivision of the ρ coordinate is essentially nonuniform. The interval size increases in geometric progression beginning at the hole edge. The region $0 \le \rho \le \rho_h$ in which the curvilinear transformation is quasi polar is subdivided into m_0 intervals, so that $\rho_h = \rho_{m_0}$. Sets of basic B-type cubic spline functions $\{R_i(\rho)\}_{i=1}^{m+3}$, $\{\Phi_i(\phi)\}_{i=1}^{k+3}$, $\{Z^{(s)}{}_i(z)\}_{i=1}^{n_s+3}$ along each coordinate are built according to recurrent procedures given by Iarve (1996). Splines along the ϕ coordinate have periodical properties at the ends of the interval. The three-dimensional approximation of displacement components was written using tensor product of three one dimensional sets of splines. The vector of the three-dimensional spline approximation functions was defined as:

$$\left\{\chi^{(s)}\right\}_q = R_i(\rho)\Phi_j(\phi)Z_l^{(s)}(z),$$

$$q = l + (j-1)(n_s+3) + (i-1)(n_s+3)k,$$

$$l = 1,\ldots,n_s+3, j = 1,\ldots,k, i = 1,\ldots,m+3.$$

Since the orthotropic material properties become location dependent in the curvilinear coordinate system, the displacement components were considered relative to x, y and z as functions of ρ, ϕ and z. The following approximation was used inside each ply:

$$\begin{aligned} u_x &= \mathbf{C}_1^{(s)}\chi^{(s)}\mathbf{U}_s^* + \\ &+\chi^{(s)}\mathbf{E}_0^* \cdot u_0 + \chi^{(s)}\mathbf{E}_L^* \cdot u_L, \\ u_y &= \mathbf{C}_2^{(s)}\chi^{(s)}\mathbf{V}_s^*, \\ u_z &= \mathbf{C}_3^{(s)}\chi^{(s)}\mathbf{W}_s^*. \end{aligned} \tag{8}$$

Bold type will be used to distinguish vectors and matrices, superscript star means transpose operation. Vectors **U,V,W** contain unknown displacement spline approximation coefficients. Non square boundary matrices $\mathbf{C}_1^{(s)}, \mathbf{C}_2^{(s)}, \mathbf{C}_3^{(s)}$ and constant vectors $\mathbf{E}_0$, $\mathbf{E}_L$ are defined so that the approximation (8) provides a kinematically admissible, i.e. satisfying boundary conditions (1) or (2), displacement field for any coefficients **U,V,W**. The components of vectors $\mathbf{E}_0$, $\mathbf{E}_L$ are equal to 1 if the same components of $\chi^{(s)}$ are nonzero at $\rho=1$, $\phi^{(1)} \le \phi < \phi^{(2)}$ (x=0) and $\rho=1$, $\phi^{(3)} \le \phi < 2\pi$ (x=L) respectively. All other components of the vectors $\mathbf{E}_0$, $\mathbf{E}_L$ are equal to zero. The boundary matrices are obtained by deleting a number of rows from the unit matrix. The deleted rows have a nonzero scalar product with $\mathbf{E}_0$ or $\mathbf{E}_L$.

Using the same spline approximation functions the interlaminar surface traction spline approximation at the lower $z=z^{(s-1)}$ and upper $z=z^{(s)}$ surface of the s-th ply was introduced

$$p_i^{(s_1)}(\rho,\phi) = \mathbf{C}_i^{(s)}\chi(\rho,\phi,z^{(s_1)})\mathbf{P}_i^{(s_1)}, \tag{9}$$

$$i = 1,2,3,\ s_1 = s-1, s.$$

The potential energy of the ply may be expressed as

$$\Pi^{(s)} = \int_0^1 d\rho \int_0^{2\pi} \left(\int_{z^{(s-1)}}^{z^{(s)}} \frac{1}{2}\sigma_{ij}\varepsilon_{ij}dz - \sum_{s_1=s-1}^{s} p_i^{(s_1)} u_i(\rho,\phi,z^{(s_1)}) \right) \det \mathbf{J} d\phi - \int_{S_T} T_i u_i ds \quad (10)$$

where summation is implied upon i,j=1,2,3. Indexes i and j correspond to directions x,y,z in the order 1,2,3 respectively. T_i- are tractions which can be prescribed at lateral sides y=0 and y=A, denoted in equation (10) as surface S_T. **J**-is the Jacobean matrix of the curvilinear transformation (7). Displacement components in equation (10) are substituted by expressions (8) and the traction components by expressions (9). Strain components are also expressed through the displacement spline approximation coefficients by taking the partial derivatives of (8) symbolically. Thus the strain components are expressed through the displacement components in each point directly. Stress components are calculated at each point through Hooke's law

$$\sigma_{ij} = Q_{ijkl}^{(s)}(\varepsilon_{kl} - t_{kl}^{(s)}\Delta T) \quad (11)$$

where ΔT - is uniform temperature change, $Q_{ijkl}^{(s)}$ are the stiffness coefficients, and $t_{kl}^{(s)}$ are thermal expansion coefficients of the s-th ply. After all parameters entering equation (10) are expressed through the displacement and traction spline approximation coefficients, the ply equations allow one to calculate the unknown displacement components if the interlaminar traction coefficients are given and vise versa can be obtained. The potential energy of the plate is calculated as

$$\Pi_p = \sum_{s=1}^{n} \Pi^{(s)}$$

Due to displacement and traction continuity conditions at the interlaminar surfaces the potential energy Π_p will only contain traction spline approximation vectors at the bottom plate surface $\mathbf{P}_i^{(0)}$ and the top plate surface $\mathbf{P}_i^{(n)}$.

5. SPLINE APPROXIMATION OF THE DISPLACEMENT AND INTERLAMINAR STRESS COMPONENTS IN THE FASTENER

A spline approximation is used for the displacement approximation in the fastener as well. Due to its isotropic elastic properties, it is reasonable to use relatively coarse subdivisions for the displacement approximation. A set of curvilinear coordinates ξ,φ,ζ is introduced

$$r = \frac{d}{2}\xi, \quad \theta = \varphi, \quad z = \zeta.$$

The fastener occupies the region $0 \le \xi \le 1, 0 \le \varphi \le 2\pi$, $0 \le z \le H$. A spline approximation of fastener displacements as functions of ξ,φ,ζ is considered. Nodal points are introduced as follows: $0 = \xi_0 < \xi_1 < \xi_2 < \ldots < \xi_{k_b} = 1$ (n_b - number of sublayers through the fastener thickness); $0 = \zeta_0 < \zeta_1 < \zeta_2 < \ldots < \zeta_{n_b} = 1$; $0 = \varphi_0 < \varphi_1 < \varphi_2 < \ldots < \varphi_{m_b} = 2\pi$. The numbers of intervals of subdivisions n_b, m_b and k_b are independent of those in the plate. Basic systems of cubic spline functions have been built upon these coordinates: $\left\{R_i^b(\xi)\right\}_{i=1}^{m_b+3}$, $\left\{\Phi_i^b(\varphi)\right\}_{i=1}^{k_b+3}$, $\left\{Z_i^b(\zeta)\right\}_{i=1}^{n_b+3}$. Similar to the plate displacement approximation, periodic properties of the spline approximation upon φ are assured. Due to isotropic elastic properties, the fastener displacement components were considered in polar coordinates as functions of ξ,φ,ζ, so that

$$\begin{aligned} v_r &= \mathbf{C}_1^b \chi_b \mathbf{U}_b^*, \quad v_\theta = \mathbf{C}_2^b \chi_b \mathbf{V}_b^*, \\ v_z &= \mathbf{C}_3^b \chi_b \mathbf{W}_b^*. \end{aligned} \quad (12)$$

where

$$\left\{\chi_b\right\}_q = R_i^b(\xi)\Phi_j^b(\varphi)Z_l^b(\zeta),$$

$$q = l + (j-1)(n_b+3) + (i-1)(n_b+3)k_b, l = 1,\ldots,n_b+3, j = 1,\ldots,k_b, i = 1,\ldots,m_b+3.$$

Vectors $\mathbf{U}_b, \mathbf{V}_b, \mathbf{W}_b$ contain the unknown spline approximation coefficients. Boundary matrices

have to be defined to satisfy the boundary conditions (4) and the condition of displacement field uniqueness in the origin of the local coordinate system:

$$\frac{\partial v_r(\xi=0,\varphi,\zeta)}{\partial\varphi}=\frac{\partial v_\theta(\xi=0,\varphi,\zeta)}{\partial\varphi}=0$$
$$\frac{\partial v_z(\xi=0,\varphi,\zeta)}{\partial\varphi}=0. \qquad (13)$$

The potential energy of the fastener can be calculated as

$$\Pi_b=\int_0^1 d\xi\int_0^{2\pi}\int_0^H\frac{1}{2}\sigma_{ij}\varepsilon_{ij}\det\mathbf{J}_b\,d\varphi d\zeta \qquad (14)$$

where strains are expressed through displacements by direct differentiation of equations (8) and stresses are calculated by using Hooke's law. Jacobean of the coordinate transformation used in the fastener is denoted $\mathbf{J}_b$.

6. CONTACT INTERACTION PROBLEM SOLUTION IN SPLINE APPROXIMATION SPACE

Consider the surface integral in the variational equation (6). We shall introduce spline approximation of the Lagrangian multiplier $\lambda(\theta,z)$:

$$\lambda(\theta,z)=\chi(\rho=0,\phi=\theta,z)\lambda^*,$$
$$\text{where } \chi^*=(\chi^{(1)^*},\chi^{(2)^*},\ldots,\chi^{(n)^*}) \qquad (15)$$

λ- is an unknown vector of spline approximation coefficients. This vector defines both the contact stress value and the contact zone geometry.

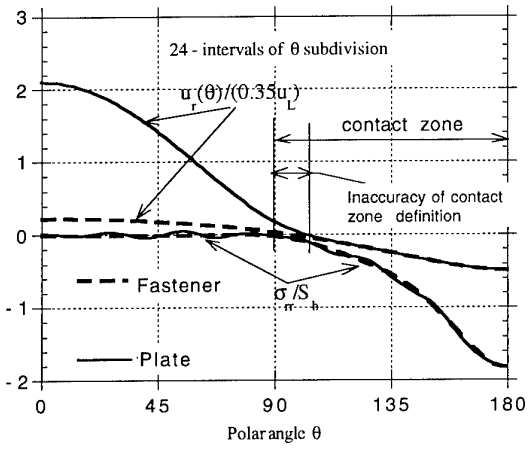
The surface integral in functional (6) is expressed through the components of vector (15). Detailed expressions are omitted due to space limitations. The equations for obtaining the unknown coefficients are derived from (6). Adjustment of the contact zone in each ply is performed during the Gauss-Zeidel block iterations.

7. BASIC COMPARISON

Contact stress behavior will be studied on an example of a square orthotropic plate loaded in bearing through a steel pin. Elastic properties of the orthotropic material are E_1=147 GPa, E_2= E_3=10.9 GPa, G_{21}= G_{31}=6.41 GPa, G_{31}=3.26 GPa, ν_{13}= ν_{12}=0.38, ν_{23}=0.45. Length to diameter ratio and diameter to thickness ratios are L/D=20, D/H=10 and L=6.35cm. The elastic properties of the pin were E=220 GPa and v=0.34. The same problem has been solved in plane stress approximation by Crews et al. (1981) by using the finite element method. Radial normal stresses and polar displacements both of the plate and the fastener at the hole edge as functions of polar angle are shown in Figure 2. The results are given on the midsurface of the plate and the fastener. The spline approximation was built by introducing n_1=1 sublayer through the thickness and m=14 intervals in the radial direction [m_0=12, $(\rho_{i+1}-\rho_i)/(\rho_i-\rho_{i-1})$=1.2], uniform subdivision into 24 and 48 intervals in circumferential direction was considered. In the fastener: n_b=1, m_b=7, $(\xi_i-\xi_{i-1})/(\xi_{i+1}-\xi_i)$=1.2 and k_b=20 in all cases. Boundary conditions (2) were applied. The polar displacements of the bolt and the plate are normalized by $0.35u_L$ to have the same scale of magnitude as for the radial stress normalized to net tension stress S_b= $A\sigma_0/D$, where

$$\sigma_0=\int_0^H\int_0^A\sigma_x(L,y,z)dydz$$

The purpose of this graphic is to illustrate radial displacement and stress continuity between the fastener and the plate in the contact zone. Solid curves show the plate displacements and stresses, and dashed curves show the results for the fastener. The radial stresses calculated in the plate with 24 interval subdivisions, Figure 2a, show slight oscillation near zero value outside the contact zone and slight oscillation around the fastener radial stress inside the contact zone. Besides, there exists a region marked as "inaccuracy of contact zone definition" in Figure 2a, where both the radial stress and the difference between the radial displacement of the bolt and the plate are nonzero. The presence of such a region is inevitable due to contact problem solution in finite dimension



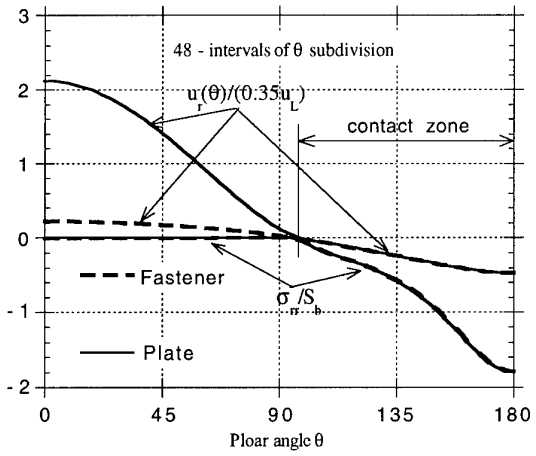


Figure 2. Orthotropic plate loaded in bearing through a steel pin. Contact zone definition accuracy: (a)- 24 intervals, (b)- 48 intervals

approximation space. However by reducing the subdivision interval size, this region must shrink.The results obtained with 48 intervals of subdivisions in Figure 2b confirm that.

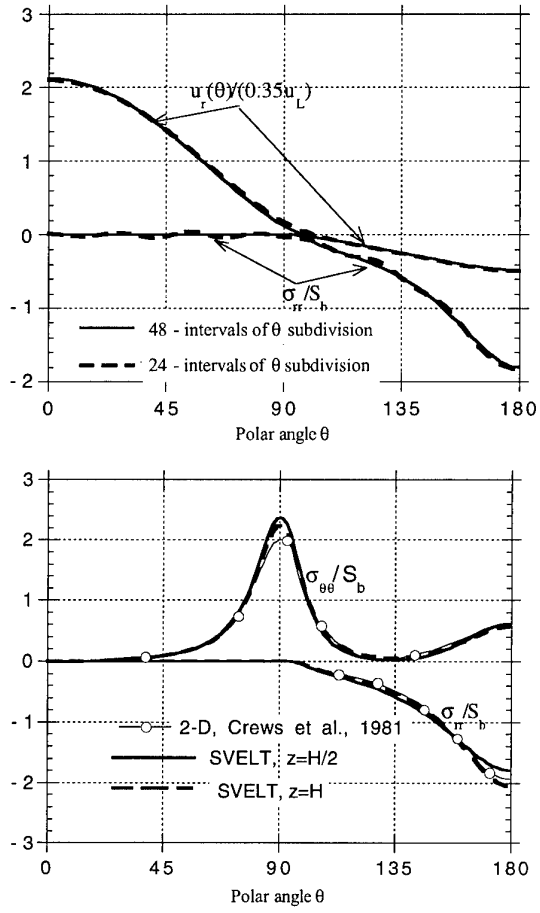


Figure 3. Orthotropic plate loaded in bearing through a steel pin. (a)-convergence, (b)-basic validation

At the same time the amplitude of the radial stress outside the contact zone reduces even more, and inside the contact zone the radial stresses in the fastener and the plate become indistinguishable as evident in Figure 2b. It is observed that rather coarse subdivisions of the fastener are acceptable.Figure 3a compares the results of stress and displacement calculation in the plate with the two subdivisions and shows that the difference is small and indicative of convergence. Figure 3b compares the hoop and radial stresses obtained with 48 intervals of subdivisions with the results of the two-dimensional analysis performed by Crews et al. (1981).

8. ASYMPTOTIC SOLUTION OF THREE BODY CONTACT

Verification of interlaminar stress calculation is a more complicated task due to lack of established baseline results in the literature. A stress singularity is expected to exist at the interface between two layers and the hole edge. The present work extends the asymptotic analysis at the orthotropic ply interface and open hole edge, performed by Iarve(1996), for the fastener hole case. A local coordinate system η, ψ, z is introduced at the interface between s and s+1 plies (Figure 1) with the origin at the point r=D/2, $z=z^{(s)}$, θ so that

$$r - \frac{D}{2} = \frac{D}{2}\eta\cos\psi,\ z - z^{(s)} = \frac{D}{2}\eta\sin\psi,$$
$$\theta = \theta;\ -\pi/2 \le \psi \le 3/2\pi,\ \eta \ge 0,\ 0 \le \theta \le 2\pi, \quad (16)$$

where η is a dimensionless parameter proportional to the distance from the origin of the local coordinate system, and ψ is an angle defining the direction in which the center of the coordinates is approached: $-\pi/2 \le \psi \le 0$ - belongs to the s- ply, $0 \le \psi \le \pi/2$ - belongs to the s+1- ply, and $\pi/2 \le \psi \le 3/2\pi$ belongs to the fastener. The following boundary conditions are imposed at the fastener-composite surfaces (hole edge) at $\psi = \pm \pi/2$, and the interlaminar surfaces $\psi = 0$:

$$u_r^{(s)} = u_r^{(f)}, \sigma_{rr}^{(s)} = \sigma_{rr}^{(f)},$$
$$\sigma_{rz}^{(s)} = \sigma_{\theta r}^{(s)} = \sigma_{rz}^{(f)} = \sigma_{\theta r}^{(f)} = 0$$
$$u_r^{(s+1)} = u_r^{(f)}, \sigma_{rr}^{(s+1)} = \sigma_{rr}^{(f)},$$
$$\sigma_{rz}^{(s+1)} = \sigma_{\theta r}^{(s+1)} = \sigma_{rz}^{(f)} = \sigma_{\theta r}^{(f)} = 0 \quad (17)$$

$$
\begin{aligned}
&u_r^{(s)} = u_r^{(s+1)}, u_\theta^{(s)} = u_\theta^{(s+1)},\\
&u_z^{(s)} = u_z^{(s+1)},\\
&\sigma_{zz}^{(s)} = \sigma_{zz}^{(s+1)}, \sigma_{zr}^{(s)} = \sigma_{zr}^{(s+1)},\\
&\sigma_{z\theta}^{(s)} = \sigma_{z\theta}^{(s+1)},\ \psi = 0.
\end{aligned}
\qquad (18)
$$

Superscripts (s), (s+1) and (f) correspond to displacement and stress components in the s, s+1 plies and the fastener correspondingly. Frictionless contact is considered. The stress components can be represented as

$$\sigma_{\alpha\beta}^{(s_1)} = \sum_{k=1}^{\infty} f_k(\theta)\eta^{\lambda_k - 1}\bar{\sigma}_{\alpha\beta}^{(s_1)}(\lambda_k, \psi, \theta);$$

where $\alpha, \beta = r, \theta, z;\ s_1 = s, s+1.$

The summation is applied to all values of λ found to provide nontrivial solution under the given boundary conditions. The solution procedure developed by Iarve(1996) is applied. The coefficients $f_k(\theta)$ are not given by the asymptotic solution and are determined by the far field solution. Special interest represents the term with λ: $0<\mathrm{Re}(\lambda)<1$. It dominates the solution for $\eta<<1$ since the stresses tend to infinity. Therefore the numerical spline approximation solution is expected to correlate with

$$\sigma_{ij} \cong f_1(\theta)\eta^{\lambda-1}\bar{\sigma}_{ij}(\lambda_1, \psi, \theta) + F_{ij}(\theta)$$

where $\lambda_1\ (0 < \mathrm{Re}(\lambda_1) < 1)$ and amplitudes $\bar{\sigma}_{ij}(\lambda_1, \psi, \theta)$ are rigorously defined by the asymptotic solution and $\bar{\sigma}_{rr}(\lambda_1, \frac{\pi}{2}, \theta) = 1$. In case of the filled hole, boundary conditions (17) and (18), we require: $F_{r\theta} = F_{rz} = 0$. The algorithm for calculating λ: $0<\mathrm{Re}(\lambda)<1$, has been described in the reference paper. Laguer's algorithm is used to calculate the determinant of the boundary condition matrix instead of permutation algorithm due to a rather large size of the matrix (18 by 18).

9. INTERLAMINAR STRESS ANALYSIS

Filled hole tension of a $[45/-45]_s$ laminated plate with L=6.35cm, A=L/2, D=0.1L is considered in the present section. The ply material is AS4/3501-6 with elastic properties E_1=138GPa, $E_2=E_3$=10.34GPa, $G_{12}=G_{13}$=5.52GPa, G_{23}=3.45GPa, $\nu_{12}=\nu_{13}$=0.3 and ν_{23}=0.55. Total laminate thickness is H=1.04 mm and will often be used as a unit of distance. The uniaxial tensile load was applied in the x direction corresponding to boundary conditions (1) with $-u_0=u_L$. Power of singularity $\lambda_1\ (0 < \mathrm{Re}(\lambda_1) < 1)$ obtained by using the asymptotic solution at the hole edge and ply ±45 interface as a function of polar angle θ under boundary conditions (17) and (18) is shown in Figure 4 for different fastener stiffnesses. The aluminum fastener has E=76 GPa, v=0.33, titanium E=103 GPa, v=0.34 and steel E=220 GPa, v=0.34.

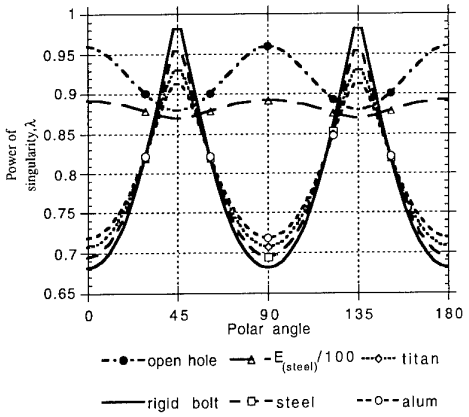


Figure 4. Power of singularity at the +/-45 interface vs. polar angle for different fastener stiffnesses.

The power of singularity for the open hole and rigid fastener hole (Iarve, 1995) is also given. In the case of the rigid fastener, no roots $\lambda_1\ (0 < \mathrm{Re}(\lambda_1) < 1)$ were found at θ =45 and θ =135. At most locations, except around 45 and 135, the power of singularity significantly and rapidly increases by increasing the fastener stiffness. The powers of singularity observed for aluminum, titanium and steel fasteners are close; they are also much closer to the rigid fastener case than that for the open hole. An artifact material E=2.2GPa, v=0.34, one hundred times more compliant than steel is also shown on the Figure 4 to illustrate how rapidly the power of singularity grows with the fastener stiffness. Increase of the power of singularity results in more rapid stress amplitude increase by approaching the interface. Two limiting cases : open and rigid fastener hole tension are considered for illustration. Stress distributions in θ =90 direction in the vicinity of the open hole edge and ply interface in the same plate under uniaxial tension where studied by Iarve(1996). The stress distributions at the same cross-section at the edge of a hole containing a rigid fastener with zero clearance will be considered below. The thickness of each ply was nonuniformly subdivided into $n_1 = n_2$=6 sublayers so that the ratio of two subsequent sublayer thicknesses was 1.5, the thinnest sublayers being near the

interface. Circumferential coordinate ϕ was uniformly divided into 32 intervals. ρ – coordinate was subdivided into m=20 intervals, with m_0=16 and a subsequent interval length ratio of 1.4.

Figure 5 shows the $\sigma_{r\theta}$ stress, normalized to the applied unidirectional load σ_0, as a function of the distance from the hole edge r-D/2 divided by half the laminate thickness. Stresses are shown at the interlaminar surface and two parallel surfaces in each ply, where $z^*=2(z-z^{(1)})/H$. Solid lines on this and the following figures represent the spline approximation method results and dashed lines represent the asymptotic solution. By comparing the stress distributions at the interlaminar surfaces of the open hole (Figure 5a) and filled hole (Figure 5b), the gradient of the stresses approaching the edge of the filled hole is considerably higher. Due to weak singularity of the open hole solution the curves $z^*= \pm 0$ on Figure 5a are almost horizontal. The unknown multiplicative factor for the open hole was determined to be equal to f_1/σ_0= - 2.231 and for the filled hole to be equal to f_1/σ_0=-0.24. These coefficients were obtained

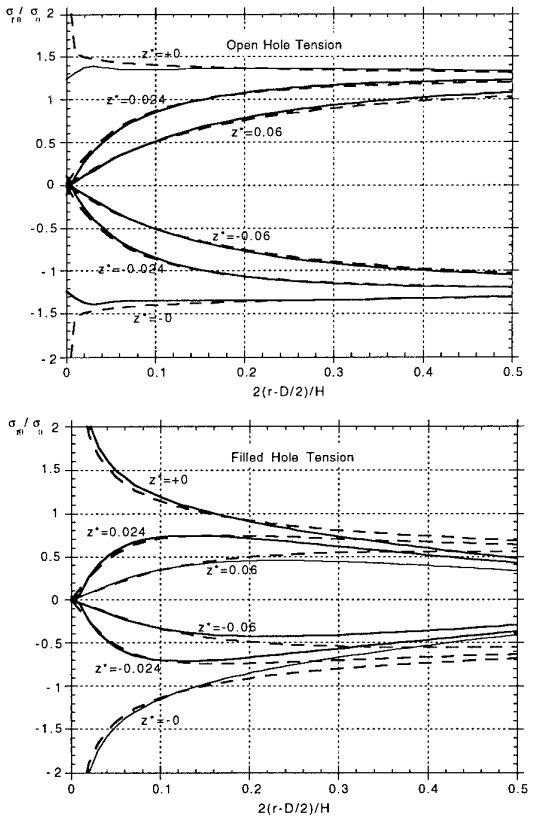


Figure 5. In plane shear stress vs. distance from the hole edge near the interface in open and filled hole tension problems.

as scaling factors to provide the amplitudes of the asymptotic solution and spline approximation solutions to be equal to each other near the hole edge. As was mentioned above, $F_{r\theta}$=0. At distances r-D/2>0.1H from the hole edge, the asymptotic solution and the spline approximation solutions for the filled hole depart from each other.

The interlaminar stresses calculated by using the spline variational approach for filled hole tension with a titanium fastener will be compared to the asymptotic solution. The stress components will be considered at a distance 0.05H from the point (r=D/2, θ=90, $z=z^{(1)}$) as functions of the local coordinate ψ, in the cross-section θ=90. Selecting an equidistant pass from the singular point as opposed to the radial distance dependencies similar to Figure 5 provides a more valid comparison since the asymptotic solution is expected to correlate with the numerical solution only near the ply interface and hole edge intersection.

The asymptotic solution can easily be plotted at these locations by defining η=0.1H/D and plotting the stress amplitude as a function of local variable ψ in the range $-\pi/2<\psi<3\pi/2$. In the spline approximation solution, all functions are defined in curvilinear coordinates (7). Since the locations of interest are in the vicinity of the hole edge, the simplified relationship between polar coordinates and curvilinear coordinates ρ and ϕ may be utilized so that

$$\rho = \eta\cos\psi,\ z = z^{(1)} + \frac{D}{2}\eta\sin\psi,\ \phi = \theta. \qquad (19)$$

An extremely attractive feature of the spline approximation analysis is that displacements and stresses can be output at arbitrary locations of the plate regardless of the meshing. In Figures 6 and 7 are shown all six stress components as functions of ψ for η=0.1H/D in the plate and in the fastener. The spline approximation solution is shown by solid lines and the asymptotic solution by dashed lines. The value of the multiplicative factor f_1/σ_0=-0.35 was obtained to match the $\sigma_{r\theta}$ stress component for the plate -90<ψ<90 with the asymptotic solution in Figure 6.

This factor is unique for all stress components inside the plate and the fastener. Inside the fastener, 90<ψ<270, the asymptotic solution gives zero $\sigma_{r\theta}$ stress value and the spline approximation solution gives small but not zero value due to far field effects. The same factor provided an excellent match between the asymptotic solution and spline approximation

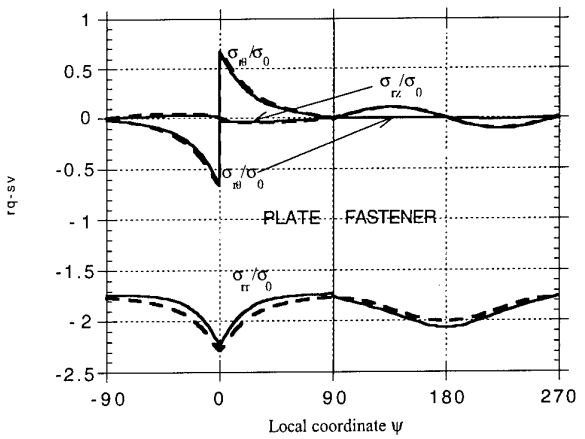
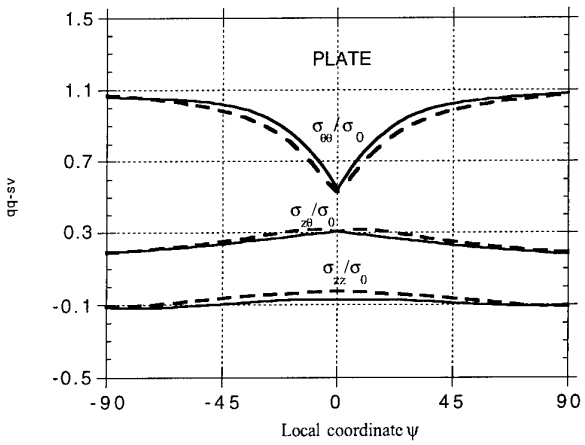


Figure 6. Comparison of stress prediction between the asymptotic solution and the spline approximation solution in the plate and the fastener. Components σ_{rr}, σ_{rz}, $\sigma_{\theta r}$.

solution for the σ_{rz} stress component both in the plate $-90<\psi<90$ and the fastener $90<\psi<270$. A constant additive $F_{rr}/\sigma_0=-1.24$ was used to account for the nonsingular terms by comparing the σ_{rr} components. The continuity of radial stress between the fastener and the plate in the +45 ply at $\psi=90$ and in the -45 ply $\sigma_{rr}(\psi=-90)=\sigma_{rr}(\psi=270)$ can be seen as well as a satisfactory match between the asymptotic and spline approximation solution. The other three stress components for the plate are shown in Figure 7a. The following additives were used to account for the nonsingular terms $F_{\theta\theta}/\sigma_0=+1.34$, $F_{zz}/\sigma_0=+0.2$, $F_{r\theta}/\sigma_0=-0.17$. The same stress components inside the fastener are given in Figure 7b, and the values of the additives used are $F_{\theta\theta}/\sigma_0=-1.44$, $F_{zz}/\sigma_0=-0.36$, $F_{r\theta}/\sigma_0=0$. Satisfactory agreement for all stress components is observed.



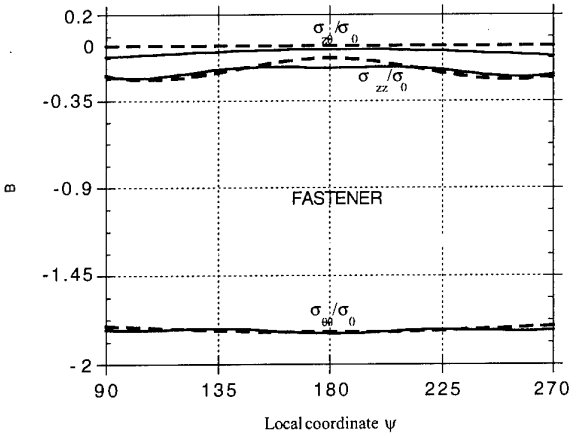


Figure 7. Comparison of stress prediction between the asymptotic solution and the spline approximation solution in the plate and the fastener. Components σ_{zz}, $\sigma_{z\theta}$, $\sigma_{\theta\theta}$. (a)- plate, (b)- fastener.

10. STRESS ANALYSIS OF A STRUCTURAL COMPOSITE LAMINATE

A common 28-ply, IM7/5250-4, laminate with a symmetric stacking sequence of $[45/0/-45/0_2/45/90/45/0_2/45/0/-45/0]_s$ was considered under uniaxial tension. Coupons were nominally 30.48 cm. [12 inches] long and 3.175 cm [1.25 inches] wide with a 0.635 cm [0.25 inch] hole drilled through the center. The average laminate thickness was 0.153 inches. The applied load was P=4,448 N [1000 lbs]. All spline approximation results were obtained using the following materials properties: E_{11} =151 GPa, $E_{22}=E_{33}=9.45$ GPa, $G_{12}=G_{23}=5.9$ GPa, $G_{13}=3.26$ GPa, $\nu_{12}=\nu_{23}=0.321$, and $\nu_{13}=0.449$.

Detailed description of the moiré interferometry procedure is provided by Schaff et al. (1996). Contour plots of moiré interferometry strains overlaid with analytical strains are shown in Figure 8. A rectangular region $[x_c-9.525\text{mm}, x_c+19.05\text{mm}]$ by $[y_c-9.525\text{mm}, y_c]$ is considered.

The spline approximation analysis predictions for axial strain, shown in Figure 8 by dashed lines, agree quite well with the experimental strains, indicated by the solid lines, both far from the hole and close to the hole edge. The major source of discrepancy appears at the edge of the lower right quadrant of the hole. In that area, the numerical model predicts a higher level of strain than was measured. This area of discrepancy extends approximately 1-2 ply thicknesses away from the edge of the hole.

Spline approximation analysis results for the transverse and shear strain components also

match quite well as demonstrated in Figures 9 and 10, respectively. Again the major regions of discrepancy are near the hole edge, but this time, the regions are deeper (2-3 ply thicknesses) and extend around much of the hole.

A=2E-4, B=4E-4, C=6E-4, D=8E-4, E=10E-4, F=12E-4, G=14E-4, H=16E-4, I=18E-4, J=20E-4

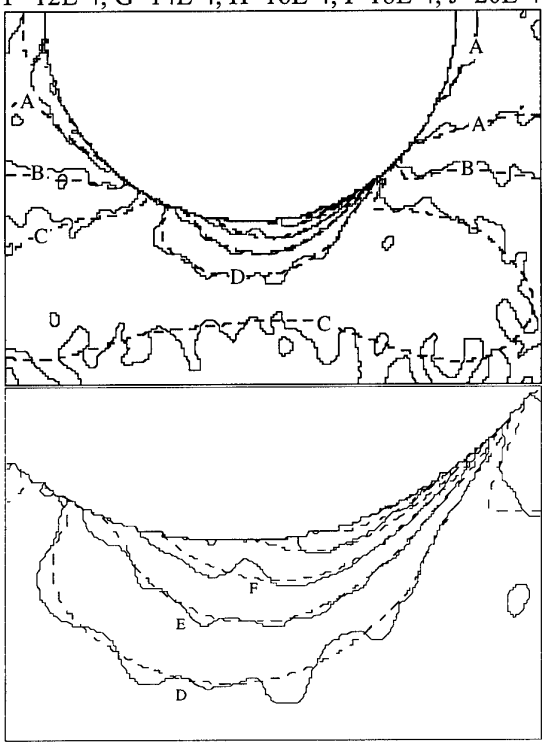


Figure 8. Comparison of measured axial strain (solid) with spline approximation (dashed) in close proximity to an open hole.

One possible cause for the discrepancies observed between the numerical and moiré results could be a slight level of drilling damage present at the hole edge. The amount of localized surface damage is not an indication of matrix cracks as no indication of latter was observed in X-rays prior to loading, Schaff et al. (1996). These chipped out regions extend approximately 1-2 ply thicknesses into the top layer of the laminate. Replication of the diffraction grating onto the specimen surface fills these chipped regions with epoxy. Overall, the comparison of experimental and spline approximation based analysis results show remarkably good agreement. This is especially the case when it is noted that the analysis was developed and run before the experimental results were available.

A=-9E-4B=-7E-4, C=-5E-4, D=--3E-4, E=-1E-4, F=1E-4, G=3E-4

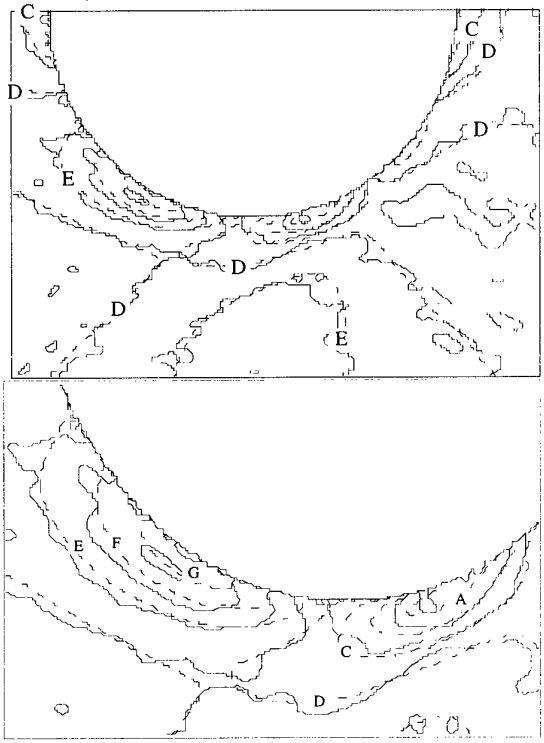


Figure 9. Measured transverse strain (solid) with spline approximation (dashed) near the hole.

A=-10E-4, B=-8E-4, -6E-4, E=-2E-4, F=0E-4, G=2E-4, H=4E-4, I=6E-4, J=8E-4

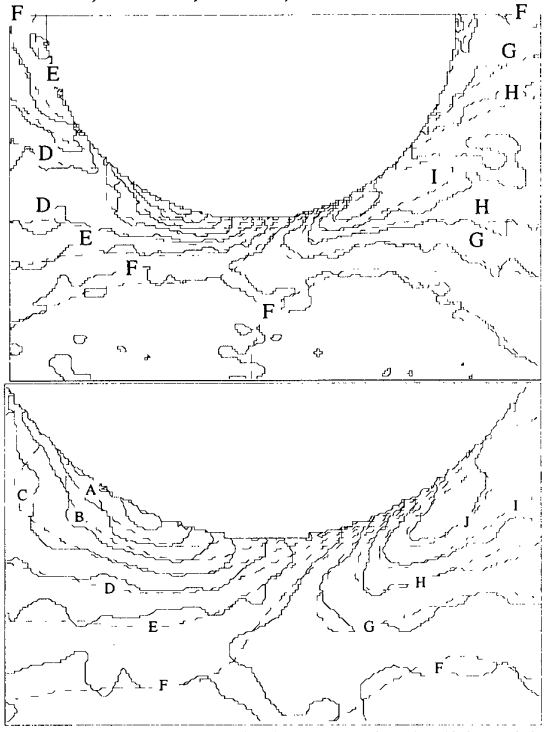


Figure 10. Measured shear strain (solid) with spline approximation (dashed) near the hole.

11. CONCLUSIONS

The spline approximation based method for three-dimensional stress analysis in elastic fastener hole composite laminates including the solution of the contact problem between the fastener and the hole edge has been developed.

An asymptotic solution of the three body contact problem arising at the intersection of the orthotropic plies and the edge of the hole containing an isotropic fastener has been developed. The power of singularity versus fastener stiffness was investigated. Good correlation between numerical solution and the asymptotic solution for a $[+/-45°]_s$ composite under filled hole tension with a titanium fastener was demonstrated.

The accuracy of stress analysis in structural 28-ply laminate containing an open hole was verified by comparing the spline approximation based predictions with moiré interferometry measurments of surface strains in the hole vicinity. Remarkable agreement between numerical and experimental results was observed.

12. ACKNOWLEDGMENT

The authors are greatly indebted to D. Mollenhauer for development of the moiré experimental results and N.J. Pagano for valuable discussions at all stages of the work. This work was funded by the Materials Directorate, Wright Laboratory, Wright-Patterson AFB OH under Contract No. F33615-95-D-5029.

13. REFERENCES

Lekhnitskii, S. G., 1954," Stress Distribution in an Anisotropic Plate with an Eliptic Elastic Core (plane problem)" *Inzhenernyy sbornic*, v. XIX., Moscow.

Crews, J.H. Jr., Hong C.S. and Raju I.S.,1981, "Stress concentration Factors for Finite Orthotropic Laminates with a Pin-Loaded Hole," *NASA Technical Paper 1862*

Snyder, D.S., Burns, J.G., Venkayya, V.B., 1990, "Composite Bolted Joints Analysis Programs," *J. of Composite Technology & Research*, Spring, Vol. 12 (1), p. 41-51.

Shyprykevich, P., (1995), "Characterization of Bolted Joint Behavior: MIL-HDBK-17 Accomplishments at Standardization," *J. of Composite Technology & Research*, July, Vol. 17 (3), pp. 260-270.

Chen, W.-H, Lee, S.-S., Yeh, J.-T., 1995, "Three-dimensional Contact Stress Analysis of a Composite Laminate with Bolted Joint," *Composite Structures*, Vol. 30, pp 287-297.

Marshall, I.H., Arnold, W.S., Wood, J., Mousley, R.F., 1989, "Observations on Bolted Connections in Composite Structures," *Composite Structures*, Vol. 13, pp. 133-151.

Folias, E. S.,1989, "On the Interlaminar Stresses of a Composite Plate Around the Neighborhood of a Hole," *Int. J. Solids Structures*, Vol. 25, pp. 1193-1200.

Iarve, E. V., 1996, "Spline Variational Three-dimensional Stress Analysis of Laminated Composite Plates With Open Holes," *Int. Journal of Solids and Structures,* Vol.33, No.14, pp.2095-2171.

Iarve, E. V., 1995, "Three-dimensional Stress Analysis of Fastener Hole Composites," *Proceeding of the ASME Materials Division*, MD-Vol. 69-1, 1995 IMECE, ASME.

Iarve, E. V., 1993, "Interlaminar Stress Analysis in Compression Loaded Composite Plates Containing Open Hole," *Proceedings of the ASC Eighth Technical Conference*, Technomic Publishing Company, Cleveland OH, October 19-21, pp. 1025-1034.

Schaff, J.R., Mollenhauer D.H. and Rose D. H., 1996, "Stress Analysis and Experimental Testing of a Structural Composite Laminate with a Hole," *Proceedings of the ASC Eleventh Technical Conference,* Atlanta, GA, October 7-9,

DEVELOPMENT OF A STRESSING METHOD FOR BOLTED JOINTS

J. Bauer, E. Mennle

Daimler Benz Aerospace AG
Military Aircraft
D-81663 Muenchen, Germany

SUMMARY

This paper describes the various steps for the development of a stressing method for bolted joints in Polymeric Composites. First a semi-empirical anlysis was generated correlating test results and the corresponding analytical data. Subsequently this predictive technique was used to derive carpet plots and diagrams which then form the basis for the stressing method. In order to cover arbitrary loading conditions the information from the diagrams is incorporated into an algorithm for final determination of the laminate strength.

INTRODUCTION

During the early 1980's the subject of stressing bolted joints was discussed intensively by several authors in the Composite Materials community. At that time the basic methodology and computer codes have been generated. In particular the strength of the Composite adherends represented the focal point of interest. One of the mostly discussed predictive techniques calculates the stress distribution around the hole and evaluates the stresses point by point around it with the target to predict the ultimate strength of the CFRP laminate.

Based on the perception that it is absolutely necessary for the design of primary Composite aircraft structure to have solved this problem satisfactoring, the Military Aircraft Division of Dasa, former MBB, decided to spend the effort and to develop some sophisticated computer codes and to collect experience with the so-called „Point Stress Criterion" (ref. 3 and 4). Since that time this prediction method had to show its applicability in real life i.e. during the design of the Eurofighter 2000 (Figure 1). This project is an international cooperation between the 4 nations Great Britain, Italy, Spain and Germany. This implies that the industrial Partners BAe, Alenia, Casa and Dasa checked all details in a collaborative manner and agreed to apply the herein detailed prediction method to stress their part of the airframe.
This paper goes back to the research work performed in 1984 to 1987. Furthermore it details the additional experiences and the subsequent amendments during the design phase of the Eurofighter and tries to sum up all the conclusions for future consideration.

GENERAL METHODOLOGY AND DEVELOPMENT STEPS

The overall purpose is to be able to predict the strength of a single hole in any CFRP laminate loaded with any type of loading. This includes for example a bolt load in any direction acting alone or passing stresses around an open hole or the most common case when both loading possibilities act superposed together. Figure 2 details these conditions. Test methods are available to test the interaction of a bolt load and longitudinal tensile and compressive stresses but these general loading conditions are not affordable to be simulated systematically.

Figure 3 presents in an overview the individual modules of the development steps. It indicates that one important part are test results. The other parts are of theoretical nature and either pure mathematics or engineering efforts. The latter is necessary to correlate test data with analytical ones. Such a semi-empirical point stress analysis computer code was generated which subsequently was used to derive diagrams or data sheets. These are forming then the information which is given into the stress offices to be used to design the aircraft.
In principle the flow chart of Figure 3 indicates that two predictive techniques have been developed. The first is represented as a pure computer tool and the second is based on diagrams. The question arises why not using the most convenient, the computer tool, instead of continuing by deriving plots? The answer can be found in the complexity of the problem and the further chance to incorporate engineering judgement based on the experience from tests. It was this step which finally generated the confidence which is required in international cooperations.
Using the identical scheme of Figure 3 Figure 4 outlines more details and gives an impression of the complexity of the problem to develop a

Paper presented at the 83rd Meeting of the AGARD SMP on "Bolted/Bonded Joints in Polymeric Composites", held in Florence, Italy, 2-3 September 1996, and published in CP-590.

stressing method for bolted joints. The basic mathematical solution for the stress distribution around a hole is restricted to a linear-elastic material behaviour and is valid for orthotropic plates from infinit extension. In the case of bolt loaded holes the fit between the bolt and the hole is analytically regarded as ideal, i.e.it is not existing. Regarding the situation in reality some discrepancies become obvious and none of these conditions remain valid regarding the technical application when Composite parts are jointed by bolts. To overcome these discrepancies semi-empirical measures are determined which provide a satisfactoring correlation of the analytically determined data with the test data. Having achieved this, it is possible to fill by analysis all the gaps which even a comprehensive test programme leaves open. Then it is possible to generate carpet plots, interaction diagrams and an algorithm combining all data for the derivation of the strength of the bolted joint.

TEST RESULTS

According to Figure 4 it is one essential of the stressing method to adapt the closed solution analysis to the test results. 5 different types of tests are necessary:

- Filled hole tension
- Filled hole compression
- Double shear pin bearing
- Single shear pin bearing
- Interaction of pin bearing and passing stresses

The quantity of test points is of major interest having in mind the accuracy of the predictive technique. Considerable effort may be saved if these are selected favourable. It is one of the major experiences that the restriction of the lay-up to allowed boundaries, in terms of fibre direction percentages, decreases the effort to find favourable semi-empirical measures. How these limitations may be shown graphically can be seen in Figure 5 and the allowed lay-up configurations are given in the so-called „Design Space". The recommended Design Space of laminates to be used in the areas of bolted joints is included in Figur 5.

Together with the common test parameters, like environmental conditions, off-axis, thickness, hole size, edge distancy, type of bolt, plain or countersunk, a considerable number of specimen is summing up to a large test programme.

DETERMINATION OF THE STRESS DISTRIBUTION AROUND HOLES

To develop a computer code for the analysis of stresses in an orthotropic plate and in the vicinity of a hole is a pure mathematical task. Two individual analytical solutions have to be superposed, the first is the solution for open holes and the second for bolt loaded holes. This is illustrated in Figure 6. The formulas and the procedure are given in the literature, e.g. Ref.1 and Ref. 4, but even more details and considerations may be found in the work of Theo de Jong (Ref. 5). The effort, which has to be spent for the generation of such a computer programme should not be underestimated. But having gone through this, it is possible to determine the stress conditions at any point in the vicinity of an arbitrarily loaded hole in an infinite orthotropic plate from linear elastic properties. These conditions represent the usual mathematical ones and therefore naturally do not coincide with the real technical ones.
In principle the stress determination may be performed as well with the Finite Element Method. Such the mathematical complexity is reduced to a minimum, but it is doubtful that this reduces the effort. Nevertheless the FEM is a perfect tool to confirm that the computer code under development is calculating correctly.

SEMI-EMPIRICAL POINT STRESS ANALYSIS

The actual technical conditions incorporate size limitations, pseudo-plastical effects at the edge of the hole and tolerances. All these influences have to be taken into account. Taking the closed solution analysis as the basis this can be achieved by suitable semi-empirical measures. The most common one is the trick with the Characteristic Distance (CA). The stresses are analysed at a certain distance away from the hole edge and interpreted by a failure criterion. Doing this point by point along the Characteristic Distance, the highest loaded location can be selected. If its failure load is regarded to be responsible for the failure of the laminate, then two items of information are received: the location where first failure occurs and the strength of the CFRP laminate.
It would be ideal if this Characteristic Distance would be a material property. For the materials Dasa investigated and gathered experience, this is not the case. For each type of loading, tension or compression, and also dependent on the content of +/-45° fibres, a different characteristic distance

leaded to satisfactoring correlation with the test results. In Figure 7 is shown how this semi-empirical measure was therefore extended. Firstly it became dependent on the +/-45° fibre content and secondly more than one was determined, each referring to one of the cases: Open hole tension, filled hole tension, filled hole compression and double shear pin bearing strength. Having in mind the accurate prediction of the arbitrary loading conditions, these Characteristic Distancies are used as detailed in Figure 7.

The failure criteria can cause some problems which become obvious if plots are generated. The failure criteria Dasa generally is using, the so-called ZTL criteria, is a modified Tsai-Hill one. In certain areas better correlation with the test results were achieved, when the failure prediction was done with the Yamada criteria (Ref. 6). It could be beneficial and reduce the development effort if further investigations include trials of other failure criterias.

During the numerous tests of the analysis another semi-empirical measure gave better correlation between test results and theoretical data and this is to increase slightly the unidirectional compression strength for the calculation of pin bearing strengths. This measure may be justified by the clamping effect. The bolt introduces into the laps a lateral force, especially in the vicinity of the bolt hole, which then is providing a better support of the fibres and the effect to increase the compressive strength.

Finally it has to be pointed out, that each individual semi-empirical measure may be favourable for a certain material but unfavourable for the next one. Not enough experience was collected up to now to extract those which lead quickly to success. Finding out promising semi-empirical measures is always an action of try and error. Bearing in mind this, the whole computer code should be prepared such that the calculation trials are performed with minimum effort. It is Dasa's experience that a large number of trials are necessary making a considerable amount of compromises necessary.

Having generated the semi-empirical point stress analysis the ability is generated to study the influence of off-axis loading, bolt-load to passing stress interaction and, may be most important, the variation originated from the lay-up's. I.e. all gaps can be closed which every test programme naturally leaves open. In addition carpet plots can be generated showing graphically the strength of notched laminates and the double shear pin bearing strength.

DERIVATION OF DATA SHEETS / DIAGRAMS

The core of the stressing method for bolted joints is detailed on Figur 7. There the normalized interaction curve of pin bearing and passing tensile and compressive stresses is presented. On the ordinate the pin bearing strength is scaled and on the negativ and positiv abszissa the filled hole compression respectively tension strength. Together with the 3 carpet plots, presenting the double shear pin bearing, the filled hole compression and the filled hole tension strength, this diagram defines the CFRP laminate strength in the case of on-axis bolt load interacting with on-axis passing stresses. The interaction curve itself resulted from analytical investigations with the semi-empirical point stress analysis computer code. During these investigations the curve was determined such that it represents all lay-ups within the limitations of the previously defined design space. This is resulting naturally to some conservatism for specific lay-ups, but this effect is of a small magnitude and such was judged acceptable. The case, when bolt load and passing stress are both directed in longitudinal direction can still be confirmed by test results.

Focussing the more complex loading conditions of Figure 2 more considerations are necessary. Three different interaction diagrams are necessary to cover the arbitrary loading conditions in a reasonable manner for further considerations:

Pin bearing stress	Longitudinal compressive and tensile stress	Shear stress
Pin bearing stress	Longitudinal compressive and tensile stress	Transverse tensile stress
Pin bearing stress	Longitudinal compressive and tensile stress	Transvers compressive stress

To generate these curves the analytical tool is the only one which remains to give advices. Tests are not feasible taking into account funding and research limitations. Following the same principles as for the easiest case of interaction, the more complex loading conditions have been handled and the Figure 9 details the conditions which have been determined when bolt load, longitudinal stress, transvers stress or shear stress are acting together.

All these interaction diagrams are normalized using the RF values for the pure bearing strength on the ordinate and the filled hole strength on the

abscizza. Taking these RF values reciprocal has the effect that the area internally of the interaction curve represents the allowed conditions of RF > 1.0. Any further parameter, like environmental conditions, off-axis, edge and width corrections etc., are possible to be considered on the basis of the carpet plots in combination with separate data sheets or plots. In general these dependencies have to be derived from test results. In the specific case of the off-axis influence, the semi-empirical point stress analysis may be helpfull in addition.

The single shear pin bearing strength is less dependent on the lay-up and therefore the semi-empirical point stress analysis is not feasible for its prediction. A more simple plot can be derived directly from test results and then be used in combination with the interaction curves. Such the application of the stressing method is extended to single shear bolted joints.

DETERMINATION OF THE RF

Assuming the most general case of a bolt loaded hole and superimposed passing stresses then two Reserve Factors can be built from the three interaction diagrams of Figure 9, one referring to the combination of longitudinal and shear stresses and the other one combining longitudinal and transvers stresses. These two RF's then have to be combined with the target to create the final one, which then is representative for the actual loading conditions. Once more the semi-empirical point stress analysis provided the guidance for the development of a procedure to determine the overall RF. I.e. it was a target to achieve with the information from the diagrams similar results as the master compuer based technique. As shown in Figure 10, this aim leaded to an unconventional method for the determination of the RF from the interaction diagrams. Even more sophisticated is the formula for the determination of the final RF taking the two previously determined as the basis as stated in Figure 11.

SUMMARY AND CONCLUSIONS

A stressing method for bolted Composite joints was developed which is based on diagrams and which was generated with the support of a semi-empirical, test results correlated point stress analysis. The effort to create all this must be regarded as massif and has in principle to be repeated for each new fibre/resin combination. In particular this statement is valid regarding the test effort which is required although extensive analytical progress was achieved.
In principle, deriving from a computer programme diagrams and plots, may be regarded as a step back. But the complexity of the problem, originated by the large number of variables, gave the direction to derive a stressing method which directly indicates all those dependencies which have to be considered. Showing these effects by plots, the required level of confidence arised. Nevertheless this was not possible to achieve without compromises and a certain degree of conservatism.

The methodology, to generate a semi-empirical point stress analysis for each new Composite material under respect, will afford a certain effort. The more often this effort will be spent in the future, the more experience will be gathered and the more the whole procedure will tend to a standardised process. An alternativ to this is, for the time being, not seen by the authors, since no stressing method came to their knowledge which would be compatible. I.e. assuming a stressing method for a new material needs to be created now, then the same methodology would be followed.

The above described stressing method could be used for standardization. It is presented by diagrams, like carpet plots, data sheets covering corrections, normalized interaction diagrams and an algorithm for the final determination of the joint strength. The grafical presentation of the various strengthes allows an effective and easy comparison between different materials. With more experience from different materials potentially it would be feasible to create a conservative standardised stressing procedure for bolted joints and valid for certain classes of fibre/resin combinations.

RECOMMENDATIONS

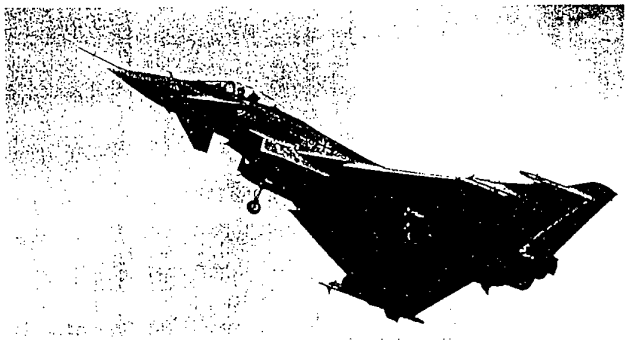
In the future the effort to create a semi-empirical point stress analysis will be reduced due to the experience which is available. Furthermore the following guidelines will serve to keep the effort near the necessary minimum:

- Define a Design Space and restrict the predictive technique accordingly
- Select the test points of the test programme such that the Design Space is covered satisfactoring
- Use a simple failure criteria
- Prepare and use a specific computer code for the computation trials during the development phase. This shall ease to find out the most

favorable semi-empirical measures and their referring values.

REFERENCES

Ref. 1: G. N. Savin, Stress Distribution around Holes, NASA-TT-F-603
Ref. 2: Lekhnitskii, Anisotropic Plates, Gordon and Breach Science Publishers
Ref. 3: F. K. Chang, R. A. Scott, G. S. Springer, Design of Bolted Composite Joints, 28th National Sampe Symposium (4/83)
Ref. 4: J. M. Whitney and R. J. Nuismer, Stress Fracture Criteria for Laminated Composite Containing Stress Concentrations
Ref. 5: Theo de Jong, Stresses in Pin Loaded Anisotropic Plates, Agard-CP-427
Ref. 6: S. E. Yamada, Analysis of Laminate Strength and Its Distribution, J. of Composite Materials Vol. 12/1978
Ref. 7: Saab, I. Ericson, Analysis Method for Bolted Joints in Primary Aircraft Structure, Agard-CP-427
Ref. 8: J. Bauer, E. Mennle, Comparison of Experimental Results and Analytically Predicted Data for Double Shear Fastened Joints, Agard-CP-427
Ref. 9: J. Bauer, Mechanism of Single Shear Fastened Joints, Agard-CP-427
Ref. 10: JST-D - 004, Issue 4, C.F.C. Properties and Allowables
Ref. 11: J. Bauer, Versagensvorhersage an offenen und bolzenbelasteten Bohrungen, MBB-FE212-TN-CFK-043/A



Single Seat Variant (SS)		Twin Seat Variant (TS)	
Length 15.965 m	Height 5.287 m	Length 15.965 m	Höhe 5.287 m
Wingspan	10.953 m	Wingspan	8.6 to 10.953 m
Max. Speed	Mach 2.0	Max. Speed	Mach 2.0
Max. Nz	9.0	Max. Nz	8.8
Thrust without/with reheat	60 - 90 KN	Thrust without/with reheat	60 - 90 KN
Structural weight	~ 10000 kg	Structural weight	~ 10600 kg
Max. Gross weight	> 21000 kg	Max. Gross weitht	über 21000 kg
Fuel	~ 4000 kg	Fuel	< 4000 kg
Max. Payload	> 6500 kg	Max. Payload	über 6500 kg

Figure 1: EUROFIGHTER 2000 - General Data

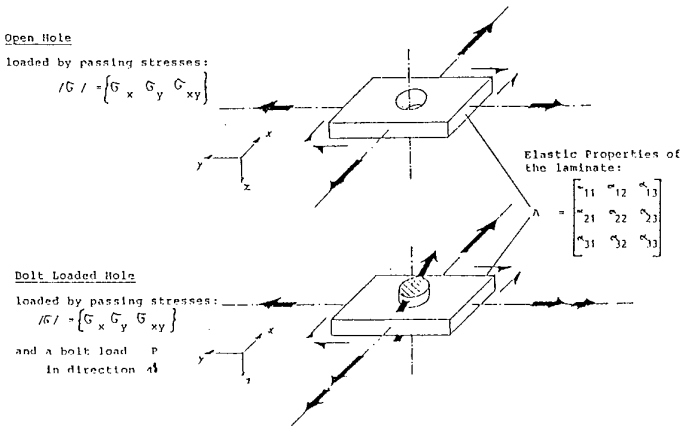


Figure 2: Loading Conditions: In-plane Stresses and Bolt Load

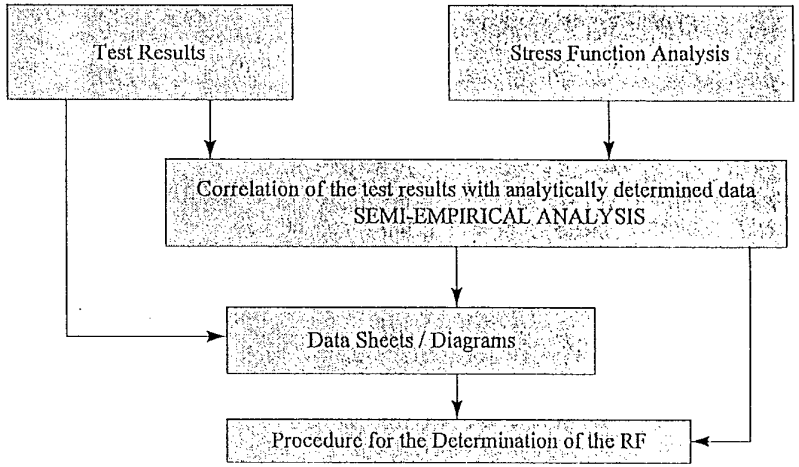


Figure 3: Basic Modules and Development Steps

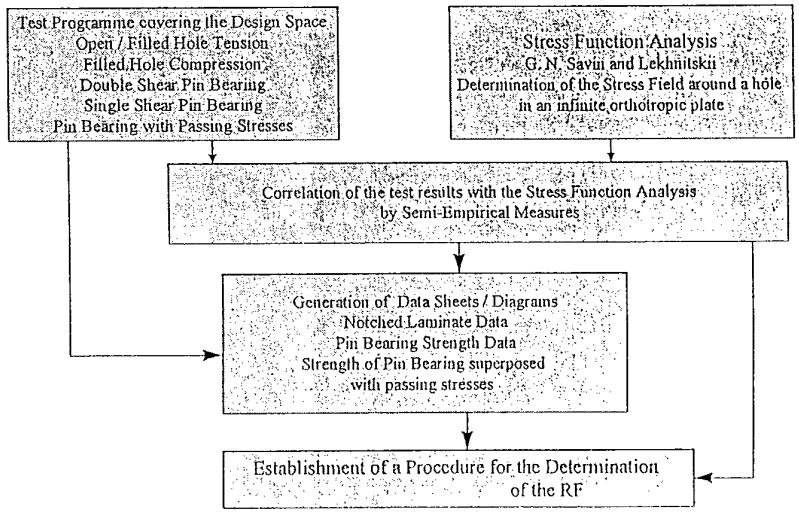
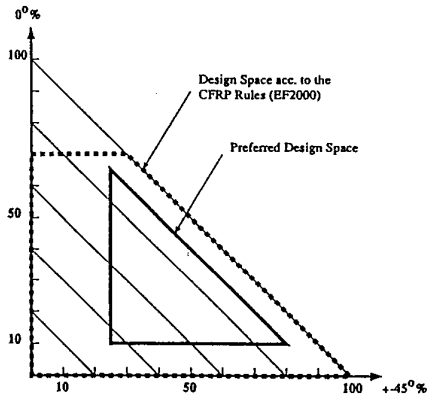


Figure 4: Items to be generated or developed

Design Space



Test Parameters:

CFRP Material:	Fibre / Resin
Bolt Material:	Steel, Titanium
Joint Configuration:	Double, Single Shear
Geometry:	Off-axis Edge Distancies (w,e) Hole Size Plain / Countersunk Thickness Bolt Fit
Environment:	RT/AR, h/w
Loading Conditions:	Tension Passing Stresses Compression P. Stresses

Figure 5: Design Space and Test Considerations

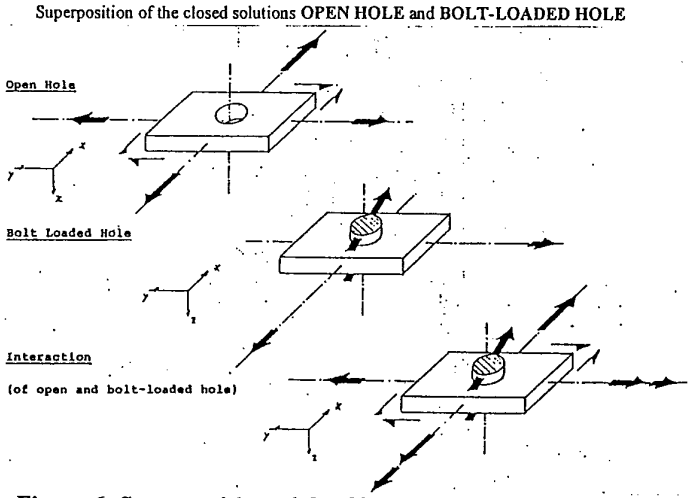
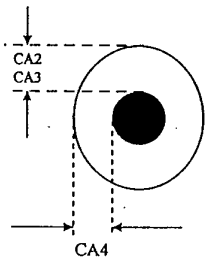


Figure 6: Superposition of the Closed Solutions OPEN HOLE and BOLT-LOADED HOLE-

1.) **Characteristic Distance:**

Open Hole Tension:	CA1 = f (45°fibre content)
Filled Hole Tension:	CA2 = f (45° fibre content)
Filled Hole Compression:	CA3 = f (45° fibre content)
Double Shear Pin Bearing:	CA4 = f (45° fibre content)



In addition the CA may be used to cover the geometrical influences.

2.) **Failure Analysis:** TSAI-HILL (ZTL)
Yamada
(Hart Smith)

3.) **Unidirectional Compression Strength**

The validity of any semi-empirical measure is determined by try and error.

Remarks: The Characteristic Distance CA is a feasible and helpfull tool to adapt the closed solution analysis to the test results. It is dependent on the material but not a material constant. Other dependencies exist in addition.

Figure 7: Semi-Empirical Measures

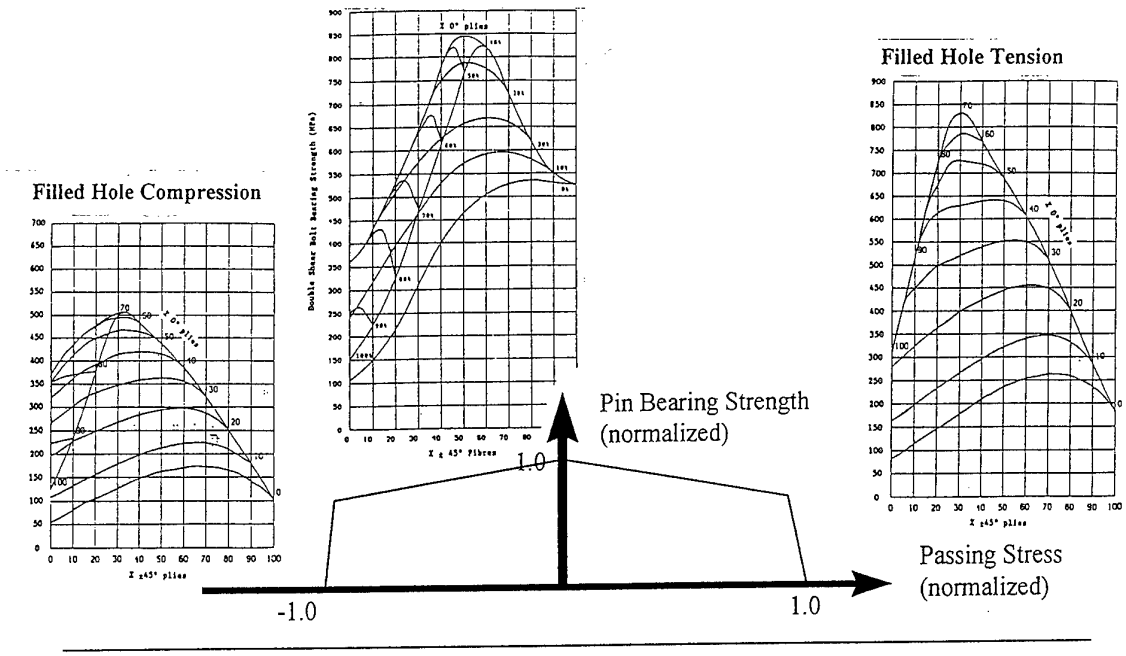


Figure 8: Interaction of Pin Bearing and Longitudinal Passing Stresses

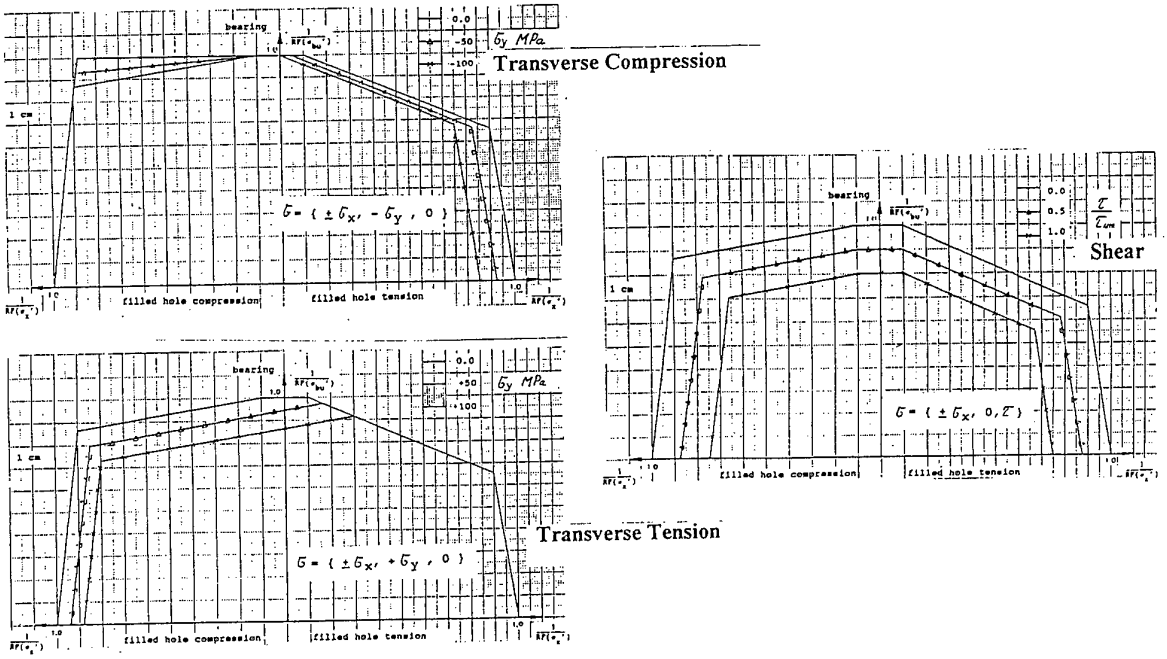


Figure 9: Interaction Curves of Pin Bearing and Passing Longitudinal, Transverse and Shear Stresses

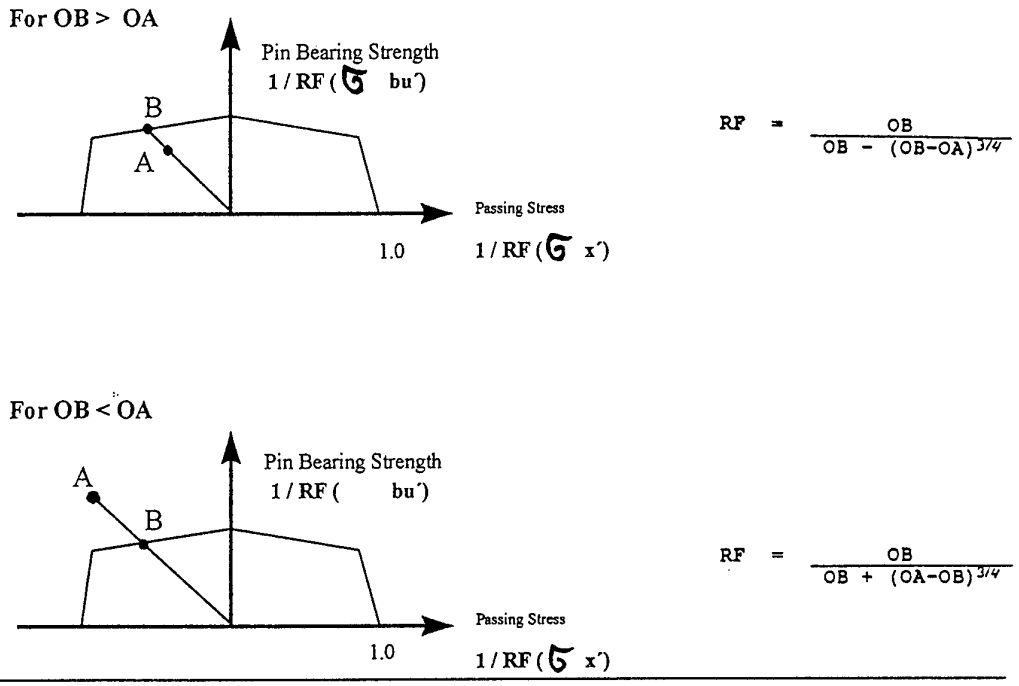


Figure 10: Determination of the RF from the Interaction Diagrams

Bolt Load : P

Passing Stresses : $\sigma_x \quad \sigma_y \quad \tau_{xy}$

Determine the RF for $P, \sigma_x \; \sigma_y \; \phi$ RF (σ_y)

Determine the RF for $P, \sigma_x \; \phi \; \tau_{xy}$ RF (τ_{xy})

Calculate the combined RF according to the formula:

$$\left[\frac{1}{RF}\right]^4 = \left[\frac{|\sigma_y|}{100} + \frac{\tau}{\tau_{all}}\right]^{-4} \cdot \left[\left(\frac{|\sigma_y|}{100}\right)^4 \cdot \left(\frac{1}{RF(\sigma_y)}\right)^4 + \left(\frac{\tau}{\tau_{all}}\right)^4 \cdot \left(\frac{1}{RF(\tau)}\right)^4\right]$$

The overall RF is then the minimum of RF (σ_y)
RF (τ_{xy})
RF

Figure 11: Procedure to Determine the Overall Reserve Factor

Development of Failure in Bolted Joints in Woven CFRP Laminates

J. L. Oakeshott
M. Gower
S. Perinpanayagam
F. L. Matthews
Centre for Composite Materials
Imperial College of Science, Technology and Medicine
London, SW7 2BY, UK

SUMMARY
A recent project at Imperial College was concerned with the development of finite element procedures for predicting the failure of bolted joints in composite laminates. Both 2-D and 3-D analyses were undertaken, one objective of the latter being to correlate the stress distributions around a fastener with the failure modes observed experimentally.

In support of the FE work an extensive test programme was carried out on single fastener joints loaded at increasing fractions of the ultimate load. The nominally 2mm thick laminates were fabricated from prepreg which consisted of balanced satin weave fabric impregnated with epoxy resin. For each load level specimens were dissected and examined under an optical microscope. A "map" of damage growth was obtained for specimen configurations exhibiting either bearing or net tensile failure. The principal failure modes observed were fibre microbuckling and through-thickness matrix shear cracking.

LIST OF SYMBOLS
d	fastener diameter
w	joint width
ε	joint end distance
t	laminate thickness
P_x	applied load
x	crosshead displacement
l	joint length
h_x	hole elongation
σ_b	bearing stress
σ_n	net-tension stress
T	bolt torque
P_t	bolt load

1. INTRODUCTION
This paper describes and presents the results from two consecutive programmes of experimental work in which the development of failure in bolted joints made from composite laminates was investigated. Tests were carried out using a carbon fibre-reinforced epoxy resin laminate material which was composed of eight layers of satin weave fabric in a balanced quasi-isotropic stacking sequence. The laminate was 2.25mm thick. Samples of the laminate were loaded in double shear by single fasteners using an experimental set-up similar to that of Kretsis and Matthews [1]. The first programme of work concerned the development of bearing failures [2] and the second programme of work the development of net-tension failures. The failure mode was controlled through the use of one of two different sample widths.

Initial samples were loaded to failure and subsequent samples to intermediate fractions of the average failure loads. Through-thickness sections were taken of the samples after loading close to the fastener holes and the sections were examined under the optical microscope. The progression of failure and failure mechanisms were monitored with the intention that appropriate criteria could be selected for incorporation into a 3-D finite element model of a region around the fasteners. The 3-D model constituted a substructure analysis of a 2-D finite element model of the experimental set-up, which in turn was based on earlier finite element representations of multi-fastener joints in composite laminates [2].

2. PROCEDURE
The laminate samples were loaded in double shear using a loading mechanism similar to that of Kretsis and Matthews [1]. This is symmetric about the centre line length and designed for samples with fastener holes located at either end. The outer laps are of 6mm thick steel and there are 6mm thick steel links to the test machine grips. The links ensure that, once a

Paper presented at the 83rd Meeting of the AGARD SMP on "Bolted/Bonded Joints in Polymeric Composites", held in Florence, Italy, 2-3 September 1996, and published in CP-590.

small initial preload is applied, the samples can be aligned axially.

The tests were carried out using a carbon fibre (T300)/epoxy resin (914) laminate composed of eight woven (5-harness satin weave) plies of continuous carbon fibres impregnated with epoxy resin. A balanced, quasi-isotropic, $[(0/90)(+45/-45)]_{2S}$ stacking sequence was used and the laminate was 2.25mm thick. The material was supplied by Westland Aerospace as four 600mm by 600mm panels and is typical of that used in the aerospace industry. Prior to cutting the panels were examined for defects using ultrasonic C-scan. No non-uniformities were found.

Sample Preparation

Sets of approximately ten samples (see Figure 1) were cut from the panels to examine the bearing and net-tension failure modes of failure and also the effect of sample orientation. All samples were 200m long and the bearing samples were 36mm (6d) wide and the net-tension samples 24mm (4d) wide. The bearing samples were oriented at 0°, 45° and 90° to the laminate axis (warp weave direction) and the net-tension samples at 0°and 45° to the laminate axis.

The samples were cut using a diamond saw and 6mm diameter holes were drilled at 36mm (6d) from either end. The 36mm end distance was to prevent shearout or cleavage modes of failure and the 128mm distance between the holes to ensure the two ends of the joint acted independently.

Joint Tests

The rig was assembled using steel fasteners, brass washers and steel nuts. The fasteners had a diameter, d, of 6mm, no thread in the region of the composite and were greased with a net fit. The washers had an outer diameter, D, of 13mm (2.2d), an inner diameter of 6mm and a thickness, t, of 2mm. The washers were placed between the composite specimen/steel links and the steel outer laps as well as beneath the bolt head and nut. In addition two extra washers (2 x 2mm thick) were placed on either side of the composite (2mm thick) to act as spacers. The extra washers ensured that the outer laps ran parallel to the inner laps and steel links (6mm thick).

The assembled rig was mounted in an Instron testing machine, fitted with a 10-tonne load cell, and an initial preload of approximately 100kN was applied. Once the mechanism had been aligned axially the bolts were tightened to a 15Nm torque. Subsequent loading of the samples was at nominal rates of 2.5mm/min or 5.0mm/min. The applied loads versus displacements were recorded with the displacements read from the relative crosshead movement. Bearing stress and net-tension stress versus hole elongation graphs were calculated from

$$\sigma_b = P_X/dt \quad (1)$$
$$\sigma_n = P_X/(w - d)t \quad (2)$$
$$h_X = x/d \quad (3)$$

For each set of samples three were loaded to failure and the average bearing or net-tension failure load for that orientation determined. The failure loads were read from the peaks in the load displacement plots. Subsequent 0°, 45° and 90° samples were loaded to 30% (in the case of the net-tension failure samples), 60%, 75% (in the case of the bearing failure samples), 90% and 95% of the average bearing or net tension failure loads. Some samples remained untested for comparative purposes and for use as spares.

One of each of the spare 0° and 45° net-tension samples were loaded to failure with no washers or through-thickness clamping applied. This was to obtain failure loads and load-displacement plots for the equivalent pin-loaded samples.

Observation of Failures

After unloading, the damage to the holes and the location of the failed hole (top or bottom) was noted. For the bearing samples this included observations of the damage caused by the washers and measurements of the final hole elongations. The washer damage was photographed at low magnifications under the optical microscope. Some of the bearing failure specimens were also sectioned parallel to the net-tension plane, gold plated and examined under the scanning electron microscope. All observations were referred to similar examinations of the untested samples.

Subsequently representative samples were cut along the bearing plane in the case of the bearing samples and along the net-tension plane in the case of the net-tension samples (see Figure 2). For the fully failed samples sections were taken of the failed and unfailed holes. After cutting the sections were mounted in epoxy resin, polished and examined under the

optical microscope. Micrographs of the unloaded samples were taken for comparative purposes.

For three of the fully failed, 0° orientation bearing samples the entire failed ends were mounted in epoxy resin. These were cut and oriented parallel to the bearing, net-tension and 45° plane (see Figure 2) and progressively ground by 1mm increments. For the fully failed net-tension failure samples additional sections were taken along the bearing and shearout planes. In these ways maps of the damage growths were obtained.

3. RESULTS

Bearing Failure Tests

The samples loaded to failure in bearing typically showed a non-catastrophic mode of failure (see Figure 3) with little acoustic emission. The majority of the samples failed at the top hole with just one of the 45° samples which failed at the bottom hole. Average failure loads of 15074N (1092MPa) for the 0° orientation samples, 15042N (1090MPa) for the 90° orientation samples and 15352N (1112MPa) for the 45° orientation samples were calculated. No discernible difference was noted between the strength and failure behaviour of the 0° and 90° samples but the 45° samples appeared to be marginally stronger, by approximately 300N (20MPa). For this reason only 0° and 45° samples were tested in the net-tension programme of work.

The fully failed samples showed significant damage on the bearing side of the fastener (see Figure 4) where the laminate had been forced over the washer. This occurred as splits and delaminations at the washer edge. Surface cracks were seen to emanate from the hole boundary at an angle from the hole centre of between 45° and 90°to the applied load. The cracks propagated roughly parallel to the applied load towards the splitting at the washer edge. It appeared that as a result of the damage at the washer edge a plug of material, contained between the washers on the bearing side of the fastener and of width approaching the diameter of the fastener, translated in the direction of the applied load. This caused the holes to elongate. Hole elongations measured directly from the fully failed samples were in the range 15-32% of the hole diameter. Similar, although less pronounced damage, was noticed in the case of the samples loaded to 95% and 90% of failure, but with no significant washer damage or hole elongations in the case of the samples loaded to less than 90% of failure. Slight impressions only of the washer were apparent.

Observations of the bearing samples under the scanning electron microscope gave very little indication of the failure mechanisms. The individual plies were hard to distinguish and enlarged views were useful only for showing the splitting and delamination at the washer edge.

Net-Tension Failure Tests

The samples loaded to failure in net-tension showed a more catastrophic mode of failure (see Figure 5) with significant amounts of acoustic emission associated with fibre breakage. Average net tension failure loads of 12320N (304MPa) for the 0° orientation specimens and 11569N (286MPa) for the 45° orientation specimens were calculated. The 45° samples appeared to be marginally weaker than the 0° samples, by approximately 800N (20MPa). Examination of the failed samples showed the failure to occur by fibre breakage and pull-out of the 0° and ±45° tows across the entire net-section.

Pin-Loaded Tests

The 0° and 45° net-tension samples which were loaded with no through-thickness clamping applied both failed in bearing. Unfortunately the load-displacement data for the 0° sample was not recorded but the data for the 45° sample showed failure to occur at a load of 3905N, approximately 34% of the failure load (11569N) of the equivalent clamped samples. As for the other bearing failure samples the failure was non-catastrophic (see Figure 3). Examinations of the samples showed there to be total disintegration of the laminate on the bearing side of the hole with widespread splitting and delamination. This was similar, but more pronounced, than that observed at the washer edge in the case of the clamped bearing failure samples.

Optical Microscopy Work

Optical micrographs were taken of the potted bearing and net tension sections to show the progression of failure.

Bearing Failure Samples

The bearing failure sections showed damage from 60% of final failure load. This consisted of fibre microbuckling and matrix shear cracking in the region where the composite was constrained by the washers. The fibre

microbuckles were apparent in the tows which were aligned with the loading direction and the matrix shear cracks in the tows which were at +45/-45° to the loading direction. The 0° and 45° orientations of the samples had the effect of changing the particular layers in which the different types of failure occurred. Figure 6 shows a typical example of the damage as seen on the bearing plane of a 45° specimen.

The fibre microbuckles formed as kink bands at angles of approximately ±45° through the thickness of the 0° oriented tows of fibres. Single and multiple kink bands were noted as the microbuckles arrested at interfaces with adjacent 90° or ±45° tows and propagated back through the 0° tows. Similarly the matrix shear cracks formed at angles of approximately ±45° through the thickness of the ±45 oriented tows. In this case the matrix shear cracks arrested at the interfaces with adjacent 0° or 90° tows but propagated through adjacent ±45° tows. Little damage was observed in the 90° tows although due to the darker image of the 90° tows damage was less easy to discern.

The damage initiated at approxiamtely 60% of final failure at the hole edge and with increasing load spread outwards to the washer edge. As the density of fibre microbuckles and matrix shear cracks increased the microbuckles and cracks tended to from a continuous line at 45° through the thickness of the laminate (Figure 6). In many instances the kink bands in the 0° tows were connected directly to matrix shear cracks in adjacent ±45° tows (Figure 6). In a few cases cracks ran along tow interfaces such that damage in adjacent plies was connected indirectly, however, very little damage was noticed in the resin rich regions between tows. This indicates how the tow geometry can affect the precise path of the damage propagation.

Once the damage had spread to the unconstrained region beyond the washer edge final bearing failure occurred with widespread splitting and delamination. The outer plies delaminated, buckled and split, whilst the inner plies buckled and crushed.

The spread of damage was determined from the fully failed samples which were progressively ground at angles of 0°, 45° and 90° to the direction of the applied load. The damage was shown to be concentrated around the bearing plane (Figure 7a) with a spread, on the bearing side of the fastener, to minimal damage on the net-tension plane. No failure mechanisms other than fibre microbuckling, matrix shear cracking and delamination and splitting at the washer edge were observed. The fibre microbuckles were restricted to the 6mm wide compressed region on the bearing side of the fastener whilst the delaminations and splits at the washer edge extended on the bearing side of the fastener to the net-tension plane. Significant damage was observed on the shearout plane which consisted mainly of matrix shear cracking with little fibre microbuckling. These matrix shear cracks were concentrated at the hole edge (on the net-tension plane) and extended up to the washer edge on the bearing side of the fastener and by the fastener radius (3mm) on the non-bearing side of the fastener (Figure 7b).

The fully failed sample which was ground at 45° to the applied load showed the microbuckles to form in the tows oriented at ±45° to the applied load as well as in the 0° oriented tows. Similarly matrix shear cracks were found in the 0° oriented tows as well as in the ±45° oriented tows. See Figure 8.

Net-Tension Failure Samples

The net-tension failure sections showed initial damage on the net tension plane at 95% of final failure. This was minimal and consisted of through-thickness matrix shear cracks in the ±45° tows close to the hole edge. On the bearing plane at net-tension failure similar damage to that observed for the partially loaded bearing failure specimens was seen (Figure 9). This would be expected since the net-tension failures occurred at approximately 82% of the bearing failure loads. The damage on the shearout plane at net-tension failure was minimal and consisted of through-thickness matrix shear cracks close to the hole edge. Damage did not extend beyond the region constrained by the washer prior to failure, and final failure was in the net-section where the laminate was unable to support the high net-tension stresses. This failure occurred as fibre breakage in the 0° and ±45° tows and matrix cracks in the ±45° and 90° tows across the entire net-tension section.

3. DISCUSSION

Comparison with Previous Studies

The effect of the 15Nm torque applied to the bolts in the joints tested was to produce a 76MPa through-thickness compression or clamp-up stress of the composite in the region of the washer. Clamp-up is known to

significantly increase the strength of bolted joints and has been noted by Collings [3] as an asymptotic relationship between bolt clamp-up and bearing strength for 0°±45° carbon fibre-reinforced laminates. Full joint strengths were found to develop at bolt clamp-ups of approximately 22MPa. Thus it would be expected that the 76MPa clamp-up applied to the joints tested here would be well within the region of full joint strength.

2-D finite element models [4] of laminated plates in tension which contain an unloaded torqued bolt have shown the peak in-plane stresses at the bolt-plate boundary to migrate from the plate through the washer to the bolt, with increasing clamping pressure. The clamping pressures were assumed to have no effect on the in-plane stress distribution. For clamping ratios (clamping pressure/applied in-plane stress) from 0 to 1 the in-plane strains, and associated free-edge effects at the hole edge, were shown to be relieved as the effective contact between the plate and bolt reduced to zero. Little effect was produced on the magnitude of the strains at the washer edge but at clamping ratios of between 0.4 and 1.0 the strain reductions at the bolt-plate boundary were sufficient that the peak strains moved to the washer outer edge. For clamping ratios from 1 to 4 only small changes were produced in the strain distributions and maximum strain values approaching, at a clamping ratio of 4, the case of a rigid inclusion of diameter equal to the outer diameter of the washer.

The case of a plate loaded in bearing by a torqued bolt is not directly analagous to the case of a plate loaded in tension which contains a torqued bolt since in the latter case no bearing stresses are developed. However, from the analyses described above, it would be expected that at high clamping ratios (low loads) the peak stresses would move from the hole edge to the washer outer edge. This is as the high stresses and associated free edge effects at the hole edge are relieved. Obviously in the case of the joints tested here the relatively low stresses developed at the washer edge are insufficient to cause failure. However, the reduction in stresses at the hole edge is sufficient to delay initial bearing failure from 3905N (pin-loaded bearing failure load of the 45° net-section sample) to 9211N (60% of the average clamped bearing failure load of the 45° bearing samples). Of most significance is the reduction in the strain in the direction of the applied load and the associated free edge effects. It is fairly obvious that the through-thickness constraint provided by the washer prevents delaminations and splits at the hole edge.

It is also interesting to note that the 45° pin-loaded net-tension sample failed in bearing at approximately 34% of the net-tension failure stresses calculated for the equivalent clamped net-tension samples. Since there is no washer to constrain the laminate and redistribute the high stresses at the hole edge in the pin-loaded sample the strength in bearing is lower than the strength in net-tension.

3-D finite element models of bolted joints [5] in laminated composites have shown that at bolt tensions of 10kN through-thickness compressive stresses, σ_{ZZ}, are generated in the region constrained by the washer and interlaminar shear stressses, σ_{ZX}, at the washer edge. In comparison the 15Nm torque applied to the bolts in the joints for which the results are presented here corresponds to a bolt tension of 8kN. Thus it would be expected that at a 8kN bolt tension a similar distribution of through-thickness direct and shear stresses would be developed.

Summary of Results

Bearing Failure

The effect of the through-thickness stress, σ_{ZZ}, is to prevent delamination, splitting and buckling within the region constrained by the washer. However, as the applied load increases, and the clamping ratio decreases, large compressive stresses are developed in the direction of the applied load, σ_{XX}. These eventually cause damage to the laminate in the form of fibre microbuckles and through-thickness matrix shear cracks. The effect is aggravated by the prevention of Poisson's expansions in the through-thickness direction.

The damage initiates at approximately 60% of the final bearing failure load on the bearing plane at the hole edge. As the load increases the damage spreads outwards in the direction of the washer edge and becomes more dense. The fibre microbuckles and through-thickness matrix shear cracks tend to align at a 45° angle through the thickness. The fibre microbuckles are concentrated on the bearing plane whilst the matrix shear cracks occur across the entire 6mm width of the fastener on the bearing side. The overall effect is to allow a small amount of through-thickness stress relief through non-catastrophic micro-failures.

Eventually the damaged region spreads to the washer edge where there are significantly reduced through-thickness compressive stresses, σ_{ZZ}, and significantly increased through-thickness shear stresses, σ_{ZX}. At this point ultimate bearing failure occurs as the laminate at the washer edge delaminates, buckles and splits. This implies that final failure could be initiated by the micro-failure events. Associated with the failure at the washer edge are cracks which emanate from the hole edge at between 45° and 90° to the applied load and run parallel to the applied load towards the washer edge. These result from the high shear stresses which are generated at the hole edge in this region. Their effect is to cause a plug of laminate to translate into the delaminated material and thus elongate the hole. Micrographs of the failed bearing samples along the shearout planes showed extensive through-thickness matrix shear damage close to the hole edge.

Net-Tension Failure

For the net-tension samples the tensile strength of the plies is exceeded on the net-tension plane before final bearing failure occurs. Damage on the net-tension plane prior to net-tension failure is minimal and initiates at approximately 95% of the final net-tension failure load. The damage occurs as matrix cracks in the ±45° plies close to the hole edge. Final net-tension failure occurs across the entire net-tension section with fibre pull-out and breakage in the 0° and ±45° tows and matrix cracking in the ±45° and 90° tows.

Choice of Failure Criteria

From the failure mechanisms observed in the joint tests it is apparent that a 3-D finite element model of the region surrounding a loaded fastener would need to include failure criteria for fibre microbuckling, matrix shear cracking and fibre breakage/pull-out. It would seem reasonable to include the fibre microbuckling and matrix shear cracking as progressive failure events in the region constrained by the washer and catastrophic failure events at the washer edge and the fibre breakage/pull-out as a catastrophic failure event on the net tension plane.

As an initial estimate, ply failures could be approximated by a maximum stress criterion which uses strengths of a $[(0/90)_4]_S$ laminate. For example, fibre breakage/pull-out could be approximated by the laminate tensile strength, fibre microbuckling by the laminate compressive strength and through-thickness matrix shear cracking by the laminate interlaminar shear strength. Once all the elements on the net-tension plane had failed due to fibre breakage/pull-out, final net-tension failure could be assumed and once one element beyond the washer edge had failed due to fibre microbuckling or matrix shear cracking, final bearing failure could be assumed.

The maximum radial stress and circumferential stress around the hole edge for an isotropic material pin-loaded by a fastener can be calculated from the failure load, P_X as follows [6].

$$\text{Maximum radial stress} = 4P_X/\pi dt \quad (4)$$

$$\text{Maximum circumferential stress} = P_X/dt \quad (5)$$

The maximum radial stress occurs on the bearing plane and the maximum circumferential stress on the net-tension plane.

The above equations give a good approximation for the case of the quasi-isotropic laminate investigated here. Assuming, for the bearing failures, that the material constrained between the washers is totally degraded, it is reasonable to replace the fastener diameter, d, used in the calculation of the maximum radial stress, by the washer diameter, D. From these equations and using the failure loads of, 15074N for the 0° bearing failure samples and 12320N for the 0° net-tension failure samples, a maximum radial stress at the washer edge of 656MPa (for the bearing failures) and maximum circumferential stress of 913MPa (for the net-tension failures) is obtained.

This shows the maximum radial stress on the bearing plane at the hole edge (656MPa), assuming the material within the washer is degraded, to be of the order of the compressive strength of the $[(0/90)_4]_S$ laminate (592MPa). Thus it might be expected that a method of progressive damage within the washer region would satisfactorily model bearing types of failures. The predicted value of the maximum circumferential stress on the net-tension plane (913MPa) is, however, 33% greater than the tensile strength of the $[(0/90)_4]_S$ laminate (687MPa). In this case it appears that some other mechanisms are contributing to net-tension failure, perhaps due to the (+45/-45) plies and/or some interaction between plies.

CONCLUSIONS

Experimental work has shown initial damage in composite bolted joints to occur at 60% of final bearing failure. The damage was apparent in laminated samples loaded in double shear as fibre microbucking and through-thickness matrix shear cracking. A quasi-isotropic laminate comprised of eight layers of woven carbon fibre tows impregnated with epoxy resin was used. The damage was concentrated on the bearing plane at the hole edge and with increasing load spread, on the bearing side of the fastener, within the region constrained by the washer. The fibre microbuckles were seen in the tows oriented at 0° and ±45° to the applied load and the matrix shear cracks in the tows oriented at ±45° and 0° to the applied load. Similar initial damage was observed for both bearing and net-tension modes of failure.

For samples with the larger width (w = 6d) further increases in the load caused the damage to spread beyond the region constrained by the washer. At this stage final bearing failure occurred as the composite delaminated and split at the washer edge. The failure was attributed to the reduced through-thickness stresses and increased interlaminar shear stresses at the edge of the washer and was thought to be initiated by the microbuckles and shear cracks.

For samples with the smaller width (w = 4d) the high stresses on the net-tension section at increased load caused the laminate to fail in net-tension before bearing failure occurred. The net-tension failure was catastrophic and damage was not apparent on the net-tension plane prior to 95% of the final failure load.

From the observed damage mechanisms it was suggested that a 3-D finite element model could be used to predict bearing and net-tension modes of failure. Progressive damage could be assumed for fibre microbuckling and matrix shear cracking within the region constrained by the washer and final bearing failure for microbuckling or shear cracking outside the washer region. Net-tension failure could be assumed for fibre breakage/pull-out over the entire net-tension plane.

Calculations were made using a simple 2-dimensional analytical model and assuming, for bearing failure, the region inside the washer was totally degraded. Fibre microbuckling was predicted from the compressive strength of a $[(0/90)_4]_S$ laminate and fibre breakage/pull-out from the tensile strength of a $[(0/90)_4]_S$ laminate. When compared to the average failure loads measured experimantally bearing failure was found to be under-predicted by 10% and net-tension failure to be under-predicted by 33%. It was suggested that the differences were due to the (+45/-45) plies and/or some interaction between plies. A 3-dimensional finite element model could incorporate these features.

REFERENCES

[1] Kretsis, G. and Matthews, F. L., "The strength of bolted joints in glass fibre/epoxy laminates", Composites, *16*, April 1985, pp 92-102.

[2] Oakeshott, J.L., Perinpanayagam, S. and Matthews, F.L., "Bearing Failure in a Woven Carbon Fibre/Epoxy Laminate", Proc. "3rd International Conference on Deformation and Fracture of Composites", University of Surrey, Guildford, England, 27-29 March 1995, pp 200-206. Institute of Materials, London.

[3] Collings, T. A., "The strength of bolted joints in multi-directional cfrp laminates", Composites, *8*, January 1977, pp 43-54.

[4] Graham, U., Wisnom, M. R. and Webber, J. P. H., "A novel finite element investigation of the effects of washer friction in composite plates with bolt-filled holes", Composite Structures, *29* (1994), pp 329-339.

[5] Matthews, F. L., Wong, C. M. and Chryssafitis, S., "Stress distribution around a single bolt in fibre-reinforced plastic", Composites, *13*, July 1982, pp 316-322.

[6] Hart-Smith, L. J., "Mechanically-Fastened Joints for Advanced Composites - Phenomenological Considerations and Simple Analyses", Douglas Paper 6748A, Proc. "Fourth Conference on Fibrous Composites in Structural Design", San Diego, California, 14-17 Nov 1978. Douglas Aircraft Corp, Long Beach, California, USA

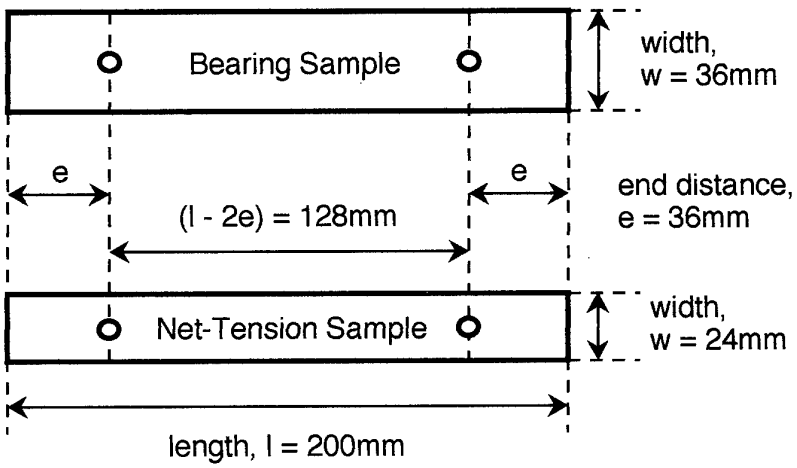


Figure 1. Sample Dimensions

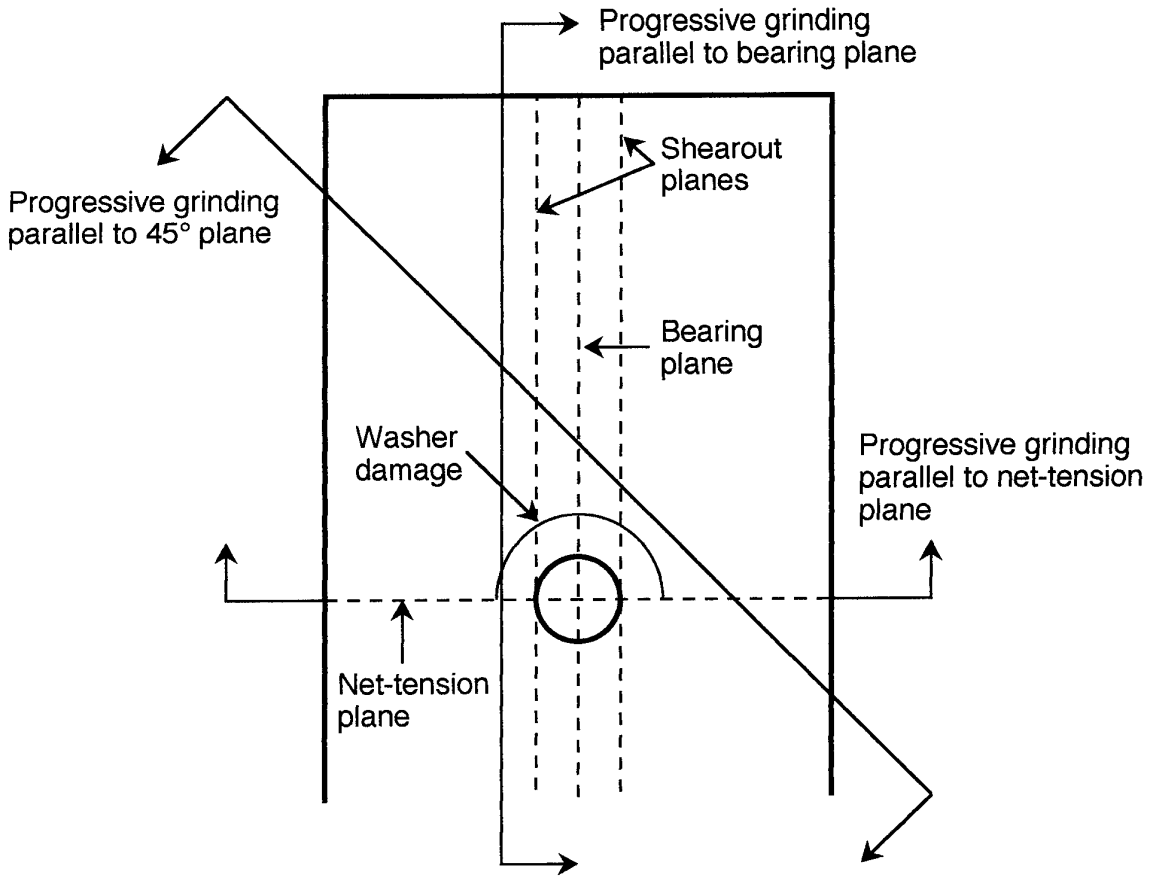


Figure 2. Sample Sections

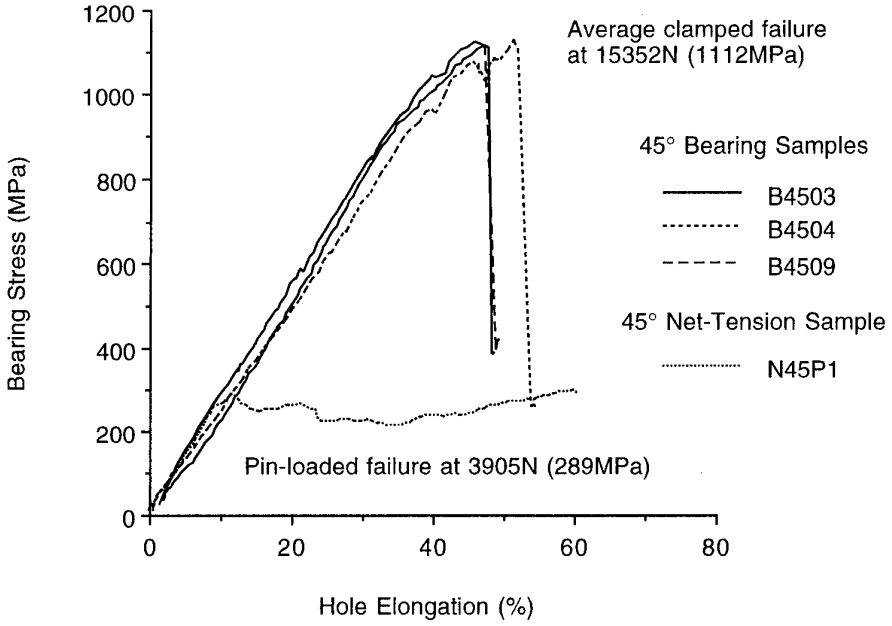


Figure 3. Deformation Behaviour of 45° Bearing and Pin-Loaded Samples

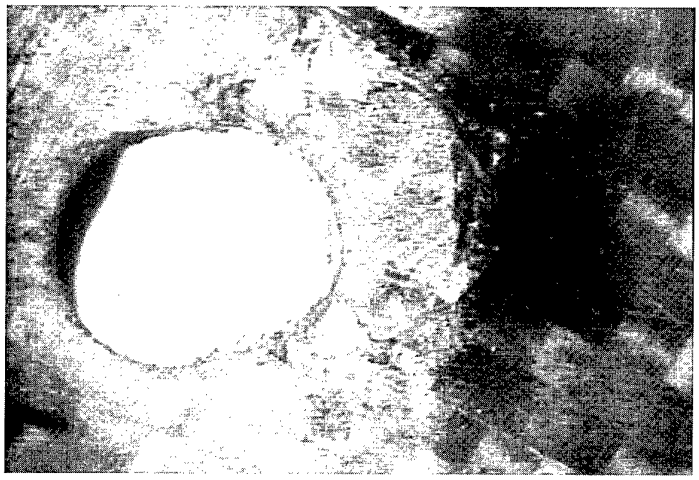


Figure 4. Damage in Fully Failed Bearing Sample (45°)

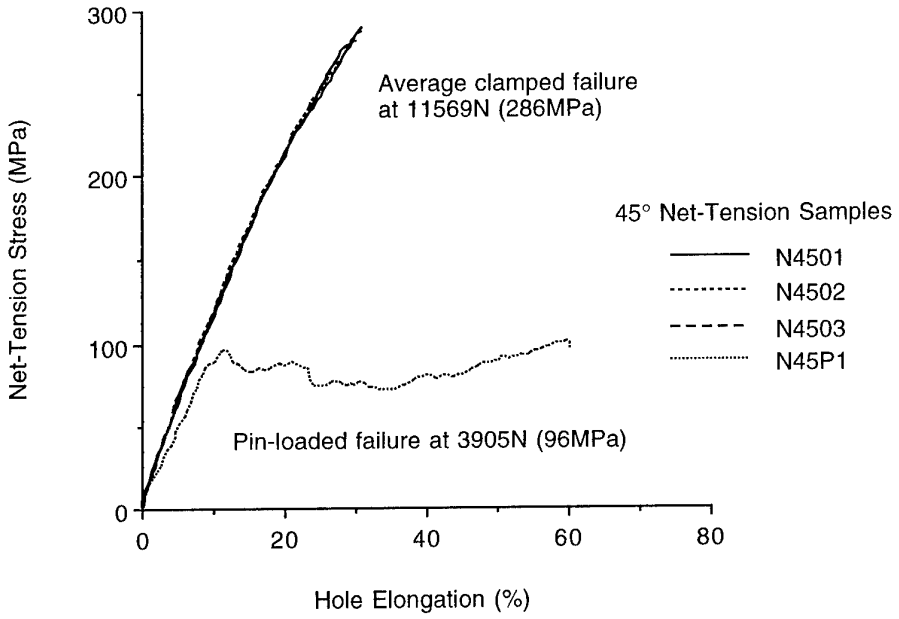


Figure 5. Deformation Behaviour of 45° Net-Tension and Pin-Loaded Samples



Figure 6. Bearing Section at Hole Edge for 45° Bearing Sample

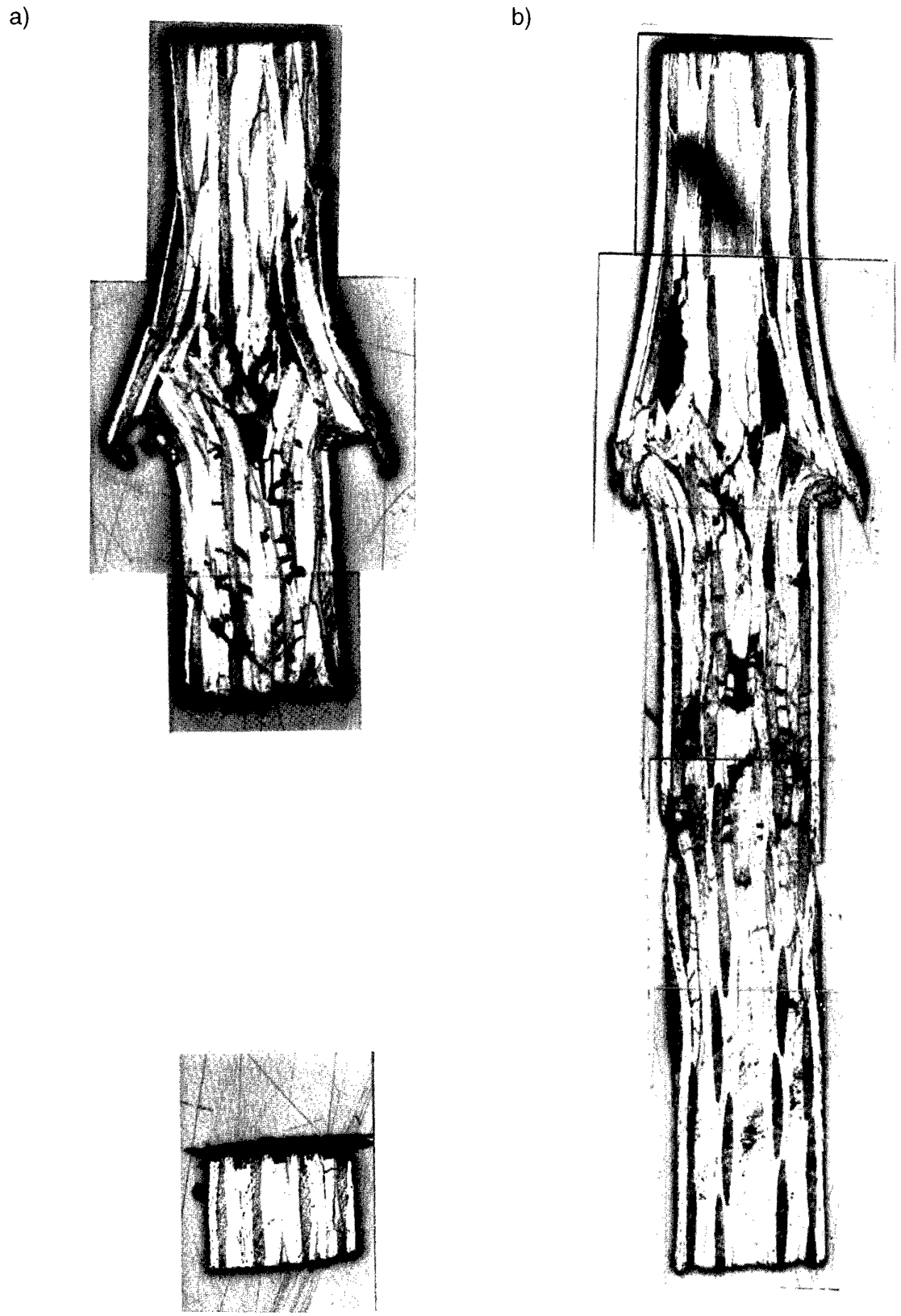


Figure 7. Sections of Fully Failed Bearing Sample (0°) taken at 0° to Applied Load; a) Bearing Plane, b) Shearout plane.



Figure 8. 45° Section through Hole Edge for Fully Failed Bearing Sample (0°)

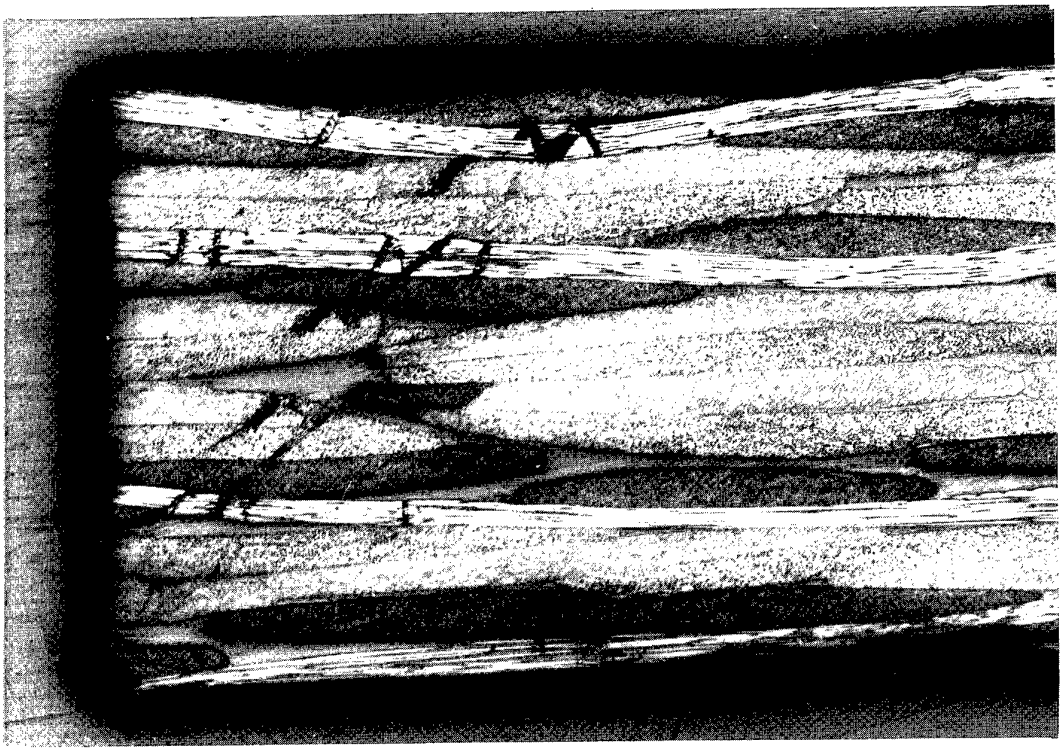


Figure 9. Bearing Plane at Hole Edge for Fully Failed Net-Tension Sample (0°)

Three-Dimensional Progressive Failure Analysis of Pin/Bolt Loaded Composite Laminates

M.M. Shokrieh, L.B. Lessard and C. Poon*
Department of Mechanical Engineering
McGill University, Montreal, Quebec, Canada
* Institute for Aerospace Research
National Research Council Canada
Montreal Road, Ottawa, Canada K1A 0R6

1. SUMMARY

A new phenomenological modeling technique, called fatigue progressive damage modeling, was established. This new modeling technique is capable of predicting the residual strength, residual stiffness, and fatigue life of pin/bolt loaded composite laminates. Stress analysis, failure analysis, and material property degradation rules are the three major components of the model. A three-dimensional, nonlinear, finite element technique was used for the stress analysis. Based on the state of stress, different failure modes were detected by a set of failure criteria. To remove the requirement of a large experimental database for the failure analysis, a normalization technique was adopted. By using this technique the restriction of the application of the failure criteria to limited states of stresses was overcome. Material properties of each element in the model were degraded by using sudden and gradual material property degradation rules. For this purpose an analytical model was established to predict the degradation of material properties of a unidirectional ply under multiaxial fatigue loading. Based on the model, a computer code was developed that simulates cycle by cycle behavior of composite laminates under fatigue loading. The modeling technique uses experimental data from a unidirectional ply under various types of uniaxial loading to predict the behavior of structures subjected to multiaxial fatigue loading. Fatigue testing of pin/bolt loaded composite laminates was performed to validate the modeling technique.

2. LIST OF SYMBOLS

E_{xx}, E_{yy}, E_{zz}	Elastic moduli
G_{xx}, G_{yy}, G_{zz}	Shear moduli
R	Stress ratio, $\sigma_{min} / \sigma_{max}$
S_{xy}, S_{xz}, S_{yz}	Shear strengths
X_t, X_c	Longitudinal strengths, tension and compression
X_l^f , X_l^S	Longitudinal fatigue and static strengths
S_{xy}^f , S_{xy}^S	Fatigue and static shear strengths
Y_t, Y_c	Transverse strengths, tension and compression
Z_t, Z_c	Normal strengths, tension and compression
ε_{xx}, ε_{yy}, ε_{zz}	Longitudinal, transverse and normal strains
Φ_{xx}^+ , Φ_{xy}	Strength normalization functions
σ_{xx}, σ_{yy}, σ_{zz}	Longitudinal, transverse and normal stresses
σ_{xy}, σ_{xz}, σ_{yz}	Shear stresses
ν_{xx}, ν_{yy}, ν_{zz}	Poisson's ratios

3. INTRODUCTION

This research involves the formulation and verification of a three-dimensional theoretical model for predicting the fatigue failure of pin/bolt loaded composite laminates. The capability to simulate the mechanisms involved in the failure of such joints in composite materials is of paramount importance to the aircraft and aerospace industry.

The model was developed in conjunction with the establishment of an experimental database. This database of basic fatigue material properties is necessary as input to the model and was developed because a full set of fatigue material properties was not available anywhere in the literature. The material used in this study was AS4/3501-6, a carbon/epoxy composite material commonly used in the aircraft industry.

The theoretical analysis presented here is in the form of a finite element simulation of the bolted joint problem with emphasis on the development of a failure analysis consistent with experimental observation. The ultimate goal was to develop a computer code for designers to simulate the fatigue failure of a pinned/bolted joint problem. With minor changes, any other structural component may also be analyzed.

The model can predict the fatigue failure of pinned/bolted joints given the geometry, ply orientation, and cycle load level. Also the model can assess the extent of damage and residual stiffness and strength for any given load level and number of cycles. To analyze the problem, the fatigue progressive damage modeling concept was used. This recently developed technique allows for isolation of failure modes of composites and for property degradation at appropriate levels of load and number of cycles. This paper presents the development of the modeling technique and experimental verification of fatigue life predictions.

4. PROBLEM STATEMENT

Consider a composite plate with a pin or bolt loaded hole, see Fig. 1. The plate has width w, length l, thickness t, edge distance e, hole diameter d, and washer diameter d_w. The composite plate is loaded through a pin or a bolt; pin load and washer load are P and P_w, respectively. The plate is a laminated composite with arbitrary ply orientation. Each ply is assumed as a transversely isotropic material with arbitrary material properties.

At the start of cyclic loading, the strength of the material is greater than the stress state, therefore there is no static mode of failure on the plate. By increasing the number of cycles from zero, based on the stress states at each point of the plate, material properties at those points are degraded as a function of the number of cycles. By increasing the number of cycles with more degradation of the material properties and redistribution of stresses, failure begins in regions where the strength of the material is less than the stress state at that point. After failure initiation, stresses are redistributed around failed regions. By further increasing the number of cycles, failure propagates in different directions. Finally after a certain number of cycles the laminate cannot tolerate additional cycles. At this point the maximum number of cycles is reached and the laminate has failed completely. Although material properties of the

Paper presented at the 83rd Meeting of the AGARD SMP on "Bolted/Bonded Joints in Polymeric Composites", held in Florence, Italy, 2-3 September 1996, and published in CP-590.

composite plate have been degraded as functions of the number of cycles, however, final mechanisms of failure in fatigue (bearing, net tension, shear-out, etc.) are similar to the mechanisms of failure in static loading.

5. COMPONENTS OF THE MODEL

Fatigue progressive damage modeling is an integration of three major components. These are stress analysis, failure analysis, and material degradation rules. A description of these components are in the following subsections.

5.1 Stress Analysis

A nonlinear, three-dimensional, finite element technique was used for the stress analysis in order to address material nonlinearity and three-dimensional phenomena such as edge effects, delamination, out-of-plane buckling, and stacking sequence effects. Assuming symmetric geometry, loading, and ply lay-up, suitable boundary conditions were used, see Fig. 2. Radial fixed displacement boundary conditions were applied on the nodes around the hole at the loaded region to simulate the pin load. To simulate a fully tightened bolt, a uniform pressure was applied on the washer region. Moreover, to simulate friction between the washer and the plate, fixed displacement boundary conditions in the radial and tangential directions were applied on the nodes on the surface of the composite plate and under the washer region. To achieve high accuracy, the isoparametric quadratic 20-node brick element was used. Also by using a large number of elements near the edge of the hole and at layer interfaces, stress singularities were considered.

In this study, inplane shear stress-strain response (σ_{xy}-ε_{xy}) and interlaminar shear stress-strain response (σ_{zx}-ε_{zx}) were considered nonlinear. The nonlinear constitutive equation for the inplane shear stress-strain response (σ_{xy}-ε_{xy}) was established based on the work of Hahn and Tsai [1]. Furthermore, by means of the transversely isotropic assumption, the nonlinear constitutive equation for interlaminar shear stress-strain (σ_{zx}-ε_{zx}) was developed [2]. There is a weak nonlinear behavior in the transverse direction for σ_{yy}-ε_{yy}, and by using a transversely isotropic assumption, in the normal direction for σ_{zz}-ε_{zz}. However, the degree of nonlinearity for these cases is not comparable to the shear nonlinear behavior. Therefore stress-strain responses in the transverse and normal directions were assumed linear. Also because of the dependency of the transverse-normal interlaminar shear modulus (E_{yz}) on the transverse modulus (E_{yy}), the corresponding interlaminar shear stress-strain response (σ_{yz}-ε_{yz}) was also assumed linear. It should be emphasized that the mentioned nonlinearities are due to inelastic behavior of the material before failure initiation. Nonlinearities due to failure are completely different phenomena and they are considered by failure analysis techniques in this study. A detailed description of the formulation of the nonlinear, three-dimensional, finite element technique is given in Ref. 2.

5.2 Failure Analysis

Failure analysis was performed using a set of stress-based failure criteria. The ability to distinguish between different modes of failure is one of the most important requirements of these failure criteria. There are different failure modes in composite laminates under fatigue loading, and each mode must be detected by a suitable failure criterion. These modes are: matrix tension, matrix compression, fiber tension, fiber compression, fiber-matrix shear out, delamination tension, and delamination compression. The failure criteria for these modes are as follows:

Matrix tension:

$$\left(\frac{\sigma_{yy}}{Y_t(N,R)}\right)^2+\left(\frac{\sigma_{xy}}{S_{xy}(N,R)}\right)^2+\left(\frac{\sigma_{yz}}{S_{yz}(N,R)}\right)^2=e_{M+}^2 \quad (1)$$

For $\sigma_{YY} > 0$, failure is predicted when $e_{M+} \geq 1$.

Matrix compression:

$$\left(\frac{\sigma_{yy}}{Y_c(N,R)}\right)^2+\left(\frac{\sigma_{xy}}{S_{xy}(N,R)}\right)^2+\left(\frac{\sigma_{yz}}{S_{yz}(N,R)}\right)^2=e_{M-}^2 \quad (2)$$

For $\sigma_{YY} < 0$, failure is predicted when $e_{M+} \geq 1$.

Fiber Tension:

$$\left(\frac{\sigma_{xx}}{X_t(N,R)}\right)^2+\left(\frac{\sigma_{xy}}{S_{xy}(N,R)}\right)^2+\left(\frac{\sigma_{xz}}{S_{xz}(N,R)}\right)^2=e_{F+}^2 \quad (3)$$

For $\sigma_{XX} > 0$, failure is predicted when $e_{F+} \geq 1$.

Fiber Compression:

$$\left(\frac{\sigma_{xx}}{X_c(N,R)}\right)^2=e_{F-}^2 \quad (4)$$

For $\sigma_{XX} < 0$, failure is predicted when $e_{F-} \geq 1$.

Fiber-matrix shear-out:

$$\left(\frac{\sigma_{xx}}{X_c(N,R)}\right)^2+\left(\frac{\sigma_{xy}}{S_{xy}(N,R)}\right)^2+\left(\frac{\sigma_{xz}}{S_{xz}(N,R)}\right)^2=e_{FM-}^2 \quad (5)$$

For $\sigma_{XX} < 0$, failure is predicted when $e_{FM-} \geq 1$.

Delamination Tension:

$$\left(\frac{\sigma_{zz}}{Z_t(N,R)}\right)^2+\left(\frac{\sigma_{zx}}{S_{zx}(N,R)}\right)^2+\left(\frac{\sigma_{zy}}{S_{zy}(N,R)}\right)^2=e_{D+}^2 \quad (6)$$

For $\sigma_{ZZ} > 0$, failure is predicted when $e_{D+} \geq 1$.

Delamination Compression:

$$\left(\frac{\sigma_{zz}}{Z_c(N,R)}\right)^2+\left(\frac{\sigma_{zx}}{S_{zx}(N,R)}\right)^2+\left(\frac{\sigma_{zy}}{S_{zy}(N,R)}\right)^2=e_{D-}^2 \quad (7)$$

For $\sigma_{ZZ} < 0$, failure is predicted when $e_{D-} \geq 1$.

5.2.1 Application of failure criteria

Summarizing the results, it is evident that all the strength parameters in Eqs. 1-7 are dependent on the number of cycles, N and the state of stress, R. In these forms, a large database is required to determine these strength parameters for a given N and R. Application of existing failure criteria for failure analysis of a unidirectional ply under multiaxial fatigue loading is restricted to a certain state of stress. The main reason for this restriction is the large experimental database required to apply the failure analysis for different states of stresses. As an example, the Hashin fatigue failure criterion [3], for fiber

failure mode in tension, and for simplicity, in plane stress condition is considered here in a modified form from that shown in Eq. 3 by ignoring the third term:

$$\left(\frac{\sigma_{xx}}{X_t^s\, f_{xx}(N,R)}\right)^2+\left(\frac{\sigma_{xy}}{S_{xy}^s\, f_{xy}(N,R)}\right)^2 = e_{F+}^2 \qquad (8)$$

In the denominators of Eq. 8, residual strengths are in the form of static strength multiplied by a function which decreases with the number of cycles. Using the present case as an example, the longitudinal tensile strength and the longitudinal-transverse shear strength in fatigue are defined in Eqs. 9 and 10, respectively.

$$X_t^f = X_t^s\, f_{xx}(R,N) \qquad (9)$$

$$S_{xy}^f = S_{xy}^s\, f_{xy}(R,N) \qquad (10)$$

It has been investigated that normalized strengths as functions of normalized number of cycles are independent of the state of stress [4,5]. Using this approach, the strength parameters defined in Eqs. 9 and 10 are normalized by the functions defined in the following equations:

$$\Phi_{xx}^+\left(\frac{N}{N_f}\right)=\frac{X_t^f-\sigma_{xx}}{X_t^s-\sigma_{xx}} \qquad (11)$$

$$\Phi_{xy}\left(\frac{N}{N_f}\right)=\frac{S_{xy}^f-\sigma_{xy}}{S_{xy}^s-\sigma_{xy}} \qquad (12)$$

The empirical functions, Φ_{xx}^+ and Φ_{xy}, have a value of one at zero cycle and decrease as damage accumulates. This normalization technique is shown schematically in Fig. 3. As it is seen from Eqs. 11 and 12, because of the normalization, Φ_{xx}^+ and Φ_{xy} are not functions of the state of stress, but only functions of the normalized number of cycles. By using these functions in the denominators of Eq. 8, the following equation is derived:

$$\left(\frac{\sigma_{xx}}{(X_t^s-\sigma_{xx})\,\Phi_{xx}^+\left(\frac{N}{N_f}\right)+\sigma_{xx}}\right)^2+\left(\frac{\sigma_{xy}}{(S_{xy}^s-\sigma_{xy})\,\Phi_{xy}\left(\frac{N}{N_f}\right)+\sigma_{xy}}\right)^2 = e_{F+}^2 \qquad (13)$$

For the other modes of failure there are failure criteria similar to Eq. 13. It must be noted that for the three-dimensional condition, the forms of the failure criteria are complicated and more parameters are needed, but they are logical extensions of the two-dimensional case. Furthermore, residual stiffnesses of the fatigued material are normalized by a similar procedure to make them independent on the stress states. Note that the reverse process is also required, that is, to predict residual strengths and stiffnesses under any state of stress given in the normalized curve shown in Fig. 3. This process has been established and will be explained in the next section on gradual material property degradation rule.

6. MATERIAL PROPERTY DEGRADATION RULES

As failure occurs in a ply of a laminate, material properties of that failed ply are changed by the material property degradation rules. For each mode of failure, there exists an appropriate sudden material property degradation rule. Some of the failure criteria are catastrophic and some of them are not. Thus for each mode of failure, a suitable rule exists. Moreover, in fatigue loading, after each cycle, material properties of each ply of a laminate are degraded, even though failure is not detected by failure criteria. This type of degradation is governed by the gradual material property degradation rule. Note that in an actual computer simulation, this degradation will take place after a fixed incremental number of cycles, ΔN .

6.1 Sudden Material Property Degradation Rules

Matrix tension and compression: For matrix tension and compression failure in a ply predicted by Eqs. 1 and 2, it is assumed that the matrix can no longer carry any load. In the failed ply, material properties which define the stiffness are reduced as follows:

$$[E_{xx}\ E_{yy}\ E_{zz}\ G_{xy}\ G_{yz}\ G_{xz}\ \nu_{xy}\ \nu_{yz}\ \nu_{xz}]\rightarrow$$
$$[E_{xx}\ 0\ E_{zz}\ G_{xy}\ G_{yz}\ G_{xz}\ 0\ \nu_{yz}\ \nu_{xz}]$$

Fiber tension and compression: The fiber tension and compression failure modes in a ply are catastrophic. When these modes predicted by Eqs. 3 and 4, it is assumed that the material in the failed region cannot sustain any additional load. Thus the material properties for the failed ply are reduced as follows:

$$[E_{xx}\ E_{yy}\ E_{zz}\ G_{xy}\ G_{yz}\ G_{xz}\ \nu_{xy}\ \nu_{yz}\ \nu_{xz}]\rightarrow$$
$$[0\ 0\ 0\ 0\ 0\ 0\ 0\ 0\ 0]$$

Fiber-Matrix Shearout: In fiber-matrix shearout failure mode, the material can still carry load in the fiber direction and in the matrix direction, but shear load can no longer be carried. When this mode is predicted by Eq. 5, the material properties for the failed ply are reduced as follows:

$$[E_{xx}\ E_{yy}\ E_{zz}\ G_{xy}\ G_{yz}\ G_{xz}\ \nu_{xy}\ \nu_{yz}\ \nu_{xz}]\rightarrow$$
$$[E_{xx}\ E_{yy}\ E_{zz}\ 0\ G_{yz}\ G_{xz}\ 0\ \nu_{yz}\ \nu_{xz}]$$

Delamination tension and compression: Although not yet formulated at this time, it is expected that the post-failure behavior in delamination should follow a logical modulus degradation law. The degradation should be such that the interface failure affects properties above and below the interface. As a result, properties involving the z-direction are reduced:

$$[E_{xx}\ E_{yy}\ E_{zz}\ G_{xy}\ G_{yz}\ G_{xz}\ \nu_{xy}\ \nu_{yz}\ \nu_{xz}]\rightarrow$$
$$[E_{xx}\ E_{yy}\ 0\ G_{xy}\ 0\ 0\ \nu_{xy}\ 0\ 0]$$

6.2 Gradual Material Property Degradation Rules

In fatigue loading, after each number of cycles, material properties of each ply (strengths and stiffnesses) are degraded,

even though failure is not detected by any of the above mentioned sudden failure criteria. For the purpose, an analytical technique was established to predict the gradual degradation of material properties of a unidirectional ply under multiaxial fatigue loading. This technique is explained by means of a flowchart shown in Fig. 4. By having material properties, constant life diagrams developed from empirical data, and states of stress of a unidirectional ply under uniaxial fatigue loading, normalized functions (Φ_{xx}^{+}, Φ_{xy}, etc.), and the number of cycles to failure (N_f for σ_{xx}, etc.) are found. By substituting these into suitable failure criteria, the number of cycles (N_f^*, * = fiber tension, etc.) under multiaxial fatigue loading are found. Then by substituting N_f^* for each stress ratio into the related constant life diagram, state of stress at final failure is found. Finally, residual material properties are found by substituting N_f^* and state of stress at final failure into the normalized functions of the material properties.

7. MODELING

As was mentioned, fatigue progressive damage modeling is an integration of stress analysis, failure analysis, and material property degradation rules. The model is explained by means of the flowchart shown in Fig. 5. First, the finite element model must be prepared. During preparation of the finite element model, material properties, geometry, boundary conditions, fatigue load, maximum number of cycles, total number of cycles, etc., are defined. Then the stress analysis, based on the fatigue load, is performed. In this step, on-axis stresses for each ply of each laminate of each element are calculated. In the next step, failure analysis is performed. In this stage, based on the maximum fatigue load, stresses are examined by a set of failure criteria. If there is a failure, then the material properties of the failed plies are changed according to appropriate sudden material property degradation rules. A stress analysis is performed again, and new stresses are examined by the set of failure criteria. In this step, if there is no failure, an incremental number of cycles are applied (e.g., $\Delta N = 100$). If the number of cycles is greater than the total number of cycles, then the computer program stops. Otherwise, material properties of the plies (strengths, stiffnesses, and Poisson's ratios) are changed according to the gradual property degradation rules, see Fig. 4. Then stress analysis is performed again and the above loop is repeated until catastrophic failure occurs, or the maximum number of cycles is reached. If catastrophic failure is reached, then fatigue life and the mechanisms of failure due to fatigue loading have been achieved. However, if the computer program stops because the user-chosen maximum number of cycles is reached, then the mechanisms of failure due to fatigue loading are found by examining the final state of damage. Furthermore, in the latter case, residual strength of the composite laminate is obtainable by applying a static progressive damage modeling on the final results of fatigue progressive damage model.

8. EXPERIMENTS AND RESULTS

In order to run the computer program developed for the fatigue progressive damage modeling of pin/bolt loaded composite laminates, the mechanical behavior of a unidirectional ply under uniaxial static and fatigue loading conditions must be fully characterized. For this purpose, both the static and fatigue material properties of a unidirectional composite laminate in the fiber and matrix directions were determined experimentally under tensile, compressive, inplane shear and out-of-plane shear loading conditions.

8.1 Static and Fatigue Tests

In the first step, all material properties of a unidirectional laminate were measured under static loading conditions to establish initial stiffnesses and strengths. Using the results from static tests as normalizing parameters, material properties of a unidirectional laminate under fatigue loading conditions were characterized experimentally. From the experiments conducted in fatigue, the following properties under uniaxial loading were determined: residual strength, residual stiffness and fatigue life. To decrease the infinite number of fatigue experiments under general stresses and stress ratios, three normalization techniques explained in Subsection 5.2.3 for stiffness degradation, strength degradation and fatigue life were used. In order to verify the simulation results obtained from the fatigue progressive damage model, a series of static and fatigue experiments were performed on different pin/bolt loaded composite laminates with different configurations under different levels of fatigue loading. The specimens used in this study were made from AS4/3501-6 graphite/epoxy material in prepreg form. The specimens were manufactured using an autoclave, cut and drilled (when needed) using standard techniques.

Tests were performed using the MTS 810 test machine equipped with hydraulic grips. A personal computer was connected to the test machine for data acquisition. Displacement, load and strain were monitored in the static tests. In fatigue tests, maximum and minimum displacement, load, strain and number of cycles were monitored. The strain was measured by using an extensometer or strain gauges. To transfer the results from the strain gauges to the controller and the computer, an accurate Wheatstone bridge was made and calibrated. Static tests were performed under displacement control, while fatigue tests were performed under load control. To avoid temperature effects, which could degrade the material properties, fatigue tests were performed at frequencies less than 10 Hz. All tests were performed in ambient temperature.

The experiments performed in this study for full characterization of unidirectional laminates and model verification are summarized in Fig. 6. Tests were designed based on the required information and data for the fatigue progressive damage model. For all six types of input tests, the appropriate ASTM test standards were used except for the compression test. A new test specimen was developed for static and fatigue compression testing [6]. For all six types of static tests performed, except for the out-of-plane shear test, the static strengths and moduli were measured. For the out-of-plane shear test, the static strength was measured while the stiffness was derived by the transverse isotropic material property assumption. The fatigue tests were performed to measure the residual moduli, strengths and life. The fatigue load was applied in a sinusoidal form. The maximum stress applied during the fatigue test was based on some percent of static strength and different stress ratios were applied. To determine the residual properties, fatigue load was stopped after some number of cycles, and then static load was applied to measure the residual moduli and strengths. To find the life of the material, different states of stress and stress ratios were applied and tests were continued until catastrophic failure. A detailed description of the input and verification test procedures and experimental results are given in Ref. 2.

8.2 Data Processing

The data obtained from the input tests [2] were processed and normalized in the form of mathematical equations to be utilized in the computer code. The theories behind all mathematical normalizations are explained in Subsection 5.2.3 and Appendix A of Ref. 2. The fatigue life, residual stiffness and residual strength are presented in normalized forms for a unidirectional laminate after data processing.

8.2.1 Fatigue life master curves

The fatigue life of a unidirectional ply in longitudinal, transverse, inplane and out-of-plane shear loading is presented in normalized form. As shown in Appendix A of Ref. 2, the effect of mean stress ($(\sigma_{max} + \sigma_{min})/2$) on the fatigue life can be presented efficiently by the constant life (Goodman-type) diagrams. However, establishing the constant life diagrams for a unidirectional ply is time consuming and expensive. By using the normalized fatigue life technique, all different fatigue life curves for different mean stress conditions collapsed to a single two-parameter master curve, which decreased the number of required experiments drastically.

Based on the results obtained from tension-tension and compression-compression fatigue tests for unidirectional laminates in the longitudinal and transverse directions, and by using the normalized fatigue life technique, the fatigue life master curves for a unidirectional ply were obtained. These master curves are shown in Fig. 7 for loading in the longitudinal direction and in Fig. 8 for loading in the transverse direction. In a similar way, the fatigue life master curves for inplane and out-of-plane shear loading conditions were obtained, see Figs. 9 and 10. The required experimental parameters for all master curves were derived by using a linear curve fitting approach.

8.2.2 Master curves for residual material properties

Based on the fatigue test results and by using the normalized residual strength and stiffness techniques discussed earlier, the master curves of a unidirectional ply under different loading conditions were obtained. The normalized residual strength and stiffness curves of a longitudinal ply under longitudinal tension-tension fatigue loading are shown in Figs 11 and 12, respectively. The required experimental parameters for residual strength and stiffness were derived by using a nonlinear curve fitting approach. By applying the same procedure, residual material curve fitting parameters were found for the fiber in compression, matrix in tension and compression, inplane shear and out-of-plane shear conditions.

8.3 Verification Tests

In order to verify the results obtained from the fatigue progressive damage modeling, static and fatigue tests were performed on different pin/bolt loaded composite laminates with different geometries and layups under different levels of fatigue loading. Static tests were performed under stroke control conditions, while fatigue tests were performed under load control conditions. First, a series of static tests was performed to measure the strength of the pin or bolt loaded composite laminates with different *e/d* and *w/d* ratios and layups ($[0/90]_S$, $[90/0]_S$, and $[\pm 45]_S$). For the bolt loaded tests a torque equal to 4.1 N.m was applied. The static test results are summarized in Table 1. As shown in Table 1, the experimental and predicted results are in good agreement. This finding demonstrates that the model is capable of predicting the static failure of a composite laminate under pin or bolt loaded conditions. By comparing the maximum strength of $[0/90]_S$ with that of $[90/0]_S$ in Table 1, it can be seen that the $[90/0]_S$ is stronger than the $[0/90]_S$ laminate. The main reason for this behavior is that the out-of-plane normal stress, σ_{zz}, for the $[0/90]_S$ laminate is higher than that of the $[90/0]_S$ laminate and therefore the $[0/90]_S$ laminate is more sensitive to delamination. This behavior was simulated successfully by the computer code.

The results of the fatigue tests are summarized in Table 2. By considering the scatter, which is unavoidable in fatigue testing, the experimental and predicted results shown in Table 2 are in good agreement. In addition to successful life predictions, the failure mode predictions by the computer code are the same as the failure mode observed experimentally.

By comparing the fatigue life of the pin and bolt loaded composite laminates in Table 2, it can be seen that using the bolt increases the fatigue life of the composite laminates. The main reason is that the bolt reduces the high stresses caused by edge effects induced on the edge of the hole between different plies. This behavior was successfully simulated by the fatigue progressive damage model.

9. CONCLUSIONS

A phenomenological modeling technique, called fatigue progressive damage modeling, which is capable of predicting residual strength, residual stiffness and fatigue life of pin/bolt loaded composite laminates, was established. To support the model, a complete static and fatigue characterization of AS4/3501-6 carbon/epoxy material was performed. The use of normalization techniques allowed the fatigue characterization to be performed with a minimum number of tests. The results obtained from the model were successfully verified against experimental results.

10. ACKNOWLEDGEMENTS

This work has been performed under NRC Project 3G3, Aerospace Structures, Structural Dynamics & Acoustics, Sub-Project JGM-02, Bolted Joint Technology in Composite Structures. The partial financial support from the Department of National Defence Financial Encumbrance 220794NRC08 is gratefully acknowledged.

11. REFERENCES

1. Hahn, H.T. and Tsai, S.W., "Nonlinear Elastic Behavior of Unidirectional Composite Laminates", J. Comp. Mat., 7, Jan. 1973, pp 102-118.
2. Lessard, L B. and Shokrieh, M.M., "Fatigue Behavior of Composite Pinned/Bolted Joints", Final Report, NRC Contract No. 31946-1-0008/01-SR, Oct. 1995.
3. Hashin, Z., "Fatigue Failure Criteria for Unidirectional Fiber Composites", J. Appl. Mech., 48, 1981, pp 846-852.
4. Charewicz, A. and Daniel, I.M., "Damage Mechanisms and Accumulation in Graphite/Epoxy Laminates", *in* "Composite Materials: Fatigue and Fracture", ASTM STP 907, 1986, pp 274-297.
5. Harris, B., Reiter, H., Adams, R., Dickson, R.F. and Fernando, G., "Fatigue Behaviour of Carbon Fibre Reinforced Plastics", Composites, *21*, 3, May 1990, pp 232-242.
6. Milette, J.F., Shokrieh, M.M. and Lessard, L.B., "Static and Fatigue Characterization of Unidirectional Composites in Compression", Tenth International Conference on Composite Materials, ICCM/10, August 1995.

Table 1. Static Test Results and Predictions of Pin/Bolt Loaded Composite Laminates

Specimen Code	E/D	W/D	Layup	Loading	Max. Load (KN)	Prediction (KN)	% Error
787-1	4	4	$[0/90]_S$	Pin	5.98	4.95	21
787-2	4	4	$[0/90]_S$	Pin	4.5 (Initiation)	----	----
787-3	4	4	$[0/90]_S$	Pin	5.96	4.95	20
787-21	2	4	$[0/90]_S$	Pin	2.8	2.24	25
787-22	2	4	$[0/90]_S$	Pin	2.63	2.24	17
787-23	2	4	$[0/90]_S$	Pin	2.71	2.24	21
787-40	5	2	$[0/90]_S$	Pin	5.04	3.97	27
787-42	5	2	$[0/90]_S$	Pin	3.93 (Initiation)	----	----
787-41	5	2	$[0/90]_S$	Pin	4.17	3.97	5
787-5	4	4	$[0/90]_S$	Pin	5.39	4.95	9
788-1	4	4	$[90/0]_S$	Pin	6.65	5.25	27
788-2	4	4	$[90/0]_S$	Pin	4.2 (Initiation)	----	----
788-3	4	4	$[90/0]_S$	Pin	6.45	5.25	23
789-1	4	4	$[\pm 45]_S$	Pin	3.47	3.23	7
789-2	4	4	$[\pm 45]_S$	Pin	3.88	3.23	20
789-3	4	4	$[\pm 45]_S$	Pin	3.4 (Initiation)	----	----
787-4	4	4	$[0/90]_S$	Bolt	10.72	9.2	16
787-6	4	4	$[0/90]_S$	Bolt	8.0	9.2	13
787-7	4	4	$[0/90]_S$	Bolt	8.03	9.2	13

Table 2. Fatigue Life Test Results and Predictions of Pin/Bolt Loaded Composite Laminates

Specimen Code	E/D	W/D	Layup	Loading	% of Max. Strength	Load Ratio	Life, N Test	Life, N Prediction	% Error
787-9	4	4	$[0/90]_S$	Pin	80	0.1	6,114	5,100	20
787-10	4	4	$[0/90]_S$	Pin	80	0.1	6,000	5,100	18
787-11	4	4	$[0/90]_S$	Pin	80	0.1	1,882	5,100	63
787-12	4	4	$[0/90]_S$	Pin	70	0.1	59,792	71,000	16
787-13	4	4	$[0/90]_S$	Pin	70	0.1	94,482	71,000	33
787-16	4	4	$[0/90]_S$	Bolt	80	0.1	133,804	110,000	22
793-9	4	4	$[0/90]_S$	Bolt	80	0.1	129,411	110,000	18
793-10	4	4	$[0/90]_S$	Bolt	70	0.1	358,482	1,000,000	64
793-11	4	4	$[0/90]_S$	Bolt	70	0.1	1,119,266	1,000,000	12

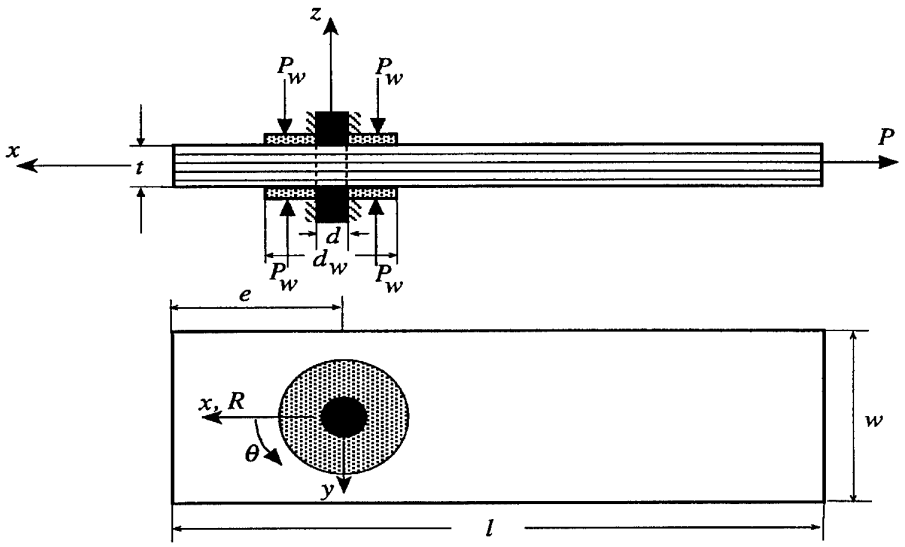


Figure 1. Parameters for a Laminated Plate Subjected to Pin/Bolt Fatigue Loading

Plane	Boundary Cond.		
	x	y	z
BCIH	0	1	0
DEKJ	0	1	0
GHKL	0	0	1

Fixed = 1
Free = 0

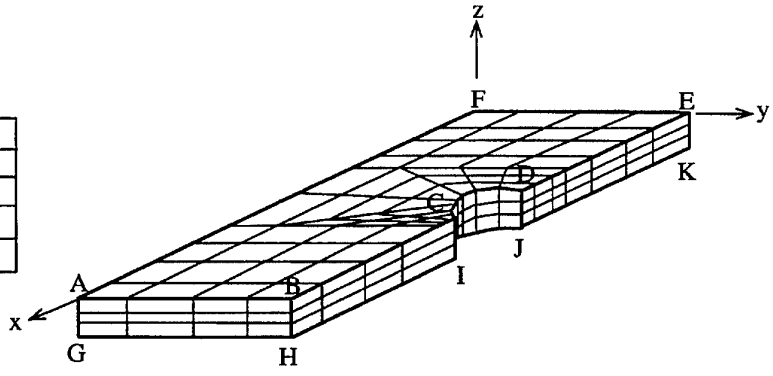


Figure 2. Finite Element Model

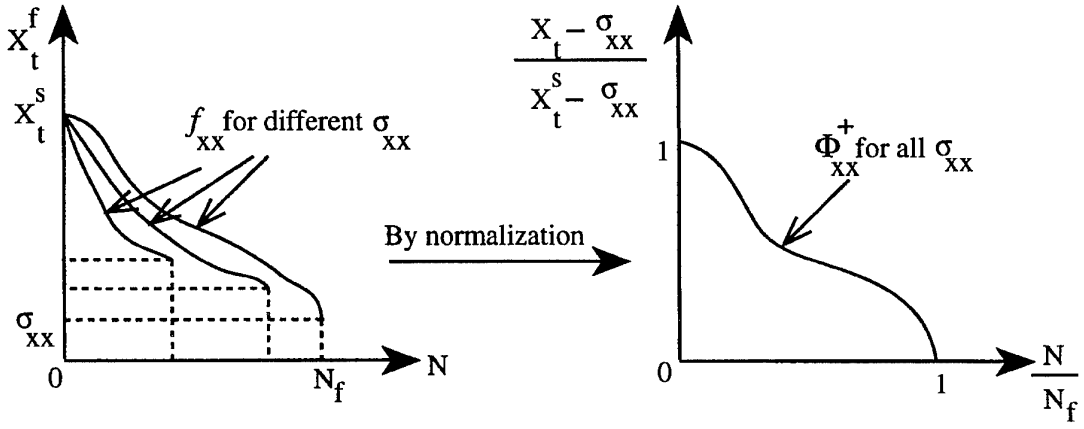


Figure 3. Normalization of the Strength Function

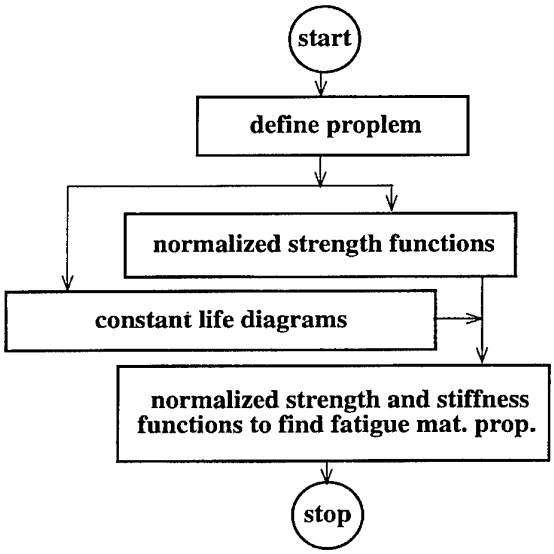


Figure 4. Flowchart of Gradual Material Property Degradation Rules

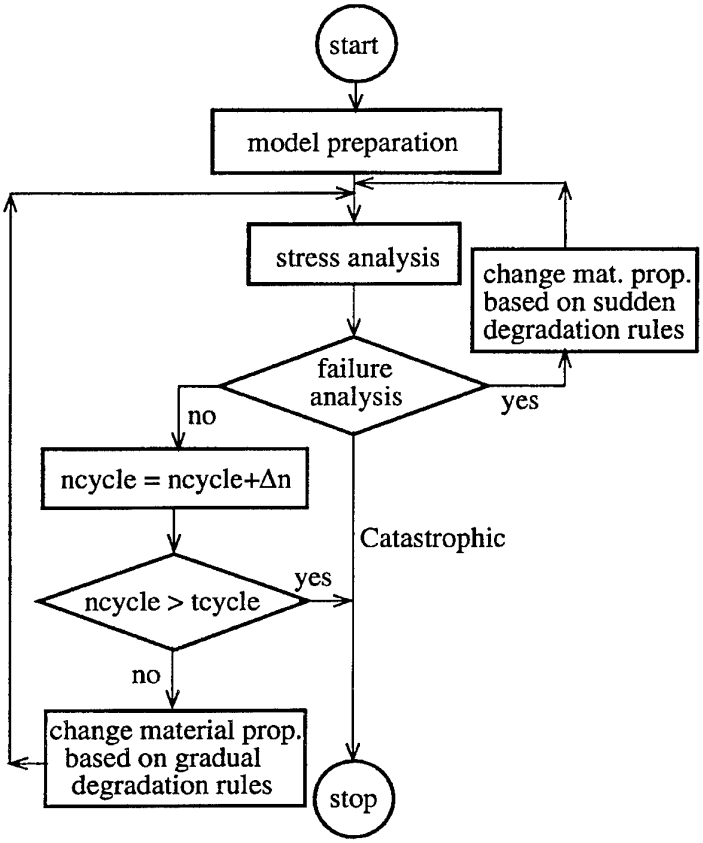


Figure 5. Flowchart of Fatigue Progressive Damage Modeling

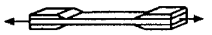
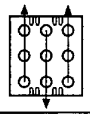
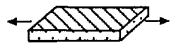
	Type of test (Static or Fatigue)	Test Specimens	Standards	Notes
Input Tests	Fiber Tension		D 3039-76 D 3479-76	With Hydraulic Grips
	Fiber Compression		———	With Hydraulic Grips
	Matrix Tension		D 3039-76 D 3479-76	With Hydraulic Grips
	Matrix Compression		D 3410-87	With Hydraulic Grips
	In-Plane Shear		D 4255-83	Modified Notched Specimen
	Out-of-Plane Shear		D 2733-70 D 2344-84	With Clamp
Verification Tests	30^{o} off-axis specimen		———	With Hydraulic Grips
	Pin/Bolt Loaded Composites		———	With Fixture

Figure 6. Specifications of Specimens Used in Static and Fatigue Tests

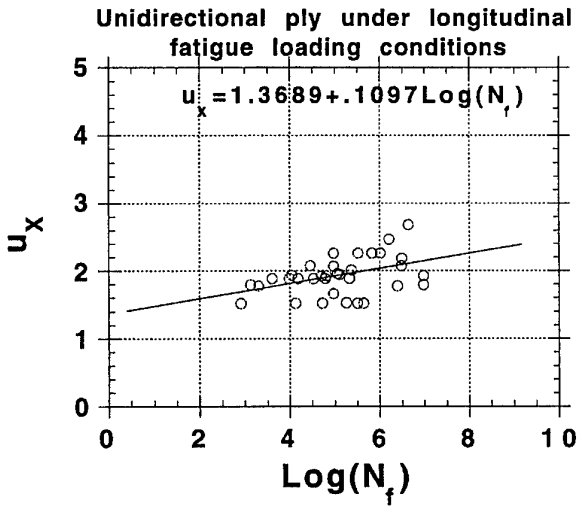


Figure 7. Master Curve for Fatigue Life under Longitudinal Loading

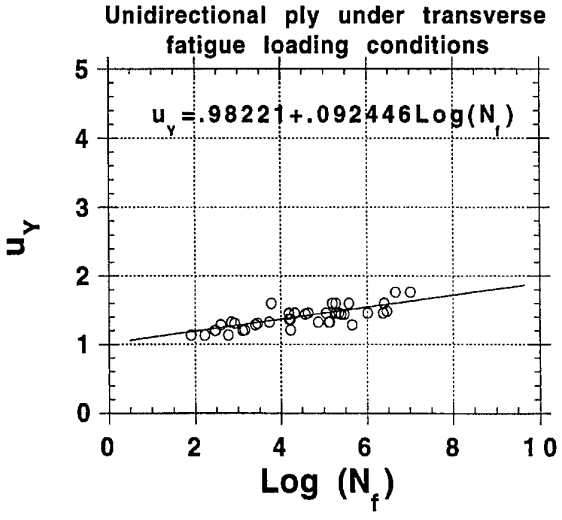


Figure 8. Master Curve for Fatigue Life under Transverse Loading

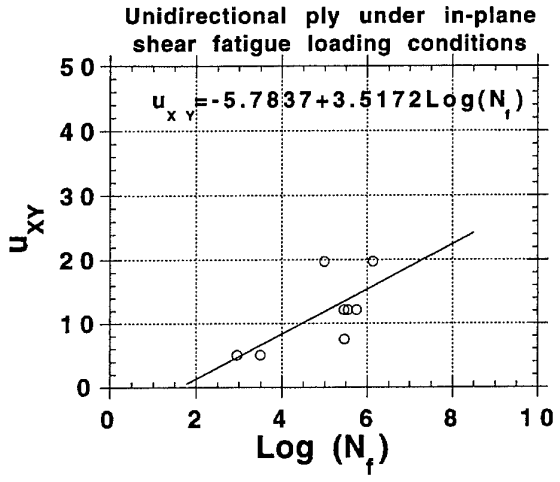


Figure 9. Master Curve for Fatigue Life under Inplane Shear Loading

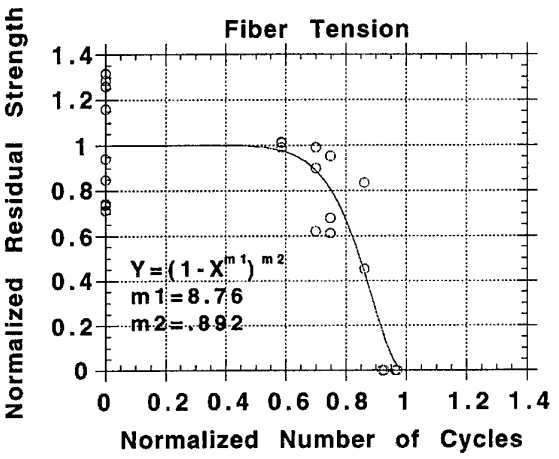


Figure 11. Normalized Residual Strength of a Unidirectional Ply under Longitudinal Tension-Tension Fatigue Loading

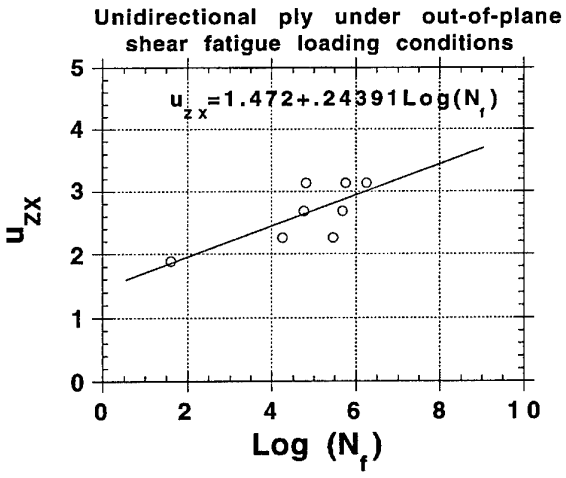


Figure 10. Master Curve for Fatigue Life under Out-of-Plane Shear Loading

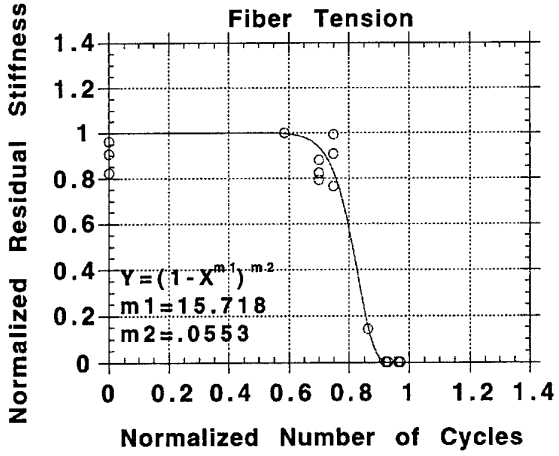


Figure 12. Normalized Residual Stiffness of a Unidirectional Ply under Longitudinal Tension-Tension Fatigue Loading

Analysis Methods for Bolted Composite Joints Subjected to In-Plane Shear Loads

Dr. L. J. Hart-Smith

Douglas Aircraft Company
McDonnell Douglas Corporation
Long Beach, California

1. SUMMARY

New analysis methods are developed for predicting the strength of bolted joints in fibrous composite laminates for geometries other than the standard test coupons, particularly in regard to in-plane-shear loads. The methods build on the author's earlier works, using the same technique of accounting for the stress-concentration relief permitted by the heterogeneous nature of fibre-polymer composites. Similar linear bearing/bypass curves, terminated by a bearing-stress cut-off, are predicted for these new joint geometries. The interactions have the same form as those which are now well accepted for the conventional case of parallel bearing and bypass loads, only with different slopes. The theory has been developed ahead of any relevant test data in the hope of encouraging an appropriate test program, so that these new solutions could be validated or refined and then added to existing joint-analysis computer codes with appropriate boundary conditions and failure criteria.

2. INTRODUCTION

Analysis methods already developed for predicting the strength of single-row and multi-row mechanically fastened joints in composite laminates have, almost without exception, been formulated and validated only for tensile or compressive loads *parallel* to the primary fibre direction, and usually *perpendicular* to a splice. These methods, for example Ref.'s 1 through 6, have been of inestimable value in furthering the applications of composite structures during the past 20 years or so. The Douglas method, the A4EJ computer code in conjunction with the "C-factor" to account for varying degrees of stress-concentration relief for different fibre patterns and hole sizes, was used in the work described in Ref. 7 to design what are still today the most efficient highly loaded bolted composite joints – in 1-inch thick laminates to a *gross-section* strain level of 0.005 [345 MPa (50 ksi) gross-section stress] in a (37.5% 0°, 50% ±45°, 12.5% 90°) carbon-epoxy laminate suitable for primary wing skins. The McDonnell BJSFM model, Ref.'s 3 and 4, was used to size all of the bolted joints in the F/A-18 and AV-8B composite wing skins, with great success except for the wing-fold area in the development test structures for the first F-18 in which the countersinks were initially too deep and the bearing stresses too high. (This should be looked upon more as the result of the time needed to fully understand the importance of designing to low bearing stresses than any shortcoming of the analysis method, however.)

Even so, these earlier methods do not cover *all* realistic boundary conditions for bolted joints in composite structures. The McDonnell BJSFM model permits the bearing load to be inclined at any direction to the fibres in the laminate, at least for infinite plates. The author attempted to formulate an extension of his earlier works, Ref.'s 2 and 6, to cover additional load components orthogonal to the primary load, see Ref. 8. Both of these developments have been limited by the virtual absence of any data with which to validate or identify the need for improvements to the models. The same handicap faces the new model to be presented here. Nevertheless, this new model is presented in the hope that, since the basic model can now be extended to in-plane-shear load transfer in multi-row bolted or rivetted joints, a case will have been presented to justify relevant testing to validate or refine the theory.

Certain key characteristics have already been firmly established by the analyses cited above, as well as by the works of other researchers, such as Eisenmann, Ref. 9 and Crews, Ref. 10. The first is that there is significant stress-concentration relief for small hole diameters, with respect to what linear elastic analysis would predict. (This is confirmed by the use of a *universal* characteristic offset dimension with the BJSFM method, regardless of the fastener diameter, and by the treatment of hole-size effects in Ref. 11.) The second is that there is a *linear* interaction between bearing and tensile bypass loads for tension-through-the-hole failures, truncated by purely bearing failures once some critical bearing stress has been attained. (The origin of this linear interaction can be traced back to experiments performed at General Dynamics during the 1970s.) There are so few test data for compressive bearing/bypass interactions that the confidence level in what has already been developed is not as great as for tensile loads. This has not been a critical deficiency, however, because compressive loads can be transmitted through fasteners in the holes, while tension loads must go around them, being confined to the net section. Consequently, tensile loads are usually the more critical for aircraft structures.

A far more serious problem, albeit largely unrecognized, has been the use of physically unrealistic failure criteria for fibre-polymer composites when the fibres were not subjected to purely longitudinal loads. This deficiency of many failure criteria was not a problem for those standard-geometry bolted joints in which tensile failures occurred at positions around the fasteners where there was no significant bearing stress, or in which bearing failures occurred in conjunction with little hoop-tension stress. However, it can be a very real problem for other joint and load geometries, in which the fibres can be stressed by significantly orthogonal loads of different signs.

Ref. 8 contains an "error" in the sense that bearing forces should not be resolved into components for so-called contact

Paper presented at the 83rd Meeting of the AGARD SMP on "Bolted/Bonded Joints in Polymeric Composites", held in Florence, Italy, 2-3 September 1996, and published in CP-590.

problems, because the area of contact is changed in the process. (Nevertheless, the degree of conservatism introduced by this physically unjustifiable empirical simplifying technique was not crucial, even though this earlier work should now be considered largely superseded by the present one.) The more significant limitation is that, when Ref. 8 was prepared, the author had yet to recognize the need for, let alone formulate, a generalization of the maximum-shear-stress failure criterion to fibrous composite laminates. Also, several more years were to pass before the importance of expressing this failure criterion on the strain, rather than stress, plane was recognized. Only now is it possible to do justice to the bearing/bypass interaction for what have in the past been considered non-standard joint geometries. The key breakthrough in this regard is the derivation in Ref. 12 of an expression relating the transverse strain in a lamina to that in its fibres. This solution is extended here to relate the stresses in a *laminate* to the transverse strain in the critical fibres, enabling the two fibre-stress components needing to be interacted in terms of bearing/bypass loads to be realistically characterized for the first time.

The techniques developed are illustrated for carbon-epoxy laminates, but when modified as indicated, can also be applied to glass-fibre-reinforced laminates. This distinction is needed because the strongest bolted joints in carbon-epoxy laminates fail in tension-through-the-hole, while it is extremely difficult to avoid bearing failures in fibreglass-epoxy laminates. This initial derivation is also limited to quasi-isotropic laminates, both to simplify the development and because laminates with fibre patterns close to this make the strongest bolted composite structures. The modifications needed to account for different C-factors for other laminates may be addressed later, if they prove to not be self evident.

3. THE STRESS FIELD AROUND A LOADED BOLT HOLE

The basis of the linear bearing/bypass interaction for the classical lug joint is that, for a homogeneous elastic isotropic plate, the *peak* tension stress alongside the bolt hole in an infinite plate is roughly equal to the *average* bearing stress, as shown in Figure 1. This result was first established by Bickley in Ref. 13. The hoop stress varies around the circumference as shown, being only about half as high in the region of the most intense bearing stress.

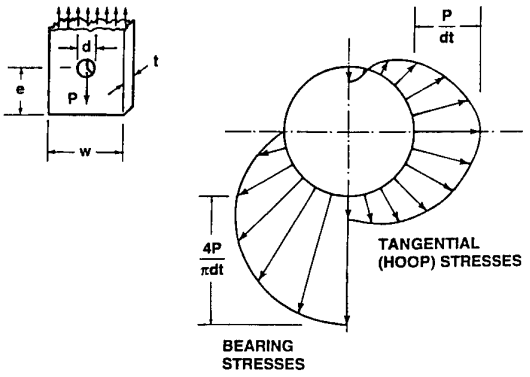


FIG. 1 BEARING AND HOOP-TENSION STRESSES AROUND A LOADED BOLT HOLE

Here, the focus will be on fibre patterns in the standard (0°, ±45°, 90°) family now used throughout most of the aerospace industry, so only the values of the hoop stresses at those angles will be of concern. The initial challenge is to so characterize the variation in the hoop stress that the same assessment is produced *after* the fastener load has been replaced by two "equivalent" increments inclined at ±45° to the true orientation of the bearing load. This is done in Figure 2, which shows that this superposition is flawed. The "error" in this technique is that the sum of the two resolved components of the bearing load makes contact with the hole over some 270°, instead of the assumed 180° for a tightly seated non-interference-fit bolt. Consequently, the superposition of these two components results in an apparent bearing load on each *side* of the hole as well, as shown in Figure 3. Remarkably, the bearing-stress distribution remains precise throughout an angle of ±45° with respect to the resultant bearing force, so resolving the bearing load does not introduce errors in those areas in which a bearing failure is most likely. This lateral bulging in Figure 3 is equilibrated by the application of remote transverse compressive loads of sufficient intensity to counteract this effect and make the *combination* of the resolved bearing load and the compensating transverse compression *equivalent* to applying the bearing load in isolation. (The need for such transverse compression, based on an unfilled hole, had been overlooked in Ref. 8.) The match in regard to hoop stresses is not perfect, but is reasonable and easy to apply. Corresponding calculations not reported here have confirmed that if the load components had been resolved by ±22.5° instead of ±45°, the same kind of superposition would work with 1/4 as much added transverse compression. However, away from the area of highest bearing stresses, the distribution is far better represented by the single resultant load than by summing the contributions of resolved components.

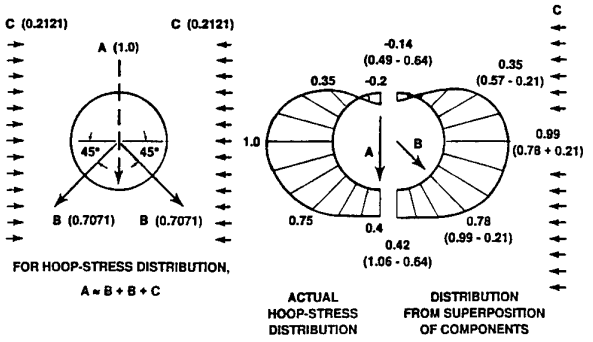


FIG. 2 REPRESENTATION OF HOOP STRESSES CAUSED BY A BEARING LOAD AS TWO RESOLVED COMPONENTS AND ASSOCIATED TRANSVERSE COMPRESSION

Failure at a loaded bolt hole in an infinitely wide quasi-isotropic carbon-epoxy plate is by bearing. Tension-through-the hole failures occur only in relatively narrow strips – *w/d* less than 4 or 5 to 1 – or in a seam of closely spaced fasteners.

It should now be possible to combine this *set* of equivalences for a bearing load with bypass loads in the same manner as has worked successfully in the past for the simpler load

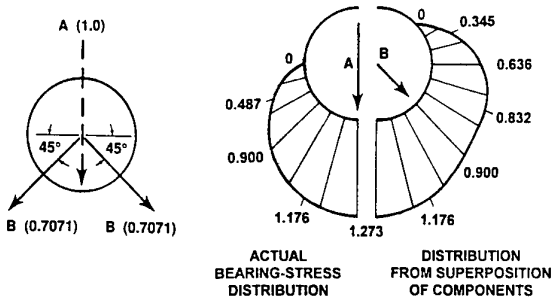


FIG. 3 REPRESENTATION OF BEARING STRESSES CAUSED BY A SINGLE BEARING LOAD AS TWO RESOLVED COMPONENTS

cases. Some progressively more complex cases are examined in turn, starting with infinitely wide plates containing a single loaded bolt hole and progressing to finite-width and finite-pitch effects in multi-fastener joints.

4. THE BASIC BEARING/BYPASS INTERACTION

It is appropriate to briefly explain the basic linear bearing/bypass interaction by the classic case of parallel load components. For simplicity, edge (finite-width or -pitch) effects are omitted initially, since they have already been adequately covered in Ref.'s 2 and 6. For the infinite elastic isotropic plate described in Figure 4, the interaction between stresses is thus that between three times the remote stress in the plate (k_{te} = 3) and the average bearing stress, with the critical conditions for tensile failures of the laminate developing *alongside* the bolt hole, where the bearing stress is nominally zero.

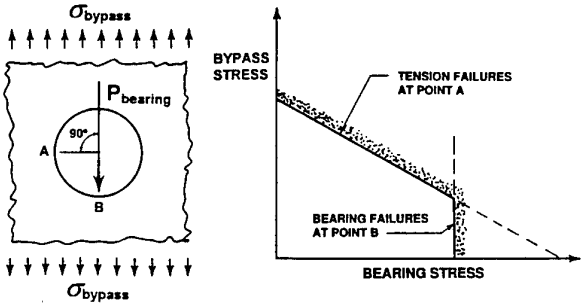


FIG. 4 CLASSICAL BEARING/BYPASS CURVE, SHOWING DECREASE IN OPERATING STRESSES UNTIL BEARING FAILURES OCCUR

In the absence of any stress-concentration relief, failure would not occur until

$$3.0 \times \sigma_{bypass} + 1.0 \times \sigma_{bearing} = F_{tu} \quad , \qquad (1)$$

in which F_{tu} is the ultimate tensile strength of the laminate. (The stress-concentration factors 3 and 1 would be different for orthotropic plates and for finite-width strips or seams of fasteners.) Using the C-factor approach for characterizing stress-concentration relief via the heterogeneous nature of the fibre-polymer composites,

$$(k_{tc} - 1) = C(k_{te} - 1) \quad , \qquad (2)$$

where k_{te} is the theoretical elastic stress-concentration factor (peak tension stress / average net-section tension stress) in the panel (3.0 in this case, but varying with the *d/w* ratio for finite-width panels), k_{tc} is the *apparent* stress concentration at failure, and C is the stress-concentration relief factor. The mechanism of this stress-concentration relief, and why it is governed by ply thickness rather than by hole diameter is explained in Ref. 11. This nonlinearity is unlike yielding of metals; it stems from the heterogeneity of fibre-polymer composites. Throughout this article, C is assigned the value 0.25, which is representative of 0.25-inch (6.35 mm) holes in quasi-isotropic carbon-epoxy laminates. Since k_{te} and k_{tc} are *both* infinite for a bearing load on an infinitely wide panel, $k_{tc} = C \times k_{te}$ in this case. Equation (1) would then be modified to read

$$(1+2C)\sigma_{bypass} + C \times \sigma_{bearing} \le F_{tu} \quad . \qquad (3)$$

In the form in which it is more usually seen, this is transformed into the relation

$$\sigma_{bypass} \le \frac{1}{(1+2C)}\left[F_{tu} - C \times \sigma_{bearing}\right] \quad , \qquad (4)$$

showing how the addition of bearing stress imposes a linear reduction in the remote stress which can be withstood by the laminate prior to failure. Given that the value of C can range from 1.0 for very large holes for which there is no stress-concentration relief down to 0.25 for quarter-inch holes in quasi-isotropic carbon-epoxy laminates, the effect of the heterogeneous behaviour of the laminates can be very significant. A similar linear reduction applies for finite-width strips and a seam of adjacent fasteners in a panel. The linear reduction in remote laminate strength as progressively more bearing load is added is eventually truncated by a bearing-stress cut-off of the type shown in Figure 5, which is the classic bearing/bypass interaction for mechanically fastened fibrous composite structures. (The sum of these two loads is the total joint or laminate strength.) Illustrative property values used here for high-strength carbon-epoxy laminates are F_{tu} = 690 MPa (100 ksi) and F_{brg} = 965 MPa (140 ksi). The bypass stresses can be converted to strains by dividing by the Young's modulus for the laminate; in this case, $E_{laminate}$ = 55 GPa (8 × 10^6 psi). The in-plane shear modulus, likewise, is $G_{laminate}$ = 21 GPa (3 × 10^6 psi). Additional material properties needed for later formulae and diagrams are the major Poisson's ratio ν_{LT}, which has a value of 0.3, and the laminate compressive strength F_{cu} of 483 MPa (70 ksi).

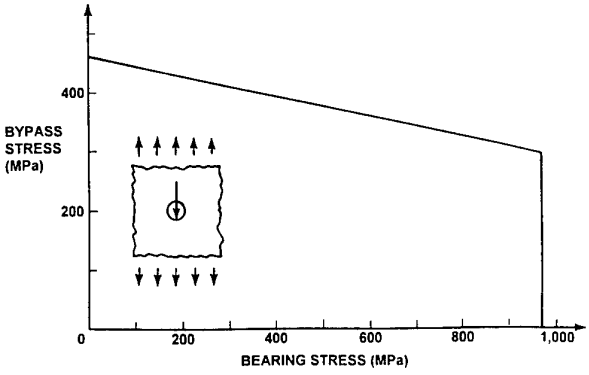


FIG. 5 BEARING/BYPASS INTERACTION FOR A LOADED HOLE IN AN INFINITE PLATE

The traditional analyses characterized above refer to tensile failure in the absence of bearing stress or to bearing failure in the presence of a small hoop-tension stress, which is neglected. It is appropriate to re-examine the bearing-stress failure, taking proper account of possible interaction with the actual hoop-tension stress in that area, the presence of which is shown in Figure 1.

Because we are concerned here with carbon fibres failing under longitudinal and transverse stresses of *opposite* sign, the truncated maximum-strain failure model can be characterized by the simple formula

$$\varepsilon_{\text{longitudinal}} - \varepsilon_{\text{transverse}} = \text{constant} = (1+\nu_{LT})\varepsilon_0 \ , \qquad (5)$$

where ε_0 is the greater of the tensile and compressive longitudinal strains-to-failure. (For simplicity here, this distinction between tensile and compressive strains-to-failure is ignored and the reader is referred to the author's papers on failure criteria for clarification.) Strictly, Equation (5) should be applied at the fibre rather than at the lamina level, but it is shown in Ref. 13 that, for carbon-epoxy type laminates, no significant error is introduced by assuming that the transverse stress within each lamina is constant throughout both fibre and matrix. What small error there does exist is conservative in regard to the strengths predicted. The same analysis, however, shows that the distinction between the transverse strains in the fibres and matrix *is* critical for fibreglass-reinforced polymer composites, for which the original (untruncated) maximum-strain failure model is superior to the truncated model described in Ref. 14, albeit slightly unconservative.

If we overlook the precise accounting of compatibility of deformations caused by Poisson effects for clarity, while acknowledging that the longitudinal load alone will induce transverse strains, Equation (5) can be expressed approximately in terms of stresses in the form

$$\left[\frac{(1+\nu_{LT})\sigma_{\text{longitudinal (laminate)}}}{E_{\text{longitudinal (laminate)}}}\right] - \frac{1}{R_\varepsilon}\left[\frac{\sigma_{\text{transverse (laminate)}}}{E_{\text{transverse (laminate)}}}\right] = \left[\frac{(1+\nu_{LT})F_{\text{tu (laminate)}}}{E_{\text{longitudinal (laminate)}}}\right] , \qquad (6)$$

in which R_ε is the amplification ratio between transverse strains in the lamina and those in the fibres. Calculations for two different carbon-epoxies in Ref. 12 found the value to be very close to 1.5. (It was found to be closer to 5 for fibreglass-epoxy laminates in which the isotropic fibres have a far greater transverse modulus.) The actual transverse stress in the specific plies of interest in the laminate is far less, in the ratio E_T/E_L for the lamina. Here, we simplify the work by restricting it to quasi-isotropic laminates, so the laminate Young's modulus E is constant throughout, permitting Equation (6) to be further simplified to the following.

$$\sigma_{\text{longitudinal}} - \frac{\sigma_{\text{transverse}}}{(1+\nu_{LT})R_\varepsilon} = F_{\text{tu}} \qquad (7)$$

The limiting strength equivalent to Equation (1) would, in the present context, then be

$$(0.4 \times \sigma_{\text{bearing}}) + \left(\frac{(4/\pi)}{(1+\nu_{LT})R_\varepsilon}\sigma_{\text{bearing}}\right) \le F_{\text{tu}} \ . \qquad (8)$$

[The change in sign between Equations (7) and (8) results from the inherently compressive bearing stress.] The factor $(4/\pi)$ relates the peak to average bearing stress in the most critical location.

The nature and characterization of the stress-concentration relief in the region of highest hoop stresses is well known and the need to include it in the analysis accepted. The same cannot be said for any stress-concentration relief in the area of highest bearing stress. Nevertheless, the bearing strength is known to improve with through-the-thickness clamp-up, from roughly the basic laminate compression strength for pin-loaded holes to roughly twice that strength for finger-tight nuts and bolts – and to even higher strengths for torqued fasteners. Without claiming any more than that there probably is *some* form of stress-concentration relief in this region also, we shall assume here that it can be characterized by the ratio of laminate compression strength F_{cu} to ultimate bearing strength F_{brg} and await the generation of test data to improve on the assessment.

Allowing for stress-concentration relief, Equation (8) would then become

$$\left[0.4C + \frac{4/\pi}{(1+\nu_{LT})R_\varepsilon}\left(\frac{F_{\text{cu}}}{F_{\text{brg}}}\right)\right]\sigma_{\text{bearing}} \le F_{\text{tu}} \qquad (9)$$

It is convenient to define a coefficient K, where

$$K = \frac{4/\pi}{(1+\nu_{LT})R_\varepsilon}\left(\frac{F_{\text{cu}}}{F_{\text{brg}}}\right) \qquad (10)$$

has a typical value of 0.3265 for the quasi-isotropic carbon-epoxy properties given earlier. We would, therefore, expect a hoop-tension failure in the peak bearing stress region only when

$$\sigma_{\text{bearing}} = \left(\frac{1}{0.4C+K}\right)F_{\text{tu}} = \left(\frac{1.0}{0.4265}\right)F_{\text{tu}} = 2.3447F_{\text{tu}} \ , \qquad (11)$$

over 67 percent higher than needed to cause a bearing failure at the same location in a quasi-isotropic carbon-epoxy laminate. However, Equation (11) also makes it quite clear that, for a highly orthotropic laminate containing too few 90° fibres, it would be quite easy to initiate tension failures in the high-bearing-stress region before the net section became critical. This may be confirmation of the well-known need for a minimum percentage of such plies (between 10 and 15 percent) to make efficient bonded fibrous composite joints.

It is also possible to use the present theory to check against the likelihood of failure in the ±45° fibres, half-way between the preceding analyses. Significantly, there is *zero* local bypass stress at these locations from any bypass load aligned with the bearing load, so the following result is of even more universal applicability. Without repeating the entire derivation, it should be self evident that Equation (11) can be modified for this new potential tensile failure site to read as follows.

$$\sigma_{bearing} = \left(\frac{1}{0.75C + 0.7071K}\right) F_{tu} = \left(\frac{1.0}{0.4184}\right) F_{tu} = 2.3902 F_{tu} , \quad (12)$$

making this site even less critical in tension than either of the other two possibilities – at the points of maximum hoop tension and of maximum bearing stress. However, Equation (12) predicts the ±45° sites to be only imperceptibly less likely to fail by hoop-tension loads than the fibres at 90°. The empirical wisdom that close-to-isotropic laminates make the strongest bolted joints is not without foundation, even if other analyses have not predicted this to be so.

5. ORTHOGONAL BEARING AND BYPASS LOADS IN AN INFINITE PLATE

Consider, next, the case of an infinite plate subjected to a uniform remote unidirectional stress and a concentrated *transverse* load at a central bolt hole, as shown in Figure 6. The *average* remote transverse load will be zero and, therefore, is not involved in this assessment. (The addition of such a bypass load can easily be handled by this method, as was done in Ref. 8, provided that all three load components contributed to a tensile laminate failure at the location being considered somewhere around the perimeter of the hole. But this step is omitted here for clarity.)

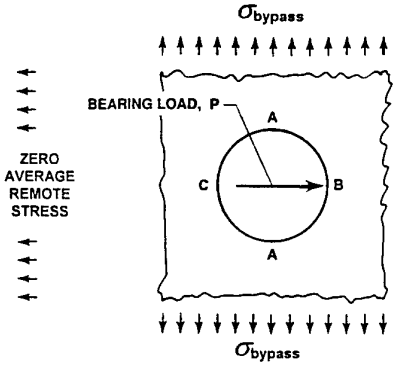


FIG. 6 COMBINATION OF ORTHOGONAL BEARING AND BYPASS LOADS IN AN INFINITE PLATE

At the location alongside the bolt hole, where the bypass load alone would cause tension-through-the-hole failures (Point B), the lateral bearing load, orthogonal to the longitudinal remote stress in the laminate, adds *two* components of stress to the peak stress caused by the bypass load. At that location, the bypass load is amplified by a nominal stress-concentration factor of 3.0, which remains the same as for the analysis above. The transverse bearing load causes a hoop-tension stress at that same location which is only some 40 percent as high as in the preceding analysis, but there is now also a transverse bearing stress acting on these same fibres.

The equation equivalent to Equation (1) would be

$$\left(3.0 \times \sigma_{bypass} + 0.4 \times \sigma_{bearing}\right) + \left(\frac{4/\pi}{(1+\nu_{LT})R_\varepsilon} \sigma_{bearing}\right) = F_{tu} \quad (13)$$

at failure. Allowing for stress-concentration relief, Equation (13) would then become

$$(1+2C)\sigma_{bypass} + (0.4C + K)\sigma_{bearing} = F_{tu} . \quad (14)$$

The final result, corresponding with Equation (4) then follows.

$$\sigma_{bypass} \le \frac{1}{(1+2C)}\left[F_{tu} - (0.4C + K)\sigma_{bearing}\right] . \quad (15)$$

The adverse effect of the transverse bearing load is predicted to be more severe than for a bearing load aligned *with* the bypass load, as is revealed by comparing Equations (4) and (15), but the failure sites can be different. If, for the present problem, only a small bypass load were combined with a dominant bearing load, tensile failure in the laminate would be predicted to occur at Points A above and below the bolt hole in Figure 6 instead of at the sides. For such a case, the elastic analysis would predict that tensile failure would not occur so long as

$$\left(1 \times \sigma_{bearing} - 1 \times \sigma_{bypass}\right) + \left(0 \times \sigma_{bearing}\right) \le F_{tu} , \quad (16)$$

there being nominally zero bearing stress at this site and a compressive component caused by the bypass stress. Allowing for the stress-concentration relief from the heterogeneity of the composite laminate, Equation (16) predicts that the critical bearing stress for a tensile failure must be as high as

$$\sigma_{bearing} = \frac{F_{tu} + \sigma_{bypass}}{C} . \quad (17)$$

At this location, the bypass stress is acting as benign preload to enhance the intrinsic strength of the laminate. (An excess of bypass would cause failure somewhere else, at point B.) This means that tensile failure in an infinitely wide strip is even less likely than in the absence of the bypass load.

There are, thus, two answers needed for this problem – Equation (15) for dominant bypass loads, and Equation (17) for dominant bearing loads. Equation (15) is plotted in Figure 7, but is somewhat misleading because of the absence of finite-width (or bolt pitch) effects needed to enable tensile failures caused by bearing loads to precede the predicted failures in bearing. This omission is even more serious for Equation (17). Nevertheless, the linear and predictable bearing/bypass interactions can easily be modified to account

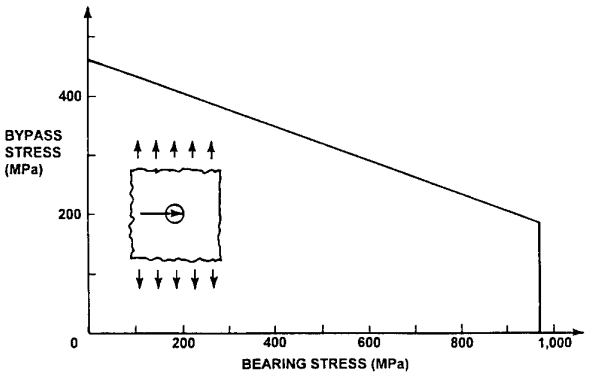


FIG. 7 INTERACTION BETWEEN ORTHOGONAL BEARING AND BYPASS LOADS IN AN INFINITE PLATE

for such effects. A comparison between Figures 5 and 7, for longitudinal and transverse bearing loads, shows the latter to be more critical, as the result of the biaxial stressing of the carbon fibres.

There is a strong bearing/bypass interaction for the problems characterized in Figure 6. For fibreglass-epoxy laminates, on the other hand, there would be very little interaction, and the slope in Figure 7 would then be less than in Figure 5. The $\{4/[\pi(1+\nu_{LT})R_\varepsilon]\}$ factor, K, would drop to almost zero because the transverse strain in each lamina would occur mainly in the matrix, with virtually none in the fibres.

6. CONCENTRATED BEARING LOAD IN AN INFINITE PANEL LOADED BY SHEAR

If an infinite panel is loaded by in-plane shear with respect to horizontal and vertical axes, a vertical or horizontal bearing load would be offset from the locations of the peak stresses at the bolt hole caused by the shear load. The stresses induced by the bearing load could be directly superimposed on these because, in this case, there has been no need to resolve the bearing load into components. Figure 8 defines the boundary conditions for this particular analysis, assuming a vertical bearing load half way between the k_{te} = ±4 axes (Points C and D). Surprisingly, two potential most critical locations, at the bottom (Point B, bearing) and sides (Points A, tension-through-the-hole) of the bearing load, are *all* associated with *zero* bypass stresses. There would be no interactions there; the panel would either fail by bearing or by tension from the remote (bypass) shear stress at an apparent stress-concentration factor of 1.75, in accordance with Equation (4), exactly as in Figure 5. A hoop-tension failure on one of the 45° diagonals (Point C or D in Figure 8) would appear to be a more interesting (and, as it transpires, more critical) potential failure site, there being an interaction between two significant hoop-stress components and a compressive bearing stress locally 0. 90 times the average (see Figure 3).

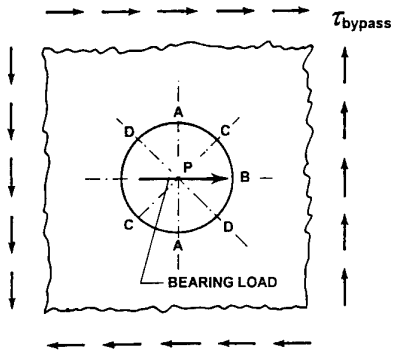


FIG. 8 GEOMETRY FOR ANALYSIS OF A SHEAR-LOADED INFINITE PLATE CONTAINING A LOADED BOLT HOLE

The hoop-tension stress at the lower-right location D consists of an increment 4.0 times as high as the nominal remote shear stress, in conjunction with a hoop-stress increment equal to 75 percent of the average bearing stress. In addition to these hoop-tension stresses, there is also a bearing stress at Point D, of an intensity $(1/\sqrt{2})$ times as high as the peak. Equation (7) would then predict no failure until

$$\left[\left(4.0 \times \tau_{\text{bypass}}\right) + \left(0.75 \times \sigma_{\text{bearing}}\right)\right] + 0.7071\left[\frac{4/\pi}{(1+\nu_{LT})R_\varepsilon}\right]\sigma_{\text{bearing}} = F_{\text{tu}} \qquad (18)$$

for hoop-tension failures, assuming no stress-concentration relief. Accounting for this effect in the same manner as in the earlier analyses, Equation (18) is transformed to read

$$\left[\left((1+3C) \times \tau_{\text{bypass}}\right) + \left(0.75 \times C \times \sigma_{\text{bearing}}\right)\right] + 0.7071K\sigma_{\text{bearing}} = F_{\text{tu}} \ , \qquad (19)$$

where K is defined in Equation (10). Hence

$$\tau_{\text{bypass}} \le \frac{1}{(1+3C)}\left[F_{\text{tu}} - \left((0.75 \times C) + 0.7071K\right)\sigma_{\text{bearing}}\right] \ , \quad \sigma_{brg} \le F_{\text{brg}} \ . \qquad (20)$$

The next analyses are for the bearing load parallel to the equivalent compressive and tensile remote stresses in the plate, corresponding with the applied shear load, (the load through Point B in Figure 8 rotated to D and C, in turn).

Aligning the bearing load with the D-D axis first, it is apparent that the initial failure would occur in the high-bearing-stress region, because the shear load induces major *compressive* hoop loads where the bolt-bearing loads caused the highest hoop-tension stresses. Equation (7) would now predict that failure would occur once the following condition was satisfied.

$$\left[\left(4.0 \times \tau_{\text{bypass}}\right) + \left(0.4 \times \sigma_{\text{bearing}}\right)\right] + \left(\frac{4/\pi}{(1+\nu_{LT})R_\varepsilon}\sigma_{\text{bearing}}\right) = F_{\text{tu}} \qquad (21)$$

After accounting for stress-concentration relief from the heterogeneous nature of the fibre-polymer composites, this equation would become

$$\tau_{\text{bypass}} \le \frac{1}{(1+3C)}\left[F_{\text{tu}} - \left((0.4 \times C) + K\right)\sigma_{\text{bearing}}\right] \ , \quad \left(\sigma_{\text{brg}} \le F_{\text{brg}}\right) \qquad (22)$$

If the bearing load were rotated through the C-C axis in Figure 8, so that the peak bearing load occurred in an area of compressive hoop stresses caused by the remote in-plane shear stress, the peak tensile stresses from both sources would combine along one *side* of the bolt, at the lower-right Point D, where there would be no bearing stress. The solution equivalent to Equation (21) would then be.

$$4.0 \times \tau_{\text{bypass}} + 1.0 \times \sigma_{\text{bearing}} \le F_{\text{tu}} \qquad (23)$$

After introducing the appropriate expressions for stress-concentration relief, and re-arrangement in the customary manner, this equation becomes

$$\tau_{\text{bypass}} \le \frac{1}{(1+3C)}\left[F_{\text{tu}} - \left(C \times \sigma_{\text{bearing}}\right)\right] \ , \quad \left(\sigma_{\text{brg}} \le F_{\text{brg}}\right) \qquad (24)$$

Equations (20), (22) and (24) are all plotted in Figure 9, using the same typical properties for carbon-epoxy laminates used in Figure 6. All predict tensile failure at the same site (Point D on the lower right in Figure 8); all are similar in form and subject to bearing-stress cut-offs. The only visible difference is in the slopes of the interactions. The predictions of Equations (20) and (22) are almost identical, representing slightly different combinations of hoop and bearing stresses.

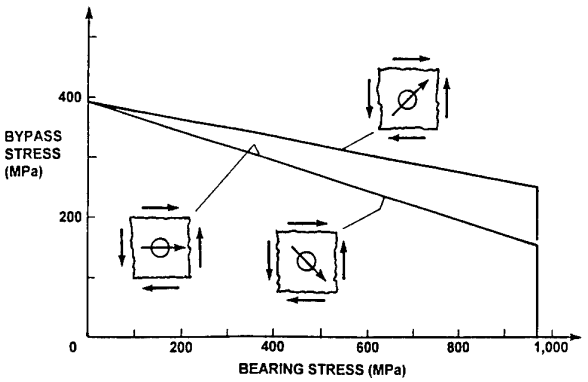


FIG. 9. BEARING/BYPASS INTERACTIONS FOR IN-PLANE SHEAR LOADS ON AN INFINITE PLATE

A significant conclusion to be drawn from Figure 9 is that the orientation of the bearing load in a shear panel is predicted not to have a substantial influence on the shear strength. (The effect would be even less for fibreglass-reinforced laminates.) This is surprising, given the very great variation in magnitude and sign of the hoop stress around the bolt hole resulting from the in-plane-shear bypass load. The similarity in form of the three solutions lends some credence to a popular empirical analysis technique used to design bolted composite joints with geometries for which there are no directly relevant test data, whereby the bearing load is realigned with the local principal bypass load and both are oriented with the nearest principal fibre axis. Having converted the problem to one for which there are test data and design coefficients for stress-concentration relief, a straightforward answer is then derived. However, Figure 9 suggests that rotating the peak bearing and bypass loads until they are collinear may not always yield a conservative solution, because doing so excludes interactions between longitudinal tension and transverse compression stresses acting on the critical fibres.

7. LOAD TRANSFER THROUGH A SINGLE ROW OF BOLTS ON THE PERIPHERY OF A SHEAR PANEL (OR THE ENDS OF TORSIONALLY LOADED TUBES)

One problem of major importance remains within the scope of the present investigation. This is the case of an infinitely long joint between two panels loaded by in-plane shear. The fastener loads are now *parallel* to the edge instead of orthogonal to it, as in standard tensile test coupons. This is the first of the present problems requiring that the bolt loads be resolved into orthogonal components parallel to tension and compression loads which are equivalent to the in-plane shear loads. Unlike the immediately preceding analyses for infinite plates, the in-plane shear stress drops to zero on one side of the fastener seam.

If the fastener loads are resolved into two orthogonal components, as shown in Figure 10, one component would be reacted by direct compressive bearing and the other by tensile bearing passing around the fastener. This model would correctly have zero *net* load on the fastener perpendicular to the edge of each panel, and there would be no prediction that the resolved fastener loads would try to spread the hole apart perpendicular to the edge of the panel – and no need, therefore, to invoke the closing increment of transverse compression that would be needed if the reactive loads had been of the *same* sign. The effective "width" to be associated with each fastener, for each resolved load component, is $p/\sqrt{2}$, where p is the fastener pitch. The equivalent tensile and compressive stresses at ±45° to the fastener seam are numerically equal to the remote shear stress, per a Mohr-circle assessment of the stresses.

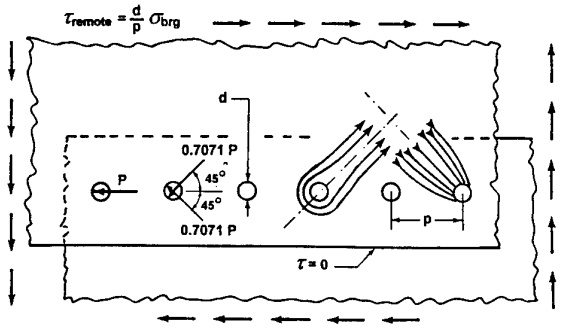


FIG. 10 JOINT GEOMETRY FOR IN-PLANE-SHEAR LOADED SPLICE

The critical location around the bolt hole, for tension-through-the-hole failures, is inclined at 45° to the edge of the panel, where the peak hoop-tension load interacts with the compression bearing stress from the other load component. The effective net section for the tensile loads is $[(p/\sqrt{2}) - d]$, on which the elastic stress concentration factor k_{te} can be approximated as $(p/d\sqrt{2})$, equivalent to the approximation w/d cited in Figure 22 of Ref. 15.

[Actually, provided that the edge distance e is sufficiently long, i.e. $e \geq w$, Equation (12) in Ref. 2 for a narrow strip isolated from a wide panel can be replaced by the much simpler expression for the net-section stress concentration,

$$k_{te} = \frac{p}{d} \quad . \tag{25}$$

Later work might provide a correction term for the higher stresses caused by short edge-distances, equivalent to that included in Ref. 2. Likewise, a new simpler formula is proposed here to replace Equation (11) in Ref. 2, for bypass loads. The stress concentration factor on the net section for a narrow strip isolated from a wide panel with many equally spaced holes can be given by

$$k_{te} = 1 + 2\left(1 - \frac{d}{p}\right)^{1.5} \tag{26}$$

The origin of this new formula, presented here for the first time, is that it is similar in form to Heywood's equation for finite-width strips, Ref. 16,

$$k_{te} = 2 + 1\left(1 - \frac{d}{w}\right)^3 \quad , \tag{27}$$

with different limiting values as the hole diameter approaches either the strip width or hole pitch, but precisely the same slope for proportionally very small holes, so that the two expressions coalesce as $d \to 0$.

Equations (1), (2), (5), and (9) in Ref. 2 are not superseded by these new formulae. Neither are any of the equations derived from them. The new Equations (25) and (26) proposed here replace Equations (11) and (12) in Ref. 2, along with solutions derived from them. The results will be numerically equivalent; the new equations are just far easier to work with. A separate article will be prepared in which joint efficiency charts equivalent to Figure 26 in Ref. 2 will be established for the new formulae.]

If the average shear stress in the skin is τ and the bolt pitch is p, the average bearing stress on each fastener of diameter d is

$$\sigma_{brg} = \frac{p}{d}\tau \tag{28}$$

where, here, the entire shear flow is reacted by bearing on the single row of fasteners. The peak elastic hoop-tension stress induced by the resolved component of the bearing load would then be

$$\sigma_{\text{hoop tension}} = \frac{\sigma_{brg}}{\sqrt{2}} \times \left(\frac{d}{\left(p/\sqrt{2}\right) - d}\right) \times \frac{\left(p/\sqrt{2}\right)}{d} = \frac{\sigma_{brg}/\sqrt{2}}{\left[1 - \sqrt{2(d/p)}\right]} \tag{29}$$

The orthogonal bearing stress, from the other resolved component of the total bearing load would be

$$\sigma_{\text{radial compression}} = \frac{\sigma_{brg}}{\sqrt{2}} \tag{30}$$

which, being the same whether arrived at as the actual local bearing stress or the peak of the resolved component, needs no correction because of errors in the distribution of the resolved bearing stresses. (This perfect match would not be achieved at some other orientations, as explained in Figure 3. For instance, the bearing stresses predicted by superposition at right angles to the true bearing axis would differ appreciably from the nominally zero value it should be. Even if the hoop stresses are formulated as the superposition of two components, use of the real bearing stress distribution would always be more reliable than the combination of resolved components.)

It remains to convert these to equivalent stress increments in the fibrous composite laminate and to interact them in the manner of Equation (7). The stress concentration factor in Equation (20) is reduced in accordance with Equation (2) to become

$$k_{tc} = 1 + C\left(k_{te} - 1\right) = 1 + \frac{1}{4}\left(\frac{p}{d\sqrt{2}} - 1\right) \tag{31}$$

[As indicated earlier, attention is focussed here on 0.25-inch (6.35 mm) holes in quasi-isotropic carbon-epoxy laminates.] Hence, the effective peak hoop-tension stress in the laminate is

$$\sigma_{t,c} = \frac{\sigma_{brg}}{4\sqrt{2}} \frac{\left(3 + \frac{p}{d\sqrt{2}}\right)}{\left(\frac{p}{d\sqrt{2}} - 1\right)} \quad . \tag{32}$$

The associated effective peak radial stress is

$$\sigma_{c,c} = -\frac{K\sigma_{brg}}{\sqrt{2}} \quad , \tag{33}$$

where K is defined in Equation (10), so that the absence of failure of the laminate by tension through the bolt hole requires that

$$\frac{\sigma_{brg}}{\sqrt{2}}\left[\frac{1}{4}\frac{\left(3 + \left(p/d\sqrt{2}\right)\right)}{\left(\left(p/d\sqrt{2}\right) - 1\right)} + K\right] \le F_{tu} \quad , \quad \left(\sigma_{brg} \le F_{brg}\right) \quad , \tag{34}$$

where, for a quasi-isotropic carbon-epoxy laminate, K is taken to be 0.3265, as indicated earlier. The usual bearing-stress cut-off applies. The corresponding remote shear stress cannot exceed

$$\tau = \frac{d}{p}\sigma_{brg} \le F_{tu} \Bigg/ \left\{\frac{1}{2\sqrt{2}}\left(\frac{p}{d}\right)\left[\frac{\left(3\sqrt{2} + p/d\right)}{\left(p/d - \sqrt{2}\right)} + 0.653\right]\right\} \tag{35}$$

The maximum gross-section shear stress sustainable can be shown to occur when

$$\left(\frac{p}{d}\right)_{opt} = \sqrt{2} + \sqrt{2 + \frac{6 - 4K}{1 + 2K}} = 3.6141 \quad , \tag{36}$$

which is remarkably similar to the optimum proportion of exactly

$$\left(\frac{w}{d}\right)_{opt} = 3 \tag{37}$$

which can be derived using the same logic, and Equation (25) for a single-row bolted joint loaded by tension rather than by in-plane shear. These solutions are obtained by differentiating the denominator of Equation (35), and its equivalent for the tensile remote loads, with respect to (d/p). (Note that both of these solutions are for carbon-epoxy materials like AS4/3501-6 and would be expected to be different for glass-fibre-reinforced polymers, for example, or for other composite materials. Indeed, it is not clear that a stationary value exists at the strongest bolted joints in fibreglass laminates; in many such cases the joint is equally critical in tension and bearing.)

If d/p is small, as when the fasteners are far apart, Equation (34) reduces to

$$\left(0.7071 \times C \times \sigma_{brg}\right) + \left(0.7071 \times K \times \sigma_{brg}\right) \le F_{tu} \quad . \tag{38}$$

These stress-concentration factors make no account of short-edge-distance effects and there would still need to be the customary bearing-failure cut-off

$$\sigma_{brg} \le F_{brg} \tag{39}$$

Tensile failure of the laminate would thus be predicted to occur when

$$\sigma_{brg} = \frac{F_{tu}}{0.7071(C+K)} = 2.4570\, F_{tu} \tag{40}$$

for a quasi-isotropic carbon-epoxy laminate. Since Equation (40) would *not* be satisfied *before* Equation (39), tensile failures would *not* be predicted to occur for this situation; instead, the bearing failures typical of a loaded fastener in the middle of an infinite plate would prevail. As a point of comparison, the corresponding factor for predicted tensile failures reacted by a direct tension load rather than by in-plane shear, Equation (11) predicts almost the *identical* strength, with a coefficient of 2.3447.

8. ANALYSIS OF SHEAR-LOADED MULTI-ROW BOLTED COMPOSITE JOINTS

This same analysis is easily modified to account for linear interactions with a shear flow passing around this seam of fasteners as one row of a multi-row joint. This bypass load would not be associated with any bearing stresses and would have a linearly elastic stress-concentration factor of +4.0 at the same critical location, for widely separated holes. For holes which are close enough for there to be a significant difference between the gross and net sections, this factor would be applied to the net-section stress. For holes which are almost touching, the ligament between the holes would bend severely under in-plane shear loads, making it most unlikely that the stress concentration factor would asymptote to 1 as it does for tensile loads. In the absence of any better data, it is assumed here that, for practical pitch-to-diameter ratios, the net-section stress concentration factor will remain at 4.

Tension-through-the-hole failure of the laminate would be predicted to occur when

$$\left[(1+3C)\tau_{bypass} + \frac{\sigma_{brg}}{\sqrt{2}}\left(\frac{1}{\left(\frac{p}{d\sqrt{2}}-1\right)}+C\right)\right] + \left[\frac{\sigma_{brg}}{\sqrt{2}} \times K\right] = F_{tu} \tag{41}$$

where τ_{bypass} is the *net*-section shear stress. The *total* remote in-plane shear load is equal to the sum of this bypass stress, corrected for the hole-out factor, and (d/p) times the bearing stress.

$$\tau_{total} = \left(1-\frac{d}{p}\right)\tau_{bypass} + \left(\frac{d}{p}\right)\sigma_{bearing} \tag{42}$$

Here, the total shear flow refers to the gross section.

The maximum operating *remote* (total) shear stress can be established by eliminating the bypass stress between Equations (41) and (42), to yield the following strength to be optimized in terms of the (p/d) and (σ_{brg}/F_{brg}) ratios in exactly the same manner as was done in Figure (26) of Ref. 2 for tensile loads on multi-row joints. The relevant equation here is

$$\tau_{total} \le \left(\frac{1-\frac{d}{p}}{1+3C}\right)F_{tu} - \left[\left(\frac{1-\frac{d}{p}}{1+3C}\right)\left(\frac{1}{\left(\frac{p}{d}-\sqrt{2}\right)}+C+K\right)-\frac{d}{p}\right]\sigma_{brg} \tag{43}$$

which is subject to two cut-offs. The total shear flow obviously cannot be less than the load carried by bearing, and the bearing stress cannot exceed the bearing strength. Thus, Equation (43) needs to evaluated in conjunction with the following constraints.

$$\sigma_{brg} \le F_{brg} \quad , \quad \tau_{total} \ge \frac{d}{p}\sigma_{brg} \tag{44}$$

Equations (43) and (44) are plotted in Figure 11, using the same material properties as in earlier examples for 0.25-inch (6.35 mm) holes in quasi-isotropic carbon-epoxy laminates, to characterize the bearing/bypass curves for this new class of problems.

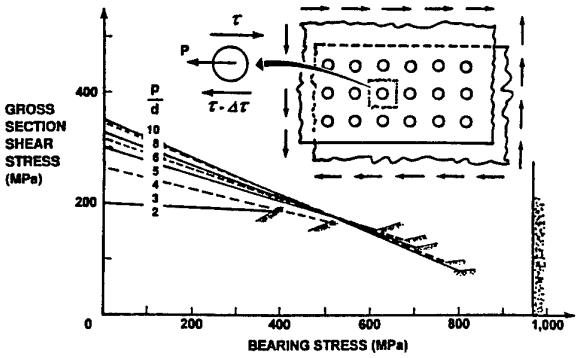


FIG. 11 BEARING/BYPASS INTERACTION FOR IN-PLANE SHEAR LOADS IN A MULTI-ROW SPLICE JOINT

A separate straight line is established for each particular (p/d) ratio, just as was shown in Ref. 17 for tensile loading. The reason why none of the lines extend to the bearing-stress cut-off, the first half of Equation (44), is the minimum strength specified by the second half of the same equation. The minimum-strength requirement is manifest as the series of radial cut-offs in Figure 11. Multi-row joints in carbon-epoxy laminates are usually more critical in tension than in bearing. Figure 11 has similar features to those in Figure 4 of Ref. 17. There is a powerful loss of strength with increasing bearing stress, and only a mild influence of the (p/d) ratio throughout the range of practical interest. Figure 11 contains the same important message as equivalent analyses of multi-row bolted joints loaded in tension have already established. This is that, at the most critical row of fasteners in the joint, it is necessary to minimize the bearing stress while keeping the fasteners far apart. These are normally mutually exclusive objectives. Satisfying these goals requires careful tailoring of the member thicknesses and fastener diameter at each station in such a way as to minimize the load transferred through the fasteners at the

most critical row in each skin, even if it requires a heavier-than-normal splice plate to do so. (Future work will include joint efficiency charts to more completely establish the influence of joint geometry, particularly in multi-row joints.)

9. CONCLUDING REMARKS

While these new analyses have yet to be confirmed by experiment, there can be little doubt that linear bearing/bypass curves could be generated for these non-classical joint geometries also.

The use of a generalized maximum-shear-stress failure criterion, or the similar truncated maximum-strain failure model, for carbon-epoxy laminates results in a predicted substantial interaction whenever the peak tension hoop stresses coincide with appreciable radial bearing stresses. This interaction would be far milder for fibre-glass-reinforced laminates, for which the original maximum-strain failure model is more appropriate because most of the transverse strain occurs in the matrix, even though it would be slightly unconservative for this class of problems.

The linearity of the previous bearing/bypass analyses for multi-row joints has involved contributions only to longitudinal fibre stresses, from two sources, in the virtual absence of any transverse stresses at that site alongside the bolt. The linear interaction in the new analyses here involves a combination of longitudinal (hoop) and transverse (bearing) stresses in the fibres. The new predicted interactions are linear *only* because of the form of composite failure criterion used here. They would not be predicted to be linear for tensor-polynomial interaction curves, for example.

The characteristic form of these new bearing/bypass interactions suggests that, if experiments were run to confirm or refine these formulae, and particularly the stress-concentration formulae and relief factors for the bearing stresses, the results could be adapted to the existing nonlinear A4EJ multi-row bolted-joint computer code.

The successful adaptation in Ref. 17 of the earlier standard bolted composite joint analysis methods for consideration of fatigue in metallic structures, particularly concerning the importance of restricting the bearing stresses and optimum *w/d* ratios, suggests that if these new analyses are validated, they should likewise be extended to metallic structures. The new formulae presented for the elastic stress concentration factors for wide panels with many equally spaced fasteners, as contrasted with the slightly different ones better suited to single-hole test coupons, could also be integrated into this prior work on bolted or rivetted metallic joints.

10. REFERENCES

1. Hart-Smith, L. J., "Bolted Joints in Graphite-Epoxy Laminates", NASA Langley Contract Report NASA CR-144899, January 1977.

2. Hart-Smith, L. J., "Mechanically-Fastened Joints for Advanced Composites – Phenomenological Considerations and Simple Analyses", Douglas Aircraft Company Paper 6748A, presented to Fourth Conference on Fibrous Composites in Structural Design, San Diego, California, November 14-17, 1978; in Proceedings, *Fibrous Composites in Structural Design*, edited by E. M. Lenoe, D. W. Oplinger, and J. J. Burke, Plenum Press, New York, 1980, pp. 543-574.

3 Garbo, S. P. and Ogonowski, J. M., "Effect of Variances and Manufacturing Tolerances on the Design Strength and Life of Mechanically Fastened Composite Joints," McDonnell Aircraft Company, USAF Contract Report, AFWAL-TR-81-3041, Vol.'s 1 to 3, April 1981.

4. Garbo, S. P., "Effects of Bearing/Bypass Load Interaction on Laminate Strength, McDonnell Aircraft Company, USAF Contract Report, AFWAL-TR-81-3144, September 1981.

5. Oplinger, D. W., "On the Structural Behavior of Mechanically Fastened Joints in Composite Structures", presented to Fourth Conference on Fibrous Composites in Structural Design, San Diego, California, November 14-17, 1978; in Proceedings, *Fibrous Composites in Structural Design*, edited by E. M. Lenoe, D. W. Oplinger, and J. J. Burke, Plenum Press, New York, 1980, pp. 575-602.

6. Hart-Smith, L. J., "Design Methodology for Bonded-Bolted Composite Joints", USAF Contract Report AFWAL-TR-81-3154, 2 Vol.'s, February 1982.

7. Nelson, W. D., Bunin, B. L., and Hart-Smith, L. J., "Critical Joints in Large Composite Aircraft Structure", Douglas Aircraft Company Paper 7266, presented to Sixth Conference on Fibrous Composites in Structural Design, New Orleans, Louisiana, January 24-27, 1983; in Proceedings, AMMRC MS 83-2, pp. II-1 to II-38; NASA CR 3710, August 1983.

8. Hart-Smith, L. J., "Bolted Composite Joints with Orthogonal Load Components", Douglas Aircraft Company, IRAD Report MDC-J2907, October 1983.

9. Eisenmann, J. R., "Bolted Joint Static Strength Model for Composite Materials", presented to Third Conference on Fibrous Composites in Flight Vehicle Design, Williamsburg, Virginia, November 4-6, 1975, in Proceedings, NASA TM-X 3377, pp. 563-602.

10. Crews, J. H. and Naik, R. A., "Combined Bearing and Bypass Loading on a Graphite/Epoxy Laminate", *Composite Structures*, Vol. 6, 1986, pp. 21-40.

11. Hart-Smith, L. J., "The Effect of Hole Size on the Strength of Cross-Plied Composite Laminates", Douglas Aircraft Company, IRAD Report MDC-K0338, November 1986.

12. Hart-Smith, L. J., "Predictions of a Generalized Maximum-Shear-Stress Failure Criterion for Certain Fibrous Composite Laminates", Douglas Aircraft Company, Technical Paper submitted to *Composites Science and Technology*.

13. Bickley, W. G., "The Distribution of Stress Round a Circular Hole in a Plate", Philosophical Transactions of the Royal Society (London), Series A, Vol. 227, 1928, pp. 383-415.

14. Hart-Smith, L. J., "The Truncated Maximum-Strain Composite Failure Model", *Composites*, Vol. 24, No. 7, 1993, pp. 587-591.

15. Hart-Smith, L. J., "Design and Analysis of Bolted and Riveted Joints in Fibrous Composite Structures", Douglas Paper 7739, presented to International Symposium on Joining and Repair of Fibre-Reinforced Plastics, Imperial College, London, September 10-11, 1986; published in *Joining Fibre-Reinforced Plastics*, edited by F. L. Matthews, Elsevier Applied Science, England, 1987, pp. 227-269.

16. Heywood, R. B., *Designing By Photelasticity*, Chapman and Hall, London, p. 268, 1952.

17. Hart-Smith, L. J., "Easily Assembled Structurally Efficient Joints in Metallic Aircraft Structures", McDonnell Douglas Paper MDC 94K0031, presented to 18th ICAF Symposium in Melbourne, Australia, May 1-5, 1995; in Proceedings, *Estimation, Enhancement and Control of Aircraft Fatigue Performance,* EMAS, Cradley Heath, England, 1995, Vol. I, pp. 331-352.

Stress and Failure Analysis of Bonded Composite-to-Metal Joints

Y. Xiong and D. Raizenne
Structures, Materials and Propulsion Laboratory
Institute for Aerospace Research
National Research Council Canada
Ottawa, Canada K1A 0R6

SUMMARY

The behavior of bonded composite-to-metal joints is examined based on the results of stress analysis and failure prediction using a quasi two-dimensional analytical model. Two joint configurations are considered which simulate the problems of bonded composite patch repair such as fatigue enhancement and crack patching. The metallic substrate is of uniform thickness, while the composite patch has a tapered region at its edges. Several typical failure modes associated with the adherends and adhesive are considered including substrate yielding, adhesive shearing, interface peeling, patch fiber breaking, patch ply shearing, and patch ply peeling. The effects of the thermal residual stresses after curing on the load transfer between the adherends are discussed. Various geometric configurations are examined from an optimal design point of view.

LIST OF SYMBOLS

b	half length of bonded joint
C_1, C_2	undetermined constants in solutions
e	tapered distance of bonded joint
E_p	longitudinal elastic modulus of patch fibers
E_s	Young's modulus of isotropic substrate
G_{a_*}	shear modulus of adhesive
G_a^*	equivalent shear modulus of adhesive
K_f	knockdown factor for patch matrix properties
p_{zp}	peel stress on patch-adhesive interface
$\bar{p}_{zp}$	peeling strength of patch-adhesive interface
p_{zs}	peel stress on substrate-adhesive interface
$\bar{p}_{zs}$	peeling strength of substrate-adhesive interface
S_m^k	safety margin of the k-th failure mode
S_{p_*}	shear strength of patch matrix
S_p^*	knockdowned shear strength of patch matrix
t_a	thickness of adhesive (uniform)
t_e	edge thickness of patch
T_o	far field stress resultant in substrate
T_o^F	failure load of joint
T_o^{AS}	failure load of joint in adhesive shearing
T_o^{PA}	failure load of joint in patch-adhesive peeling
T_o^{PFC}	failure load of joint in patch fiber compression
T_o^{PFT}	failure load of joint in patch fiber tension
T_o^{PP}	failure load of joint in patch interlaminar peeling
T_o^{PS}	failure load of joint in patch interlaminar shearing
T_o^{SA}	failure load of joint in substrate-adhesive peeling
T_o^{SY}	failure load of joint in substrate yielding
t_p	full thickness of patch
T_p	stress resultant in patch
t_s	thickness of substrate (uniform)
T_s	stress resultant in substrate
U_s	shear strain energy of adhesive
X_p	tensile strength of patch ply in fiber direction
X'_p	compressive strength of patch ply in fiber direction
Y_{p_*}	tensile strength of patch ply in transverse direction
Y_p^*	knockdowned tensile strength of patch ply in transverse direction
y	axial coordinate of joint
z	transverse coordinate of joint
α	patch tapered angle
α_p	thermal coefficient of patch
α_s	thermal coefficient of substrate
β	stiffness ratio parameter
ΔT	temperature difference between operation and curing conditions
η	thermal effect parameter
γ_e	maximum elastic strain of adhesive
γ_{max}	maximum failure strain of adhesive
$\bar{\sigma}_k$	maximum stress of the k-th failure mode
$\sigma^k_{\max}$	strength allowable of the k-th failure mode
σ_s^y	yield stress of substrate
σ_{yp}	axial stress in patch
σ_{ys}	axial stress in substrate
σ_{zp}	transverse normal stress in patch
σ_{zs}	transverse normal stress in substrate
τ_a	shear stress in adhesive
$\bar{\tau}_a$	shear strength of adhesive
τ^*_{max}	equivalent maximum shear strength of adhesive
τ_{xyp}	shear stress in patch
τ_{xys}	shear stress in substrate

1. INTRODUCTION

Bonded composite patch repair is a developing technology that has been used in the aerospace industry for the purpose of enhancing the fatigue resistance of structure and restoring the stiffness and strength of damaged/cracked structure, see, e.g., [1~3]. In the application of this technology to aircraft structures, the design and analysis of bonded patch repair are important steps [4]. Two phases are involved in the analysis of a patch repair. One is the global stress analysis which determines the effect of the bonded patch on the global stress redistribution. This is usually done by finite element methods for complex geometries and by analytical modeling such as the hard inclusion analogy [5] for simple geometries. The effectiveness of the patch on reducing the stress intensity or concentration factor in a cracked or damaged substrate is also examined in this phase of the work [6]. The other phase is the local stress and failure analysis of the joint focusing on the

Paper presented at the 83rd Meeting of the AGARD SMP on "Bolted/Bonded Joints in Polymeric Composites", held in Florence, Italy, 2-3 September 1996, and published in CP-590.

behavior of the bondline. This latter phase is the subject of the present paper.

The objective of the present work is to develop an efficient analytical model for the stress analysis and failure prediction of bonded composite-to-metal joints. The problems under consideration simulate such bonded composite patch repairs as fatigue enhancement and crack patching [4]. The model must be capable of dealing with patch thickness tapering, mechanical and thermal stresses, and various joint failure modes associated with the patch and adhesive. Emphasis is placed on ease of use in a PC environment.

Bonded composite joint analysis has been studied quite extensively and capabilities exist from simple analytical models to complex 3D finite element methods. The main advantages of analytical approaches, due to various assumptions, include the efficiency and the avoidance of the stress singularities at the bi-material interfaces so that consistent results can be obtained, see the original work of Goland and Reissner [7]. The efficiency of analysis is very important in the stage of preliminary design. In contrast, numerical procedures such as finite element methods [8, 9], although capable of dealing with various material and geometry effects on the joint performance, are not ideal for parametric studies or design optimization iterations, particularly in a PC environment, because of the requirement for extensive labor and computing time. In addition, numerical difficulties may arise when modeling the thin layer of adhesive because of the high aspect ratios of elements and the stress singularities at the bi-material interfaces may cause inconsistent results from models of various meshes.

In 1970's and 80's, Hart-Smith proposed a series of analytical approaches to deal with various material behavior and geometry configurations of bonded joints [10~15]. The work by Hart-Smith based on closed-form solutions and the associated PC software A4EI [16] have been widely used in the aerospace industry. The program A4EI predicts load transfer between adherends and adhesive and shear failure strength. Elastic-plastic behavior of the adhesive has been taken into account. However it does not consider the interface peeling between adherends and adhesive and within the composite adherend. In addition, the data input phase for A4EI involves many manual calculations which is inconvenient, particularly for joints with a tapered thickness.

Two dimensional stress analysis approaches have been proposed by Allman [17], Chen and Cheng [18], and by Adams and Mallick [19] for single- or double-lap bonded joints without tapered thickness. These two dimensional models have good accuracy in stress calculations including the effects of bending, stretching, shearing and peeling but they are cumbersome in theoretical derivations and thus in computer implementations. The effects of different assumptions in several analytical approaches were discussed by Carpenter [20].

A quasi two dimensional model has recently been developed at the Institute for Aerospace Research [21]. The conventional 1D beam model is employed for calculating the load transfer between the substrate and the patch via the adhesive. After the axial normal stresses in the adherends and the shear stress in the adhesive are calculated, a general two dimensional stress state is considered for both the substrate and the patch. By solving the two dimensional equilibrium equations and using appropriate boundary conditions, the transverse stresses in the substrate and patch as well as the peel stresses on the interfaces are determined. With these stress results and appropriate material strength allowables, the joint failure load is predicted. Safety margins are determined for eight typical failure modes which are substrate yielding, patch fiber breaking in tension, fiber failing in compression, adhesive shearing, substrate-adhesive peeling, patch-adhesive peeling, patch interlaminar peeling, and patch interlaminar shearing.

In the discussion below, the joint configuration and assumptions are first described. A brief outline of the quasi-2D analysis model is given. Case studies and parametric studies are conducted and some conclusions are made.

2. JOINT CONFIGURATION AND ASSUMPTIONS

The problems under consideration originate from the bonded composite patch repair of a metallic substrate for fatigue enhancement and crack patching. For the stress analysis along the bondline, a strip of the bonded region with unit width is considered, as shown in Figure 1, which is under a far field tensile or compressive load, T_o. The joint is single-lap in configuration, symmetric with respect to the mid-span and the bonded region consists of both tapered and un-tapered portions. The distinction between fatigue enhancement and crack patch is shown in Figure 1 by a vertical dashed line at the mid-span of the substrate which demonstrates a central crack in the case of crack patching.

The half length of the bonded region is b and the distance for the tapered portion is e. The substrate is of uniform thickness t_s, while the patch has a tapered thickness specified by t_p and t_e. The thickness of the adhesive is t_a. The patch tapering is also characterized by the taper angle α.

To simplify the problem, the following assumptions are made: (i) the materials of all joint members are linearly elastic; (ii) the patch fibers are uni-directional along the loading direction; (iii) the patch and substrate are perfectly bonded together; (iv) the adhesive layer is so thin that the shear stress is constant through the thickness; and (v) the secondary bending due to load eccentricity is ignored. The impact of these assumptions is discussed in later sections.

3. QUASI-2D ANALYTICAL MODEL

3.1 Half of Joint Model

Because of the symmetry, only half of the joint needs to be modeled. The applied load and stress resultants acting on this half model are shown in Figure 2. For fatigue enhancement the stress resultants, which are functions of coordinate y, will be dependent of the stiffness ratio between the substrate and patch. To determine these stress resultants, the symmetry conditions are used which are written as:

$$\begin{aligned} T_p(y) &= T_p(-y) \\ T_s(y) &= T_s(-y) \quad 0 \le y \le b \end{aligned} \tag{1}$$

where T_s and T_p are the stress resultants in the substrate and patch, respectively. For crack patching these stress resultants are readily determined as:

$$T_p(0)=T_o, \qquad T_s(0)=0 \tag{2}$$

Because of the tapered patch thickness, the bonded region is divided into n segments, as shown in Figure 3. In each of these segments, the patch thickness is assumed to be uniform, denoted by t_{pi}, in order to derive closed-form solutions. For accurate computations, a relatively small length is used for the segments close to the edges and the juncture between the tapered and un-tapered portions

3.2 Axial Forces and Shear Stress

Consider the load transfer from the substrate to the patch via the adhesive. The conventional one dimensional model is employed which simulates the adherends as one dimensional beams and assumes uniform axial stresses in the cross sections. The axial normal stress in the adhesive is ignored. Solving the differential equations established for the i-th segment, closed-form solutions are obtained for the axial stress resultants in the patch and substrate, respectively, as:

$$T_p^i(y)=C_1^i \operatorname{Sinh}(\beta_i y)+C_2^i \operatorname{Cosh}(\beta_i y)+\eta \tag{3}$$

$$T_s^i(y)=T_o-C_1^i \operatorname{Sinh}(\beta_i y)-C_2^i \operatorname{Cosh}(\beta_i y)-\eta \tag{4}$$

and for the shear stress in the adhesive as:

$$\tau_a^i(y)=\beta_i [C_1^i \operatorname{Cosh}(\beta_i y)+C_2^i \operatorname{Sinh}(\beta_i y)] \tag{5}$$

where

$$\beta_i^2=\frac{G_a}{t_a}\left(\frac{1}{E_s t_s}+\frac{1}{E_p t_{pi}}\right)$$
$$\eta=\frac{T_o}{E_s t_s}-(\alpha_s-\alpha_p)\Delta T \tag{6}$$

and E_s and t_s denote the Young's modulus and thickness of the substrate, E_p and t_p are the elastic modulus in the fiber direction and the thickness of the patch, respectively, G_a is the shear modulus of adhesive, α_s and α_p are the thermal coefficients of the substrate and patch, respectively, and ΔT is the temperature difference between the operating and curing conditions.

The two constants in Eqs (3~5), C_1^i and C_2^i, are to be determined by the boundary conditions at the ends of the segment. For a division of n segments, there are $2n$ constants to be determined. Using the boundary conditions at the two ends of the joint and the continuity conditions at the junctures of segments, a recurrence process is established, see Ref. [21] for details.

3.3 Transverse Stresses in Patch and Peel Stresses

Consider now the transverse stresses in the substrate and patch. The major concerns are the peel stresses on the substrate-adhesive and patch-adhesive interfaces and the transverse stresses in the patch. Consider the substrate first. Assume a general 2D stress state which satisfies the following equilibrium equations:

$$\frac{\partial \sigma_{ys}^i}{\partial y}+\frac{\partial \tau_{xys}^i}{\partial z}=0, \qquad \frac{\partial \tau_{xys}^i}{\partial y}+\frac{\partial \sigma_{zs}^i}{\partial z}=0 \tag{7}$$
$$(0\le y\le y_i,\ 0\le z\le t_s)$$

where τ_{ysx}^i and σ_{zs}^i are transverse shear and normal stresses in the substrate, respectively.

Integrating Eqs. (7) with respect to z and satisfying the condition that τ_{ysx}^i and σ_{zs}^i vanish at the bottom face (z = 0) of the substrate, the transverse shear and normal stresses in the substrate are obtained as:

$$\tau_{yzs}^i(y,z)=\frac{z\beta_i}{t_s}[C_1^i \operatorname{Cosh}(\beta_i y)+C_2^i \operatorname{Sinh}(\beta_i y)] \tag{8}$$
$$0\le z\le t_s$$

$$\sigma_{zs}^i(y,z)=-\frac{z^2\beta_i^2}{2t_s}[C_1^i \operatorname{Sinh}(\beta_i y)+C_2^i \operatorname{Cosh}(\beta_i y)] \tag{9}$$
$$0\le z\le t_s$$

It is seen that the shear stress on the top face of the substrate is identical to that in the adhesive, see Eq. (5). The peel stress on the substrate-adhesive interface is readily obtained from Eq. (9) as:

$$p_{zs}^i(y)=-\frac{t_s\beta_i^2}{2}[C_1^i \operatorname{Sinh}(\beta_i y)+C_2^i \operatorname{Cosh}(\beta_i y)] \tag{10}$$

In a similar procedure, the transverse shear and normal stresses in the patch are derived as:

$$\tau_{yzp}^i(y,z)=\frac{(t_{pi}-z)\beta_i}{t_{pi}}[C_1^i \operatorname{Cosh}(\beta_i y)+C_2^i \operatorname{Sinh}(\beta_i y)],$$
$$0\le z\le t_{pi} \tag{11}$$

$$\sigma_{zp}^i(y,z)=\frac{(z-t_{pi})^2\beta_i^2}{2t_{pi}}[C_1^i \operatorname{Sinh}(\beta_i y)+C_2^i \operatorname{Cosh}(\beta_i y)],$$
$$0\le z\le t_{pi} \tag{12}$$

These stresses satisfy the vanishing conditions on the top face of the patch. Also the shear stress on the bottom face of the patch is identical to that in the adhesive, see Eq. (5). On the same face, the transverse normal stress in the patch is the same as the peel stress on the patch-adhesive interface which is obtained as:

$$p_{zp}^i(y)=\frac{t_{pi}\beta_i^2}{2}[C_1^i \operatorname{Sinh}(\beta_i y)+C_2^i \operatorname{Cosh}(\beta_i y)] \tag{13}$$

Note the difference in the peel stresses on the two interfaces due to the adhesive shear stress. That is the peeling failure of a bonded joint under load can be either substrate-adhesive or patch-adhesive separation. Eqs. (3~5, 8~13) are the analytical solutions for a representative segment. Running through i = 1, 2, ..., n, the solutions for the whole bonded region are obtained.

3.4 Failure Loads and Modes

With the stress solutions at hand, the failure load of the bonded joint can now be predicted against the strength allowables of the joint member materials. Since the quasi-2D model developed is capable of calculating all stress components of concern, eight different failure modes are considered. Associated with these failure modes is the margin of safety which is defined as:

$$S_m^k = 1 - \frac{\sigma_{\max}^k}{\bar{\sigma}^k} \tag{14}$$

where $\sigma_{\max}^k$ and $\bar{\sigma}^k$ are the maximum stress and the strength allowable, respectively, corresponding to the k-th failure mode. The value of S_m^k represents the degree of safety of the joint under the applied load. A negative value of S_m^k indicates that the joint has exceeded the strength allowable and has therefore "failed".

For the purpose of convenience, the failure prediction in the present discussion is constrained to the cases with applied load T_o alone. The failure load of the joint to be predicted is the maximum applied load $(T_o)_{\max}$ that the joint can carry without failure. The eight failure modes are examined below:

(i) substrate yielding when the maximum axial normal stress in substrate exceeds its yielding strength σ_s^y:

$$(\sigma_{ys}^i)_{\max} = \sigma_s^y \;\Rightarrow\; T_o^{SY} = \frac{\sigma_s^y}{(\sigma_{ys}^i)_{\max}/T_o} \tag{15}$$

(ii) patch fiber breaking in tension when the axial normal stress in patch is in tension and exceeds the tensile strength of a ply in the fiber direction X_p:

$$(\sigma_{yp}^i)_{\max} = X_p \;\Rightarrow\; T_o^{PFT} = \frac{X_p}{(\sigma_{yp}^i)_{\max}/T_o} \tag{16}$$

(iii) patch fiber failing in compression when the axial normal stress in the patch is in compression and exceeds the compressive strength of a ply in the fiber direction X'_p:

$$(\sigma_{yp}^i)_{\max} = X'_p \;\Rightarrow\; T_o^{PFC} = \frac{X'_p}{(\sigma_{yp}^i)_{\max}/T_o} \tag{17}$$

(iv) adhesive shearing when the shear stress in the adhesive exceeds its shear strength $\bar{\tau}_a$:

$$(\tau_a^i)_{\max} = \bar{\tau}_a \;\Rightarrow\; T_o^{AS} = \frac{\bar{\tau}_a}{(\tau_a^i)_{\max}/T_o} \tag{18}$$

(v) substrate-adhesive interface peeling when the peel stress on this interface exceeds the corresponding peeling strength $\bar{p}_{zs}$:

$$(p_{zs}^i)_{\max} = \bar{p}_{zs} \;\Rightarrow\; T_o^{SA} = \frac{\bar{p}_{zs}}{(p_{zs}^i)_{\max}/T_o} \tag{19}$$

(vi) patch-adhesive peeling when the peel stress on this interface exceeds the corresponding peeling strength $\bar{p}_{zp}$:

$$(p_{zp}^i)_{\max} = \bar{p}_{zp} \;\Rightarrow\; T_o^{PA} = \frac{\bar{p}_{zp}}{(p_{zp}^i)_{\max}/T_o} \tag{20}$$

(vii) patch interlaminar peeling when the transverse normal stress in a patch ply is in tension and exceeds the matrix tensile strength of a ply Y_p:

$$(\sigma_{zp}^i)_{\max} = Y_p \;\Rightarrow\; T_o^{PP} = \frac{Y_p}{(\sigma_{zp}^i)_{\max}/T_o} \tag{21}$$

(viii) patch interlaminar shearing when the shear stress in a patch ply exceeds the matrix shear strength of a ply S_p:

$$(\tau_{yzp}^i)_{\max} = S_p \;\Rightarrow\; T_o^{PS} = \frac{S_p}{(\tau_{yzp}^i)_{\max}/T_o} \tag{22}$$

The actual joint failure load and mode are determined by the minimum of the values from Eqs. (15~22), that is:

$$T_o^F = \text{Min}\{T_o^{SY}, T_o^{PFT}, T_o^{PFC}, T_o^{AS}, T_o^{SA}, T_o^{PA}, T_o^{PP}, T_o^{PS}\} \tag{23}$$

3.5 Failure Strength Allowables

It is noted that joint failure predictions rely on the strength allowables associated with various failure modes and are affected by many factors. Ideally all the strength allowables should be obtained from test work conducted specifically for the joint materials and configuration under consideration. Unfortunately this kind of test data is not readily available. Most analytical work uses manufacturer suggested values. These values are generated from idealized test specimens and conditions which may be different from those of a joint. Therefore discrepancies occur between analysis and test results. To pursue accurate predictions, some failure criteria need to be modified.

3.5.1 *Equivalent adhesive shear properties*

Adhesive shearing is one of the most common failure modes predicted for a bonded joint. It has been realized that the adhesive shear failure strength predicted by pure elastic analysis is well below the actual failure strength because of the elastic-plastic behavior of the adhesive. To take into account the adhesive plasticity without losing the simplicity of an elastic analysis, a shear failure criterion based on the shear strain energy is employed. Consider an elastic-pure plastic behavior for the adhesive, as shown by line ***OAB*** in Figure 4. The energy criterion states that the adhesive fails when the shear strain reaches its maximum. In this case, the maximum strain energy is the area under line ***OAB*** in Figure 4 which can be written as:

$$U_s = \frac{1}{2} G_a \gamma_e^2 + (\gamma_{\max} - \gamma_e) G_a \gamma_e \tag{24}$$

where γ_e and γ_{max} are the elastic and failure shear strain of the adhesive, respectively. An equivalent elastic behavior is then assumed for the adhesive described by line ***OC*** in Figure 4 with which the adhesive has the same amount of shear strain energy at the failure state. That is the area under line ***OC*** is

equal to that under line *OAB*. Based on this, an effective shear modulus of the adhesive can be derived as:

$$G_a^* = (2 - \frac{\gamma_e}{\gamma_{\max}}) \frac{\gamma_e}{\gamma_{\max}} G_a \qquad (25)$$

and the equivalent maximum failure shear stress is determined as:

$$\tau_{\max}^* = G_a^* \gamma_{\max} \qquad (26)$$

This effective maximum shear stress is used in Eq. (18) for adhesive shear failure mode replacing $\bar{\tau}_a$. Equation (15) is a maximum shear stress criterion, it is now, with this replacement, a maximum strain criterion. It has been realized that for ductile adhesives, the maximum strain criterion gives more accurate predictions than the maximum stress criterion [22].

3.5.2 *Knockdown factor for patch matrix properties*

Great variations exist in the strength allowables of composite patches. For a cocured patch repair, these allowables, particularly for matrix failure, can be reduced by as much as 40% from those in manufacturer's specifications [23]. Therefore a knockdown factor is employed in this work for the matrix tensile and shear strength allowables of the patch, i.e.

$$Y_p^* = K_f Y_p, \qquad S_p^* = K_f S_p \qquad (27)$$

The value of the knockdown factor K_f is to be determined case by case. The factored matrix tensile strength allowable is also used for the interface peeling failure prediction in this paper because the peeling strength allowables are not available.

4. CASE STUDIES

The above analytical approaches for stress analysis and failure prediction of bonded joints have been evaluated through case studies.

4.1 Fatigue Enhancement Under Compression

This is a fatigue enhancement case simulating the test work presented in [23] with a cocured patch. The substrate was Aluminum 7075-T651 with a uniform thickness. The patch was fabricated with 23 plies of uni-directional Textron 5521/4 boron prepreg with a single ply drop-off and a 1.25° taper angle. Two layers of an epoxy nitrile structural adhesive --- Cytec FM73M OST, were used to bond the patch in place. The joint was under an axial compressive stress of -67 *Ksi*. This is equal to the yield strength of the substrate, that is, the substrate under this load will be in a yield state. Since substrate yield is not a catastrophic failure mode, the discussions below will focus on other failure modes associated with the patch and adhesive. The geometry data of the joint are: b = 5.49 *in*, e = 4.49 *in*, t_s = 0.334 *in*, t_a = 0.018 *in*, t_p = 0.1196 *in*, t_e = 0.0052 *in*. Material properties from [23] are listed in Table 1.

The stresses along the bondline calculated using the baseline material properties listed in Table 1 are displayed in Figure 5 and Figure 6, respectively. The most critical location is at or close to the tapered edge where high stress concentrations occur and the possible failure modes are adhesive shearing, patch matrix shearing, and patch fiber failure as well as substrate yielding. The interfacial peeling is not a problem in this case because of the edge tapering. The thermal residual stresses after curing due to the thermal mismatch between the substrate and patch have unfavorable effects on the possible failure modes associated with the patch and adhesive. The effects of the thermal stresses would be reversed if the applied load were in tension, as demonstrated in Figure 7 and Figure 8.

Table 1. Material properties

AL 7075-T651
E_s = 10.6 *Msi*, α_s = 13 *PPM / °F*, Y_s = 67 *Ksi*
Boron 5521/4 (0°)
E_p = 33.4 *Msi*, α_p = 2.5 *PPM / °F*, X_p = 192 *Ksi* X'_p = -282 *Ksi*, Y_p = 8.3 *Ksi*, S_p = 15.3 *Ksi*
FM73 Adhesive
G_a = 51.5 *Ksi*, $\bar{\tau}_a$ = 5.15 *Ksi*, γ_e = 0.1, γ_{max} = 0.6
Effective: G_a^* = 51.5 *Ksi*, $\bar{\tau}_a^*$ = 5.15 *Ksi*,

To examine how the material properties affect the failure behavior of the same joint, stresses are calculated and the safety margins associated with various failure modes are determined. Three material property options are used:

1) the baseline properties,
2) effective adhesive properties without knockdown of the patch properties, and
3) effective adhesive properties with a knockdown factor of 0.6 for the patch properties.

The results are shown in Table 2. It is seen that only the analysis using the material property option 3 predicts matrix shearing in the patch as the dominant failure mode. This agrees with the experimental observations [23] and indicates the necessity of using effective adhesive properties in a simple elastic analysis and knocking down the patch properties. It is also noted in Table 2 that patch fiber failure in compression can be a potential mode since the safety margin of this mode is significantly lower than those of other modes. This is because of the high compressive stress in the patch ply close to the tapered edge, see Figure 5.

Table 2. Safety margins of fatigue enhancement

Failure mode	Material properties		
	option 1	option 2	option 3
substrate yield	0.00	0.00	0.00
adhesive shear	***(-0.96)***	***(0.26)***	0.26
patch-adhesive peel	0.96	0.97	0.95
substrate-adhesive peel	1.00	1.00	1.00
patch matrix peel	0.96	0.97	0.95
patch matrix shear	0.34	0.55	***(0.24)***
patch fiber in tension	1.00	1.00	1.00
patch fiber in compression	0.28	0.40	0.40

4.2 Crack Patching Under Tension

For the same joint materials and geometry configuration, assume a central crack existing in the substrate which is subject to an axial tensile stress of 67 *Ksi*. This is a case called crack patching. The stresses along the bondline calculated

using the baseline material properties are displayed in Figure 9 and Figure 10, respectively. It is seen that in this case, the most critical location is at the crack surface rather than at the tapered edge as in the fatigue enhancement application discussed above because there is no edge tapering at the crack location. The possible failure modes are adhesive shearing, patch matrix shearing, patch fiber failure in tension, patch-adhesive interface peeling, and substrate-adhesive peeling if the substrate yielding is not considered. The thermal residual stresses after curing due to the thermal mismatch between the substrate and patch have mixed effects on the possible failure modes. While the axial stress in the patch and the substrate-adhesive peel stress are reduced due to the thermal mismatch, other stresses are increased.

Similarly the safety margins associated with various failure modes are determined using the three material property options. The results are shown in Table 3. Again, the patch matrix shearing is predicted as the dominant failure mode when the material option 3 is used. Patch fiber failure in tension is predicted as a very possible mode using all the three material options.

Table 3. Safety margins of crack patching

Failure mode	Material properties		
	option 1	option 2	option 3
substrate yield	0.00	0.00	0.00
adhesive shear	***(-2.46)***	***(-0.10)***	-0.10
patch-adhesive peel	0.60	0.81	0.69
substrate-adhesive peel	0.75	0.92	0.87
patch matrix peel	0.60	0.81	0.69
patch matrix shear	-0.16	0.32	***(-0.13)***
patch fiber in tension	0.03	0.03	0.03
patch fiber in compression	1.00	1.00	1.00

5. PARAMETRIC STUDIES

The behavior of a bonded joint is dependent of various parameters related to the materials and geometry configurations. The quasi-2D model can be used for material selection and for parametric studies. This section is devoted to discussions of several parametric studies.

5.1 Effects of Edge Thickness t_e

Consider the case of fatigue enhancement under compression and examine the effects of the edge thickness t_e on the axial stress in the patch and the shear stress in the adhesive. The design variable t_e varies in the range of $0 < t_e < t_p$, while other parameters remain unchanged. The axial stress in the patch and the adhesive shear stress are plotted in Figure 11 and Figure 12, respectively. It is seen that while the maximum axial compressive stress in the patch decreases as the edge thickness becomes larger, the maximum shear stress in the adhesive as well as in the patch increases by a similar percentage. The optimum value of t_e should be determined by considering all stresses of concern. This is discussed below.

5.2 Failure Loads and Modes of Fatigue Enhancement

Parametric studies with respect to the failure loads and modes are conducted by taking the edge thickness t_e and the tapered distance e as the design variables. For convenience of this discussion, thermal stresses have not been considered in calculating the failure loads and determining the modes.
The edge thickness t_e and the tapered distance e vary in the ranges of $0 < t_e < t_p$ and $0.1\,b < e < 0.99\,b$, respectively. The failure loads and modes for the case of fatigue enhancement under compression discussed in 4.1. are determined using the material property option 3 and are shown in Table 4. The numbers in the parenthesis indicate the failure mode as discussed in Section 3.3. The substrate yielding is not included in the results because it is not a catastrophic failure mode as mentioned earlier. It is seen that the joint may fail in patch-adhesive interface peeling when the tapered distance and the edge thickness are small, while the dominant failure mode of the joint in most of the cases is patch matrix shearing. The results are also shown graphically in Figure 13. The failure load increases with the edge thickness when the tapered distance is relatively small (below 20% of the half length of the joint). This trend is reversed when the tapered distance becomes larger than about 20% of the half length of the joint. The highest failure load of 41.6 *k-lb/in* in compression is achieved when the tapered distance e reaches the half length of the joint with the patch thickness tapered down to one ply of fibers at the edge.

A similar parametric study has been conducted for the case of fatigue enhancement with a thinner full patch thickness, i.e., t_p = 12 plies of fibers. The full patch thickness is usually determined by the required degree of enhancement. This study examined the behavior of different patch thicknesses. The predictions of the failure loads and modes are shown in Table 5 and the change trends of the failure load with the tapered distance e and the edge thickness t_e are graphically shown in Figure 14. It is seen that when the tapered distance is small, the failure load is not sensitive as the edge thickness changes, but when the tapered distance is large, a thin edge thickness is required for a strong joint. It is also noted that the highest failure load in this case is 43.9 *k-lb/in* in compression which is larger than that for the above case. This is because less load is transferred from the substrate to the patch via adhesive in a joint with a thinner patch. In general, joint failure load increases with the full patch thickness t_p when it is relatively thin (less than 10 plies in this case), as shown in Figure 15. However when the patch thickness is increased (more than 10 plies in this case), the failure load decreases with t_p. Further increase of the patch thickness will have unfavorable effects from the joint failure point of view. It is also noted in Figure 15 that the tapered angle α, which gives the maximum failure load, is about 1.1 degrees when the full patch thickness is greater than 10 plies.

6. CONCLUSIONS

Stress and failure analysis of bonded composite-to-metal joints are discussed in this paper. The development of a quasi two dimensional model for the analysis is outlined. The salient features of this model include an ability to (i) handle tapered composite patches, (ii) calculate interface peel stresses and transverse stresses in the patch as well as adhesive shear stress, (iii) determine thermal residual stresses after curing due to thermal mismatch, and (iv) predicte joint failure load and safety margin for eight typical modes. Because of the closed-form solutions in the model, parametric studies can be carried out efficiently on the joint failure load with respect to materials and geometry configurations. Equivalent shear properties of the adhesive have been examined in order to account for the

plastic behavior using an elastic analysis. In addition, the degradation of patch matrix properties is discussed.

Case studies and parametric studies were conducted for fatigue enhancement and crack patching applications using different material property options. Some conclusions can be drawn from these studies.

(i) In the case of fatigue enhancement under compression, the most critical location is at the tapered edge and the possible failure modes are adhesive shearing, patch matrix shearing, and patch fiber failure. The thermal residual stresses have unfavorable effects on these failure modes.

(ii) Predictions of failure load and mode, particularly the dominant failure mode, are dependent of the selection of material property options. The equivalent adhesive shear properties result in higher failure load which is more realistic. The knockdown of the patch matrix properties is necessary particularly when the edge thickness is small.

(iii) In the case of crack patching under tension, the most critical location is at the crack edge rather than the tapered edge. The possible failure modes are adhesive shearing, patch matrix shearing, and patch fiber failure in tension, patch-adhesive peeling, and substrate-adhesive peeling. The thermal residual stresses have mixed effects. The dominant failure mode is patch matrix shearing if the equivalent adhesive properties and the degraded patch matrix properties are used.

(iv) Tapered patch thickness is desirable to reduce the shear stress concentration at the tapered edge. However a thin edge thickness may result in high axial tensile or compressive stress in patch plies close to the edge.

(v) Appropriate edge thickness, tapered distance and full patch thickness need to be determined by considering all stresses of concern. The full patch thickness is usually determined by the amount of enhancement required and, in general, the maximum joint failure load is achieved at an edge thickness of one ply of fibers. Therefore the tapered distance is a key variable specifying the taper angle in the design of an optimum bonded joint. In the case of the fatigue enhancement application discussed above, the best taper angle is about 1.1 degrees.

Three issues require further examination: (i) bending effects due to load eccentricity, (ii) elastic-plastic behavior of adhesive, and (iii) debonding at the joint extremities.

ACKNOWLEDGMENT

This work is carried out under IAR Program 3G3, Aerospace Structures, Structural Dynamics and Acoustics, Project JGN-00, Composite Repair Techniques for Primary Aircraft Structures.

REFERENCES

1. Baker, A. A. and Jones, R. (eds.), 1988, Bonded Repair of Aircraft Structures, Martinus Nijhoff Publishers, Dordrecht/Boston/Lancaster.
2. Jones, R. and Miller, N. J. (eds.), 1991, Proceedings of International Conference on Aircraft Damage Assessment and Repair, The Institution of Engineers, Australia.
3. Raizenne, D. (ed.), 1993, Composite Repair of Metallic Aircraft Structures, Proceedings of the Third Workshop, IAR/NRCC, Ottawa.
4. Xiong, Y. and Raizenne, M. D., 1995, On design and analysis of composite bonded repair in aircraft structures, LTR-ST-2014, Institute for Aerospace Research, National Research Council Canada, Ottawa.
5. Rose, L. R. F., 1981, An application of the inclusion analogy for bonded reinforcement, Int. J. Solids Structures, Vol. 17, 827-838.
6. Rose, L. R. F., 1988, Theoretical analysis of crack patching, in Bonded Repair of Aircraft Structures (eds. Baker, A. A. and Jones, R.), Martinus Nijhoff Publishers, Dordrecht, Boston, Lancaster.
7. Goland, M. and Reissner, E., 1944, The stresses in cemented joints, ASME Journal of Applied Mechanics, Vol. 11, A17-A27.
8. Tong, L., Sheppard, A. and Kelly, D., 1994, A numerical study of Adhesively bonded composite panel-flange joints, Composite Structures, Vol. 28, 449-458.
9. Kurita, M. and Fujita, M., 1995, Three-dimensional FEM stress analysis for bonded dissimilar plates with various thicknesses, JSME International Journal, Series A, Vol. 38, 333-339.
10. Hart-Smith, L. J., 1973, Adhesively-bonded double-lap joints, NASA-CR-112235.
11. Hart-Smith, L. J., 1973, Adhesively-bonded scarf and stepped-lap joints, NASA-CR-112237.
12. Hart-Smith, L. J., 1973, Adhesively-bonded single-lap joints, NASA-CR-112236.
13. Hart-Smith, L. J., 1974, Analysis and design of advanced composite bonded joints, NASA-CR-2218.
14. Hart-Smith, L. J., 1980, Further developments in the design and analysis of Adhesively-bonded structural joints, Douglas Paper 6922, McDonnell Douglas Corporation.
15. Hart-Smith, L. J., 1982, Design methodology for bonded-bolted composite joints, Vol. 1 analysis derivations and illustrative solutions, *AFWAL-TR-81-3154-Vol-1*.
16. Hart-Smith, L. J., 1983, A4EI bonded joint program, Douglas Report A8372, McDonnell Douglas Corporation.
17. Allman, D. J., 1976, A theory for elastic stresses in adhesive bonded lap joints, Journal of Mechanics and Applied Mathematics, Vol. XXX, Part 4.
18. Chen, D. and Cheng, S., 1984, An analysis of Adhesively-bonded single-lap joints, ASME Journal of Applied Mechanics, Vol. 50, 109-115.
19. Adams, R. D. and Mallick, V., 1992, A method for stress analysis of lap joints, Journal of Adhesion, Vol. 38, 199-217.
20. Carpenter, W. C., 1991, A comparison of numerous lap joint theories for Adhesively bonded joints, Journal of Adhesion, Vol. 35, 55-73.
21. Xiong, Y., 1996, A quasi-2D model for bonded composite-to-metal joints with tapered edges, LTR-ST-2051, Institute for Aerospace Research, National Research Council Canada, Ottawa.
22. Adams, R. D. and Mallick, V., 1993, The effects of temperature on the strength of adhesively-bonded composite-aluminum joints, Journal of Adhesion, Vol. 43, 17-33.
23. Gaudert, P. C., Raizenne, M. D., et al, 1994, Fractographic investigation of boron epoxy 5521/4 patches, LTR-ST-1973, Institute for Aerospace Research, National Research Council Canada, Ottawa.

Table 4. Failure loads *(k-lb/in)* and modes of fatigue enhancement (t_p = 23 plies)

e	Edge thickness t_e *(=plies of patch fibers)*											
(in)	1	2	3	4	5	6	7	8	9	10	11	12
0.55	8.11 (6)	9.64 (6)	11.5 (6)	13.7 (6)	16.5 (6)	20 (6)	24.6 (6)	25.6 (8)	25.6 (8)	25.6 (8)	25.6 (8)	25.5 (8)
1.09	27.2 (8)	26.9 (8)	26.7 (8)	26.5 (8)	26.4 (8)	26.3 (8)	26.2 (8)	26.1 (8)	26 (8)	26 (8)	25.9 (8)	25.8 (8)
1.63	28.9 (8)	28.3 (8)	27.9 (8)	27.5 (8)	27.3 (8)	27 (8)	26.9 (8)	26.7 (8)	26.5 (8)	26.4 (8)	26.3 (8)	26.2 (8)
2.18	30.7 (8)	29.7 (8)	29.1 (8)	28.6 (8)	28.2 (8)	27.8 (8)	27.5 (8)	27.3 (8)	27.1 (8)	26.9 (8)	26.7 (8)	26.5 (8)
2.72	32.6 (8)	31.2 (8)	30.3 (8)	29.6 (8)	29 (8)	28.6 (8)	28.2 (8)	27.9 (8)	27.6 (8)	27.3 (8)	27.1 (8)	26.9 (8)
3.26	34.6 (8)	32.7 (8)	31.5 (8)	30.6 (8)	29.9 (8)	29.3 (8)	28.8 (8)	28.4 (8)	28 (8)	27.7 (8)	27.4 (8)	27.2 (8)
3.81	36.4 (8)	34.1 (8)	32.6 (8)	31.5 (8)	30.6 (8)	29.9 (8)	29.4 (8)	28.9 (8)	28.4 (8)	28.1 (8)	27.7 (8)	27.4 (8)
4.35	38.2 (8)	35.4 (8)	33.6 (8)	32.3 (8)	31.3 (8)	30.5 (8)	29.9 (8)	29.3 (8)	28.8 (8)	28.4 (8)	28 (8)	27.7 (8)
4.89	39.9 (8)	36.6 (8)	34.5 (8)	33.1 (8)	31.9 (8)	31 (8)	30.3 (8)	29.7 (8)	29.1 (8)	28.7 (8)	28.3 (8)	27.9 (8)
5.44	41.6 (8)	37.7 (8)	35.4 (8)	33.8 (8)	32.5 (8)	31.5 (8)	30.7 (8)	30 (8)	29.4 (8)	28.9 (8)	28.5 (8)	28.1 (8)

Table 5. Failure loads *(k-lb/in)* and modes of fatigue enhancement (t_p = 12 plies)

e	Edge thickness t_e *(=plies of patch fibers)*											
(in)	1	2	3	4	5	6	7	8	9	10	11	12
0.55	31.4 (8)	31.2 (8)	31 (8)	30.9 (8)	30.8 (8)	30.7 (8)	30.6 (8)	30.5 (8)	30.5 (8)	30.4 (8)	30.4 (8)	30.4 (8)
1.09	33.7 (8)	32.9 (8)	32.3 (8)	31.9 (8)	31.6 (8)	31.3 (8)	31.1 (8)	30.9 (8)	30.8 (8)	30.6 (8)	30.5 (8)	30.4 (8)
1.63	36.5 (8)	34.9 (8)	33.8 (8)	33.1 (8)	32.5 (8)	32.1 (8)	31.7 (8)	31.3 (8)	31 (8)	30.8 (8)	30.6 (8)	30.4 (8)
2.18	39.4 (8)	36.9 (8)	35.4 (8)	34.3 (8)	33.4 (8)	32.8 (8)	32.2 (8)	31.7 (8)	31.3 (8)	31 (8)	30.6 (8)	30.4 (8)
2.72	42.2 (8)	38.8 (8)	36.8 (8)	35.3 (8)	34.2 (8)	33.4 (8)	32.7 (8)	32.1 (8)	31.6 (8)	31.1 (8)	30.7 (8)	30.4 (8)
3.26	43.9 (3)	40.6 (8)	38 (8)	36.3 (8)	35 (8)	33.9 (8)	33.1 (8)	32.4 (8)	31.8 (8)	31.2 (8)	30.8 (8)	30.4 (8)
3.81	42 (3)	42.2 (8)	39.1 (8)	37.1 (8)	35.6 (8)	34.4 (8)	33.4 (8)	32.6 (8)	31.9 (8)	31.3 (8)	30.8 (8)	30.4 (8)
4.35	40.6 (3)	43 (3)	40.1 (8)	37.8 (8)	36.1 (8)	34.8 (8)	33.7 (8)	32.8 (8)	32.1 (8)	31.4 (8)	30.9 (8)	30.4 (8)
4.89	39.5 (3)	41.9 (3)	41 (8)	38.4 (8)	36.6 (8)	35.1 (8)	34 (8)	33 (8)	32.2 (8)	31.5 (8)	30.9 (8)	30.4 (8)
5.44	38.7 (3)	41 (3)	41.7 (8)	39 (8)	37 (8)	35.4 (8)	34.2 (8)	33.2 (8)	32.3 (8)	31.6 (8)	30.9 (8)	30.4 (8)

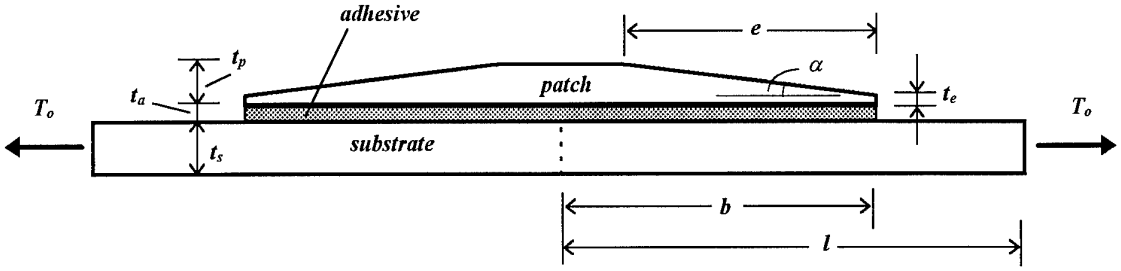


Figure 1. A composite-to-metal joint with tapered edges

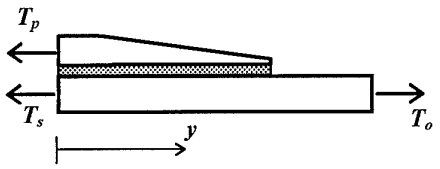


Figure 2. A half of joint model

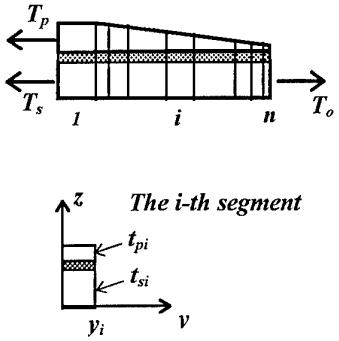


Figure 3. Segmentation of bonded region

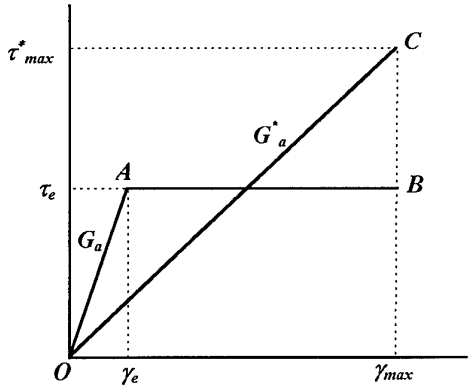


Figure 4. Effective shear behavior of adhesive

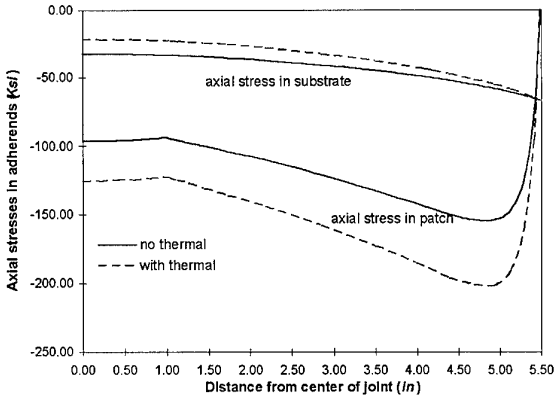


Figure 5. Axial stresses along bondline in adherends of fatigue enhancement under compression

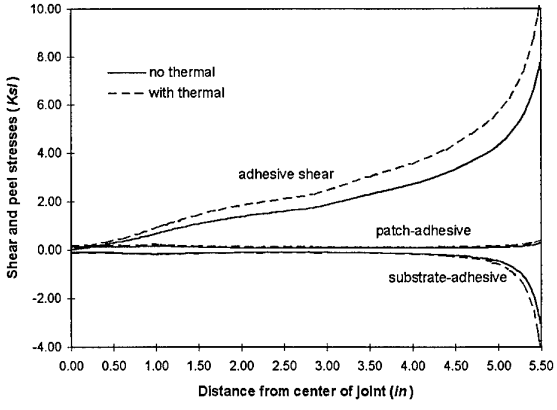


Figure 6. Shear and peel stresses along bondline of fatigue enhancement under compression

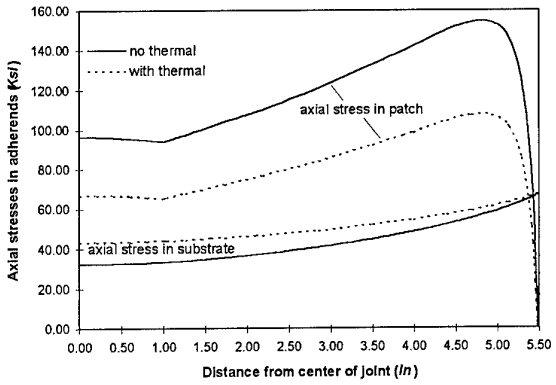


Figure 7. Axial stresses along bondline in adherends of fatigue enhancement under tension

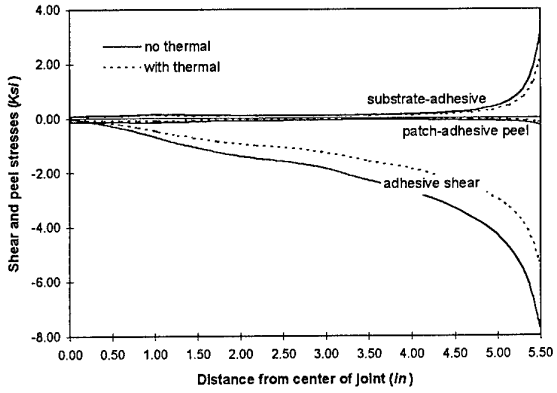


Figure 8. Shear and peel stresses along bondline of fatigue enhancement under tension

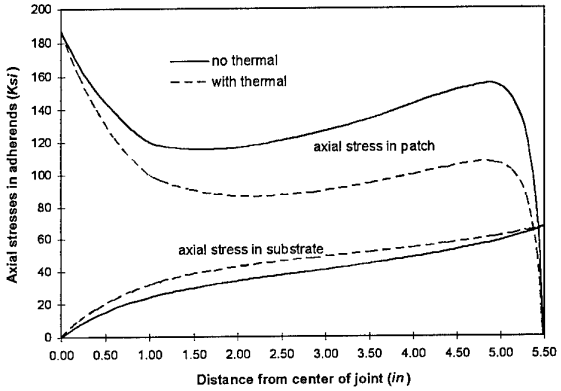


Figure 9. Axial stresses along bondline in adherends of crack patching under tension

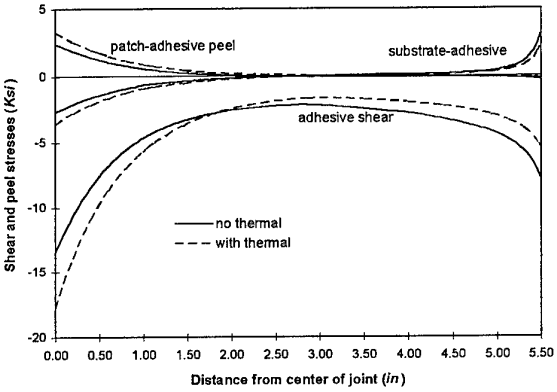


Figure 10. Shear and peel stresses along bondline of crack patching under tension

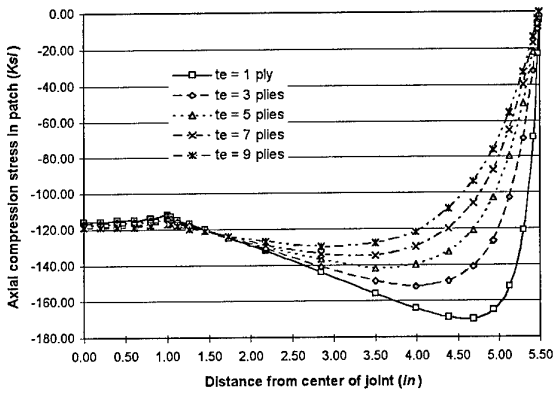


Figure 11. Effects of edge thickness on axial stress in patch of fatigue enhancement under compression

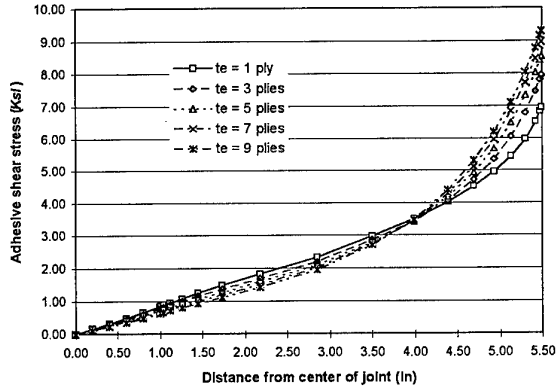


Figure 12. Effects of edge thickness on shear stress in adhesive of fatigue enhancement under compression

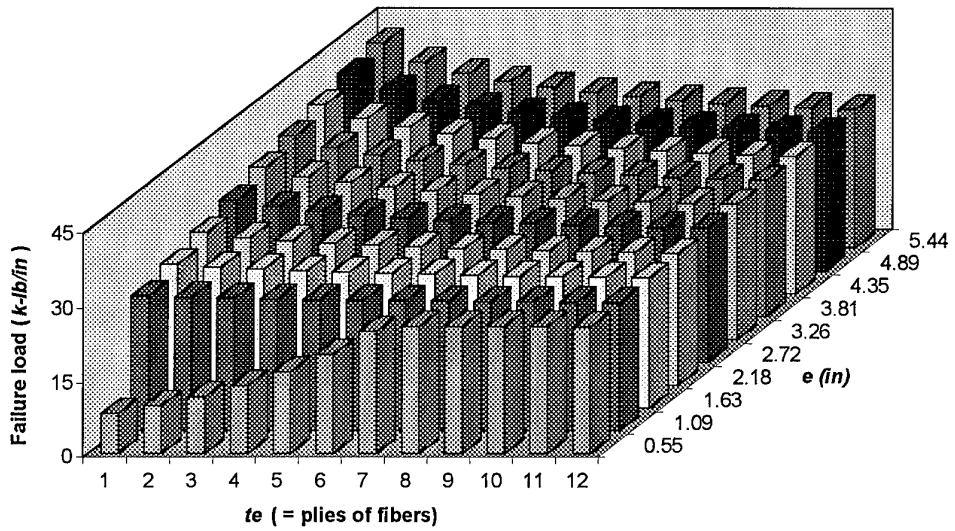


Figure 13 Failure load of fatigue enhancement under compression (t_p = 23 plies)

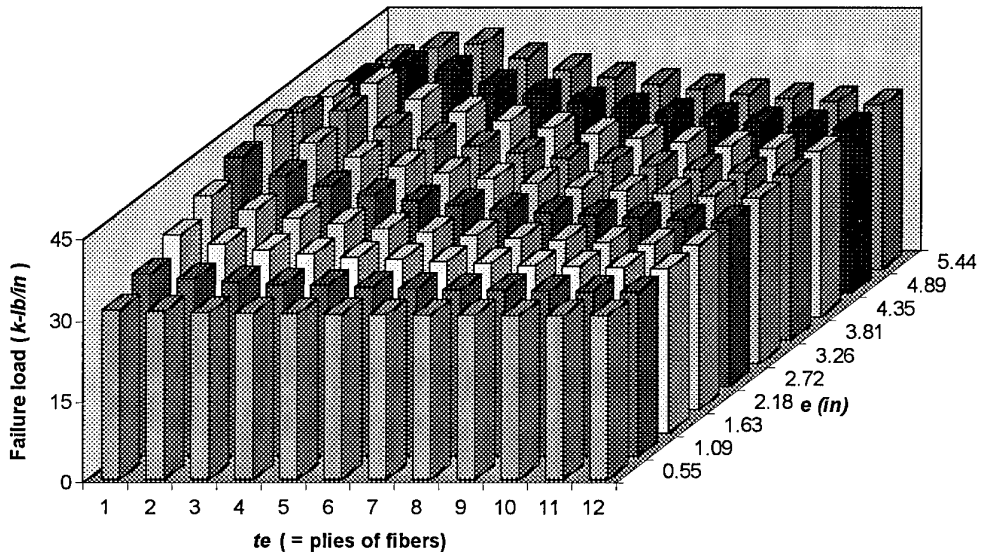


Figure 14 Failure load of fatigue enhancement under compression (t_p = 12 plies)

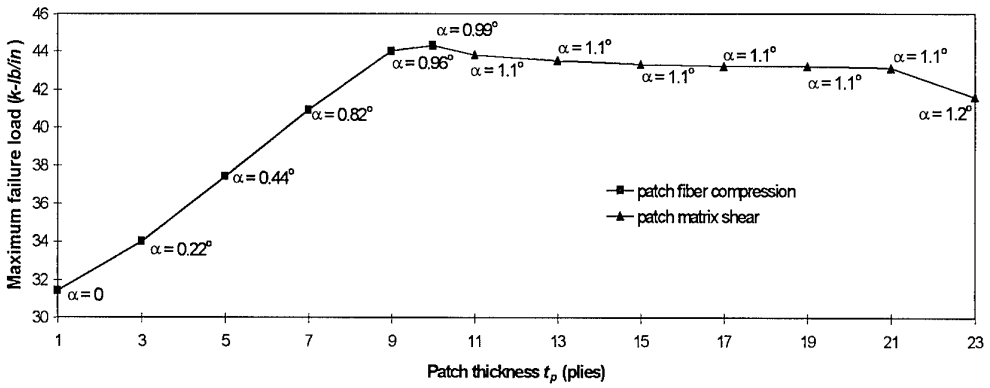


Figure 15. Maximum failure load of fatigue enhancement under compression (t_e = 1 ply)

STRENGTH PREDICTION OF BONDED JOINTS

M. N. Charalambides
A. J. Kinloch
F. L. Matthews
Mechanical Engineering Department & Centre for Composite Materials
Imperial College of Science Technology & Medicine
London SW7 2BX

SUMMARY

The performance of carbon fibre / epoxy repair joints bonded with an epoxy film adhesive, under static and fatigue loading has been investigated. The joints have been immersed in water at 50°C for a period of 16 months and the effect of the hot/wet environment on the static and fatigue strengths was evaluated. In addition, residual strength tests, i.e. static tests of pre-fatigued repair joints were performed. The mechanical properties of the substrate and the adhesive forming the joint were also determined. Apart from the experimental study, it was also desirable to determine a failure criterion which will accurately predict the experimental strength of this joint. A parallel study on double lap joints prepared from the same substrate and adhesive as the repair joints, was performed. Static tests on lap joints of various overlap lengths were conducted. The experimental failure loads were used in conjunction with finite element analysis to examine the validity of proposed failure criteria.

1. INTRODUCTION

The use, development and understanding of adhesive joints has been continually growing during the last 50 years due to the many advantages they offer compared with other techniques for fastening materials. However, there is a great concern about possible performance degradation when the joints are subjected to a hot/wet environment. In the current study, the fatigue as well as the static performance of environmentally conditioned repair joints is examined. In addition, there is a great need for a failure criterion to be developed for use in design. For the criterion to be of any use, it has to be applicable to a wide range of joint geometries and materials. In the current research programme, it was decided to test both repair and double lap joints. The intention is that the failure criterion has to successfully predict the experimental failure loads for both geometries. The stress analysis is performed with the aid of the ABAQUS Finite Element software package (Ref. 1).

2. EXPERIMENTAL

In this section, the details of specimen geometries and test methods are first given, followed by the experimental results.

2.1 Test methods

The materials used throughout were Ciba Geigy carbon fibre / epoxy composite (T300/914) and epoxy film adhesive (Redux 319). The effect of the hot/wet environment on the performance of the repair joints was studied by immersing the specimens in distilled water heated at 50°C for various periods.

The repair specimen geometry is shown in Figure 1. One of the adherends, i.e. the parent, was precured according to the manufacturer's specifications. This represents the original material that has undergone damage and is in need of repair. After autoclave curing, the parent plate was machined at an angle of 2°, sanded and degreased. The adhesive and the other adherend, i.e. the repair, were then co-cured under vacuum pressure only, simulating a typical repair procedure used in industry. The lay-up of the repair is such that the same slope (1:30) is obtained. The lay-up of the parent and the repair was quasi-isotropic, $(\pm 45/0/90)_{2s}$, with two extra adhesive layers and two 0° plies on the upper and lower surfaces of the repair joint. The adhesive thickness was 0.17 mm and the joint width was 25 mm.

The composite adherends of the double lap joints had a unidirectional lay-up and were cured in an autoclave according to the manufacturer's specifications. The joints were symmetric, i.e. the thickness of the outer adherends was half the thickness of the central adherend, as shown in Figure 2. The central adherend thickness was 4 mm, the adhesive thickness was 0.1 mm and the joint width was 20 mm. The areas of the composite panels to be bonded were sanded and degreased prior to bonding.

Dumbbell specimens, 0.25 mm thick and 7 mm wide, were used to measure the tensile properties of the film adhesive. Thick - adherend lap - shear specimens (Ref. 2) were also manufactured to enable measurement of the shear properties of the adhesive. Steel substrates of dimensions 110 x 25 x 6.5 mm were used. The glue line thickness was 0.1 mm and the length of the lap test section was 5 mm.

The longitudinal, transverse and shear properties of the unidirectional composite were obtained from tensile tests on coupon specimens, as specified by the CRAG test methods (Ref. 3). Composite coupon specimens of quasi-isotropic layup were also made. These were tested in fatigue, so that a comparison could be made between the performance of the repair joint and the parent material.

For reasons which will be obvious in a later section of this paper, the failure locus of the adhesive had also to be determined. For this, Mode I (opening) and Mode II

Paper presented at the 83rd Meeting of the AGARD SMP on "Bolted/Bonded Joints in Polymeric Composites", held in Florence, Italy, 2-3 September 1996, and published in CP-590.

(shear) Double Cantilever Beam (DCB) tests are needed (Ref. 2). Once the critical Mode I (G_{ic}) and Mode II (G_{iic}) strain energy release rates are determined, the failure locus can be approximated with a straight line passing through the two points (Ref. 10). DCB joints were prepared with 2 mm thick unidirectional carbon fibre epoxy substrates. The glue line thickness was 0.1 mm and the joint width was 20 mm. A polytetrafluoroethylene film of 12.5 μm thickness was inserted between the two substrates at one edge of the joint before curing to act as a starter crack. After curing, two aluminium end blocks were bonded on the sides of the specimen which provided the means for applying the load. Finally, one edge of the specimen was coated with a white typewriter correction fluid and fine marks were inscribed at 5 mm intervals. This enabled monitoring of the crack length during the test.

All static tests were performed using an INSTRON tensile testing machine at a constant crosshead rate. Extensometers were used to record the displacement of the joints, dumbbells and transverse composite test specimens. Strain gauges were used for the longitudinal and shear composite tests. The fatigue experiments were performed under tensile load control, at a frequency of 5 Hz and a stress ratio of 0.1, using a servo-hydraulic fatigue machine.

2.2 Results

Typical tensile stress - strain curves obtained from the "dry" adhesive dumbbells are shown in Figure 3. The results from all series of tests, i.e. "dry" and "conditioned" are tabulated in Table I. By comparing the results, it is apparent that there is no significant change in the Young's modulus and 0.1% offset yield stress and strain. However, a notable decrease is observed in the ultimate tensile stress and strain to failure of conditioned samples.

Figure 4 shows the shear stress vs. shear strain curve as obtained from the thick - adherend lap - shear tests. Tests on "dry" joints only were performed.

Tables II, III, IV show the longitudinal, transverse and shear properties of the unidirectional composite. In Table II, there are no changes observed as a result of conditioning. This was expected since the longitudinal properties are governed by the carbon fibres which should not be affected by conditioning in water. The transverse properties are also unaffected. The shear properties show a noticeable increase in strength and failure strain after the 4 month conditioning period. This was also observed by Joshi (Ref. 5) who suggested that the reason for this increase could be related to the release of residual strains induced during the cooling of the composite from its cure temperature.

The static test results of the repairs are shown in Table V. A small increase in the failure load was observed in the "4 month conditioned" specimens. Thereafter, the strength starts falling to the original "dry" values. The failure loads can be converted to failure "stresses" by dividing by the cross sectional area of the parent side. For comparison purposes, the failure stress of the parent composite was measured to be 611 MPa. All static failures occurred in the parent side of the joint and most seemed to have originated from the end of the longest of the overlapping plies.

The fatigue data are shown in Figure 5, in the form of S-N curves. The maximum stress was calculated using the cross section of the parent side of the repair. Only four samples conditioned at 8 and 11 months were tested, at 240 MPa maximum stress. Fatigue data for the parent material are also plotted on the same graph, for comparison purposes. It is obvious that there are no significant changes between the "dry" and the "conditioned" repairs whereas there is a noticeable decrease in fatigue life when compared to the parent data.

"Dry" repair joints were tested in fatigue at a maximum stress of 240 MPa. The cycling was stopped at various fractions of the expected number of cycles to failure, i.e. before the specimens failed. Static tests were then performed on the pre-fatigued specimens to determine their residual strength. The results are shown in Figure 6. It is observed, that fatigue did not have an effect on the static strength of the joints. The tests were repeated for joints conditioned for 4 months and similar results were obtained. A video camera fitted with a macro lens was used to magnify and record the static tests. During the majority of the tests, small cracks were observed in the area marked by the ellipse in Figure 1. Specifically, the cracks originated from the end of the longest overlapping adhesive and 0° ply. Figure 7 shows a photograph of one such crack at the instant just before joint failure. The average crack length from all the tests was 2.6 ± 0.8 mm.

The results from the double lap static tests are shown in Figure 8 where the load per unit width at joint failure is plotted against the overlap length. The trend shown in Figure 8, i.e. increasing strength with increasing overlap until a plateau value is reached, has been observed and explained before by other researchers (Ref. 6). The double lap joint failures were predominantly cohesive in the adhesive.

The average Mode I critical energy release rate (G_{ic}) of the adhesive was found to be 335 J/m^2.

3. FINITE ELEMENT ANALYSIS

Two dimensional Finite Element Analysis (FEA) was performed on the scarfed repair and the double lap geometries. The ABAQUS software package was used with plane strain quadratic elements (Ref. 1).

3.1 Repair joint

One end of the repair joint was clamped. The other was restrained in the vertical direction whereas its horizontal nodal deflections were prescribed to be equal. The total load as measured from the static tests was then applied on one of these nodes.

Two models were used for the repair joints. In the first one, the composite substrates were modelled as a single material with linear elastic orthotropic properties. This will be referred to as the "single material" model. In the second, one row of elements was used to represent each of the composite plies. The 0° and 90° plies were modelled as orthotropic and the +45° and -45° were modelled as anisotropic. This model will be referred to as the "ply" model.

The data shown in Tables II, III and IV together with laminate analysis were used to determine all the composite material constants required by the ABAQUS orthotropic and anisotropic material models. The adhesive was modelled as a Linear Elastic material.

3.2 Double lap joint

For the double lap geometry, only one half of the joint was modelled due to symmetry. One end of the joint was clamped and the other was restrained in the vertical direction and loaded through a fixed displacement in the horizontal direction. The applied displacement was such that the resulting load reactions were equal to the failure loads measured experimentally.

The composite was modelled as a linear elastic orthotropic material using the data in Tables II, III and IV. The adhesive was modelled as a linear elastic - plastic material. The Raghava's pressure dependent yield criterion was used (Ref. 7). The full stress - strain curve as measured from the tensile and shear tests was used in the modelling, i.e. work hardening was included (Ref. 8). The Young's modulus and yield stress values of Table I were used. Comparisons between the experimental and the numerical approximations of the tensile and shear stress - strain curves are shown in Figures 3 and 4. A close agreement is observed.

4. FAILURE CRITERIA

Failure criteria have been the subject of many research projects. More work has been published on lap than repair joint geometries. In the first subsection some of these criteria are employed to get failure load predictions for the double lap joints of the current work. The second subsection summarises the prediction results concerning the repair joint.

4.1 Double lap joint

The most widely used and simplest criterion that appears in many design analyses is that the joint will fail when a certain stress or strain component reaches a critical value (e.g. Ref. 5). The latter is usually measured from simple uniaxial tensile or shear tests. In this study, the FE analysis for the shortest overlap (L = 10 mm) was used to define the critical values of the proposed stress or strain criterion. This was then used in conjunction with the analysis of the longest overlap (L = 80 mm) to predict the failure load for the L = 80 mm overlap. The validity of the argument was examined using various parameters: von Mises stress, maximum principal strain, equivalent plastic strain, shear strain and shear stress. When the critical values of these parameters, deduced from the L = 10 mm analysis, were used in the L = 80 mm analysis errors of 55 - 60 % in the predicted failure loads were observed.

Other proposed failure criteria are based on values of stress or strain acting over a finite distance. For example, such a criterion was proposed in Ref. 9. It states that the largest distance measured normal to the mean direction of the maximum principal stress, in the zone bounded by the ultimate tensile strength of the adhesive, reaches a critical value when the adhesive fails catastrophically. The ultimate tensile strength of 65 MPa (Figure 3) was used in the analyses of the shortest (L = 10 mm) and longest (L = 80 mm) overlaps. A spew fillet was introduced in the model in order to be consistent with the work described in Ref. 9. The critical distance was determined from the L = 10 mm analysis. This was used in conjunction with the L = 80 mm analysis to predict the failure load, i.e. the load corresponding to the same critical distance. The error in the predicted load for the L = 80 mm joint was 68 %. This error did not improve when different fillet sizes and different values of ultimate tensile strength were used.

An alternative criterion based on Fracture Mechanics was examined. A micro-crack, or flaw, is assumed to be present in the adhesive halfway through its thickness and at the most severely loaded end of the joint. The submodelling option of ABAQUS (Ref. 1) was used to create a fine mesh at the crack area. Figure 9 shows a schematic of the submodelled region. The J-integral is then calculated, as a function of the crack length, for both short and long overlaps. The results are shown in Table VI. The aim is to compare the calculated J-integral values of Table VI with the failure locus of the adhesive. However, mode II tests have yet to be performed. Preliminary observations can be made regarding the results from this analysis so far. The calculated J-integral is much larger for the longer overlap. It was apparent that a higher Mode II component was present in the long overlaps. Therefore, some of the observed discrepancy between the J-integral values corresponding to the short and long overlaps, might be accounted for once the exact failure locus of the adhesive is determined.

4.2 Repair joints

Following the inaccurate failure load predictions from the maximum stress/strain and the stress over a distance criteria for the double lap joint, it was decided to use a Fracture Mechanics based criterion for the repair joint. As stated in the earlier section, cracks were obvious in the parent side of the pre-fatigued joints. Since the residual strength of these joints were very similar to the static strength of joints that had not been fatigued, a crack of 2 mm was introduced to both "single material" and "ply" models in the area indicated by the ellipse in Figure 1. The crack was assumed to lie between the first +45° and -45° plies and the area around this crack was again submodelled, so as to obtain accurate J-integral values from the finer mesh. Figure 10 shows a schematic of this submodel with the crack line indicated by a black

solid line. The Vitrual Crack Closure Method (VCCM) (Ref. 10) was also used to calculate the fracture energy and this was found to be identical to the J-integral value, as expected for a linear elastic material. The advantage of the VCCM method is that it can determine the mode mix, i.e. the ratio of G_i to G_{ii}. The numerically calculated fracture energy was then plotted on the failure locus obtained from T300/914 DCB specimens with the crack running between +45° and -45° plies (Ref. 11). The results are shown in Figure 11 where the black solid line indicates the failure locus. It is obvious that the more detailed "ply" model yields a more accurate prediction than the simplified "single material" model.

In order to obtain the actual error in the failure load prediction, the mode mix as calculated from the "ply" model was used to determine the "correct" fracture energy, i.e. the fracture energy that lies on the failure locus of the composite (point A in Figure 11). This was found to be 823 J/m^2 compared to the numerically calculated J-integral of 950 J/m^2 (point B in Figure 11). The "ply" model was then run with various applied loads so as to get a plot of J-integral vs. corresponding applied load. The results are shown in Figure 12, where the applied load is normalised with the experimentally measured load. At a J-integral of 823 J/m^2, the corresponding ratio of applied to experimental load is 0.93. This means that the fracture mechanics based criterion used with a crack length of 2 mm in the parent side of the repair, results in a 7% error in the predicted failure load. This is an acceptable error.

In order to find out how the accuracy of the prediction varies with the assumed crack length, two additional "ply" models were run with cracks lengths of 1 and 5 mm. These correspond to the minimum and maximum crack lengths that were observed during the residual strength static tests. The same submodelling procedure was followed as above. The calculated J-integral for both cases was within 3% of the J-integral corresponding to the 2 mm crack length case. The mode mix was also very similar. Therefore, the error in the load predictions is once again very small. It is not clear at this stage why the fracture energy is insensitive to the crack length when the latter varies between 1 and 5 mm.

5. CONCLUSIONS

From the experimental data, it is concluded that conditioning for 16 months in water heated at 50° C has no noticeable effect on the static and fatigue performance of the repair joints. Whilst the static properties of the repair joints are not significantly different from those of the parent composite, the fatigue performance is significantly inferior.

The failure criteria studies on the double lap joint showed that both "critical stress or strain" and "critical distance" criteria result in very large errors in the predicted failure loads. Note that the "critical stress or strain" criterion inherently suffers from mesh dependent results, since the maximum values of stresses or strains occur at the corner of the adhesive, i.e. the singularity point. In this study the mesh density was kept constant for both the short and the long overlap models. However, even then, the predictions are not reliable. Following the unsuccessful use of the above criteria to predict the correct failure load, an alternative analysis based on fracture mechanics was used. Preliminary results showed that for the same crack length, the longer overlap results in a larger J-integral than the shorter overlap.

The fracture mechanics based criterion was also applied to the repair joint. The "ply" model resulted in more accurate predictions than the "single material" model. The error in the predicted load when the "ply" model is used is 7%. Very similar predictions were obtained when the assumed crack length was changed to 1 or 5 mm. The reason for this was that the calculated J-integral was insensitive to the crack length.

ACKNOWLEDGEMENTS

The authors would like to thank EPSRC for the funding of the project. Dr E. Busso is acknowledged for his assistance in the numerical part of the work and permitting the use of his ABAQUS User Material subroutine. Messrs L. Vaughn of Bristol University and I. Pearson of Warwick University are also acknowledged for performing the thick - adherend lap - shear tests and Mr J. Hogan for performing the Double lap joint tests.

REFERENCES

1. ABAQUS User's Manual, Version 5.4, Hibbit, Karlsson & Sorensen, USA, Inc. 1994.
2. Kinloch, A.J., "Adhesion and Adhesives", Chapman & Hall, Cambridge University Press, 1987, (ISBN 0 412 27440 X).
3. "CRAG test methods for the measurement of the engineering properties of fibre reinforced plastics", Royal Aerospace Establishment, Technical report 88012, ed. PT Curtis, UK, 1988.
4. Hashemi, S., Kinloch, A.J. and Williams, J.G., Proceedings of Americal Society for Testing and Materials meeting, Orlando, Florida, "Composite Materials: Fatigue and Fracture", ed. T.K. O'Brien, Volume 3, ASTM STP 1110, 1991, pp 143 - 168.
5. Joshi, O.M., Composites, Volume 14, 1983, pp 196 - 200.
6. Hart-Smith, L.J., "Developments in Adhesives-2", ed. AJ Kinloch, Applied Science Publishers, London, 1982, pp 1 - 43.
7. Raghava, R., Caddell, R.M. and Yeh, G.S.Y., J. Mater. Sci., Volume 8, 1973, pp. 225 - 232.
8. Busso, E., Electrical / Electronic Packaging (ASME Transactions), Volume 11, Application of Fracture Mechanics in Electronic Packaging and Materials, ed. T.Y. Wu, W.T. Chem, R.A. Pearson and D.T. Reid., 1995, pp 134-140.
9. Clark, J.D. and McGregor, I.J., J. Adhesion, Volume 42, 1993, pp 227 - 245.
10. Rybicki, E.F. and Kanninen, M.F., Engineering Fracture Mechanics, Volume 9, 1977, pp 931 - 938.
11. Gilchrist, M., Kinloch, A.J., Matthews, F.L. and Osiyemi, S., to be published.

Conditioning	E (GPa)	UTS (MPa)	$\varepsilon_{max.}$ (%)	σ_y (0.1%)	ε_y (0.1%)
"dry"	3.783 ± 0.2	64.5 ± 2.6	2.31 ± 0.04	34.7 ± 3.4	1.03 ± 0.13
4 months	3.995 ± 0.5	46.7 ± 2.4	1.67 ± 0.38	35.6 ± 3.3	1.01 ± 0.13
12 months	3.466 ± 0.4	38.5 ± 3.6	1.53 ± 0.20	30.6 ± 3.4	0.98 ± 0.16
16 months	3.822 ± 0.4	38.7 ± 4.3	1.28 ± 0.18	30.3 ± 4.6	0.88 ± 0.15

Table I: Adhesive tensile properties.

Conditioning	E_{11} (GPa)	Strength (MPa)	$\varepsilon_{max.}$ (%)	ν_{12}
"dry"	141.5 ± 2.68	1733 ± 199	1.24 ± 0.09	0.31 ± 0.01
4 months	140.4 ± 6.38	1584 ± 201	1.15 ± 0.08	0.31 ± 0.01
16 months	141.3 ± 2.42	1544 ± 131	1.14 ± 0.09	0.30 ± 0.01

Table II: Longitudinal properties of unidirectional composite.

Conditioning	E_{22} (GPa)	Strength (MPa)	$\varepsilon_{max.}$ (%)
"dry"	8.37 ± 0.29	36.8 ± 4.00	0.44 ± 0.04
4 months	9.92 ± 0.66	38.2 ± 2.71	0.40 ± 0.04
16 months	7.92 ± 0.26	32.7 ± 0.48	0.42 ± 0.01

Table III: Transverse properties of unidirectional composite.

Conditioning	G_{12} (GPa)	Strength (MPa)	$\varepsilon_{max.}$ (%)
"dry"	4.59 ± 0.21	103 ± 3.30	14.2 ± 2.3
4 months	4.31 ± 0.17	120 ± 1.73	17.3 ± 2.2
16 months	4.21 ± 0.29	107 ± 2.12	17.4 ± 0.8

Table IV: Shear properties of unidirectional composite.

Conditioning	Max. load (kN)	"Stiffness" (kN/mm)	"Stress" (MPa)
"dry"	26.32 ± 1.25	131.13 ± 3.52	526
4 months	29.69 ± 1.41	125.27 ± 5.34	594
11 months	28.65 ± 0.49		546
16 months	26.16 ± 2.30	103.3 ± 14.6	523

Table V: Static test results of repair joints.

Overlap (mm)	Crack length (mm)	J-integral (J/m^2)
10	0.05	358
80	0.05	2115
10	0.025	184
80	0.025	976

Table VI: Numerically calculated J-integral values.

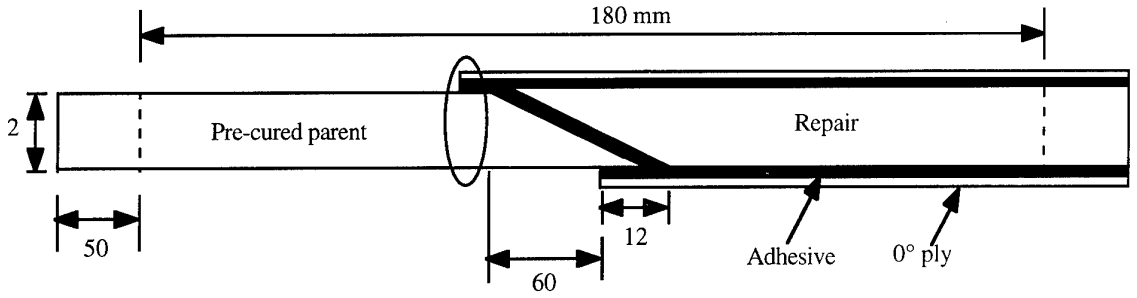


Figure 1: Repair specimen geometry; ellipse shows submodelled region for Finite Element Analysis.

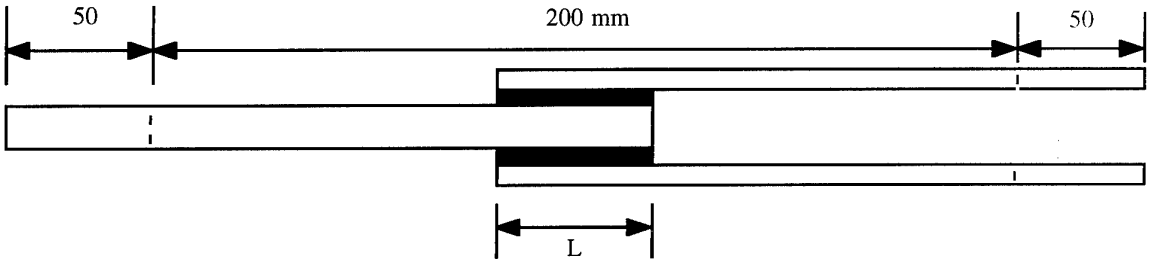


Figure 2: Double lap specimen geometry.

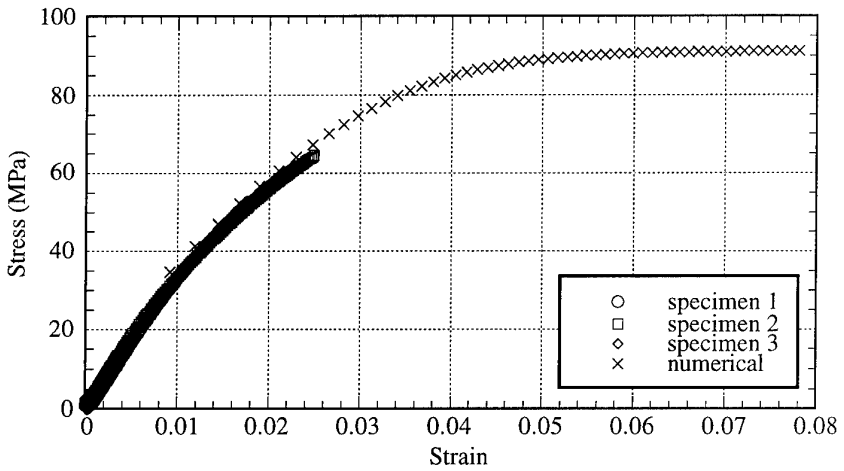


Figure 3: Tensile stress - strain curves of adhesive and comparison with numerical approximation.

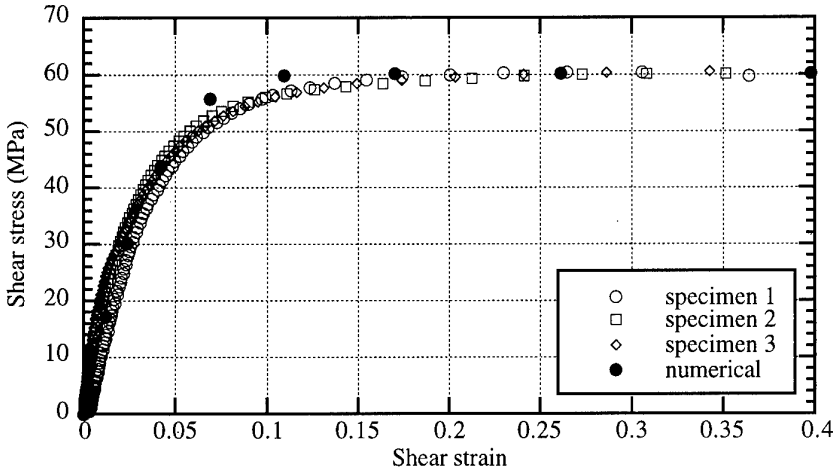


Figure 4: Shear stress - strain curves of adhesive and comparison with numerical approximation.

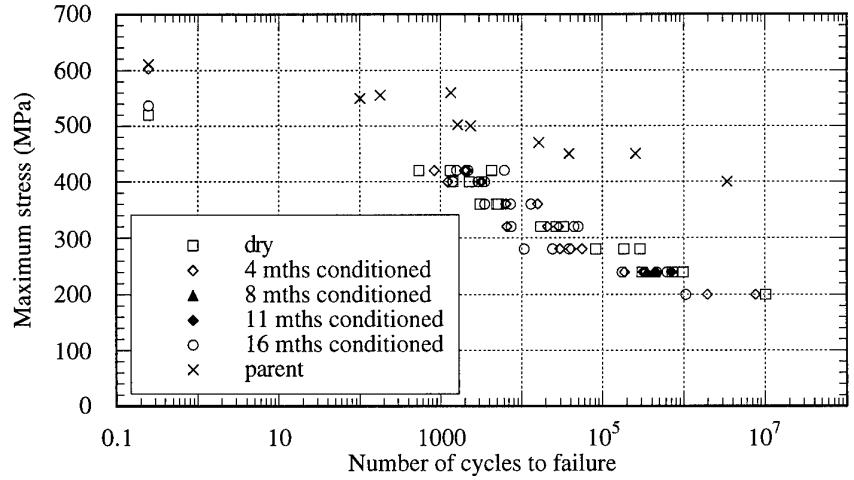


Figure 5: S - N curves for repair joints and parent samples.

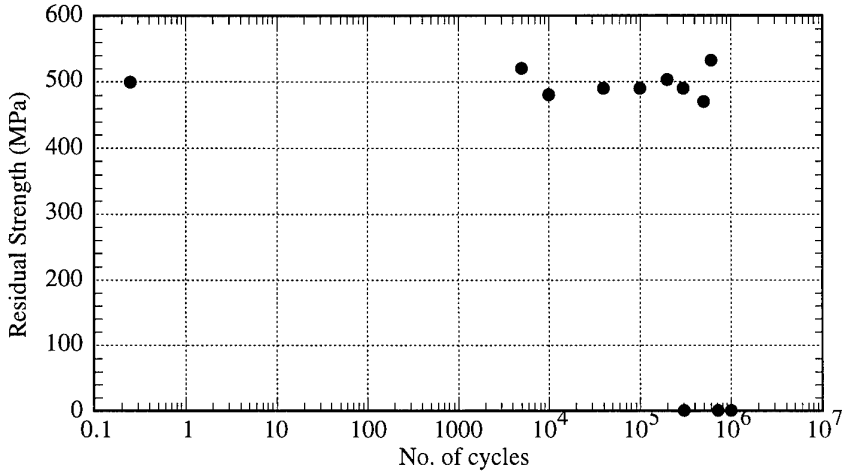


Figure 6: Residual strength vs. no. of cycles for "dry" repairs.

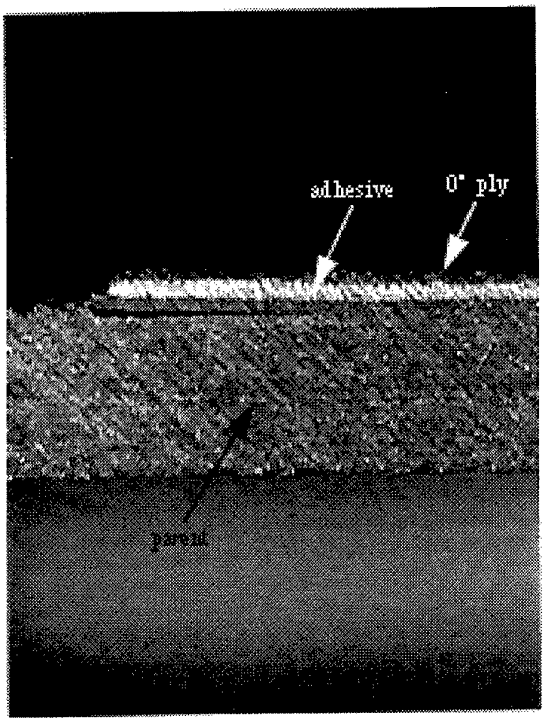


Figure 7: Crack in parent side of repair joint observed during residual strength testing.

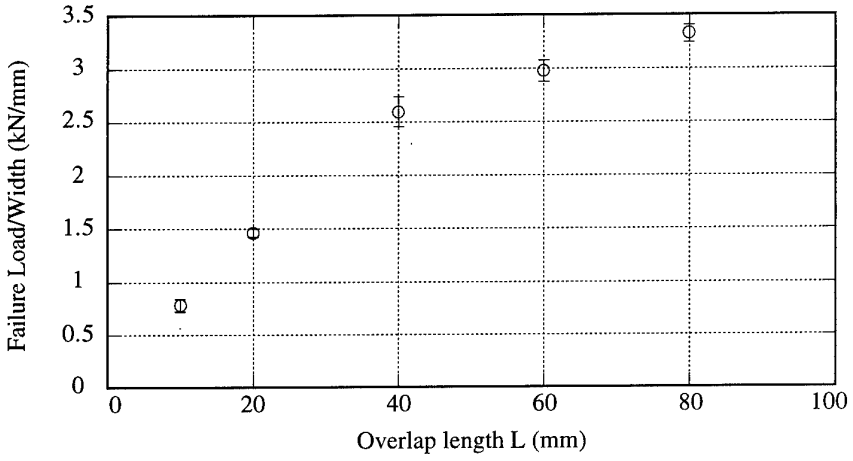


Figure 8: Load per unit length versus overlap length for double lap joints.

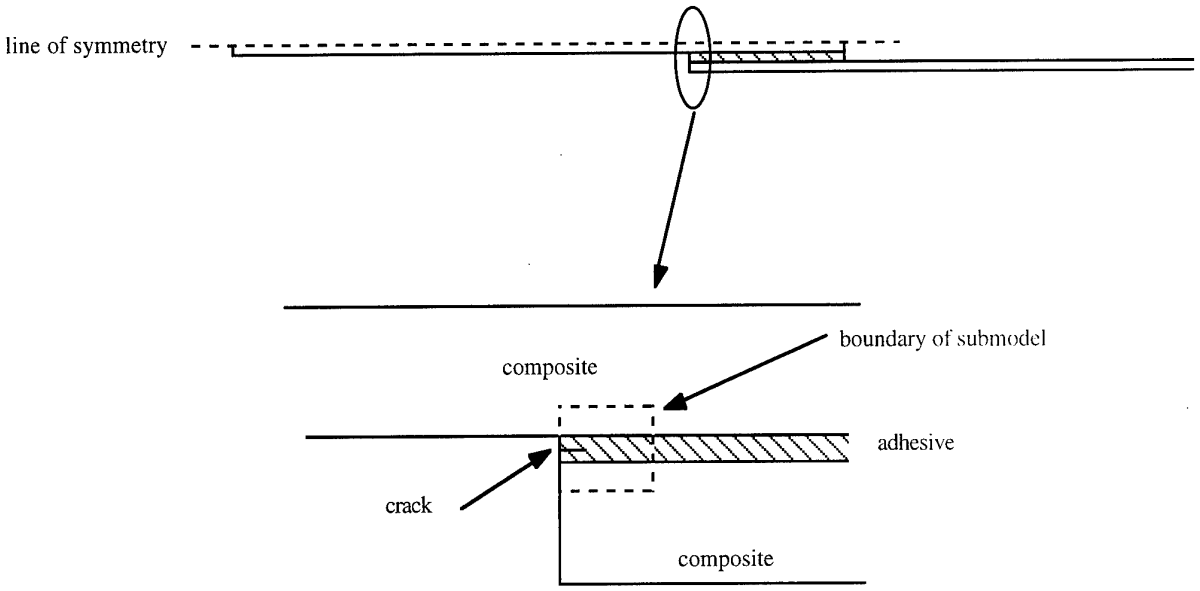


Figure 9: Schematic of submodel region for double lap joint.

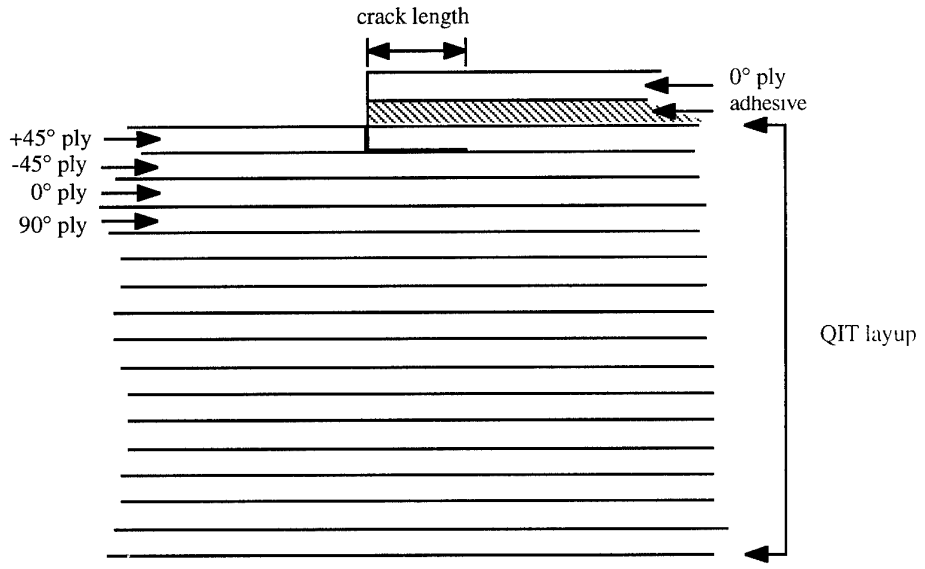


Figure 10: Schematic of submodel region for repair joint.

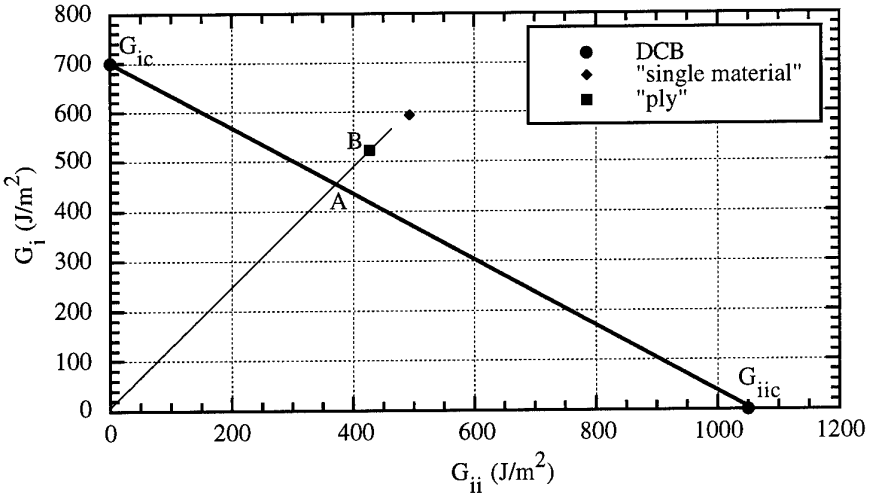


Figure 11: Fracture energy predictions from "single material" and "ply" models; comparison with failure locus of composite obtained from DCB specimens (Ref. 11).

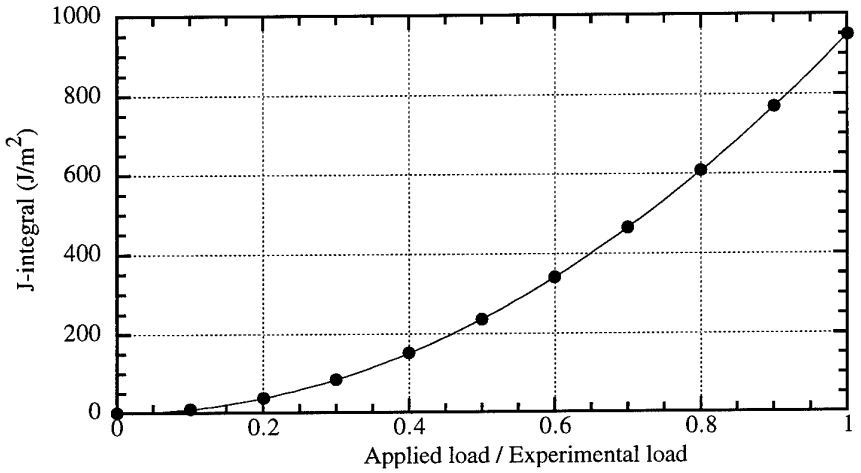


Figure 12: J-integral vs. corresponding applied load / experimental load for repair joint.

NUMERICAL STRENGTH PREDICTIONS OF ADHESIVELY BONDED MULTIMATERIAL JOINTS

G. LASCHET

senior research engineer
ACCESS e.V., Intzestrasse 5, D-52072 Aachen, GE

SUMMARY

Numerical tools have been developed in order to improve the strength prediction of adhesively bonded multimaterial joints. At first, a specific elastoplastic model based on the Raghava yield criterion is introduced for adhesives. Furthermore, in order to evaluate the strength reserve of a joint after local failure initiation, a simple smeared 2-D and 3-D crack propagation model is developed. Then, to improve this simple failure model, a new isotropic damage model for adhesives is presented, which is coupled with the specific elastoplastic one. Finally, the accuracy of this approach is illustrated by numerical strength and failure mode predictions of several single and double-lap joints.

1. INTRODUCTION

During the last decade, structural adhesive bonding has become a major joining technique which can replace successfully conventional fasteners like bolts and rivets for a wide range of industrial applications. Adhesive bonding is of particular interest in the case of multimaterial joining and of lightweight structures made of composite materials since stress concentrations due to drilled holes can be so avoided.

To correctly design an adhesive joint, mathematical tools are needed which can predict accurately the stress/strain state of the joint, but also its load-bearing capacity. A recent review [1] of several analytical and numerical models developed in the past in order to evaluate the stresses in the adhesive layer of a single or double lap-joint has clearly pointed out the necessity to develop a special non-linear adhesive model in our finite element program for the numerical prediction of the stress/strain state, the strength and the failure modes of adhesive joints.

In order to take into account the different yield behaviour of adhesives in tension and compression, a specific elastoplastic model, based on the Raghava yield criterion [2], has been developed. This model, briefly recalled in section 2, has been introduced in the 2-D and 3-D volume finite elements for the numerical analysis of any kind of adhesive joints.

Then, in order to evaluate the joint strength reserve after local failure initiation, more realistic failure criteria for triaxial extension states and *a simple smeared 2-D and 3-D crack propagation model* [1] have been developed in relation with the elastoplastic adhesive model. In this local failure approach a virtual crack normal to the direction of the maximum principal stress or strain is assumed to exist locally in each failed Gauss point.

A significant improvement of this model is only possible by considering the main micro-mechanical toughening mechanisms of the epoxy adhesives ameliorated either by rubber or inorganic particles.

Actually, only few micro-mechanical adhesives models [3] exist in order to describe such phenomena, but they are not linked with a structural stress/strain and damage analysis. So, in order to improve the simple local failure model, *a new isotropic damage model for adhesives* is presented in section 4. This model is based on Continuum Damage Mechanics (CDM) [4] and coupled with our specific elastoplastic model. Its mean feature is that *each principal micro-mechanical deformation mechanism is characterised by a specific scalar damage variable.*

In order to validate these models and to quantify their accuracy, several numerical strength and failure mode predictions on single lap-joints with spew fillet are presented in section 5. These joints are built of a great variety of adhesives in combination with the same high yield aluminium [1,5].

Finally in section 6, an other more practical point is discussed : *the choice of the non-linear adhesive reference curve.* It can be either deduced from an uniaxial tensile test or from a pure shear one. In order to determine its influence, two numerical strength and failure mode predictions of a mixed double-lap joint with spew fillet are compared with experimental results. This joint is built of two interior bevelled steel pieces and a carbon-epoxy laminate.

2. ELASTOPLASTIC MODEL FOR ADHESIVES

2.1. Adhesive mechanical behaviour and choice of the non-linear reference curve

Structural adhesives, like epoxy resins, present a pronounced non-linear behaviour even at low load levels. *This behaviour is different in uniaxial extension, compression and pure shear.* It is mainly due to the fact that the plasticity of many polymers depends on both the *deviatoric* and the *hydrostatic* stress components. This behaviour induces a difference between the uniaxial yield stress in tension T and compression C. The corresponding ratio S = C/T is nevertheless relatively constant and close to 1.3 for epoxy resins.

In order to connect these experimental curves to a 3-D elastoplastic model, an equivalent stress (Raghava), an equivalent strain (equivalent plastic strain) and a non-linear reference curve must be defined. Classically, the uniaxial extension curve is used as reference : for example, for metals and brittle adhesives. But, for ductile adhesives, it is not the best choice. Indeed, as illustrated at figure 1 for an epoxy resin modified by rubber particles, its failure behaviour is very different in uniaxial extension and pure shear. This different behaviour is mainly due to fact that different deformation micro-mechanisms govern the failure in tension and shear : a stability phenomenon coupled with a localisation one (necking of the test specimen) are the origin of tensile failure, but only damage accumulation leads to shear failure [1]. Therefore, *the experimental pure shear curve is preferred as reference curve for the strength prediction of toughened adhesive joints.*

2.2. The Raghava yield criterion

Raghava & al. [2] suggest for polymers the following modified von Mises yield criterion, depending on both the deviatoric and the hydrostatic stress components :

Paper presented at the 83rd Meeting of the AGARD SMP on "Bolted/Bonded Joints in Polymeric Composites", held in Florence, Italy, 2-3 September 1996, and published in CP-590.

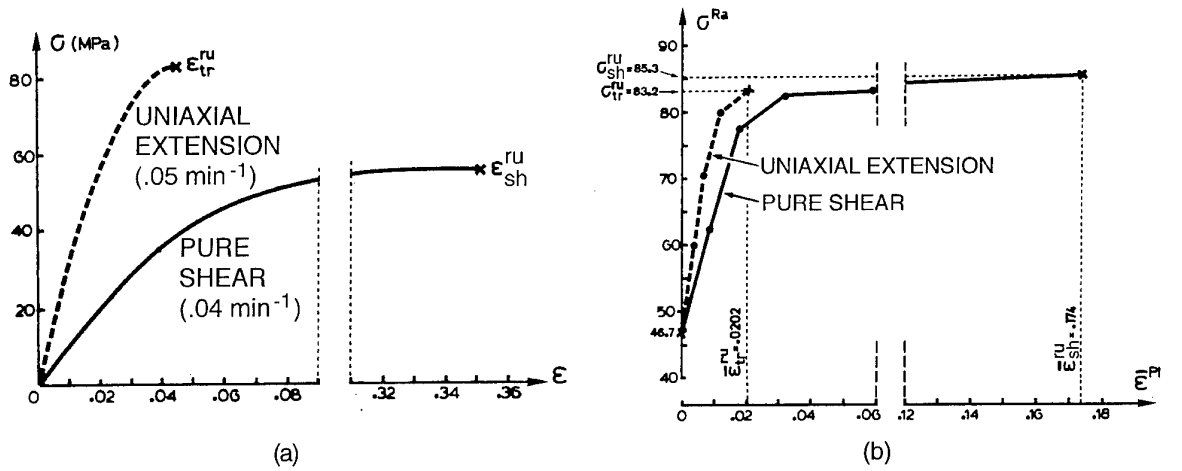


Figure 1 : Uniaxial (a) and equivalent (b) stress/strain curves of a modified epoxy resin in uniaxial extension and pure shear.

$$F(\sigma) = \sigma_{eq} - T = \frac{J_1(S-1) + \sqrt{J_1^2(S-1)^2 + 12\,S J_{2D}}}{2S} - T = 0 \qquad (1)$$

where: - J_1 is the first invariant of the stress tensor σ_{ij}
- J_{2D} is the second invariant of the deviatoric stress tensor s_{ij}
- σ_{eq} is the equivalent stress.

This yield criterion defines a convex surface which describes in the 3-D stress space a paraboloïd and in 2-D one an ellipse whose centre is given by [T-C, T-C]. This yield surface is in good agreement with several biaxial tests results for polymers like PVC, PS, PC and epoxy resins. Note that this criterion reduces to von Mises one, when S = 1.

2.3. Model features : flow rule, hardening behaviour

As polymers are standard materials, an *associated* flow rule is used to describe the plastic strain increase. Its expression is given by :

$$d\varepsilon_{ij}^{pl} = d\lambda \left\{ \frac{(S-1)}{2S} \left[1 + \frac{J_1(S-1)}{\sqrt{J_1^2(S-1)^2 + 12 S J_{2D}}} \right] \delta_{ij} + \frac{3\,s_{ij}}{\sqrt{J_1^2(S-1)^2 + 12 S J_{2D}}} \right\} \qquad (2)$$

where $d\lambda$ is a proportional factor and δ_{ij} the Kronecker symbol.

In order to model the adhesive hardening behaviour, an additional assumption has been introduced : the ratio S = C/T is independent of the hardening parameter h. In this model, the equivalent plastic strain notion is used to characterise the hardening behaviour.

The main feature of this elastoplastic model is the possibility to choose between three different hardening laws : an isotropic one, a linear kinematic one (the yield surface translation is either governed by Prager's rule or by Ziegler's one) or a mixed hardening law.

The establishment of the corresponding elastoplastic constitutive equations and their introduction in an explicit subincrement integration scheme is more detailed at reference [1].

2.4. Finite element library for structural adhesives

This elastoplastic model has been integrated in all 2-D and 3-D volume elements of the SAMCEF code, building so a F.E. library for adhesives which allow to model any kind of adhesively bonded structures. This library contents :

- quadrangular and triangular 2-D isoparametric volume elements;
- a cubic isoparametric volume and thick shell element;
- an isoparametric pentahedron and tetrahedron.

3. SMEARED CRACK PROPAGATION MODEL

Instead of classical fracture mechanic tools, a local failure approach [1,4] has been chosen in order to localise the failure initiation and to predict the joint strength and the failure mode. This choice is mainly governed by the fact that ameliorated adhesives present important inelastic strains before their ductile failure.

In this paper, successively an uncoupled local failure approach, a simple crack propagation model, and a coupled one, a new isotropic damage model, are presented in order to describe the failure behaviour of any kind of adhesives (brittle or ductile ones).

3.1. Failure criteria

As there exists no critical damage value in this uncoupled approach, a macroscopic failure criterion is needed to decree local initiation of a macro-crack. Actually, as suggested by Harris & Adams [5], the following 5 simple failure criteria are available :

- maximum equivalent plastic strain criterion $\bar{\varepsilon}_{max}^{pl}$, corresponding to the last point of the uniaxial reference curve;
- maximum principal stress criterion *combined* with the precedent one;
- maximum principal strain criterion combined with the first one;
- the precedent two simple failure criteria *not combined* with the first one.

3.2. Model assumptions

Locally, in each failed Gauss point, *a virtual crack is assumed to exist normally to the direction of the maximum principal stress (s^1) or strain (e^1)*, according to the chosen failure criterion. This crack induces locally, in the principal stress or strain axis system, *an anisotropic stress relaxation and stiffness reduction*. Furthermore, only at the crack initiation time, the strains are assumed to be unaltered.

According to the adopted 2-D or 3-D finite element model, two different cases must be considered, but only the 2-D one will be described here (see fig. 2).

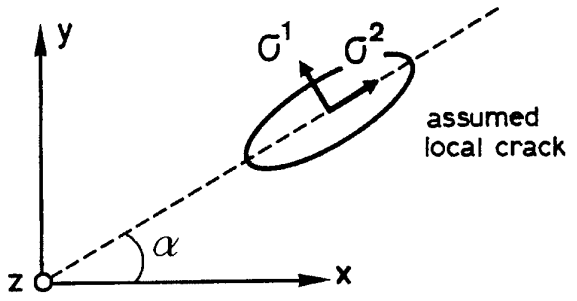


Figure 2 : 2-D virtual crack in the principal stress or strain axis system.

The virtual local crack induces the following new stress state:

$s^1 \approx 0$; $s_z = 0$ (plane stress)

or $s_z \approx 0$ (plane strain)

only s^2 is different from zero.

3.3. Definition of the degraded Hooke matrix

In order to describe this anisotropic stress relaxation and to identify the equivalent Hooke matrix, two numerical stiffness reduction parameters, P_1 and P_2, are introduced in the Hooke matrix of the principal stress or strain axis system. Furthermore, the Poisson's coefficients are assumed to be reduced to zero, so that all coupling between the stress and strain components disappear. Moreover, *the Young and shear modula become insignificant except the modulus in the crack direction, which is reduced but still significant*. So, for a plane strain state, the mechanical behaviour of the cracked zone is governed by the following equivalent Hooke matrix :

$$H_{12}^{degr} = \begin{vmatrix} E_d & 0 & 0 & 0 \\ 0 & \mathbf{P_2 E} & 0 & 0 \\ 0 & 0 & E_d & 0 \\ 0 & 0 & 0 & G_d \end{vmatrix} \qquad (3)$$

where: $$E_d = P_1 . E \; ; \; G_d = \frac{P_1 . E}{2(1+\nu)} \qquad (4)$$

- The degraded modulus E_d is very small but different from zero in order to avoid numerical mechanisms due to zero pivots in the structural stiffness matrix : *P_1 is always chosen equal to 10^{-4}*.
- *The main adjustable parameter is P_2, which characterises the residual stiffness in the crack direction.* Numerical correlation tests with experimental strengths must be achieved respectively for brittle and ductile adhesives in order to determine its specific validation domain and its standard value.

3.4. Post-degradation constitutive equations

Defined by the angle α (see fig. 2), the rotation matrix **A** permits to evaluate the degraded Hooke matrix $\mathbf{Q}_{str}$ in the structural axis system. Furthermore, as the strains are assumed to be unaltered, the adhesive post-degradation behaviour is governed by the following expression :

$$\sigma_{str}^{degr} = Q_{str} : \varepsilon_{str}^{mec} \qquad (5)$$

This relation defines *a pseudo-linear behaviour with a constant Hooke matrix* during the crack propagation.

Remark :

The main weakness of this simple crack propagation model is its constant Hooke matrix after crack initiation, which is not related to an internal damage variable. So, it does not take into account further stress relaxations during crack growth.

4. COUPLED ISOTROPIC DAMAGE MODEL FOR ADHESIVES

4.1. Micromechanical deformation mechanisms

In order to develop for brittle and tough adhesives a new macroscopic damage model coupled with the specific elastoplastic one, it is important to identify, at first, the different micro-deformation mechanisms which dissipate the most energy. As reviewed by Garg & Mai [3], the fracture behaviour of rubber modified epoxy resins involves the following micro-deformation mechanisms :

- strain localisation in shear bands near the inclusion particles;
- nucleation, growth and coalescence of microvoids around the inclusions;
- stretching, tearing and debonding of rubber particles;
- plastic zone at the crack tip and diffuse shear yielding.

The two most energy dissipating deformation mechanisms are : *shear band yielding (a pure deviatoric process) and nucleation, growth and coalescence of microvoids (a pure dilatatoric process)*. Furthermore, in resins ameliorated by inorganic particles, the crack front pinning mechanism contributes also significantly to their fracture toughness.

4.2. Model assumptions and features

As the macroscopic mechanical behaviour of adhesives is *isotropic* in a first approximation, its damage behaviour is also assumed to be isotropic. This implies that scalar damage variables, which are easier to identify by experiments than tensorial ones, are introduced.

Classical isotropic damage models [4] and also Edlund & Klarbring's recent adhesive damage model [6] are characterised by only one scalar damage variable D, which is able to describe the variation of the Young modulus with the damage progress but not the variation of the Poisson's coefficient. So, we prefer to develop *a new isotropic damage model based on two scalar damage variables d et δ : the first one, d, defines the deviatoric component of the damage and the second one, δ, its hydrostatic component.*

Moreover, this choice allows to represent *each principal failure micro-mechanism by its own specific damage variable :*

- the damage variable d, associated with the deviatoric stress tensor, characterises well the shear band formation, mainly governed by deviatoric stresses;
- the variable δ, linked to the hydrostatic stress component, describes well the nucleation, growth and coalescence of microvoids, mainly governed by

This model is an extension and application to the adhesives of the isotropic version of *Ladevèze's model* [7], initially introduced to describe the anisotropic damage behaviour of composite materials. This damage model is based on *the equivalence of the total deformation energy* between the virtual undamaged material and the real damaged one.

4.3. Thermodynamic formulation

1. In this model the equivalent plastic strain $\bar{\varepsilon}^{pl}$, the damage variables δ, d and w, defining a cumulative damage, are adopted as internal variables. The homogenised free energy $\Psi\left(\varepsilon_{ij}^{el}, \bar{\varepsilon}^{pl}, d, \delta, w\right)$ is chosen as thermodynamic potential. ε_{ij}^{el} are there the elastic strains and $\bar{\varepsilon}^{pl}$ the equivalent plastic one. This potential must be convex and verify the following Clausius-Duhem's inequality :

$$\sigma_{ij}\, d\varepsilon_j^{pl} - Rd\bar{\varepsilon}^{pl} - Y_d dd - Y_\delta d\delta - Bdw \geq 0 \qquad (6)$$

where the following thermodynamic forces has been introduced :

- R : measures the increase of the plastic yield surface due to hardening;
- B : by analogy, measures the increase of the damage surface due to w;
- Y_d and Y_δ : respectively associated to d and δ correspond to the total energy release and dissipation rate.

2. *Dissociation of the free energy* : as the plastic strains contribute also to damage accumulation in ductile materials [1], it is important to introduce in this formulation a *strong coupling between the dissipative terms : plasticity and damage.* This coupling is realised by the following original dissociation of the free energy :

$$\Psi\left(\varepsilon_{ij}^{el}, \bar{\varepsilon}^{pl}, d, \delta, w\right) = \overline{W}^{el}\left(e_{ij}^{el}, d\right) + W_{ij}^{el}\left(e_h, \delta\right) + \Psi_d^{el}(w) + \Psi_{pl}\left(\bar{\varepsilon}^{pl}, d, \delta\right) \qquad (7)$$

- $\overline{W}^{el}$ is the deviatoric part and W_h^{el} is the hydrostatic part of the elastic deformation energy;
- Ψ_d^{el} is the elastic free energy due to w and Ψ^{pl} is the plastic one, which depends *explicitly from d and δ and implicitly from w.*

Consequently, Y_d *and* Y_δ *include not only the classical elastic energy release rate but also a plastic dissipation term* [1].

3. *Dissipation potentials* : as plastic flow could occur without damage and otherwise damage could exist without significant plastic flow, the damage and plastic dissipations must *separately* verify Clausius-Duhem's inequality (6) :

$$\sigma_{ij}\, d\varepsilon_{ij}^{pl} - Rd\bar{\varepsilon}^{pl} \geq 0 \;\; ; \;\; -Y_d dd - Y_\delta d\delta - Bdw \geq 0 \qquad (8)$$

An elegant way to ensure these inequalities is to assume the existence of a dissipation potential ϕ and its dual ϕ^* composed of two *independent* parts F_{pl} and F_d :

$$\Phi^* = F_{pl}\left(\sigma_{ij}, R\right) + F_d\left(Y_d, Y_\delta, B\right) \qquad (9)$$

Finally, the expressions:

$$F_{pl} = 0 \quad \text{et} \quad F_d = 0 \qquad (10)$$

define respectively the plastic yield surface and the damage one.

4.4. The plastic and damage yield surfaces

The plastic yield surface defined by the Raghava criterion (1) depends on both damage variables d and δ and not only on the deviatoric one, as the von Mises criterion. Their influence on the Raghava criterion is illustrated at figure 3 : *the deviatoric damage variable d reduces the initial threshold and the ratio S but the hydrostatic one , δ, still increases the initial ratio S.*

As damage yield surface, we adopt Ladeveze's energy expression [7]:

$$F_d = -Y_d - \langle\tau\rangle Y_\delta - B_0 - B(w) = 0 \qquad (11)$$

where $\langle\tau\rangle = \dfrac{\delta}{d}$ for $\tilde{\sigma}_h > 0$; $\langle\tau\rangle = 0$ for $\tilde{\sigma}_h \leq 0$ (12)

B_0 is the initial damage threshold and B(w) defines the increase of this threshold due to the cumulative damage w.

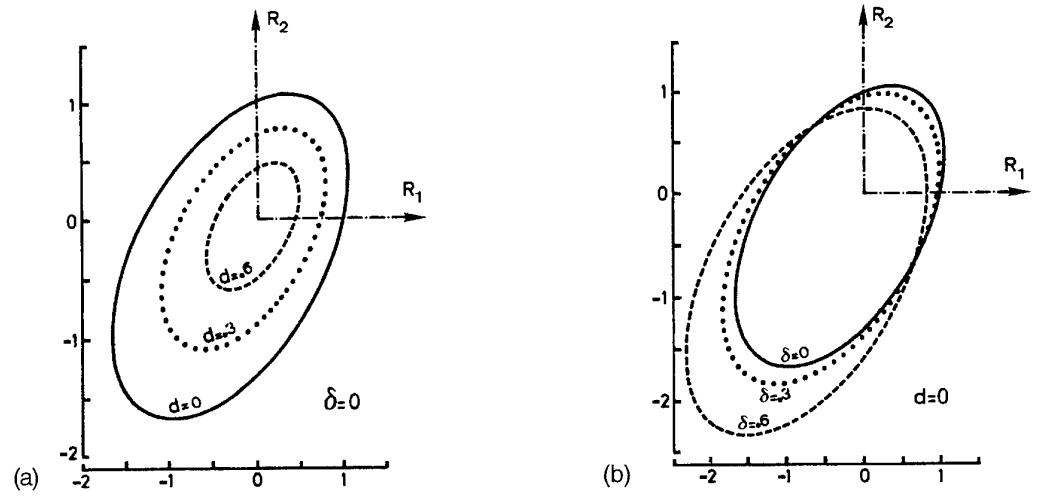


Figure 3: Damage influence on the Raghava yield surface : (a) pure deviatoric damage (b) pure hydrostatic damage.

The parameter <τ> indicates that a compressive hydrostatic state does not contribute to the damage evolution, but well a tensile one. So, *a different hydrostatic damage behaviour is introduced in tension and compression.*

4.5. Damage evolution and incremental constitutive equations

As the damage criterion is expressed by energy quantities, the damage evolution equations are naturally deduced from *the principle of maximum damage dissipation*, like as for plasticity. Their expressions are given at reference [1]. The incremental constitutive equations of our model are then established by using the consistency condition of the two yield surfaces : $dF_{pl} = 0$ and $dF_d = 0$.

This coupled adhesive damage model has been then introduced in an implicit integration scheme, *the closest-point-projection algorithm*. In order to take into account a strong coupling between plasticity and damage, a coupled damage/plasticity corrector phase has been adopted in this algorithm. Finally, the consistent incremental Hooke matrix is evaluated by a simple perturbation technique.

5. NUMERICAL STRENGTH PREDICTION OF SINGLE-LAP JOINTS

In order to validate our simple crack propagation model and to quantify its accuracy, several numerical strength and failure mode predictions have been realised on single-lap joints with spew fillet (see figure 4). These joints correspond to the ASTM D1002-72 specifications and are built of a great variety of adhesives (see figure 5) in combination with the same high yield aluminium adherent (2L73).

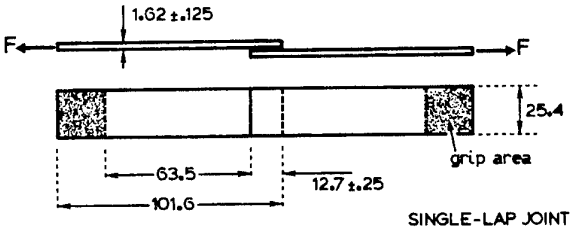


Figure 4 : Single-lap joint corresponding to the ASTM D1002-72 specifications.

In this paper, strength results will only be presented for the semi-brittle adhesive AY-103 and the ductile one MY-750 + 15% CTBN. Results for the other adhesives will be found in reference [1]. Material properties of the retained adhesives and the aluminium adherent can be found in references [1] and [5]. Their uniaxial non-linear stress/strain curve is given at figure 5.

In order to estimate the influence of the F.E. mesh on the strength predictions, two different 2-D plane strain F.E. meshes are adopted :

- the reference mesh: the same as Harris & Adams [5]. This mesh has only one 2^{d} degree element over the glue thickness, which leads to a model with 1367 D.O.F.;
- the refined mesh (see ref. [1]) : it has three 1^{st} degree elements over the glue thickness but only 1133 D.O.F.

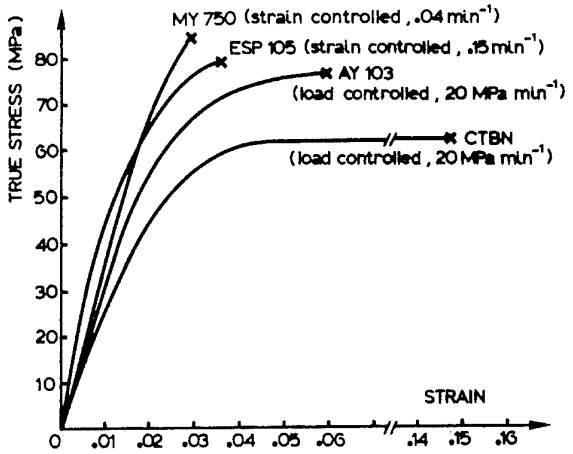


Figure 5 : Uniaxial tensile curves of bulk structural adhesives.

5.1. Semi-brittle adhesive AY-103

A first numerical investigation phase [1] has been realised with the reference model in order to define a correct value of the stiffness reduction parameter P_2. It leads to following recommendations for P_2 :

- values below 10^{-2} have no influence on the predicted joint strength, but values above 6.10^{-2} have a significant but bad influence;
- so, *its validation domain for brittle adhesives is : $10^{-2} \leq P_2 \leq 6.10^{-2}$ and $P_2 = 3.10^{-2}$ is adopted as standard value.*

As suggested by Harris & Adams [5], the combination of the maximum principal stress criterion and $\bar{\varepsilon}^{pl}_{max}$ is adopted as the most appropriate failure criterion for this semi-brittle adhesive. Our numerical strength predictions are reported at table 1, where they are compared with Harris & Adams numerical and experimental results. These results need some comments :

- as the failure initiation already overestimates the experimental strength by 6.8 %, our strength predictions with the reference mesh are really too stiff. So, *the reference mesh is not appropriate* to predict accurately failure initiation and joint strength;
- the influence of the F.E. mesh on the joint strength is really *significant*. Indeed, *the use of a finer mesh* where the critical Gauss point is at a distance of 22.8 μ from the singular point (corner), *gives excellent predictions* : only an error of 1.7 % is observed !;
- for this refined mesh, the choice of the parameter P_2 in its validation domain has no significant influence on the joint strength prediction;
- *these results justify the development of the simple failure model* and indicate clearly that Harris & Adams assumption [5] of instantaneous cohesive failure with no further load increase after local failure initiation is inconsistent for this assembly.

The predicted failure mode, which corresponds to mode III (see Harris & Adams notations [5]) is illustrated at figure 6.

models	crack initiation		strength	
	value	error	value	error
a) *experience* **5.9 kN ± 1.03 kN**				
b) *reference mesh*				
$P_2 = 10^{-4}$	6.3 kN	6.8 %	8.4 kN	42.4 %
$P_2 = 5.10^{-2}$	6.3 kN	6.8 %	9.2 kN	55.9 %
Harris & Adams	5.5 kN	-6.8 %		
c) *refined mesh*				
$P_2 = 10^{-2}$	4.97 kN	-15.7 %	**5.8 kN**	-1.7 %
$P_2 = 5.10^{-2}$	4.97 kN	-15.7 %	**5.8 kN**	-1.7 %

Table 1 : Strength predictions of the AY-103 / 2L73 joint.

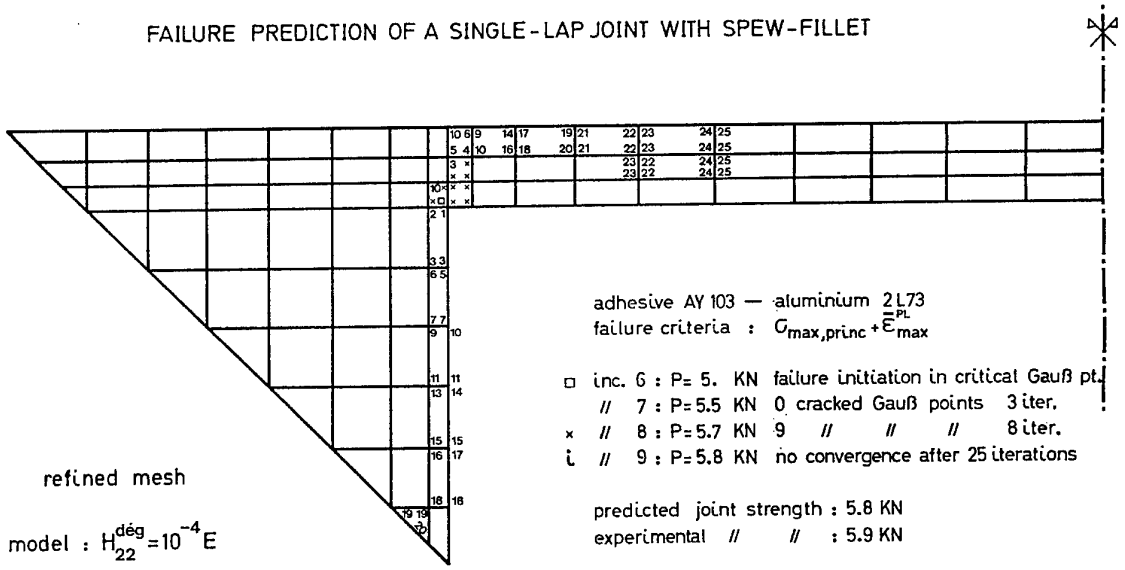


Figure 6 : Predicted failure mode of the AY-103 / 2L723 joint.

At first, the crack spreads along the adherent boundary of the spew fillet and through the glue thickness in the critical area and, then, only in the adhesive layer. This mode III has been also observed experimentally by Harris & Adams.

5.2. The ductile adhesive MY-750 + 15% CTBN

The addition of rubber particles in the proportion 100:15 leads the brittle epoxy resin MY-750 (see figure 5) to *a ductile and tough behaviour*. Indeed, the uniaxial tensile test curve presents large deformations (> 14 %). As suggested by Harris & Adams [5], the maximum principal strain criterion combined with $\bar{\varepsilon}^{pl}_{max}$ is the most suitable failure criterion for these adhesives.

The experimental strength and several joint strength predictions with the refined mesh are reported at table 2.

These results need some comments :

- the simple failure model with values of the stiffness reduction parameter P_2 comprised between 10^{-2} and 6.10^{-2} - validation domain of brittle adhesives - underestimates significantly (≈ 17 %) the experimental strength of this tough joint. But, using values of P_2 comprised between 8.10^{-2} and 10^{-1}, *our strength predictions become really better and acceptable for an engineer*. Indeed, only an error of 5% is recorded when $P_2 = 9.10^{-2}$.
- So, in order to take implicitly into account the micro-mechanical toughening mechanisms of modified epoxy resins, an other specific validation domain of P_2 is defined for these adhesives :

$$8.10^{-2} \leq P_2 \leq 10^{-1} \quad \text{(standard value : } P_2 = 9.10^{-2})$$

models	criterion	failure initiation		strength	
		value	error	value	error
a) *experience 15.9 kN* (± 0.53 kN)					
b) *refined model*					
$P_2 = 3.10^{-2}$	$\varepsilon^{max}_{princ} + \bar{\varepsilon}^{pl}_{max}$	12.9 kN	-18.9 %	**12.9** kN	-18.9%
$P_2 = 6.10^{-2}$	$\varepsilon^{max}_{princ} + \bar{\varepsilon}^{pl}_{max}$	12.9 kN	-18.9 %	**13.4** kN	-15.7%
$P_2 = 8.10^{-2}$	$\varepsilon^{max}_{princ} + \bar{\varepsilon}^{pl}_{max}$	12.9 kN	-18.9 %	**14.4** kN	-9.4 %
$P_2 = 9.10^{-2}$	$\varepsilon^{max}_{princ}$	13.2 kN	-17 %	**15.1** kN	-5 %

Table 2: Strength predictions of the MY-750 + 15 % CTBN / 2L73 joint.

6. STRENGTH PREDICTION OF A CFRP/STEEL DOUBLE-LAP JOINT

Double-lap bonding is an appropriate technique to assembly two metal pieces with a composite plate. Among the design configurations tested experimentally and numerically by Adams & al. [8], the most resistant one is here retained. This design, illustrated at figure 7, is characterised by an interior bevelled steel end and a spew fillet of 30°.

The central CFRP adherent is built up on UD carbon-epoxy plies oriented at 0°. Adams & al. [8] use as adhesive, the modified epoxy resin whose tensile and pure shear response are given at figure 1. Their main difference occurs for the equivalent failure strain : $\bar{\varepsilon}^{ru}_{tens}$ 2.02 % again $\bar{\varepsilon}^{ru}_{sh}$ 17.4 %. The material properties of the retained adhesive, steel and composite adherents can be found in references [1] and [8].

Aim:
Determine the influence of the choice of the non-linear reference curve on the joint strength prediction. Therefore, two complete non-linear analyses with strength prediction have been achieved respectively with the uniaxial extension and the pure shear curve as reference one.

Experimental results:
Adams & al. [8] observe that this double-lap joint fails at *3.05 kN* by transverse matrix cracking of the 0° plies under the spew fillet at the bevelled overlap end.

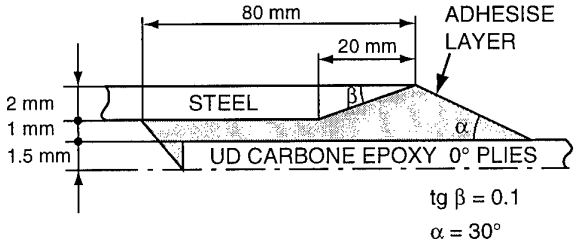


Figure 7 :Interior bevelled mixed double-lap joint with spew fillet.

6.1. Non-linear analysis and strength prediction with the uniaxial extension curve as reference curve

The plasticity in the joint is confined around the bevelled steel end at low load levels (P < 2. kN). But, the yielding of the steel adherent at P = 2.4 kN modifies completely the plastic growth in the adhesive layer : it increases now more in the first spew fillet than in the bevelled region [1]. This local plasticity increase is so pronounced that a macro-crack initiation is predicted at P= 2.6 kN. This crack grows along the free boundary of the first spew fillet until the ultimate load: P= *2.68 kN*. This failure load underestimates the experimental one by 12.1 %. But worse, *a wrong failure mode - cracking of the adhesive layer - is predicted.* Moreover, at this load level, the Tsai-Wu criterion confirms that all 0° plies are always intact.

6.2. Strength prediction with the pure shear curve as reference curve

As the failure plastic strain is now greater, no premature failure initiation occurs at P = 2.6 kN. Further load increments are applied until 2.8 kN. At this load, the Tsai-Wu criterion is verified in the composite adherent under the second spew fillet, as illustrated at fig. 8.a, and the UD plies degrade by transverse matrix cracking. Moreover, the adhesive modelled with the pure shear curve is always intact at this load level, as confirmed by the plastic flow diagram given on fig. 8.b.

After matrix degradation, the transverse stresses in a damaged ply are assumed to be maintained at their failure value. With this simple post-degradation behaviour few further load increments have been applied up to P= *2.97 kN*, load at which the joint failure is decreed. *This predicted strength is in excellent agreement with the experimental one (2.6 % error).*

Note that at 2.93 kN, the plastic strain in the adhesive reaches also locally, in the first spew fillet, its failure value. So that, for the last 3 increments, *a complex failure mode* is predicted : matrix cracking at the bevelled end and adhesive crack propagation at the other end.

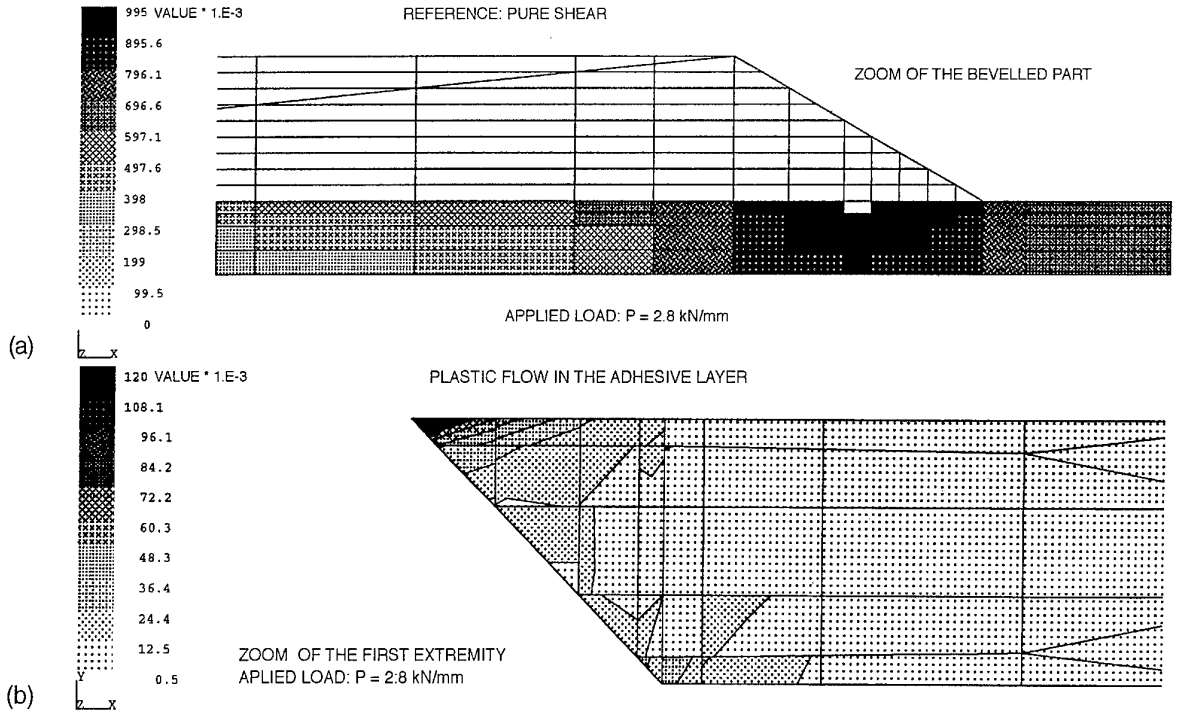


Figure 8 : a) Partial degradation of the composite adherent decreed by Tsai-Wu at P = 2.8 kN;
b) Plastic flow in the adhesive layer near the first overlap end.

7. CONCLUSIONS

The new simple failure model, combined respectively with the maximum principal stress or strain criterion, localises accurately the failure initiation and determines the possible joint strength reserve. Furthermore, with a judicious F.E. model, it predicts correctly the failure mode and the joint strength of brittle adhesives and provides satisfying results for ductile and modified resins. As the last predictions are always conservative, it will be interesting to respect these values as bonds during the joint design phase.

In order to improve and to remedy the main drawbacks of this simple failure model (significant influence of the F.E. mesh, constant Hooke matrix,...), a new coupled isotropic damage model for adhesives has been developed. This model linked in the future with an appropriate localisation technique [1] will be able to describe more physically and accurately all adhesive degradation mechanisms until the joint failure.

Finally, the strength predictions of a mixed double-lap joint show obviously the superiority of the pure shear test curve over the uniaxial extension one as reference curve in the adhesive elastoplastic model.

REFERENCES

[1] G. LASCHET : "Prediction par éléments finis du comportement non linéaire et de la résistance d'assemblages multimatériaux collés", Ph. D. thesis, University of Liège, July 94.

[2] R. RAGHAVA, R.M. CADDELL & G.S. YEH : "The macroscopic yield behaviour of polymers", J. Mater. Scien., Vol. 8, 1973, pp 225-232.

[3] A.C. GARG & Y.W. MAI : "Failure mechanisms in toughened epoxy resins - a review", Compos. Scienc. & Techno., Vol. 31, 1988, pp 179-223.

[4] A. BENALLAL, R. BILLARDON & J. LEMAITRE : "Continuum damage mechanics and local approach to fracture : numerical procedures", Comp. Meth. Appl. Mech. & Engng., Vol. 92, 1991, pp 141-155.

[5] J.A. HARRIS & R.D. ADAMS : "Strength prediction of bonded single-lap joints by non-linear finite element methods", Int. J. Adhes. & Adhesives, Vol. 4, n° 2, 1984, pp 65-78.

[6] U. EDLUND & A. KLARBRING : "A coupled elasto-plastic damage model for rubber modified epoxy adhesives", Int. J. Sol. & Struct., Vol. 30, n° 19, 1993, pp 2693-2708.

[7] P. LADEVEZE : "Sur une théorie de l'endommagement anisotrope", rapport interne n° 34, L.M.T. de Cachan, 1984.

[8] R.D. ADAMS, R.W. WATKINS, J. A. HARRIS & A.J. KINLOCH : "Stress analysis and failure properties of carbon-fibre-reinforced-plastic/steel double-lap joints", J. Adhesion, Vol. 20, 1986, pp 29-53.

Structural Efficiency of Different Assembly Methods for Stiffened Composite Panels: Cocuring and Secondary Bonding

F.Elaldı
Technical Department
Turkish Land Forces , Ankara 06100, Turkey

S.Lee
Structures, Materials and Propulsion Lab.
IAR, Nationai Research Council, K1A 0R6, Ottawa, Canada

SUMMARY

The recent introduction of composite materials in aircraft primary structures has resulted in lower weight and improved performance. These improvements require the development of new design concept and manufacturing techniques for weight and cost efficient structures. Current manufacturing approaches are focused on cocurring, where the skin and stiffeners are cured together in a single autoclave cure, and secondary bonding, where stiffeners and skin are cured separately and then bonded together with an adhesive film. For this study, cocurring and secondary bonding manufacturing techniques were used to produce four stiffened panels. Experience gained with those techniques is discussed. Ultrasound C-scan inspection was carried out to detect any defects in the panels. These panels were tested in compression to verify their structural efficiency of assembling technique.

This paper presents the details of different assembly methods, and identifies and discusses the advantages and disadvantages of each manufacturing technique.

1. INTRODUCTION

The use of advanced composites in aircraft structures has demonstrated the potential for decreasing structural weight. Weight savings result from the high stiffness-to-density and high strength-to-density properties of fibres such as carbon. The technologies used for a civil aircraft may not be the same as those used for a military aircraft (fighter type) since the priorities are different. Performance is usually the top priority for military aircraft [1]. In most cases this means that the structure must achieve a given task with minimal weight. Life cycle cost which includes the original equipment cost, direct operating cost and inspection and maintenance cost (including repair) is important for any type of aircraft. Traditionally, stiffened panels and shell structures are designed to reduce the weight of the aircraft [1-7].

In order to optimize the design of stiffened structures, design concepts must be verified by experiments. In addition, new fabrication techniques have to be developed in order to produce integrally stiffened panels. Integrally stiffened composite panels will result in reduced part count when compared to equivalent metal structures, thus reducing assembly time.

This study is concerned with the design, fabrication and testing of stiffened composite panels. Current manufacturing approaches are focused on cocuring, where the skin and stiffeners are cured together in a single autoclave cure, and secondary bonding, where stiffeners and skin are cured separately and then bonded together. In this report, both manufacturing techniques are discussed on the basis of structural efficiency and advantages and disadvantages are emphasised.

2. STIFFENER-SKIN ATTACHMENT DESIGN

The influence of the stiffener-skin attachment design on the performance of the stiffeners on a skin was investigated by several researchers [1-3]. In reference [3], several different attachment designs were evaluated on a static strength basis. The test data from this study are summarized in Figure 1. Among these alternate designs, the tailored flange and the tailored flange-skin designs seem to be more efficient, especially for the post-buckling loading range. The tailored flange design concept was also found to contribute to longer fatigue life. The baseline design with stitching exhibited some improvement in strength, but it is still difficult to stitch the flange to the skin due to the lay-up complexity. The stitching can arrest delamination growth, but the stitching may also provide a potential failure site.

It was found that the use of a smooth radius in joining the web to the skin maximized joint strength and also that joint strength increased as the radius of the joint increased [3,4].

3. MANUFACTURING CONCEPTS

The producibility of advanced composite structures is based on a compromise between design requirements and the manufacturing characteristics and limitations of the materials. Hence, the manufacturing process is one of the most critical factors in the successful use of advanced composite materials in aircraft structures. The objective of developing a manufacturing process is to establish manufacturing techniques for compatible design approaches and to achieve the goal of cost-effective manufacture of composite structures. For manufacturing of stiffened composite panels, **tooling and fabrication** are considered to be critical.

3.1 Tooling

General experience has indicated that certain characteristics are essential for tooling used to cure large and complex parts. The researchers [4,5] have indicated that the most important parameters of tooling for large and complex composite parts are;

a. thermal properties
b. structural properties

Paper presented at the 83rd Meeting of the AGARD SMP on "Bolted/Bonded Joints in Polymeric Composites", held in Florence, Italy, 2-3 September 1996, and published in CP-590.

c. surface characteristics
d. maintenance
e. reasonable costs and lead time

There are two important curing tools for stiffened composite structures such as the skin of a fuselage or wing skin components; one is the caul plate (skin tool) and the other is the mandrel. The caul plate is used for the manufacture of skin components while mandrels are used for the fabrication of stiffeners. The materials for the caul plates and mandrels should be selected according to above parameters.

It is usually difficult to achieve compatible thermal expansion between the part and the tool unless the tool is composed of the same material as the part and has the same ply orientation. This is not to say that steel, aluminum or plastic material should not be used to make tools for stiffener and skin components. Tools made of these materials are also used for making flat or slightly contoured skins where thermal distortion can be controlled by design.

The latest investigations show that the most suitable tooling materials for stiffeners are elastomeric and foam materials. Carbon fibre reinforced composite materials are suitable for making caul plates. Elastomers were found [1-7] to have more of the properties required for making the tools for open or closed section stiffeners than other available materials. The caul plates for the manufacture of fuselage and wing skin components are generally manufactured from carbon fibre cloth using a wet lay-up technique with a high service temperature curing resin.

3.2 Fabrication

Stiffeners are usually assembled by following the designed ply orientation and stacking order for proper placement of prepreg tapes, ply by ply, on the tool. Open-section stiffeners are laid either on the mandrels directly or on a flat base plate and then placed on the mandrels. All lay-ups are vacuum bagged for compacting the plies. To enhance the forming and to ensure conformance with the mandrel, hot air is used in addition to vacuum. This is a debulking process that is sometimes referred to as hot-forming.
The lay-up technique for closed-section stiffeners is almost the same as for an open-section stiffeners except that inserts (mandrels) in combination with machined molds are used to form the stiffeners. Similarly, hot air and steel rollers are used to ensure that the prepreg layers conform to the mold. After forming the stiffeners there are two methods for assembling stiffeners and skin [6];

a. **Cocuring**: Stiffeners are integrally cured with the skin in one cure cycle, see Figure 2.

b. **Secondary bonding**: Stiffeners and skin are cured separately and bonded together with an adhesive film in a secondary operation , see Figure 3.

4. PANEL SIZE AND CONFIGURATION

The selection of the appropriate panel size and configuration for experimental examination should be based upon two main factors. First, the panel configuration should be such that it simulates closely the geometry and loading conditions in a real structure such as one might find in fuselages of a future V/STOL airplane, second, the panel size should be such that it is feasible to test it with commonly available test equipment at a reasonable cost.

In this study, the structural component that was selected was a J-stiffened panel designed to perform in post-buckling. The J-sections were selected because of structural efficiency over other types of stiffeners (except hat stiffeners) particularly when used as axial load members to carry fuselage bending moments and common use in aerospace vertical and horizontal stabilizers, fuselage, wing structures of aircraft.
The stiffened panels were designed and fabricated at National Research Council of Canada, Institute for Aerospace Research. The test panel consists of two bays containing three cocured J-stiffeners which simulate stringers on a fuselage skin. As an example consider the sketch shown in Figure 4.

In the absence of any better ultimate stress criteria a compression stress of 225.3 MPa [1,3] was assumed to be the ultimate compression allowable for the panel. The minimum panel thickness required to carry an ultimate compression load of 350 KN/m will thus be 3.14 mm. Since the nominal thickness per ply of IM6/5245C carbon-epoxy prepreg chosen is 0.129 mm, the laminate configuration requires twelve unidirectional plies of tape. Eight of these plies are chosen ± 45 degrees with respect to loading axis to compensate shear loads, two plies are chosen zero degree and two plies are chosen 90 degree plies to get a quasi-isotropic structure. Thus the panel configuration is $(\pm 45/90/0/\pm 45)_s$ where reference axis is in the longitudinal direction. It is noted that this configuration is midplane symmetric. To prevent the stiffener from being buckled until the total failure occurs, additional twelve zero degree plies were inserted to the cap (outer flange) of the stiffener.

5. PANEL FABRICATION

Two manufacturing process which are cocuring and secondary bonding, were used and in total, four panels were produced. Each panel was assigned a code so that all the information and data pertaining to a particular panel could be retained and identified.

5.1 Material and Tooling

The composite materials used in this study were unidirectional tape of carbon fibre pre-impregnated with modified epoxy resin (prepreg). The carbon fibres were Hercules IM6 and the epoxy resin was Narmco 5245C. Narmco IM6/5245C material was chosen for this study since utilized modified epoxy-resin system with improved resin toughness.. A common characteristic of the tougher resin systems is their greater ductility and higher strain to failure. The prepreg material was relatively dry and lacked adequate tackiness for the lay-up. To ensure that any trapped air and wrinkles were removed, the prepreg plies were smoothed with a piece of teflon and moderate heat from a heat gun was applied to improve tack. Typical physical and mechanical properties of this material can be found in the open literature.

A skin lay-up tool was machined from 12.7 mm thick aluminum plate stock, 625 mm wide and 865 mm long. The surface of the tool was sanded and polished. The forming

and curing tools for stiffeners and three sets of angle supports were machined from aluminum material and positioned on the lay-up. The aluminum sheets; 0.55 mm thick, 635 mm long were used to cover the skin lay-up which was not occupied by stiffener flanges.

5.2 Fabrication of Cocuring Panels

Four successive manufacturing sequence plans were prepared for adaptive development with successive modification efforts aimed at removing some steps and consolidating others to reduce the total number of sequences in the manufacturing process.

In the evolutionary development of the cocurring technology, all of the tools for fabricating stiffeners and skin were coated with a non-silicone release agent prior to lay-up to ensure that the cured composite parts would easily separate from the tools. All stiffeners and skin plies were cut in accordance with the configuration by using templates. Following the stacking sequences, plies were placed on the curing tools one by one for the U, Z and skin parts. The plies were then tightly pressed against the forming and curing tools with a teflon block, The curing tools for the stiffeners were assembled and secured with C-clamps. Later, unidirectional material was cut to a width of 63.5 mm, hand rolled into a rod shape and then placed into the cavity which ran the full length of the flange-skin joint. Accordingly, it was compacted by means of air heater and roller. All stiffener lay-ups and curing tools were then placed on the flat skin plies after aluminum cover sheets for the skin were positioned properly. A layer of parting film and a layer of bleeder were applied over the whole assembly. Also, one ply of breather was placed around the edges of the laminate.

The entire assembly was then vacuum bagged for the autoclave cure. The bagged assembly was pre-compacted for 30 minutes at a pressure of 690 KPa and a temperature of 125°C in the autoclave before curing. The prepreg manufacturer's recommended cure cycle for IM6/5245C is then applied. Three stiffened panels were made using the cocuring technique and were identified as J1, J2 and J3, see Figure 5.

5.3 Fabrication of Secondary Bonded Panel

In the lay up, tooling and curing techniques of the skin and stiffeners the fabrication process are the same with the cocurred ones. The only difference is that the cured stiffeners were bonded with the thermally activated epoxy film system, FM 300, on the cured skin in a second curing operation. Only one panel was made using the secondary bonding technique and identified as J4.

5.4 Scanning and Panel Preparation

The four panels were inspected in the IAR ultrasonic inspection facility using C-scan in both the pulse-echo and reflection pulse-echo modes of inspection. Examination of the surfaces of the panels revealed areas that corresponded to the indications on the C-scan plots which appeared to be a small amount of distortion (warpage). Since the pulse-echo technique is sensitive to surface distortion the inspection was repeated in reflection pulse-echo in an attempt to determine whether these apparent defects were delaminations. All four panels exhibited areas which appear to be distortions, and except a few minor defects in one stiffener web, no other defects were detected.

After trimming and cleaning, the panels were mounted and cast into a steel U shape channels using room temperature cured epoxy resin. These U-shape channels act as a mould for potting the ends of the panel and serve as an end plate for transferring the load from the test machine to the test panel. Except one panel, which had 24 strain gauges (J2), test panels were instrumented with 20 strain gauges.

6. TESTING AND TEST RESULTS

Panels were tested in compression with a 2.7 MN Baldwin test machine. Loads were taken by means of pressure a transducer mounted to the hydraulic system of the machine. After the panel was carefully centered in the platen of the test machine, the test panel was axially loaded in compression with constant increments of loads. The load was increased until the ultimate failure of the test panel occurred. Strains and loads were gathered by a data acquisition system (Sciemetric System 200) and recorded by a computer.

The load-strain curves for each strain gauge pair were obtained from the data recorded by the data acquisition system. Strain data from longitudinal back to back strain gauges located at the skin edges, bays between stiffeners, stiffener caps, flanges, and web of the four test panels are shown in Figure 6. Failure load and failure strains are also given in Table 1.

7. DISCUSSION

Compression strains in the cap section showed that the caps did not buckle but deformed slightly prior to collapse of the stiffeners. The caps were the basic load carrying elements of the stiffeners which was consistent with the post buckled design.

The data from the longitudinal back-to-back strain gauges located on the stiffener flange are shown in Figure 6. Higher strains were recorded as the applied load increased and this indicated that the flange element remained intact prior to the ultimate failure. Apparently, these higher strains at the stiffener flanges may have contributed to a local failure in the skin-stiffener interface region.

The first three panels (J1, J2, and J3), which were fabricated by cocurring the skin with the stiffeners, failed at a average load of 21500 kg. The fourth panel was fabricated by secondary bonding the skin to the stiffener in a second operation and it failed at 25360 kg, which is about 18 % higher than the cocurred ones. Panel J3 failed at lowest load, which was 20230 kg. This might be attributed to the existence of some small defects which were found on the stiffener web. The failure of this panel occurred at the section containing the defects .

The failure mode was associated with compression failure of the caps, local delamination in the flange-skin section and failure along the 45° lines in the skin. The maximum strains for all the test panels were in the range from 5 % (5255 microstrain) to 6 % (5911 microstrain), see Table 1. It appears that the failure initially occurred due to the separations or delaminations of the stiffeners from the skin,

but it is noted that the separations (delamination) are local in nature and are believed to have been caused by the compression failure of the stiffener caps. The global failure modes of the test panels are also presented in Figure 7.

8. STRUCTURAL EFFICIENCY OF TEST PANEL

To evaluate the structural performance of the test panels a structural efficiency method [7] was used. The structural efficiency of the panel is:

$$K = (AL / W).(\overline{N} / L)^{1/2}$$

where K is the structural efficiency coefficient, W is the weight of the panel, A is the area of panel, L is the length of the panel and $\overline{N}$ is the applied load/width. This coefficient can serve as a measure of relative merit for various configurations. The efficiency coefficients in Table 1 are based on experimental data.

The coefficient of structural efficiency for the cocurred panels was $2.39*10^{-2}$, while the theoretical values for a J-stiffened aluminum panel and a carbon-epoxy J-stiffened panel from [7] are $3.52*10^{-2}$ and $2.10*10^{-2}$ respectively. This indicates that the panels manufactured in this study would be slightly heavier than the theoretical carbon-epoxy J-stiffened panel but much lighter than the minimum-weight aluminum J-stiffened panel designed to carry an identical compression load.

The similar comparison revealed that the secondarily bonded J-stiffened panel which had a structural efficiency coefficient of $2.26*10^{-2}$ would be 1.07 times heavier than theoretical minimum-weight carbon-epoxy J-stiffened panel with the same load carrying capability. The cocurred J-stiffened composite panels had structural efficiencies that were approximately 32 % greater than that of the J-stiffened aluminum panel, while for the secondarily bonded J-stiffened composite panel it is about 36 % greater.

9. CONCLUSIONS

1. Simple technique have been developed to lay up plies efficiently for the stiffener elements,
2. The tools for the stiffeners were satisfactory,,
3. No significant separation between skin and stiffeners was observed before failure, only local separation occurred around the failure section,
4. Secondary bonded stiffened panels may carry slightly higher loads than cocurred stiffened panels but perhaps at the expense of additional fabrication cost,
5. Considering the data obtained , it can be concluded that the secondary bonding technique is easier to apply than the cocuring technique for complex structures and it usually costs less in tooling due to its simplicity. However, the cocuring technique offers the following advantages;

a. large one-piece structures can be made, thus eliminating joints and discontinuities and improving structural integrity,

b. the manufacturing process involves fewer operations, and

c. fewer fit-up problems occur and less sealing is required in assemblies which reduce costs.

6. The results showed that J-stiffened carbon-epoxy panels can be designed to carry a specified compression load with 32-36 % less weight than is required by the most efficient aluminum J-stiffened configuration.

10. ACKNOWLEDGEMENT

The support of DND CRAD-DIRD through the Defence Research Fellowship Program is acknowledged. The authors would like to thank Dr. W. Wallace, Director of the Structures and Materials Laboratory of IAR, for his support of this work and also to thank Mr. C.E. Chapman, Mr. W. Ubbink and Mr. P.A. Adams for their technical support.

11. REFERENCES

1. Agarwal, B.L., "Postbuckling Behaviour of Composite Shear Webs", AIAA Journal, 19, No. 7, 933 (1981).

2. Cope, R.D., and R.B. Pipes, "Design of the Spar-Wingskin Joint", Fibrous Composites in Structural Design, E. Edward, D.W. Oplinger, and J.J. Burke, Eds., Plenum Press, New York (1980).

3. Renieri, M.P., and R.I. Garret, "Stiffener/Skin Interface Design Improvements for Postbuckled Composite Shear Panels", NADC-80134-60, Naval Air Development Centre (1982).

4. Starnes, J.H.Jr., N.F. Knight, and M. Rouse, "Postbuckling Behaviour of Selected Flat Stiffened Grp/Ep Panels Loaded in Compression", AIAA Paper, No. 82-0777, 464 (1982).

5. Bell, J.E., and I.J. Muha, "Integrally Stiffened Co-Cured Shear Panel", Fibrous Composites in Structural Design , M. Edward, D.W. Oplinger, and J.J. Burke, Eds., Plenum Press, New York, 187 (1980).

6. Elaldı, F., S. Lee, and R.F. Scott, NRC LTR-ST-1872, p.8, (April, 1992).

7. Williams, J.G., and M.M.Jr. Mikulas, "Analytical and Experimental Study of Structurally Efficient Composite Hat-Stiffened Panels Loaded in Axial Compression", Paper presented at the 16th Structures, Structural Dynamics and Materials Conference, Denver, USA (May, 1975).

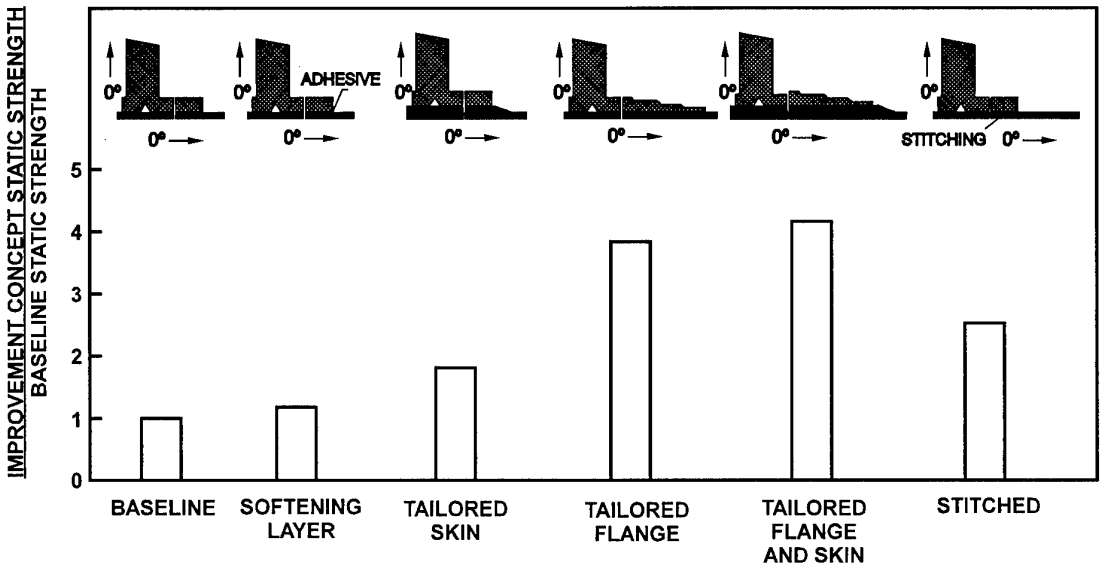


FIGURE 1. COMPARISON OF STATIC STRENGTH FOR SEVERAL STIFFENER-SKIN INTERFACE DESIGN

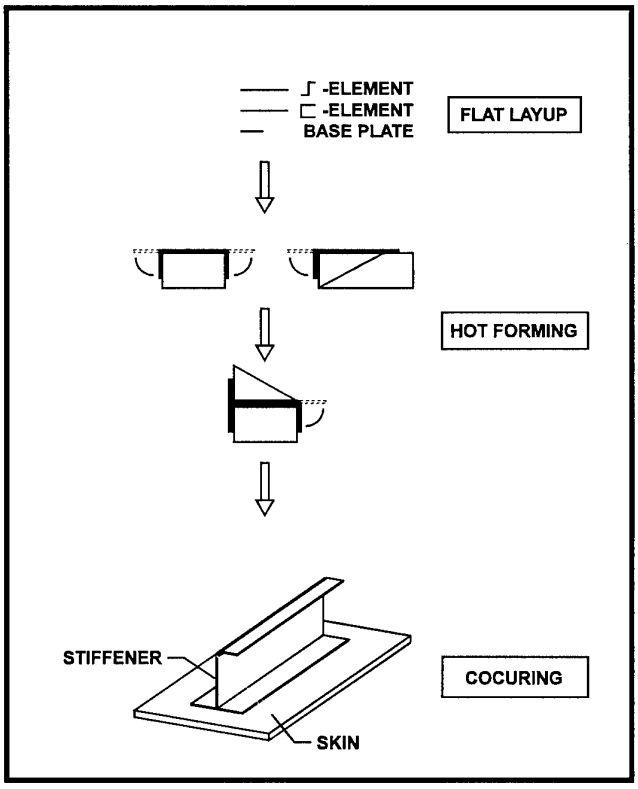


FIGURE 2. SCHEMATIC VIEW OF COCURING TECHNIQUE

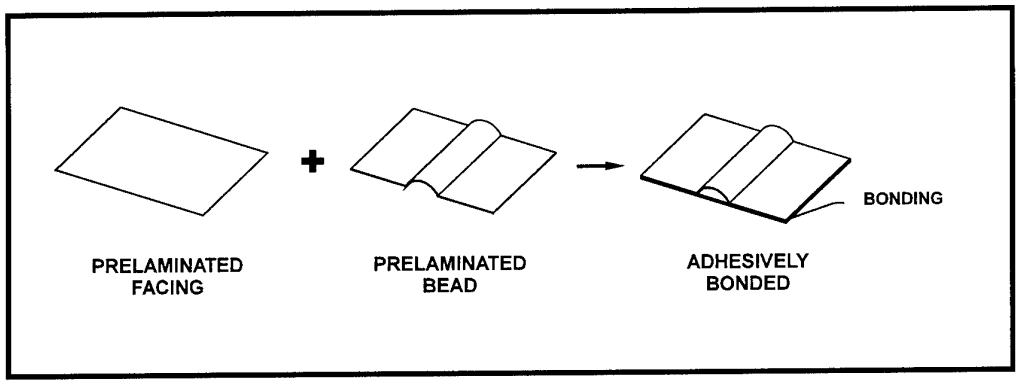


FIGURE 3. SCHEMATIC VIEW OF SECONDARY BONDING TECHNIQUE

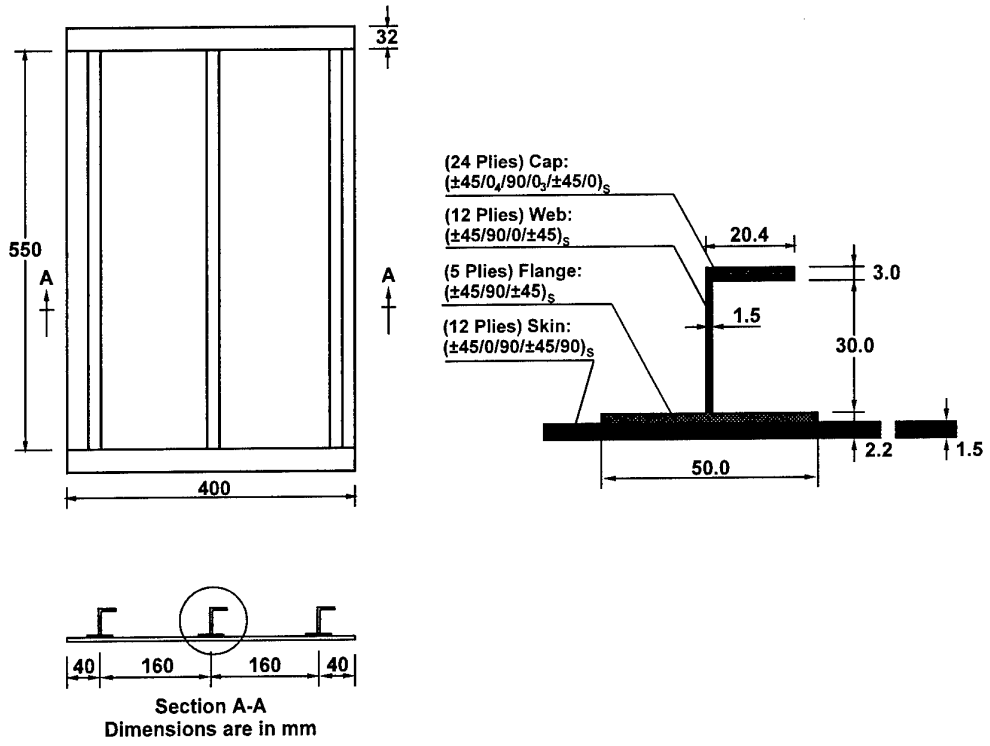


FIGURE 4. STIFFENED COMPOSITE PANEL GEOMETRY AND LAY-UP SEQUENCE

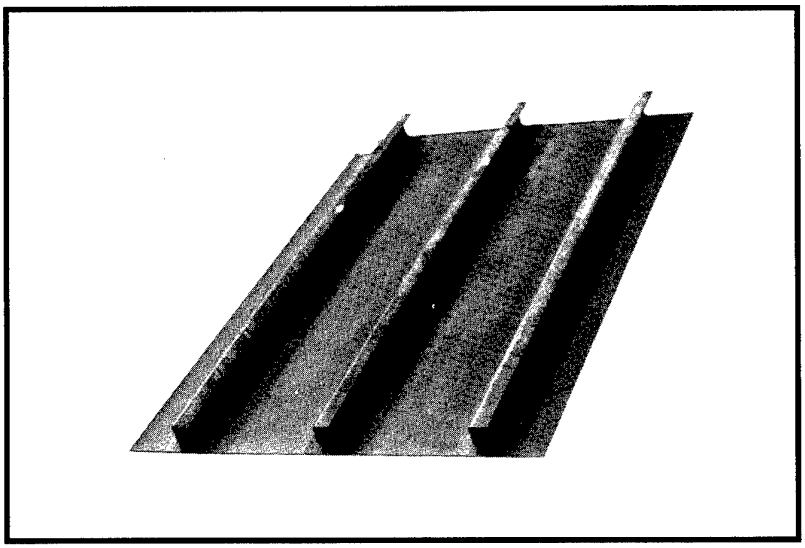


FIGURE 5. FABRICATED STIFFENED COMPOSITE PANEL

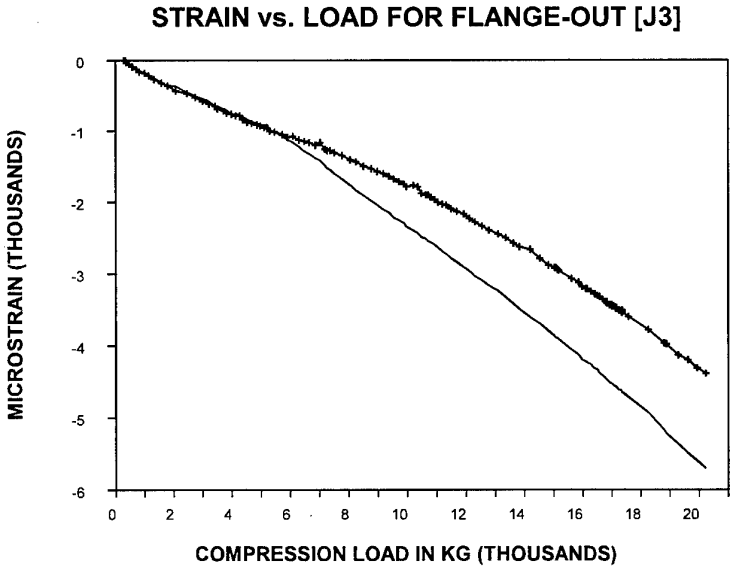


FIGURE 6. COMPRESSION LOAD VS AXIAL STRAIN FOR THE FLANGE OF STIFFENER / SKIN INTERFACE

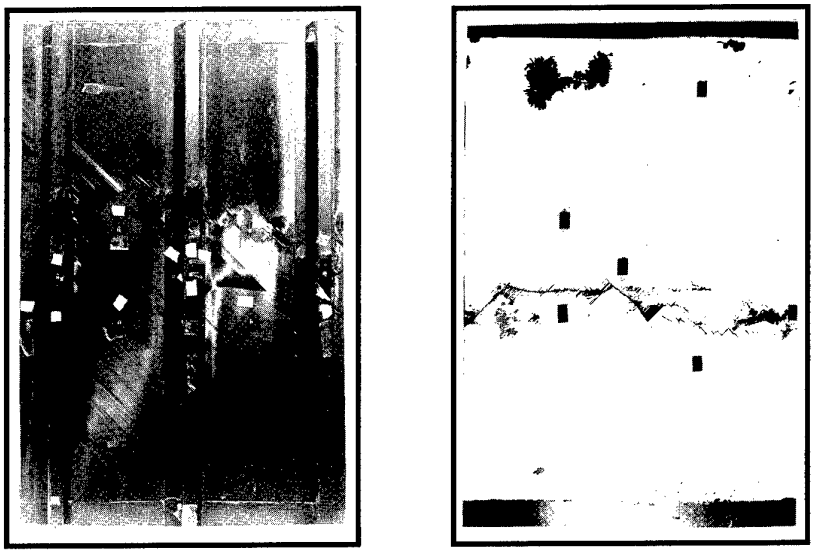


FIGURE 7. GENERAL FAILURE MODELS OF THE TEST PANELS

TABLE 1. FAILURE LOAD/FAILURE STRAINS AND STRUCTURAL EFFICIENCY OF THE PANELS

Panel	**Type**	**Buckling**		**Failure**		**The Coefficient of Structural Efficiency K,** $(kN)^{1/2}/m^2$
		Load(kN)	μ Strain	Load(kN)	μ Strain	
J1	Cocured	54,9	900	224,2	6123	$2.32x10^{-3}$
J2	Cocured	63,7	1000	208,3	6070	$2.35x10^{-3}$
J3	Cocured	55,9	1080	198,7	5708	$2.48x10^{-3}$
J4	Secondary Bonded	51,9	900	249,1	7482	$2.23x10^{-3}$
Averages		56,6 (58,1)	970	220,0 (210.9)	6346 (5967)	

( )= An average J1, J3, and J3 only.

Surface Treatment and Bonding of Thermoplastic Composites

S J Shaw*, J Comyn†, L Mascia, †

*Structural Materials Centre
Defence Research Agency,
Farnborough, Hampshire GU14 6TD

†Institute of Polymer Technology and Materials Engineering
Loughborough University of Technology
Loughborough, Leicestershire, UK

1 INTRODUCTION

The use of structural adhesives in engineering applications can offer substantial benefits in comparison to more traditional joining techniques such as mechanical fastening and welding. These include:

a. Improved fatigue performance.

b. Ability to join dissimilar materials.

c. Ability to join thin gauge materials and honeycomb constructions.

d. Simpler and cheaper component construction.

Operational benefits which can result from the significant use of bonding include improved equipment performance, resulting largely from the significant weight reductions which adhesive bonding can provide, together with substantial reductions in both procurement and life-cycle maintenance costs. In particular, the use of adhesive bonding in the construction of advanced lightweight composite structures will be of major importance since mechanical fastening would impose penalties in terms of mechanical integrity and weight.

Traditionally, engineering structures have been produced from materials such as steel and aluminium alloys, where adhesive bonding has often been viewed as the preferred joining method. With each material type, surface treatment is often seen as the vital prerequisite to successful bonding with various standard treatments emerging over the years for various alloy types.

In recent years a new generation of materials, most notably polymer composites, have emerged for a range of potential applications. Offering substantial advantages over traditional metal alloys in terms of density and fatigue properties, in most cases a reconsideration of surface treatment requirements has been necessary. With thermosetting based fibre composites, surface treatment requirements have been shown to be relatively simple and straightforward. Thus surface treatments designed to essentially remove contaminants e.g. abrasion and degrease, have usually been considered sufficient. However, due primarily to surface energetic considerations, thermoplastic based composites are usually difficult to bond frequently resulting in low joint strength and durability. Consequently more sophisticated and/or aggressive treatments have been considered necessary for successful bonding of these more recently introduced materials.

The work described in this paper is based upon an extensive study which has considered several surface treatment approaches for thermoplastic composites, with emphasis placed upon arguably the most commonly employed thermoplastic matrix resin i.e. polyether ether ketone (PEEK).

2 EXPERIMENTAL

2.1 Materials

Three types of surface treatment were investigated i.e. plasma, corona discharge and chemically based treatments. For the plasma and corona discharge studies, amorphous PEEK film, 250 μm thick, was used as adherend whereas a carbon fibre PEEK composite was used for chemical treatment studies. With the plasma and corona discharge work a 120°C cure carried epoxy film adhesive was employed. Several adhesive types were considered in the chemical treatment investigation, all based on epoxy resins.

Paper presented at the 83rd Meeting of the AGARD SMP on "Bolted/Bonded Joints in Polymeric Composites", held in Florence, Italy, 2-3 September 1996, and published in CP-590.

2.2 Surface treatments

Prior to laser or corona discharge treatments, PEEK film adherends were cleaned with acetone so as to minimise surface hydrocarbon contamination.

Theoretically a plasma treatment can be defined as any form of surface treatment in which material is exposed to an ionised gas (plasma). Corona discharge can be included in this definition, the main difference between the two techniques being that plasma generally refers to low pressure treatments requiring vacuum equipment. Depending on the gas used to generate the plasma and the plasma parameters, three different forms of treatment are possible. The first involves noble gas plasmas, the principal objective being the elimination of weak boundary layers. The second involves reactive gas plasmas (e.g. oxygen, nitrogen etc) where the primary effect is the introduction of functional groups onto the surface based on the chemical structure of the gas, with the third involving polymerisable gas plasmas capable of depositing and developing a polymeric film on a surface. The plasma types employed in this study were largely taken from the second category i.e. oxygen, ammonia, sulphur dioxide and air, with just one noble gas, argon, being employed.

Plasma treatments were carried out in a Plasma Technology 'System 80' barrel type apparatus. The operating frequency available was 10^5 Hz with power availability up to 1000 watts. Processing pressures of approximately 260mtorr were provided by the use of a rotary vacuum pump. The above mentioned gases were introduced into the chamber during surface treatment.

Corona treatments were conducted in a corona generator capable of a power output range of 0 to 30 Hz. During treatment specimens were placed on a polyethylene support plate installed between two electrodes. The gap between electrode and specimens was maintained at 1.1 mm with both sides of the PEEK being treated separately under identical conditions. During treatment, gas was injected into the apparatus from a compressed gas cylinder at a constant flow rate of 10l min^{-1}.

The energy output per unit area from the electrode was determined from:

$$E = \frac{PN}{LV} \qquad (1)$$

where E is the energy output per unit area (termed the treatment level) P the power of the generator, N the number of passes between electrodes experienced by the supporting plate and specimens, L the electrode length and V the velocity of the supporting plate.

The chemical surface treatments investigated were:

a. Chromic acid etch at room temperature followed by a 20 minute wash in cold running tap water with air drying at 60°C.

b. Concentrated sulphuric acid/ orthophosphoric acid/water in ratio by volume of 5:2:2 with and without addition of potassium permanganate, followed by washing in cold running tap water and air drying at 60°C.

In addition, for comparison purposes PEEK composite specimens were also subjected to simple acetone wipe and grit-blast procedures prior to bonding.

2.3 Joint preparation and testing

Both T-peel and lap-shear joints were employed to characterise plasma and corona discharge treated PEEK specimens. For the former, dimensions were approximately 125 mm by 25 mm wide with a bonded area of 75 by 25 mm. Following the appropriate surface treatment adhesive was applied and cured at 120°C for 1.5 hours under 175kPa pressure, followed by natural cooling. Joint testing was conducted at 20°C at a crosshead speed of 25.4 cm min^{-1}.

Lap-shear joints of unreinforced PEEK were prepared according to ASTM D3164-73. PEEK film, previously subjected to plasma or corona discharge treatment, was sandwiched in the overlap regions of the joint between steel adherends, film adhesive being used to bond PEEK to steel. Following assembly, joints were cured at 120°C for 1.5 hours under pressure followed by natural cooling. Testing of bonded joints was conducted at 20°C at a crosshead speed of 1.3 mm min^{-1}.

Failure analysis of peel and lap-shear specimens was conducted using both visual examination and scanning electron microscopy. In addition both untreated PEEK film and specimens previously plasma or corona treated were subjected to surface analysis using contact angle, x-ray photoelectron spectroscopy (XPS) and time of flight secondary ion mass spectroscopy (TOF-SIMS) techniques.

3 RESULTS

3.1 Plasma treatments

The extent of the bonding difficulties which exist with thermoplastics such as PEEK is demonstrated by the data shown in Table 1 which shows both lap-shear and peel strength data for joints prepared from PEEK adherends previously subjected to a simple solvent wipe. As indicated the level of adhesion between essentially untreated PEEK and adhesive was negligible, with no detectable load recorded during the peel test procedure. Locus of failure was entirely interfacial between adhesive and PEEK, indicating clearly the need for an improved surface treatment. A moderate lap-shear strength was however obtained, this difference being due to stress condition variations provided by the two test geometries, with the peel test being more revealing of adhesive - adherend interface weakness.

Table 1. Joint strength values and locus of failure for untreated PEEK joints

T-peel strength N(mm)	Lap-shear strength (MPa)	Locus of failure
0	--	I
--	16.9±1.3	I+C

I: Interfacial failure between adhesive and PEEK
C: Cohesive failure within adhesive

Joint strength results obtained from the various plasma treatments employed to surface modify PEEK are shown in Tables 2 to 4. The data reveals clearly that all the plasma treatment variations considered i.e. gas type, treatment time, power level and pressure, with the exception of one, resulted in substantial increases in strength and, most importantly, a transfer of the locus of failure away from the adhesive - PEEK interface to within either the adhesive layer or the PEEK. This can of course be regarded as achieving the ultimate objective, with surface treatment modifying the nature of the PEEK surface to such an extent that, upon bonding, failure is not associated with that surface.

3.2 Corona discharge treatments

Joint strength results obtained from the corona discharge treatments, with gas type and treatment level being the main experimental variables studied, also revealed significant improvements in strength with a similar change in locus away from the adhesive - PEEK interface (Table 5 and 6). From this data, corona treatment is clearly having a highly beneficial effect on adhesion, with extent of treatment having no significant effect on both strength and locus of failure beyond an obvious minimum necessary treatment condition.

Table 6 shows the effect of different gas environments on lap-shear strength,. As indicated, the type of gas employed i.e. air, oxygen, argon, ammonia or sulphur dioxide, has little influence on joint strength and locus of failure beyond the obvious improvements over the untreated PEEK systems.

Table 2. Effect of oxygen plasma processingparameters on the T-peel joint strength of PEEK

Parameters	T-peel strength(N/mm)	Locus of failure
Untreated	O	I
300 w, 0.3 torr, 0.5 min	0.84±0.04	I+C
1 min	4.23±0.34	C
2 min	4.18±0.09	C+P
6 min	3.90±0.02	C
10 min	3.80±0.35	C+P
30 min	4.07±0.06	C
1 min, 0.3 torr, 300w	4.23±0.34	C
400w	4.29±0.03	C+P
500w	4.64±0.02	C+P
600w	4.84±0.11	C+P
10 min, 0.3 torr, 300w	3.80±0.35	C+P
400w	3.88±0.06	C
600w	3.72±0.29	C+P
600w, 1 min, 0.3 torr	4.84±0.11	C+P
0.4 torr	4.13±0.10	C
0.5 torr	4.42±0.16	C+P
600 w, 10 min, 0.3 torr	3.72±0.29	C
0.4 torr	3.77±0.35	C

I: Interfacial failure between adhesive and PEEK film.
C: Cohesive failure within adhesive.
P: Failure within PEEK film.

Table 3. Effects of plasma treatment gas on the T-peel joint strength

Treatment condition	Peel strength (N/mm)	Locus of failure
O_2, 1 min, 500 w, 0.3 torr	4.64±0.02	C+P
1 min, 600w, 0.4 torr	4.13±0.10	C
Ar, 1 min, 500w, 0.3 torr	3.36±3.36	C
5 min, 500w, 0.3 torr	3.85±0.27	C+P
Air, 1 min, 500w, 0.3 torr	4.19±0.07	C+P
1 min, 600w, 0.4 torr	4.00±0.38	C
NH_3,1 min, 500w, 0.3 torr	4.05±0.11	C
1 min, 600w, 0.4 torr	4.00±0.09	C

Table 4. Effect of plasma treatment gas on the lap-shear joint strength

Treatment gas*	Shear strength (MPa)	Locus of failure
Untreated	16.9±1.3	I+C
Oxygen	34.0±1.4	C+P
Ammonia	32.2±2.1	C+P
Sulphur dioxide	32.8±0.9	C+P
Air	29.1±1.8	C+P

* Treatment condition: 1 min, 500w, 0.3 torr.

Table 5. Effect of air corona discharge treatment on lap-shear strength of PEEK.

Treatment level (J/mm^2)	Shear strength (MPa)	Locus of failure
0	16.9±1.3	I+C
0.05	28.3±0.9	C+P
0.2	28.9±2.2	C+P
0.4	28.5±1.8	C+P
0.6	29.1±0.4	C+P
0.8	29.5±0.6	C+P
2.0	29.3±0.5	C+P

Table 6 Effect of gas injecting into the corona discharge on the lap-shear joint strength of PEEK.

Treatment level (J/mm^2)	Gas	Shear-strength (MPa)	Locus of failure
0.05	Air	28.3±0.9	C+P
	Oxygen	29.9±0.5	C+P
	Argon	28.1±0.3	C+P
0.4	Air	28.5±1.8	C+P
	Oxygen	30.2±0.7	C+P
	Argon	28.8±0.8	C+P
	Ammonia	28.0±1.7	C+P
	Sulphur dioxide	32.0±1.2	C+P

Table 7 Boeing wedge test results

Adhesive	Pretreatment	a_0, mm	G_{1c}, KJ/m^2	Failure
Epoxy	GB	48.77±2.84	0.08±0.02	I
	2 min. CE	mostly max.	0.031±0.026	I
	30 min. CE	mostly max.	0.012±0.022	I
	GB+2 min. CE	44.65±2.61	0.313±0.074	C/I
	GB+30 min. CE	42.28±3.29	0.419±0.122	C/I
	repeat	48.44±2.62	0.206±0.044	C/I
	GB+A	52.30±2.27	0.170±0.04	C/I
	GB+A+0.5%P	37.63±1.39	0.610±0.08	C/I
	GB+A+1.0%P	33.90±1.80	0.920±0.20	A
	repeat	34.99±2.17	0.810±0.20	C/I

Pretreatments:
GB - grit blast
CE - chromic acid etch
A - Sulphuric acid + phosphoric acid
P - + potassium permanganate

Failure:
C - in adherend
A - in adhesive
I - at interface
C/I - in composite near interface

3.3 Chemical treatments

As stated previously a total of five surface treatments were considered namely acetone wipe, grit-blast, chromic acid etch and sulphuric acid/orthophosphoric acid/water with and without the addition of potassium permanganate. Boeing wedge and lap-shear joint designs were employed to assess joint behaviour.

As expected the simple treatments i.e. acetone wipe and grit-blast were ineffective with high crack propagation and low fracture energy values obtained from the wedge experiments and low joint strengths from lap-shear tests. Although the sulphuric acid/orthophosphoric acid/ water treatments were also ineffective, the addition of 1% potassium permanganate, a strong oxidising agent, resulted in strong bonds with failure predominantly away from the interfacial zone. Table 7 shows representative data from the chemical treatment study.

4 DISCUSSION

4.1 Proposed mechanisms for bondability enhancement.

In an attempt to develop mechanisms which could account for the joint strength improvements and locus of failure modifications noted above, three main surface characterisation approaches were employed namely, wettability studies, scanning electron microscopy and surface specific analytical techniques.

One of the most important factors likely to influence the strength of an adhesive joint is the ability of the adhesive to wet and spread on the adherend surface. This most important characteristic can be quantified in terms of the contact angle which a liquid (adhesive) forms when placed in contact with a solid surface. Considered initially by *Young* in 1805, he related contact angle to the surface energies of the two contacting materials e.g. adherend and adhesive, as indicated in equation 2.

$$\gamma_{SV} = \gamma_{SL} + \gamma_{LV}^{\cos\theta} \qquad (2)$$

Where γ_{SV} is the surface free energy of the adherend in contact with the vapour of the liquid (adhesive), γ_{SL} is the interfacial free energy and γ_{LV} the liquid (adhesive) surface free energy. Since a contact angle of 0° would clearly be a desirable objective (demonstrate spreading of adhesive across the adherend surface and thus intimate molecular contact between the two phases), equation 2 can be employed to demonstrate a simple wetting criteria in which the adhesive will spread on an adherend when,

$$\gamma_{SV} \geq \gamma_{SL} + \gamma_{LV} \qquad (3)$$

This equation quite simply demonstrates that to enhance adhesive wetting and spreading behaviour, the surface free energy of the adherend, γ_{SV} should be maximised to at least greater than the surface free energy of the adhesive phase. Indeed, the need for surface treatments, be they metals, composites or plastics can be attributed, partly at

least to the simple criterion indicated in equation 3. Bearing in mind the improvements in bondability which have been shown from the various treatments described here, it is of interest to determine whether these trends can be attributed to enhancements in surface free energy.

Within this context, although the surface tension of a liquid, γ_{LV} can be determined using well established techniques, γ_{SV} the surface free energy of a solid is more difficult to determine. In recent years contact angle values exhibited by a range of organic liquids on various adherend surfaces have been used to provide surface free energy values, and this approach has been adopted in this study to assess surface free energy effects. In this work four liquids were employed in the contact angle studies, i.e. liquids having differing inter-molecular force characteristics necessary to achieve an accurate picture of both the magnitude of solid surface energy and the various intermolecular force types which contribute to it.

For all the liquids considered, surface treatment of PEEK showed substantial reductions in liquid contact angle thereby indicating improved wettability from each of the various surface treatments employed. In order to determine PEEK surface free energies from liquid contact angle values, the concept of intermolecular force contributions to surface free energy requires consideration. Proposed initially by *Fowkes* in the early 1960s, he suggested that surface free energy could be expressed by two terms, namely a dispersion and a polar component representing the two principal types of intermolecular interaction present in most materials. Thus

$$\gamma = \gamma^d + \gamma^p \qquad (4)$$

where γ^d is the dispersion force component γ^p the polar force component.

In an attempt to determine surface free energies and related dispersion/polar force components for the PEEK surfaces studied in this work, it is necessary to consider the interaction energies which would exist between an adherend such as PEEK and an adhesive. Within this context it has been proposed that the geometric mean of the dispersion force components is a reliable predictor of the interaction energies caused by this type of force. Thus for interactions involving only dispersion forces,

$$\gamma_{SL} = \gamma_{LV} - 2(\gamma_{SV}^{\,d}\gamma_{LV}^{\,d})^{1/2} \qquad (5)$$

However, in recognising that, with some adherend/adhesive combinations, polar force interactions would undoubtedly exist, equation 5 can be modified to express this combination thus,

$$\gamma_{SL} = \gamma_{SV} + \gamma_{LV} - 2(\gamma_{SV}^{\,d}\gamma_{LV}^{\,d})^{1/2} - 2(\gamma_{SL}^{\,p}\gamma_{SV}^{\,p})^{1/2} \qquad (6)$$

In considering a solid-liquid system, this relationship may be combined with equation 2 to eliminate the interfacial free energy term resulting in,

$$1+\cos\theta = \frac{2(\gamma_{SV}^{\,d})^{1/2}(\gamma_{LV}^{\,d})^{1/2}}{\gamma_{LV}} + \frac{2(\gamma_{SV}^{\,p}\gamma_{LV}^{\,p})^{1/2}}{\gamma_{LV}} \qquad (7)$$

From a knowledge of contact angle, Υ_{LV}^{d}, Υ_{LV}^{p}, and Υ_{LV} for two liquids, simultaneous equations of (7) can be solved to yield the dispersion component of the solid (PEEK) surface, Υ_{SV}^{d} and the polar component Υ_{SV}^{p}. From this a value of solid surface free energy can be deduced simply from equation (4). Using this approach, values for, Υ_{SV}^{d}, Υ_{SV}^{p} and Υ_{SV} for the various PEEK surfaces were calculated from the contact angle values together with published data for liquid Υ_{LV}^{d}, Υ_{LV}^{p} and Υ_{LV} values. Data for both plasma and corona discharge treated PEEK are shown in Table 8 and 9 respectively. The surface polarity values indicated are simply a quantifiable expression of the polar nature of the surface, obtained simply from the expression,

$$\text{Surface polarity} = \frac{\gamma^p}{\gamma} \qquad (8)$$

As can be seen from Table 8, the three plasma treatments shown, namely oxygen, ammonia and sulphur dioxide plasmas, resulted in significant increases in both total surface free energy Υ_{SV} and polar force component Υ_{SV}^{p}, with Υ_{SV}^{d} undergoing a modest decline. Due to the substantial increase in Υ_{SV}^{p}, the surface polarity values also underwent substantial increases following treatment. Since high values of both Υ_{SV} and Υ_{SV}^{p} would be expected to enhance both wettability and adhesion, an oxygen plasma treatment would be expected to yield the greatest joint strength results. The data shown in Table 3 reveals that this was indeed the case.

Similarly, corona discharge treatments (Table 9) also resulted in increased levels of Υ_{SV}, and surface polarity, although not to the extent of that obtained

Table 8 Effect of plasma treatment on the surface free energy and polarity of PEEK films

Treatment condition	Surface energy (mJm^{-2}) γ_s^p	γ_s^d	γ_s	Surface polarity
Untreated	7.2± 3.9	31.5± 8.3	38.7	0.186
O_2, 1 min, 500w, 0.3 torr	42.5±18.1	23.5±13.6	66.0	0.644
O_2, 1 min, 600w, 0.4 torr	43.5±17.6	22.6±12.8	66.1	0.658
NH_3, 1 min, 500w, 0.3 torr	32.4±11.6	22.7± 9.8	55.1	0.587
NH_3, 1 min, 600w, 0.3 torr	34.6±11.7	23.2± 9.7	57.8	0.598
SO_2, 1 min, 500w, 0.3 torr	26.3±11.2	26.0±11.3	52.3	0.503
SO_2, 1 min, 600w, 0.3 torr	19.5± 9.7	27.5±11.6	47.0	0.416

Table 9 Effect of corona discharge treatment on the surface free energy and polarity of PEEK films

Gas	Treatment level (J/mm^2)	Surface energy(mJm^{-2}) γ_s^p	γ_s^d	γ_s	Surface polarity
Untreated		7.2± 3.9	31.5± 8.3	38.7	0.186
Air	0.05	28.6±12.1	26.5±11.7	55.1	0.519
	0.2	22.8± 7.6	26.9± 8.3	49.7	0.460
	0.4	34.5±14.3	24.0±12.0	58.5	0.590
	0.6	30.1±11.9	25.4±11.0	55.5	0.543
	0.8	33.0±13.4	26.4±12.1	59.4	0.555
	2.0	33.6±13.8	26.2±12.3	59.8	0.562
Ammonia	0.05	24.6± 9.2	25.2± 9.4	49.8	0.494
	0.4	25.9± 8.7	25.7± 8.7	51.6	0.502
Sulphur dioxide	0.4	24.6± 8.3	28.0± 9.0	52.6	0.467
Oxygen	0.05	21.0± 6.6	28.2± 7.7	49.2	0.428
	0.4	28.7±11.3	26.8±11.0	55.5	0.518
Argon	0.05	26.1± 9.1	27.2± 9.4	53.3	0.489
	0.4	29.8±11.1	26.2±10.5	56.0	0.532

with plasma treatments. Thus, the surface free energy and polarity results indicate that both plasma and corona discharge treatments change surface molecular structure and increase surface polarity so as to contribute greatly to improved bondability.

SEM analysis of both plasma and corona discharge treated PEEK revealed no enhanced surface topographical effects in comparison to the untreated surface, implying that both treatments are mechanically very mild, causing no erosion or etching of the PEEK surface. This suggests that both the bondability and wettability improvements previously discussed, can be attributed primarily to surface chemical modification.

The surface specific analytical techniques of X-ray photoelectron spectroscopy (XPS) and time of flight secondary ion mass spectrometry (TOF-SIMS) were used to assess surface chemistry modifications ensuing from the treatment procedures. Both techniques revealed that both plasma and corona discharge treatments resulted in substantial changes in the chemical structure of the PEEK surface with, in particular, evidence to indicate the introduction of oxygen and/or nitrogen containing species onto the surface. The presence

of such species would be sufficient to enhance the polarity of the surface and to provide scope for the formation of interfacial chemical bonds between the PEEK surface and adhesive, both of which would be a considerable aid to improved adhesion and resultant joint strength.

That the treatments employed to surface modify PEEK increase free energy has already been established. Although this implies the attainment of improved wettability characteristics, it is important to establish whether this is the main contributor to the improved adhesion and joint strength values obtained.

The simple criterion developed above and highlighted by equation 3 suggests that thorough wetting of an adherend, Υ_{SV}, by an adhesive, Υ_{LV}, should occur when $\Upsilon_{SV} \geq \Upsilon_{LV}$. Contact angle measurements obtained with liquids in contact with cured adhesive revealed a surface free energy, Υ_{LV}, of 33.1 mJ/m^2 with dispersion and polar contributions of 21.2 and 11.9 mJ/m^2 respectively. This compares with Υ_{SV} of 38.7 mJ/m^2 for untreated PEEK film and 66.1 mJ/m^2 for the best surface treatment (oxygen plasma). Thus, the criterion indicated above would suggest that thorough adhesive wetting would occur with all of the films investigated including the untreated PEEK. However, a more detailed analysis, involving the wettability envelope concept, would provide a more accurate prediction of wettability and is therefore worthy of consideration.

For wetting to occur, equation 3 (repeated for convenience) revealed that:

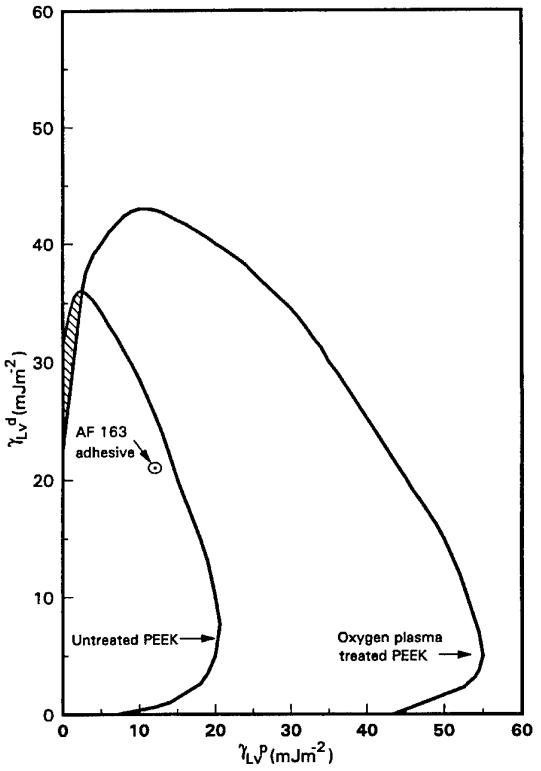
$$\gamma_{SV} \geq \gamma_{SL} + \gamma_{LV} \qquad (3)$$

By substituting for Υ_{SL} from equation 6 into equation 3 and re-arranging, the condition that wetting will just occur becomes,

$$\gamma_{LV} - (\gamma_{SV}^{d}\,\gamma_{LV}^{d})^{1/2} - (\gamma_{SV}^{p}\,\gamma_{LV}^{p})^{1/2} = 0 \qquad (9)$$

Thus, knowing values of Υ_{SV}^{d} and Υ_{LV}^{p} for the adherend surface enables equation 9 to be solved to yield values of Υ_{LV}^{d} and Υ_{LV}^{p} for liquids (adhesives) which would just wet the solid surface and so allow a wettability envelope for the solid to be constructed. This procedure was employed to construct envelopes for untreated PEEK and an oxygen plasma treated PEEK which are shown in Figure 1. Also shown are the values of Υ_{LV}^{d} and Υ_{LV}^{p} for the adhesive employed in this work. As indicated, the Υ_{LV}^{d} and Υ_{LV}^{p} values lie inside both envelopes, indicating wetting of both treated and untreated surfaces by the adhesive. Thus, this result would suggest that inadequate wetting of the untreated PEEK by the adhesive was not the main cause of the poor bondability exhibited by this surface . Figure 1 does, however, show clearly the improved wetting potential which results from surface treatment. The treated surface has a much larger wettability envelope which would allow wetting by various adhesives exhibiting a wide range of Υ_{LV}^{d} and Υ_{LV}^{p} values. Although wettability benefits would therefore be expected from either plasma or corona discharge treatments, Figure 1 does, interestingly, indicate a small envelope region (dashed) where the reverse would be expected i.e. where an adhesive with the Υ_{LV}^{d} and Υ_{LV}^{p} combinations shown, would be expected to wet the untreated surface but not the treated surface.

Figure 1 Wettability envelopes for untreated and oxygen plasma treated PEEK



Since a wetting 'go/no go' scenario based upon a 0° contact angle value is unable to explain the differences in adhesion and joint strength performance between untreated and treated PEEK surfaces, it is of interest to consider the surface modifications brought about by surface treatment on PEEK-adhesive interfacial interactions.

As previously outlined, surface analytical techniques had indicated the presence of polar functional groups on treated surfaces. In addition to potential for formation of chemical bonds at the

interface, the presence of these groups would enhance surface polarity with a resultant improvement in adhesion. The likelihood of this can be assessed by determining work of adhesion values for the various PEEK-adhesive interfaces.

Theoretically the thermodynamic work of adhesion required to separate a unit of two phases forming an interface, W_A, can be related to the surface free energies of the materials in contact, together with the interfacial free energy by the Dupre equation,

$$W_A = \gamma_{SV} + \gamma_{LV} - \gamma_{SL} \qquad (10)$$

Strictly this equation should only apply to a solid/liquid or a liquid/liquid interface but, by assuming that the surface free energy of a liquid does not change significantly upon solidification and ignoring shrinkage stresses, it may be applied to solid adhesive/adherend interfaces. By using equation 6 to eliminate the interfacial free energy term Υ_{SL}, then work of adhesion can be expressed by,

$$W_A = 2(\gamma_{SV}{}^d \gamma_{LV}{}^d)^{1/2} + 2(\gamma_{SV}{}^p \gamma_{LV}{}^p)^{1/2} \qquad (11)$$

By use of equation 11, together with the dispersion and polar force contributions to surface free energy, work of adhesion values can be calculated. W_A values obtained using this approach, shown in Table 10, indicate significant differences between the treated surfaces and the untreated PEEK, suggesting a change in the nature of the interfacial interactions on going from untreated to treated PEEK. Thus, although the introduction of both surface polarity and chemical functional groups on to the PEEK surface does not, with the adhesive currently employed, influence wettability behaviour, the surface modifications do appear to substantially enhance interfacial interactions between PEEK and the epoxy adhesive. From this aspect alone, improvements in joint strength and a change in locus of failure away from the adhesive-PEEK interface would be expected.

Table 10 Thermodynamic work of adhesion for PEEK/adhesive interfaces

Treatment condition*	Work of adhesion (mJm^{-2})
Untreated	70.2
Oxygen plasma	89.7
Ammonia plasma	83.1
Sulphur dioxide plasma	82.3
Air corona	85.6
Ammonia corona	81.2
Sulphur dioxide corona	82.9

4.2 Solvent and surface ageing effects

Although adhesive bonding should ideally be conducted immediately following surface treatment, in many practical applications this is often unrealistic. In such circumstances contamination of the treated surface by, for example, atmospheric hydrocarbons, grease etc is possible. Thus in such circumstances a simple solvent wipe prior to bonding would appear desirable. In addition, industrial practice could involve treated material undergoing transportation, storage or other operational procedures during which ageing of the surface prior to bonding could occur. It was therefore deemed necessary to study factors such as the above and determine their influence on wettability and adhesion.

Experimentally, the solvents employed in the programme, namely water, acetone and 2-propanol, were applied by simply wiping with a cloth immediately following either plasma or corona treatment. Such surfaces were then subjected to contact angle analysis and bonding followed by joint strength evaluation. The results obtained were surprising and of major theoretical interest and practical relevance. Analysis of the contact angle data revealed surface energy changes to the solvent treated PEEK film which would, upon bonding, suggest substantial reductions in both adhesion between PEEK and adhesive joint strength. In practice however this was not observed as shown in Table 11, where solvent treatment would appear to have little effect on joint strength.

Table 11 Effect of solvent washing on the lap shear joint strength of plasma and corona discharge treated PEEK films

Treatment condition*	Solvent	Lap shear strength(MPa)	Failure locus
Untreated		16.9±1.3	I+C
Oxygen plasma	Before	34.0±1.4	C+P
	Acetone	33.8±1.4	C+P
	IPA	35.8±0.5	C+P
Ammonia plasma	Before	32.2±2.1	C+P
	Acetone	32.3±1.6	C+P
	IPA	33.7±1.7	C+P
Sulphur dioxide plasma	Before	32.8±0.9	C+P
	Acetone	31.7±0.5	C+P
	IPA	31.9±0.5	C+P
Air corona	Before	28.5±1.8	C+P
	Acetone	28.2±2.4	C+P
	IPA	29.6±0.9	C+P
Ammonia corona	Before	28.0±0.7	C+P
	Acetone	31.1±1.2	C+P
	IPA	28.3±1.5	C+P
Sulphur dioxide corona	Before	31.9±1.2	C+P
	Acetone	31.1±0.7	C+P

* Plasma treatment condition: 1 min, 500w, 0.3 torr
Corona discharge level: 0.4 J/mm^2

In an attempt to assess surface ageing effects, treated PEEK film was subjected to laboratory atmospheric exposure at predetermined intervals followed by wettability and joint strength behaviour as above. Identical behaviour to that obtained from the solvent treatment work was found with increased exposure time resulting in surface energy changes sufficient to theoretically inhibit adhesion and joint strength. The latter was in fact found to be virtually independent of ageing time

Thus although data obtained from the surface wettability study suggested that both solvent and surface environmental ageing related problems could occur which would pose serious practical difficulties, joint strength data did not agree with this pessimistic prediction.

5 CONCLUSIONS

Both plasma and corona discharge treatments markedly enhance the bondability of amorphous and crystalline PEEK films to the extent that failure is no longer associated with the PEEK surface. These improvements are achieved by the introduction of chemical groups onto the PEEK surface which promote a general increase in polarity and allow the potential for chemical reaction with epoxy adhesive, both factors substantially enhancing adhesion between PEEK and adhesive.

Although both subsequent solvent wipe and surface ageing produce changes in surface characteristics, this change has no harmful effect on bondability. This is important because manufacturing processes often involve a significant delay between surface treatment and bonding.

Etching APC-2 composite with a solution of 1% potassium permanganate in a mixture of sulphuric and orthophosphoric acids produces a surface which can produce strong bonds to epoxy adhesives, comparable with those obtained from laser treatment.
A range of surface treatments have been developed and studied which show that composites based upon PEEK can be bonded satisfactorily.

©British Crown Copyright DERA/1996
Published with the permission of the Controller of
Her Britannic Majesty's Stationery Office.

Hygrothermal fatigue of composite bonded joints

V. Giavotto, C. Caprile, G. Sala
Dipartimento di Ingegneria Aerospaziale
Politecnico di Milano
Via Golgi, 40
20133 Milano
Italy

1. SUMMARY

Adhesive bonding is the optimal technique to join composite laminates, because it does not induce stress concentrations, fibres cutting, resin delaminations and problems due to electro-chemical non-compatibility. Notwithstanding, in many cases bolted and riveted joints have to be used, mainly in hot-wet environmental conditions, as well as when composites have to face chemically aggressive fluids, as hydraulic and de-icing fluids, oils and fuels. Moreover, the influence exerted on bonded joints by technological defects (voids, inclusions) and barely visible damages (due to low-energy impacts) should be addressed. The results of a research on the fatigue behaviour of wet-conditioned, impacted and defective composite bonded joints are reported. Single and double lap geometry carbon fabric/epoxy joints are considered, bonded with high-toughness adhesive. The specimens were wet-conditioned in hot water (70° C) up to saturation. Barely visible damages were produced in the bonded region (influencing both the composite adherents and the adhesive layer) by means of low-energy impacts (0.5 J per mm laminate thickness) imparted by a spring-propelled horizontal apparatus with 20 mm hemispherical steel impactor). Defective bondings were simulated by including copper inserts, located in different positions. Defective, impacted and wet-conditioned specimens were subjected to static and constant amplitude fatigue testing (tension-compression, R=1, 6Hz frequency); their performances were compared to the behaviour of plain specimens. The stiffness decrease and the damage growth were continuously monitored during the testing by means of extensometers and NDI techniques (ultrasonic scanning and dye penetrant radiography). The results consist in the comparison of the static stress-strain curves relevant to plain, defective, impacted and wet-conditioned specimens, the curves of stiffness decrease vs. number of cycles and the Woehler curves. Finally, the static characteristics and the fatigue performances are correlated with the damage growth and the adhesive progressive degeneration by analysing the radiographs and the SEM micrographs of the failed bonded region, in order to propose an interpretative model.

2. INTRODUCTION

The aircraft structures must be in the same time light and structurally efficient. These requirements deserve the introduction of shallow structures and innovative materials, like composites and honeycomb; as a consequence, in the last decades, bonded joints became more and more attractive, being particularly suited for this type of structural philosophy.

A potential weight saving of 25% for secondary structures and 5-10% for primary ones can be envisaged, such a reduction leading to a remarkable increase of paying load. The bonded joints allow an efficient load transfer and, in the same time, contribute to damp the structural vibrations; besides, they reduce, in comparison to bolted joints [1-4], the problems due to stress singularities and do not suffer from clearance recovery.

The adhesives allow to design smooth and aerodinamically efficient joints; because the bonded line is continuous, the adhesive can be used as a sealant for gases or liquids as well (e.g. in integral fuel tanks) [5].

Thanks to their chemical nature, they do not undergo galvanic corrosion [6] and can also be used as insulators between electro-chemical non-compatible adherents. For the same reason, they behave well as electric insulators, even if - through the addition of suitable additives - they can act as conductors

The bonded joints allow to make large integral assemblies, connecting components of complex geometry which should be hardly produced through conventional mechanical techniques; in many cases they can lead to a cost reduction, because the time required to prepare a bonded joint does not depend on the extension of the connection (contrary to the mechanical joints), but only on the plants and the tools to be used, as well as on the adhesive curing parameters [7].

However, the bonded joints show some disadvantages and limitations as well: in fact, they require an accurate chemical and mechanical preparation of the surfaces to be joined, complex and time-consuming curing cycles in ovens or autoclaves and the employment of skilled personnel.

The bonded joints, being made of polymeric materials, possess marked visco-elastic characteristics and show low creep performances: they strain under constant load components (even if due to pulsating fatigue loads) [8,9]. The bonded joints are particularly sensitive to the adhesive thickness: a layer non-uniformity can lead to a notable reduction of the characteristics [10]. Further disadvantages consist in the difficulty to inspect the joint through NDI techniques and in the impossibility of disassembling the adherents to repair or maintain the structure; moreover, an accurate design of the joint geometry is required, in order to minimise the peeling stresses [11,12].

The bonded joints are particularly sensitive to environmental effects, such as high temperature and moisture content (hot-wet conditions), leading to a rapid decrease of the mechanical characteristics [13-15]. Furthermore, the bonded joints can undergo severe and uncontrolled deteriorations owed to technological defects (voids, impurities and residual of release films) and damages due to the use (barely visible impact

Paper presented at the 83rd Meeting of the AGARD SMP on "Bolted/Bonded Joints in Polymeric Composites", held in Florence, Italy, 2-3 September 1996, and published in CP-590.

damages owed to the low-energy impacts of gravel during the taking off/landing and hail during the flight) [16,17].

In the following, the results of an experimental study are reported, aimed to investigate the fatigue behaviour of the bonded joints of composite materials, in presence of technological defects, environmental wet conditioning and barely visible damages.

3. MATERIALS AND SPECIMENS

Hysol XEA 9361 is a epoxy-based, high elongation, two component paste adhesive that may be cured at room temperature. Hysol XEA 9361 has a good combination of high shear, peel strength and flexibility. It is suitable for general purpose bonding as well as uses which require high elongation, such as sealing and cryogenic applications. The main features are high elongation, long pot life, ability to bond many substrates, excellent low temperature properties. The adhesive requires complete mixing of the two components together (mix ratio by weight: 100 Part A, 140 Part B) just prior to application to the parts to be bonded. The accelerated cure cycle consisted of 1 hour at 82 °C.

The the uncured adhesive properties and the typical bond strength performances and are summarized respectively in Tabs. 1 and 2.

COLOR	PART A	PART B	MIXED
Viscosity‡	130 Pa·s	70 Pa·s	100 Pa·s
Density	1.33 g/ml	1.26 g/ml	1.28 g/ml
Shelf-Life‡	1 year	1 year	-
Pot Life‡	-	-	120 minutes

‡ at 25 °C

Table 1: Uncured adhesive properties

TEST METHOD	TEMPERATURE	STRENGTH
Lap Shear †	-196 °C	27.6 MPa
"	-55 °C	27.6 MPA
"	25 °C	24.1 MPa
"	71 °C	5.9 MPa
"T" Peel ‡	-55 °C	1.8 N/mm
"	25 °C	4.4 N/mm

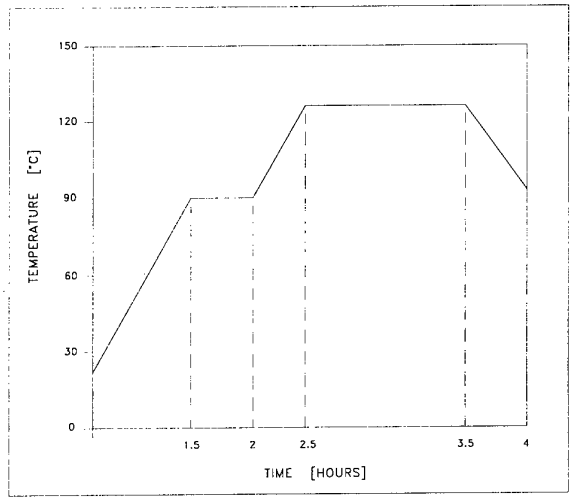
† per ASTM D-1002
‡ per ASTM D - 1876

Table 2: Typical bond strength

The adherents surfaces were prepared by solvent (MEK) degreasing and light abrasion with medium-grit emery paper without exposing the reinforcing fibres

The adherents were made of carbon fabric (8 harness weave style, 3K HTA-7 high strength tow) reinforced epoxy (CYCOM 759). This composite system has been formulated to be used in load bearing structural composites, combining good moisture resistance with damage tolerance and thermal performance; it has extremely forgiving processing characteristics to enable it to meet the diverse available moulding conditions.

It claims good hot-wet properties up to 80 °C and guarantees structural performance up to 130 °C; resin content 40% +/- 3%, volatile content 2% maximum, shop life 4 weeks at 23 °C and shelf life at -18 °C. The cure cycle is shown in Fig. 1, while the RTD mechanical properties are reported in Tab. 3.



Heating rate 1-3 °C per minute

Figure 1: CYCOM 759 autoclave cure cycle

	WARP	WEFT
Tensile Strength [MPa]	903	757
Tensile Modulus [GPa]	66	64
Compressive Strength [MPa]	806	762
Compressive Modulus [GPa]	63	57
Flexural Strength [MPa]	1019	-
Flexural Modulus [GPa]	52	-
ILSS [MPa]	61	-

Table 3: Laminate mechanical properties

The specimens (ASTM D-907) are shown in Fig. 2; the thin adherents were made of 7 pre-preg layers (layer thickness 0.27 mm, total thickness 1.79 mm); the thick ones of 14 layers.

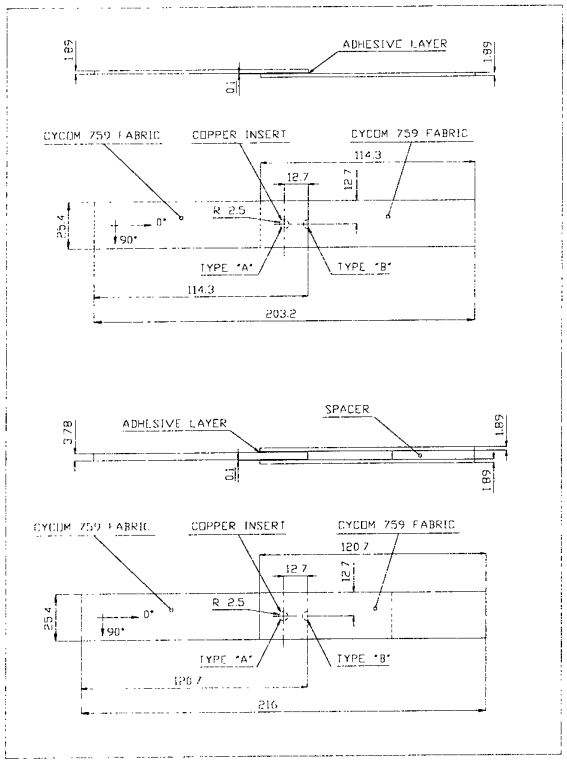


Figure 2: ASTM D-907 adhesive bonded specimens

4. TEST PROCEDURES

The two typologies of specimen (single and double lap) were divided in five batches (defective type A, defective type B, plane dry-conditioned, plane wet-conditioned and impacted), resulting in ten different groups to be subjected to both static and fatigue testing.

The defective specimens had a circular (2.5 mm diameter) copper insert placed respectively in the middle (type A) and at the edge (type B) of the bonded region (Fig. 2); the conditioned and the impacted specimens were prepared according to the procedures described in the following.

When a polymer composite is exposed to the action of humid air, the moisture content changes, impairing its thermal and mechanical characteristics and inducing a general reduction of the glass transition temperature, thermal conductivity, elastic modulus, static strength and fatigue endurance. To assess the change of properties, the material is exposed to the humid environment until the required moisture content is reached; then it is tested and its performances measured. Such a conditioning methodology, reproducing the real life of the material, can last years. To reduce up to few weeks the conditioning times, the accelerated ageing procedures were developed, exploiting the dependence of the absorption mechanism on two parameters, i.e. the diffusivity D:

$$D = D_0 e^{-\left(\frac{A}{T}\right)}$$

and the relative humidity :

$$M_m = a(\Phi)^b$$

Because the methods exploiting the increase of environmental relative humidity leads to a non-uniform moisture distribution, an alternative route was chosen, which requires the material to be immersed into distilled water and exploits the temperature increase to speed-up the kinetics of the phenomenon. The conditioning temperature cannot be increased at will, but has to be lower than the composite and adhesive service temperature. In fact, conditioning performed at temperature levels close to the glass transition temperature of the resin can induce permanent cracks. Moreover, because of the immersion in water, a huge quantity of moisture is forced to soak through the material in a very short time; this induces a distortion of the crystalline structure, an abrupt swelling and the onset of further cracks, which modify not only the mechanical performances of the material, but also its absorption characteristics (maximum moisture content M_m at saturation). These occurrences were avoided paying attention to maintain the absorption mechanism within reversibility limits.

The specimens tested to assess the hygrothermal effects were dry-conditioned in order to remove the initial moisture content, then half of them was wet-conditioned up to saturation; finally, both the batches were statically tested and fatigued.

Dry-conditioning was performed in a vacuum furnace at 60 °C temperature; the specimens were weighed with an analytical balance (range 120 g, accuracy 0.1 mg) and put into the oven; at regular time intervals the specimens were extracted, cooled and weighed again; the process was completed when no weight variations occurred between two subsequent weighings; before to be tested, the specimens were maintained into a sealed glass tank with hygroscopic salts. Wet conditioning to saturation was performed in a thermally controlled vessel containing distilled water at 60 °C, according to the same procedure used for dry-conditioning (extraction, cooling, wiping the superficial moisture and weighing); the procedure was iterated untill no weight variations occurred between two subsequent weighings. Before testing, these specimens were maintained immersed in a sealed glass tank containing distilled water at room temperature in order to keep their moisture content constant.

The moisture content (expressed as a mass percentage of the dry material) is reported in Fig. 3 as a function of the square root of the conditioning time. Through the initial slope of the curve and the maximum moisture content, the value of the diffusivity D can be computed:

$$D = \pi\left(\frac{h}{4M_m}\right)^2\left[\frac{M(t_2) - M(t_1)}{\sqrt{t_2} - \sqrt{t_1}}\right]^2$$

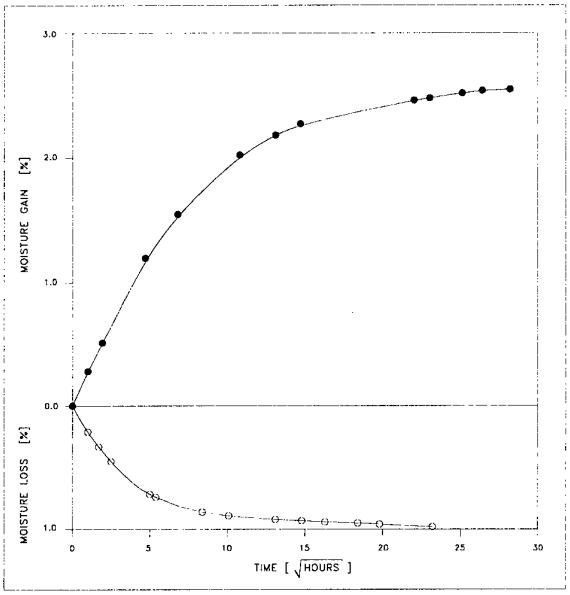


Figure 3: Wet and dry conditioning.

One of the main problems of the aerospace structures made of composite materials consists in the possible onset of barely visible damages due to low-energy impacts (falling of tools during the fabrication, hits of gravel during the take off and landing or hail during the flight); in literature several studies are available, dealing with the influence exerted by these types of damages on the fatigue behaviour of the composites laminates; on the contrary, very little is known about the consequences suffered by a composite bonded joint subjected to a low-energy impact.

Controlled impact damages were produced by means of a low-energy impact apparatus consisting of a computer-controlled spring propelled horizontal device, able to impart slight impacts and to circumvent the problems due to friction and rebound. The arrangement was equipped with an electro-magnetic release system, an hemispherical impactor (12.5 mm diameter) and an interchangeable modular mass (1.0 kg). The acquisition system consisted of two photo cells to measure the dart velocity just before the impact, one encoder (2,700 PPR, 10,000 RPM) to measure the displacement time-history, one accelerometer (500 g range, 5,000 Hz frequency response) integrated with the impactor to measure the acceleration time-history, one digital oscilloscope (1 MHz sampling rate), an acquisition board and a

supervising personal computer. This experimental arrangement supplied the curves of force or energy vs. time or displacement reported in Fig. 4.

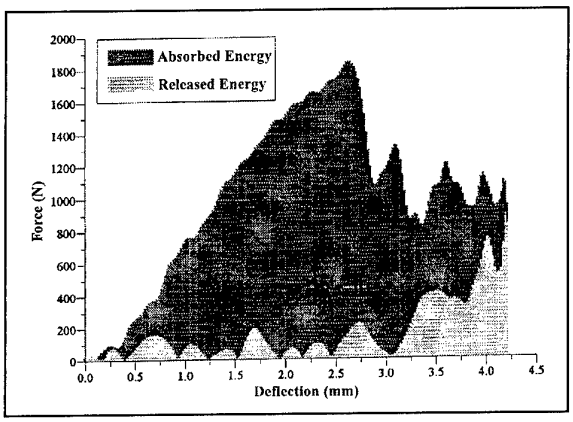


Figure 4: Absorbed and released energy (typical).

Both single and double lap specimens were impacted at 1.5 J energy, corresponding to 0.75 and 0.375 J/mm specific energy. A number of specimens sufficient to verify the repeatability and to guarantee the reliability of the results was statically tested to measure the complete stress-strain curve of the joint and to evaluate its stress ultimate σ_{ult}.

The constant amplitude tensile fatigue tests (0.1 $\sigma_{min}/\sigma_{max}$ stress ratio and 10 Hz frequency) were performed at different $\sigma_{max}/\sigma_{ult}$ stress levels; the stresses and the strains were continuously monitored by means of load cells and estensometers (accuracy class 0.1, gauge length 50 mm). At pre-determined life intervals (25,000 cycles), static tests were performed to evaluate the instantaneous stiffness, to be compared to the initial value for obtaining the diagrams of the residual stiffness vs. the number of cycles and the Woehler curves. Meanwhile, on-line opaque-enhanced dye penetrant x-radiographs were taken to monitor the damage extension and to correlate it with the stiffness decrease. Finally, SEM micrographs of the bonded surfaces allowed to investigate the causes of the failures and to point-out the influence exerted by conditioning, impacting or defecting.

5. RESULTS

The results of the static tests are summarized in the following Tab. 4, which reports the strength N, the shear stress ultimate τ and the stiffness E of the specimens.

	PLAIN		CONDITIONED		IMPACTED	
	Single	Double	Single	Double	Single	Double
F [N[	11,517	30,358	10,982	24,916	6,543	16,010
τ [MPa]	17.85	23.53	17.02	19.30	10.14	12.41
E [GPa]	3.25	3.43	2.49	3.36	1.98	3.33

Average values on 5 tests

Table 4: Static strength and stiffness of the specimens

The Figs. 5 and 6 show the static stress strain curves of the single and double-lap specimens; in Figs. 7-9 the fatigue residual stiffness of single-lap specimens is summarized, to be compared to the behaviour of double lap-specimens, shown in Figs. 10-12.

Finally, the Woehler curves of single (Figs. 13-15) and double-lap specimens (Figs. 16-18) are reported.

The curves of residual stiffness are reported as a function of the per cent ratio R between the maximum fatigue stress and the static stress ultimate; the Woehler curves as a function of the per cent stiffness decrease.

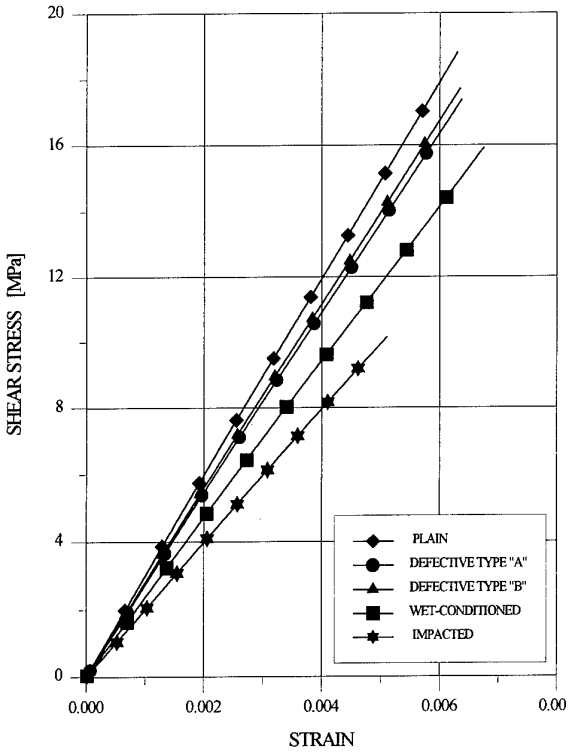


Figure 5: Stress-strain curves of single-lap specimens.

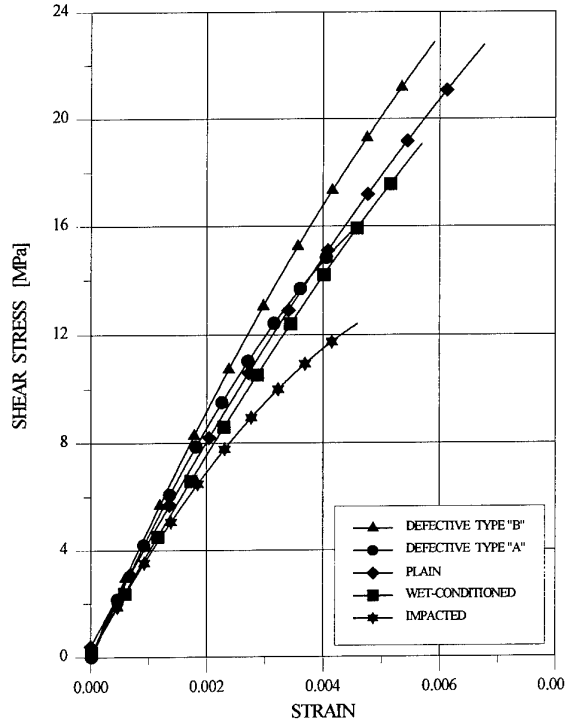


Figure 6: Stress-strain curves of double-lap specimens.

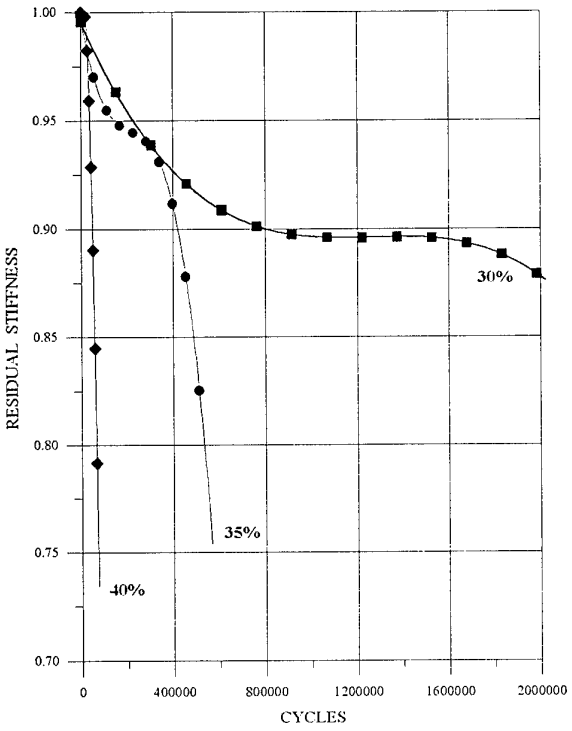


Figure 7: Plain single-lap specimens: residual stiffness.

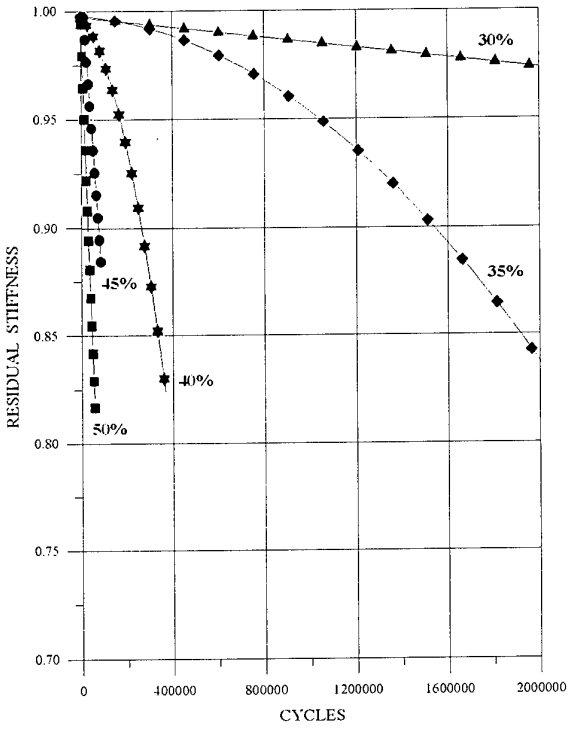


Figure 10: Plain double-lap specimens: residual stiffness.

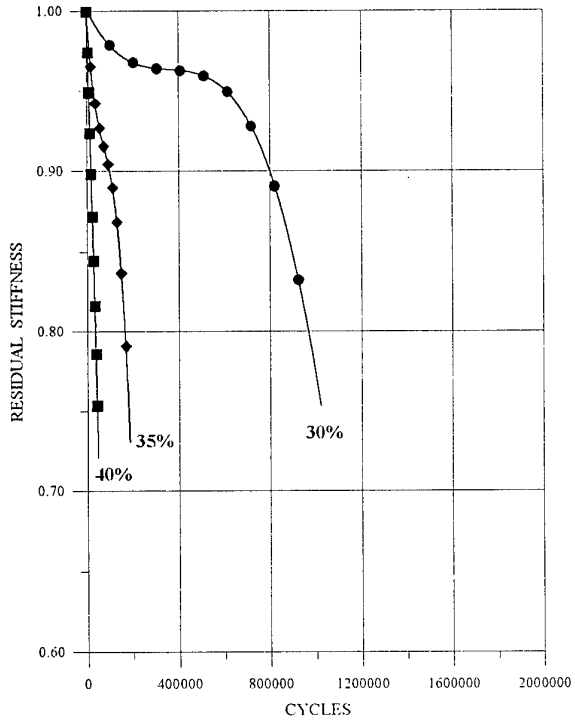


Figure 8: Conditioned single-lap specimens: residual stiffness.

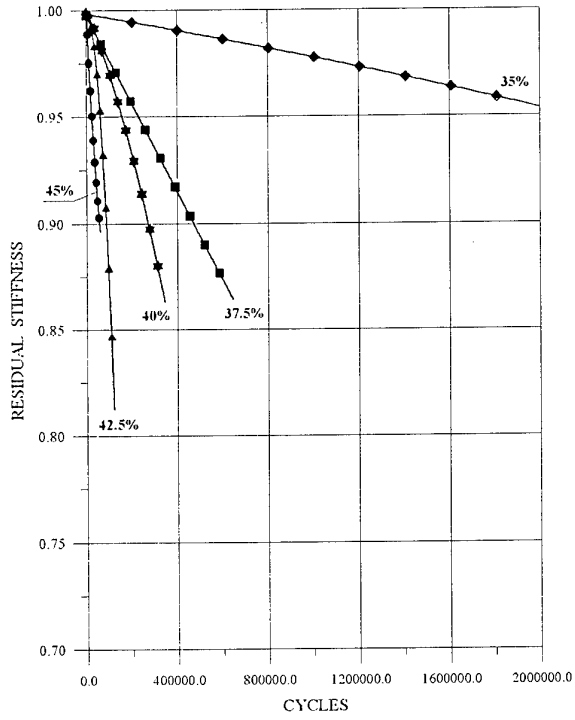


Figure 11: Conditioned double-lap specimens: residual stiff.

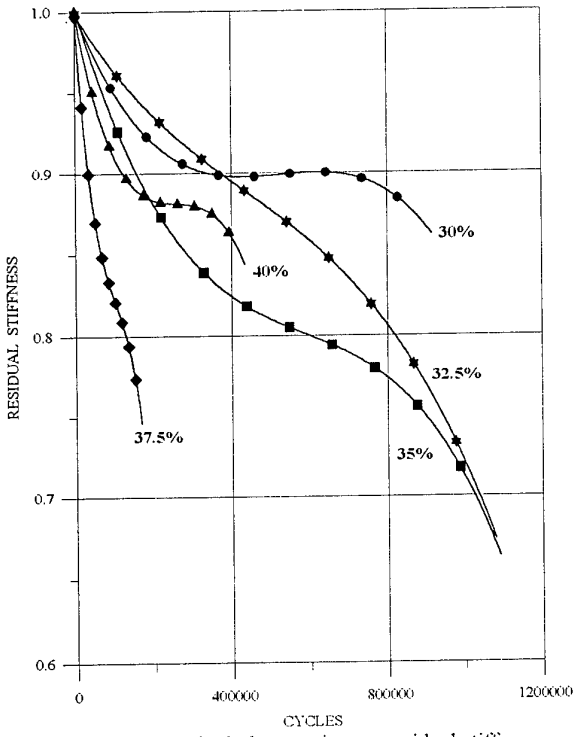


Figure 9: Impacted single-lap specimens: residual stiffness.

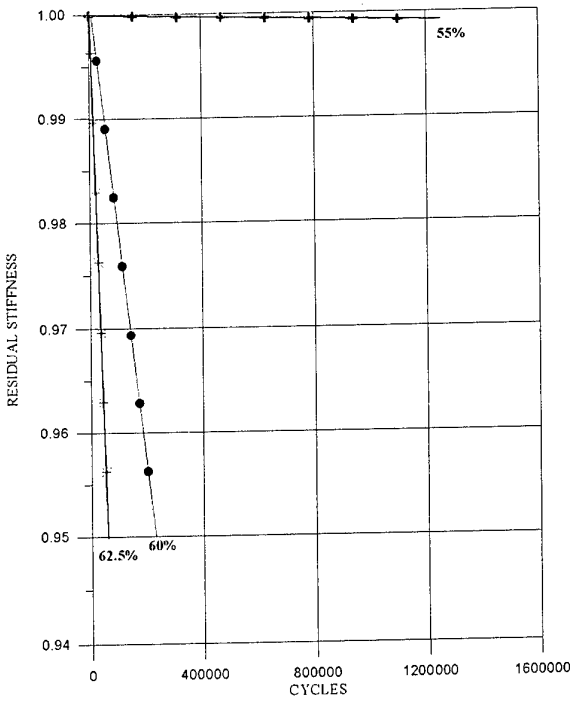


Figure 12: Impacted double-lap specimens: residual stiffness.

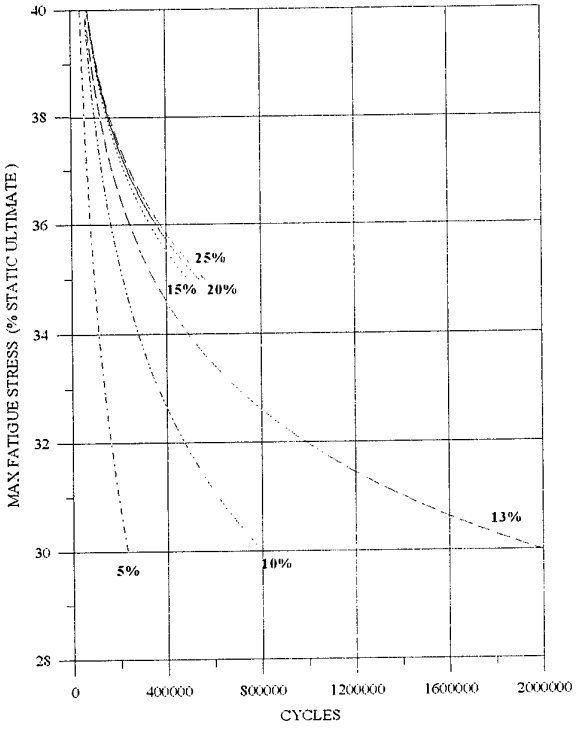


Figure 13: Plain single-lap specimens: Woehler curves.

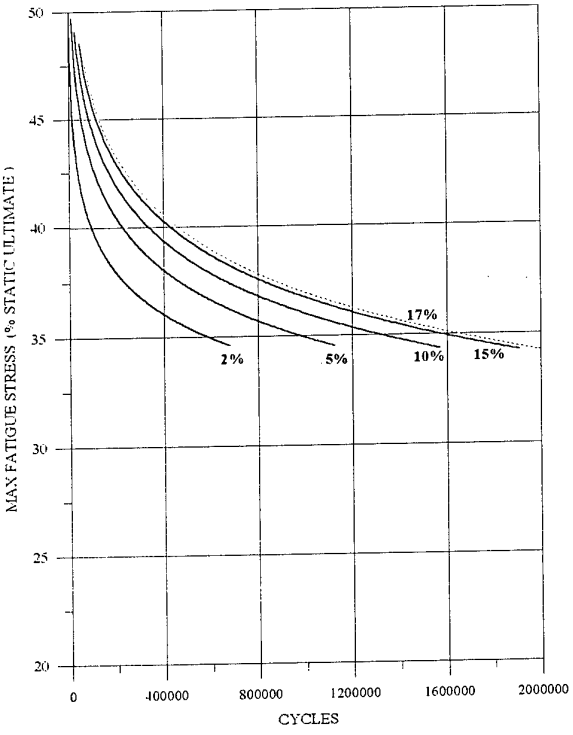


Figure 16: Plain double-lap specimens: Woehler curves.

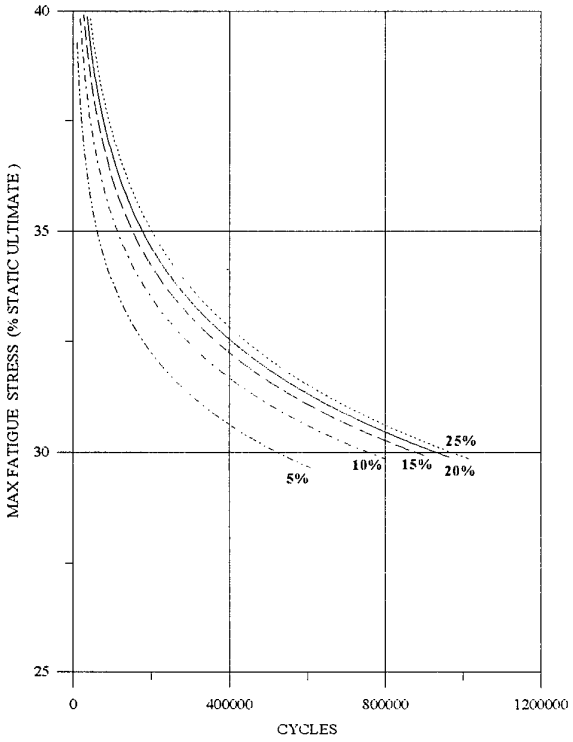


Figure 14: Conditioned single-lap specimens: Woehler curves.

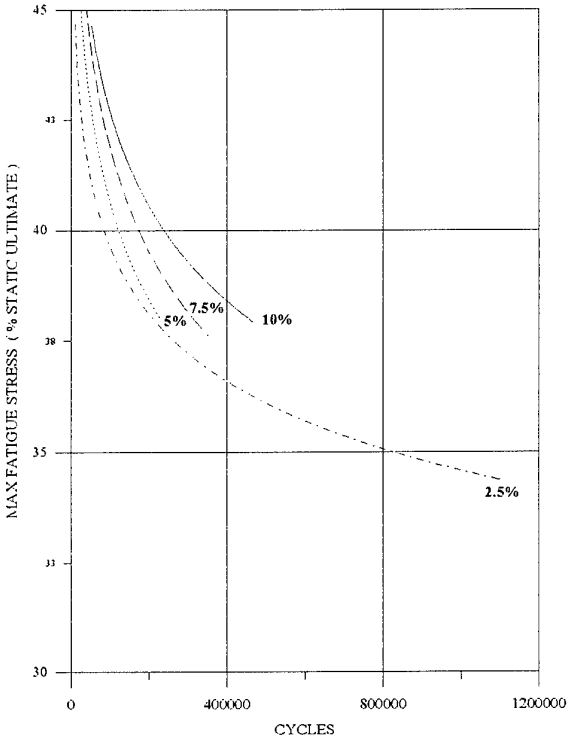


Figure 17: Conditioned double-lap specimens: Woehler curves.

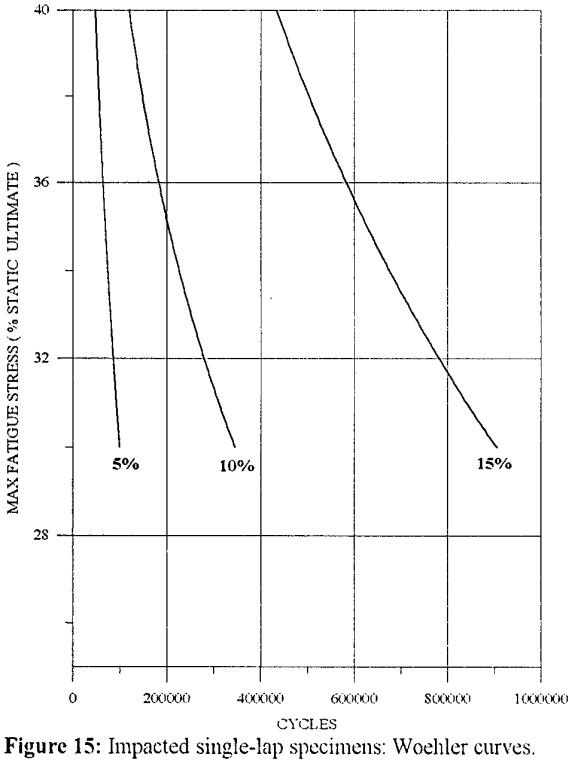


Figure 15: Impacted single-lap specimens: Woehler curves.

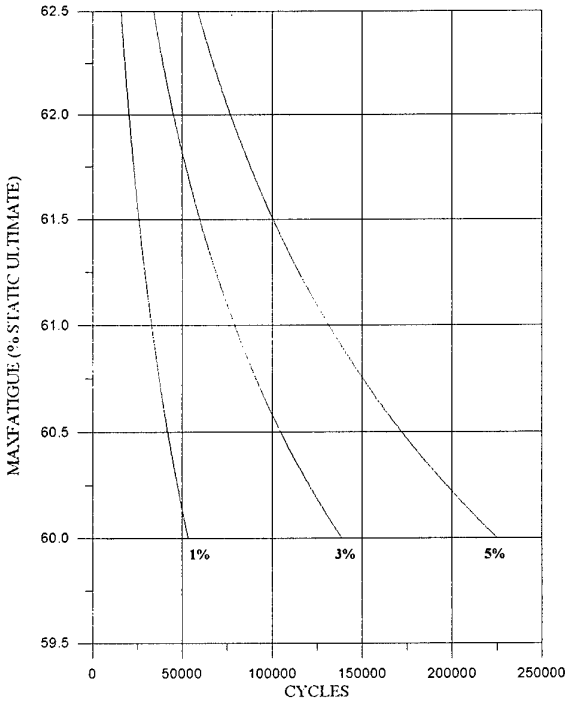


Figure 18: Impacted double-lap specimens: Woehler curves.

6. DISCUSSION

The results of the static tests, summarised in Tab. 4 and Figs. 5 and 6, show that the presence of defects like disbonded inserts, independently of the position, does not notably influence the joint performances: in fact, the stress-strain curves of the defective specimens are not different from the curves of the plain ones and the possible slight reduction of strength is proportional to the reduction of bonded area. The fracture surface is cohesive, even close to the insert, (Fig. 19).

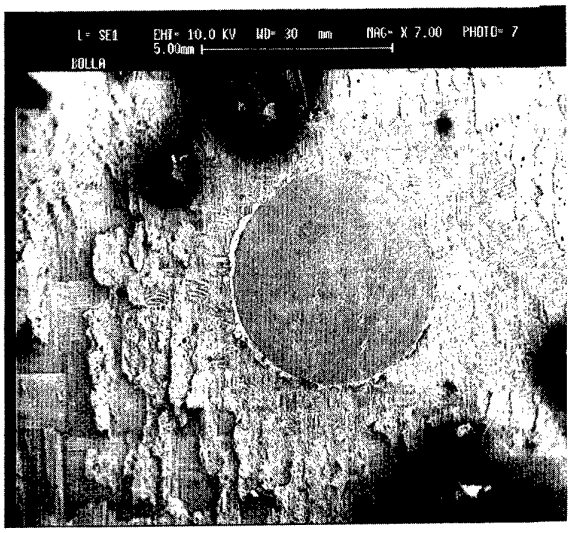


Figure 19: Fracture surface close to the insert.

On the contrary, the wet-conditioned specimens show a reduction of both the stress ultimate and the stiffness; even more remarkable is the performance decrease of the impacted specimens: in this case, the cracks due to the impact induce a macroscopically non-linear behaviour of the stress-strain curve, as shown in Fig. 6. In general, the strength and stiffness decrement are larger for single-lap specimens, owing to the presence of peeling stresses in the adhesive layer: besides, they are more sensitive to the wet-conditioning and to the impacts as well.

The fatigue behaviour of the plain specimens, reported in Figs. 7 and 10, summarised in the Woehler curves of Figs. 13 and 16, does not show any fatigue limit: in fact, for R = 30%, the stiffness decrement at 2 millions cycles exceeds 10% for single-lap specimens and 3% for double-lap ones, the trend being continuously decreasing. The failure due to oligocyclic fatigue is reached for R = 40% (single-lap) and 50% (double-lap specimens).

Some technological remarks have to be made with regard to the double-lap plain specimens. Owing to production reasons, the surfaces of the single adherent are different: the one close to the vacuum bag during the curing process is rough and rippled; the other being in direct contact with the caul plate is smooth and even. As shown in Figs. 20 and 21, which refer to a specimen tested at R = 50%, the adhesion on the rough surface gives a cohesive fracture, while the adhesion on the smooth surface induces a failure which implies a wide delamination in the adherent and the separation of its outer layer, which remains bonded to the adhesive layer and tears away from its laminate of origin. This is due to the fact that an uneven surface induces a non-uniform adhesive thickness and leads to stress concentrations, which allow the onset and propagation of a cohesive fracture inside the adhesive: the adhesive itself becomes the weak link of the whole joint; vice versa, if the surfaces of the adherents are smooth and even, the adhesive has a constant thickness and the weak link of the joint is represented by the interlamina between the adherent laminate and its outer layer(s).

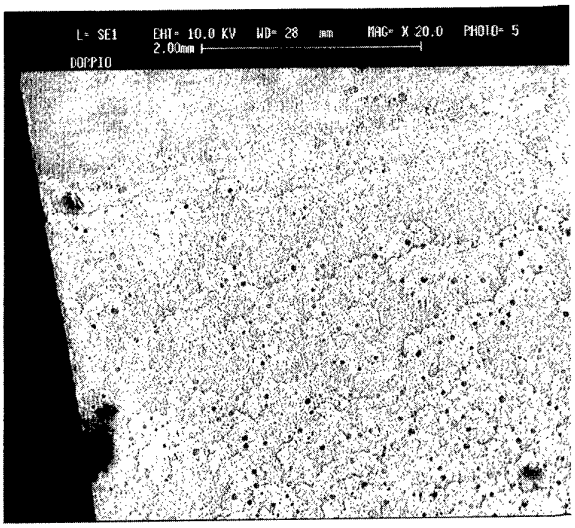


Figure 20: Cohesive fracture at the rough surface.

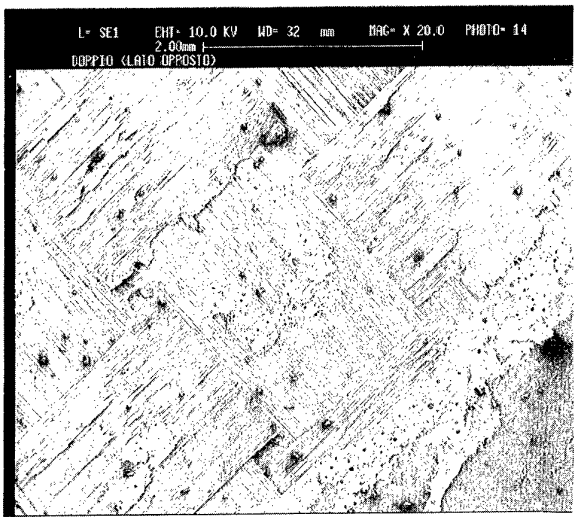


Figure 21: Layer separation at the smooth surface.

The wet conditioning deteriorates the fatigue endurance of both single- and double-lap specimens; the decrement is not very notable in case of oligocyclic fatigue, but it gets dramatic at low R ratios: the stiffness decrease doubles and the fatigue life halves (especially for single-lap specimens). Such a behaviour is mainly due the reduction of adhesive performances: in fact, while the plain single-lap specimen tested at R = 35% shows an adhesive-cohesive failure (Fig. 22), the corresponding wet-conditioned specimen is characterised by a quite cohesive fracture (Fig. 23), which means that the joint fails owing to the adhesive inadequacy, lasts a lower number of cycles and suffers an higher stiffness decrease.

The behaviour of the impacted specimens can hardly be assessed in an univocal manner and according to a well-established trend. Notwithstanding the repeatability of the impact energy values and the reliability of the fatigue testing methodologies, owing to

the randomatic defects and in-homogeneity characterising the structure of the adherents and the adhesive, identical impacts cause different damages and different damages lead to different fatigue behaviours.



Figure 22: Adhesive-cohesive fracture of a plain specimen.

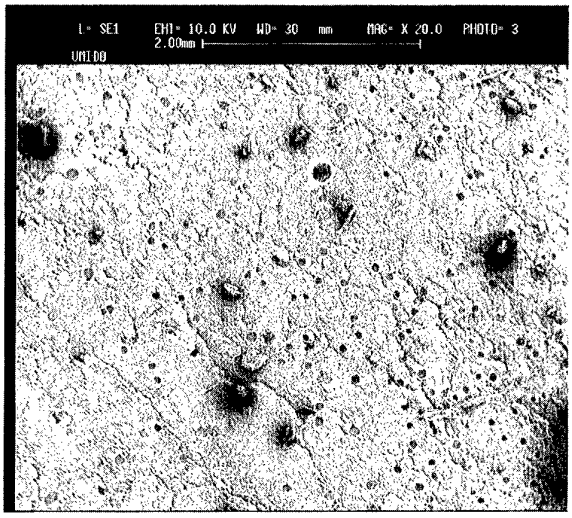


Figure 23: Cohesive fracture of a wet-conditioned specimen.

In general, on the microscopical scale, the impact induces the localised breakage of the fibre, the brittle failure of the matrix and the disbonding of the fibre-matrix interface (Fig. 24); on the macroscopical scale, the impact can induce the cohesive failure of the adhesive, the adhesive failure at the adhesive/adherent interfaces or the interlaminar failure of the adherents, as shown in Fig. 25, which refers to a single-lap specimen impacted with a specific energy of 0.75 J/mm.

In consequence of the prevailing of the one or the other of these mechanisms, the fatigue behaviour notably varies as well. All the specimens referred to in Fig. 9 suffered large cohesive failures of the adhesive, due to the impact; the two specimens tested at R = 30% and 40% also suffered a macroscopical damages of one of the adherents, consisting in a through-the-thickness intralaminar crack perpendicular to the axis of the specimen. This induces an anomalous behaviour, implying a wide *plateau* where the residual stiffness does not change, followed by an abrupt stiffness decrease (typical fatigue behaviour of the composite laminates); it causes the sudden final failure of the joint, owing to the brittle fracture of the adhesive. Vice versa, the other curves show a smoother stiffness decrement, due to the uniform growth of the crack in the adhesive; this induces a cohesive fracture which propagates up to the final brittle failure of the residual bonded area, no more able to sustain the static loads. The crack propagation is reported in Fig. 26, showing the sequence of enhanced X-rays corresponding to 25, 50, 100 and 150 fatigue chilocycles.



Figure 24: Fibre breakage and matrix failure due to the impact.

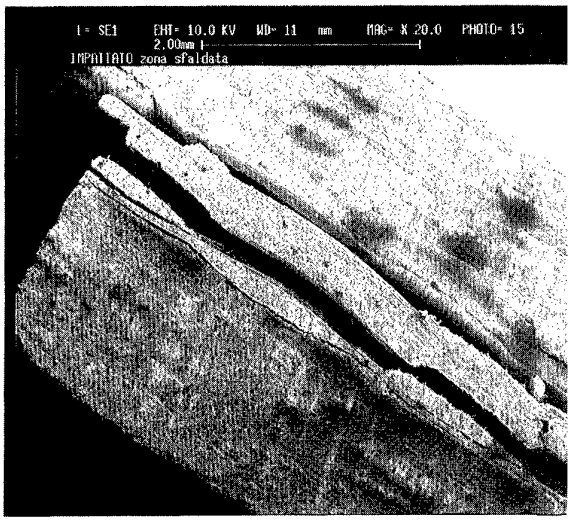


Figure 25: Interlaminar cracks due to the impact.

However, the fatigue behaviour of the impacted double-lap specimens shows some noteworthy aspects. Their static ultimate is halved owing to the impact, while the fatigue tests, performed at stress ratios R deriving from the static strength of the impacted specimens, show stiffness decreases extremely less pronounced than plain specimens: this means that the impact exerts an influence more severe on the static behaviour than on the fatigue endurance. Even though hidden by the complex phenomena previously described, the same trend can be envisaged for the single-lap specimens as well, only if the impact does not cause initial damages to the adherents, but induces a mere delamination in the adhesive layer.

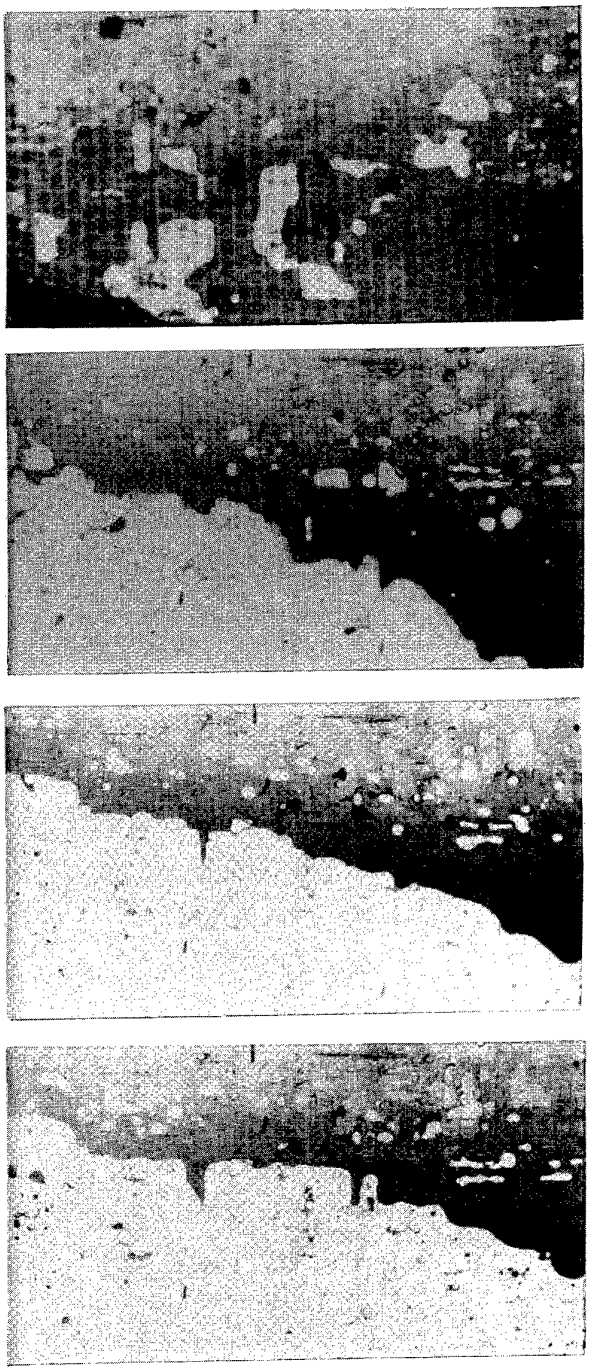


Figure 26: Crack growth (25, 50, 100 and 150 chilocycles).

7. CONCLUSION

Finally, the following main synthetic conclusions can be drawn:

- the presence of defects (disbonded inserts) independently of the position, does not affect the static behaviour of the joint;
- if the surface of the adherents is smooth, layers tear-off is likely to occur; otherwise a cohesive failure appears;
- the wet-conditioning notably reduces the fatigue endurance and turns the adhesive-cohesive failure into purely cohesive;
- the fatigue behaviour of impacted joints is more sensitive to the type of damage than to the fatigue stress level;
- the impact exerts an influence more severe on the static behaviour than on the fatigue endurance.

8. REFERENCES

1. Caprile, C., Sala, G., "Fatigue Behaviour of CFRP Jointed Specimens", l'Aerotecnica, Missili e Spazio, Vol.65, No.4, pp.176-185, December 1986.

2. Caprile, C., Sala, G., "Alcuni Risultati Sperimentali sulla Fatica di Giunzioni Meccaniche nei Compositi" (in Italian), Procs. I AIFA National Symposium, Milano, 16-17 March 1987.

3. Giavotto, V., Caprile, C., Sala, G., "Damage Growth in Composite Bolted Joints", AGARD CP-427.

4. Caprile, C., Sala, G., "Stiffness and Residual Strength Variations on Mechanical Joints in CFRP Specimens in Cycling Loading", AGARD CP-427.

5. Sala, G., "Fatigue Performance of Riveted, Bonded, and Fusion-Bonded Joints of Thermoplastic Composites for Automotive Application", Procs. XXV ISATA International Symposium, Firenze, 1-5 June 1992.

6. Caprile, C., Sala, G., Cardinale, M., "Valutazione di Rivetti Speciali per Strutture Aeronautiche in Materiale Composito" (in Italian), Procs. X AIDAA Natioanl Congress, Pisa, 16-20 October 1989.

7. Kinloch, A.J., "Adhesion and Adhesives - Science and Technology", Chapman and Hall, London-New York, 1987.

8. Romanko, J., "Behaviour of Adhesively Bonded Joints Under Cyclic Loading", AGARD LS 102, 10-1979.

9. Sancaktar, E., "Fatigue and Fracture Mechanics", in "Adhesives", ASM International, 1990., pp.501-520.

10. Thrall, E.W., "Failures in Adhesively Bonded Structures", AGARD LS 102, 10-1979.

11. Penado, F.E., "Numerical Design and Analysis" in "Adhesives", ASM International, 1990, pp. 477-500.

12. Hart-Smith, L.J., "Rating and Comparing Structural Adhesives: A New Method", in "Adhesives", ASM International, 1990., pp.471-476.

13. Nak-Ho Sung. "Moisture Effects on Adhesive Joints", in "Adhesives", ASM International, 1990., pp.622-627.

14. Good, G., "Combined Temperature-Moisture-Mechanical Stress Effects on Adhesive Joints", in "Adhesives", ASM International, 1990., pp.651-655.

15. Kollek, H., "Weathering and Aging Effects onAdhesive Joints", in "Adhesives", ASM International, 1990., pp.656-662.

16. Giavotto, V., Caprile, C., Sala, G., "Fatigue and Damage Mechanics of Notched, Impacted and Jointed Thermoplastic Composites", Procs. XVII ICAF Symposium, Stockholm, 7-11 June 1993.

17. Brockmann, W., "Durability Assessment and Life Prediction for Adhesive Joints", in "Adhesives", ASM International, 1990, pp.663-672.

CYCLIC FATIGUE AND ENVIRONMENTAL EFFECTS WITH ADHESIVELY BONDED JOINTS

I.A. Ashcroft, R.B. Gilmore and S.J. Shaw
Structural Materials Centre
DRA Farnborough
Hampshire GU14 6TD
U.K.

SUMMARY

The influence of service environment, bonding method and adherend properties on the fatigue resistance of adhesive bonded CFRP joints has been investigated. It was seen that environment had a significant effect on joint performance, with hot/wet conditions proving extremely damaging. Composite lay-up also had a significant effect on the fatigue performance of joints and co-bonding was seen as an advantageous joining technique.

1. INTRODUCTION

The use of structural adhesives in aircraft applications can offer numerous advantages over traditional joining techniques such as mechanical fastening. Major benefits include improved aircraft performance e.g. agility, payload and range, together with considerable scope for reductions in both procurement and life-cycle maintenance costs. Additionlly, adhesive bonding would be of paramount importance in the development and construction of advanced lightweight composites.

One of the major concerns in using adhesive bonded joints is in predicting their life to failure. This is usually determined by the environmental conditions and stresses experienced in service. It is critical therefore to simulate these conditions in laboratory tests in order to better understand the failure mechanisms, aid in joint development and to predict the safe life of a joint in the field. There are many variables to consider when designing a programme of accelerated fatigue testing including frequency, temperature, environment, bondline thickness, substrate thickness, displacement and load ratios, and mean displacement. The main aim of such programmes is to simulate the mechanisms of failure experienced by the structure under actual long-term service conditions in a much shorter period of time.

At DRA the effect of test environment on the fatigue performance of adhesive joints is being investigated using the following methods.
(i) Crack initiation is studied by fatigue loading joints with constant amplitude cyclic loads to determine the threshold load for fatigue crack propagation in different environments. It has been proposed that the strain energy release rate calculated at this threshold load (G_{th}) can be used to calculate the threshold loads in other geometries[1].
(ii) Crack propagation is studied by measuring crack growth in a pre-cracked sample in constant amplitude displacement fatigue loading. A fracture mechanics approach can be used to calculate strain energy release rate (G) as a function of crack propagation rate (da/dn). The resultant plot can be used to obtain threshold strain energy release rates and Paris law relationships for stable crack growth regions. These can then be used to predict threshold loads in other geometries and to predict the number of cycles to failure in joints loaded above this threshold figure[2]. It should be noted however that the exponent in the Paris law relationship for bonded composites is usually considerably greater than that seen with metals indicating that the crack growth rate is more sensitive to changes in the applied load. This fact and the scatter seen in results means that predicting fatigue crack growth rates using this method can lead to inaccuracies.
(iii) The fracture path may vary with test environment and/or materials parameters and in some cases has been seen to change as a crack propagates through a sample. This would be expected to influence the fatigue resistance and hence it is important to determine the fracture path associated with fatigue failure. This is achieved on a 'macro' scale by optical microscopy and x-ray radiography of tested joints.
(iv) A more detailed study of the fracture surfaces is required to determine the fracture mechanisms. Fracture surfaces are therefore studied on a 'micro' scale by electron microscopy techniques.

This paper will be restricted to discussion of items (i) and (iii).

2. EXPERIMENTAL

The aim of this work was to determine a threshold load below which fatigue failure will not occur for a given service life. 10^6 cycles was chosen as the threshold limit for this study in order to study a range of environments in a reasonable time.

2.1 Materials

Current work is focused on the joining of carbon fibre reinforced polymers (CFRP). The CFRP in the current work has a modified bismaleimide/epoxy matrix and T800 fibres. The pre-preg material is laid up as 'unidirectional' (16 ply at 0°) or 'multi-directional' (8 ply at 0°, 4 at -45° and 4 at +45°) panels which are cured at 182° C for 2 hours with an initial autoclave pressure of 90 p.s.i. The adhesive used was a modified epoxy which was supplied in film form either with a nylon carrier or unsupported. The adhesive was cured for 1 hour at 120°C.

2.2 Joint Design

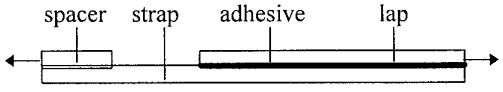


Figure 1 Lap/strap joint

Paper presented at the 83rd Meeting of the AGARD SMP on "Bolted/Bonded Joints in Polymeric Composites", held in Florence, Italy, 2-3 September 1996, and published in CP-590.

Most of the fatigue testing of adhesive joints has been with the lap/strap joint shown in figure 1. This is basically the same geometry as the cracked lap shear sample, however, a starter crack is not introduced in order to study crack initiation in a realistic joint. The sample has a spacer bonded to the strap to ensure that the applied load is aligned with the bondline and aluminium end tabs are bonded to the adherends to aid gripping. Features of this joint are that the stresses at the crack tip are a mixture of modes I and II, the crack growth is limited to a single bondline and there is no well defined failure point of the joint. At DRA the sample is also used in a pre-cracked form to study crack propagation rates.

The stresses in the joint are a mixture of modes I and II and the magnitude and proportion of these will depend on a number of factors including the applied stress and the mechanical properties of the adherends and adhesive. The ratio of mode I/mode II in the uncracked sample can be controlled by altering the thickness of the lap and strap components of the joint and by tapering the end of the lap[1]. It has been shown[3] that for equal thickness adherends with a square edged lap end GI/GII ≅0.3. This ratio decreases as the lap end is scarfed. A mixed mode stress distribution can be seen as an advantage in that it is more representative of stresses in real joints than the predominantly mode I failures seen in joints such as the DCB, however analysis of the joint is more complex as stresses and strain energy release rates need to be differentiated into mode I and mode II components. Strain energy release rates in the joints can be calculated by analytical methods or by F.E techniques for the uncracked joint[3]. Brussat[4] derived the following expression for the total strain energy release rate, G_t in a cracked lap shear joint.

$$G_t = \frac{P^2}{2b(EA)_s}\left[1 - \frac{(EA)_s}{(EA)_t}\right] \qquad 1$$

Where P is the applied load, b is the sample width and $(EA)_s$ and $(EA)_t$ are the tensile rigidities of the strap and the lap and strap respectively. This expression gave similar results to FE derived values for equal thickness adherends[3].

During crack propagation G_t ($=G_I+G_{II}$) can be calculated from equation 2.

$$G_t = \frac{P^2}{2b}\frac{dC}{da} \qquad 2$$

Where dC/da is the change in sample compliance with crack length.

Samples were made either by adhesive bonding pre-cured CFRP panels or by co-bonding. In the latter process the pre-preg and adhesive were cured in a single operation. The curing conditions used in the co-bonding are as for the composite and therefore the adhesive wasn't cured under optimum conditions. Co-bonding resulted in a less distinct adhesive region in the joint due to interdiffusion of adhesive and composite resins and the formation of a markedly different adhesive fillet at the end of the lap adherend. This is shown schematically in figure 2.

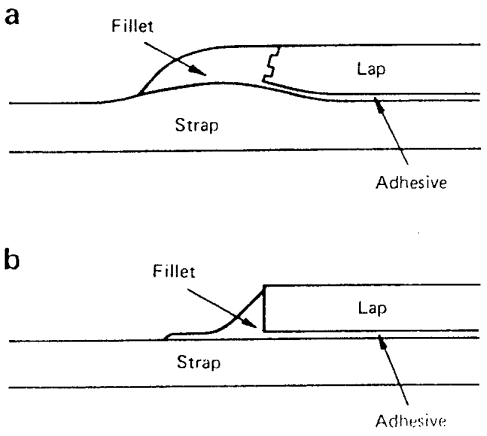


Figure 2 Adhesive fillets in (a) co-bonded and (b) adhesive bonded joints

Samples to be tested dry were stored at 50°C under vacuum and samples to be tested in a humid environment were conditioned in a humidity chamber at 60°C, 85% R.H. prior to testing. A test coupon of the adherend material was conditioned at the same time as the test samples and weighed at periodic intervals to monitor water uptake. The samples were only tested once equilibrium had been reached.

2.3 Fatigue testing

Fatigue testing was carried out using servohydraulic fatigue testing machines. One machine was fitted with a humidity chamber capable of testing from ambient to 150°C. Another machine had a temperature chamber capable of testing dry in the temperature range -60 to 180°C. Current testing environments are dry testing at -50, 25 and 90°C. High humidity testing was at 25°C, 85%R.H. and 90°C, 65%R.H. All testing was at 5Hz, with various maximum fatigue loads and test periods employed to determine threshold values. Testing was in load control with constant load amplitude and a load ratio of 0.1.

2.4 Post Fatigue Examination

Optical microscopy of the sample edges was used to detect first signs of crack growth in the sample. After fatigue testing, optical microscopy and x-ray radiography were used to determine the fracture path on a 'macro' scale and to measure the crack length. On the basis of the preceding examinations selected samples were sectioned in order to study the fracture surfaces.

3. RESULTS

The results from the fatigue tests with the adhesive bonded CFRP samples are summarised in tables 1-6. A more complete set of results can be found in reference 5.

It should be remembered that in this report 'adhesive bonding' refers to the process of first curing the composite panels, and then curing the adhesive in a second operation whereas 'co-bonding' refers to the adhesive and composite being cured in the same operation.

Key to failure modes

A	cohesive failure in the adhesive
S/A	adhesive failure at the strap/adhesive interface
L/A	adhesive failure at the lap/adhesive interface
S	failure in the composite strap

The failure modes quoted in tables 1-6 indicate the dominant fracture path only, in many cases other failure modes were observed in small areas due to material variations and manufacturing imperfections.

3. 1 Unidirectional CFRP adhesive bonded with unsupported adhesive

Table 1

Test environment	Maximum load, kN	Cycles to failure	Failure mode
25°C, Dry	10 17	$>10^6$ $1.5x10^5$	S/A, S
90°C, Dry	10 17	$>10^6$ $9x10^4$	A
-50°C, Dry	10 17	$>10^6$ $1.5x10^5$	S
25°C, Wet	10 17	$>10^6$ $2x10^5$	S/A
90°C, Wet	5 10	$8x10^5$ $<10^4$	S/A, A

It can be seen from the table above that for the unidirectional composite bonded with the unsupported adhesive a maximum fatigue load of 10 kN was only sufficient to initiate failure in those samples tested wet at 90°C. In these conditions failure was seen after $< 10^4$ cycles. Failure, in this enviroment, was also seen with a maximum load of only 5kN. At 17kN failure was observed in all test conditions at $< 10^6$ cycles. The samples tested at 25°C gave similar results whether tested wet or dry. The samples tested at -50°C showed similar fatigue resistance to those tested at 25°C whereas those tested dry at 90°C had slightly lower fatigue resistance.

In all cases fatigue crack initiation was in the adhesive fillet. The crack propagated through the adhesive fillet at approximately 45° to the applied load, as shown in figure 3.

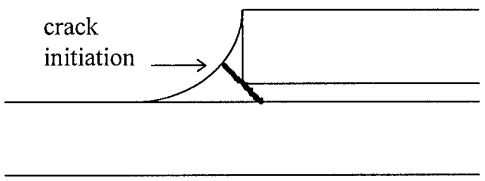


Figure 3 Locus of fatigue crack initiation in adhesive bonded joints

The samples tested at 25°C failed mainly at the strap/adhesive interface, although some interlaminar failure between plys in the composite strap was also seen in the samples tested dry at 25°C. Samples tested at -50°C failed almost entirely by interlaminar fracture of the composite strap close to the interface. This indicates that the composite matrix resin becomes less fatigue crack resistant than the adhesive at low temperatures. This is not surprising as the composite resin is designed for a higher maximum service temperature (177°C) than the adhesive (121°). Composite failure was associated with longitudinal cracking in the x-ray radiographs, as shown in figure 4. This indicates debonding of the fibres from the matrix. Note that isolated pockets of delamination can be seen ahead of the actual crack front.

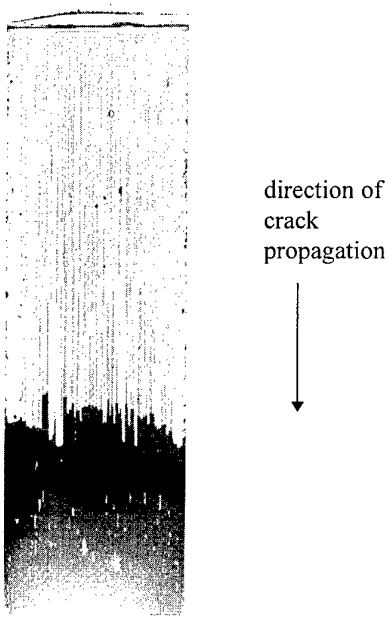


Figure 4 X-radiograph showing longitudinal cracking associated with composite failure.

The samples tested dry at 90°C failed entirely by cohesive failure in the adhesive whereas the samples tested wet at 90°C exhibited a mixture of cohesive failure in the adhesive and adhesive failure at the strap/adhesive interface. X-ray radiographs of samples exhibiting cohesive failure of the adhesive showed extensive 'transverse cracking' across the sample width, as shown in figure 5. Again, some delamination can be seen ahead of the crack front.

SEM study of the fracture surfaces revealed plate like fractures in the adhesive with crack fronts approximately perpendicular to the crack propagation direction, as shown in figure 6.

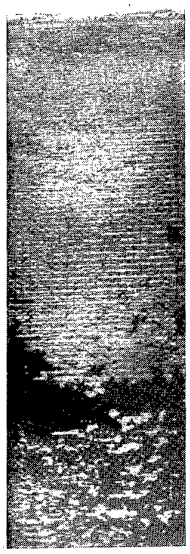


Figure 5 X-radiograph showing transverse cracking associated with cohesive failure in unsupported adhesive.

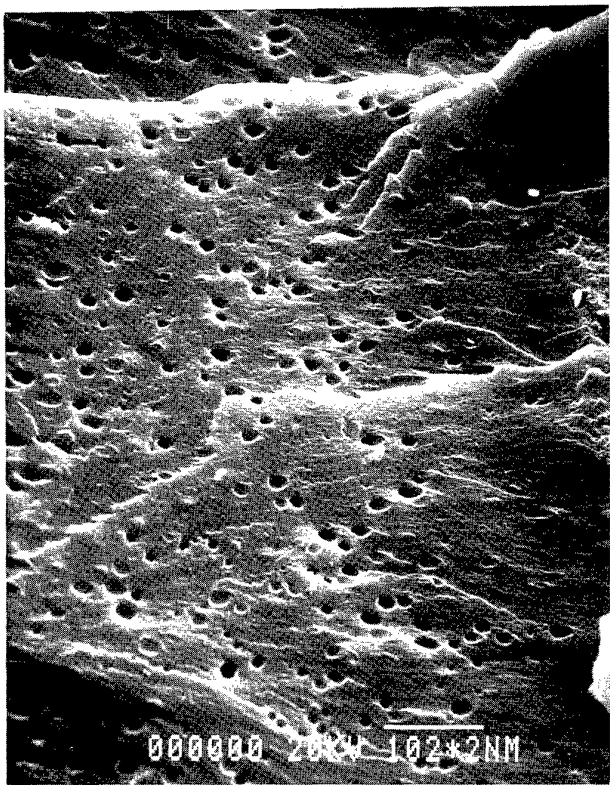


Figure 6 SEM micrograph showing crack fronts perpendicular to the crack direction.

3.2 Unidirectional CFRP adhesive bonded with supported adhesive

Table 2

Test environment	Maximum load, kN	Cycles to failure	Failure mode
25°C, Dry	10 17	$>10^6$ 10^5	S/A, S, A
90°C, Dry	10 17	$>10^6$ $4x10^4$	S/A, S
-50°C, Dry	10 17	$>10^6$ $4x10^4$	S
25°C, Wet	10 17	$>10^6$ $2x10^5$	S/A, A
90°C, Wet	10 17	$9x10^4$ $<10^4$	S/A, A

As with the supported adhesive, the only joint failures with a maximum fatigue load of 10kN were those tested wet at 90°C. At 17kN samples tested at 25°C proved the most fatigue resistant (whether in wet or dry conditions) followed by those tested dry at -50°C and then those at 90°C. Samples tested at 90°C in a wet environment exhibited significantly lower fatigue strength than those tested under any other conditions.

Crack initiation was in the adhesive fillet as with the unsupported adhesive.

In most cases similar fracture paths to those described for joints with the unsupported adhesive were observed, with two notable exceptions. Firstly, it can be seen that whereas with the unsupported adhesive transverse cracking was associated with cohesive failure of the adhesive, with the supported adhesive multi-directional cracking was seen, as shown in figure 7.

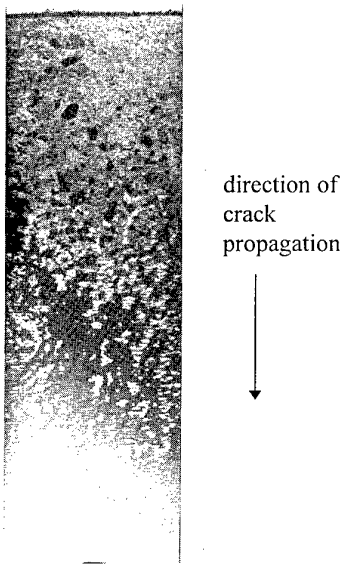


Figure 7 X-radiograph showing multi-direcional cracking associated with cohesive failure in supported adhesive.

The obvious explanation for this difference is that the carrier fibres in the supported adhesive interfere with the fracture path.

A second interesting observation is that whereas with the unsupported adhesive failure was entirely cohesive in the adhesive when tested dry at 90°C, with the supported adhesive under these conditions failure is a mixture of adhesive failure at the strap/adhesive interface and interlaminar cracking of the composite in the strap. A possible explanation for this is that in the case of the unsupported adhesive the adhesive is sufficiently weakened on heating to become the easiest path for crack propagation whereas with the supported adhesive the carrier mat helps to provide the adhesive with additional strength when the adhesive resin has been weakened. The supported adhesive would be acting as a fibre reinforced composite under these conditions, with the fibres acting as stressed members and increasing the toughness of the adhesive by a combination of mechanisms which could include crack deflection, fibre pull out and fibre bridging of cracks. The reason why this effect is not apparent at lower temperatures is firstly because the epoxy matrix is more rigid and secondly because the main mechanism of toughening at these temperature is associated with the dispersed rubber particles in toughened epoxies.

3. 3 Multi-directional CFRP, adhesive bonded with unsupported adhesive

Table 3

Test environment	Maximum load, kN	Cycles to failure	Failure mode
25°C, Dry	10 14	$>10^6$ $5x10^4$	L/A, S/A, S
90°C, Dry	5 10	$>10^6$ $9x10^4$	S/A, A
-50°C, Dry	10 14	$8x10^5$ $<10^4$	S/A, A, S
25°C, Wet	5 10	$>10^6$ $8x10^4$	S
90°C, Wet	5 10	$8x10^4$ $<10^5$	S/A, A, S

The table above shows the results from the fatigue testing of adhesive bonded multi-directional CFRP with the unsupported adhesive. The first thing to note is that in all environments significantly lower fatigue strength is demonstrated with multi-directional CFRP adherends as compared with the unidirectional composite. This can be attributed to the fact that multi-directional adherends will be considerably weaker than unidirectional adherends in the direction of loading and hence will deform a greater amount for a given applied load. This will have the effect of increasing the stresses in the adhesive and at the interface. This can be demonstrated by studying equation 1. It can be seen that G_t is inversely proportional to the adherend modulus for a given load if geometric factors remain constant. It can also be seen that for a given G_{th} the load required for crack initiation will be greater for the sample with the higher modulus adherends. With a G_{th} of $300J/m^2$ (determined experimentally in recent work) equation 1 predicts a threshold load of 8kN with the unidirectional adherends and 6kN with the multi-directional adherends.

With a maximum fatigue load of 10 kN failure is seen in all the test environments except dry at 25°C. The next best environment in terms of resistance to crack initiation is -50°C. It can be seen that testing wet at 25°C is more detrimental to the fatigue life of the joint than testing dry at 25°C. This is in contrast to the tests with the unidirectional CFRP adherends, which showed little difference in the fatigue life of joints tested wet or dry at 25°C. It can also be seen that the failure mode when testing wet at 25°C with the multi-directional CFRP adherends is interlaminar failure in the CFRP strap. It can be concluded therefore that the wet environment must weaken the CFRP adherend. The unidirectional CFRP tested wet at 25°C must also be weakened to some degree but remains stronger than the strap/adhesive interface and the adhesive. In this case the cohesive strength of the adhesive and the adhesive strength of the strap/adhesive interface, which are relatively insensitive to humidity at 25°C control the fatigue behaviour of the joint. The multi-directional adherend, however, is significantly weaker than the unidirectional adherend and on exposure to moisture is further weakened to such an extent that it is becomes the preferred path for fatigue crack propagation.

As with the unidirectional adherends transverse cracking is associated with cohesive failure of the adhesive and in all test conditions, except dry at 90°C, interlaminar failure of the composite strap has become an important failure mechanism. The composite material is much stronger when loaded in the direction of the fibres than when loaded perpendicular to the fibres. In the multi-directional material the plys at 45° to the direction of loading will therefore have a significant stress component in their weak direction. It is not surprising therefore that composite failure is observed. The x-ray radiographs of these joints show cracking at 45° to the loading direction in the areas of composite failure. This indicates fibre debonding in the 45° plys.

3. 4 Multi-directional CFRP adhesive bonded with supported adhesive

Table 4

Test environment	Maximum load, kN	Cycles to failure	Failure mode
25°C, Dry	10 14	$>10^6$ $5x10^4$	L/A, S/A, S, A
90°C, Dry	5 10	$>10^6$ $8x10^4$	L/A, S/A, S, A
-50°C, Dry	10 14	$>10^6$ $5x10^5$	S/A, S
25°C, Wet	5 10	$>10^6$ $4x10^5$	S/A, S
90°C, Wet	5 10	$<10^5$ $<10^5$	S/A, S

The multi-directional composite joints bonded with the supported adhesive also show significantly poorer fatigue strength than comparative tests with unidirectional composite, see table 2. Hot, wet testing is the most detrimental environment and -50°C appears to be the most favourable. As noted with the unidirectional adherends cohesive failure of the supported adhesive was accompanied by multi-directional cracking. In most cases

failure in these joints was a mixture of adhesive failure in the adhesive, interlaminar failure of the strap and cohesive failure at the strap/adhesive interface.

3. 5 Multi-directional CFRP co-bonded with unsupported adhesive

Table 5

Test environment	Maximum load, kN	Cycles to failure	Failure mode
25°C, Dry	14 17	$>10^6$ $2x10^5$	S, S/A, A
90°C, Dry	5 10 14	$<10^6$ $5x10^5$ $5x10^4$	S, S/A, A
-50°C, Dry	10 14	$>10^6$ $<10^6$	S

The results for the co-bonded joints with the unsupported adhesive are presented in table 5. Firstly, it can be seen that has only been in 'dry' conditions for the co-bonded joints. This is because moisture equilibrium has not yet been attained for the co-bonded joints being conditioned, however it is expected that co-bonded joints will be tested in wet conditions in the near future. Fatigue resistance is greatest at 25°C followed by -50°C then 90°C.

In all environments the first sign of damage with the co-bonded joints is interlaminar cracking in the strap in front of the adhesive fillet, as shown in figure 8. This is in contrast to the adhesive bonded joints, where in most cases the first sign of damage is cracking in the adhesive fillet. This can be explained by studying the schematic figure of the adhesive fillets in figure 2. The fillet in the co-bonded joint represents less of a discontinuity than that in the adhesive bonded joint and therefore lower stress concentrations would be expected. Also, it can be seen that in the co-bonded joint there is a region just ahead of the fillet where the top plys in the strap are distorted. This is a consequence of the way the samples are jigged in the autoclave and the effect of the vacuum pressure distorting the uncured plys where plate pressure is not applied. This will obviously weaken the strap in this region and account for the cracking observed there. This effect may be less noticeable if the unidirectional CFRP adherends were used.

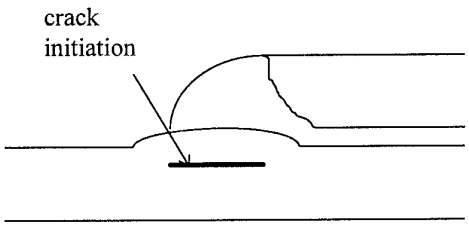


Figure 8. Locus of fatigue crack initiation in co-bonded joints

Crack propagation is a mixture of interfacial failure at the strap/adhesive interface, interlaminar cracking in the strap and cohesive fracture of the adhesive (with transverse cracking). Compared with adhesive bonded samples, the co-bonded joints appear to be more fatigue resistant. This is probably because crack initiation is more difficult in the fillet of the co-bonded sample and that interdiffusion of composite and adhesive resins when co-bonding increases resistance to fatigue crack propagation along the bondline.

3.6 Multi-directional CFRP co-bonded with supported adhesive

Table 6

Test environment	Maximum load, kN	Cycles to failure	Failure mode
25°C, Dry	10 14	$>10^6$ $8x10^4$	S/A, A, S
90°C, Dry	10 14	$<10^5$ $<10^4$	S, S/A, A
-50°C, Dry	10 14	$>10^6$ $<10^4$	S

The samples co-bonded with the supported adhesive also tend to exhibit interlaminar failure in the strap prior to adhesive failure. Crack propagation is again a mixture of mechanisms, except for those tested at -50°C where failure is only in the composite strap. As with the unsupported adhesive the co-bonded joints provide greater fatigue resistance than comparative adhesive bonded joints. Compared to the co-bonded joints with the unsupported adhesive the supported adhesive joints are less fatigue resistant at 25 and -50°C but are more fatigue resistant at 90°C.

4. DISCUSSION

4.1 Locus of failure in bonded joints

In the case of the 'adhesive bonded' samples (i.e. those in which the pre-preg was cured prior to bonding) fatigue crack initiation was in the adhesive fillet and progressed through the fillet at approximately 45° to the loading direction towards the bondline. This can be explained by studying figure 9 which shows the principal stresses in the adhesive fillet of a lap/strap joint with unidirectional adherends and a load of 5kN. Obviously the crack follows a path at 90° to the direction of the maximum principal stresses in the adhesive fillet until the bondline is reached.

In the case of the 'co-bonded' samples crack initiation was in the strap at a point below the adhesive fillet. This was partly explained by noting that the strap in this region is weakened during the curing process. It can also be seen from figure 10 that this region is the location for the maximum stresses in the adherend.

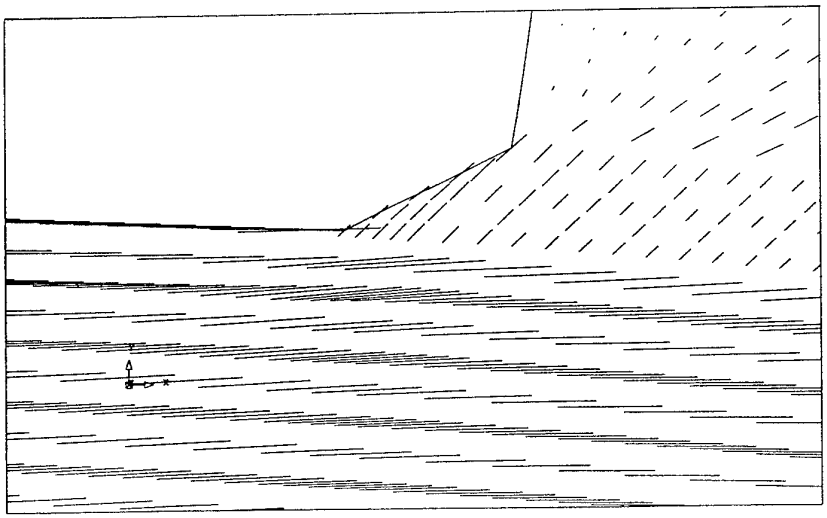


Figure 9 Principal stresses in adhesive fillet of strap/lap joint.

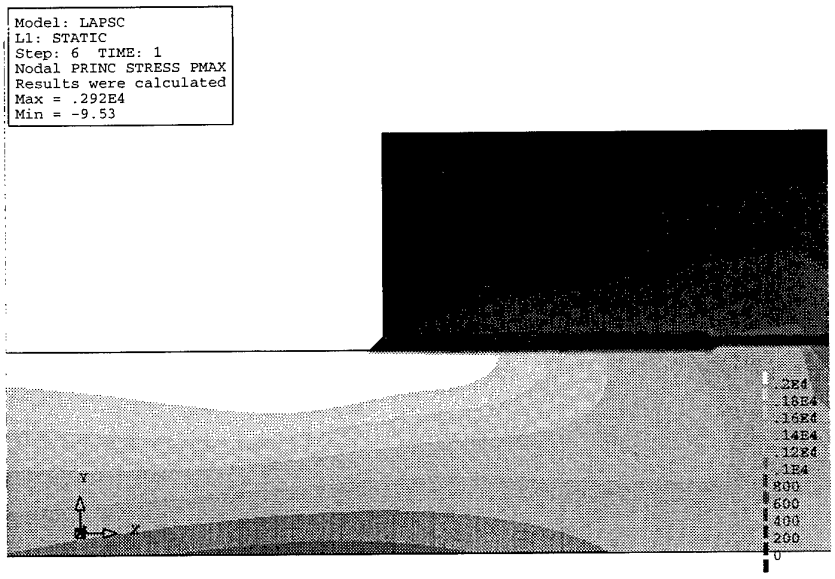


Figure 10 Stress contours in strap/lap joint

4.2 Effect of test environment on fatigue strength

In the case of unidirectional CFRP joints there appears to be little difference in the fatigue resistance of joints tested wet or dry at 25°C. This is in contrast to most metal/adhesive joints which will have reduced strength when subjected to a high humidity environment at 25°C. This can be explained by the fact that the work of adhesion at the adhesive/adherend interface remains positive for the CFRP/adhesive joint[6]. It should be noted that those samples tested wet at 25 and 90°C had undergone the same conditioning treatment (approx. 1 year at 60°C, 85%R.H.). Therefore the conditioning must be of secondary importance, in terms of fatigue strength, compared to the test environment for these joints. In the case of samples constructed with multi-directional CFRP adherends, the fatigue strength was reduced when testing wet at 25°C as compared to testing dry at this temperature. This was attributed to a weakening of the adherend material in the

wet conditions, which is more critical for the multi-directional adherends than for the stronger unidirectional adherends.

Increasing the test temperature to 90°C tends to reduce the fatigue strength of bonded composite joints as both the matrix resin and adhesive weaken as T_g is approached. This effect is not great, however, as the composite is designed for high temperature service and is not expected to be weakened significantly at 90°C. Also the weakening of the adhesive in terms of reduced stiffness may be partially offset by increased toughness at elevated temperatures.

It is obvious that by far the most detrimental test condition in terms of the fatigue strength of composite joints is 90°C in a humid environment The combination of humid environment and high temperature appears to have a detrimental effect which is greater than the sum of the individual effects of temperature and humidity. It has already been noted that high temperatures will tend to weaken the adhesive and to some extent the CFRP matrix resin. Heating will also cause an expansion of the adherends and the adhesive which will enable the absorption of a greater amount of water. Moisture absorption has the effect of lowering the T_g of polymeric materials and therefore it would be expected that the strength of the CFRP adherends and the adhesive would decrease in a humid environment. In hot wet conditions then, we have an accumulated effect of weakening of adhesive and adherend materials which will both increase the stresses on the adhesive for a given applied load and reduce the ability of the adhesive (and composite) to resist these stresses. Qualitatively then, it is not surprising that hot, wet conditions are so damaging to bonded composite joints, however, a more detailed investigation to isolate the effects of water absorption and heat on the strength of adhesive and composite is required to explain this more quantitatively.

Testing at low temperatures does not seem to significantly effect crack initiation but the locus of the fracture shifts to the strap adherend indicating that at low temperatures the composite matrix resin has a lower fracture toughness than the adhesive.

4.3 Effect of adhesive carrier on fatigue strength
In most cases the fatigue resistance of the bonded composite joints with the supported and unsupported adhesives are similar, any differences being secondary to the effects of environment, adherend and bonding technique. In the case of cohesive failure in the adhesive different fracture surfaces are observed with the different adhesives. The unsupported adhesive has a plate like fracture surface with extensive transverse cracking across the sample width. In contrast the supported adhesive exhibits a multi-directional, cracked fracture surface which has been attributed to crack deflection by the carrier fibres.

4.4 Effect of bonding technique on fatigue strength
It has been seen that co-bonding increases the fatigue resistance of the joints compared with adhesive bonding. This has been attributed to the reduction in material discontinuities at the overlap and along the bondline. However, a drawback to the technique is that the composite strap is weakened near the end of the overlap which results in interlaminar failure of the strap adherend prior to failure in the joint itself. This is a symptom of the curing method and it is possible that this could be addressed in future work.

4.5 Effect of composite ply on fatigue strength
It is clearly seen in tables 1-6 that the fatigue resistance of adhesively bonded composite joints is significantly reduced by using multi-directional adherends as compared to unidirectional adherends. It should be noted therefore that laboratory work on biaxial loading of unidirectional composites will give unrealistically high performance data and these results should not be used as a basis of joint design incorporating multi-axial loading of the composite. In this work only two lay-up configurations were used to fabricate the CFRP panels whereas in practise many other configurations may be found. As the fatigue strength is so sensitive to the composite lay-up pattern it is suggested that in future work other lay-up configurations are investigated and attempts are made to develop a predictive capability to enable the results from mechanical tests to be extended to other composite panel configurations.

5. CONCLUSIONS

It has been demonstrated that the service environment affects the initiation and fracture path of fatigue cracks in adhesive bonded composite joints. By far the most detrimental environment for the joints was hot/humid.

Fatigue lay-up was also shown to affect the fatigue performance of the joints. It may be possible to predict the performance of composites with different lay-ups and loading configurations by establishing a threshold strain energy release rate for the adhesive in fatigue loading. However, more testing is required to establish the applicability of this method.

'Co-bonding' was seen as preferable to 'adhesive bonding' in terms of bond integrity, however the curing method used in this work resulted in a weakening of the strap in the area of greatest stress concentrations. Co-bonding is seen as a cost effective bonding process, reducing fabrication time and therefore costs, compared with the adhesive bonding of cured panels.

6. REFERENCES

1. Johnson, W.S. and Mall, S., 'A fracture mechanics approach for designing adhesively bonded joints', ASTM STP 876, Ed. W.S. Johnson, ASTM, Philadelphia, 1985, pp. 189-199.

2. Kinloch, A.J. and Osiyemi, S.O., 'Predicting the fatigue life of adhesively bonded joints', J. Adhesion, 36, 1993, p. 79.

3. Brussat, T.R., Chiu, S.T. and Mostovoy, S., 'Fracture mechanics for structural adhesive bonds-final report', AFML-TR-77-163, Air Force Materials Laboratory, Ohio, 1977.

4. Johnsson, W.S., 'Stress analysis of the cracked lap shear specimen: an ASTM round robin, JTEVA, 15(6), 1987, p.303.

5. Ashcroft, I.A., Gilmore, R.B. and Shaw, S.J., 'Fatigue of adhesively bonded joints', DRA/SMC/CR961079, Structural Materials Centre, DRA Farnborough, 1996.

6. Kinloch, A.J., 'Adhesion and adhesives: science and technology' Chapman and Hall Ltd., London, 1987.

Attachment of Ceramic Matrix Composites to AFR700B Composites for Exhaust Washed Airframe Structures

Mr. Steven Atmur, Dr. Mary Colby, Mrs. Mary Tomasek,
Mr. Michael Hagen, Mr. David Sherrill
Northrop Grumman Corporation, Military Aircraft Systems Division
Pico Rivera, CA, USA,
Mr. Charles Foreman
Northrop Grumman Corporation, Advanced Technology Development Center
Dallas, TX, USA
AND
Mr. Douglas Dolvin
Wright Patterson AFB, OH, USA

SUMMARY

Current industry practice separates the design of an air vehicle's propulsion system from the design of its airframe. This practice causes many problems and inefficiencies particularily for advanced exhaust nozzle designs. It results in redundant aircraft structure to be insulated and shielded from the engine thermal and acoustic emanations. Perhaps, most importantly, it causes buckling and cracking at the joint interfaces where the thermally induced stresses are reacted. The critical joint interfaces are the co-cured/bonded joints between layers of dissimilar materials and the mechanical joints between structural components. Northrop Grumman's concept is to modernize the design, analysis, and construction of future high performance aircraft by integrating the exhaust nozzle/ exhaust washed structural components into the primary airframe structure through a combination of organic and ceramic matrix composite materials. Designing bolted and bonded joints to carry induced loads efficiently, then, is critical to an integrated structural approach.

Northrop Grumman has evolved a variety of approaches to transfer loads, including co-bonding of dissimilar materials and unique joint designs. Ceramic matrix composite/ AFR700B bolted and bonded joints have been identified as a critical need, and under Air Force-contracted research, joints have been designed and analyzed and will be fabricated. Sub-element testing, including static and fatigue, will validate the design and analytical methodologies. Durability and maintainability will be validated through testing and nondestructive evaluation. Trade-off analysis performed on the bolted and bonded joints will address structural efficiency, reliability, supportability, and battle damage tolerance.

1.0 INTRODUCTION

Over the last 20 years, and particularly since the advent of stealth technologies, propulsion system and aft-fuselage weights have significantly increased as an overall percentage of total aircraft weight. These weight increases were typically offset by increases in overall aircraft performance and vehicle survivability. However, these benefits in performance and survivability came at the price of significantly increased acquisition and operational costs. In order to reverse this trend, future high performance aircraft will have to rely more heavily on airframe integrated exhaust structures in order to reduce the weight and costs associated with the manufacturing and operation of these air vehicles.

The use of high temperature composites, combined with innovative design and manufacturing techniques, will enable airframe contractors to produce affordable, highly survivable, high performance aircraft for future military requirements. The joining technology developed, and in development, by Northrop Grumman provides critical data needed to design and fabricate a layered composite integrated aft fuselage exhaust nozzle structure. Efforts funded by the U.S. Air Force will expand on the basic Northrop Grumman technologies to provide a more detailed understanding through the design, analysis, fabrication, and testing of representative element specimens.

Northrop Grumman's goal is to modernize the design, analysis, and manufacturing methodology required to implement new high temperature tolerant material combinations into the "Extreme Environment Zone". Northrop Grumman has developed a new approach to the problem of integrating advanced exhaust systems/ nozzles into future air vehicle designs. The approach; co-bonding polymer matrix composite (PMC) to ceramic matrix composite (CMC) helps to manage thermal and acoustic loads, minimizing weight, manufacturing cost and maintenance while integrating the exhaust nozzle into the airframe structure.

Northrop Grumman has been performing research in-house and jointly with the U.S. Air Force in a building block approach to establish the basic design data and operational experience required to transition an integrated exhaust system into an air vehicle. Key research efforts (described in more detail later) have included CMC heat shield, AFR700B/CMC co-bonding studies, heat shield pyro-bonding, Mechanically fastened CMC joint allowables program, and CMC nozzle demonstration. As depicted in Figure 1, all of these efforts

Paper presented at the 83rd Meeting of the AGARD SMP on "Bolted/Bonded Joints in Polymeric Composites", held in Florence, Italy, 2-3 September 1996, and published in CP-590.

feed into the Air Force Structural Technology and Analysis Program (STAP), Ceramic Composite Exhaust Washed Structures Delivery Order contract. Under the STAP effort the major focus has been on CMC to AFR700B composite joining for application to an integrated aft fuselage advanced technology demonstration component (ATDC).

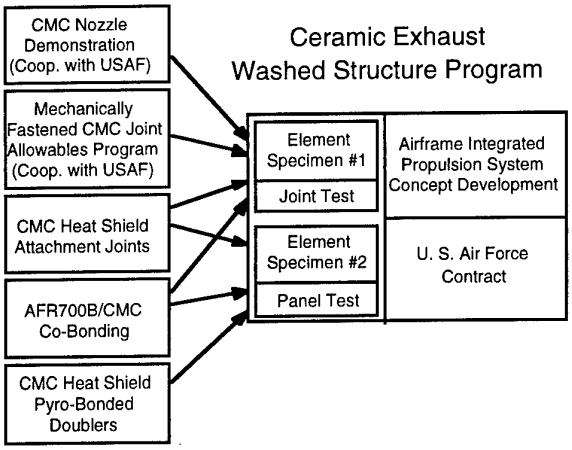


Figure 1. Key Development and Demonstration Activities Provide the Base for the STAP Program

1.1 Design Integration Problems

Advances in propulsion technology have increased air vehicle costs due to the added weight, complexity and maintenance required in the exhaust nozzle systems. This has created the need to integrate the advanced exhaust systems into the airframe in a manner that reduces the adverse effects.

For the integrated exhaust system, the issues of the attachment to the metal airframe, the thermal expansion differences between the polymer composite, ceramic composite and the metal, and the thermo-acoustic durability are critical. The availability of test data on ceramic joints is minimal. The closest comparable systems are polymer composite joints which have not been studied at temperatures and acoustic levels associated with the exhaust environment. The STAP Program being performed consists of analytical modeling of a integrated aft fuselage concept and the selection of representative ceramic attachment joints to investigate fastening and bonding techniques and thermo-acoustic durability. Subsequent mechanical testing is planned to verify the analytical results.

1.2 Description of CMC Joint Applications Experience

Northrop Grumman has extensive design and manufacturing experience in airframe and exhaust integration and in high temperature composites, both organic matrix composite (OMC) and CMC. This experience gained during flight testing of the Northrop Grumman advanced air vehicle systems has been instrumental in formulating the designs developed for the STAP contract. In the development and demonstration of high temperature components the joints and attachment techniques are critical. Northrop Grumman continues to work on nozzle sidewall liners, nozzle flaps, ceramic honeycomb and a variety of truss and sandwich core structures. In order to validate design, analysis and manufacturing methodologies Northrop Grumman is actively pursuing demonstration opportunities such as a CMC heat shield, a CMC engine nozzle, an aft deck thermal protection shield, an engine exhaust component, and hot trailing edge thermal protection systems. In all of the above applications, a common design philosophy is applied: transfer the loads over as wide an area as possible, minimize the thermal expansion mismatch, and when large thermal expansion mismatch is unavoidable, compensate with strain isolation systems.

1.3 Overview of STAP Ceramic Exhaust Washed Structure Program (Air Force Contract)

A combined effort on the STAP program between the Northrop Grumman Military Aircraft Systems Division, the Northrop Grumman Advanced Technology Development Center, and the USAF Wright Laboratories is dedicated to the development of a structurally integrated exhaust system with significant reductions in weight and complexity. The advancements will be accomplished through the use of co-bonding CMCs to organic PMCs in a lightweight airframe integrated exhaust system that will less expensive to build and maintain than current metal exhaust systems.

The goal of the program is to evaluate innovative concepts for exhaust nozzle/ airframe integration and to modernize the design, analysis and manufacturing methods required to implement new material combinations. The project is focusing on attachment / joints as the critical need. As of the writing of this paper the representative joints, both co-cured/co-bonded and mechanically attached, have been identified , designed, and analyzed. Fabrication and test of the test sub-elements is scheduled for 3rd and 4th quarter of 1996.

2.0 NORTHROP GRUMMAN JOINTS TECHNOLOGY BROUGHT TO THE STAP PROGRAM

Over the past three years, CMC development work has been conducted at Northrop Grumman, which provides much of the joining technology required for the USAF STAP Program. This development work was conducted under four different company internal research and development (IR&D) programs. One of the CMC materials used in all of these development efforts consisted of Nicalon™ [1] fiber (with a Northrop Grumman proprietary fiber coating system) in a pyrolyzed Blackglas™ [2] polymer matrix.

---

[1] Nicalon is a registered trademark of the Nippon Carborundum Corporation.

[2] Blackglas is a registered trademark of the Allied Signal Corporation.

CMCs may be joined with metallic or composite structures by bolting, bonding, or a combination thereof. The approach selected depends on a variety of design criteria, including, but not limited to, the stage of the design, the size of the transition region, and the temperature extremes. Discussed below are the different approaches investigated by Northrop Grumman prior to the STAP contract. The CMC heat shield attachments (Figure 2) were designed to facilitate the retrofit of the current metallic heat shield with a lower life-cycle-cost CMC heat shield.

Attachment Design Considering Thermal Expansion Stresses Is a Key to Successful Use of CMC in Aircraft Structure.

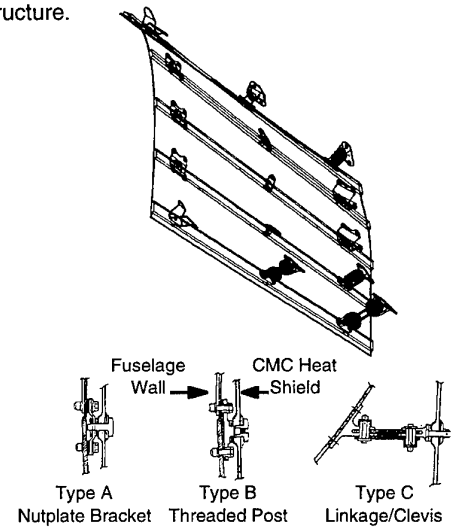


Figure 2. Heat Shield and Attachments

The CMC nozzle demonstration component (Figure 3) provides insight into attachment of CMC to metal engine flanges, gas path seals, and thermo-acoustic fatigue behavior of the CMCs in the exhaust environment. The other prior activities have application to the development of analysis methods, design techniques, and manufacturing methodology required to transition these material systems to production.

2.1 AFR700B to CMC Co-Bonding

After identifying attachment of CMCs to airframe structures as a critical need, Northrop Grumman began evaluating a range of approaches to minimize the stresses induced at joints and interfaces between dissimilar materials. The combination of materials investigated included OMC to CMC, metal to CMC, and CMC to CMC. The attachment techniques investigated for these three couples are discussed in the sections below.

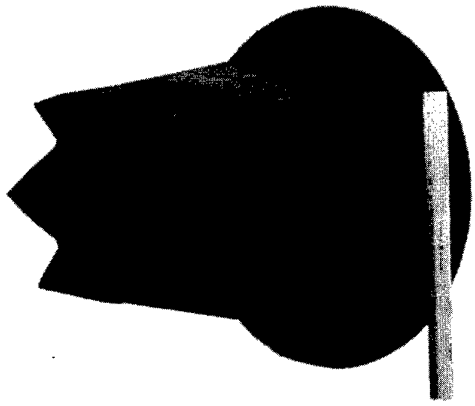


Figure 3. Ceramic matrix composite demonstration exhaust nozzle for an aircraft ground test.

2.1.1 Materials and Processes Description

Numerous OMCs have been bonded directly to CMCs. The process involves forming the CMC structure and then using the CMC as the "fly-away" tool for the OMC portion of the hybrid structure. The bonding mechanism appears to be both mechanical and chemical in nature and, in some cases, is stronger than the interlaminar strength of the CMC. A variety of couples have been evaluated. Table 1 lists the OMCs and the CMCs that have been directly bonded together. Blackglas™ is a siliconoxycarbide matrix made from a polymer precursor supplied by Allied Signal. Applied Poleramic is an aluminosilicate CMC, made from an organic slurry reinforced with ceramic powder supplied by Applied Poleramic.

Table 1. Ceramic and Organic Matrix Composites Evaluated for Co-Bonding

Ceramic Matrix Composites Reinforcements Can Include Woven Cloth or Uni-Tape
Blackglas™ with Nextel™ 312 Reinforcement [3]
Blackglas™ with Nicalon™ Reinforcement
Blackglas™ with Graphite Reinforcement
Blackglas™ with S-Glass Reinforcement
Applied Poleramic with Nextel™ 440 Reinforcement
Organic Matrix Composites Reinforcement Is Woven Cloth
BMI with Fiberglass Reinforcement
BMI with Graphite Reinforcement
AFR700B with Fiberglass Reinforcement
AFR700B wutg Graphite Reinforcement
Epoxy with Fiberglass Reinforcement
PMR15 with Fiberglass Reinforcement

[3] Nextel is a registered trademark of the 3M Corporation.

Because of the design criteria of high temperature (greater than 500C) and high strain (greater than 0.4%) in the presence of vibro-acoustic loads, Blackglas™/Nicalon and AFR700B were selected as the materials of choice to couple together. The selection process was based on the temperature requirements; thus, designs for other less extreme environments may be able to utilize the other systems.

2.1.2 Materials Selected

Blackglas™ Ceramic Matrix Composite

The Blackglas™/Nicalon CMC system was selected for incorporation into the STAP Program because of its high strength and high strain to failure. Additionally, the material is one of the most mature systems available with a design allowables database generated. Table 2 summarizes the design properties of the Blackglas™/Nicalon™ system. The specific interface coating utilized is Northrop Grumman proprietary.

Table 2. Design Data For CMC

Typical Properties of Blackglas™/Nicalon™	
Young's Modulus (GPa)	58.6
Poisson's Ratio	0.01
Shear Modulus (Gpa)	17.9
Density (kN/m3)	21.4
Coefficient of Thermal Expansion (/°C)	$2.7x10^{-6}$
Tensile Strength (Mpa)	68.9
Compressive Strength (Mpa)	213.7
In-Plane Shear (MPa)	17.2

AFR700B Organic Matrix Composite

The OMC selected for co-bonding evaluation to the Blackglas™/Nicalon™ system is AFR700B/graphite. A Northrop Grumman proprietary process is used to fabricate the AFR700B/graphite composites. The same AFR700B processing parameters can be used to fabricate the organic-ceramic couples.

AFR700B-Blackglas™ Couple

Prior to the STAP Program a series of experiments were conducted to generate design data on the CMC to OMC co-bond joint. Nextel™312 reinforced Blackglas™ and AFR700B/S-Glass composites were prepared. The thickness of the AFR700B composites and the Blackglas™ CMC were varied to study organic matrix in-flow into the CMC during fabrication. Couples were machined into double notch shear coupons. The 8-ply Blackglas™ CMC/ 10-ply AFR700B OMC failed in the AFR700B in shear (8.0 MPa). Typically the couples that failed in shear had a higher interlaminar shear strength than the parent CMC.

Additional work continues to add to the understanding of the bonding mechanism between Blackglas™ and AFR700B matrices. In some areas the AFR700B has infiltrated the Blackglas™ microcracks; however, the extent of the infiltration does not appear to be sufficient to explain the shear strengths measured. Microstructural analysis is continuing to study the reactivity of Blackglas™ and AFR700B.

2.2 Mechanically Fastened Joint Allowables for CMC Materials

Northrop Grumman Advanced Technology Development Center is conducting a cooperative program with the United States Air Force to develop a data base of design allowables for mechanically fastened joints in CMC materials(independent of the STAP Program). For this program, which is about fifty percent complete, Northrop Grumman is fabricating the test specimens and the Air Force is conducting the mechanical testing.

Test specimens are cut from 8-ply (~3.0mm thick) Blackglas™/Nicalon™ CMC panels. The lay-up orientation for the Bi-directional Nicalon™ woven fabric is $(0°/90°/45°/0°)_{sym.}$. Sixty coupon specimens were initially tested to establish baseline material properties.

Tension, compression, interlaminar shear, and in-plane shear tests were conducted at room temperature, 815°C, and 982°C. Tensile and compression ultimate strengths obtained are presented in Figure 4.

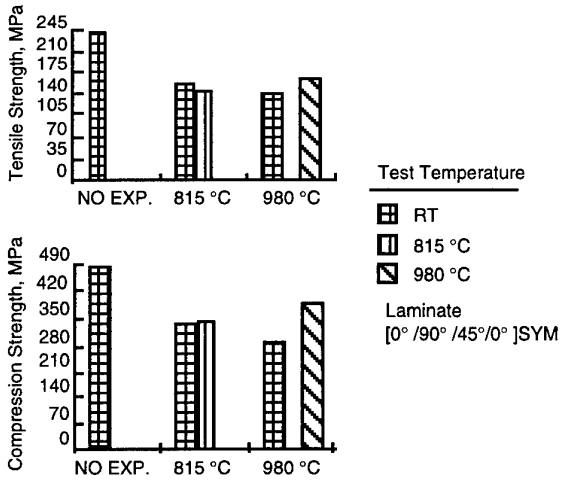


Figure 4. Tensile and Compressive Data from Mechanical Joint Design Allowables Program

Joint allowable bearing property tests being conducted by the Air Force are listed in Table 3. To date, all CMC laminates have been fabricated, one-half of the specimens have been machined, and testing is underway. These initial tests were conducted to determine the "optimum" hole edge distance to be used for CMC joint design. The optimum design would be the edge distance that results the maximum strength to weight efficiency of the joint.

Table 3. Allowables Bearing Strength Testing Matrix.

				No Temp. Exposure		100 Hours at 815 °C Test Temperature			
				Room Temp.		Room Temp.		815 °C	
Fastener Diameter ~ mm				4.7	6.4	4.7	6.4	4.7	6.4
Static Bearing Strength	Double Shear (Pin Bearing)	e/d	2.0	-	-	-	6	-	-
			2.5	-	6	-	6	-	6
			3.0	-	-	-	6	-	-
	Single Shear, Countersunk			6	-	6	-	6	-
Open Hole	Tension			-	-	-	6	-	6
	Compression			-	-	-	6	-	6
Creep	Double Shear (Pin Bearing)			-	-	-	-	-	3 [a]
Thermal Cycling	Single Shear, Countersunk			3 [b]	-	-	-	3 [b]	-
Cyclic Fatigue	Cantilever Reed			-	-	15	-	15	-
	Single Shear, Countersunk			-	-	-	-	15	-
Total Tests				15		51		60	
Grand Total Tests				126					

(a) 100 hours under load.
(b) 1,000 cycles: RT to 815 °C to RT.

Testing to-date indicates that an e/d of 3.5 would be a good design value for double shear specimens. The process of establishing edge distance design values is illustrated in Figure 5. Single and double shear specimens with higher e/d ratios have been fabricated and will be tested. These tests will establish the hole to edge distance design values. Upper limit design stress allowables for CMC laminates with unloaded holes will be established by open hole tension and compression tests. Bearing creep tests will be conducted at 815°C to determine the amount of bearing deformation with time at the initial bearing yield stress. Single shear countersunk bearing specimens will be loaded while subjected to thermal cycling.

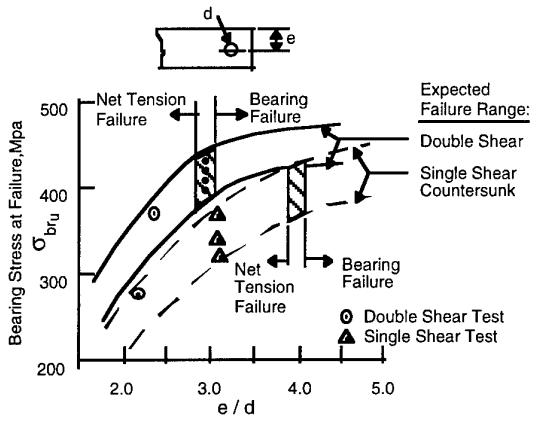


Figure 5. e/d Determination Methodology

Single shear bearing specimens will be fatigue tested at 815°C under a typical flight loading spectrum. Tests will be conducted at several bearing stress levels so that a bearing SN curve can be constructed.

2.3 CMC HEAT SHIELD

Northrop Grumman has developed an aircraft CMC heat shield under a cooperative program with McDonnell Douglas Aerospace. The CMC heat shield design provides a weight savings, and a reduction of ownership costs by eliminating most of the maintanence associated with the metallic heat shield.

2.3.1 CMC Heat Shield Attachment Joints

The production heat shields are constructed using a high temperature stainless steel alloy. Although the current shields perform adequately they have exhibited cracking problems at low flight hours, resulting in frequent maintenance and repair.

Two CMC heat shields have been fabricated and instrumented for testing. Ground and flight tests will be conducted during August and September of 1996.

2.3.1.1 Joint Design

The heat shield is approximately 58 cm wide and 79 cm long with five horizontal hat section stiffeners. The hest shield is attached to the fuselage by 15 brackets arranged in five rows (corresponding to the five stiffeners). Figure 2 illustrates the

heat shield attachment scheme as well as the three distinct attachment bracket types.

The CMC heat shield is of solid laminate construction (including the hat stiffeners) and was designed to the production heat shield envelope and environment. Existing fuselage attachment brackets were used. In-plane thermal growth is accommodated by using oversized and slotted holes in the heat shield. All out-of-plane motion is restrained by incorporating Inconel Belleville spring disc washers at each panel attachment bolt. These spring washers provide positive clamping pressure, but still allow the panel to slide in-plane.

2.3.1.2 Sub-element Attachment Testing

Three attachment designs were tested to determine if they could survive the simulated cyclic temperature and vibration environment associated with an advanced aircraft. The test success criteria was for the ceramic coupon to exhibit minimal wear at the end of the test cycle and for the attachment design to maintain clamp-up pressure throughout the test.

Figure 6 describes the setup that was used to test the attachment designs. The ceramic heat shield is represented by a CMC test coupon. The basic setup has a CMC test specimen attached on either side to in-plane sliding mechanism arms. The center of the CMC specimen is attached to an 0.127 cm bracket that corresponds in thickness to the actual fuselage attachment design.

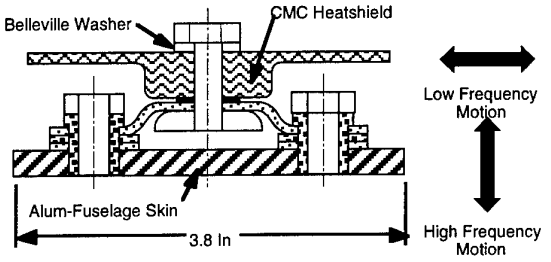


Figure 6. Attachment Design Test Setup

The design called for Belleville disc spring washers to provide a secure attachment for the entire temperature range. Several sizes of Belleville washers were tested at room temperature and at 649°C for load capacity, hysteresis effects, and displacement to yield point. These tests demonstrated that the Belleville washers maintained clamp-up pressure while accommodating thermal growth at the elevated temperatures.

Two representative attachment joints were tested at 649°C with broadband transverse vibration and low cycle in-plane translation. Test duration was 30 hours for each joint specimen. The CMC coupons were examined after the tests to determine the wear around the attachment bolt hole. Sliding friction forces were recorded continuously to track the performance of the Belleville washers.

2.3.1.3 Test Results

The wear on the CMC coupon was minimal. Figure 7 shows the test specimen parts at the conclusion of the tests. The tests demonstrated that the joint materials and attachment design should survive the planned ground and flight tests with minimal wear and with retention of joint clamp-up.

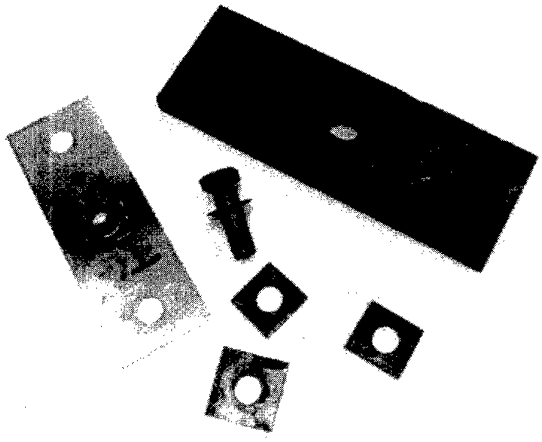


Figure 7. No Wear Visible on Joint Test Coupons

2.3.2 CMC Heat Shield Pyro-Bonded Doublers

Detailed structural analysis of the CMC heat shield indicated that reinforcement of five of the fifteen attachment holes was required. Because the heat shield outer mold line/ inner mold line (OML/IML) tooling was already fabricated, it was necessary to reinforce the holes with doublers bonded to the exposed (exhaust washed) surface. Doublers were machined from a CMC laminated of the same material and thickness as the heat shield web.

Doublers were bonded to the two heat shields using Blackglas™ polymer resin and other proprietary materials. The doublers were held in position during curing by tooling pins in the fastener holes. The doublers were cured to the heat shield using the standard Blackglas™ autoclave cure cycle. After curing, the doublers and bond joints were impregnated with Blackglas resin and the heat assembly was pyrolyzed in a furnace. This process was repeated once more for a total of two processing cycles.

Bond joint specimen tests were conducted to determine the shear strength of the CMC-to-CMC pyro-bonding. Two small CMC panels were pyro-bonded together and four notched compression specimens, shown in Figure 8, were cut from these bonded panels. This specimen design is similar to, but slightly larger than, a standard notched interlaminar shear specimen. The bond surface in this specimen is 1.80cm x 1.27cm, with an area of 2.29cm^2. The specimens were loaded in compression using a standard ASTM D695 fixture.

The average failing stress for the four specimens was 11.7 MPa (1700psi). This bond shear strength is about fifty percent

of the interlaminar shear strength of the CMC material, but it provides sufficient strength for the heat shield doubler bondline shear loads. It is felt that the shear strength of pyro-bonded CMC joints could be increased significantly with further development of bonding materials and processes.

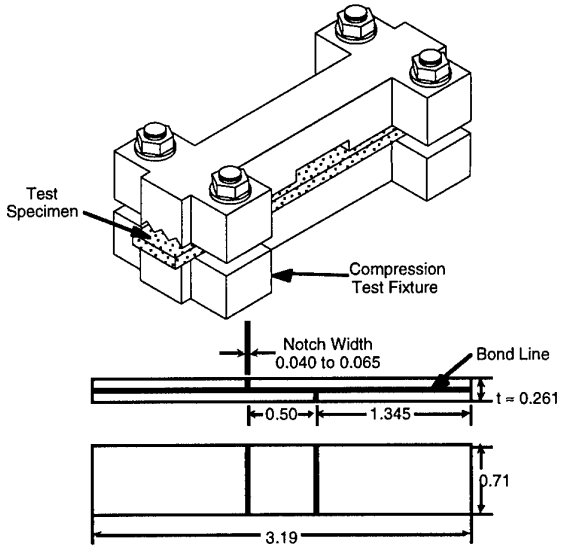


Figure 8. Notched Compression Shear Test Coupon

3.0 STAP CMC AIRFRAME INTEGRATED EXHAUST NOZZLE STRUCTURE DEVELOPMENT

Northrop Grumman Corporation's past experience has been applied to the STAP program; Figure 1 depicts a sample of the broad range of efforts Northrop Grumman has focused on for exhaust washed ceramic applications.

3.1 Applications in the Structure

Air vehicle structural complexity and cost are increasing due to advances in propulsion technology and the increased thermo-mechanical stresses those advances impose. A prime area of concern and the focus of the STAP program is the aft fuselage. The aft fuselage contains the engine nozzle section which can include an afterburner and a variable area exhaust nozzle with movable components. The aft fuselage also incorporates the aft aero-control surfaces and other subsystems, including but not limited to, tail-hooks, auxiliary power units, and antennae.

Achieving the STAP Program goals of modernizing design, analysis and manufacturing methodology, requires the implementation of new high temperature material couples into this extreme temperature zone. Current design practices separate the propulsion system from the airframe. The nozzle attaches to the engine's aft face and the engine and nozzle assembly is insulated from the adjacent structure. Fire shields, ducted air, and parasitic insulation materials are required to control heat transfer into the airframe.

The STAP program will demonstrate key PMC to CMC bonding technology that can be incorporated into an integrated nozzle and airframe design capable of sustaining high thermo-acoustic and mechanical loads. The attachment techniques to be evaluated include PMC to CMC co-bonding, co-curing and bolting.

Figure 9 compares schematically a conventionally mounted exhaust system versus a fully airframe integrated exhaust system. The fully integrated exhaust system requires the unique design features being validated on the STAP program. The STAP program leverages the technologies discussed above along with configuration and system trade study results.

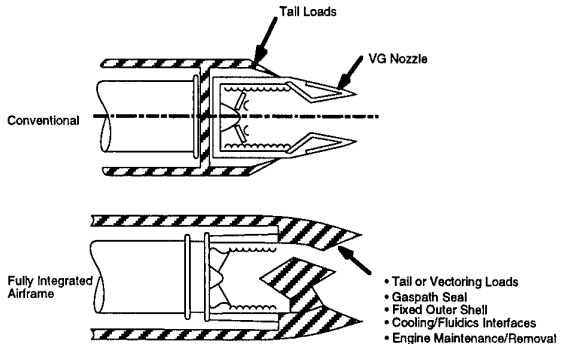


Figure 9. Comparison of a conventionally mounted nozzle to an integrated nozzle/airframe design.

3.2 Design Trades

Design trades have focused on the STAP program specific requirements of integrating a heat and load tolerant airframe/exhaust system. The design trades have examined key structural attachment methods and nozzle structural details with the goal of minimizing weight, system complexity and fabrication cost, while enhancing durability of the finished exhaust assembly. The trades have included AFR700B data and Blackglas™ CMC data from Northrop Grumman supported research.

The STAP Advanced Technology Demonstration Component (ATDC), shown in Figure 10, is a fixed aperture composite exhaust system. The ATDC was analyzed to provide load and environmental definitions to determine realistic test conditions for sub-element testing of joining and attachment concepts.

Engine thermodynamic cycle models were used to determine exhaust flow path conditions (static and dynamic pressures, temperatures, and velocities) inside the nozzle. Critical aerodynamic and thermal loading conditions were derived using representative flight conditions. Structural analysis using finite element models of the internal loading was performed to size the structure. The design integration team composed of materials, processing, observable, and propulsion engineers worked with structural designers to prepare the ATDC design .

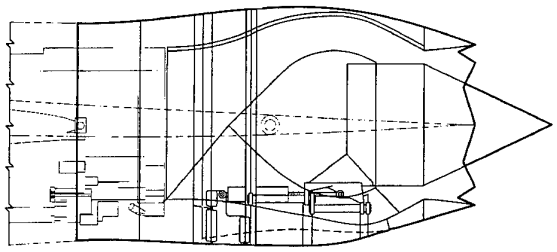


Figure 10. Schematic design of the STAP ATDC

3.3 Verification in Sub-element Specimen Tests

Sub-element specimen tests will be performed to verify the structural integrity, validity of analytical methods, and life of the critical joining technologies. Figure 11 shows the ATDC finite element model (FEM) with a highlighted section representing the location of the detailed FEM analysis.

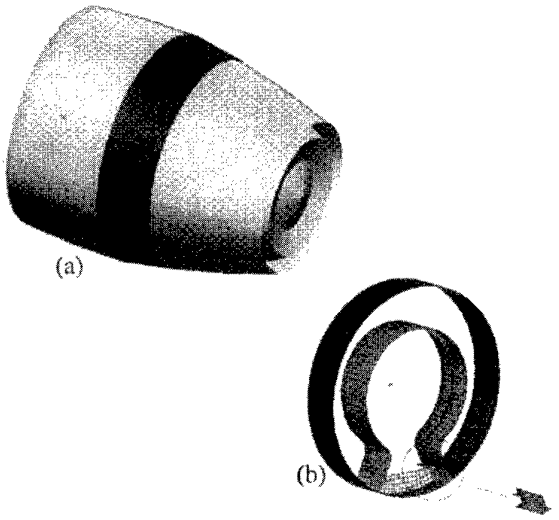


Figure 11. a) STAP ATDC Airframe Integrated Ceramic Composite Nozzle, b) Detailed Model with Cruciform Joint.

Two types of joints have been identified and are both represented in the detailed FEM analysis. The first sub-element is representative of the layered sidewall construction where the critical joining technology is the co-curing/co-bonding of the dissimilar materials into a heat tolerant sandwich structure. The second sub-element is representative of the "cruciform" joint of the ATDC The cruciform joint attaches the layered sidewall outer surface to internal composite structure supporting the nozzle lower access door as shown in Figure 11(b).

The ATDC test section has been analyzed using MSC/NASTRAN finite element analysis tools to predict specifically the performance of the cruciform CMC joint and, more generally, the bonded PMC to CMC structure under the nozzle's predicted mechanical loads and the combined thermal/vibro-acoustic environment. To test the layered construction of the first sub-element a panel approximately 30 cm by 30 cm will be fabricated and tested in the Wright Laboratory Acoustic facility. To test the cruciform joint double lap shear tests will be performed on a representative joint as shown in Figure 12. PMC to CMC bolted attachments, bonded attachments and co-cured attachments will be evaluated.

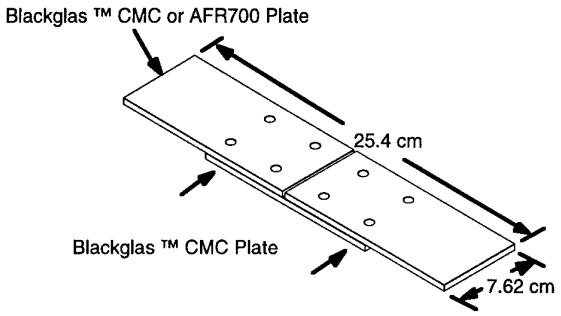


Figure 12. Representative Blackglas™ joint (double-lap shear test specimen).

These representative cruciform joint test specimens will be evaluated by simulating the dynamic environment on a vibration shaker table at elevated temperature. Analytical predictions will be compared to test data to asses the ability to analyze CMC structures and predict failure using conventional analysis tools.

4.0 CONCLUSIONS

Preliminary design data, like edge distance criteria and mechanical properties of CMC, have been generated to a sufficient level that detailed structural designs can be developed and analyzed using traditional composite analysis techniques. CMC hardware demonstrations have increased design confidence as well as maturing the CMC manufacturing processes. However, as background design data and design confidence has increased the complexity of the proposed concepts has also grown. It has become clear that the understanding of joining and attachment mechanisms has not kept pace and is a critical limiting factor in the introduction of large scale CMC structure into production aircraft.

The STAP program has developed a detailed structural concept for an airframe integrated exhaust system, suitable for high performance aircraft, by leveraging both government and contractor experience. Primary effort under the STAP Program was to develop an innovative composite structure that offered revolutionary benefits to future aircraft while performing detailed engineering design and analysis to assure the viability of the end product. The current STAP Program has completed the design and analysis phases. The joining and attachment methodology was identified as the critical

need. Sub-elements have been design and are in fabrication. Testing of the sub-elements will allow the contractor validate the analytical techniques used in the development of the ATDC as well as provide specific data about the performance of CMC to AFR700B joints.

Current efforts have been focused on understanding the behavior of the Ceramic composite materials in the exhaust environment along with the behavior of joints between dissimilar materials. Design and analysis methodologies will be verified through testing of selected representative sub-element specimens.

Future efforts will be aimed at the ground testing of full scale integrated aft fuselage sections that are representative of a next generation fighter aircraft. The test fixtures would be designed to enable the investigation of the structural interactions of the multi-layered construction particularly related to the dissimilar material interactions. Attachment of the materials whether bolted, bonded, or co-cured will be the critical areas of interest.

5.0 ACKNOWLEDGMENTS

The authors gratefully acknowledge the financial support of U.S. Air Force and the Northrop Grumman Corporation in the preparation and presentation of this research and paper. The authors gratefully acknowledge the technical guidance given by Chris Clay of the U.S. Air Force. Additionally the authors gratefully acknowledge the support received from other Northrop Grumman staff including Kendall Young, John Ramon, Steve Pauletti, Don Box, Stephen Grossman, and William Haub.

3-D Composites in Primary Aircraft Structure Joints

Larry Bersuch
Keith Hunten
Lockheed Martin Tactical Aircraft Systems
Fort Worth, Texas

Bill Baron
James Tuss
Wright Laboratory, Dayton, Ohio

Abstract

Three-dimensional woven and braided inserts and preforms, when cocured into primary wing and fuselage laminate structure, offer reduced weight, increased performance, lower costs, and improved damage tolerance and ballistic survivability for future aircraft. To achieve these benefits, three-dimensional (3-D) weaving and braiding technologies must be characterized through the development of design criteria, design methods, structural concepts, and manufacturing processes. In addition to 3-D weaving and braiding, z-direction reinforcement can be achieved through in-process fiber insertion with processes such as z-spiking, stitching, and short fiber additions to adhesives. Innovative applications of these technologies, combined with net shape curing processes such as resin transfer molding (RTM), electron beam cure, diaphragm forming, fiber placement, and cocuring, will result in the elimination of machined metal load fittings, fasteners, and reduction in weight at composite joints on future aircraft. Wing applications for 3-D composites would be at the intersection of spars and ribs and in the radius area between spars/ribs and the lower skin of a cocured wing assembly. In fuselage structure, 3-D composites eliminate the need for machined fittings and fasteners at concentrated load joints such as those at inlet duct, weapons bay, gun-trough, and fuel floor intersections with bulkheads/frames. This paper is directed at design for manufacturing of 3-D composite structures to best exploit the structural properties that they exhibit.

KEYWORDS: Composite materials, 3-D preforms, Z-fiber reinforcement, graphite/epoxy, failure criteria and design criteria for 3-D composite materials.

Introduction

The use of 3-D composite structural concepts will enable effective management of out-of-plane loads. This key feature opens the door to novel composite airframe designs with both breakthrough performance improvement and cost reduction. Composite integration in state-of-the-art fighter air vehicles has been typically limited to under twenty-five percent by vehicle weight. The primary barriers to increased composite utilization are high fabrication and assembly cost, overly conservative design criteria, lack of high fidelity design tools, poor ballistic survivability, and poor interlaminar/out-of-plane mechanical properties. The use of 3-D composite structural concepts will eliminate these barriers.

A variety of structural concepts based on complex, yet low cost, woven and braided fiber textile reinforcements are currently under development. Figure 1 shows a collage of these technologies. Intersecting structure with continuous fiber reinforcement through the intersection and woven three-dimensional fiber preforms for highly loaded composite wing carry-through bulkheads are being investigated. Ultra-high strength pultruded carbon fiber rods featuring extremely straight fiber alignment are being incorporated in advanced designs to enable highly controlled and tailored load path management and important survivability improvements. The development of Z-direction or through the thickness (Z-fiber) reinforcement to greatly increase the interlaminar strength and toughness of laminated composite structures is enabling the local tailoring of out-of-plane strength. Emphasis is being placed on coupling complex textile based fiber architecture with low temperature RTM, resin film infusion, and electron beam curing materials. Since electron beam curing is

Paper presented at the 83rd Meeting of the AGARD SMP on "Bolted/Bonded Joints in Polymeric Composites", held in Florence, Italy, 2-3 September 1996, and published in CP-590.

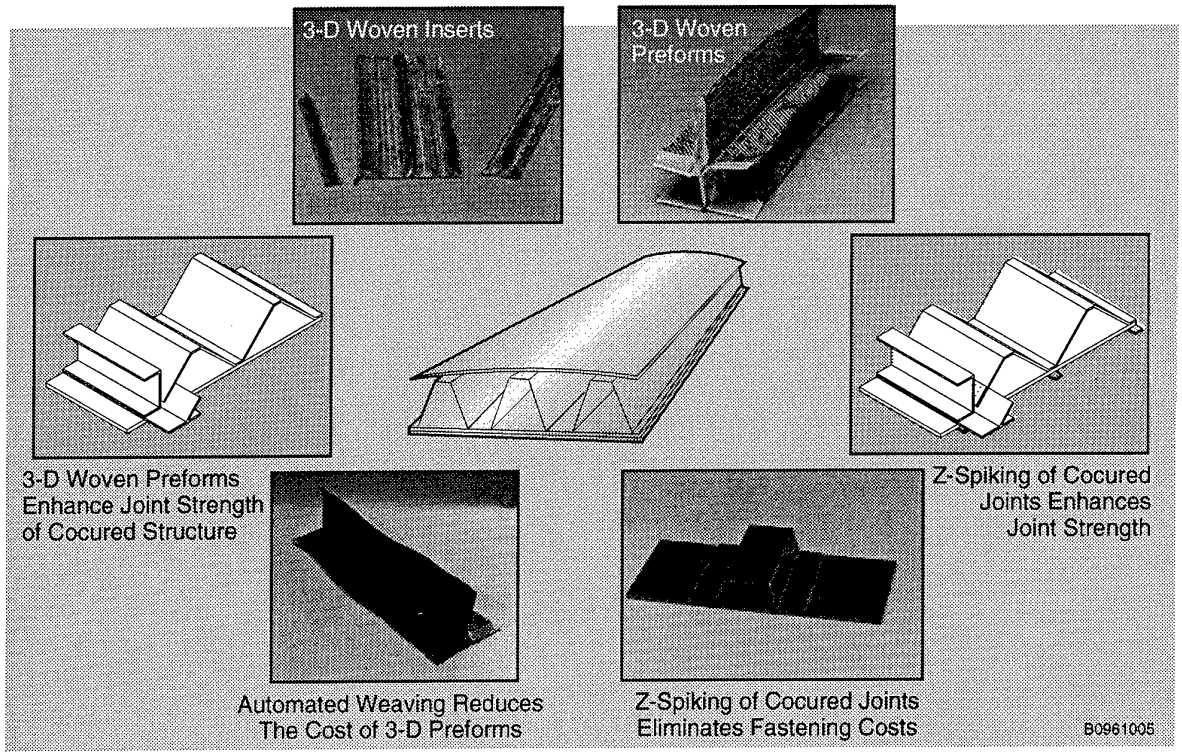


Figure 1 3-D Woven Preforms, Z-Spiking, and Low Energy Processing Will Enhance Joint Strength and Reduce Costs

essentially a low temperature process, extremely low cost tooling materials can be used. This enables designers to consider innovative structural arrangements that are highly efficient but previously were prohibitive in cost because of the complex tooling needed for autoclave cure.

3-D Woven and Braided Composite Technologies

Woven preforms can be produced by a number of techniques, including the following:

- **Orthogonal pattern**. Z-fibers are pulled through the warp (0 degree direction) and fill (90 degree direction) fiber, intersecting the layers at a 90 degree angle.

- Through-the-thickness angular interlock. Z-fibers are woven through the layers of the fabric, intersecting the layers at an angle. These Z-fibers may be the same type and filament count as the warp and fill fibers. In some cases a finer fiber is preferred for through-thickness reinforcement because it allows tight packing of the warp and fill fibers.

- Layer to layer interlock. Warp fibers are woven into adjacent layers within the weave at designated intervals. This process improves interlaminar shear strength but does not provide true through-thickness reinforcement.

Braiding technology for 3-D preforms interlocks fibers in a cylindrical grid arrangement by shifting columns of fiber carriers in opposite directions, then oscillating rings in opposite directions. A wider array of fiber orientation and distribution is achievable with braiding compared to weaving.

To make 3-D woven and braided preforms more affordable will require standardization of shapes (T, cruciform, special shapes) in stepped sizes for various loads. These could be standardized in a manner similar to aluminum extrusions. To reduce storage costs, preforms should be impregnated with resin just prior to cocure into laminated composite structure. Reducing the cost of 3-D preform weaving will require automation of the more complex shape preforms and the addition of bias (+/- 45 degree plies) for efficient shear of loads into web structure.

Z-Fiber Reinforcement. The "Z-fiber reinforcement" (also called Z-spiking) process incorporates through-thickness reinforcement into preimpregnated or staged composite details. The Z-fiber reinforcement process is illustrated in Figure 2. A foam block containing Z-fibers is

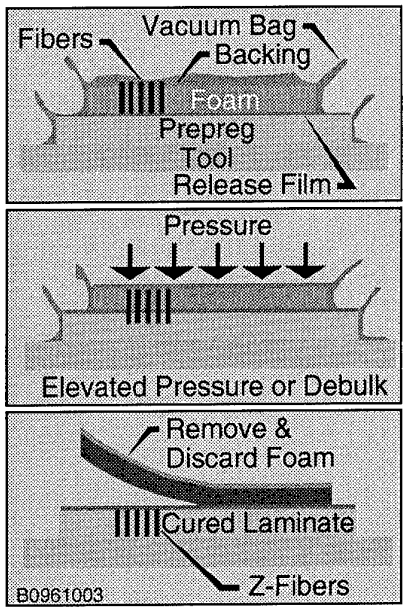


Figure 2 The "Z-Fiber Reinforcement" Concept

placed on the component prior to curing at the specific locations where damage tolerance and/or through-thickness reinforcement is desired. The Z fibers are small, pultruded rods made from whatever reinforcement and matrix is desired for the application. During cure or debulk, the foam compacts and the Z-fibers are forced through the component.

Z-fiber reinforcement can be used in damage-prone areas such as blade- and hat-stiffened laminates, in sandwich joints where 3-D woven preforms and 2-D materials intersect, and as edge reinforcements to prevent delamination. Z-fiber reinforcement provides a number of advantages in composite structures. Empirical testing has shown only minimal decreases in in-plane properties compared to 2-D components with no through-thickness reinforcement. Knockdowns in tensile and compressive strengths are less than five percent. Z-fiber reinforcement provides a 30-50 fold improvement in interlaminar fracture toughness. This translates into a significant improvement in damage tolerance and ballistic survivability when applied in cocured composite structure. Z-fiber reinforcement is especially important for hat- and blade- stiffened structure where the Z-fibers improve initial and ultimate pull-off failure loads. In addition, the Z-fibers eliminate the need for radius blocks and fasteners at the stiffener ends. These improvements will prevent catastrophic failure from propagation of a manufacturing flaw or in-service damage.

Current composite structure designs require labor intensive fabrication and assembly which account for 60% to 90% of the total cost. The use of 3-D structures will allow unitization, i.e., reduced fastener and part count. In addition, the long term support costs will be reduced since the majority of repair actions in fielded fighter air vehicles are conducted on mechanically fastened joints which will be reduced through the use of unitized structure.

Design and Manufacture 3-D Composite Application for Bulkheads and Frames

Composite utilization in the heaviest parts of the airframe such as highly loaded fuselage bulkheads and moderately loaded frames has been virtually non-existent because of the poor interlaminar properties of conventional laminated or two-dimensional reinforced composites. Because of these low interlaminar properties, composites have not been used in structures subjected to high out-of-plane or complex loads without costly integration of metallic fittings and fasteners. This also often results in an increase in the amount of composite material required to accommodate the low bearing strength of typical polymer matrix composite structures. Figure 3 shows a moderately loaded composite bulkhead fabricated from conventional laminated materials. The bulkhead consists of a composite web with blade-stiffeners cocured to the web. Machined metal fittings are mechanically attached with fasteners to carry the concentrated out-of-plane loads resulting from engine hammershock and gun recoil conditions.

The development of composite structures that can react out-of-plane loads will greatly reduce the reliance on bolted joints and will offer improved structural efficiency. One of the primary keys to lowering the cost of composite structures is to minimize touch labor, part count, and fastener count through unitized structural assemblies. Figure 4 shows a moderately loaded bulkhead that reacts engine hammershock and longitudinal body bending pass- through loads with 3-D preforms. In this bulkhead the preforms are staged and cocured with conventional laminated composite details during final cure. The staged details are net shape prior to the final cocure assembly. The 3-D fibers in the out-of-plane direction are capable of carrying the high engine hammershock and fuselage bending pass-through loads without the costly machined

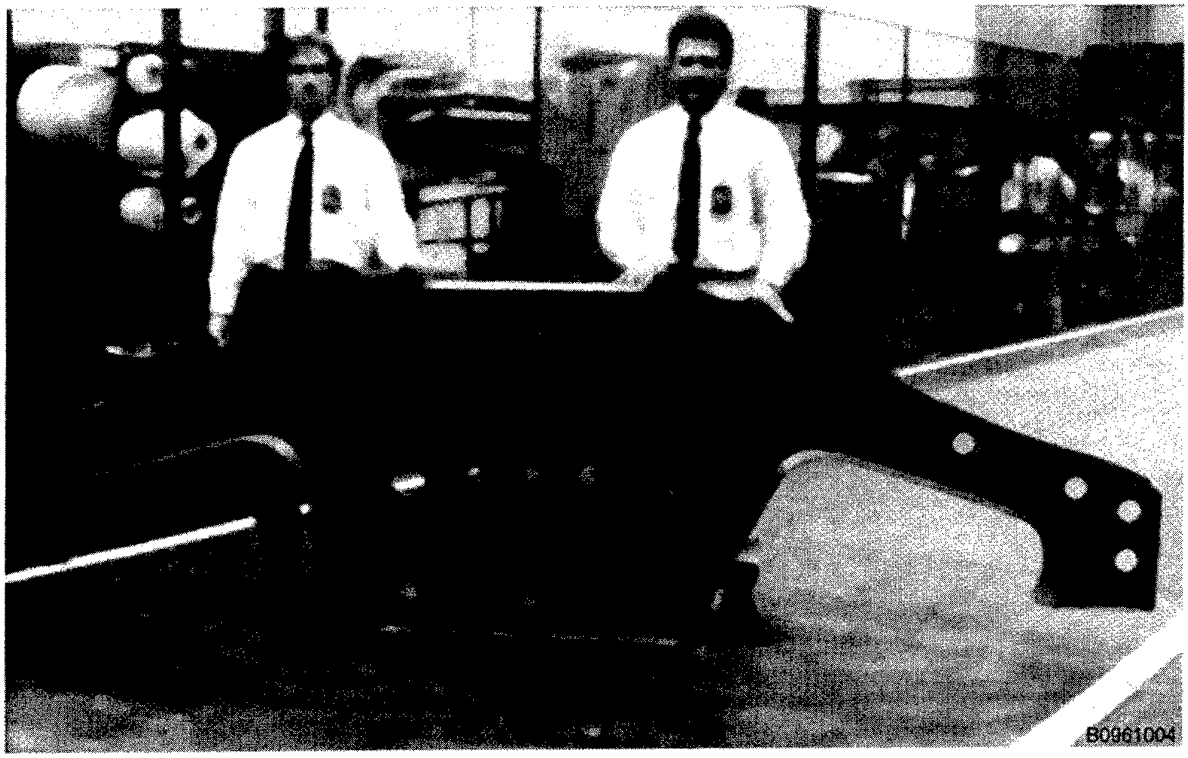


Figure 3 Moderate Loaded Composite Bulkhead

fittings and fasteners. The insert data show that the 3-D inserts carry approximately twice the load of the baseline uni-tape insert. The cruciform data demonstrate that the bonded joint with embedded cruciform carries three times the load of the baseline bonded joint.

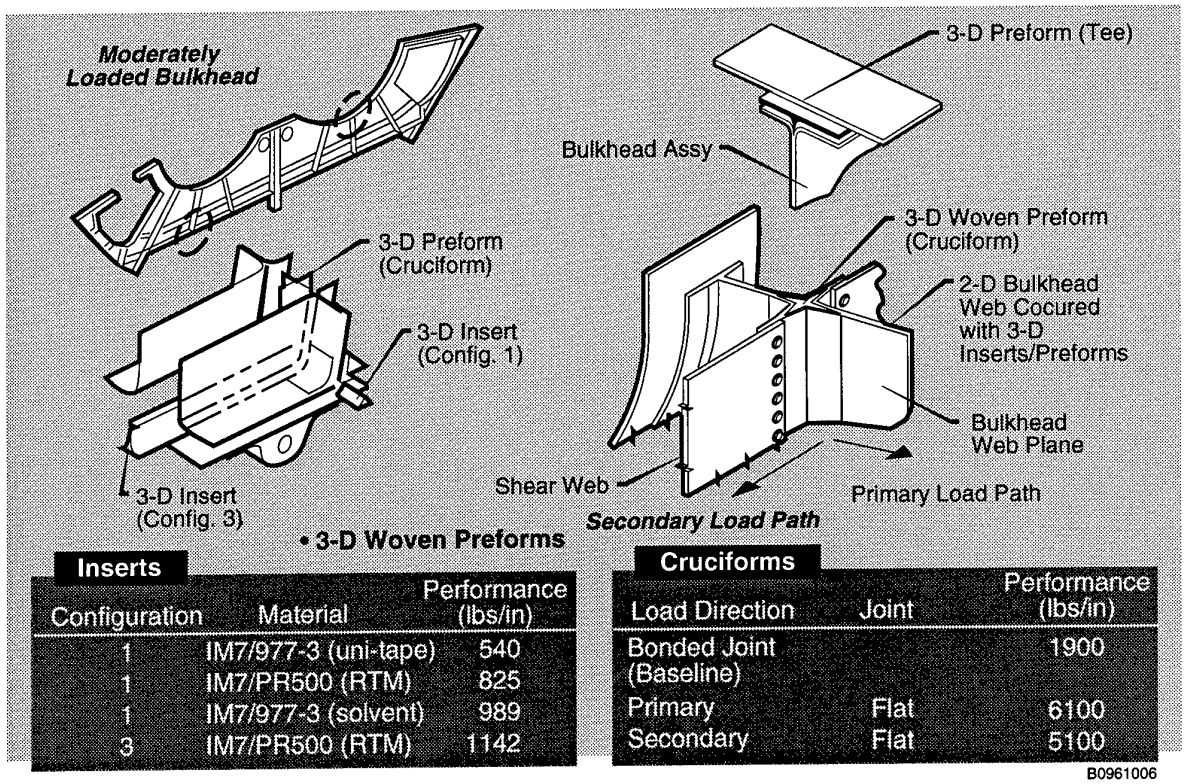


Figure 4 Generic F-22 Laminated Composite Bulkhead with Embedded 3-D Preforms

3-D Composite Application for Sandwich Structure

Sandwich structure is the most weight efficient design for a large percentage of an aircraft structure because of buckling stability requirements. Unfortunately, use of sandwich structure is limited on state-of-the-art aircraft due to the high manufacturing and supportability costs associated with metallic honeycomb structure on earlier aircraft. Figure 5 shows the B-58, which use a high percentage of aluminum sandwich construction. The illustration shows a typical wing joint in which the sandwich was full depth through the joint with a metallic insert (internal slug) for joining the skin to the spars. The spars were spaced fifteen inches apart to reduce the parts count. The mission requirements of the B-58 dictated low structural weight fraction (0.24) and good thermal and sonic fatigue properties; this drove the design to sandwich construction.

These structures, however, experienced high maintenance costs due to moisture retention, severe corrosion, and damage tolerance problems. The emergence of composite materials, novel core concepts, tougher adhesives, textile preforms and z-fiber reinforcement have now created a new opportunity to take advantage of the superior structural efficiency of sandwich construction without the penalty of maintainability problems. These emerging technologies apply non-corrosive honeycombs, utilize foam filling to reduce moisture retention and improve damage tolerance, and employ design concepts that eliminate leak paths.

Current high-payoff applications feature the use of sandwich in highly loaded mid-fuselage and aft-fuselage structure. The unitized center fuselage shown in Figure 6 makes extensive use of advanced composite sandwich structure and 3-D composite preforms and z-spiking in the joint intersections. Extensive integration of the wing and fuselage will significantly reduce weight, fabrication costs, and maintenance costs. Parts count is reduced by cocuring the lower wing skin with ribs and subspars, and building the upper skin in one piece, tip-to-tip. Longeron, spar, and bulkhead caps are embedded in the skins using either unidirectional tape or Neptco rods to provide unbroken primary load paths. Reducing parts count will lead to a more cost effective airframe and the unitized, efficient structural approach will reduce airframe weight fraction.

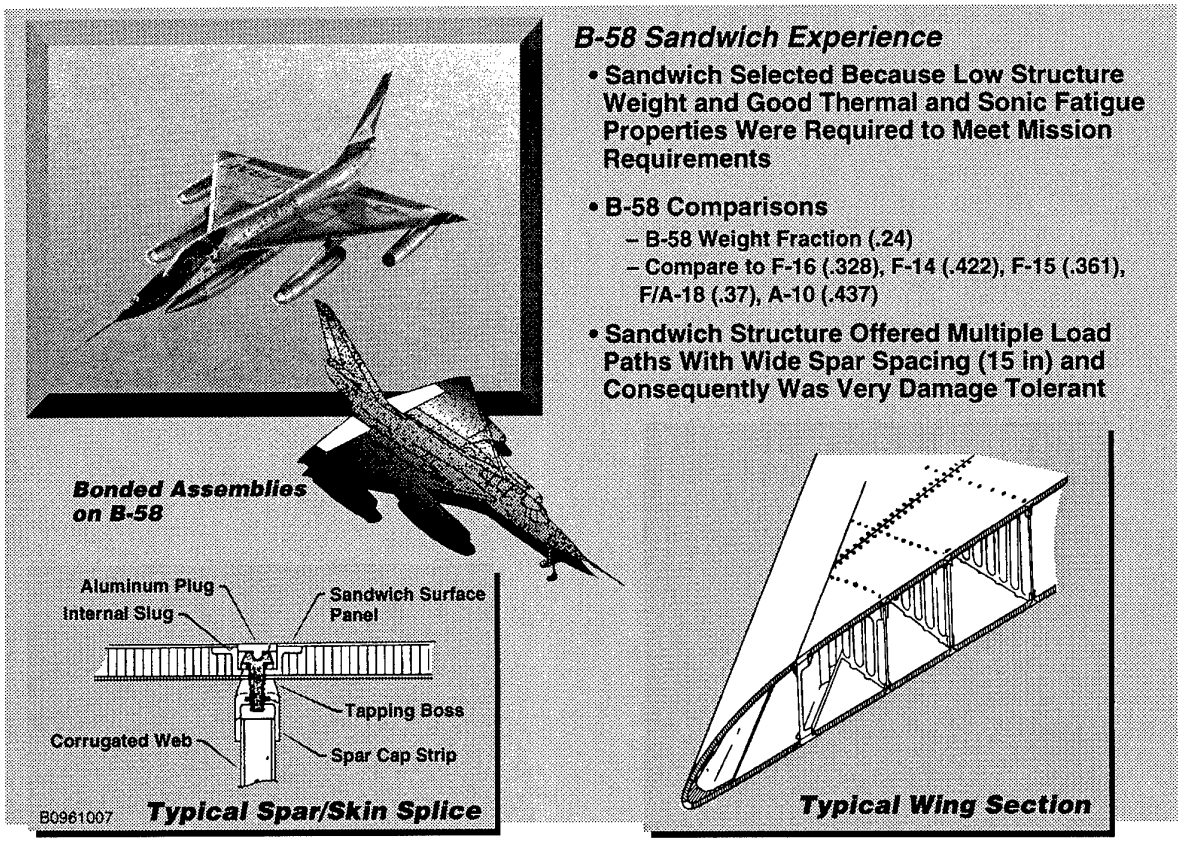


Figure 5 B-58 The Bonded Bomber

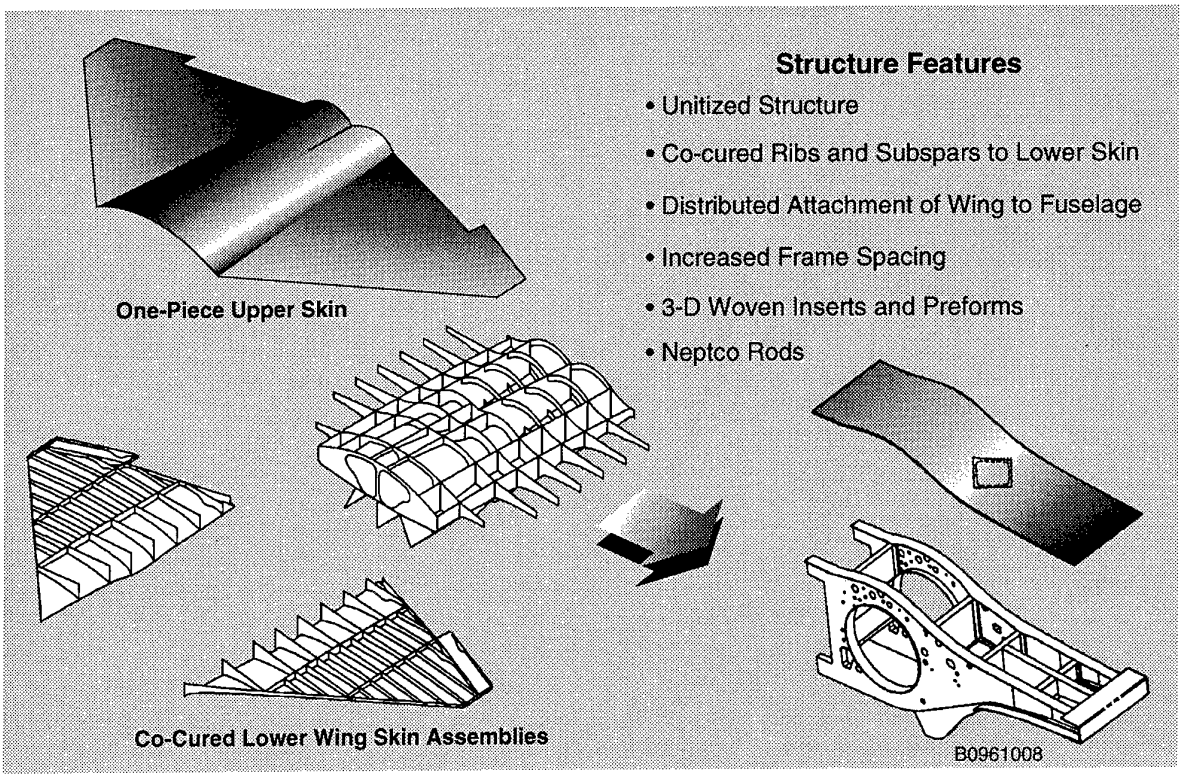


Figure 6 Unitized Center Fuselage Application of Advanced Sandwich Structure for a 21st Century Fighter

Neptco rods offer attractive features for sandwich construction – options that have just recently become available. Embedding these rods in sandwich structure improves compressive strength with respect to an equivalent design made with unidirectional tape. Compressive strength is improved since the fibers in the rods are much straighter than in the tape. Maintenance will be reduced for two reasons: (1) there are substantially fewer joints to fatigue and (2) most of the fasteners in the lower skins have been eliminated so fuel leak paths are greatly reduced. Figure 7 shows how Neptco rods could stiffen a sandwich skin for reinforcement over a bulkhead. In this case the bulkhead is of sandwich construction.

Highly supportable composite sandwich concepts are under development featuring non-corrosive moisture resistant foam cores reinforced with integrally woven facesheets and core webs and pultruded carbon fiber pins embedded in the sandwich facesheets. Figure 8 shows two such sandwich concepts. In the first concept, pultruded fiber rods penetrate through foam core into the laminate facesheets. Both foam filled and hollow core (foam is removed) concepts are possible. In the second concept, 3-D woven preforms are impregnated and cured into truss core. Conventional laminate facesheets are cocured to the 3-D woven truss core. Again both foam filled and hollow core are possible. These concepts mechanically tie the cores to the facesheets, compared to traditional joining by weaker adhesive bonds.

"Z-spiked" Cocured Wingbox Application

Testing has been conducted at Wright Laboratory to determine the response of cocured wingbox composite designs with z-spiked joints to high explosive incendiary ballistic threats.

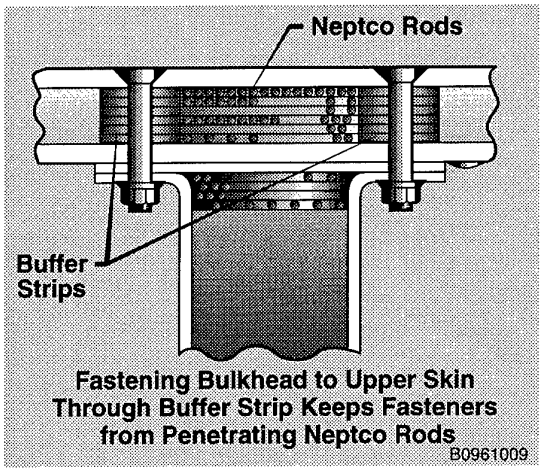
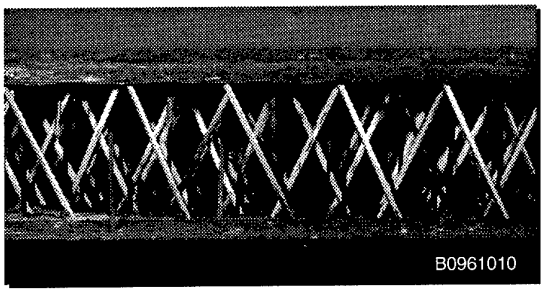
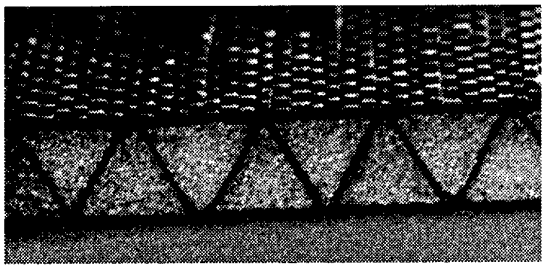


Figure 7 Neptco Rods Embedded in Skin Structure Offer Efficient Load Paths



Z-Spiked Core



3-D Woven Core

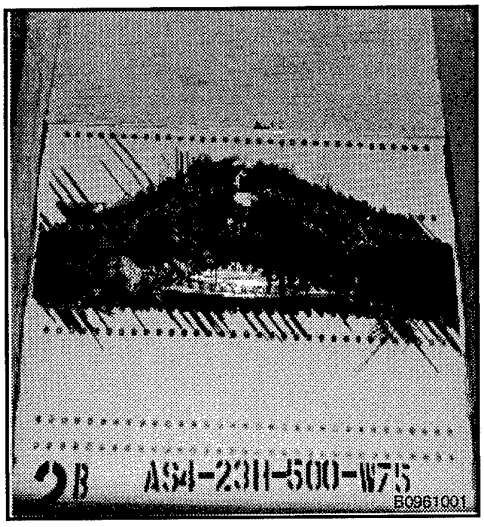
Figure 8 3-D Reinforced Sandwich Concepts

This testing evaluated the merits of a cocured lower skin to I-section spars concept with Z-spiking in the joint interface against a conventional composite skin with aluminum substructure design. The ballistic tests were conducted under fully simulated combat conditions which included airflow, ballistic impact, structural load, hydraulic ram and blast from a high explosive incendiary projectile.

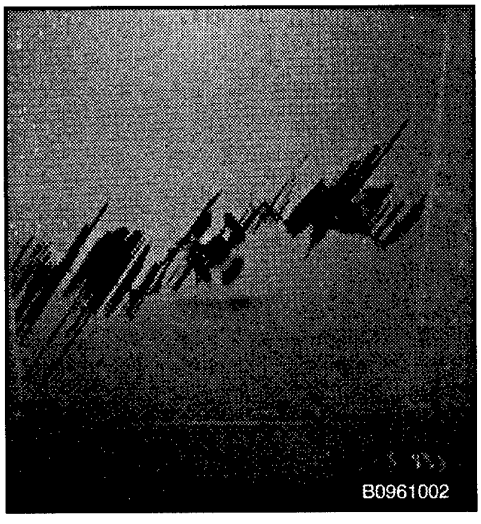
The composite cocured design allowed the joint to rotate as the explosive pressures impinged on the skin/spar substructure and placed the entire fuel cell in tension. The cocured design enabled the joint to act as a fully integrated assembly. This was unlike the skin of the mechanically fastened baseline design that rotated independently from the substructure. By designing the cocured wingbox with laminate plies blended from the skin into the substructure the z-spiked spars were able to rotate and the skin did not fail at the fastened joints as in the baseline tests. The skin was loaded as a tension membrane that initiated a spanwise crack across the impacted bas of the test section. Figure 9 shows the results of the ballistic test for the baseline fastened wingbox and for the cocured Z-spiked wingbox.

Analysis and Certification

The certification issues and design methodologies for 3-D composites center around the measurable quality of the as-manufactured structure, and the resulting allowables. The quality of a part is typically measured by non-destructive inspection (NDI) techniques such as ultrasonic and x-ray. The NDI of 3-D composite joints will be less critical because of the increased strength and enhanced damage tolerance. The ability to resolve flaws in complex 3-D joints (such as those using inserts, preforms, Z-fibers, and cocured assemblies) will to a large extent drive the manner in which allowables will be calculated for a particular joint technology. Analysis tool and methodology development, physical tests, and design and certification advisors will all reflect the flaw



Mechanically Fastened



Cocured Z-spiked Design

Figure 9 Baseline and Z-Spiked Wing Box Test Results

resolution limitations imposed by quality inspection capabilities. Though advanced inspection techniques such laser ultrasonics can be readily applied to inspect 3-D composites with a high degree of accuracy, structural load, stress, and strain allowables development needs to reflect manufacturing variability so that flaws produced by typical manufacturing capability are accounted for in the allowables determination. Allowables development will also be based on the manufacturing process (e.g., RTM, solvent impregnation, resin film infusion, and electron beam) and the knowledge gained from testing 3-D joints manufactured with these technologies.

The many advantages of 3-D composites have already been discussed above. However, there is much work to be done to provide a production structural certification capability to allow the structural designer to take advantage of all these promises.

The structural certification of 3-D preforms will center around the development of design specific mechanical properties, allowables, and analysis development. The calculation of woven or braided properties, particularly at intersections, has proven to be very difficult. To develop a-priori certification techniques the properties and allowables for the woven or braided inserts alone (not in a joint) must be developed, along with insert in a joint allowables. This is particularly necessary when calculating margins of safety for the insert, and when specifying material response properties for detailed finite element analyses. As previously noted, mechanical allowables will be processing-, structure-, and materials-dependent. Because of the lack of maturity in complex 3-D composite material response prediction, a comprehensive testing and analysis correlation will be needed in the near-term. Figure 10 shows the test results for IM7/977 3-D woven preforms. The data shows the loads carried in each of the legs of the preforms. Figure 11 shows the results of these preforms cocured into a sandwich subelement joint. These were thin preforms that failed in tension.

The methodology and criteria must be updated to account for the effects of manufacturing defects and delaminations in Z-fiber reinforced structures if the advantages of the delamination arrestment capabilities are to be realized. Static test programs to date have shown that significant gains in delamination arrestment are possible. However, a comprehensive test program to document the behavior of post-delaminated Z-fiber reinforced joints and components must include not only static strength but service life testing for multiple lifetimes under realistic loading spectrums. Once the behavior of post-delaminated Z-spiked structure has been completely characterized the possibility of changing aircraft certification criteria to allow

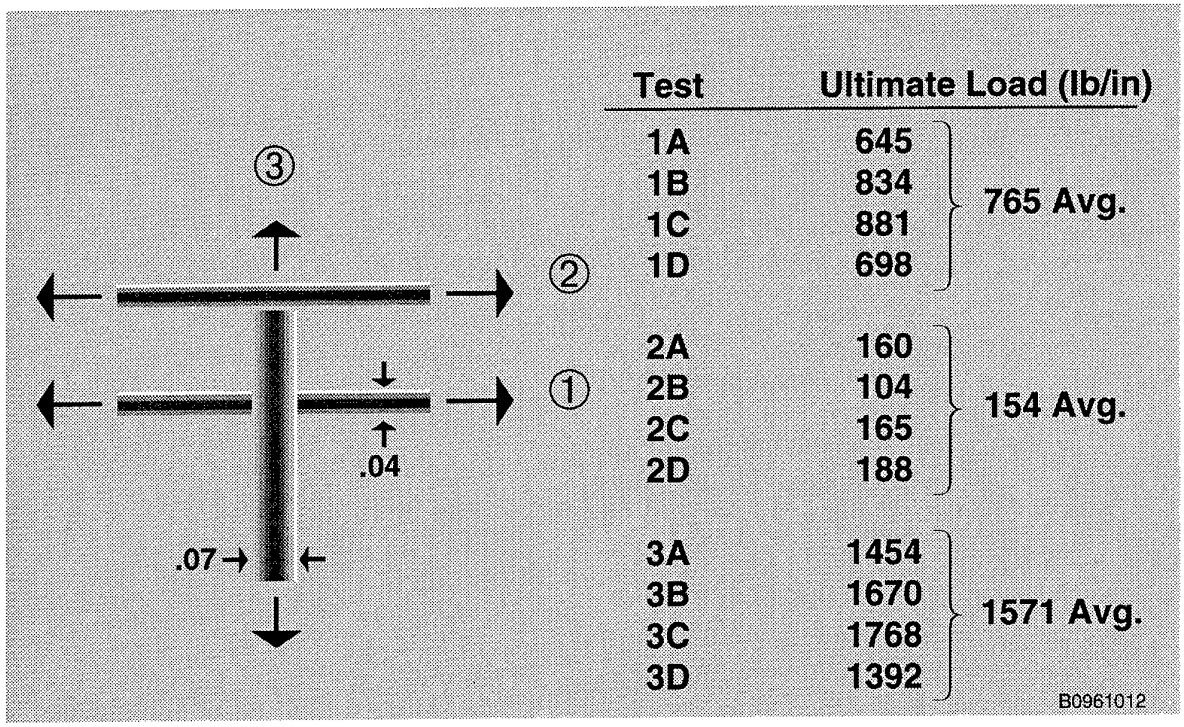


Figure 10 Tension Test Results for 3-D Woven Preforms Only

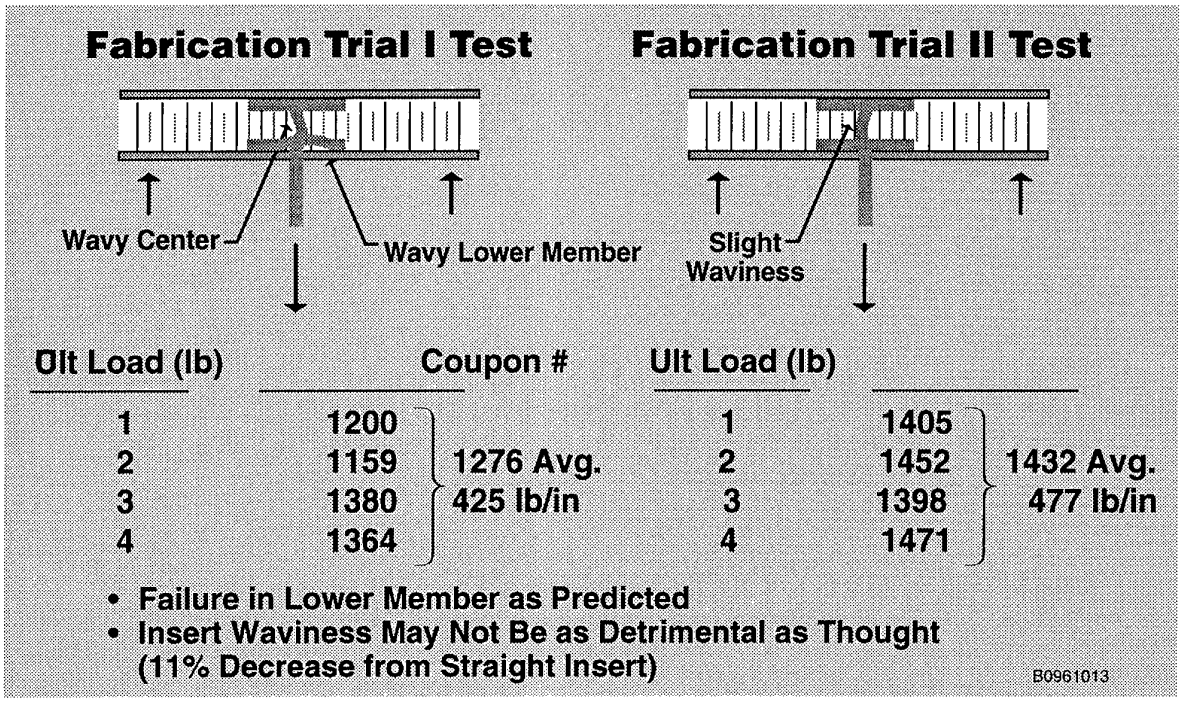


Figure 11 Test Results for Subelement Joint with Embedded 3-D Preform

flight of delaminated structures will become a possibility. This will make possible the potential weight and safety benefits promised by the early Z-spiked structural tests.

There are many gaps in the capabilities of 3-D composite joint analysis tools and methodologies. As previously mentioned, tools to reliably a-priori calculate material properties will provide the cornerstone that will enable detail design and structural certification. Building upon this methodology will be the application of finite element analysis (FEA) techniques for certification. Both 2-D (plane stress/strain and shell elements) and 3-D (solid elements) FEA analysis techniques must be developed and verified by test comparisons. The 2-D modeling idealizations include micro plane stress/strain modeling where individual or groups of plies are modeled, macro plane stress/strain where entire materials or aspects of a structure (such as face-sheet, insert, core) are modeled with one layer of elements, and shell element modeling where the laminate (or sandwich) is represented by matrices that represent the membrane, bending, and coupling responses of the structure. The 3-D modeling techniques similarly are micro or macro approaches. In all of the 2-D and 3-D modeling techniques fully characterized (and therefore accurate) 3-D properties are essential to the success of the analyses.

Testing will perform a crucial role in the development of 3-D structural certification tools and methodology. Each of the aspects of 3-D materials and joints must be characterized both within a structure and individually. Examples already discussed include woven or braided inserts and Z-fiber reinforcement. One of the most difficult aspects of testing is the accurate determination of out-of- plane properties for 3-D laminates. This is only made more complicated by the extremely complex geometries of fiber placement in the woven and braided intersections. A comprehensive program to test these properties combined with the development of mathematical material response property calculation tools will provide the optimum approach to the development of tools and methodologies capable of accurate a-priori predictions of structural strength and margins of safety. Once this has been completed the physical tests can be minimized and maximum advantage gained by the virtual certification tools and methodologies.

It is clear from the above discussions that the design and certification of 3-D woven insert joints will require the application of a large body of knowledge gained from test and analysis. Durability and damage tolerance approaches will have to be a mix of experience - based heuristics and analyses until much more sophisticated mathematical models are available. The complex

body of knowledge for 3-D composite joint structural certification, design technology, and methodology is very suitable to automation in either a procedural or rule based advisor system. The advisor will enable information and skill sharing in the integrated design - analysis environment in today's product development approach by minimizing the chance that one of the many aspects of 3-D composite joint design and certification are not considered.

SUMMARY AND CONCLUSIONS

The application of 3-D preforms and Z-fiber reinforcement in continuous fiber reinforced composite materials offer future aircraft significant improvements in aero-performance, maintainability, and survivability over current in-service composite structures. 3-D inserts make it feasible to use polymeric composite materials for structural applications such as bulkheads that were previously not possible. To obtain these benefits will require continued maturation of the processing and manufacturing technologies required to (1) fabricate net shape preforms and (2) cure these preforms into precision affordable assemblies. Composite certification and design methodology development is also underway, however it will require continued attention to be brought to full maturity.

Z-fiber reinforcement offers improvements in out-of-plane joint strength, damage tolerance, and ballistic survivability compared to current cocure structures. The Z-fiber manufacturing process is readily adaptable to current cocure tooling approaches. The cost of in-process z-fiber insertion will be offset by elimination of fasteners currently employed for joint strength or to meet damage tolerance or ballistic survivability requirements.

Emerging 3-D composite and innovative sandwich structures will offer future generation aircraft both weight reduction and cost reduction through unitization and through significant improvements in load carrying capability and survivability.

REFERENCES

1. Burgess, K., Paradis, S., "Application of 3-D Woven Preforms to Laminated Composites," Paper No. 95-3890, Proceedings of the 1st AIAA Aircraft Engineering, Technology, and Operations Congress, September 1995.

2. Fisher, K., "3D Reinforcements: on the Verge?," High Performance Composites Magazine, March/April 1996.

3. Gause, L. W., Alper, J. M., "Braided to Net Section Graphite/Epoxy Composite Shapes," Journal of Composites Technology & Research, 1988.

4. Baron, W., "Survivability of Multispar Cocured Composite Wing Structure," 37th Structural Dynamics and Materials Conference, April 1995.

Z-Fiber Technology and Products for Enhancing Composite Design

G. Freitas, T. Fusco
Aztex, Inc.
303 Bear Hill Road
Waltham, MA 02154
USA
T. Campbell, J. Harris and S. Rosenberg
Foster-Miller, Inc.

ABSTRACT

Z-Fiber™ technology uses small, solid, cylindrical pins to greatly enhance the performance of composite structures. These pins, typically 0.25 to 0.50 mm in diameter, can be used for many strucural applications. Z-Fibers, either composite or metal, are inserted through the thickness of a composite laminate to increase out-of-plane strength, damage resistance, and through thickness thermal conductivity. Z-Fiber is also used for structural joints and can be designed to be the structural network of the core material in an extremely weight and cost efficient sandwich structure.

Z-Fiber technology has been under development for over ten years. The growth of this technology, originally developed by Foster-Miller Inc., has begun to move at a very accelerated rate under Aztex Inc. during the past two years. Despite this extended development period, the revolutionary advances in the performance of composite structures made possible by this technology are only now becoming fully apparent. When used at the conceptual stage of aircraft design, when the overall structural arrangement is being formulated, Z-Fiber technology can completely change the current design approaches.

This paper presents a general overview of Z-Fiber technology and products and focuses on the work to date to form structural joints. The paper demonstrates, even at this early stage of development, Z-Fiber's capability to outperform fasteners and significantly increase the static survivability of composites.

BACKGROUND

As composite materials were introduced into aircraft structures over the last 30 years, it became increasingly apparent that the material itself could not meet the lofty expectations set for it if it was merely substituted for metals. While composite materials offer many advantages, the disadvantages tend to have an offsetting effect in actual designs. Of all the difficulties in designing with composite materials, lack of out-of-plane strength is probably the most difficult to overcome. Designers have become so accustomed to the characteristics of metals and the standard metal approaches, they tend to approach a composite in much the same way, as if it were just another alloy. Z-Fiber technology is the first new strengthening, joining, and sandwich structure approach to be developed solely for and uniquely applicable to composite structures.

An assessment of composite usage in mostly military aircraft over the past 20 years is largely a study in unmet expectations. In general, the weight savings have been less than projected and the costs have been higher. This has mainly been caused by the lack of an innovative, aggressive approach in design, choosing rather to proceed with material substitution in conventional designs. Setting aggressive cost and weight goals and then attempting to meet them with conventional design and manufacturing approaches, relying solely on the material for success is a certain formula for failure. Z-Fiber offers the first real opportunity to break this cycle. Z-Fiber will allow composites to realize their true potential by adopting the more innovative and aggressive designs that are required for success. Z-Fiber offers the opportunity to take the revolutionary step forward in design concepts which is pivotal in achieving the intended weight and cost savings.

The kind of global design decisions made during the preliminary design phase tend to dominate the final cost and weight results. Once the overall structural configuration is chosen, 80 percent of the outcome is fixed, leaving only 20 percent that can be optimized throughout the remainder of the program. Z-Fiber has the potential to completely alter the way that engineers think about designing with composites. Therefore, if Z-Fiber is introduced early in the process, an entirely different product is likely to result. Firstly, Z-Fiber will reduce the designer's need to design around the lack of through-the-thickness strength inherent to composite structures. By incorporating the structural benefits of Z-Fiber, they will be more free to design as though they are using an isotropic material , and then only apply Z-Fiber where it is actually needed. Secondly, structural attachment using Z-Fiber will allow the formation of complex shapes not presently possible, by connecting simple, easy to form components with pins. Major benefits will come from both the design of more efficient structures as well as the weight, cost and structural efficiency characterized by Z-Fiber attachment. Thirdly, advanced structural core products manufactured with Z-Fiber will not only drastically reduce the cost of sandwich structures but they will also yield a lightweight, more robust structure capable of broadening the application of sandwich core.

In summary, Z-Fiber can be employed as:

- A global or local reinforcement for increased through-the-thickness strength, improved damage tolerance and through thickness thermal conductivity.
- A secondary structure attachment method for greatly improved joint performance at a reduced cost and weight.
- The structural network used to manufacture a highly efficient, low cost sandwich core.

Z-Fiber Sandwich Core Products: X-Cor™ and Hollow Core™

Sandwich structure has long been recognized as an extremely efficient structural product, but one plagued by a poor service usage reputation. The high cost of maintaining honeycomb structures has led to them being banned by some airworthiness authorities and denounced by others. The problems with honeycomb generally fall into one of the following categories:

- Water intrusion. Trapped water adds weight, and in control surfaces and rotor blades can cause dynamic imbalance.

Paper presented at the 83rd Meeting of the AGARD SMP on "Bolted/Bonded Joints in Polymeric Composites", held in Florence, Italy, 2-3 September 1996, and published in CP-590.

- Core degradation. Aluminum core corrodes while Nomex core actively absorbs moisture.

- Skin to core debonds. With no core penetration into the skin the bonded joint is extremely fragile.

Aztex's Z-Fiber based core products solve these problems. Figure 1 shows the two product forms of Z-Fiber structural core, X-Cor™ and Hollow Core™. X-Cor has a layer of foam inserted with a structural network of Z-Fibers. During processing (i.e., addition of the skins), the Z-Fibers penetrate both skins creating a continuity between the two facesheets that does not occur in honeycomb structures. Additionally, the foam layer is bonded to the skin during processing. Hollow core is an identical product form of X-Cor without the foam layer. Figure 2 shows a Hollow Core specimen being tested in three point bend.

With Z-Fiber structural core products, water intrusion is eliminated in two ways. During manufacture, the skins in the core structure are co-cured with full autoclave pressure. Since they are fully supported during the cure cycle by a continuous core material, they will be less porous than co-cured honeycomb skins, which must be cured at low pressures so as not to drive the composite material into the cells of the honeycomb. Being a co-cured structure, X-Cor will have a superior core to facesheet seal than that of separately cured and secondarily bonded skins. Additionally, there are no open cells to trap water as there is in honeycomb. If water enters the Hollow Core system, it can be moved via a few drain holes. Secondly, the pin material typically used in Z-Fiber structural core products is either titanium or carbon. The mechanical properties of both materials are minimally affected by moisture intrusion, unlike aluminum or Nomex honeycomb. Thirdly, Z-Fiber structural core products are designed so that the truss network of pins penetrates the skins during the manufacturing process , thus there is no reliance on an edge bond as is the case with honeycomb. Additionally, each pin bond is an independent structural joint. Unlike honeycomb, where any debond predisposes the adjacent bonds to fail and the disbond to grow, adjacent Z-pins are not affected by the failure of surrounding pins.

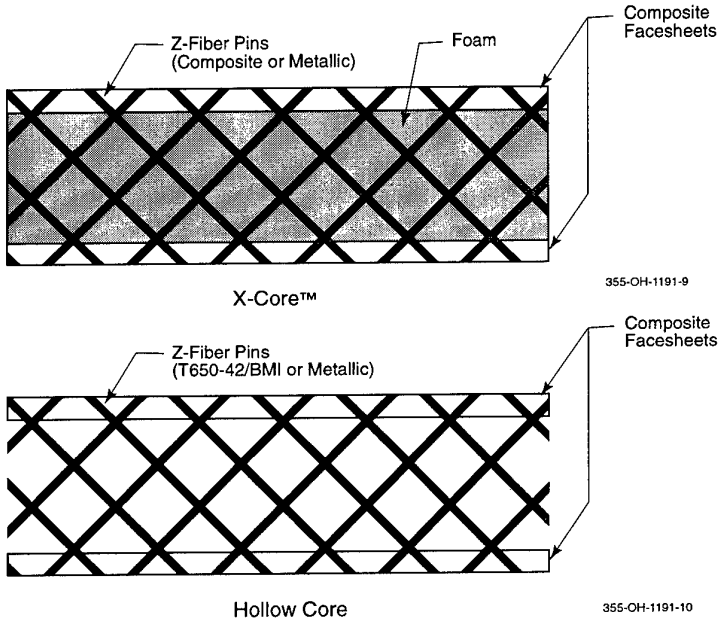


Figure 1. Z-Fiber Structural Core Products

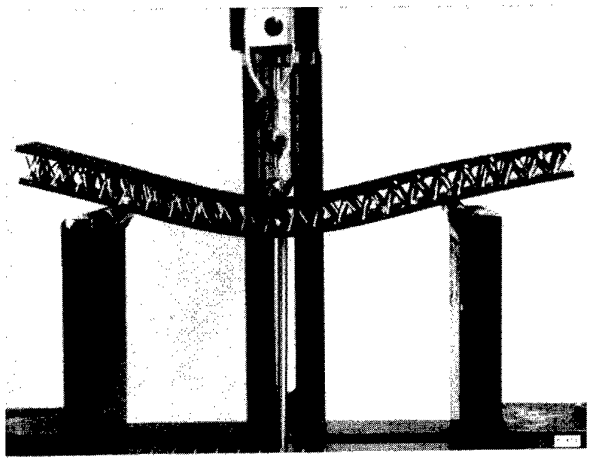


Figure 2. Mechanical Testing of a Hollow Core Specimen

A comparison of the properties of Z-Fiber structural core products with the best grades of aluminum core is shown in Table 1. From this table, it is apparent that Z-Fiber core products are equivalent to or outperform aluminum honeycomb in every category. X-Cor and Hollow Core structures are currently being tested for flexural fatigue properties. Because there are no facesheet disbonds X-Cor acts more like a ductile structure with initial failure the yielding. Initial testing has shown failed X-Cor to withstand 20,000 cycles at a high loading without significant additional failure or loss of stiffness. This phenomenal performance is not completely understood and is currently under study.

Most airworthiness authorities are currently averse to the usage of sandwich cores, particularly in primary structure due to years of poor experience with honeycomb parts. Therefore, designers tend to avoid honeycomb whenever possible. However, Z-Fiber structural core products have the potential to not only make existing core applications less expensive and more robust, but to greatly expand the use of sandwich structure. The majority of the skins on aircraft are designed by buckling criteria, hence, the advantage of sandwich structure to increase skin thickness and resistance to buckling. The key requirement is to stabilize the skin so that it can be loaded without buckling. Previous attempts in this area to use a thin layer of foam at the center of the skin to give it more thickness have proven unworkable in most cases, but there have been some successes. If this were possible with Z-Fiber core and the spacing of the stiffening members like wing skin stringers and ribs or fuselage frames and stringers could be increased, the weight and cost savings would be tremendous.

These Z-Fiber products will produce a major paradigm shift in how composite aircraft structural design is thought about. The inherent flexibility and efficiency of composite materials, largely unused thus far, could now be brought to bear on the complete range of aircraft structural applications. The local benefits of the ability of Z-Fiber to toughen skins, attach stiffeners, form core, etc., will be small compared to the large synergistic effect of allowing it to affect the entire design by introducing it at the outset. Used at the outset, Z-Fiber technology will provide sufficient weight savings to allow a newly designed aircraft to be resized. Hence, it will act as an efficiency multiplier on both the composite structure and the overall performance of the aircraft.

The Z-Fiber Insertion Process (for non-core applications)

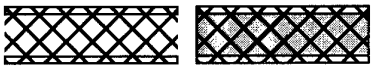
The Ultrasonically Assisted Z-Fiber (UAZ) process and insertion equipment developed by Aztex, Inc. offers quick, flexible 3D reinforcement for composite structures. UAZ is a simple, two stage, room temperature process for inserting Z-Fibers into thermoset prepregs, dry fiber preforms, and consolidated thermoplastics. UAZ employs a basic Z-Fiber preform which is partially compacted, in the first stage of the process, under forces applied by an ultrasonic horn. The residual foam layer is then removed and a second pass is made with the ultrasonic horn to set the pin ends flush with the part surface. Figure 3 shows a schematic of the two stage UAZ process. Access is needed to only one side of the composite layup. Special tips can be configured for areas which are partially obstructed or difficult to access. Hand-held or bench top insertion units are commercially available from Aztex, Inc. UAZ systems can also be configured to function as an end effector for a robot, gantry system or tape laying machine.

The UAZ process can also be used to insert metallic pins into a cured composite for potential repair applications. One repair scheme involves removing the damaged material, applying a film adhesive and wet lay-up patch followed by the insertion of Z-Fibers through the repair area into the cured substrate. The part can then be vacuum bagged and cured. UAZ is also being evaluated for repair of disbonds in honeycomb sandwich panels.

Select Z-Fiber Properties

Z-Fiber changes the way we think about composites. Typically, 2D laminates have constant fracture toughness whereas Z-Fiber reinforced laminates actually get tougher with crack length. In practice, as a crack propagates the number of reinforcing fiber rows which are activated increases resulting in increased fracture toughness. The increased fracture toughness eventually reaches equilibrium as reinforcing fibers, several rows behind the crack front, begin to pull out. However, this equilibrium often occurs at a point 50 times in excess of the baseline composite fracture toughness and requires significant crack growth to achieve.

Table 1. Comparison of Z-Fiber Structural Core Properties with Honeycomb



Core Properties	Hollow Core T650-42 BMI 12.7 gm Core	X-Cor™ T300/977 12.7 gm Core		5052-.007 Aluminum	5052-.007 Aluminum	5056-.001 Aluminum
Density, kg/m^3 (psi)	27.3 (1.7)	44.9 (2.8)	68.9 (4.3)	68.9 (4.3)	49.7 (3.1)	36.9 (2.3)
Shear Strength, Mpa (psi)	1.16 (169)	1.65 (240)	2.16 (313)	2.20 (320)	1.45 (210)	1.17 (170)
Specific Shear, Mpa/kg/m^3 (psi/pcf)	4.25 (99)	3.67 (86)	3.14 (73)	3.19 (74)	2.92 (68)	3.17 (74)
Compress Strength, Mpa (psi)	4.37 (634)	3.17 (460)	7.37 (1070)	3.45 (500)	2.00 (290)	1.45 (210)
Specific Compression, Mpa/kg/m^3 (psi/pcf)	0.16 (330)	0.07 (164)	0.11 (249)	0.05 (116)	0.04 (94)	0.04 (91)

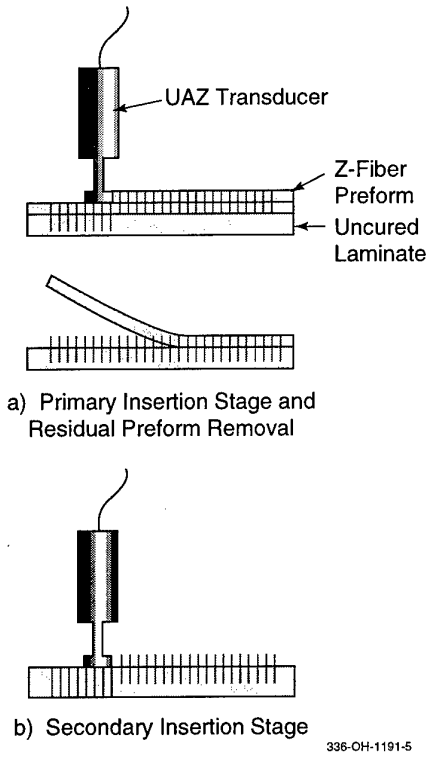


Figure 3. Schematic of Two Stage UAZ Process

One question with Z-Fiber is: what 2D properties are compromised to achieve the benefits of 3D reinforcement? For densities less than 1.5 percent a negligible reduction in tension or compression strength is seen. Some of the secondary structure attachment designs require greater local areal densities, however. Figures 4 and 5 display Z-Fiber's effect on in-plane tensile strength and ultimate tensile strain respectively. Tension was selected for evaluation because it is considered much more sensitive to through thickness penetrations. Strain was included because interestingly enough the strain carrying capability of Z-Fiber reinforced laminates is not significantly changed. This phenomenon is due to the fact that the cured laminate thickness increases as areal densities in excess of 1.5 percent are inserted into the composite. In essence it is the thickness increase that causes the strength reductions at greater densities, not in-plane fiber damage.

Comparison of Structural Joining Options

One of the key elements in the design of an aircraft structure is how to stiffen the skins. The accepted choices are increasing the skin thickness (too heavy), sandwich structures (too fragile) and the normal sheet/stringer approaches. Using the sheet/stringer approach with composites raises great concern about how to safely and securely attach the two components. The options are:

1. Co-cured, co-bonded or secondarily bonded attachment.
2. Fasteners.
3. Stitching.
4. Z-Fiber technology.

Option 1 has proven to be very fragile and has resulted in major redesigns in many programs. Total reliance on any form of bonding alone is risky, particularly when the damage tolerance and impact requirements are considered.

Option 2, fasteners, is too expensive, increases weight, decreases in-plane properties and introduces the threat of fuel leaks, lightening strikes and increased observables. One has to realize that the low cost, fuel tight, squeezed rivets that work so well in aluminum aircraft structures are not an option with composites. Expensive, close tolerance bolts with O-rings, or even more expensive sealed nut plates in fuel areas, are the extremely unattractive fastener options.

Option 3, stitching, has been tried many times, thus far without success. One might ask, how can Aztex support through thickness reinforcement yet conclude stitching is not a viable solution for attachment? The reason for this is simple, stitching is much too limited a process. Imagine if designers were told the only materials they could use to react in-plane loads were Kevlar and glass, the two most prominent stitch materials. If this were true composites usage would be minimal. There are several additional reasons stitching is viewed as an inadequate reinforcement process:

- Stitching threads are buckled during consolidation and cure, severely limiting their ability to effectively carry load.
- The manufacturing process is slow and can not access the critical regions; stiffener radii, intersections of stiffening elements and areas close to a perpendicular structure. Unfortunately these are the primary areas where through thickness reinforcement is needed.
- Stitching can not be effectively applied to prepregs because the in-plane fiber damage is too substantial and a debulked laminate can not easily be penetrated.

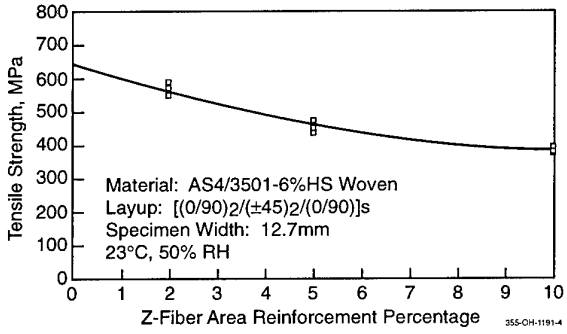


Figure 4. In-Plane Tensile Strength versus Areal Density of Z-Fiber Reinforcement

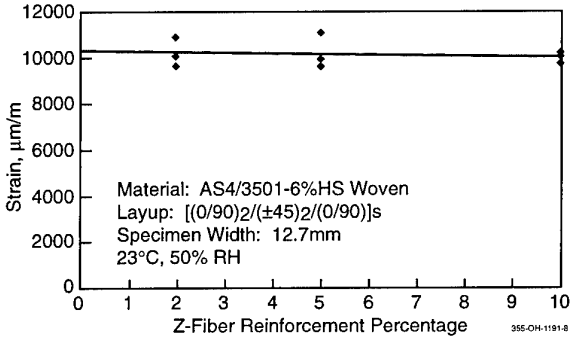


Figure 5. Ultimate Tensile Strain versus Areal Density of Z-Fiber Reinforcement

- Stitching can not be applied in the areal densities or materials required to quickly react out of plane loads. It is strictly a damage tolerance process.

- Stitching requires a significant capital machinery investment.

- Stitching has no repair option.

The Z-Fiber process was developed with all of stitching's inadequacies in mind. In the Z-Fiber process, any rigid material can be used as reinforcement so Z-Fiber composites structurally outperform stitched components. Z-Fiber does not require a major capital investment and with the development of Ultrasonically Assisted Z-Fiber (UAZ) through cured laminates a viable repair option now exists.

Potential advantages of Z-Fiber over conventional fastening techniques include:

- Mechanically fastened composite joints usually fail in bearing and the numerous small diameter pins provide a much larger bearing area than a single fastener.

- Composites are statically notch sensitive and the many small pins allow the elimination of the stress concentration caused by the fastener hole.

- The net section lost due to the fastener hole is regained.

- The load transfer is now evenly distributed across the entire specimen, rather than being forced through the fastener.

- The volume of Z-Fibers needed to replace a fastener represent only a portion of the shank section of the fastener, the head and the nut are eliminated thus reducing weight.

- Z-Fibers are either manufactured from commercially available wire, mainly titanium or steel, or in the case of composite pins made from a simple pultrusion process. Hence, there is no expensive forming, machining and finishing process as is the case with fasteners.

- Z-Fibers can be inserted with the layup on tool prior to the cure cycle using an ultrasonic system. Hence, no secondary processes (i.e., drilling, reaming, hole inspection, rework) are required.

Z-Fiber as an Attachment Method

Initial Approach - Replace Fasteners

Initially the Z-Fiber process was evaluated directly against co-cured and fastened joints. A blade stiffened design provided by McDonnell Douglas was selected. Stiffened panels were manufactured and machined into pull off specimens. A basic finite element analysis was conducted to determine load distribution during testing. As expected, most of the critical loads were found to occur at the radius of the stiffener and at the flange terminations. Based on these early indications a Z-Fiber reinforcement scenario, as depicted by Figure 6, was adopted. Four different specimen reinforcement configurations were tested:

1. Co-cured baseline.
2. Huck fastened.
3. 2 percent, 0.5mm Z-Fiber titanium reinforced.
4. 5 percent, 0.5mm Z-Fiber titanium reinforced.

Static pull off testing was completed and the test results are shown in Figure 7. All the specimens reached approximately the same load when initial failure, delamination at the stiffener radii/noodle interface, occurred. It is well documented that in bonded/fastened structures, fasteners are ineffective until a disbond occurs and that they act primarily as a secondary load path. Our data support this assumption. The significant aspect of this testing was the characteristics of the Z-Fiber specimens after initial failure. Unlike the co-cured and fastened structures, Z-Fiber specimens did not result in a catastrophic disbond of the stiffener from the skin. In fact, after initial failure Z-Fiber specimens climbed to about 70 percent more load than the fastened structures. At this point instead of a catastrophic failure, pull off of the stiffeneing element, the Z-Fiber specimens showed a delamination in the skin, then reached an equilibrium load approximately equivalent to the virgin co-cured specimen.

The initial testing demonstrated that Z-Fiber can do the job of a fastener, providing damage tolerance and fail safety, better than a fastener. The far superior fracture toughness of Z-Fiber joints showed the potential for designers to be less concerned with damage progression. Based on this early testing two possible scenarios could be assumed which would make major strides forward in composite structure performance:

- Alter acceptance criteria - If Z-Fiber could demonstrate the ability to limit crack growth in fatigue, new designs could be incorporated based on ultimate strength rather than initial failure.

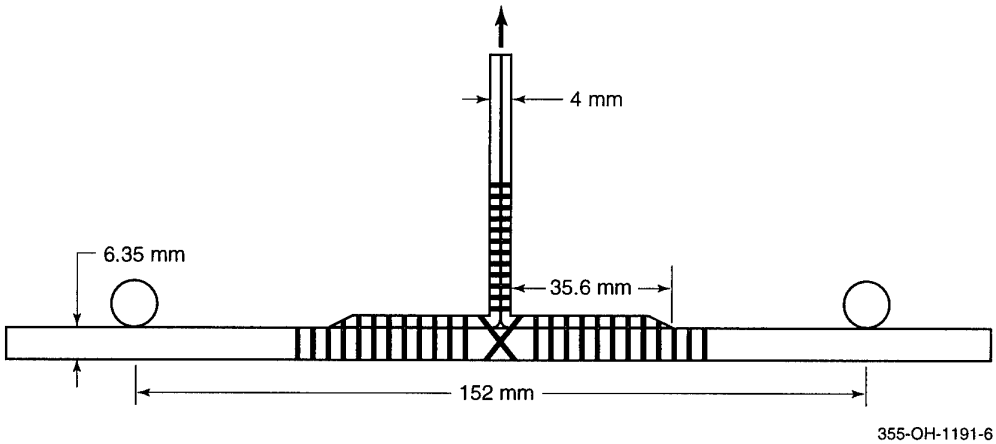


Figure 6. Blade Stiffener Pull-Off Configuration 1

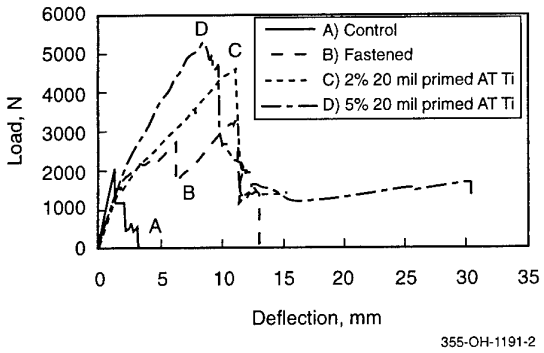


Figure 7. Stiffener Pull-Off Test Results

- Increase initial failure loads - Previous work suggests initial failure loads can be increased when combining innovative design practices with Z-Fiber.

Aztex is aggressively pursuing both scenarios. Success with both scenarios would have a major impact on composite aircraft design. Obviously, increasing initial failure load levels is an easier sell and one welcome by airframers. To that end we are focusing design and testing efforts in this area.

Increasing Initial Failure Loads

Under a routine screening matrix single lap shear testing was conducted comparing co-cured, co-cured/fastened, and Z-Fiber reinforced specimens. The results are plotted in Figure 8. The results point to the need for detailed design of the joint interface. As expected, the co-cured specimens loaded until bond failure then the joint failed catastrophically. Bolted/bonded joints load to initial matrix failure then transfer the load to the fastener until bearing failure occurs. The co-cured Z-Fiber configuration showed a modest increase in initial failure load and a large increase in ultimate load. The most interesting result was a specimen made with Z-Fibers and a PTFE film layer in the bondline (i.e., no bond at the lap joint). This specimen displayed over six times the initial strength of co-cured or fastened joints and the specimen ultimately had a net section tension failure. This indicates that if load sharing between the pin and the matrix can be optimized initial failure loads could be significantly increased.

In an effort to delay the onset of initial failure in stiffened structures, it was theorized that a low modulus interlayer, located at the stiffener radius/noodle interfaces, used in combination with Z-Fiber would allow the stresses to be carried by the pins and not the resin matrix. Additional test specimens were manufactured using configuration 1 to verify this theory. A co-cured stiffener with the interlayer but without pins was manufactured and tested. Two additional stiffeners with the interlayer and Z-Fiber, one each at 2 percent and 5 percent reinforcement in the radii, were also manufactured and tested. These test results were added to the previous data base, for configuration 1, and are summarized by the bar chart in Figure 9. For this configuration, a co-cured stiffener with the interlayer alone yielded the lowest initial failure load of all the specimens tested. However, the two sets of specimens that incorporated the interlayer in combination with Z-Fiber proved to have the highest initial failure loads, 50 percent greater than all of the other specimens tested.

A study was then conducted investigating the effects of several design variables on pin/matrix load sharing based on the significance of the preliminary lap shear and stiffener pull off results described above. The idea of this analysis was to better understand the mechanics of increasing initial failure load in stiffened panel joints. Our basic approach was to vary blade stiffener radius, Z-Fiber reinforcement pin diameter and density, and noodle modulus and analyze the effects. The use of a soft interlayer to aid transfer of the load directly into the pin was also investigated. From this investigation, a second blade stiffener configuration, configuration 2, with a stiffener radius of 9.6 mm was evaluated. A larger radius has the benefit of being able to distribute the stresses more evenly over a larger area. Figure 10

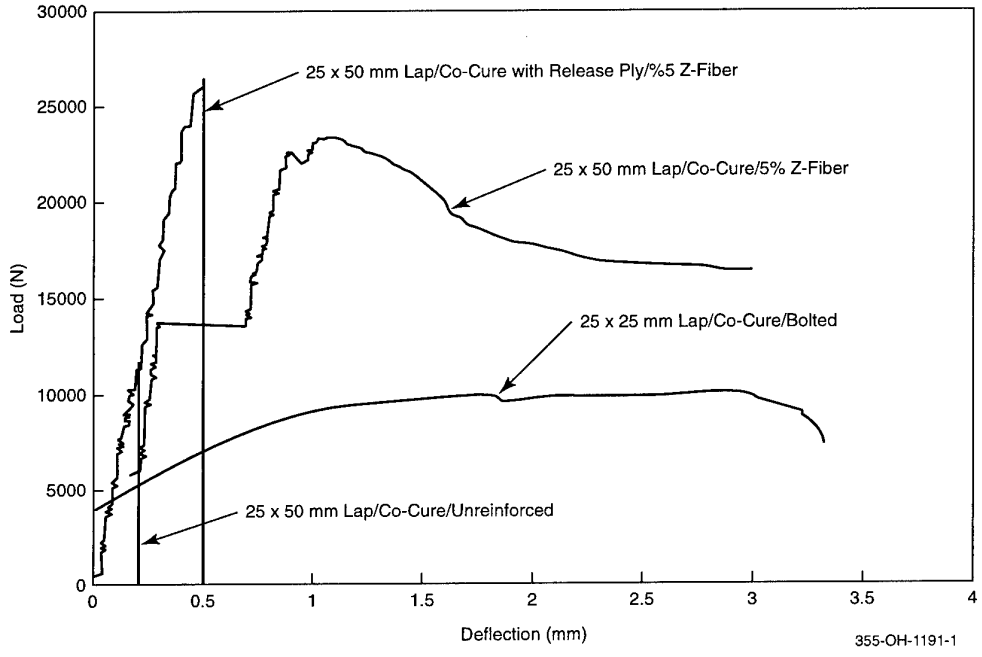


Figure 8. Lap Shear Screening Results

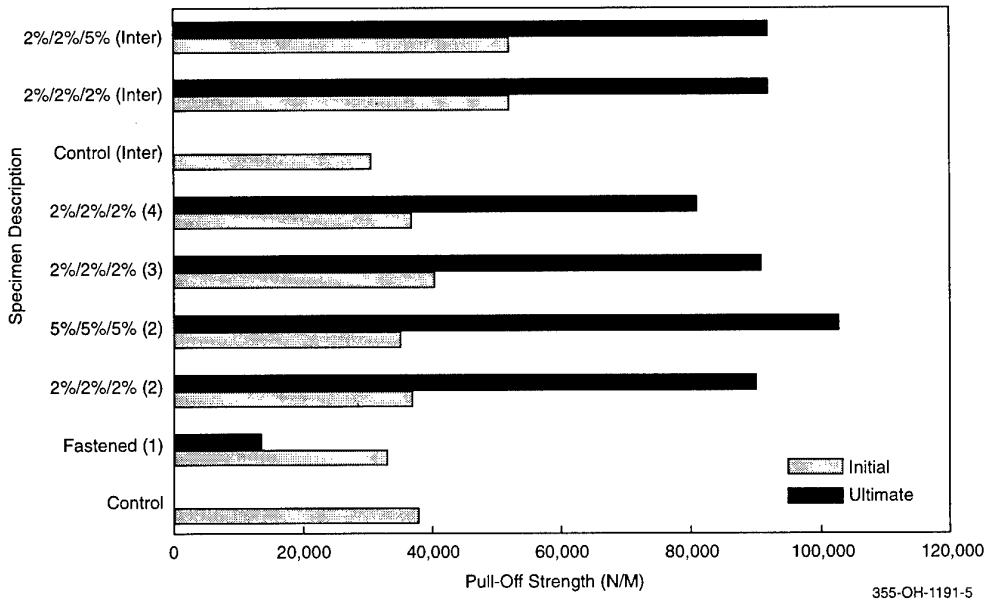


Figure 9. Increase in Initial Failure Load for Stiffener Configuration 1

summarizes the effects of the design variables on the expected test results based on a finite element analysis. Various design configurations were included in the analysis. Based on the model, a viable solution to delay the onset of initial failure was determined. Z-Fiber reinforcement at a varied areal density in combination with a thin, low modulus interlayer at the radius/noodle interfaces was selected for testing.

Preliminary manufacture and testing has begun on the new baseline stiffener, configuration 2 (Figure 11). A thin, soft interlayer was included at the radii/noodle locations during the layup process. Z-Fiber reinforcement was added to the flange/skin interface, within the web area and at the stiffener radii/noodle interfaces. The Z-Fiber reinforcement for the majority of the stiffener was 0.5 mm 6Al-4V titanium inserted at an areal density of 2 percent. However, at the critical stress points, the reinforcement was changed to 0.25 mm 6Al-4V titanium inserted at an areal density of 5 percent. This change in Z-Fiber size and areal density was deemed necessary to react the stress concentrations located at the tip of each noodle/radius interface.

Typical load-deflection plots for the stiffener pull-off tests are shown in Figure 12. Plot A shows the test results for a thin skinned stiffener manufactured with a rubber interlayer but without Z-Fiber. Initial failure occurred in the interlayer. Another stiffener was manufactured identical to the second but with Z-Fiber added. Plot B shows that the addition of Z-Fiber to the interlayer approximately doubled the initial failure load.

The above test results indicate that Z-Fiber is effective in delaying the onset of initial failure of various stiffener configurations while yielding damage tolerance far superior to that of a co-cured or fastened structure.

Configuration	Result		Comment		Solution
Control	High stresses	→	Need to reduce stresses	→	Add Z-Fiber
Pins, no interlayer	High stresses	→	Need to transfer loads into pins	→	Add rubber interlayer
Pins, thick interlayer, constant pin %	Low stresses; high pin loads	→	Need to reduce pin loads	→	Reduce interlayer thickness
Pins, thin interlayer, constant pin %	Acceptable stresses	→	Still need to reduce pin loads	→	Add more pins to distribute load amongst pins
Pins, thin interlayer, varied pin %	Acceptable shear/interlaminar; acceptable pin loads	→	Pin loads relatively even at all locations; viable solution	→	Change noodle modulus
Pins, thin interlayer, varied pin %, low modulus noodle	Low stresses, low pin loads	→	Viable solution		

Figure 10. Effects of Design Variables

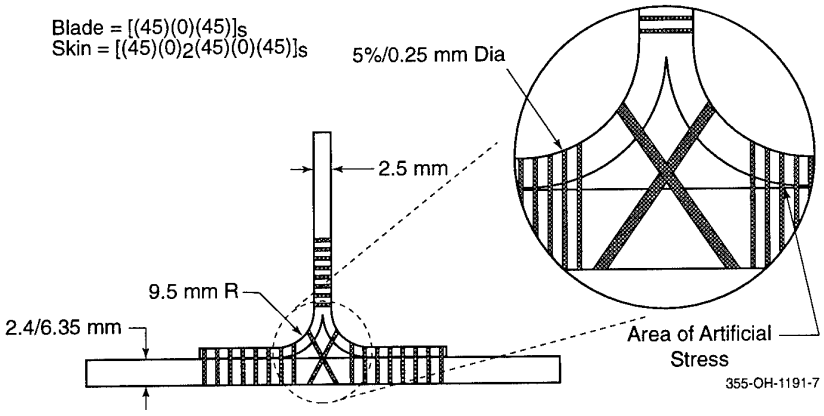


Figure 11. Stiffener Configuration 2

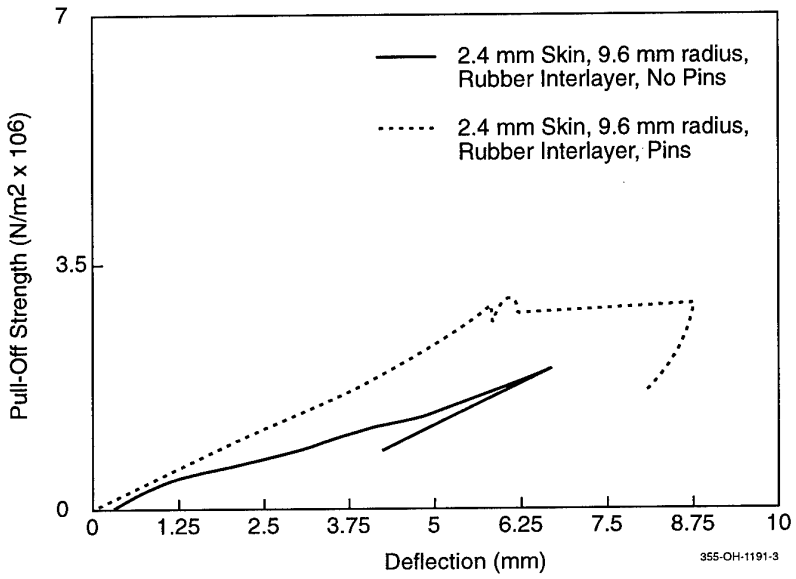


Figure 12. Typical Load-Deflection Plots for Large Radius Stiffeners

SUMMARY

The current family of Z-Fiber products is capable of revolutionizing the way composite aircraft structures are designed and fabricated. Z-Fiber should be viewed as an enabling technology that will allow composite structures to achieve their much talked about, but seldom achieved, weight savings. Further, by eliminating reinforcing metal fittings and reducing the number of fasteners and skin support members, the cost of composite structure could become competitive with aluminum.

It is important that this technology be introduced at the outset of the design process, such that the global, synergistic effect of Z-Fiber can be maximized. There is ample experience to demonstrate that without a major step forward, such as that offered by Z-Fiber, designs will gravitate toward fewer composites, more metal and fasteners, and fewer large unitized parts leading to a greater part count. The benefit of Z-Fiber is not solely to attach structures, improve damage tolerance, etc., rather it is to provide the design flexibility and confidence necessary to embrace an extremely efficient, but unconventional design.

AN INVESTIGATION ON A BOLTED-COLD BONDED JOINT FOR LARGE DIAMETER STRUCTURES

M. Montabone, M. Nebiolo and C. Vigada

Alenia Spazio S.p.A.
Corso Marche 41
10146 Torino
Italy

ABSTRACT

A study is hereafter described to investigate the structural behaviour of cold bonded/bolted and simply cold bonded joints.
These joints are representative of connections at the interface of large diameter structures (over 4 m) in which sandwich composite panels have to be fixed to aluminum fork - shaped rings.
They find practical application as adaptor structures for satellite launchers, providing high strength/stiffness performances, and are peculiar of areas fitted with continuous separation systems.
Special low preload bolts have been introduced in order to avoid the use of through inserts in sandwich panels necessary to prevent the crushing of the core so optimising mass and manufacturing cost/time but still maintaining very high load capabilities.
A Finite Element analysis has been carried out to detect load distributions at the bolted/ bonded interfaces of the joints.
A test campaign is planned for the manufactured specimens and a final test correlation will be performed to compare experimental and theoretical results.

INTRODUCTION

The selected configuration is intended to be applied to large diameter structures. The bolt added to bonding is due to the necessity of introducing a further element of safety in a particularly critical area in which the shock load, consequent to pyrotechnic explosion during separation, could cause local adhesive failure.
In addition, in the real structure the adhesive application might not guarantee constant thickness and completely avoid unbonded areas, so the accommodation of a close tolerance fit bolt is strongly recommended as a safe solution.
Bolt introduction has led to the need for a local doubler to be added to the basic laminate thickness in order to increase the bearing/ shear-out load carrying capability of the skin.
It must be pointed out that the manufactured specimens are intentionally flat because curvatures on large diameters are clearly low and they are consequently representative of these interfaces without introduction of stiffness/strength errors.

GENERAL REQUIREMENTS AND DESIGN DESCRIPTION

The baseline concept of the bolted/bonded joint design has been based on the following requirements:
- high structural stiffness
- use of cold setting adhesive with high gap filling capability and extended curing time
- tensile failure over 300 N/mm
- minimum mass impact w.r.t. full bonded option
- maximum simplicity in the joint assembly operations
- on assembly possibility of adjustment of the overall component due to manufacturing tolerances.

The detailed design is illustrated by Fig.1.
The joint consists of a honeycomb sandwich panel with CFRP skins reinforced by means of internal doublers; the panel is joined to an external fork type end-fitting in aluminum alloy, which is considered a quasi standard application for interface rings and separations.
The sandwich panel is made of aluminum honeycomb core with CFRP skins and doublers, both cured with hot setting adhesives.

Paper presented at the 83rd Meeting of the AGARD SMP on "Bolted/Bonded Joints in Polymeric Composites", held in Florence, Italy, 2-3 September 1996, and published in CP-590.

The skins and doublers are first cured and then bonded to the core in a further manufacturing step, but for their cure process the same male mandrel of the panel (if applied to cylindrical shape) can be utilized due to small curvatures in a real application. For the specimen manufacturing, the utilized mandrel is obviously flat.
The sandwich panel is eventually cold bonded to the external fork.
The use of cold bonding is mandatory for large diameter parts as autoclaves of such a great size are not always available and large cylindrical structures are usually manufactured by assembling 4 or more curved sectors.
The skins are made of M55J - Cycom 950-1 prepreg in unidirectional style with a lay-up of $(0_2,90,+45,-45,90,0_2)$ while the doubler is given by a stacking sequence of $[0_2,(0,+45,-45,0)_5,0_2]$ of the same material.
Titanium alloy bolts are then used for fastening the aluminum to the sandwich panel.

MATERIALS

The CFRP skins are made of M55J - Cycom 950-1 pre-preg which is commercialised by Cyanamid. It is a UHM carbon fibre with epoxy low cure temperature (125°C) resin system.
The main characteristics of this unidirectional prepreg are listed in Table. 1.
The aluminum honeycomb core is a 3/16-5056-0.0007P commercialised by Hexcel.
The fork-shaped flanges are made of machined aluminum alloy 7075-T7351 but in the real application a large ring flange could be obtained from a forging of the same base material.
The bonding between aluminum forks and composite skins is obtained with EA934NA that is a structural adhesive paste commercialised by Dexter Hysol, qualified in accordance with MMM-A-132 type I class 3 and well experienced in potting, filling, and liquid shim applications.
This adhesive is made of two components, and has enough low viscosity to allow good accommodation or injection into shallows and grooves (if any) and in addition is a good room temperature curing paste from the point of view of strength.
Its characteristics derived from thick adherent shear test are reported in Fig 2.

Table 1 M55J/950-1 Properties

Property	Value	Unit
Axial Elastic Modulus	292000	MPa
Transverse Elastic Modulus	6510	MPa
Shear Modulus	4015	MPa
Axial Tensile Stress	1500	MPa
Transverse Tensile Stress	52	MPa
Ultimate Shear Stress	69	MPa

SPECIMEN MANUFACTURING PROCESS

The manufactured specimens are shown in Fig.3.
The length of specimens is 191 mm for the sandwich panel part plus the two aluminum fork fittings to its end parts.
The sandwich panel has been manufactured with aluminum honeycomb previously milled at its ends to allow CFRP tapered doublers accommodation.
The skins and doublers in carbon fibre M55J-CYCOM 950-1 are then co-bonded with REDUX 312-L adhesive film to the honeycomb panel and they have been cured separately with peel ply on each surface at a temperature of 125°C following the cure cycle provided by the supplier.
The performed prebonding treatment on aluminum forks consists of an alkaline degreasing followed by water rinsing.
Immediately after drying, a thin layer of BR127 Primer commercialised by Cyanamid has been sprayed onto the adherents surfaces and then cured to increase the prebonding

treament lifetime.
A thin layer of Hysol EA 934 NA (0.15 mm thick) has been spread on the aluminum parts to be bonded to the sandwich panels.
After adhesive curing completion (7 days at room temperature in clean room conditions) the manufacturing process has been completed by riveting aluminum buttstraps on aluminum forks and fastening the forks to the sandwich panels.
The specimens have been assembled by means of a dedicated support tool in order to guarantee adherents alignment.
A total number of 5 specimens has been manufactured with the following characteristics concerning their end parts:
end A having a larger extension area of 480 mm^2 and end B having an area of 340 mm^2.
The overall typologies of specimens is reported in Table 2.

Table 2 Specimen Configuration

Specimen	End "A"	End "B"
1	Bonded	Bonded
2	Bonded	Bolted
3	Bonded	Bond/Bolt
4	Bonded	Bond/Bolt
5	Bond/Bolt	Bond/Bolt

JOINT ANALYSIS

The analysis of the joints has been performed following the listed approaches.
- Hand Calculation: this type of analysis has been used for the design of the joint.
- Finite Element computation: this type of numerical analysis has been used for the final verification of the joint load carrying capability.

These analysis approaches have been carried out considering both the pure elastic and the elastic perfectly-plastic adhesive stress-strain behaviours.

HAND CALCULATION

The preliminary design approach for bonded/ bolted composites structure is normally based on hand calculation, which is very useful for the current understanding of strength problems, as well as very efficient for design trade-off.
These analyses are based on a common well known analytical method which enables the designer to calculate the stress/strain distributions in the adhesive layer of simple joint configurations (on condition that simplifying constraint rules are applied to the analysis).
Typically, for these analyses the RD[1 and 2] are the currently applied methods.
For the pure elastic approach it must be underlined that this simplified method does not consider the through-to-thickness bending effect; however, it can be easily used for a preliminary assessment of load carrying capability, limited to the fully elastic behaviour (i.e. γ=0.04).
The obtained shear distribution for a typical adhesive thickness of 0.15 mm is shown in Fig. 4.
The maximum shear stress (τ=22. MPa) is reached on the side of the external adherent junction.
Hence, for different adhesive thicknesses η in pure elastic field, the Table 3 allowable loads Pe are calculated.

Table 3 Pure Elastic Load

η [mm]	Pe [N/mm]
0.075	350.
0.1	405.
0.125	450.
0.15	493.
0.175	530.
0.2	565.
0.25	625.

After the elastic region the adhesive will start behaving in the elasto-plastic way.
In this region the composite adherents might still behave in the elastic way while the glue is already in its plastic field.

Fig. 1 Sample Drawing

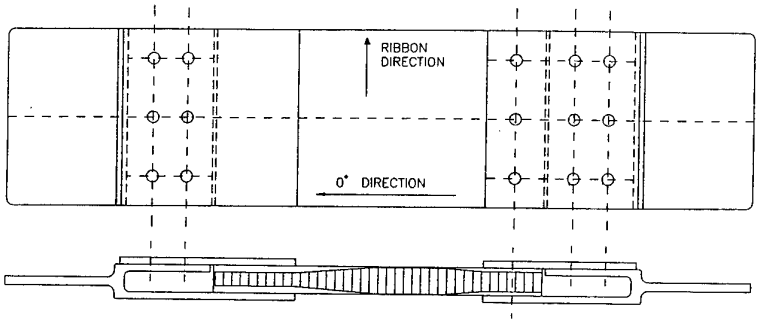


Fig. 2 EA 934 NA Properties and Hart-Smith Elasto-plastic Curve.

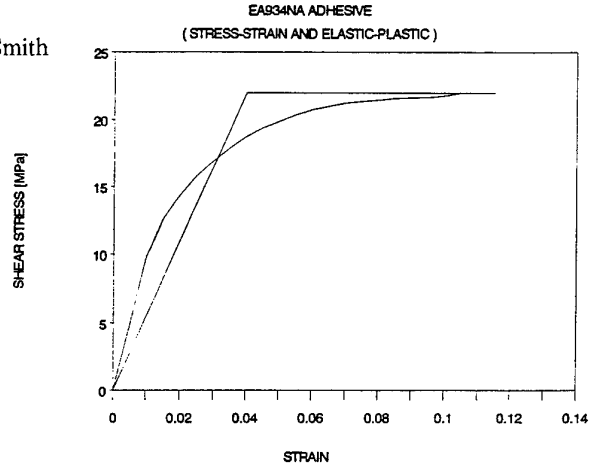


Fig. 3 Typical Specimen

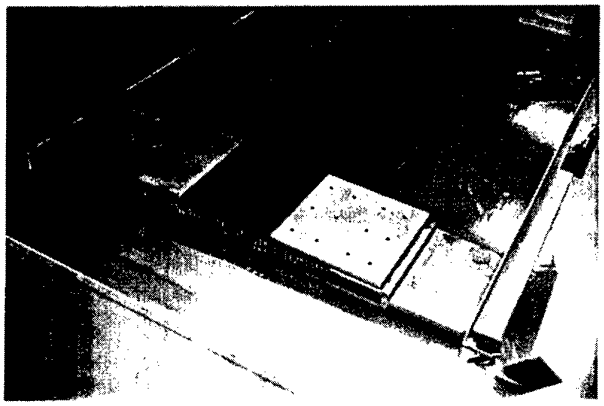
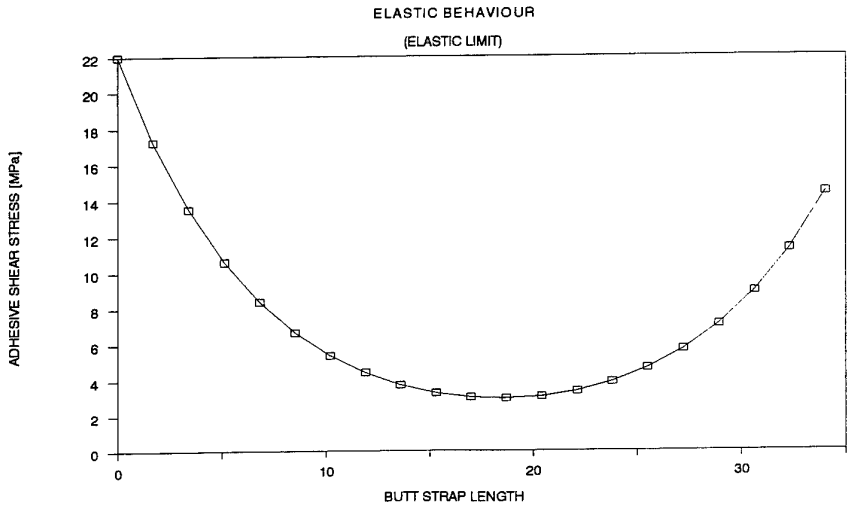


Fig. 4Adhesive Shear Stress (Elastic behaviour)



This part of the strength might therefore be used as a margin for the load carrying capability of the joint, i.e. up to the elastic region the proof load can be applied and then the plastic region can be utilised as a reserve for the ultimate strength load capability and margin of safety evaluation.
The failure load of adhesive can be evaluated using RD[1-2] and taking into account the perfect plastic behaviour, the applied peel stress σp and the estimation of the maximum thickness of outer adherent not causing peel problems, can be calculated as reported in Table 4.

Table 4 Elasto-Plastic Behaviour

η [mm]	Pu [N/mm]	σpeel [MPa]	toa [mm]
0.075	765	28.7	2.56
0.1	884	26.6	3.42
0.125	988	25.1	4.25
0.15	1083	24.0	5.13
0.175	1169	23.0	5.98
0.2	1250	22.3	6.83
0.25	1397	21.0	8.54

As appears from the Table, the failure load with a fully plastic behaviour (i.e. about 1400 N/mm) of the glue is nearly reached for a 0.25 mm adhesive thickness.
The above analyses apply only to the bonded solution, while for the bolted option the RD[3] analysis program has been used.
In performing this analysis, the effect of bonding contribution of course has been neglected, so the pure load carrying capability of the CFRP skins is evaluated.
Such estimation leads to a load flux value of Pu=320 N/mm with a bearing/shear-out failure mode. Considering that, for any reason, the bonding application might not be as good as designed (e.g. wrong prebonding treatments or excess of glue thickness, voids or delaminations), a sort of strength reserve factor is anyway reached with a negligible mass impact on the whole structure by coupling bonding with bolting.

However, this last load carrying capability appears lower with respect to the only bonded option.

FEM DESCRIPTION

In order to assess the mechanical behaviour of the joints under tensile load, a dedicated FE mathematical model has been prepared for each of the three following joint configurations:

a) Simply Bonded Joint (see Fig. 5)

b) Simply Bolted Joint (see Fig. 6)

c) Bonded/Bolted Joint (see Fig. 7)

Each FE model is representative of half a joint thickness because of symmetry considerations for loads and constraints, so the simmetry constraints have therefore been placed to re-establish the complete joint behaviour.
In the width direction, only one bolt has been considered for the determination of the failure load fluxes, both for simplicity and symmetry considerations.
A solid element modellization has been chosen for all the constitutive materials of the joint.
Both elastic and elasto-plastic behaviours for the typical adhesive layer (0.15 mm thickness) have been taken into account for the Simply Bonded Joint Shear and Peeling stresses distribution evaluation.
The Static Analyses have been performed by solving the FE models with MSC/NASTRAN V68 Solution 101 (Fully Elastic Behaviour) and Solution 106 (Elasto-Plastic Behaviour).

FEM ANALYSIS RESULTS

A different analysis approach has been considered for the three joint typologies.
Starting from the Simply Bonded Joint, the analysis has been set up in accordance with the following procedure: the γ-deformations coming from the thick adherent shear test on adhesive and represented as $\gamma = 0.04$ (Elastic Limit) and $\gamma = 0.115$ (Plastic Limit at Adhesive Failure) have been considered to establish the loads for both Elastic and Elasto-Plastic behaviour and the resulting stresses on

adhesive.
The stress distribution in terms of σp (Peeling Stress) in the interfacing adhesive and composite layers is reported in Fig. 8 and Fig. 9 while the τ (Shear Stress) in adhesive layer is shown in Fig.. 10 for the Elastic Limit (γ = 0.04) coincident to A) Fully Elastic and B) Elasto-Plastic behaviours.

A) Fully Elastic Behaviour

For this behaviour a load flux of 522 N/mm for γ= 0.04 (Elastic Limit) and a load flux of 1498 N/mm for γ = 0.115 (Plastic Limit) have been obtained, the latter is fictitious because it gives a τ= 63 MPa out of glue range with an elastic shear modulus of 550 MPa.
The stress distribution in terms of σp (Peeling Stress) in interfacing adhesive and composite layers is reported in Fig. 11 and Fig. 12, while the τ (Shear Stress) in adhesive layer is shown in Fig. 13 for the Plastic Limit (γ = 0.115).

B) Elasto-Plastic Behaviour

For this behaviour, the same load flux of 522 N/mm for γ= 0.04 (Elastic Limit) and a load flux of 953 N/mm for γ = 0.115 (Plastic Limit) have been obtained; this latter load is theoretically correct and corresponds to a τ = 22 MPa.
The stress distribution in terms of σp (Peeling Stress) in interfacing adhesive and composite layers is reported in Fig 14 and Fig. 15 while the τ (Shear Stress) in adhesive layer is shown in Fig. 16 for the Plastic Limit (γ = 0.115).

The difference between A) and B) behaviours in the plastic range comes clearly out of the consideration that in fully elastic adhesive the real τ-γ curve is not taken into account and as the considered curve is a linear one, the deformation γ= 0.115 is obtained with a false failure load flux of 1498 N/mm at a resulting false shear ultimate stress τ = 63 MPa, as said before.
In the elasto-plastic adhesive approach, a more realistic value of failure load flux of 953 N/mm at a ultimate stress of τ = 22 MPa is obtained.

Bolted Joint

The analysis for the bolted joint has been performed in order to evaluate its global load carrying capability: a fully elastic behaviour of the components has been considered.
The whole load is now completely sustained by the bearing load capability of doublers and skins.
Load transfer from titanium bolt to sandwich panel has been simulated in the mathematical model with a radial connection between the bolt elements and the sandwich elements in order to guarantee pressure load application at the hole edge.
The load flux under which failure is estimated to occur in the most stressed elements around the hole edge of the composite skin is 380 N/mm.

Bonded/Bolted Joint

The same considerations made for the previous type of joint are still valid except that in this case the load is now sustained by both the bearing and bonding load carrying capability of the joint.
The load flux under which failure is estimated to occur in the most stressed elements around the hole edge of the composite skin is 1195 N/mm, so the presence of the adhesive layer causes a good increase in the strength to failure of the simply bonded joint (953 N/mm).
The advantage of having bonded/bolted joints is therefore not only limited to a strength reserve approach but leads as well to a considerable improvement in the load carrying capability of the joint itself.
As is clearly shown, the resulting load flux for a bonded/bolted joint is obtained by the quasi-addition of the simply bonded and simply bolted contributions.

Fig 5 Simply Bonded FEM

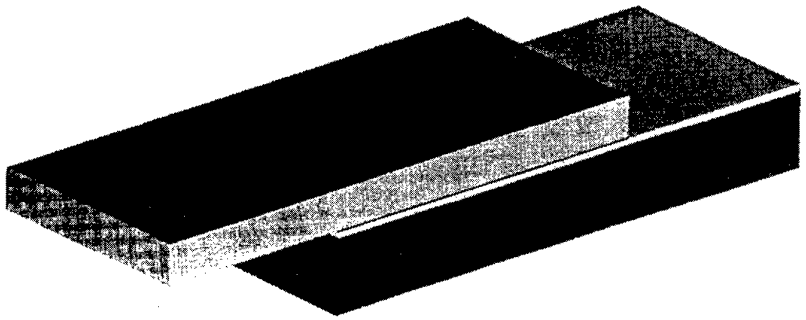


Fig 6 Simply Bolted FEM

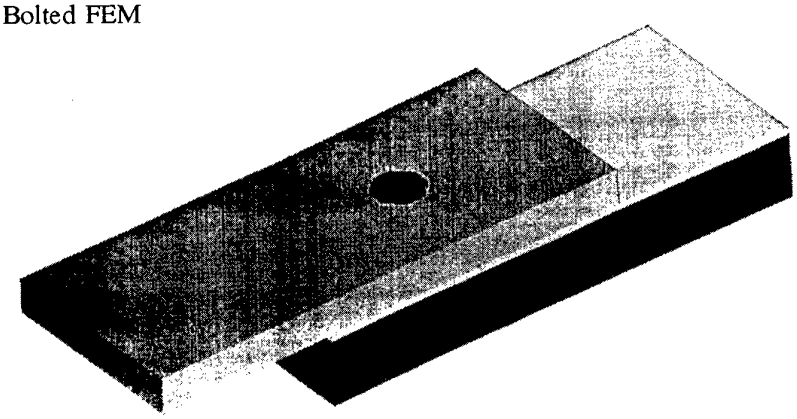


Fig. 7 Bonded/Bolted FEM

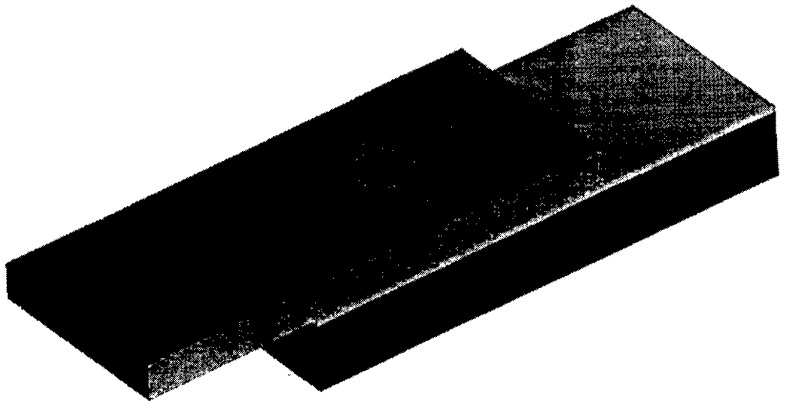


Fig. 8

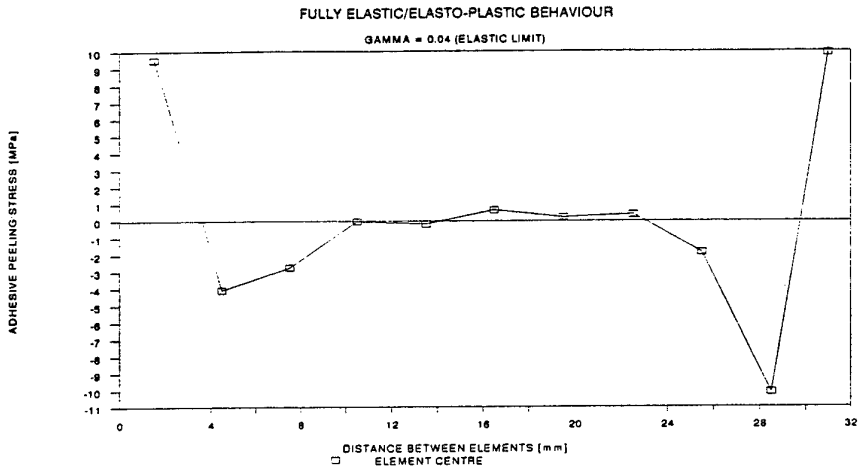


Fig. 9

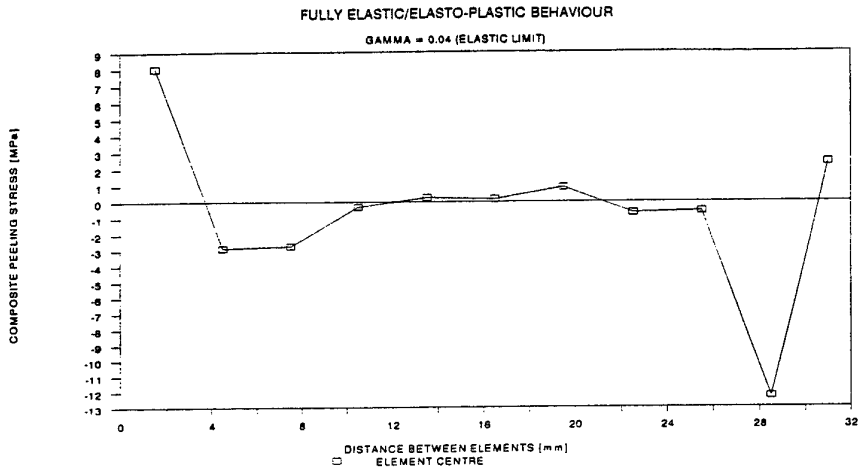


Fig. 10

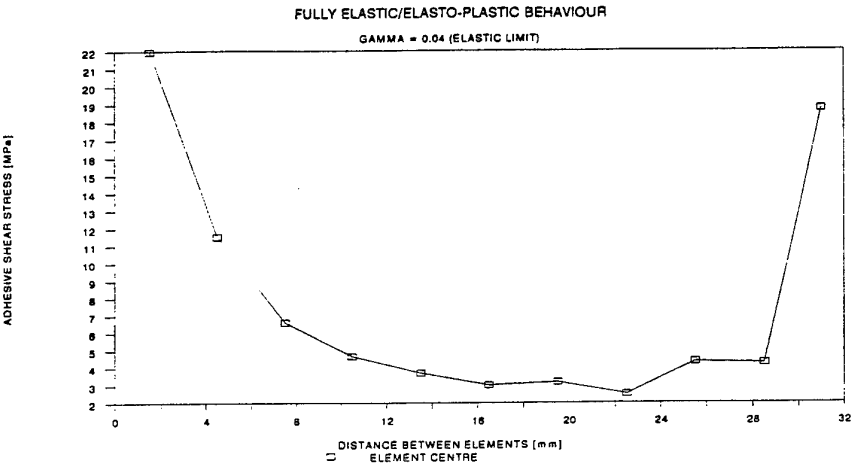


Fig. 11

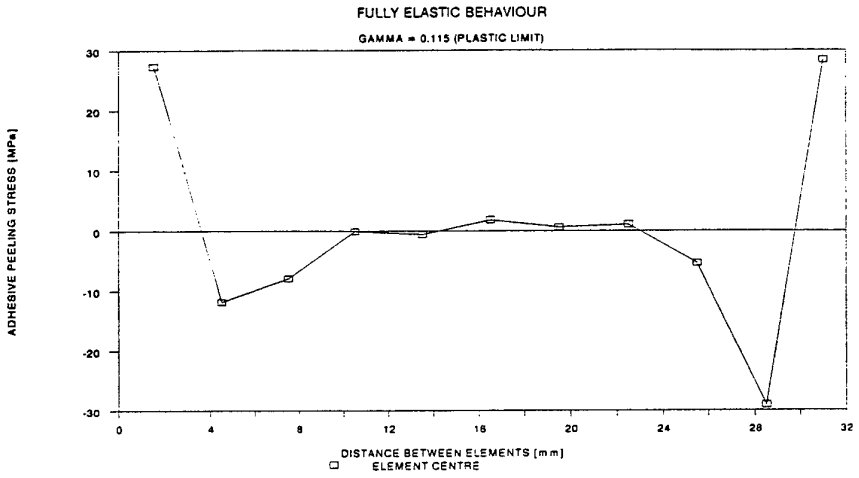


Fig. 12

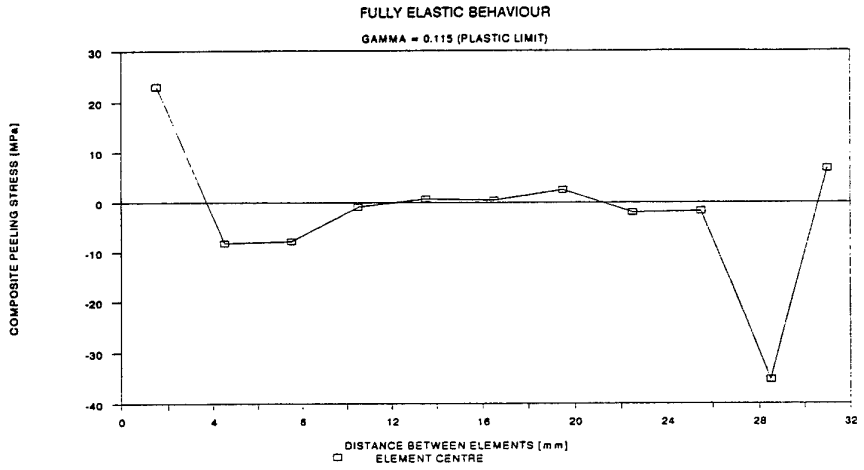


Fig. 13

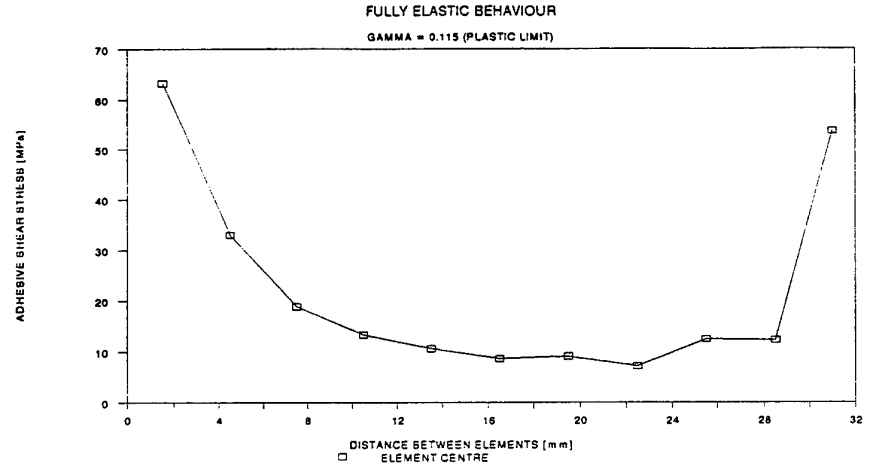


Fig. 14

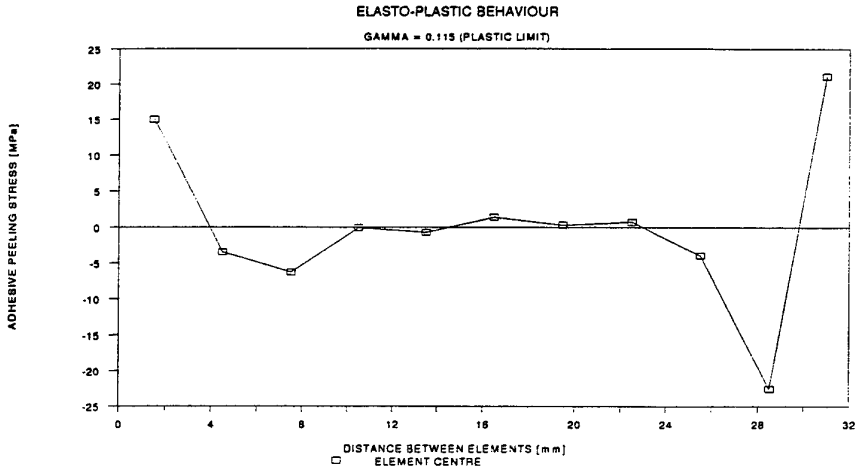


Fig. 15

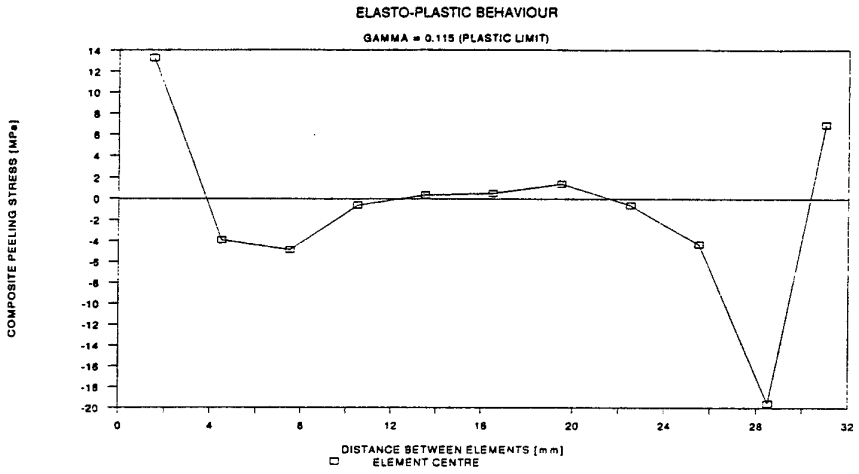
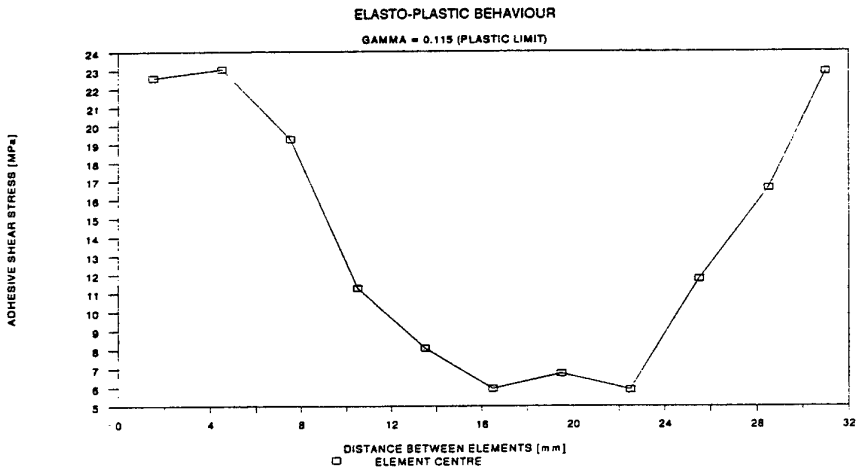


Fig. 16



MECHANICAL TEST

A short test campaign has been conducted on a limited number of 5 specimens in order to assess their strength characteristics practically. The used tensile test machine was a Zwick with a maximum load capability of 25 tons. The load has been applied at a speed rate of 0.15 KN/min and the failure load fluxes obtained for each one of the 5 specimen configuration previously reported in Table 2 are here below listed in Table 5.

Table 5 - Specimen Test Results

Specimen	Failure Fluxes [N/mm]	Type of Failure
1	350	Peeling of CFRP skin at end B
2	250	Bearing at end B
3	300	Peeling of CFRP skin at end A
4	340	"
5	430	" at end A plus Bearing at end B

As it is possible to see from this Table in none of the specimens (1,3,4,5) is the failure mode due to adhesive failure so it can be practically said that the adhesive layer, at the experimentally evaluated failure load fluxes, is just working in its elastic field and the plastic region is therefore never reached because of a lower limit in strength imposed to the joint by the peeling of the CFRP layer directly close to the glue and the resin interlaminar shear strength capability.
It must be underlined that, generally speaking, a limitation in the failure load of the joints, is currently due to the composite material and not to the adhesive behaviour; this is applicable also to other types of resin-to- fibre combination

The occurring type of peeling failure is represented in Fig.17 and practically shown in Fig. 18.
A different matter is the bearing behaviour of the joint (specimen 2) for which a lower value in load flux of 250 N/mm has been obtained, but again due to the resin behaviour.

Fig. 17 Peeling/Interlaminar Shear Failure

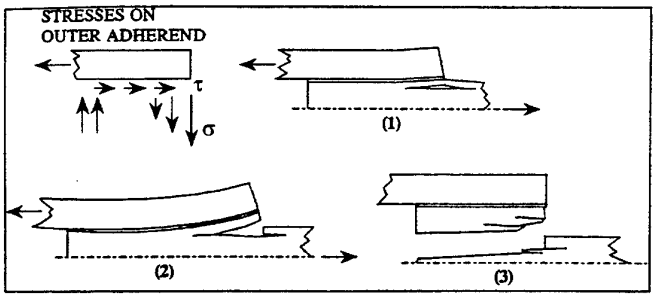
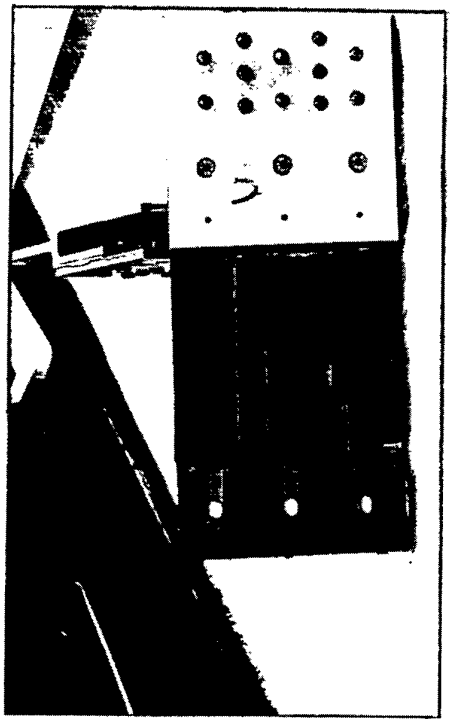


Fig. 18 Tested Specimen



ANALYSIS AND TEST RESULTS COMPARISON

First, a comparison is reported for hand calculations and FE analysis results.
For the adhesive thickness of 0.15 mm under pure elastic behaviour, very close values for load fluxes of 493 N/mm (hand calculation) and of 522 N/mm (FE analysis) have been found.
The same consideration can be made for the elasto-plastic behaviour for which load fluxes of 1083 N/mm (hand calculation) and of 953 N/mm (FE analysis) have been evaluated.
Then, good comparison is also obtained for the σpeel stresses.
The very slight differences between the two calculation methods are therefore a further confirmation of formulae validity for bonded joints preliminary evaluation.
For simply bolted joints, a strict similarity in load fluxes has been demonstrated between a dedicated software [RD3], i.e. (320 N/mm), and the FE analysis (380 N/mm).
For bonded/bolted joint the only evaluation has been carried out by means of FE analysis and a load flux of 1195 N/mm has been estimated so confirming the advantage of having both bonding and bolting w.r.t. simply bonding (953 N/mm) as a strength reserve for the joint.
Second, the comparison to the test results must be carefully evaluated, mainly due to the limited number of specimens.
In any case, it is possible to say that a fairly good correlation can be made as long as the adhesive behaves in the elastic way because, as previously said, its plastic behaviour is never developed due to a premature failure in composite skin.
For the just bonded option, the estimated load of about 500 N/mm (pure elastic) and the obtained results of 300 to 350 N/mm must be seen as the peeling/interlaminar shear effects on the resin which imposes a strong elastic behaviour on the glue.
For the just bolted option, the obtained result of 250 N/mm is comparable with the about 300 N/mm analytically evaluated.
Finally, the superimposition of glue and bolt increases the actual load capability significantly as demonstrated by calculations.

CONCLUSIONS

The results of the mechanical tests have demonstrated the suitability of the joint design. The measured properties have met the initial strength requirement, as the achieved values are above the acceptance limit.
However, the type of joint failure suggests some general considerations concerning design optimization and further studies could be dedicated to modifying doubler extension and thickness as well as to extend its tapering length for a better distribution of the load.
Changes in the design of external adherent free ends (such as tapering) could reduce peel stress concentration.
In any case, even considering that there is still enough room for improvement, the initially foreseen research objectives are considered achieved.

REFERENCES

[1] NASA CR-112236
Adhesive-Bonded Single-Lap Joint
L.J. Hart-Smith
[2] NASA CR-112235
Adhesive-Bonded Double-Lap Joint
L.J. Hart-Smith
[3] BOLT PROGRAM
University of Michigan
Fu-Kuo Chang, R.A.Scott, G.S. Springer

The Assembly of Thermoplastics by Adhesive Bonding: Process and Control.

J.LECOMTE
CRIF
Parc Scientifique de la Cense Rouge
rue Bois Saint-Jean, 12
4102 OUGREE-SERAING
BELGIQUE

1. ABSTRACT

Nowadays, the manufacturing techniques include more and more frequently the assembling of different materials, each dedicated to fulfil one or several requirements of the final assembly. Product designers are therefore induced to consider adhesive bonding of thermoplastic materials, either between themselves or to other materials. Adhesive bonding offers several advantages: weight reduction, better stress distribution in the joint, sealing and insulation,...

However, this type of assembly, especially when the adherents are thermoplastics, raises many questions about the performances in terms of mechanical resistance, durability, and also about the reliability and the control of the joints.

This presentation will consider the four design steps which are of primary importance for the conception of an assembly by adhesive bonding:

- **adhesive selection**: simple rules will be presented for the selection of the families of adhesives that will meet the requirements of the assembly. Additional qualification tests will be suggested, which will help refine and optimise the selection.

- **material behaviour**: the second part will show how the performance of the bonded joint are influenced by the properties of the adherent material, by the presence of additives like demoulding agents, fillers, plasticizers and stabilisers, by slight modifications in the formulation of the thermoplastics, and even by processing conditions during fabrication of the adherents.

- **surface treatment**: the third topic will be the importance of surface treatment before bonding, the parameters of which have to be carefully determined
in order to have good and reproducible performances.

- **overall joint shape**: Finally, the paper will address the problem of the overall design of the joint shape, which must be optimised by taking into account the various constraints applied to that assembly.

2. INTRODUCTION

Assembly techniques have evolved very much in those 20 last years, mainly in order to meet the requirements of more and more dedicated and sophisticated products, gathering the specifications for the design (shape, ergonomics), the mechanical performances, and the reliability. In all the sectors of the industry, new materials are joined together.

Thermoplastic materials are well known today for their ability to give rise to parts with complex shapes in one shot, by injection moulding mainly. But they often need to be joined to other materials to improve, in most of the cases, their mechanical performances (stiffness, static resistance,...) or their external aspect.

One of the most effective techniques, sometimes the only one, for the assembly of thermoplastic materials together or with other materials, is the adhesive bonding. However, a careful management of the process must be carried out, from the design of the bonded joint until the control of the process parameters, in order to insure the reliability and the durability of the assembly.

Paper presented at the 83rd Meeting of the AGARD SMP on "Bolted/Bonded Joints in Polymeric Composites", held in Florence, Italy, 2-3 September 1996, and published in CP-590.

3. ADHESIVE SELECTION: THE DIFFERENT TYPES OF ADHERENTS AND ADHESIVES.

Thermoplastic materials are a priori difficult to assemble by adhesive bonding. The main reason for this is the weakness of their surface energy, that prevents them from insuring a good wettability of the adhesive on the substrate. Some of them are particularly critical in this respect: PTFE's, the polyolefines, and, to some extent, the polyamides.

The first question to answer in the selection process of the adhesive system, is the functionality of the assembly.

3.1. Adhesive bonding of identical thermoplastic substrates.

When the assemble concerns two identical thermoplastic substrates, three solutions are to be taken into account at first:

- Design of a unique part. Injection moulding allows to realise complex parts and one of the most important advantages of this manufacturing technique is to reduce the number of components of an assembly. The decision to replace an adhesive bonding by the design of a unique part, will depend on:

- The cost of the modifications to bring to the mould, in terms of machining of the mould, and in production time.
- The size of the series
- The cost and time of surface preparation and bonding operations.

- Welding of the adherents. This is practicable by fusion of the materials, or by ultrasonic methods. The design of the joint must be adapted to the technique used.

- Adhesive bonding with solvent-based adhesives of the same polymer as the substrates. Some thermoplastics, like PVC, PMMA, polystyrene, polyamide, may be solved easily with adhesives containing the same polymer in solution. The upper layers of the substrates are dissolved, and when the solvent evaporates, the joint is similar to the result of a welding.

- Welding and solvent-based adhesive bonding have their drawbacks. One of the most important is the weakness of the joint in terms of mechanical resistance, due to stress cracking, and also to the fact that, with adherents made of filled thermoplastics, the material of the joint is not identical to the one of the substrates.

3.2. Adhesive bonding of different materials

When the two adherents are completely different, or when the former solutions did not give satisfactory results, it is necessary to find an adhesive compatible with the two substrates.

At this time, the overall functionality of the assembly must be defined, and a choice has to be made between:

- Adhesive bonding for positioning or tightness, that do not participate to the mechanical performances of the assembly.

- « Structural » adhesive bonding, that may be defined, in the case of thermoplastic adherents, as a bonding where the joint has a mechanical resistance at least as good as the substrate, for the constraints to which it will be submitted.

In the first case, the adhesive will be chosen between pressure sensitive tapes, mastics, elastomeric adhesives, hot melts, and the criteria will be the cost of the adhesives and of the application material, and the manufacturing parameters (cycle time, automation, pressure, temperature).

In the second case, the choice will probably be made between thermoset adhesives (epoxys, acrylates, polyurethanes). Between those adhesives, the best suited will be chosen by comparing the requirements of the assemble and the mechanical behaviour of the adhesive, in terms of static and dynamic stresses, temperature resistance, durability, flexibility.

As the most critical problems occur when dealing with structural bonding, only those assemblies will be considered in the following.

When the substrates have been carefully chosen, taking into account their intrinsic characteristics but also their ability to be bonded, some simple rules may be applied for the choice of one or two families of adhesives. From the analysis of the specifications sheet of

the assembly, it is easy to determine the most important of those specifications, what we will call « priority 1 » specifications.

Some examples of simple rules:

- If the assembly asks a very fast curing, if the joint is very thin, if the temperature and humidity in service are low and the loads are static, cyanoacrylates may be considered as a solution.

- If the assembly must receive very high static loads during a long time, epoxy resins will be a good choice.

- When the adherents are subjected to high decreases and increases in temperature, polyurethane may be the first choice.

Though it is possible, in each family of adhesives, to find special formulations who will decrease the weaknesses of the common adhesives of this family, it is better to select the family whose general properties will meet the « priority 1 » specifications.

The other specifications will help afterwards to choose two or three adhesives belonging to the selected family, or families. It is worthwhile that this final choice is assessed with the help of tests. Those tests will be performed on samples (standardised tests) or on the assembly itself when possible (tests in « real » situation).

4. THE BEHAVIOUR OF THE MATERIAL.

There is a huge variety of adhesives (between 2000 and 3000). There is also a great number of possible applications, in different sectors of the industry, for the adhesive bonding of thermoplastics. But the types of adherents offer also a big variety of chemical and physical properties.

It is therefore important to identify the determining factors leading to a constant quality in the behaviour of the joint, and to control those parameters throughout the manufacturing process. For the thermoplastic adherent itself, those parameters are numerous. The characteristics of the adherent, and therefore its ability to be bonded, depend on its composition and on its manufacturing parameters.

4.1. The components

Two thermoplastics from the same family, but coming from different manufacturers, may have different adherence properties: those materials contain different kinds of fillers and additives, and the manufacturers do not reveal the exact nature and ratios of all those additives:

- Internal demoulding agents are often added to injected thermoplastics, in order to allow an easy demoulding of the part from the mould. Those agents act by migration towards the surface of the part, and have therefore an harmful influence on the adherence performances of the substrate. This bad influence may grow with the time, if for example the assembly is submitted to high temperatures and if the adhesive is not able to prevent the migration of the demoulding agent.

- Antioxidants are added to thermoplastics to prevent fast ageing of the materials. Those antioxidants react with the free radicals generated by the UV rays. However, this oxidation is sometimes needed to increase the surface energy, and so the adherence properties, of the material.

- Fillers are mixed to the material to decrease its price and modify its physical (mechanical, electrical, optical,...) properties. The fillers will generally have an influence on the adherence properties of the material. This influence is often beneficial.

- Plastifiers and stabilisers, added to the plastics to improve their impact behaviour, are also subject to migration towards the surface, which becomes fat and oily. This happens mainly with polyolefines and with the materials that are manufactured at high temperatures.

The polymers themselves, even belonging to the same family, may have different chemical compositions. Let us consider for example, the different kinds of polyamides (PA 6, PA 66, PA 12,...). Their mechanical characteristics (Young modulus, stiffness, flexibility, surface energy) may differ very much from one to another. The surface energy differs from one polyamide to another, depending also, as we have previously seen, on their contents in additives. Consequently,

the ability of those plastics to be bonded, differ very much.

Some thermoplastics like ABS or SAN, are copolymers, or alloys of different polymers. The control of the ratio of the different polymers allows to control the mechanical properties, the surface appearance, the chemical characteristics (resistance to chemical agents, ageing) of the final copolymer. Necessarily, variations in the ratios will influence the adherence properties.

In conclusion, if the adherence of one substrate, with a given composition, is well known and characterised with one type of adhesive, it is really essential that the chemical composition, the contents in additives, fillers, and eventually reinforcing materials is strictly controlled and guaranteed by the supplier. When modified, the material must be tested again with adherence tests or surface energy measurements. But the variations in the composition of the material must also be combined with the processing conditions.

4.2. The processing conditions

The manufacturing conditions of the plastic parts have also a strong influence on the physical properties, the surface state and therefore the adherence properties, of the material.

When modifying the temperature, pressure, injection speed in the injection moulding process, for example, the following properties of the substrate may change:

- The crystallinity ratio, and the size of the crystallites will change, influencing the possibilities of migration of certain additives to the surface.
- The molecular chains will be more or less oriented, depending of the flow orientation during the injection stage.
- Shrinkage phenomena will be more or less important, depending on the injection parameters. With the shrinkage, the flatness of the surface to be bonded, and therefore the thickness of the joint, may be affected.
- Depending on the processing conditions, some polymers (polyamide, PET) will tend to absorb water and to swell, inducing internal stresses in the joint.

We can see that if the assembly is critical, that is, if the mechanical performances must be well known and controlled, or if the durability of the assembly must be guaranteed, it is important, not only to control the assembly process itself, but also the manufacturing process of the thermoplastic components.

This is not always possible to do. In many cases, however, a suitable surface treatment will bring the material in a state where the most significant variations in the manufacturing processes will be rubbed out.

5. THE SURFACE TREATMENTS.

At the light of the former chapter, the aim of the surface treatment of the thermoplastics, may be described as a double aim:

- To get as much as possible a reproducible state for the substrates surface,
- To optimise the adherence properties by increasing the surface energy.

We will distinguish three types of pre-treatments:

- The surface preparation (degreasing)
- The mechanical treatments (grinding, blasting)
- The physical pre-treatments (flame, plasma, CORONA)

The first operation (degreasing with solvents) is always required, mainly in order to achieve the first aim (reproducible results). This will remove dust and oils, demoulding agents and, to a certain extent, the additives that had moved towards the surface of the substrate. However, this treatment does not have any influence on the adhesive strengths of the substrate, and gives rise to environmental problems.

The second operation (grinding or blasting) is not required with thermoplastic substrates, and gives good results only if the demoulding agents may not be removed by degreasing. the improvement of the surface roughness does not improve the adherence properties of the material.

5.1. Physical pre-treatments

Physical pre-treatments are required for the substrates with a weak surface energy. The aim of this surface treatment is to increase the polar part of the surface energy. This is obtained by an oxidation of the surface. The three available treatments for this are CORONA, plasma and flame treatment.

The benefits and drawbacks of those treatments have been described by several authors, and each treatment has its supporters and its opponents. When applied properly, each of those pre-treatments improves the adherence properties of the substrates. To summarise, CORONA treatment is mainly applicable for the pre-treatment of plastic films, the flame treatment is efficient when the surface to be treated is not too complex, and plasma treatment is applicable to complex shapes, but is a batch process that takes a lot of time.

For each of these treatments, a careful setting and control of the treatment parameters is requested. For the plasma treatment, for example, the use of common values for the parameters (pressure, time and intensity of the treatment), will give adherence strengths on substrates like polyolefines which do not have any adherence strength without a treatment, but a thorough tuning of those parameters, varying with the type of plasma chamber, the type of substrate and the gas used for the plasma, will increase the adherence strengths by a factor of two or three!

The flame treatment has been criticised, namely for its lack of precision and the bad reproducibility of the results. But if the composition of the flame and the distance between the surface and the flame are constant and well controlled, and if the substrates passes at least two times in the flame, the increase in the adherence strengths are even better than with the plasma treatment, and the variation in the results, when measuring the adherence strengths, may be less than 5%.

For an industrial process, the flame treatment is well suited if the surface to be treated is simple, so that the distance between the flame and each point of the surface to be treated is always the same. The process must be automated and is very fast.

Following the conditions of process, the type of substrate and the type of treatment, the thickness of the treated layer on the surface will be different. The durability of the treatment, that will drive the time between the pre-treatment and the bonding operation, will depend on the type of substrate and the thickness of the treated layer.

If the intensity of the treatment is too low, the layer is too thin and not homogeneous. If the intensity of the treatment is too high, the surface energy of the upper layers is very high, but those layers are damaged, and the cohesive strengths between these layers and the bulk material are lowered.

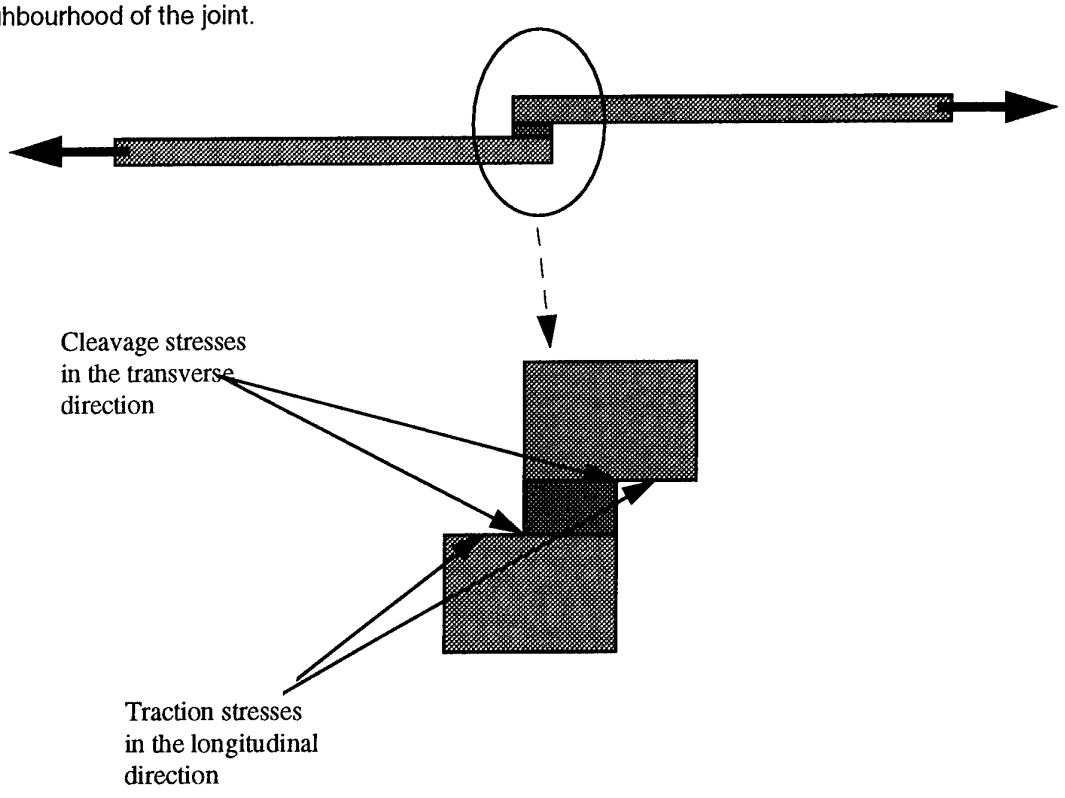
6. DIMENSIONING OF THE JOINT.

One of the main advantages of the adhesive bonding on the other methods of assembly, is the better distribution of the constraints throughout the joint. This is only true when the joint has been well designed. Amongst the static loads to which the joint is submitted (cleavage, pealing, compression, traction, shear), only shear strengths guarantee that the distribution of the constraints throughout the joint is almost uniform.

The joint will therefore be designed to be mostly constrained in the shear direction. Even in those conditions, and particularly with the thermoplastic substrates, who have rather poor mechanical resistance, the bonded joint itself may introduce secondary constraints, and weaken the substrate in the neighbourhood of the joint.

Let us consider the single lap shear test, where the shear stresses are obtained by traction on the two substrates. The non symmetric character of the joint induces flexion constraints in the neighbourhood of the joint. Those localised constraints cause the substrate to break for values of the traction strengths notably lower than the traction strength needed to break a traction test piece of the same thermoplastic.

In fact, the introduction of a discontinuity in the material, like a bonded joint stiffer than the material itself, causes parasitic strengths weakening the substrate.



7. CONCLUSION.

The structural adhesive bonding of thermoplastic substrates asks to know very well, not only the mechanical behaviour of the cured adhesive, but also the characteristics of the substrate and even the history of its manufacturing process. This will come to the design of a high performances and high durability bonded joint. The adhesive suppliers set up new adhesives, more and more dedicated to specific applications and specific substrates, but in each case, the design of the joint must integrate and take into account all the parameters described before. Adhesive bonding must not be considered as an alternative to another solution, or a repairing technique, but as one part of the product, taken into account in all the stages of the design and manufacturing operations, from the choice of the basic adherents to the application of the adhesive.

8. BIBLIOGRAPHY :

Les colles et adhésifs et leurs emplois industriels, *J.J.Meynis de Paulin et Ph.Cognard,* Editions Le Prat.

Analysis and Design Data for Adhesively Bonded Joints, *J.P.Jeandreau,* Int.J.Adhesion and Adhesives, Vol.11, N°2, April 1991

Recherche sur la théorie des assemblages collés, *O.Volkersen,* Constructions mécaniques, n°4, 1965, pp3-13.

Structural Adhesive Joints in Engineering, *R.D.Adams & W.C.Wake,* Elsevier applied science publisher, 1986.

Adhesion and Adhesives - Science and Technology, *A.J.Kinloch,* Chapman and Hall, London, 1987

Surface preparation of Plastics (COMETT/FORMACOL module)

Concevoir les collages, *D.Benazet,* Assemblages n°127, 1991.

Adhesive Bonding (Ed. Lieng-Huang Lee, 1991)

Handbook of Adhesives, Irving Skeist Ed., 1977

Flame Treatment for Adhesive Bonding of Polypropylene: the Influence of Filling Content and Storage Conditions, *F.Demblon,* Proceedings of JADH'94.

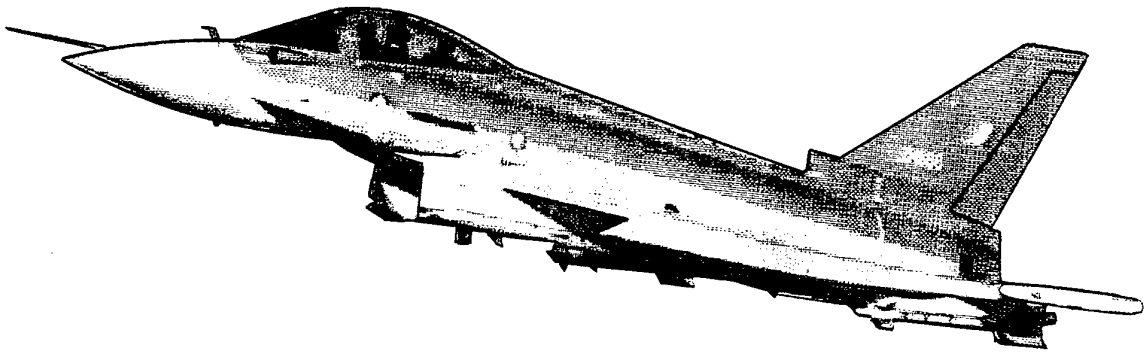
Plasma Surface Modification and Plasma Polymerisation, *N.Inagaki,* Technomic publishing Company, 1996.

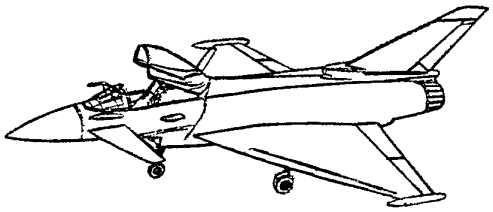
Plasma Treatment for Improved Bonding: a Review, *Edward T.Liston,* J.Adhesion 1989, Vol.30, pp 199-218)

DESIGN LOADS FOR BONDED AND BOLTED JOINTS

M. J. Broome BSc CEng MRINA

Warton Structures Department - 3rd September 1996





EF 2000

Paper presented at the 83rd Meeting of the AGARD SMP on "Bolted/Bonded Joints in Polymeric Composites", held in Florence, Italy, 2-3 September 1996, and published in CP-590.

DESIGN LOADS FOR BONDED AND BOLTED JOINTS

Section 1

NON-LINEAR LOADS IN THE BONDED RAMP REGIONS OF HONEYCOMB SANDWICH PANELS

Section 2

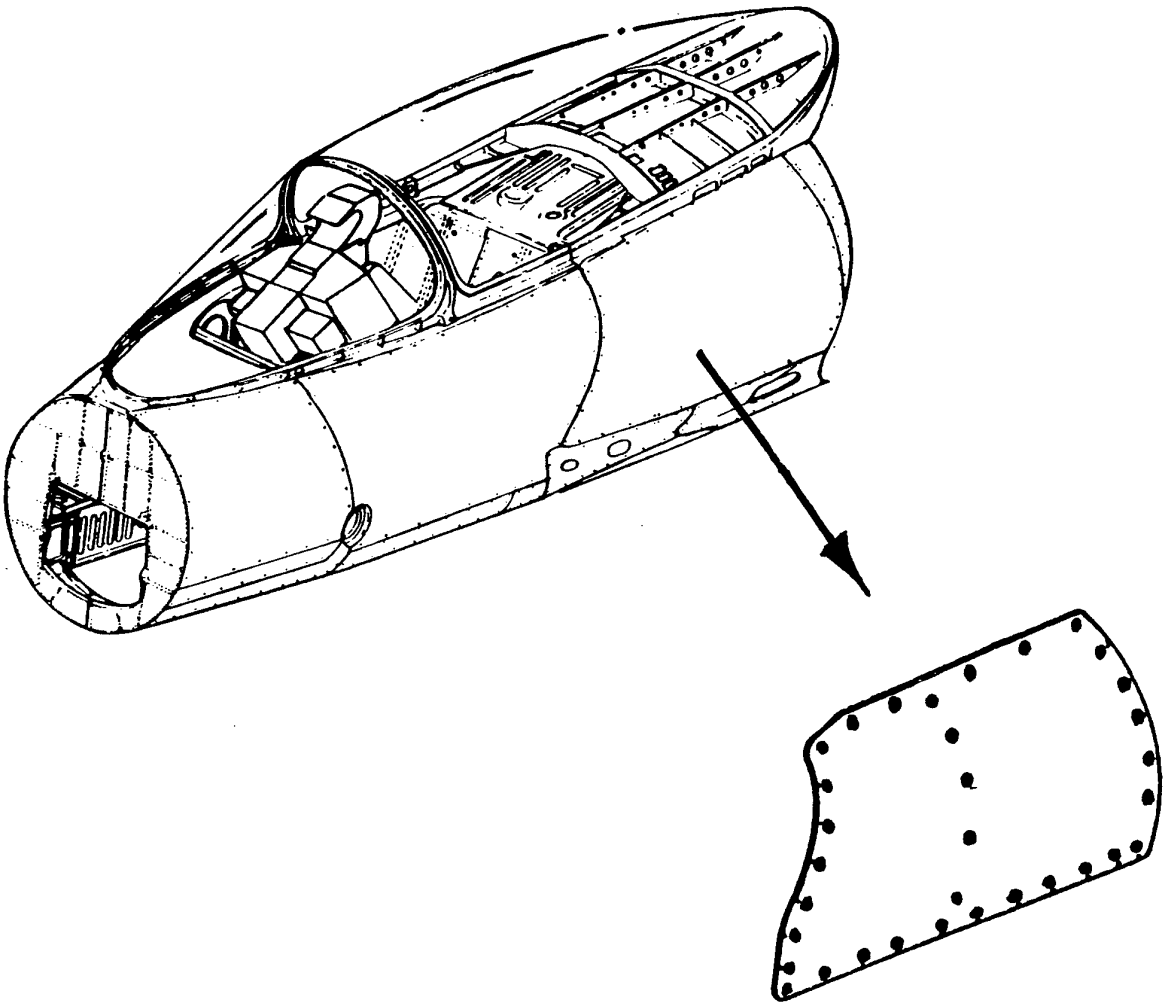
BOLT LOADS IN STATICALLY INDETERMINATE STRUCTURES

EF2000 AVIONICS BAY

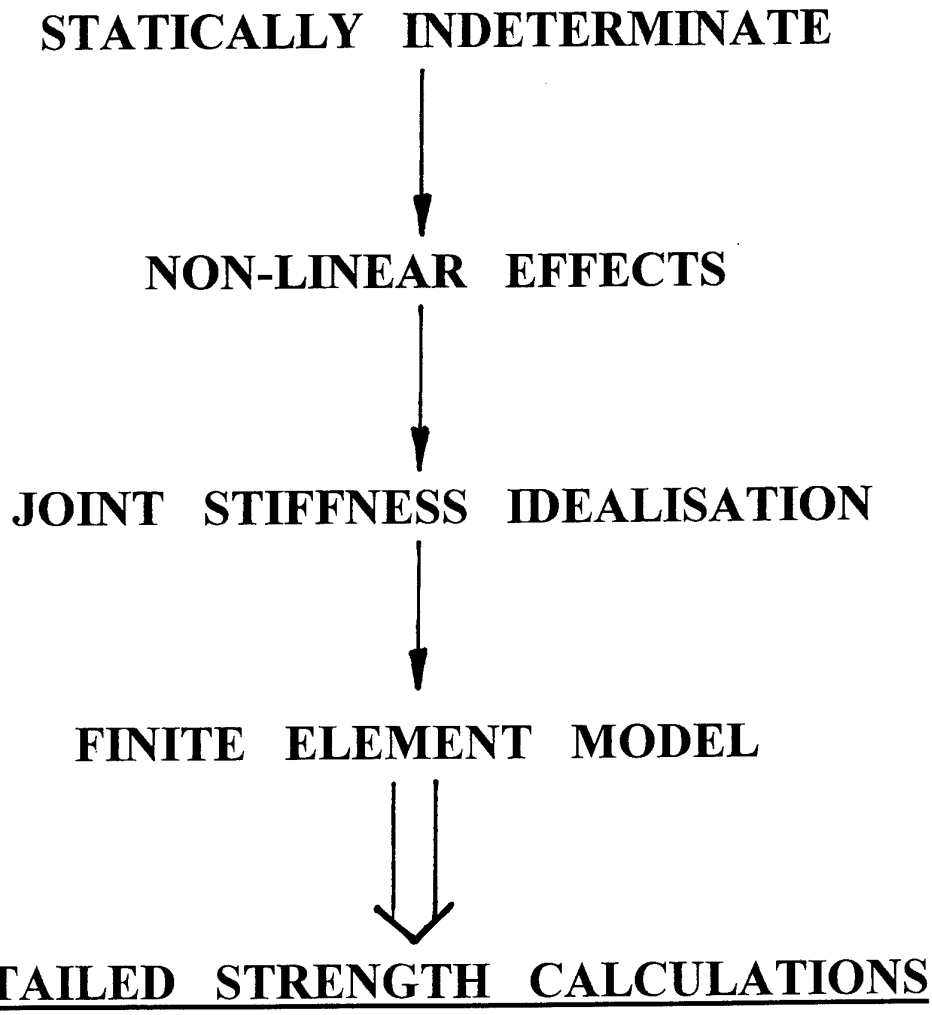
ACCESS DOOR

HONEYCOMB CONSTRUCTION

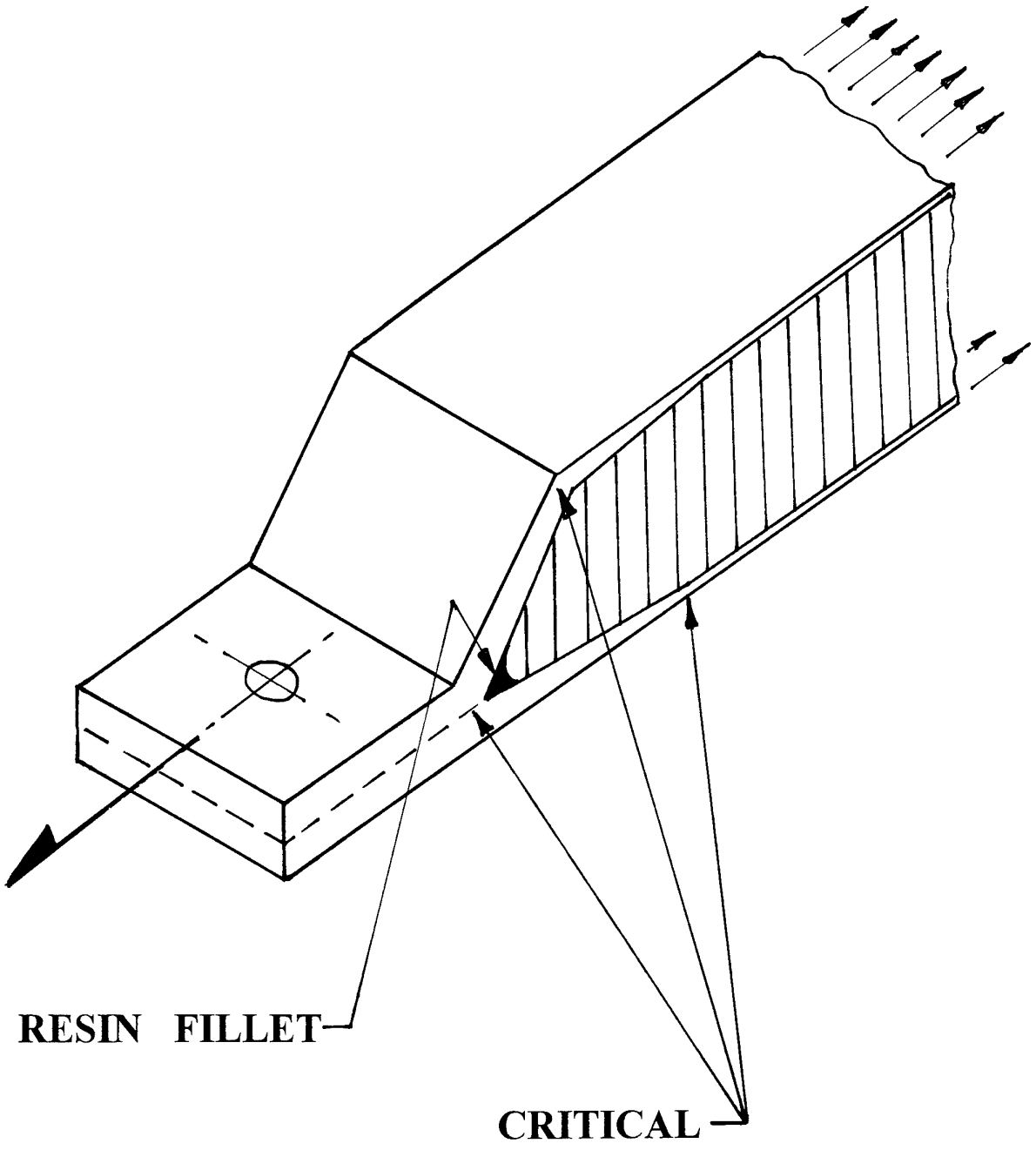
BOLTED JOINTS (WIDE FASTENER PITCH)



BOND AND BOLT LOADS IN STATICALLY INDETERMINATE STRUCTURES



CRITICAL RAMP REGIONS



NON-LINEAR LOADS IN HONEYCOMB PANEL RAMPS

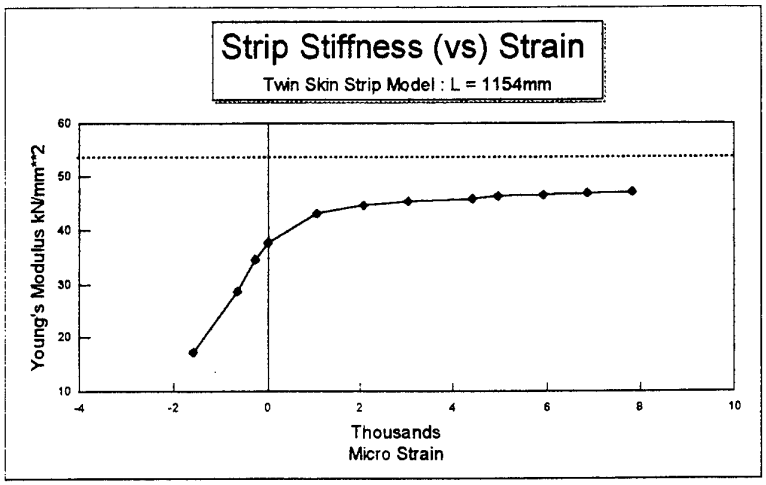
1. ACCURATE APPLIED FORCES AND MOMENTS ARE REQUIRED BEFORE ANY STRESS CALCULATIONS CAN BE DONE.

2. ASYMMETRIC HONEYCOMB PANEL SKIN LOADS ARE NON-LINEAR FOR END LOADING.

3. BAe IS DEVELOPING A METHOD OF CALCULATING THE STRENGTH OF THE CRITICAL RAMP REGIONS.

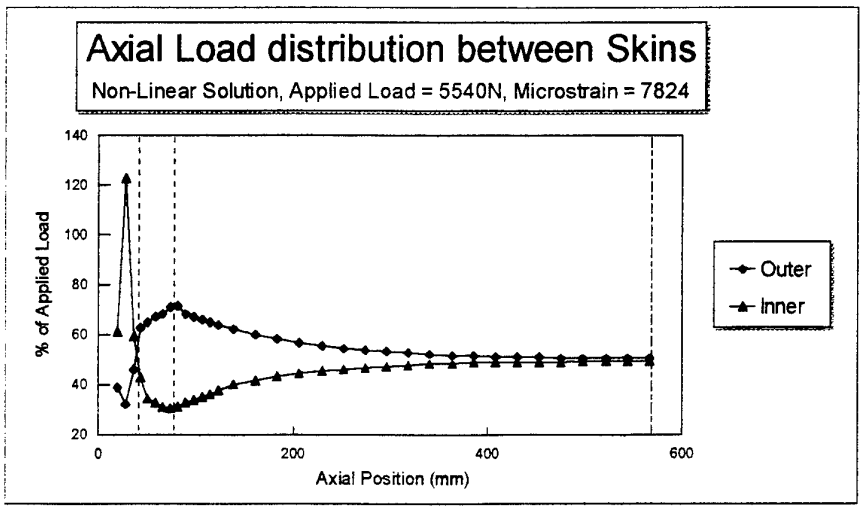
OVERALL END-LOAD NON-LINEARITY

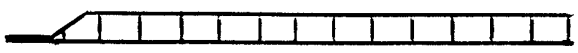
(TOTAL PANEL)



RAMP NON-LINEAR END-LOAD

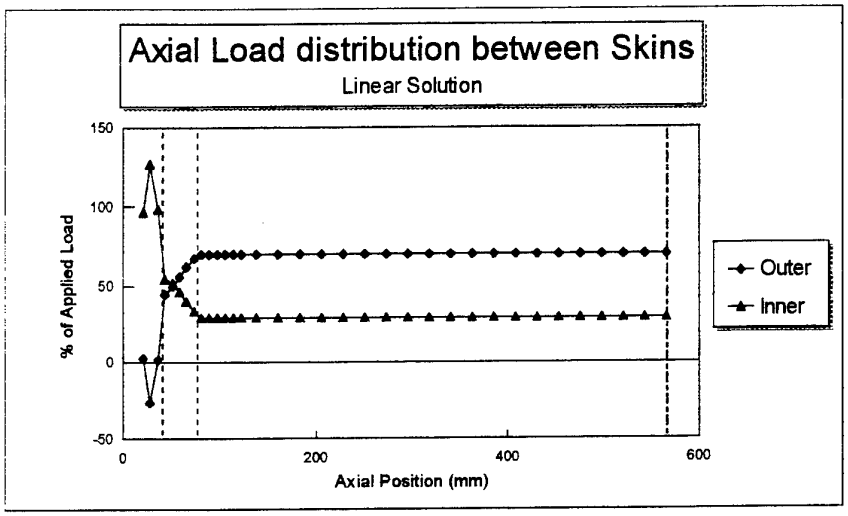
DISTRIBUTION BETWEEN SKINS

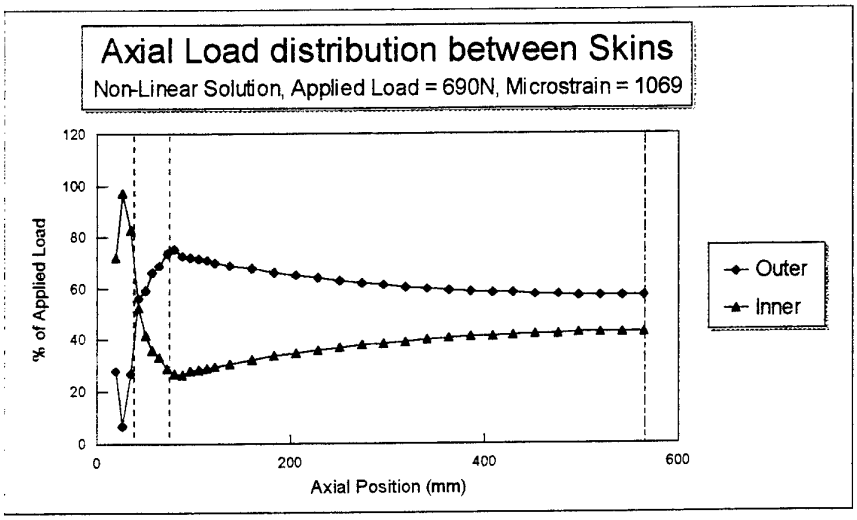


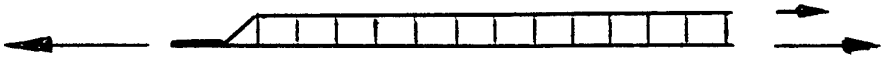


COMPARISON OF SKIN LOADS

LINEAR AND NON-LINEAR ANALYSIS







SUMMARY OF NON-LINEARITY

1. THE ASYMMETRY OF THE PANELS SHOULD BE CORRECTLY MODELLED TO HAVE THE CORRECT END-LOAD STIFFNESS.

2. OVERALL END-LOAD NON-LINEARITY OF A COMPLETE PANEL IS SMALL AT TYPICAL AIRCRAFT STRAIN LEVELS.

3. LOCAL NON-LINEAR EFFECTS CAN BE QUITE LARGE AND SHOULD BE CONSIDERED.

SHEAR IDEALISATION

$$G_{12\ \text{Effective}} / G_{12} = \frac{1}{1 + n P^2 G_{12} T / (K a b)}$$

G_{12} = shear modulus of panel

(Effective means panel + bolts)

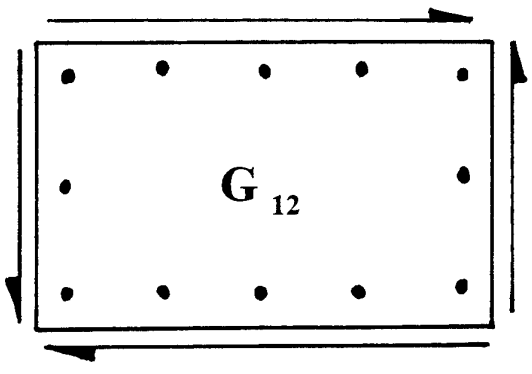
n = number of fasteners

P = fastener pitch

T = panel thickness

a = panel length

b = panel width



END LOAD IDEALISATION

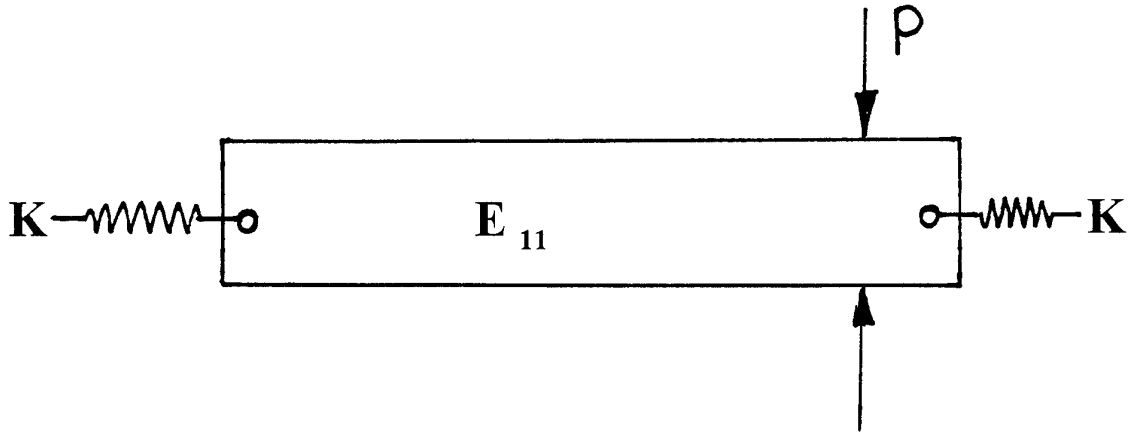
$$E_{11\ \text{Effective}} = \frac{1}{1 / E_{11} + 2 P T / (a K)}$$

E_{11} = end load modulus of panel

(Effective = panel + bolts)

P = fastener pitch

Other terms as above



SHEAR AND END LOAD STIFFNESS

(MATRIX FORMAT)

$$M_{Modified} = 1/T \cdot [F/T + B]^{-1}$$

$M_{Modified}$ = Reduced in-plane stiffness matrix

(NASTRAN MAT2 CARD)

T = Thickness F = In-plane flexibility matrix

B = diagonal bolt flexibility matrix

$$B = \begin{bmatrix} \frac{2b}{nKa} & 0 & 0 \\ 0 & \frac{2a}{mKb} & 0 \\ 0 & 0 & \frac{2b}{nKa} + \frac{2a}{mKb} \end{bmatrix}$$

CONCLUSIONS

1. DETAILED STRESS CALCULATION METHODS FOR BONDED AND BOLTED JOINTS REQUIRE THE INPUT OF ACCURATE LOADS.

2. THE OVERALL STIFFNESS OF HONEYCOMB PANELS AND BOLTED JOINTS MUST BE CORRECTLY REPRESENTED IN FE MODELS.

3. LOCAL NON-LINEAR EFFECTS SHOULD BE CONSIDERED IN HONEYCOMB PANEL RAMPS.

TILTROTOR TRANSPORT BONDED WING DESIGN SUMMARY

Robert V. Dompka
Structures Research and Development
Bell Helicopter Textron, Inc.
Fort Worth, TX 76101-0482, USA

Richard C. Holzwarth
Structures Design Development Branch, Flight Dynamics Directorate
USAF Wright Laboratory
WPAFB, OH 45433-6553, USA

SUMMARY

This paper presents the results of research and development activities conducted under Air Force contract by Bell Helicopter Textron, Inc. (Bell) to apply advanced design and manufacturing technology to reduce production costs of a composite tiltrotor transport vehicle wing. Strength, stiffness, and weight requirements dictated the utilization of advanced composites. This paper will provide a description of the effects of these requirements on wing torque box design and the analysis used to size major structural components and joints. Component verification test results are provided to support the design decisions and validate the analyses and structural integrity. Future plans are presented for a full-scale torque box structural test as demonstration of the viability of the final design.

INTRODUCTION

The Design and Manufacture of Low Cost Composites (DMLCC) program is jointly funded and managed by the USAF Wright Laboratory Manufacturing Technology and Flight Dynamics Directorates. The objective of this effort is to identify, develop, and demonstrate through manufacture and test new structural design concepts and manufacturing processes that will significantly reduce the acquisition cost of advanced composite structures. The goal of the program is to demonstrate that the application of these processes through effective design can reduce the manufactured cost of advanced composite structures by 50% relative to current advanced composite structure technology, and simultaneously reduce the support cost by 25%. The DMLCC – Bonded Wing (DMLCC–BW) contract with Bell is one of these programs. The cost and performance baseline from which progress is measured is the wing torque box from the Full-Scale Development version of the V–22 tiltrotor aircraft. A new wing torque box structure, matching the existing loft line and accounting for all system integration requirements, was designed under this program. The design exploits several high-risk/high-payoff technologies that have potential to both increase performance and reduce cost for a wide range of future aircraft. Unique features of the design include (1) a relatively soft all-bias-ply skin, (2) application of high-stiffness pultruded carbon rods to wing skin stiffeners, (3) bonding of fabric-based RTM rib chords to these stiffeners and skins, and (4) thermoplastic rib shear webs with bonded-on thermoplastic stiffeners. The application of these technologies is described in further detail within this paper.

The DMLCC–BW program was initiated in 1991. It was established as a three-phase effort, planned and executed around a building-block approach:

- Phase I – Advanced wing design, and element and coupon level tests.
- Phase II – Manufacturing process demonstration through production of subcomponents and engineering verification through test of those articles.
- Phase III – Manufacture of two full-scale wing box technology demonstration articles. Currently, these demonstration articles are being modified to prepare for static, durability, damage tolerance, and survivability testing. These tests will be conducted by the USAF Structures Test Branch at Wright Laboratory, with assistance from the contractor, Bell.

All three phases are described within this paper.

Demonstration of low cost and structurally effective bonding processes was critical to the success of the DMLCC–BW program. The baseline structure cost analysis indicated that fabrication of small composite parts was a very prominent contributor to the final manufactured cost. Additionally, the assembly of these numerous small details was a significant contributor to the total assembly cost of the structure. Therefore, recurring cost was dominated by small parts. A driver in the DMLCC–BW approach was to eliminate these small parts through designs that maximized "structural unitization" within the constraints of subsystem integration and required structural performance. Although cocured wing skins were identified early as high payoff, it was also recognized early in the program that adhesive bonding was required in order to achieve the desired structural unitization without the tooling cost or manufacturing complexities of a fully cocured wing box.

Paper presented at the 83rd Meeting of the AGARD SMP on "Bolted/Bonded Joints in Polymeric Composites", held in Florence, Italy, 2-3 September 1996, and published in CP-590.

DESCRIPTION OF DMLCC BONDED WING DEMONSTRATION ARTICLE

The structural concepts and cost benefits identified in the DMLCC–BW program are being demonstrated through the fabrication and testing of two wing torque box demonstration articles. The demonstration articles represent a full-scale section of the DMLCC-BW wing, designed to meet all V–22 mission performance requirements, but also designed to utilize low-cost manufacturing processes identified within the DMLCC–BW program. The demonstration articles are a constant cross section, located outboard of the sweep/dihedral break, but inboard of the wingtip feed tank (Fig. 1). This allows the DMLCC demonstration articles to capture all of the critical technology features and provide high-fidelity representation of the manufacturing process. The design approach for the DMLCC–BW program was to simplify fabrication by minimizing tooling aids and to reduce assembly by designing large cocured structure, while meeting all structural requirements of the baseline concept.

The demonstration articles are a five-rib, four-bay section having the correct aerodynamic contours. Upper and lower wing skins are "soft" laminates, essentially all ±45-degree plies fabricated using an automated tape-laying machine. Hat-shaped wing skin stiffeners, containing pultruded rod packs, run continuously from tip to tip, with five stiffeners on the top skin, four on the bottom. The bottom skin panel contains an access door representative of access doors on the baseline aircraft. The unique pultruded rod-reinforced wing skin stiffeners and the forward and rear spar caps are manufactured using the layer of rods machine (developed by Bell) and are integral (by means of cocuring) with the wing skins. The wing rib upper and lower chords are fabricated using a resin transfer molding (RTM) process and are adhesively bonded to the upper and lower wing skin and skin stiffeners. The rib shear webs are fabricated separately using a combination of thermoplastic compaction with bonded-on stiffeners fabricated from the same material. The spars are essentially flat shear webs stiffened to resist buckling. The web section is fabricated using the tape-laying machine; the separately fabricated spar stiffeners are cocured to the webs.

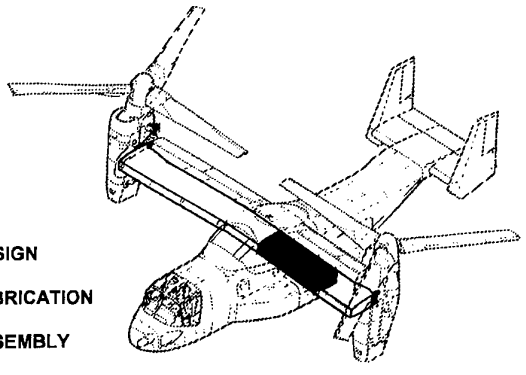


Fig. 1. Tiltrotor showing location of demonstration box.

The assembly concept consists of locating the upper and lower skin/rib chord segments in place and mechanically attaching the rib shear webs to the rib chords. The spars are then mechanically fastened to the spar web attach flanges integral to the upper and lower skins and the rib shear webs. The installation of access doors, which are a structural part of the rib shear webs, completes the assembly of the structure. The full-span DMLCC bonded wing would be manufactured in the same manner as the demonstration article.

TORQUE BOX DESIGN

The basic design concept is a straightforward beam and shear panel design. Almost all webs are shear resistant to ultimate load. The wing skin and web areas are soft, made from bias plies only, and carry the majority of shear loads. The stringers and spar caps are made predominantly with zero-degree material and carry axial compressive and transverse loading. The load-carrying portion of the wing is a semi-monocoque single-cell thin-walled section with the forward spar at 5% chord and the aft spar at the 50% chord location. The wing consists of five large cocured components: the upper and lower skins, the front and rear spars, and the ribs (Fig. 2). The overall loads and geometry were taken directly from V–22 tiltrotor design, which already addresses fail-safe design features. The overall bending at the tip had to meet the proprotor stability requirements and overall tip deflection of the original design. Torsional and chordwise bending stiffness matched the original design. No strain allowables were assumed to start this design. Strains were calculated based on the material required to fulfill constant bending stiffness requirements. The constant bending stiffness feature created a requirement for a 30% increase in strength at the inboard section of the wing, where the design becomes strength critical instead of stiffness critical (see Fig. 3).

WING SKINS

The wing skins are made from IM7/E7T1-2 prepreg tape. This is a toughened resin system. The integral hat stiffeners are made from the same graphite material with precured carbon-epoxy rods and syntactic resin core interleaved to provide axial load-carrying capability. The rods consist of carbon fibers, which remain straight during the curing process and provide minimal fiber waviness to increase compression carrying capabilities (see Ref. 1). The stringer taper angles were sized based on tooling requirements, which enabled the rib shear ties to fit up in one step during

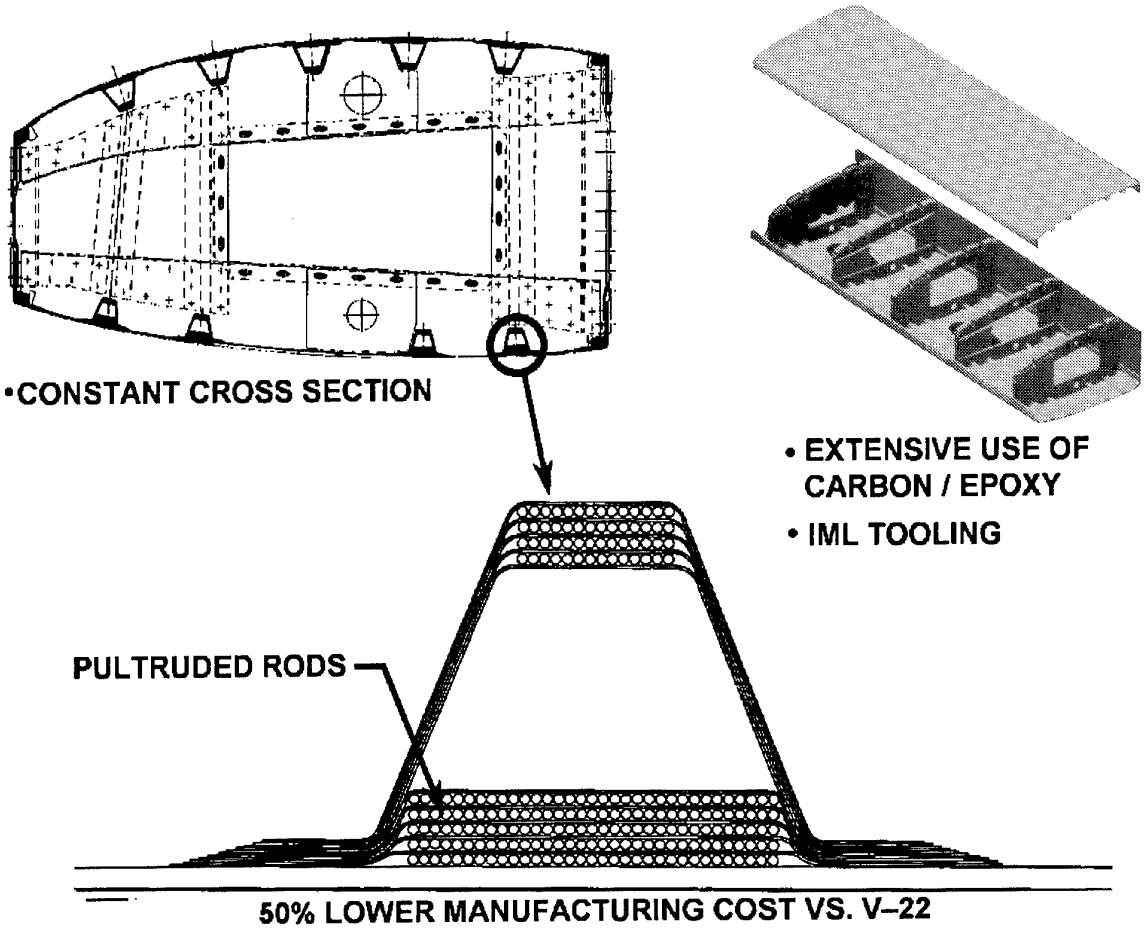


Fig. 2. Exploded view of torque box, showing hats and rods, bondline, and exploded view of rib.

assembly. On the lower skin, the middle stringer was eliminated from access hole bays and skin pad-ups were added to the tooled surface. The access holes enable installation of fuel bags and maintenance for this dry wing design. The skins have a unique design in that the soft skins are entirely made up of bias plies. The axial load is focused into the hat stringers. Other unique features are the damage tolerance of the design, the skin/rib/hat all-bias ply interfaces, and the higher compression capability of the stringers. This system of precured rods, the toughened resin system, and the all-bias skin provided the inherent damage-tolerance needed for the requisite 30% increase in strength due to the simplified cross section. This increase in damage tolerance has been demonstrated by component tests.

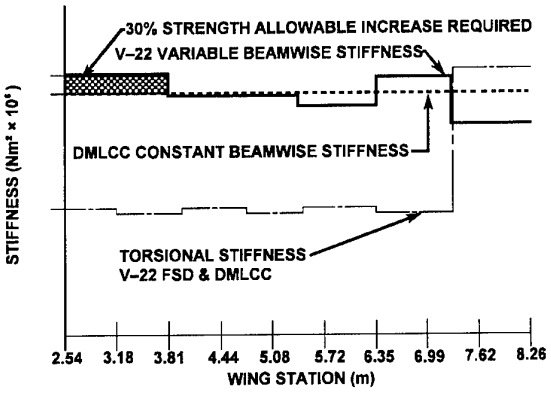


Fig. 3. Bending stiffness vs. wing station.

Assembly and cost considerations drove the need to minimize the use of fasteners. No fasteners were used in the skins on aerodynamic surfaces. The only fasteners in the skins were at the spar web-to-skin interfaces. The leading-edge (LE) and trailing-edge (TE) attach features were incorporated into integral flanges by splitting the skin plies fore and aft between the flange, which is perpendicular to the skin for spar attachment, and a horizontal piece for LE/TE attachment. An angle that matched the flange and overhang portions was produced separately to enable the closeout features of the wing to be attached.

The maximum skin strain requirements called for -4,500 microinch/inch (μin/in) (–4,500 micro-millimeter/millimeter [μmm/mm]) in compression and 5,000 μin/in (5,000 μmm/mm) in tension. The tiltrotor

environment provides a highly reversible load requirement. The lower skin is predominately in tension and the upper skin in compression, but each skin sees up to 80% reverse load during certain maneuvers. Analysis of the skins consisted of standard column buckling, shear panel buckling under combined shear and compression loads, and point-stress analysis using an open-hole compression allowable. A global finite-element model (FEM) using ANSYS was made (see Fig. 4) to determine the internal load distributions of each portion of the structure. Critical aerodynamic, fuel, and mechanical loads from the tiltrotor pylons were applied for a series of maneuvers to establish the critical load conditions for various parts of the structure. These loads were then transferred to in-house programs based on classical lamination theory to determine the local margins of safety for structural details.

SPAR DESIGN DETAILS

The spars were fabricated using IM7/E7T1-2 tape. Both the front and rear spars are flat laminates consisting mainly of bias plies. They attach to the integral flanges of the skin. No shear buckling is allowed below ultimate load. Various portions of the spar are sized by fail safe, flight maneuver, jacking, and tiedown design features in progression from root to tip. Based on the analysis, strains are not critical, because 16 bias plies are required in the web for torsional stiffness requirements. Panel breakers were located to maintain buckling stability to ultimate load. Rib-to-spar joints were sized to resist bending due to a local joggle and interrivet buckling. Both spars have zero-degree tape added at the upper and lower skin attachment locations to meet local bending stiffness requirements. At system penetrations, four-ply padups were added to prevent buckling. Local details including stiffener spacing and systems penetrations were analyzed using local and interrivet buckling analysis.

RIB DESIGN DETAILS

The ribs were sized for skin pulloff loads determined from the ANSYS FEM to resist aerodynamic, fuel pressure, and hydraulic ram considerations. Local areas between stiffeners were sized for plate buckling and shear resistant stability to ultimate load. Laminate strain for an open-hole compression condition sized the part to .1 inch (2.54 mm) thickness.

ASSESSMENT OF STRUCTURAL DESIGN/ INTEGRITY

Analysis and Test

Determination of shear load transfer, tension and compression load carrying capability, effects of low-speed impact damage, environmental effects, and fatigue life were investigated through limited design support tests. A building block approach of coupon, component, and subelement test specimens was used as tooling became available commensurate with program development. The tests are depicted graphically in Fig. 5 and the results summarized in Table 1. Each of the tests were correlated with analysis used to size wing components or joints as described below.

Towards a Bonded Wing

Two primary load-carrying joints, the integral hat section wing stringer cocured interface and the rib-chord-to-skin interface, rely solely on resin or adhesive to transfer the load. No fasteners were used in these joints, which alleviated the time-consuming and costly processes of drilling countersunk holes in composites, and avoided the stress concentrations associated with fastener holes.

Skin-to-stringer interface (cocured joint)

There are several key questions which analysis had to answer. First, is the skin-to-stringer joint going to be the weak link in a compression after impact scenario? This is the critical design feature for most of the wing skin area. Second, does the bias ply transfer the loads to the axial load members, the rods, efficiently enough to develop the full axial capabilities of the rods? The ramifications of these issues are addressed in Refs. 2 and 3. Although there is no adhesive between the skin and stringers, this interface experiences significant load transfer and the laminating resin acts as the attachment feature. This joint posed some unique

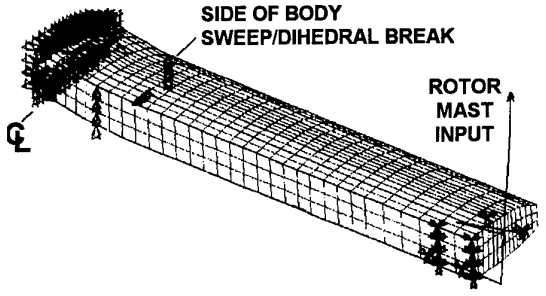


Fig. 4. Wing ANSYS finite-element model.

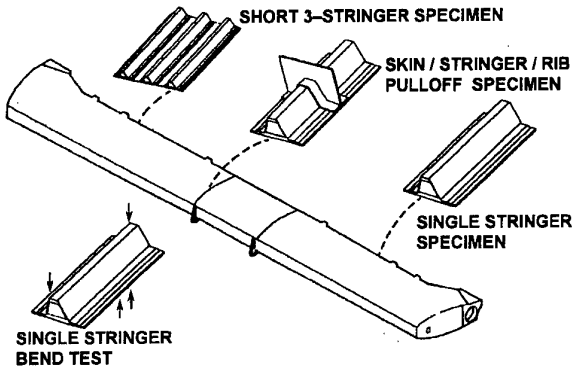


Fig. 5. Structural test elements.

Table 1. DMLCC – BW test results.

A. Single stringer compression.

Configuration	Load (N)	Measured strain (μmm/mm)	Rod stress (MPa)	Comments
No damage	613,824	–7,800	1,130	Skin buckled
Impact at edge	684,992	–8,200	1,365	Skin buckeld
Impact at center	636,064	–7,400	1,220	Skin buckled
1/4-inch holes in WE	658,304	–8,200	1,213	Skin buckled
Average	640,512	–7,900	1,200	

–6,700 microstrain (μmm/mm) desired.
Adequate margin achieved to account for scatter and environmental effects.

B. Single stringer bending.

Test type	Damage	Load (N)	Strain (μmm/mm) Tension	Strain (μmm/mm) Com-pression	Cycles	Com-ments
Static	None	124,988	14,800	–8,300	–	Tension in cap
Fatigue	None	44,480	5,500	–2,500	1,000,000	No failure
Residual strength		116,982	13,800	–7,200	–	Tension in cap
Fatigue	None	44,480	5,500	–2,800	500,000	No failure
Fatigue	1,327 J and a scratch	44,480	5,500	–2,800	500,000	No damage growth

No significant loss of residual strength at 1 million cycles design ultimate load.
No damage growth for barely visible impact damage (BVID) or scratch.

C. Rib-to-skin joint pulloff.

Rib chord type	Test type	Environmental conditions	Failure load (N)	Failure mode
TS	Static	Cold dry	44,480	Tension in rib chord
TS	Static	Room temp	46,259	Tension in rib chord
TS	Static	Hot wet	51,152	Tension in rib chord
RTM	Static	3 cold dry	41,366	Tension in rib chord
RTM	Static	3 room temp	41,144	Tension in rib chord
RTM	Static	2 hot wet	36,648	Tension in rib chord
RTM	Fatigue	1 hot wet	24,464	Bondline

Design ultimate load = 19,282 N
TS = thermoset
RTM = resin transfer molded

D. 3-stringer compression panels.

Panel No.	Design	Impact energy (J)	Environmental conditions	Failure load (kN)	Calculated linear failure strain (μmm/mm)
1	Baseline	2,212	Room temp	1,869	6,720
2	Baseline	2,212	Room temp	1,623	5,840
3, 4	Baseline	2,212	Hot wet	1,531	5,510
5	Baseline	10,617	Room temp	1,242	4,470*
6	90 plies	1,327	Room temp	1,978	7,115
7	Z spikes	2,212	Room temp	1,835	6,600

Design ultimate load = 1,252 kN
Design ultimate strain = 4,500 μmm/mm
*Compare to 1.3 limit = 3,900 μmm/mm due to impact energy

challenges to classical FEM plate elements due to the thickness of the rod packs and planks. Some issues also arise when considering the conventional approach to generating allowables for the rod packs themselves. Ref. 3 provides discussion of material allowables generation. An in-depth study of the stringer-to-skin interface (Ref. 2, Fig. 6) suggests that the syntactic-resin-core–to–bias-ply-skin interface does have enough load transfer capability to develop the required strength capabilities. An ANSYS FEM predicted failure of the rodpack between the syntactic core and skin in local stability. Global local analysis of the single-stringer hat stiffener showed the axial stress component S_x in all three levels of modeling to be the critical component in a zone shown by section A-A of Fig. 6. The most realistic result, which has the rod/syntactic resin core interface and bias ply modeled independently, suggests that a positive margin of 0.74 in compression is the predicted failure stress that correlates to approximately –6,700 μmm/mm strain. These numbers compare favorably with single-stringer subcomponent tests when looking at calculated linear *(P/AE)* strains (see Table 1A). The strain gage data are somewhat higher due to out-of-plane deformation, which reached a minimum of –7,400 μin/in (–7,400 μmm/mm) of strain. The hat and skin interfaces were exercised more completely in fatigue using 48-inch (1.2-m) single stringer four-point bending specimens during Phase I, and by three-stringer subcomponent tests in Phase II of the program. The single-stringer bending specimens exhibited the capability to run one million cycles at ultimate load without any significant loss of residual strength or growth of imposed damage. These specimens verified the damage tolerance and durability of the new designs at the component level (Table 1B). The three-stringer panels provide more realistic biaxial loading conditions and sufficient energy to exercise the type of failure mechanisms that a wing skin might experience. No specific analyses were performed for correlation purposes at the three-stringer compression panel level. The three-stringer test panels were 24 inches (610 mm) long and 20 inches (508 mm) wide. They were potted on each end with 1 inch (25.4 mm) of potting compound in an aluminum frame. The tests were performed on a 500,000-lb (2,225 kN) Baldwin test machine in pure compression. The panels had enough size to experience the type of biaxial loads that a section of the wing skin would experience in compression. Two failure modes were evident from these tests. One failure mode is caused by an apparent delamination of the hats away from the skin at the syntactic resin core interface, leading to sublaminate

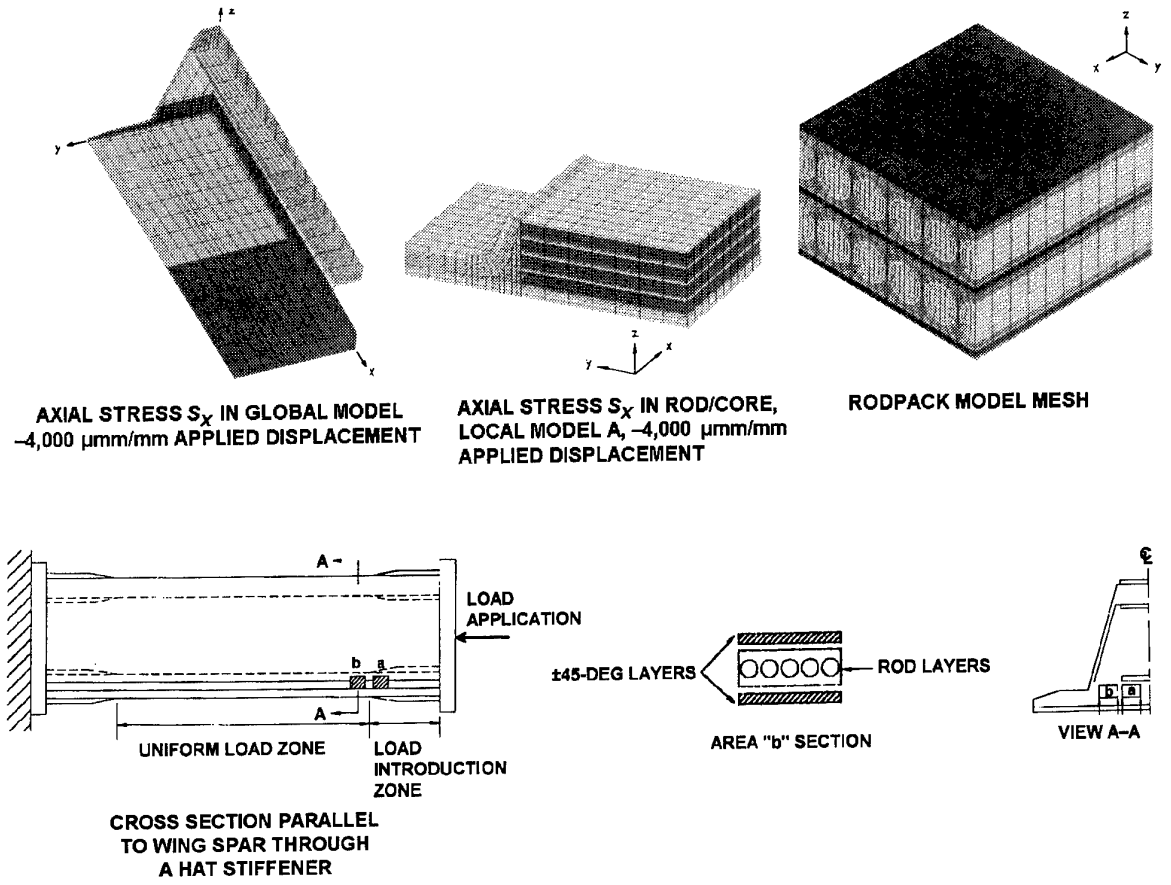


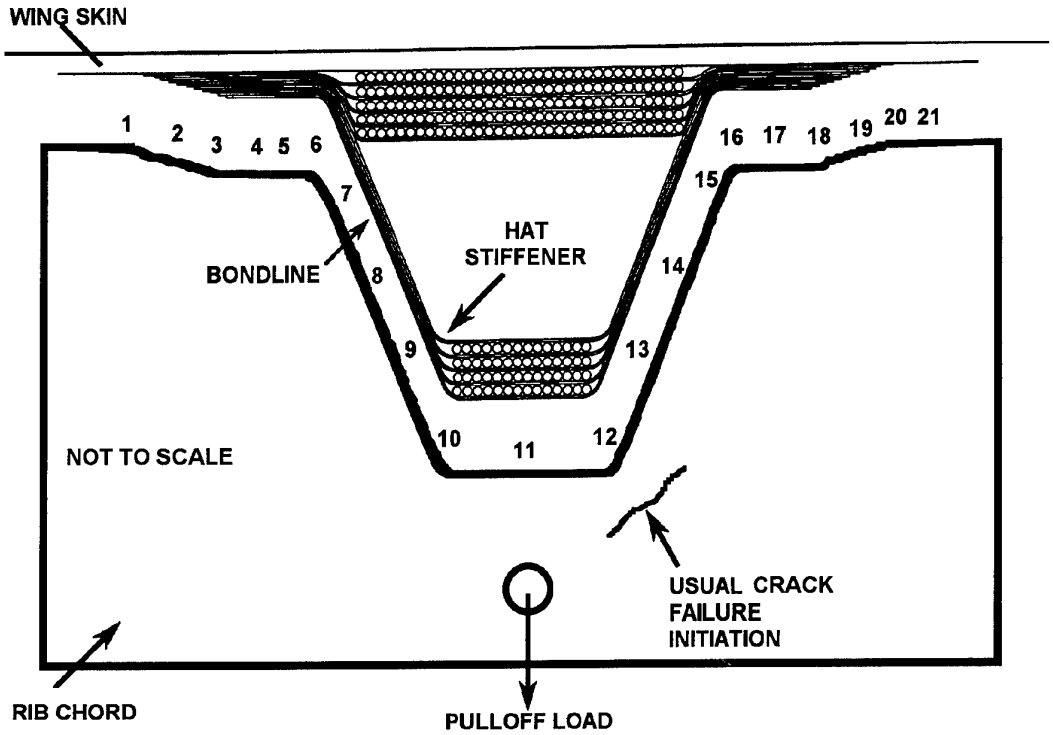
Fig. 6. Skin-to-stringer FEM.

buckling of the skin. This is a common phenomenon for hat-stiffened structure. The other failure mode is a net section failure of the entire panel. These two failure modes occurred at the same strain levels and appeared to alternate randomly for various test specimens. Both failures occurred at approximately 275% limit load and provided the necessary strength requirements for the system. The average strain to failure at ambient conditions was –7,900 μin/in (–7,900 μmm/mm), which is enough margin to absorb environmental and test data scatter knockdowns and still achieve the desired strain allowable of -4,500 μin/in (–4,500 μmm/mm) in compression (Table 1D).

Rib-to-skin interface (secondarily bonded joint)

The ribs resist vertical pulloff loads from aerodynamics, fuel pressure, and ballistic events quite differently in this design than the baseline. The base-line design had a conventional "mousehole" in the rib to allow continuous skin stringers to pass through. Me-chanical attachment points were at the tops of the stringers and in the soft skin areas between the stringers. The maximum pulloff load capability for this "mousehole" joint is significantly less than the current design based on test results. The most prominent feature of the DMLCC–BW rib-to-skin joint is that the design provides for shear continuity, which lends itself to bonding, since bonded joints transfer shear loads more efficiently than they transfer peel loads. The loads are reacted by the rib in tension and the bondline in shear and tension. The load path to the rib is through the adhesive bond joint in shear with the stringer webs and in tension with the stringer cap and wing skin. The stiffest and strongest path from the hat to the rib is the bond between the hat web and the sloping flanges of the ribs. This interface is predominantly in shear and is quantified in the analysis described below.

During Phase 2 of DMLCC, twelve rib pulloff specimens were tested to evaluate the capability of the joint and rib laminate normal to the skin plane. A section of the upper wing skin and a portion of the rib chord were loaded in tension through a clevis. All specimens failed the rib laminate due to interlaminar tension near the top of the hat in the radius of the rib web and cap flange (see Fig. 7). All failures were above design ultimate load, as shown in Table 1C. These tests are the basis for correlating the FEM.



Specimen number:	ML5	ML5	ML6	ML6	ML7	ML7	ML8	ML8	ML9	ML9
Measurement location	Near side dim (mm)	Far side dim (mm)	Near side dim (mm)	Far side dim (mm)	Near side dim (mm)	Far side dim (mm)	Near side dim (mm)	Far side dim (mm)	Near side dim (mm)	Far side dim (mm)
1	0.330	0.229	0.686	0.152	0.813	0.127	0.991	0.356	0.838	0.254
2	0.330	0.203	0.737	0.076	0.838	0.127	0.914	0.356	0.864	0.178
3	0.406	0.152	0.762	0.076	0.762	0.127	0.838	0.254	0.813	0.076
4	0.508	0.152	0.762	0.127	0.508	0.152	0.762	0.127	0.940	0.076
5	0.508	0.127	0.762	0.127	0.660	0.076	0.787	0.076	0.813	0.076
6	1.854	1.092	1.727	1.016	1.270	1.041	1.727	1.219	1.905	1.143
7	1.016	0.178	0.635	0.305	0.229	0.305	0.457	0.279	0.762	0.203
8	1.041	0.305	0.635	0.305	0.330	0.305	0.381	0.229	0.762	0.152
9	0.965	0.279	0.660	0.330	0.254	0.254	0.254	0.254	0.660	0.152
10	0.813	0.229	0.559	0.279	0.127	0.254	0.102	0.254	0.610	0.152
11	0.635	0.127	0.762	0.102	0.584	0.076	0.533	0.127	0.762	0.076
12	0.076	0.279	0.584	0.203	0.737	0.127	0.711	0.305	0.457	0.254
13	0.254	0.381	0.635	0.305	0.711	0.127	0.838	0.381	0.533	0.254
14	0.305	0.406	0.762	0.254	0.762	0.127	0.813	0.381	0.635	0.203
15	0.305	0.330	0.711	0.152	0.737	0.127	0.762	0.279	0.533	0.305
16	1.600	1.219	2.083	1.143	1.651	1.118	1.473	1.168	1.905	1.295
17	0.660	0.051	0.940	0.102	0.381	0.076	0.381	0.203	0.787	0.076
18	0.559	0.152	0.914	0.076	0.533	0.127	0.406	0.152	0.813	0.076
19	0.635	0.076	0.940	0.127	0.356	0.127	0.305	0.229	0.914	0.076
20	0.762	0.127	0.864	0.203	0.330	0.127	0.279	0.178	0.991	0.178
21	0.864	0.178	0.864	0.203	0.406	0.127	0.254	0.152	1.016	0.305

ML5 – cocked towards the rear, corner noodles big due to tooling, left vert and right horiz larger

ML6 – cocked twds rear, corner noodles big, vert and horiz more uniform

ML7 – cocked twds rear, noodles big, backside barely scrim thickness deep, right vert and left horiz larger

ML8 – cocked twds rear, corner noodles big , left vert and right horiz larger

ML9 – cocked twds rear, noodle large, left vert and right horiz larger, backside scrim barely in thickness

Fig. 7. Rib pulloff specimen bondline variability measurements.

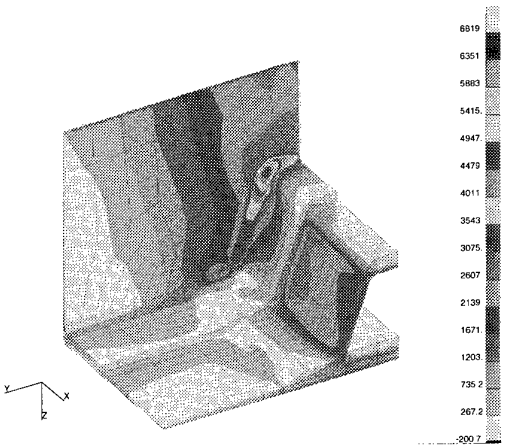


Fig. 8A. Major principal overall 1/4 model.

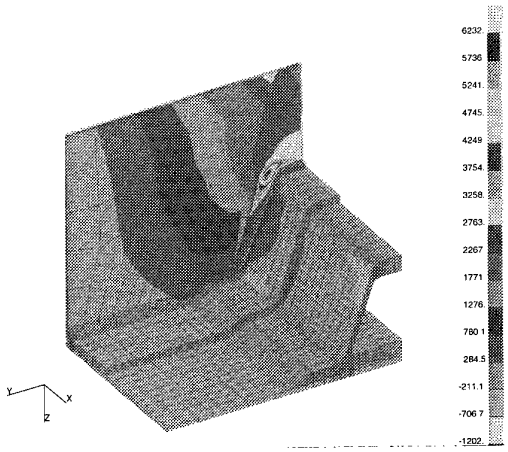


Fig. 8B. Global vertical (z).

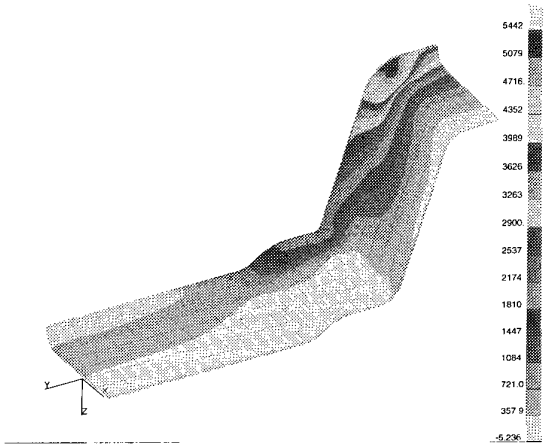


Fig. 8C. Major principal innermost rib flange ply.

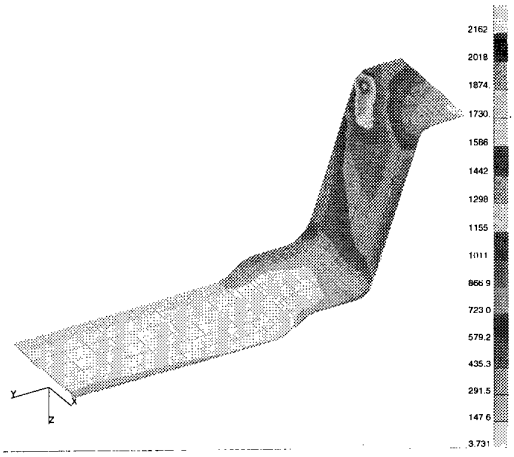


Fig. 8D. Major principal nomianl adhesive.

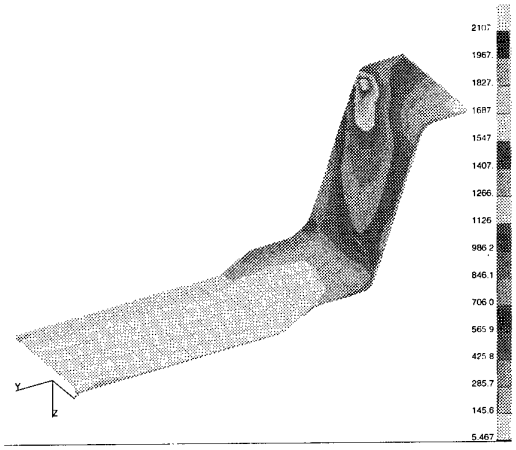


Fig. 8E. Major principal thin adhesive.

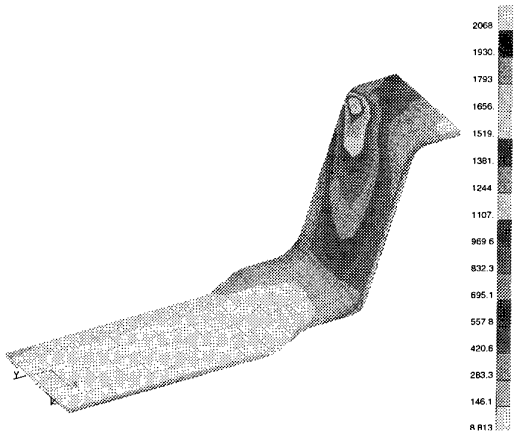


Fig. 8F. Major principal thick adhesive.

Fig. 8. Select rib-to-skin bondline stress gradients under 1,000-lb (4,448-N) load.

An independent analysis of the rib pulloff specimens was performed after the design phase of DMLCC–BW was complete. A NASTRAN FEM was created to provide a correlated analytic tool that could be used to demonstrate the capabilities of the joint for future optimization efforts. The FEM was used to investigate stress distribution and the effect of bondline thickness variation, since some of the fabricated parts exhibited

variations in the bondline beyond those deemed acceptable by engineering tolerances. An isometric of 1/4 of the pulloff specimen FEM with two planes of symmetry is shown in Fig. 8. The model included the vertical rib web, half its flange, the bondline, and the hat stiffener and skin segment. Solid hexagonal nondeformable elements were used with orthotropic material properties in a linear static analysis. The FEM had approximately 60,000 degrees of freedom. Nonlinear adherend properties or geometric analysis were not accounted for.

Based on tooling constraints, the nominal bondline was established at 0.020 inch (0.51 mm) thick. In actual practice, bondlines varied from 0.003 to 0.050 inch (0.076 – 1.27 mm) for the test specimens used in the rib-to-skin pulloff tests. These variations were determined by destructive investigations after the test were performed. Fig. 7 shows measurement locations and resultant bondline variation for five specimens. Each rib has two flanges, one on either side of the rib web, to form a T-joint. Measurements were taken on both sides of the rib web and are labeled "near side" and "far side" in Fig. 7. The specimens were tested at three various environmental conditions, yet no significant data scatter was seen. This is attributable to the fact that all the rib pulloff tests failed in the laminate, not the bondline; therefore, the bondline variability was not the critical factor. All specimens were within 10% load at failure and significantly above anything achievable with the previous bolted shear tie joint. All failures occurred well above the pulloff load requirements of 4335 lbf (19,282 N). (See Table 1C.)

A 1000-lbf (4448-N) load was applied to the FEM for all the results discussed here. Major principal stresses for the outer plies are shown in Fig 8A. The highest stress gradient is shown at the rib web to cap flange. The stress components of the major principal stress will be discussed in some detail, but not shown graphically due to space limitations. Also of interest is that the FEM predicted another local high stress gradient region inside the hat at the lower rod pack interface with the web directly under the rib flange dropoff. The peak values at this gradient were approximately 75% of the peak stress gradients at the rib flange. After the tests, the destructive investigations found matrix cracks at this same location. It had not led to complete failure, but probably would have continued to propagate and eventually caused failure of the joint.

For various reasons, an attempt to correlate absolute magnitudes of the stresses with the tests will not be pursued. For one reason, no peel allowable for the adhesive or the laminate interlaminar shear is available. However, the trends can be used to assess the viability of this design. Future optimization efforts should concentrate on shear and peel interaction curves to determine how much margin of safety exists in this joint.

Element stresses in the direction of the load are shown in Fig 8B. The global vertical stress is the predominant component of the principal stress in the rib web. This stress distribution, in addition to some Poisson's effect shrinkage, contributes to the stress concentration at the top of the hat and the radius of the rib web flange. Views of the major principal stresses in the first ply of the rib laminate and the adhesive are shown in Figures 8C and D. One should notice that the relative magnitudes of the stresses in the adhesive versus the laminate suggest that the laminate experiences stress gradients approximately three times larger than the adhesive at the critical radius location. This compares favorably with the observation from test that all failure modes initiated in the rib web laminate at this radius. Both of these contour plots show how the load lags into the rib flange/adhesive at a 45-deg angle. This is the usual assumption for calculating effective area when sizing the joint by classical stress analysis. Further review of the stress components comprising the adhesive principal stress shows that shear stresses contribute over 90% of the stress to these values. This is consistent with the objective of this design to provide an efficient means of transferring load through a bondline by minimizing peel loads.

Several references (Refs. 4 and 5) have shown that bonded joint shear strength will exceed the strength of a composite adherend within reasonable thickness limitations of the bondline. The FEM was used to try and quantify the effect of the bondline variation found in the test specimens and determine if it was within these limitations. The rib portion of the FEM was translated back and forth from nominal to approximate the effects of varying bondline thickness. These variations are shown in Figs. 8D, E, and F. A thin bondline (0.005 in , 0.127 mm) and a thick bondline (0.050 in, 1.27 mm) were analyzed. The FEM only shows approximately a 10% change in the peak principal stress levels. Although variability in the actual specimens was more random, and there were thick and thin portions in close proximity which would cause more severe stress variation, it does suggest that the engineering tolerances may be too stringent. Engineering often bases the tolerances on variations in bondline thickness in small coupon tests to determine the effects on mechanical properties. This phenomenon is explained in detail in Fig 1. of Ref 4, where short overlap coupons, used to force the failure out of the adherend into the adhesive, do not represent the behavior of that same adhesive in a more typically proportioned joint. The results of the bondline variation studies suggest that there is sufficient margin to allow

some variation as long as normal quality issues are addressed. Also, porosity must still be minimized, but this is something that nondestructive inspections can identify for accept/reject criteria of a bonded joint.

FULL-SCALE TEST PLAN

The low-cost design concepts and manufacturing processes developed under the DMLCC–BW program have been verified for cost through production of the two wing box demonstration articles. The structural performance of the demonstration articles will be confirmed through testing of the completed article, as though it were a structural component. The tests will be conducted by the USAF Wright Laboratory Structures Test Branch, with support from Bell. A schematic of the full-scale test setup is shown in Fig. 9. The current test plan consists of a series of proof tests up to 1.2 design limit load, a single lifetime of fatigue testing, inspection, and then deliberate damage at critical locations, and a second lifetime of fatigue. If the demonstration article survives the second fatigue application, it will then be inspected once more, followed by a one or two shot ballistic survivability test.

The test program is being conducted to confirm the performance of the new design concepts and manufacturing processes selected, and is not intended to validate the DMLCC–BW concept for V–22 service. Therefore, full load spectrum testing of all flight conditions will not be performed. Static testing will be conducted to demonstrate the overall strength and stiffness of the pultruded rod reinforced structure. The test will also demonstrate the strength of the front and rear spars and the ability of the ribs to react chordwise shearing loads. The objective of the fatigue test is to demonstrate that the pultruded rod reinforced skin, the rib chords, and the adhesive joint between these elements are capable of sustaining two lifetimes of fatigue damage. Impact damage will be applied to the upper and lower skins after one lifetime of random spectrum fatigue testing. A second lifetime fatigue spectrum will then be applied. The residual strength of the structure will be confirmed through proof testing to design ultimate load. The ballistic test will be conducted under applied beamwise bending load to realistically demonstrate the survivability of the design concept with respect to hydrodynamic ram threats. The selected shotlines will emphasize damage to critical areas such as bondlines, rod reinforced areas, and integral flanges.

The DMLCC–BW demonstration article represents a midwing section of the V–22 wing design. This presented several challenges with respect to introducing the correct loads to the test region. Additionally, the program budget could not afford to design and fabricate large complex load introduction and transition structure, and the demonstration article structure ribs and spars were not designed to react the concentrated loads necessary. These problems were resolved by developing a test structure that utilized one of the demonstration articles, sectioned into two halves and reinforced with skin and spar doublers fabricated from a new low-cost, room-temperature-cure composite material system to introduce loads. The test load introduction fixture matches the stiffness of the DMLCC article in order to prevent local overloading.

Critical load conditions from the V–22 provided the required test conditions. These consist of maximum

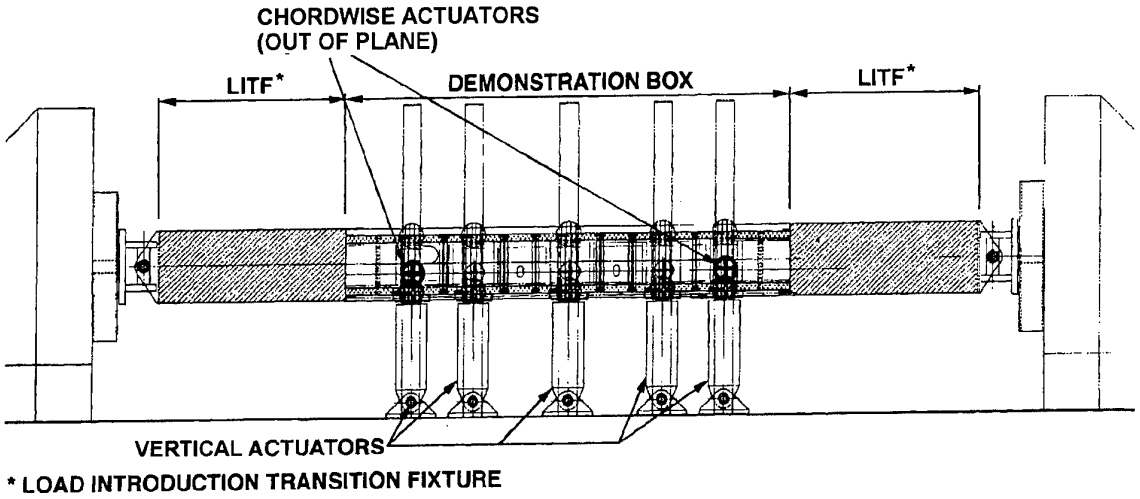


Fig. 9. Schematic of the full-scale test setup.

chordwise bending (vertical takeoff), maximum beamwise bending (2-*g* taxi), minimum beamwise bending with low and high torsion (rolling pullout in helicopter mode), and maximum torsion (rolling pullout in airplane mode). These test conditions were selected in order to demonstrate that the loads that sized the DMLCC–BW demonstration structure were accounted for and that performance requirements had been met, and that the maximum load envelope for beamwise bending, chordwise bending, and torsion had been covered.

Fatigue loads will consist of a 10,000-flight hour flight-by-flight random spectrum based on a 100% helicopter mode. The fatigue spectrum is derived from a critical point-in-the-sky and includes 32,429 load pairs. Hot-wet conditioning will be accounted for through the application of a 22% load factor to the applied maximum and minimum loads.

CONCLUSIONS

The DMLCC–BW program reproduced a section of a tiltrotor transport wing torque box to demonstrate the viability of an affordable primary structure made with advanced polymer composites. This was a successful collaboration of manufacturing and design engineers that demonstrated a 50% cost reduction while meeting or exceeding all performance capabilities of the original design. The costs were verified through the fabrication of two full-scale demonstration articles that were built and assembled in a production environment. Costs were gathered and compared directly to the original industrial engineering cost figures. Performance has been measured through a building block test approach to verify the structural integrity of the DMLCC–BW as the program developed. All tests have exceeded requirements to date. Static, fatigue, durability, damage tolerance, weight, and cost objectives were all obtained. The results of this program suggest that a cost effective alternative for a primary wing box composite design is achievable. This conclusion is based on a fairly unbiased series of manufacturing and engineering development tasks. In 1997, a full-scale test program will be performed to verify the overall structural integrity of the wing torque box, to include static, fatigue, and ballistic tests. This test will exercise more of the full-scale joints and the overall interaction of the torque box that no combination of subcomponent tests can possibly address.

Several analytical challenges arose from the final design. The axial load-carrying material in the wing skins used pultruded carbon rods embedded in syntactic resin core and prepreg tape known as a rod pack. This rod pack concept was critical to achieving the damage tolerance compression allowables which enabled this concept to succeed. Analytical capabilities to support this design approach have been developed and successfully demonstrated during this program. This provides a very important tool required to transfer this technology into production for future applications. The rod pack concept also proved to be a challenge to classical FEM plate element representation. Local–global techniques with various constituent property representations have been successfully demonstrated and correlated with test results to verify the load transfer mechanism in this new structural design.

Another challenge to design and analysis was the representation of the bondline between the ribs and skins of the torque box. A bonded joint in primary airframe structure requires significant development to address the myriad of questions concerning quality control, reliability, inspection and, in military applications, survivability and vulnerability. The critical design feature in this application was that the majority of the load is transferred through the skin-to-rib bondline in shear and not peel. This has been successfully demonstrated through test and analysis and provides a level of confidence that the bondline will not be the weak link in this joint. A detailed FEM of this joint confirms that the preponderance of the stress in the bondline is shear, and that peak values appear to be well below critical levels. Also, the FEM suggests that the rib web laminate highest stress is three times larger than adhesive stresses and the predicted high stress gradient regions in the laminate compare favorably with onset of failure. All test specimens to date have failed in the rib laminate and suggest that the critical feature in this joint is the laminate. The joint has also exceeded ultimate design strength requirements by two to three times, providing a high margin of safety to accommodate manufacturing defects, environmental effects, overpressures, and other anomalies. Further optimization of this joint should be feasible with this correlated FEM.

Finally, the DMLCC–BW program has verified that an integrated design team which addresses a common set of ground rules can provide cost-effective primary composite structure and meet the myriad of requirements (cost, weight, damage tolerance, survivability) that an aerospace application requires.

ACKNOWLEDGMENTS

The authors would like to thank the DMLCC team for their collective effort presented here. This was a collocated group of design, cost, manufacturing and maintainability engineers that deserve credit for the product described in this paper. Also, appreciation is expressed to Mr. John McCullough for his FEM analysis of the rib pulloff specimens.

REFERENCES

1. Rai, H. G., Rogers, C. W., and Crane, D. A., "Mechanics of Curved Fiber Composites," *Journal of Reinforced Plastics and Composites*, Vol 2, (5), May 1992.

2. Rousseau, C. Q., Baker, D. J., and Chan, W.S., "Analysis and Testing of a Graphite Rod Reinforced Hat section stringer," Paper 95-1509, 36th AIAA/ASME/ASCE/AHS/ASC Structures, Structural Dynamics ,and Materials Conference, New Orleans, LA, Apr 1995.

3. Baker, D. J., Nunn, K. E., Rogers, C. W., Dompka, R. V., and Holzwarth, R. C. "Design, Development, and Test of a Low-Cost, Pultruded-Rod-Stiffened Wing Concept and Its Application to a Civil Tiltrotor Transport," 10th DOD/NASA/FAA Conference on Fibrous Composites in Structural Design, Hilton Head, SC, Nov. 1993.

4. Hart-Smith, L. J., "Adhesive-Bonded Joints for Composites – Phenomenological Considerations," Technology Conferences Associates Conference on Advanced Composites Technology, El Segundo, CA, 14–16 March, 1978.

5. Davis, M. J., "The Development of an Engineering Standard for Composite Repairs," AGARD CP-550, *Composite Repair of Military Aircraft Structures*, 79th Meeting of the AGARD Structures and Materials Panel, Seville, Spain, 3–5 October 1994.

ROYAL AIR FORCE EXPERIENCE OF MECHANICALLY-FASTENED REPAIRS TO COMPOSITE AIRCRAFT STRUCTURES

Squadron Leader S H Chicken
Royal Air Force Repair Design Authority
Royal Air Force St Athan, Barry, Vale of Glamorgan
United Kingdom

1. SUMMARY

The RAF has been repairing helicopter composite rotor blades, fibreglass radomes and panels on a variety of combat aircraft types for many years. However, the Service's main experience in the maintenance of carbon fibre composite (CFC) material has been related to the Harrier II aircraft. This paper describes the main CFC structures of the Harrier II and outlines the variety of RAF peace-time, bolted structural repairs applied to the aircraft. Examples are provided of various simple and complex repairs.

2. INTRODUCTION

The RAF's experience in the repair of CFC material is largely based around the maintenance of the structure of the BAe/McDonnell Douglas Harrier II aircraft, also known as the AV8B in US Marine Corps use. Although there are repairable composite panels and doors on other RAF fixed-wing aircraft, not least the Tornado, and glassfibre repairs are common on radomes and gliders, it is the Harrier II which has taught the RAF the most lessons regarding the repair of composite materials, particularly in regard to bolted repairs to carbon/epoxy structures. This paper concentrates on repairs to damage sustained in the normal peace-time operating environment; battle damage repair is a different subject altogether.

The Harrier II in its GR5 version was introduced into service in 1986 and is the RAF's main battlefield interdiction and close support aircraft, equipping 4 squadrons with 87 aircraft in the modified GR7 form. It can carry an impressive weight of ordnance over a militarily useful range and can use its unique short take-off and vertical landing ability to provide support to ground forces from austere bases very close to the front line. The Harrier II structural design is based on that of the Harrier I; the main difference being the large-scale use of CFC as a build material.

3. CONSTRUCTION

3.1 Materials

The Harrier II forward fuselage, wing and horizontal tailplane are constructed of CFC, along with other structural components such as the control surfaces (see Figure 1). For brevity the flap will be the only control surface considered in detail in this paper. The main materials used in the Harrier II structure are as follows:

a. Carbon epoxy cloth to McDonnell Douglas Material Specification MMS 544 is used for monolithic structures. This material can withstand temperature environments of -53°C to 156°C and comes in 7 types of differing harness satin weave, thickness, resin content and method of impregnation.

b. Carbon epoxy unidirectional tape to McDonnell Douglas Material Specification MMS 549 is used for both monolithic and sandwich structures. This material can withstand temperature environments of -53°C to 156°C and comes in 5 differing resin contents and thicknesses.

Paper presented at the 83rd Meeting of the AGARD SMP on "Bolted/Bonded Joints in Polymeric Composites", held in Florence, Italy, 2-3 September 1996, and published in CP-590.

c. Carbon bismaleimide (BMI) cloth used for monolithic structures requiring high temperature resistance up to 267°C.

3.1 Forward Fuselage

The forward fuselage extends from the aircraft's nose to Frame 8 forward of the air intakes and includes the nose cone, windscreen, canopy and cockpit structure (see Figure 2). The forward fuselage is a semi-monocoque shell of laminated CFC reinforced with longerons, stringers, frames, floors and bulkheads. Two CFC bulkheads form the forward and rear limits of the pressurised cockpit. The rear bulkhead supports the ejection seat mounting rails. In the case of the nose cone the lay-up of the CFC is augmented by bi-directional Kevlar cloth to enhance the birdstrike protection provided by the structure. The nose cone is hinged for access to the interior of the front fuselage.

3.2 Mainplane

The Harrier II mainplane is a one piece, swept back, super-critical section wing which not only functions as a load carrying member but also includes integral fuel tanks (see Figure 3). The wing is constructed of complete, monolithic CFC upper and lower skins which are bolted onto the CFC and metal substructure. Most of the torque box is sealed and acts as a fuel tank. Access can theoretically be gained to all internal components and structure by removal of the top skin. The torque box is of a multi-spar design and is constructed as a continuous unit from tip to tip (see Figure 4). Vertical, shear and torque loads are transmitted inboard along the spars to the main wing to fuselage attachment ribs and distributed to the 6 fuselage attachment fittings. Other ribs are located within the torque box at points of local load introduction. There are 3 primary and 5 auxiliary spars. A small aft spar acts as a closure member for the fuel tank. Small access panels in the upper skin permit limited access to the fuel tank. The entire torque box is assembled with titanium fasteners. Titanium bolts with corrosion-resistant steel anchor nuts are used to attach the skins. The spar to rib joints use titanium Hi-lok fasteners. The CFC spars embody integral flanges and sinewave webs, the sinewave design providing a structurally effective means of transmitting shear loading. Three auxiliary spars are located between the front and centre spars and 2 between the centre and rear spar. An all-metal non-sinewave intermediate front spar section strengthens the area of the outrigger undercarriage and provides support for the middle pylon. The spars are locally reinforced with additional plies and metal fittings where concentrated loads are introduced. There are 15 ribs in the torque box, 10 of which are of CFC sinewave construction and 5 of metal. The centre line fuel tank closure and wing tip ribs are aluminium machinings. The wing to fuselage CFC attachment rib redistributes wing shear and torque through fittings bolted to the bottom surface of the wing. The inboard and outboard pylon ribs and outrigger rib are all of composite sinewave construction. The leading edge is aluminium alloy, both to act as birdstrike protection and as a likely lightning attachment point. The aluminium leading edge is attached to an internal titanium web which also acts as a heat-shield for the reaction control system duct which runs to the wing tip. The wing tip is of aluminium alloy construction, includes the reaction control system nozzle and is supported by a titanium machining.

3.3 Flap

The flap is of multi-spar and rib construction and, unlike the wing, has the spars co-cured to the upper skin. The leading edge skin assemblies are CFC but the trailing edge skins and inboard skin assemblies which impinge in the jet efflux are made from carbon BMI (see Figure 5).

4. REPAIR INFORMATION

The RAF relies on 2 main sources of repair information for CFC structures: the structural repair manual (SRM) and Design Authority (DA) approved schemes. In the case of the Harrier II the DA is BAe (Military Aircraft Division) Farnborough.

4.1 SRM Repairs

The purpose of the SRM is to provide the operator with a readily available source of relatively simple repairs to areas of the structure which are commonly damaged. The Harrier II SRM includes repairs to slight surface damage, laminate crazing and surface and edge ply delamination. Simple bolted and adhesively bonded patch repairs are also included for skin and stiffeners. All SRM repairs begin with a non-destructive inspection (NDI) to establish damage limits and confirm that there are no internal delaminations.

4.2 DA Repair Schemes

When the extent of the damage exceeds that detailed in the SRM the details are sent to the DA. The DA then designs the repair scheme and authorises its use, usually on a specific aircraft. In some cases a staged examine, remove damage, re-examine process is required, with information flowing to and from the DA until a final, fully comprehensive repair scheme is agreed.

4.3 Repair Policy

The structural repair policy of the Harrier II has to reflect the fact that the aircraft's operational environment is very much based on austere, semi-prepared airstrips. Thus the structure is extremely robust. At the time of design there was much debate on the effect of barely visible impact damage. This potential problem was solved by designing the structure such that any likely internal delamination which was not detectable by visible means would be deemed acceptable. Only when a damage signature was visible, either by a surface irregularity or fuel leak, would the delamination be significant enough to warrant repair. This conscious "over-design" has a mass penalty, but has resulted in an aircraft which can accept a lot of damage before repair is necessary.

5. SRM REPAIR EXAMPLES

5.1 Bolted Lap Patch Repairs

Damage which can be repaired using a SRM bolted metal lap patch is limited depending on location. For example, for the majority of the forward fuselage, 101.6 mm (4 in) diameter damage is the maximum which can be repaired without a DA repair scheme. The damage is routed out and the area is lightly sanded, vacuumed and cleaned with trichloroethane. A chamfered and primed titanium patch is manufactured to a size and shape to suit the damage location. Fastener pitch must be a minimum of 4D between fasteners and 3D from the material edge. Sealing compound is applied and the patch wet assembled using Composi-lok Jo-bolts (see Figure 6). This technique has been applied to the wing to repair lightning damage.

5.2 Bolted Aluminium Flush Patch

For aerodynamic considerations repairs to the forward fuselage skin are restricted in some areas to flush repairs only. For example, forward fuselage damage up to 101.6 mm (4 in) in diameter can be repaired using a SRM scheme (see Figure 7). The damage is routed out and the area vacuumed and cleaned with trichloroethane. Splice and backing plates are manufactured to a size and shape to suit the specific repair scheme. Note that fastener pitch must be a maximum of 4D between fasteners and 3D from the material edge. The splice plate and smaller backing plate are rivetted together and the assembly clamped onto the internal side of the repair area. Pilot

or full size fastener holes are then drilled through skin and backing plate. The smaller backing plate assembly is then removed and the process repeated for the larger backing plate. The external skin is then countersunk using a carbide countersink cutter rotating at a maximum of 2000 rev/min. The repair area is then cleaned again. PR1750 sealing compound is applied to both backing plates and open weave nylon cloth added. The smaller backing plate assembly is loosely attached to the internal side of the repair with a single temporary fastener at one corner. The assembly is then swung away from the repair opening. The larger half backing plate is then located on the internal side of the repair and secured with temporary fasteners. The small backing plate is then rotated back into its final position and the whole backing plate assembly wet-assembled with Jo-bolts and PR1750 sealing compound. A filler plug mixture is prepared and applied to the repair hole and is cured at room temperature for 2 hours. When cured the plug is sanded down to the skin contour and surface finish re-applied. This type of repair has been carried out on a wing following a wire-strike.

5.3 Non-structural Plug Repairs

In certain locations where routed out damage does not exceed 25.4 mm (1 in) diameter a non-structural plug can be used to fill the resulting hole. There are 4 types of plug: simple nylon, fuel-proof expandable and for high temperature applications, Torlon and titanium. All plugs are wet assembled to the skin with PR1755 sealant.

6. DA REPAIR SCHEMES

6.1 Repairing Wing Skin Delamination

Subsurface delamination comprises of delamination within the monolithic structure which cannot be detected visually. This type of damage is only detectable by NDI or, in the case of fuel tanks, leakage. If the damage is caused by maintenance error operator honesty is also a significant factor. In a recent example a CO_2 cylinder from one of the underwing pylon weapons release units sprang from the pylon and hit the underside of the wing. Slight surface damage was visible and a fuel leak was noted in the area. NDI indicated delamination over an area of approximately 6cm x 3cm. However, no indication of possible `christmas tree' damage inside the tank was available. This type of loose fibre damage is extremely significant inside fuel tanks where the fibres can migrate to fuel lines and clog filters. As no SRM scheme existed for this type or extent of repair the DA was provided with details and a repair instruction requested. The wing was removed and vented of all fuel. As the particular fuel cell involved was not accessible via a removable panel, and the task of completely de-skinning the wing was deemed unacceptable, a 25.4 mm (1 in) inspection hole was drilled in the upper skin. No `christmas tree' delamination was visible. The DA repair scheme was to drill a pattern of holes through and around the delamination and install 26 x Composi-lok fasteners to clamp the delaminations together (see Figure 8). The inner surface was sealed with EA956A/B resin and PRC. The small inspection hole in the upper wing surface will be sealed with a fuel-tight expandable plug, although at the time of writing this has yet to be delivered.

6.2 Repairs to Delaminated BMI

The underside of the starboard flaps has suffered particularly bad edge delamination. This is caused by the flap's operational environment, in that not only does the jet blast impinge upon the panel but it is also downstream of an oil drain. The resultant high velocity hot oil spray severely delaminates the flap trailing edge. There are 2 possible repair solutions to the damage. The first solution is a large, bolted titanium lap patch which largely uses existing fastener lines (see Figure 9). This not only uses the fasteners to pull the delamination together but also adds a layer of heatshielding

material. This repair is now only used if the delamination extends beyond the BMI panel. A more elegant solution is to replace the damaged BMI panel with a similar titanium panel. This is completed using Visu-lok 100° countersunk fasteners with titanium loadspreaders where access is available to both sides of the structure, but large footprint Composi-lok fasteners where access is only available to one side.

6.3 Fastener Misalignment

Many of the Harrier II replaceable panels come with pre-drilled fastener holes. It is not uncommon for these pre-drilled holes to be found to be misaligned with the relevant holes in the aircraft structure. In a recent case this type of misalignment occurred in an upper leading edge panel. Research work has been carried out in a MOD-sponsored proof-of-concept programme at BAe (Military Aircraft Division) Warton which indicated that holes mis-drilled normal to the load line could be filled with EA934N/A, redrilled and countersunk with good static strength and fatigue performance at room temperature/wet and hot/wet conditions. However, similar repairs with the holes mis-drilled parallel to the load line suffered severe bearing deformation, particularly in hot/wet conditions. This failure was also the case when short chopped fibres were added to the EA934N/A at approximately 5% volume ratio. As the misalignment of the holes in the leading edge panel were deemed to be parallel to the load direction the principles of this proof-of-concept method were modified by the DA to include titanium washer plugs to improve bearing performance (see Figure 10). Note that 2 plies of CFC are added over the repaired fasteners.

6.4 Repair to Longeron

In a recent incident a low-flying Harrier hit a high voltage electricity pylon in Germany. Damage to the lower surface of the forward fuselage and the gun pods was significant but repairable. In particular, damage to the main lower longeron is being repaired using a cut-down spare longeron. Existing build fasteners are augmented by Composi-loks. The interface between the CFC and the aluminium alloy fittings is protected by a nylon interfay layer and the repair is room temperature, wet assembled with EA956A/B adhesive.

7. WORKING WITH CFC

Many of the repair procedures for CFC structures require that the material is drilled, scarfed, sanded or otherwise mechanically worked. Note that when drilling, reaming or cutting composite materials the tool exit area is always supported with a backing plate to prevent splintering and delamination. Also, any cutter is always rotating before contact with the material to ensure that splintering does not occur. There is also a very high awareness of both the health and safety aspects of any fibre waste and the effects of contaminates on surface preparation for bonded repairs. Thus, when vacuum cleaning of a semi-prepared piece of work is required, it is done with a dedicated cleaner. Sumps are used to collect dust and drill waste. Personnel wear filter masks and other specialist clothing. If the damaged component cannot be removed to a dedicated clean composite repair bay the surrounding area must, in essence, be converted into such a controlled environment by the construction of a sealed plastic tent.

8. CONCLUDING REMARKS

The RAF's experience in maintaining the Harrier II aircraft has illustrated the practicality and safety of repairing composite military aircraft structures with bolted repairs. Proven techniques are available for repairing edge and internal delamination with fasteners. Similarly, titanium and, in some cases, aluminium alloy patches can be fitted and offset fastener holes repaired.

ACKNOWLEDGEMENTS

The author acknowledges the essential and constructive help and guidance of the repair design staff of BAe (Military Aircraft Division) Farnborough in the production of this paper. Similarly, thanks go to the composite repair trainers of the Harrier Maintenance School at RAF Wittering and the technicians from the Aircraft Engineering Squadron at RAF Laarbruch and Repair Support Squadron at RAF St Athan. The input of the Harrier II Support Authority at HQ Logistics Command at RAF Wyton is also gratefully acknowledged.

© British Crown Copyright 1996/MOD Published with the permission of the Controller of Her Britanic Majesty's Stationery Office

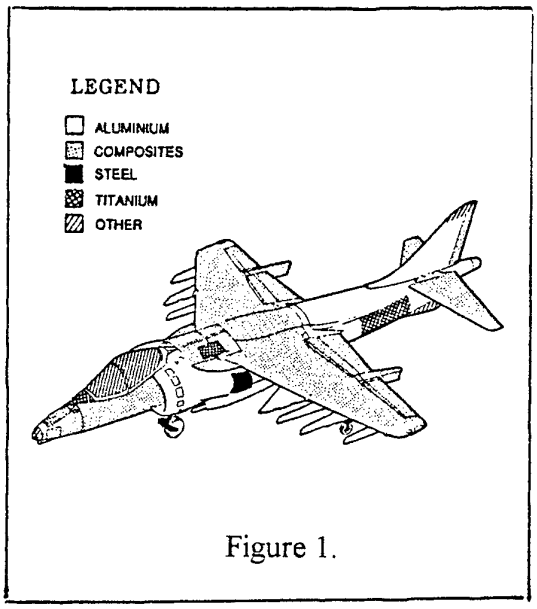


Figure 1.

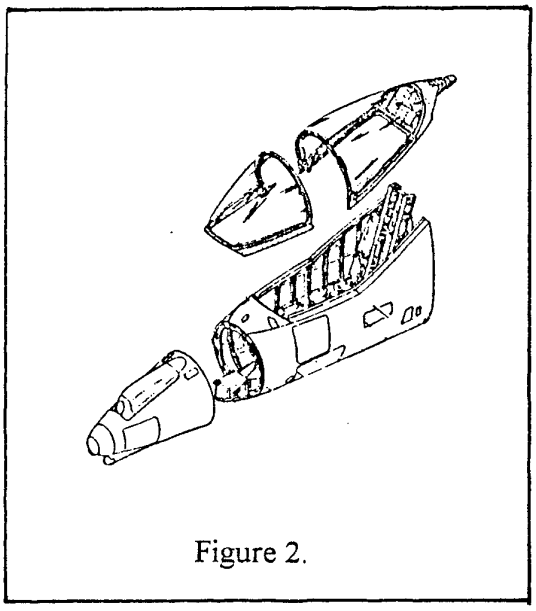


Figure 2.

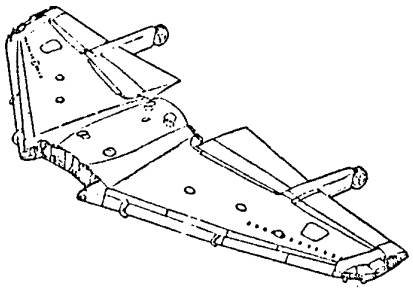


Figure 3.



Figure 4.

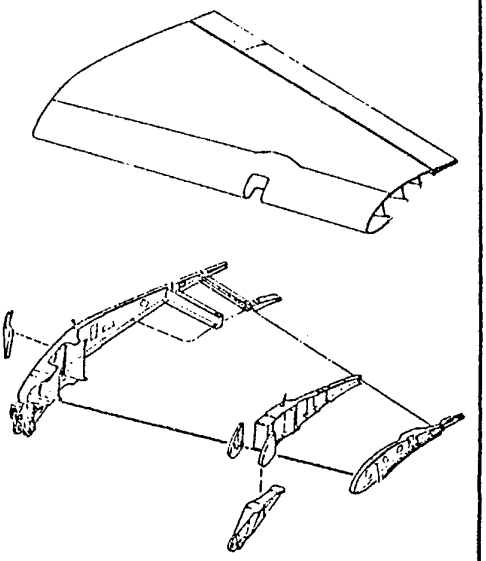


Figure 5.

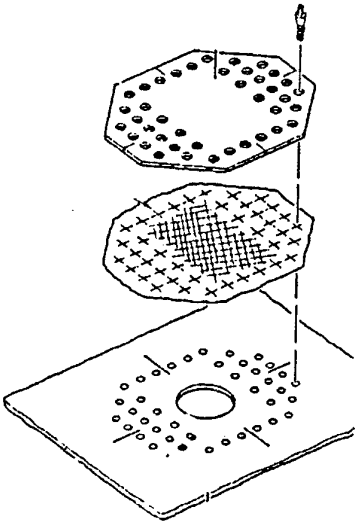


Figure 6.

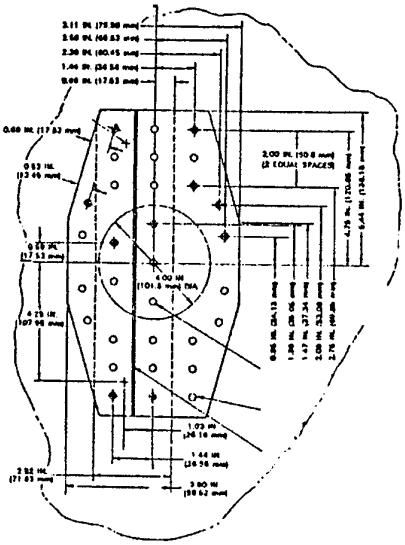


Figure 7.

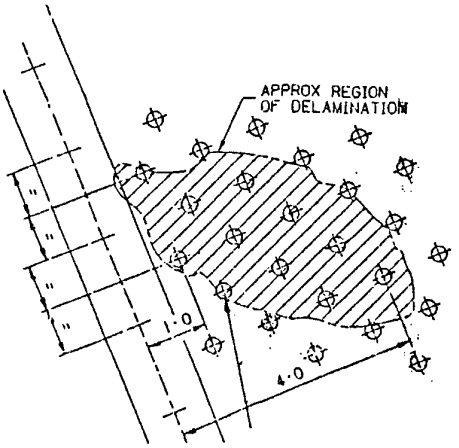


Figure 8.

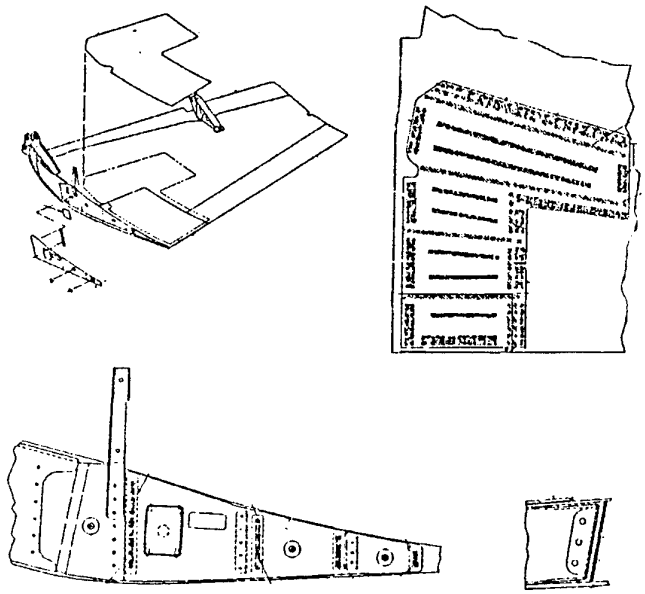


Figure 9.

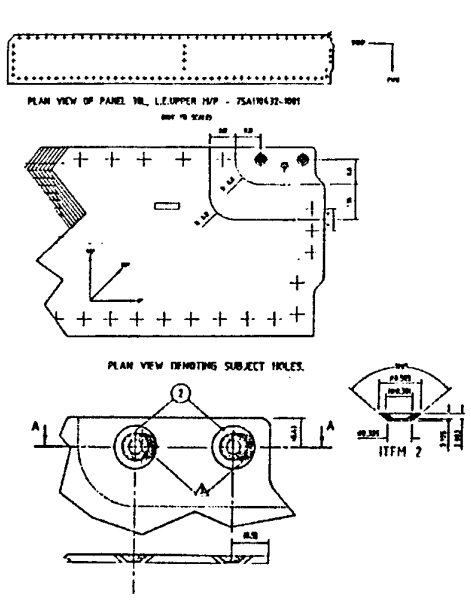


Figure 10.

Quality Assurance and Certification Procedures for Bonded Joints in On-Aircraft Scenarios

A. Maier
G. Günther
Daimler Benz Aerospace AG
Military Aircraft Division
München, Germany

Abstract:

As the repair of primary composite aircraft structures using composite materials has become a matter of "world wide interest and activity", the requirement of certification methods and engineering standards for composite repairs have become evident.
Bonded joints for principal load transfer within the structure have to run through an extensive certification / qualification procedure during development phase and are subject to rigerous quality control during the original component manufacturing.
However, within typical "On-Aircraft" repair scenarios bonding procedures and manufacturing conditions are in almost every technical aspect different from original processes and require therefore more extensive vertification.
Methods to certify repair design, repair procedures, repair methodology and quality control depend on specific repair levels (i.e. SRM, Engineering Disposition, ABDR) and are not yet standardised.
The paper describes DASA's current approach to certify bonded repairs for damages which require "Engineering Disposition" for "On-Aircraft" application.

1.0 Introduction

The constant demand for improved performance in the development of new fighter aircraft together with reduced structural weight limits has led to new design techniques and the application of advanced fibre reinforced materials for the load carrying structure. Fighter aircraft with extensive usage of composite, i.e. CFRP material have now been in service for some years. Although the trend for composites in structural applications in percent of structural weight will show an asymtotic limit of approx. 30-35% in future, (Fig.1.0-1), the wetted area will be made almost exclusively from thermoset composites like CFRP, which is used in most cases as a combination of a high strength/modulus carbon fibre and a hot curing thermoset resin.
For the *Eurofighter* about 70% of the aircraft´s exterior surface is covered with composite skins Fig.1.0-2, including fuselage, wings, horizontal and vertical stabilizer. All of this graphite epoxy skin surface is load carrying, most of it primary structure made of high temperature (175°C) curing CFC/Ep system cured in an autoclave with vaccum and high pressure.
With the structural requirement of high mechanical loads for the primary load pathes in combination with local load introductions and stability criteria, the result is very often either thin-walled stiffened skin design and/or sandwich structures. The large amount of integrated structural elements with reduced number of fasterners dictate the requirement for maintainability and repairability of these elements, especially under the consideration of part costs and assembly effort.
Maintainability aspects are partly covered due to the damage tolerant design approach, in general todays composite structures are designed using a "Limited Fibre Strain Approach" at ultimate design loadcases, where the reduced material allowables account for a low energy impact damage level, respectively the visibility threshold of damages ("Barely Visible Impact Damage", BVID),that can be sustained without compromising structural strength over the entire life of the aircraft.
However, damages exceeding these limits should not lead to immediate replacement of parts or extensive A/C-downtime for disassembly, autoclave repair, reinstallation and inspection.
The alternative of designing most components as exchangeable parts between A/C´s is also limited for practicability and cost restrictions.
Therefore the "Repair on Aircraft" capability for the structure becomes an important part of the maintenance concept for highly integrated structures, that need to be considered during design and qualification phases.

Paper presented at the 83rd Meeting of the AGARD SMP on "Bolted/Bonded Joints in Polymeric Composites", held in Florence, Italy, 2-3 September 1996, and published in CP-590.

2.0 Structural Design Concepts for Bonded and Bolted Joints

The overall task for bolted and bonded joints in aircraft structures are identical: Permanently attaching two load carrying structures up to a defined load-level over the entire life of the aircraft. However, the engineering properties and manufacturing processes of both methods are different and have led to distinct applications for both types of joints, i.e.:

* Bonded joints are up to a magnitude stiffer in shear than bolted joints.
* Mechanical interface versus chemical reacted joint material.
* Good combined shear and cross-ply tension behavior of bolted joints compared to bonds.
* Load transfer along joints are nonuniform for both types.
* Bolted joints show redundant loadpathes, where bonds are "Single Fastener Systems".
* Bolted joints are fatigue sensitive in the adherents, well designed bonds show almost unlimited mechanical life.
* Quality assurance procedures are based on visual, mechanical checks for bolts, whereas chemical processes for adhesives and surfaces are far more complex to control.
* Bonded joints can act as sealings between structural elements.

The above list is not complete, but gives an indication why bonded joints historically have been applied to aircrafts mainly to thin structures and honeycomb panels with low load transfer and conservative design approaches in a production environment with good process control.
Unlike metal fatigue design concepts of slow and controlled crack-grow under cyclic loading, defects in bonded joints will either never grow under mechanical load (providing adhesion of the glue to the adherend is existing) or very rapidly with no predictable life remaining.
Therefore high loaded load-introductions in A/C strucures are still the dominant area for "close tolerance bolted joints", where read across of quantitative joint strength from coupon testing is easy and production control is limited to material and geometric checks.
Still today no satisfactory technique is available for the detection of poor adhesion, so these possible defects must be eliminated by checking the adherends prior to bonding and careful process control. Time elaborating ultrasonic-, sonic vibration and X-Ray-techniques are the methods most commonly used for the detection of physical disbonds and porosity.
The most appropriate method depend on the type of structure , test environment and on the minimum size of defect which must be detected. In composite joints, the minimum detectable defect size is often larger than in metal to metal joints. /1/
In summary, the application of primary bonded joints is always linked to extensive engineering and manufacturing development phases for a special component and qualification/ certification programs within the aircraft development phase.

3.0 Damage Scenario for Composite Structures in Service

The threat of structural damage to composites is not limited to inservice scenarios, but includes production and assembly phases of components and aircrafts, a summary of possible damage sources and -types is shown in Fig. 3.0-1.
Not all of these require structural repair activities and the majority of damages are limited to the surface and edges of parts, covered by the structural repair manuals, however, more extensive damage on highly integrated parts occur and require the capability of tailored repair methods applied on the aircraft. These repaires are usually handled by a socalled "case by case" method, which implies that no specific procedure for the NDI and manufacturing tasks exist and all activities have to be managed through "engineering dispositions".

4.0 Joints Techniques for Repairs

The primary repair technique for composite structure is to bolt-on a metal sheet or machined doubler made of aluminium, titanium or steel and is the same as applied to metal structures for years. The big advantage of using metal is that aircraft mechanics are used to work with it and no special tools are required. Also metal patches can be applied in a comparatively short period of time.
There are drawbacks, however, because tailoring this technique to the needs of composite material is sometimes difficult. Metal patches are usually heavier than the composite materials they are replacing (some control surfaces often have "repair weight limits"), and they can chance the local stiffness of the original component.
In areas, where the orthotropic behavior of high modulus fibre composites has been used extensively (i.e. longerons or integrated spar caps) these doublers soon become quite thick therefore high load transfer bolted joints are required in the composite.
Aerodynamic considerations ("Out of Loft Limits") or thin honeycomb facesheets with reduced load introduction capability for bolts are two other reasons for the application of bonded scarf-repairs in these tasks, as are bonded composite patches on cracked metal skins where additional rivets are geometrically impossible or create new stress concentrations in high

load transfer zones. Boron reinforced epoxy composite patches are mainly used to repair cracked and fatigued metallic parts as well as reinforcing undamaged structure to reduce local stess levels and therefore preventing crack initiation.
This technique will gain more importance with the requirement to maintain fleets of aging aircraft and extend their structural life.
Stealth aircraft will pose an even larger repair challenge than common fighter aircrafts with regard to preserving the low radar cross section, not to be altered by riverted doublers.
Adhesively bonded repairs are therefore a common type of repair carried out with composite material. Bonded, scarfed repairs can restore a component to its full design strength without unacceptable change in stiffness and provide the original shape and finish to a component which has an aerodynamic critical surface. For honeycomb constructions with relatively thin skin laminates bolted repairs and scarfed repairs are impossible, thus these repairs have to be designed as external doublers, bonded to the repaired core area and the surrounding skin by film or paste adhesives; Fig. 4.0-1.

5.0 The Challenge of Bonded Joints "On Aircraft"

While bonded joints are extensively used in the production phase of aircrafts, the challenge of producing reliable bonds "on A/C" becomes evident when the conditions and manufacturing parameters of this task are considered:

* Qualified orginal processes are not applicable
* Manufacturing environment is different (depot manufacturing, single side access only, tooling and space limited, etc.)
* Simplified techniques and references required (repair kit, mobile NDI)

Other "problems" with repairing aircraft structures with adhesives are often linked to the fact, that thermoset composites and adhesives are originally cured by a chemical reaction that takes place at temperatures of 175°C (350°F) and a pressure of at least 3 bar (40 psi) in an autoclave.
Additionally, the **qualification** for this material and therefore all engineering properties are also **based** and linked to this process only!
In a repair situation, particulary if removal of the component from the structure is difficult or impossible, only "hot-bonders" including heat blanket and a vacuum pump that can provide high temperatures but only vaccum pressure can be used for repairs on the aircraft. The alternative use of a room temperature curing adhesive system is usually not possible since these systems are unable to provide the required strength in the "hot/wet"-environment for fighter aircraft. /2/

Therefore not only the production environment is affected, but:

* New materials are often required for repair processes (reduced pressure and temperature)
* Manufacturing risk is high (component integration, aircraft system installation, repairs are often "unique" cases)
* Additional nonproduction processes (redrying of composites, non tank surface treatment for metalics, decontamination, removing debris from tank compartments etc.)
* Surface and/or assembly related design features must be restored (lightning strike protection, sealing systems, etc.)
* Tolerances for curing parameters are higher than during production (heat blanket temperature distribution and heat-up/cool-down rates)

One of the major risks is the application of excessive temperature through the heat blanket, causing serious problems to the surrounding structure and fully assembled parts since they are not designed for such high thermal loads. High temperature causes also problems to composite components which have been in service and have picked up a significant amount of moisture. Expansion of new the moisture during cure can cause delamination or disbonds in the repair area. /2/
While typical cure temperature tolerances for autoclaves are ±5°C (±9°F) and heat-up rate tolerances are as small as ±0,5°C (±1°F) the respective values of heat-blankets are up to 4-6 times larger.
It should be noted that this demand does not exclude usage of advanced laboratory equipment and the best expertise available to evaluate and judge the results of the process development steps, but quality checks for acceptance of individual work steps must be performed and qualified by staff and equipment available "On-Aircraft"!
For these reasons it is beneficial to use a lower temperature/extended time for cure and also to dry the component before repairing.

Summarizing, the requirements for "On A/C bonding" differ significantly from production processes and experience gained during the original manufacturing of components and aircrafts cannot be automaticly transfered to the repair task or:

"Manufactures who have familiarity with autoclave bonding processes may not be competent in the performance of the same processes using localised heater blankets and vacuum bags." /3/

6.0 Repair Process Development

If repairs, performed on aircraft, fail during service, insufficient strength of the adhesive is rarely the reason, instead process related deficiencies like curing degree, surface preparation, adhesive thickness distribution etc. are the governing factors for insufficient bonds. Therefore the quality assurance of the complete process and its associated activities in a retraceable form is absolutely mandatory to ensure structural integrity of a repair.

Tests during development of repair methods are generally performed in laboratories for the production of repair specimen with "state off the art" -equipment and by expert supervision of disciplines like materials-, design-, stress- and manufacturing-engineering. The artificial implementation of damages also allows the prediction of the best NDI method. Decisions and modifications often take place in direct contact and without extensive documentation, the common background of the repair-method development project helps in avoiding "labourous formalismen" like specifications, acceptance sheets and Go/NoGo-criteria. Quality acceptance and NDI during this "development-phase" is also "State of the art", both for the damage accessment phase and the repair, simply because the results need to be evaluated in a form, that allows to judge on individual influences of parameters, therefore US-3D-squirter-technique and X-ray is used rather than manuel A-Scan to find the best information available. Strength testing of these coupons evaluate the efficiency of the repairs in a quantitative form both static and longterm fatigue and the data can be linked to performance and quality of the repair in other words, the task and the results are correlated via NDI and numerical test data, Fig. 6.0-1. The important fact, that these correlations are **only valid if the complete process** is repeated and repeatable, is often forgotten when the repair development is transfered to On-Aircraft application, Fig. 6.0-2.

7.0 Process Qualification for "On-A/C"-Repairs

The different aspects of a repair process qualification that need to be considered and their influence are shown in Fig. 7.0-1. The most important lesson to be learned is the recognition and acceptance of the boundary conditions for any engineering and manufacturing task "On-A/C" and the need for design criteria that take the possibility of these repairs during service into account.
If the repair process development is tailored to the "On-A/C-Repair" needs and the available NDI-methods and-results are used to verify the repair on a "step by step" basis together with the analytical checks of the repair a certification of repairs even for structurally critical components is possible.

Fig. 7.0-2 shows the required inputs and disciplines involved in the development of a repair procedure as part of the overall process "From procedure development to application". Typical output of this phase are drafts of a process- and NDI-Spec for this type of repair, often developed in manufacturing/depot-environment and facilities.
All the same time the design concept for the repair and the analysis methodology are established.

7.1 The "On Aircraft" - Qualification Program

7.1.1 Purpose of Qualification Program

The qualification program should establish all data needed for a save application of the repair method to a flight structure and satisfy the certification requirements. Primary attention must be paid to realistic damage for the type of structure the repair is focussing on, i.e. a "standard 2 inch round hole after clear-out" in a non tapered sandwich skin of a flat panel, well away from edges and recess-areas might not be the ideal representation for a real damage scenario and methods and techniques that work well for this type of repair specimen might show some "new" aspects when applied to a curved, tapered sandwich area of a load carrying cover/door with bonded-in metal hinges or frames, close to the edge.
Therefore, a "Test-Request for Realistic Repair Specimen" is a major item of any qualification and should not be mixed-up with standard coupons or even components, tested for process development and -variation purposes, Fig. 7.1-1.

7.1.2 Process Relevant Influences during Qualification

In order to establish confidence in a repair method for a given damage and type of structure, the different parameters influencing the quality of a repair need to be evaluated and quantified where possible, shown in Fig. 7.1-2 for the manufacturing facilities and-staff and quality assurance equipment and-staff; i.e. effects of porosity in bondlines or repair laminates and their influence on US-Scan/-interpretation as well as strength properties can only be assessed, if considered in this part of the program.
The "natural" aim of asking for perfect bonded joints, inspected by highly trained and perfectly equipped laboratory quality assurance personal is of questionable value, if later "some porosity" is found with less sophisticate NDI-equipment on the real aircraft and nobody is able to conclude the effects of these findings! So there is a need to establish "process-windows" and NDI-margins, where mechanical properties can be based on.
These "windows" and margins again need to be tailored to "On-A/C-repair" conditions, i.e. heat-up rates and max./min. temperature distribution as well as

bondline thicknesses will not be the same as for autoclave production! Tolerances that are to be met by material, equipment and staff-expertise are to be evaluated and documented in the Procedure Verification Phase, as shown in Fig. 7.1-3.
The correlation of mechanical and QA-inspections, both for process and repair results is the major step to overall qualification and certification, before a method can be applied to load carrying structures on the aircraft.
The same attention is paid for personal qualification and any primary or auxiliary material used during production of the "repair components".
Only those materials and equipment that can be used later on-aircraft should be used to manufacture the specimen and only personal, experienced with the limitations of performing repair work for composites on the aircraft should manufacture them.
The final step, "Application of a new repair method", with the important factor's summarized for the repair procedure, is illustrated in Fig. 7.1-4 where the main objective is to perform a "qualification checklist" for each discipline in order to ensure the applicability of the designed repair to the previous qualification program. Any deviation of the actual repair scenario from the performed qualification phases should be carefully considered and should initiate additional qualification tasks, if needed. Special attention must be paid to the "human factor" or "expertise", since the type of repairs addressed is a typical "unique case" task, not a routine and standard process like component production!

8.0 Summary of Qualification Approaches for "On-Aircraft Bonded Repairs"

The "traditional" approach for repair method- and process-development and the modified current "DASA-Approach" for this task are shown in Fig. 8.-1 and Fig. 8.-2.
In the "traditional" approach data like adhesive strength were tested with "standard" specimen (i.e. "Thick adherand specimen"), their data then referred as "Design Allowables" and used for the design and analysis of coupons (most of these are company standards from previous production development programs) to verify the analytical methodology for bonded joints, later "verified" on typical structural components like stiffened skin panels to establish the repair limits of these structures for a given design load/stress level of the particular aircraft. This procedure was "traditionally" accepted as verification for a repair method and any effects (besides direct material properties; i.e. influence of lower cure temperature or staging of adhesives) due to "On-Aircraft Limitations" were left to the materials/stress engineer to account for.

The new proposed qualification approach shown in Fig. 8.-2 starts with these "On-aircraft limitations" focusing on processes- and NDI-limits and although the three major phases (specimen/coupons/structural components) are still identical, every step is checked against the "On-Aircraft" scenarios, focusing on the evaluation of process tolerances and their influence on qualitiy and therefore strength.
The manufacturing specification of this procedure is therefore not a "modified copy" of a production specification for bonded joints but a specification for "On-Aircraft" bonded repair methods where all parts needed for the certification of a structural repair consider the requirements of "On-Aircraft" scenarios.

9.0 References

/1/ P. Cawley
"Non-destructive testing of Composite bonds"
Bonding and repair of composites, 14 July 1989, Metropole Hotel, Birmingham, UK

/2/ A.E. Maier
"Repair of Aircraft Structures
using 'Hard' Composite Patches"
ICCM-9, 12-16 July, 1993
Madrid. Spain

/3/ M.J. Davis
"The Development of an Engineering Standard for Composite Repair"
AGARD Conference Proceedings No. 550-24, 1995

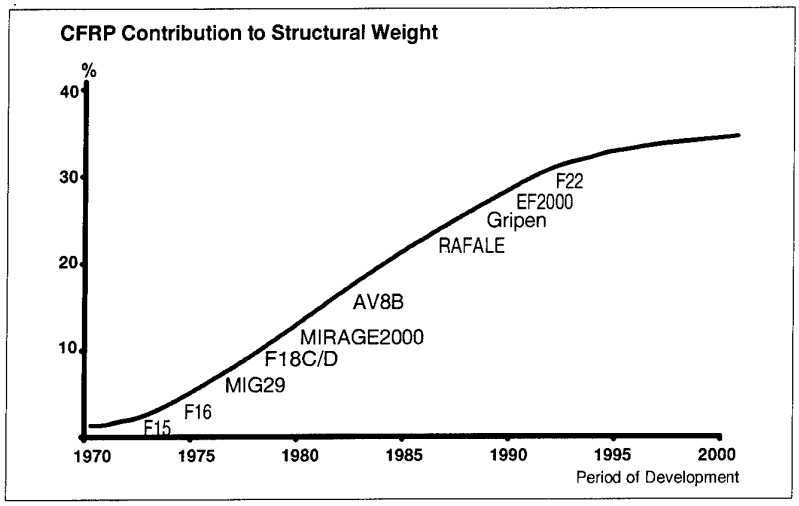
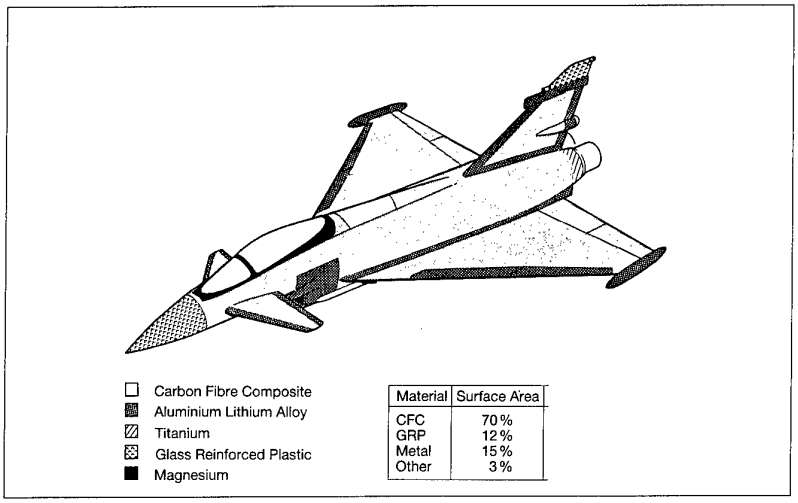


Figure: 1.0-1



Material	Surface Area
CFC	70 %
GRP	12 %
Metal	15 %
Other	3 %

Figure: 1.0-2

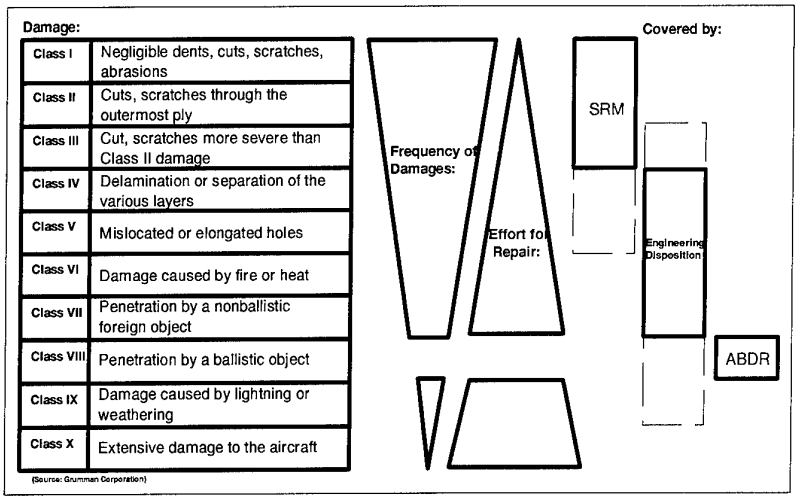


Figure: 3.0-1

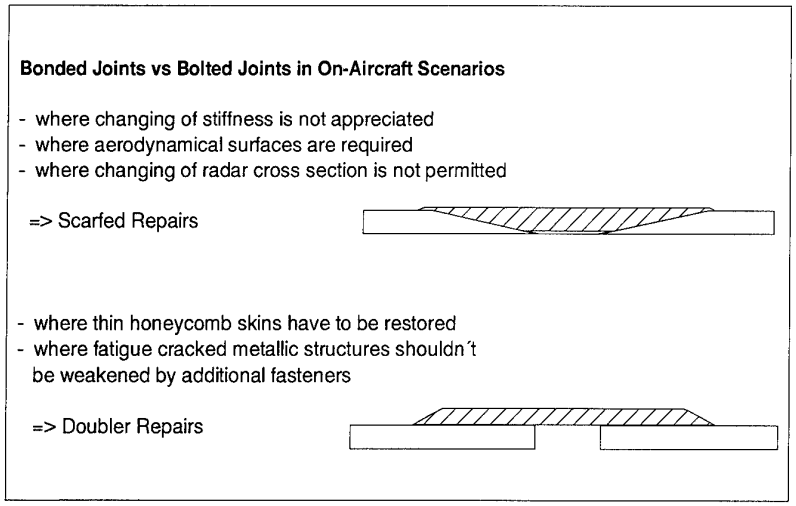


Figure: 4.0-1

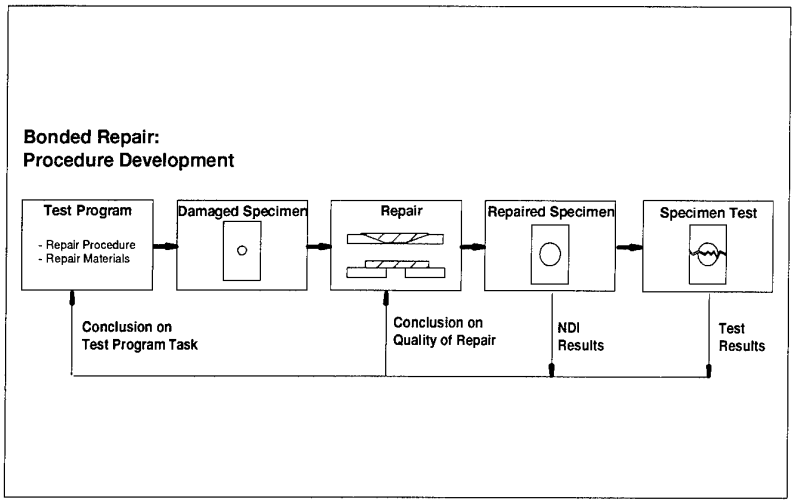


Figure: 6.0-1

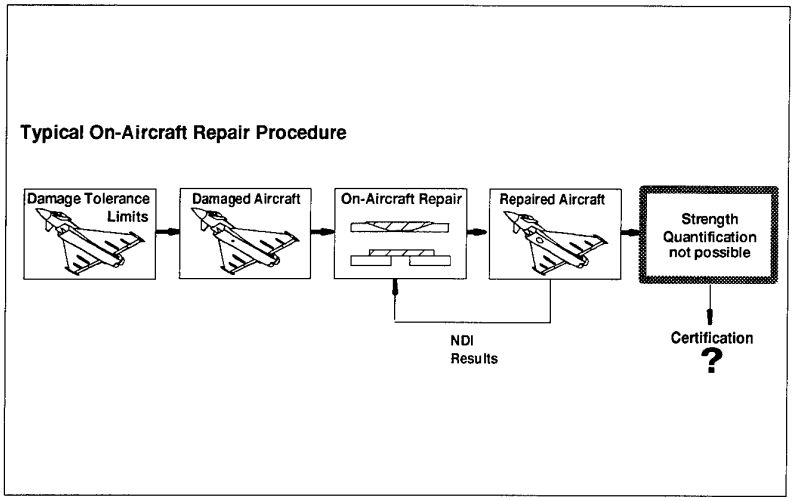


Figure: 6.0-2

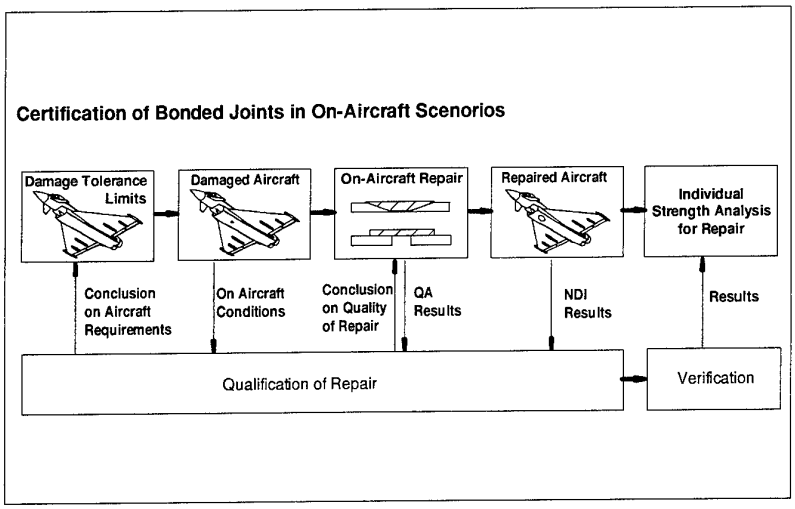


Figure: 7.0-1

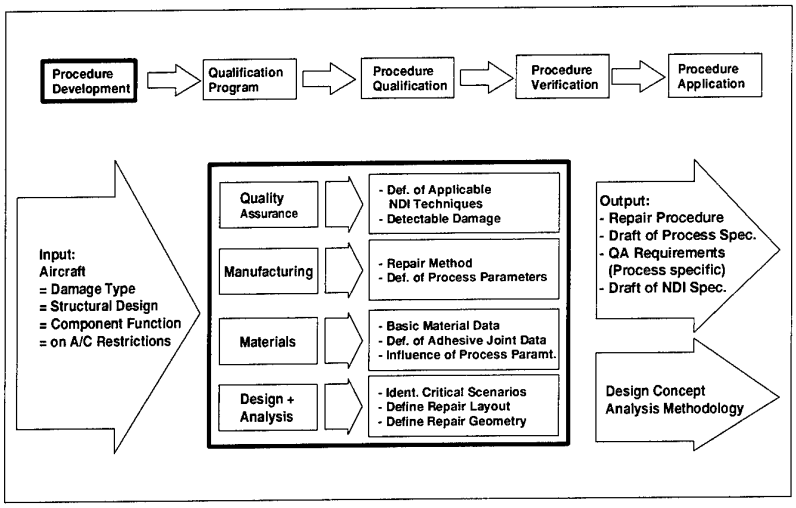


Figure: 7.0-2

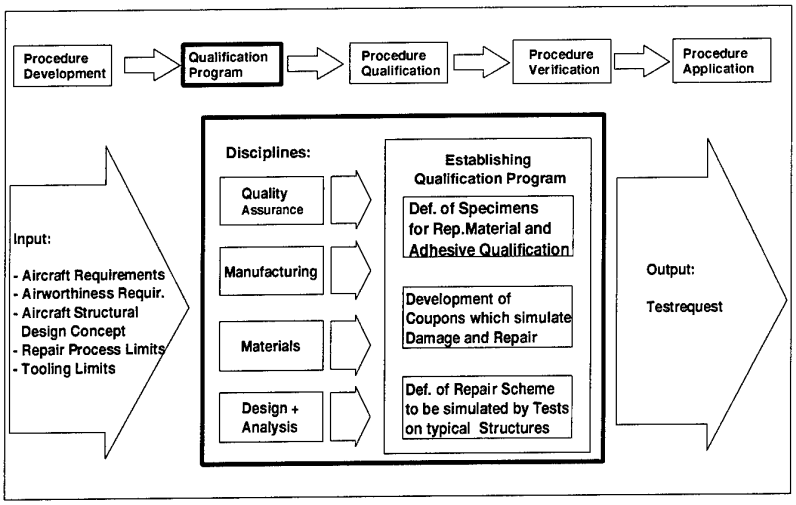


Figure: 7.1-1

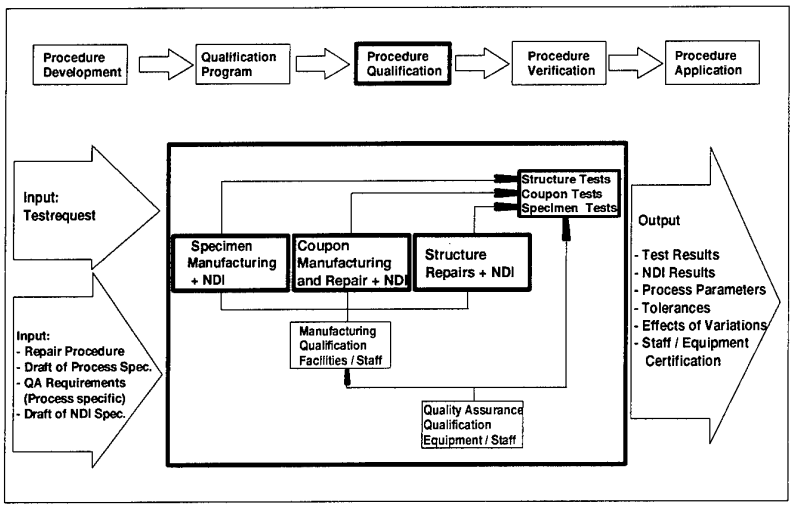


Figure: 7.1-2

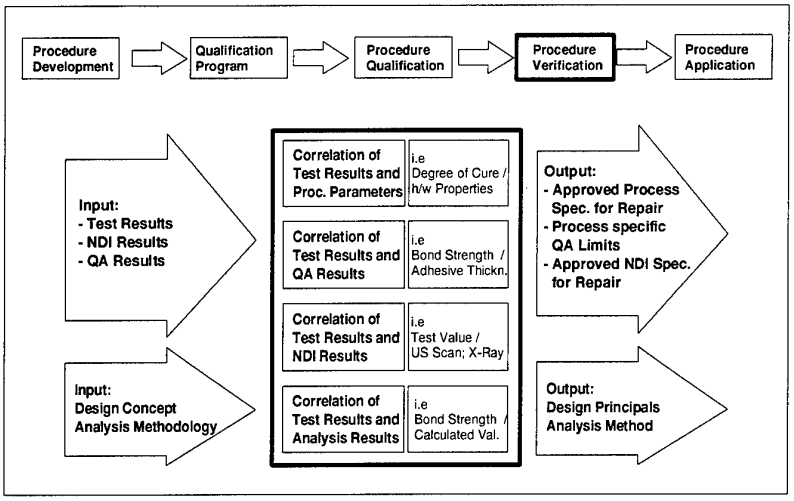


Figure: 7.1-3

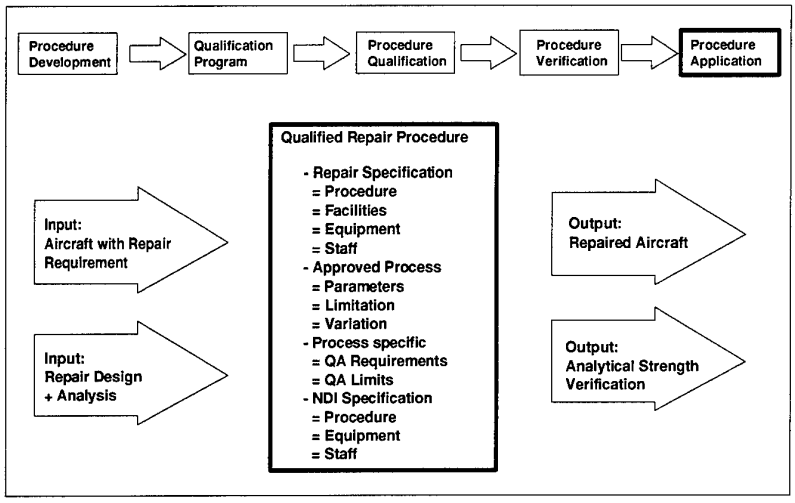


Figure: 7.1-4

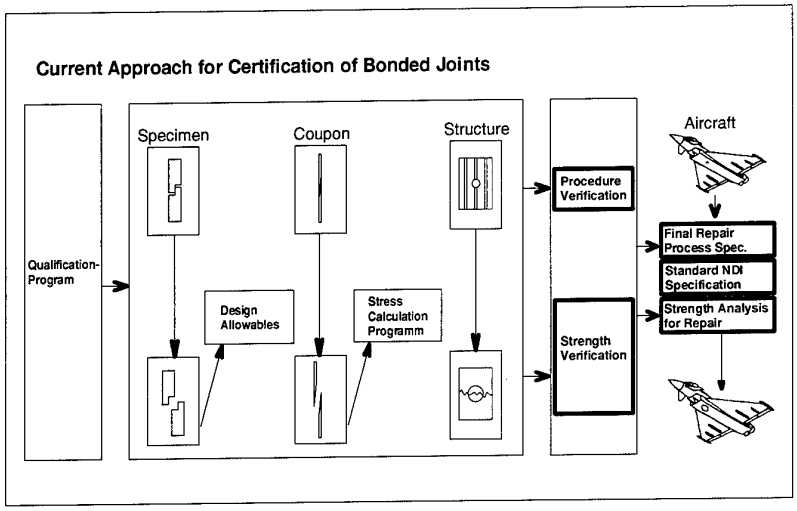


Figure: 8.0-1

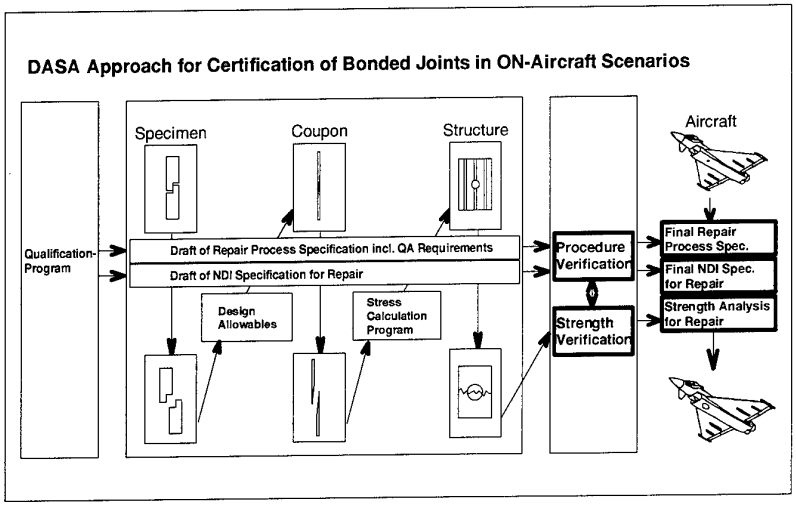


Figure: 8.0-2

PROBABILISTIC EVALUATION OF BOLTED JOINTS IN POLYMER MATRIX COMPOSITES

C. C. Chamis
NASA Lewis Research Center
Cleveland, Ohio 44135

L. Minnetyan
Clarkson University, Potsdam, New York

ABSTRACT

Computational methods are described to probabilistically simulate fracture in bolted composite structures. Progressive fracture is simulated via an innovative approach independent of stress intensity factors and fracture toughness. The effect on structure damage of design variable uncertainties is quantified. The Fast Probability Integrator is used to assess the scatter in the composite structure response before and after damage. Sensitivity of the response to design variables is evaluated. The methods are demonstrated for bolted joint polymer matrix composite panels under end loads. The effects of fabrication process are included in the simulation of damage in the bolted panel. The results show that the most effective way to reduce the end displacement at fracture is to control the load and ply thickness.

1. INTRODUCTION

Flawed structures, metallic or composites, fail when flaws grow or coalesce to a critical dimension such that (1) the structure cannot safely perform as designed and qualified or (2) catastrophic global fracture is imminent. However, fibrous composites exhibit multiple fracture modes that initiate local flaws compared to only a few for traditional materials. Hence, simulation of structural fracture in fibrous composites must include: (1) all possible fracture modes, (2) the types of flaws they initiate, and (3) the coalescing and the propagation of these flaws to critical dimensions for imminent structural fracture.

The phenomena of fracture in composite structures is further compounded due to inherent uncertainties in the multitude of material properties, structure geometry, loading, and service environments. The effect of all these types of uncertainties must be designed-in for satisfactory, reliable, and affordable structures. The various uncertainties in traditional designs are accounted for via safety factors with generally unknown reliability. An alternate approach to quantify those uncertainties on fracture of jointed structures is to use probabilistic methods as described herein.

The objective of the present investigation is to present methods/codes for (1) computationally simulating the initiation and progression of damage in joints for composite structures and (2) probabilistically assessing the effect of joint design variable uncertainties on the structural fracture. The methods and corresponding computer codes are demonstrated for the uncertainty in the damage load in select bolted joint of polymer matrix composite panels.

2. COMPUTATIONAL SIMULATION PROCEDURE

The comprehensive simulation of progressive fracture presented herein is independent of stress intensity factors and fracture toughness parameters. Concepts governing the structural fracture simulation are described in reference 1. Based on those concepts, a computational simulation procedure has been developed for (1) simulating damage initiation, progressive fracture, and collapse of composite structures and (2) evaluating probability of structural fracture in terms of global quantities which are indicators of structural integrity.

Progressive Fracture

The methodology for a step-by-step simulation of

Paper presented at the 83rd Meeting of the AGARD SMP on "Bolted/Bonded Joints in Polymeric Composites", held in Florence, Italy, 2-3 September 1996, and published in CP-590.

individual and mixed mode fracture in a variety of generic composite components is described in reference 1 to 3. The methodology has been incorporated into an integrated computer code, CODSTRAN (Composite Durability Structural Analysis - references 4 and 5). The damage stages are quantified by the use of composite mechanics while degradation of the structural behavior is quantified by the finite element method where the damaged part of the structure does not contribute to the resistance but is carried along as a parasitic material.

The combination of composite mechanics with the finite element method to permit formal description of local conditions to global structural behavior is normally handled through an integrated computer code as shown schematically in Figure 1. The bottom of Figure 1 describes the conditions of the material (microstress versus resistance) and where the criteria for damage initiation, growth, accumulation and propagation are examined. The left part of Figure 1 integrates (synthesizes) the effects of local damage conditions through the various composite scales to global structural behavior (response). The right part of Figure 1 tracks (decomposes) the effects of global changes (loading conditions for example) on the local (micro) material stress/resistance. Increases in damage are induced at the micro scale while increases in the load conditions are applied at the global structural model. Overall structural equilibrium is maintained by iterations around the "cartwheel" in Figure 1 until the damage growth or progression stabilized.

The approach has been applied to computationally simulate structural fracture of various composite structures including panels subjected to in-plane loads. Typical results for through-the-thickness delamination are available in reference 1.

Probabilistic Assessment of Structural Fracture

The effects on the fracture of the structure of uncertainties in all the relevant design variables are quantified. The composite mechanics, finite element structural simulation, and Fast Probability Integrator (FPI) have been integrated in IPACS (Integrated Probabilistic Assessment of Composite Structures - reference 6). A schematic of IPACS is shown in Figure 2. FPI, contrary to the traditional Monte Carlo Simulation, makes it possible to achieve order-of-magnitude computational efficiencies which are acceptable for practical applications. Therefore, a probabilistic composite assessment becomes feasible which can not be done traditionally, especially for composite materials/structures which have a large number of uncertain variables.

IPACS starts with defining uncertainties in material properties at the most fundamental composite scale, i.e., fiber/matrix constituents. The uncertainties are progressively propagated to those at higher composite scales (subply, ply, laminate, structural), as shown in Figure 2. The uncertainties in fabrication variables are carried through the same hierarchy. The damaged/fractured structure and ranges of uncertainties in design variables (such as material behavior, structure geometry, supports, and loading) are input to IPACS. Consequently, probability density functions (PDF) and cumulative distribution functions (CDF) can be obtained at the various composite scales for the structure response. Sensitivity of various design variables to structure response is also obtained.

3. DEMONSTRATION CASE

The methods and computer codes discussed above are demonstrated for (1) simulating the fracture in a bolted joint of a composite panel and (2) evaluating the probability of the damage initiation load of the panel.

A polymer matrix composite (8.0 x 4.0 x 0.25 inch) panel is fastened by a 1.0 inch diameter bolt at 2 inches from one of its ends and is subjected to a uniformly distributed load at the other end (Figure 3). The composite system is made of AS-4 graphite fibers in a high-modulus high-strength epoxy matrix (AS-4/HMHS). The fiber volume ratio is 0.60 and the void volume ratio is two percent. The constituent material properties and their respective uncertainties scatters are summarized in Table 1. The laminate consists of forty eight 0.00521 inch plies. The laminate configuration is $[90/\pm45/0]_{12}$. The 90^{o} plies are in the y direction and the 0^{o} plies are in the x direction. The effect of fabrication-induced residual stresses is simulated via a cure temperature of 350^{o} F. The bolt is modeled using

high strength steel properties. The finite element model of the bolt jointed panel is also shown in Figure 3. The bolt is fixed with respect to all displacement and rotational degrees of freedom at its center. The composite system is subjected to gradually increasing load until it is fractured and broken into two pieces.

Figure 4 shows the simulated damage progression with increasing load on the panel. During the first load increment of 800 lbs (=0.8 kips), finite element connectivities between the bolt and the composite are released where generalized membrane stress N_x and N_y are both tensile. Under a 6.8 kip loading, damage is initiated around the right half circumference of the panel at the bolted joint by matrix cracking in the 90° plies. When the load is increased, damage grows outward of the bolted joint. Gradual damage accumulation in selective plies continues until a 32.8 kip load is reached when fracture begins around the right half circumference of the panel at the bolted joint. Fracture is rapidly propagated to cause the ultimate break of the joint due to the fracture line that started from the bottom connection point.

The deterministically simulated panel fracture provides no information on its respective reliability. The end displacement (a global indicator of structural integrity) is probabilistically assessed. The end displacement depends on uncertainties in relevant panel geometry and material properties of the panel and bolt, bolt hole geometry and the load.

The cumulative distribution function of the panel end displacement before damage initiation is shown in figure 5. The probability that the panel end displacement before damage initiation will be less the 0.002 inch is about 0.001 and the probability of it being less than 0.0065 inch is about 0.999. There is about 0.50 probability that the end displacement will be 0.0043 inch.

The sensitivity of the 0.001 and 0.999 cumulative probability for the panel end displacement to uncertainties in design variables is shown in Figure 6. The load is the most significant design variable which affects the end displacement before damage initiation. The effect of uncertainties in ply thickness on end displacement is also substantial. The effect of uncertainties in composite material properties on end displacement is minor. These effects are the same on both probability levels. These results indicate that: (1) the damage initiation is strongly dependent on uncertainties in the load and (2) the panel end displacement damage initiation can be most effectively reduced by controlling the ply thickness.

Cumulative distribution functions of longitudinal stress in various plies (at point A - Figure 3) before and after damage are shown in Figure 7. The damage is initiated by 90° ply therefore, the 90° ply will not carry any load after damage initiation. The stresses were redistributed to the remaining plies (±45° and 0°) as shown in Figure 7. Also shown in this figure is that the major part of the load carried by the 90° ply before damage initiation is now carried mostly by +45° plies. The sensitivity of 0.001 probability for the ply longitudinal stress to uncertainties in design variables is shown in Figure 8. For 90° ply, it is most sensitive to load followed by thermal expansion coefficient of the matrix, fiber volume ratio and ply thickness. For 0° ply, it is most sensitive to the load followed by fiber volume ratio and ply thickness. For ±45° plies, the probability of their respective longitudinal stresses is most sensitive to the load followed by ply thickness. The remaining random variables have little contribution to the cumulative probability.

Cumulative distribution functions of transverse stress in various plies (at point A - Figure 3) before and after damage are shown in Figure 9. Again, the 90° ply will not carry any load after damage initiation. The unbalance in load due to damage initiation is redistributed to remaining plies. The sensitivity of 0.001 probability for the ply transverse stress to uncertainties in design variable is shown in Figure 10. For all plies, their respective probability is most sensitive to the thermal expansion coefficient of the matrix followed by fiber modulus in the transverse direction. The fiber volume ratio and matrix modulus contribute similarly to the probability for each transverse ply stress. Cumulative distribution functions of in-

plane shear stress before and after damage are shown in Figure 11. The stress and its scatter for each ply is insignificant. The 0.001 probability for ply shear stress in the respective ply is most sensitive to the load followed by longitudinal fiber modulus, fiber volume ratio and ply thickness.

4. CONCLUSIONS

Methods and corresponding computer codes were discussed to probabilistically assess jointed composite structures fracture. The progressive fracture in these composite structures was simulated via an innovative approach independent of stress intensity factors and fracture toughness parameters. This approach is inclusive in that it integrates composite mechanics (for composite behavior) with finite element analysis (for global composite structural response) and incorporates probability algorithms to perform a probabilistic assessment of composite structural fracture. The effect on the composite structure fracture of all the design variable uncertainties was accounted for at all composite scales. Probabilistic scatter range and sensitivity factors are key results obtained from the probabilistic assessment of fractured jointed composite structures. The sensitivity factors provide quantifiable information on the relative sensitivity of structural design variables on the respective reliability of that structure. The results obtained indicated that: (1) the scatter range of the end displacement is about 0.005 inch; (2) the end displacement at fracture is most sensitive to the load followed by the ply thickness; (3) the most effective way to reduce the end displacement at fracture is to control the load and ply thickness; (4) after the damage initiated in the 90^{o} ply, unbalanced stresses are redistributed to the remaining plies; (5) the cumulative probability for longitudinal stress is most sensitive to the load and the ply thickness has important contribution to the cumulative probability for the stress in all plies; (6) the cumulative probability for transverse stress is most sensitive to the thermal expansion coefficient of the matrix. Fiber volume ratio and fiber transverse modulus both contribute significantly to the cumulative probability for stress in all plies.

5. ACKNOWLEDGEMENT

The authors thank their cglleagues Dr. S. N. Singhal and Dr. M. C. Shiao, NYMA, Inc., for their assistance in the probabilistic simulations.

6. REFERENCES

1. T. A. Wilt, P. L. N. Murthy, and C. C. Chamis: "Fracture Toughness, Computational Simulation of General Delamination in Fiber Composites". NASA TM 101415, 1988.

2. P. L. N. Murthy and C. C. Chamis: "Interlaminar Fracture Toughness: Three-Dimensional Finite-Element Modeling for End-Notch and Mixed-Mode Flexure". NASA TM 87138, 1985.

3. P. L. N. Murthy and C. C. Chamis: "Composite Interlaminar Fracture toughness: 3-D Finite Element Modeling for Mixed Mode I, II, and III Fracture". NASA TM 88872, 1986.

4. C. C. Chamis and G. T. Smith: "Composite Durability Structural Analysis". NASA TM 79070, 1978.

5. C. C. Chamis: "Computational Simulation of Progressive Fracture in Fiber Composites". NASA TM 87341, 1986.

6. C. C. Chamis and M. C. Shiao: "IPACS -- Integrated Probabilistic Assessment of Composite Structures: Code Development and Application". Third NASA Advanced Composites Technology Conference, Long Beach, CA, June 1992.

Table 1. Constituent Material Properties and Respective Uncertainties Used in the Probabilistic Simulation

Random Variables	Mean Value	Assumed Scatter	Distribution Type
Fiber:			
Normal Modulus E_{f11}	32mpsi	8%	Normal
Normal Modulus E_{f22}	3 mpsi	8%	Normal
Poisson's ratio ν_{12}	0.23	8%	Normal
Poisson's ratio ν_{23}	0.25	8%	Normal
Shear modulus G_{f12}	2.5 mpsi	8%	Normal
Shear modulus G_{f23}	2.5 mpsi	8%	Normal
Thermal Expansion Coefficients α_{f11}	0.55 μin/in/°F	8%	Normal
$\alpha_{f22,33}$	5.6 μin/in/°F	8%	Normal
Tensile strength S_{fT}	400 ksi	8%	Normal
Compressive strength S_{fC}	400 ksi	8%	Normal
Matrix:			
Normal Modulus E_m	0.45 mpsi	8%	Normal
Poisson's ratio ν_m	0.41	8%	Normal
Thermal Expansion Coefficients α_m	38μin/in/°F	8%	Normal
Tensile strength S_{mT}	6.7 ksi	8%	Normal
Compressive strength S_{mC}	39 ksi	8%	Normal
Shear strength S_{mS}	8.9 ksi	8%	Normal
Fabrication Variables:			
Fiber volume ratio (fvr)	60%	8%	Normal
Void volume ratio (vvr)	0.01%	8%	Normal
Ply thickness:	0.0055in.	5%	Normal
Ply misalignment:	0	0.9*stdv	Normal

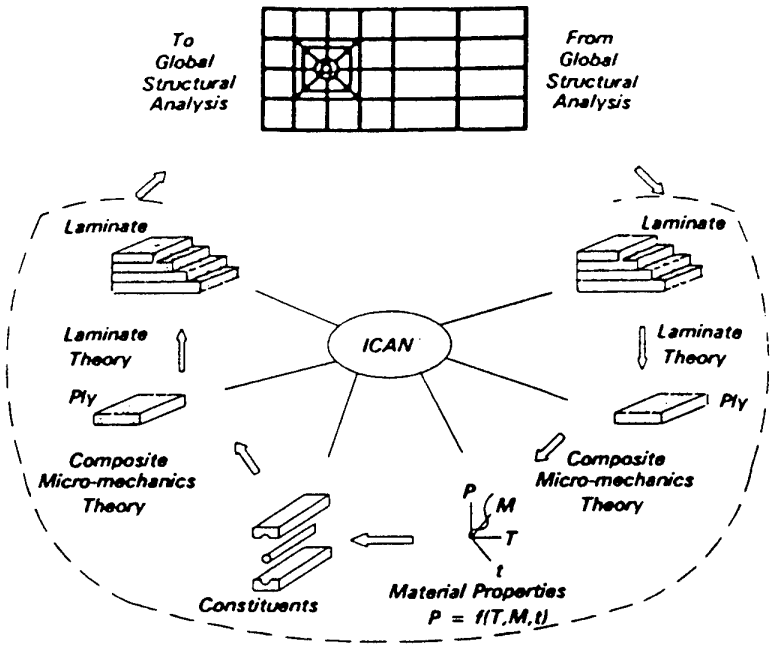


Figure 1 - Composite Durability Structural Analysis (CODSTRAN)

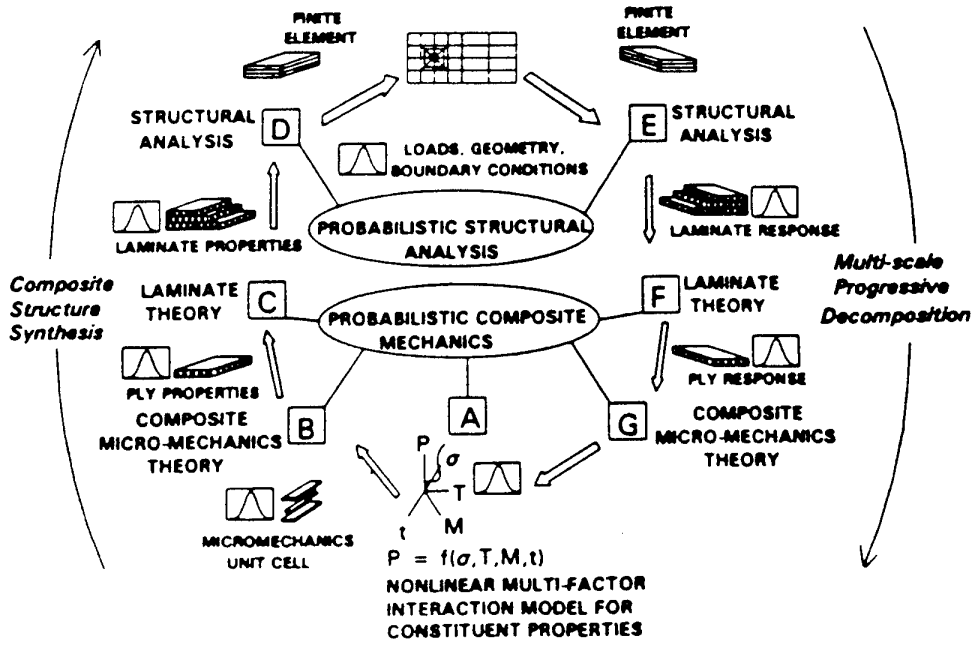


Figure 2 - Integrated Probabilistic Assessment of Composite Structures

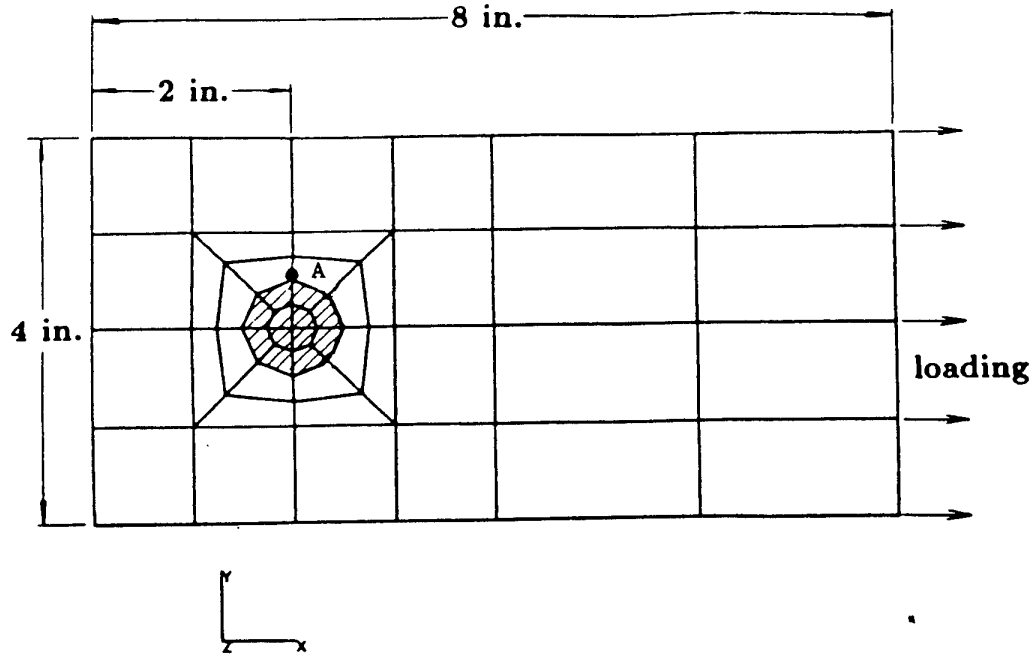


Figure 3 - Bolted Joint Composite Panel and Finite Element Model

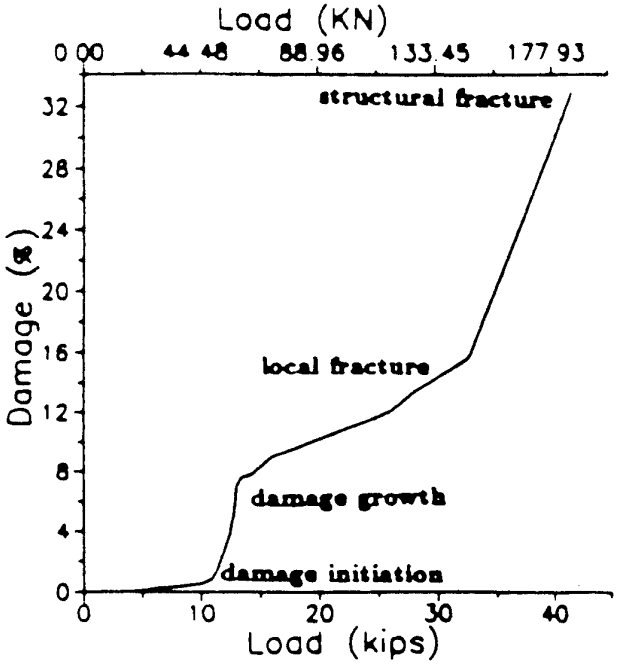


Figure 4 - Damage Progression for Bolted Laminate

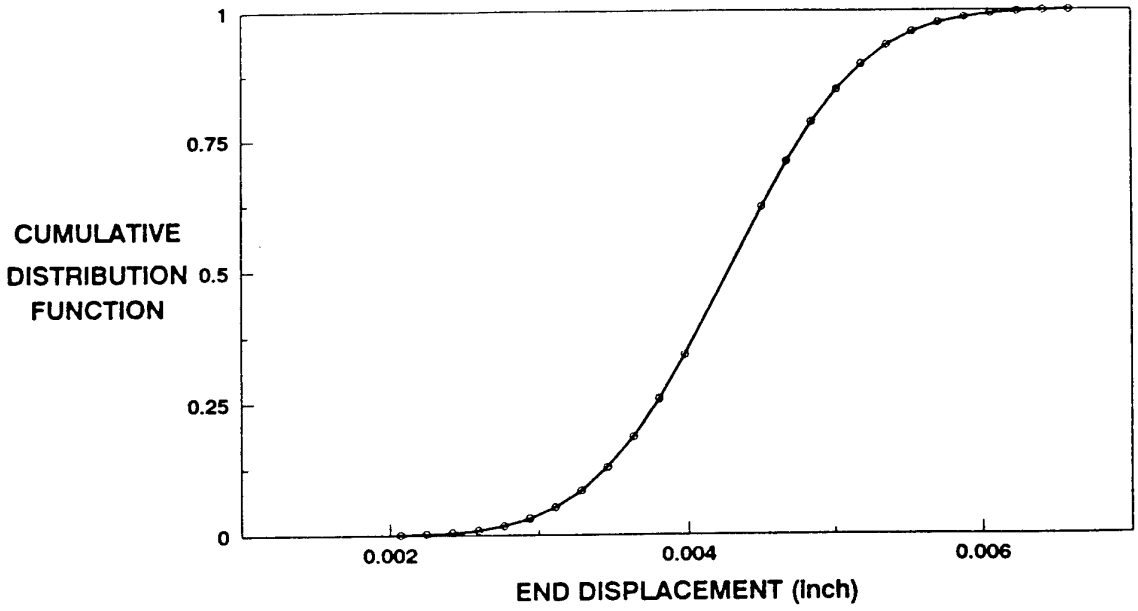


Figure 5 - Cumulative Distribution Function of Bolted Laminate End Displacement Before Damage Initiation

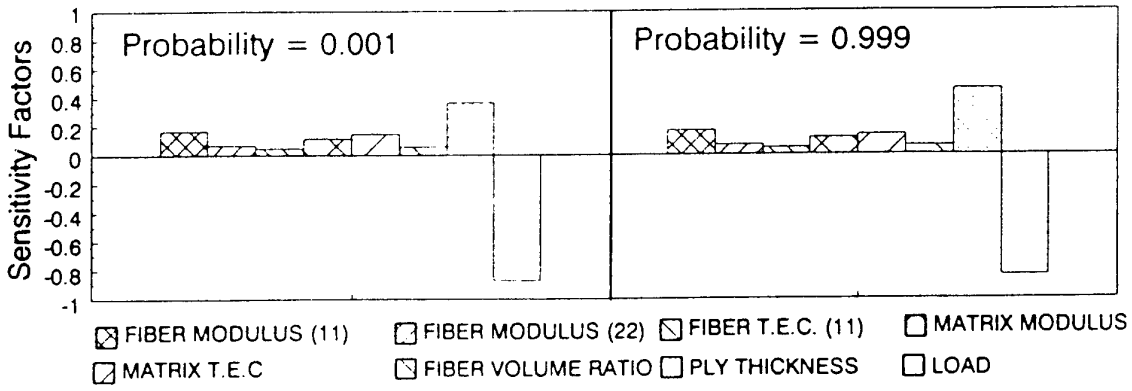


Figure 6 - Sensitivities of Uncertainties in Design Variables to Bolted Laminate End Displacement Before Damage Initiation

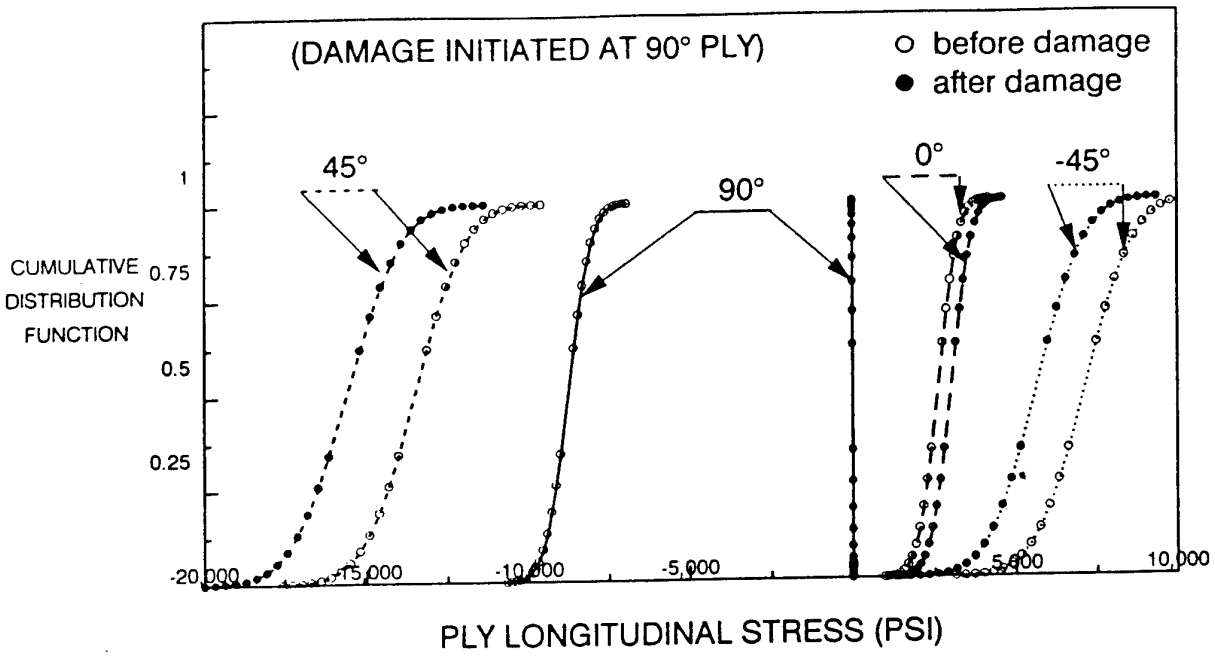


Figure 7 - Ply Longitudinal Stress Before and After Damage

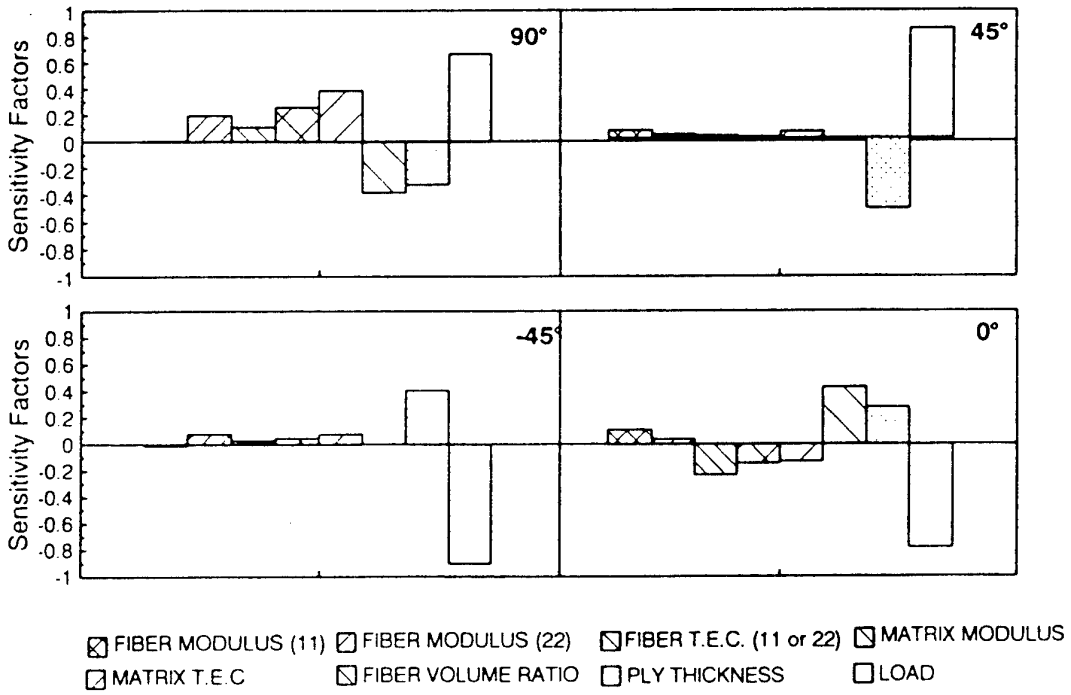


Figure 8 - Sensitivity Factors For 0.001 Cumulative Probability of Ply Longitudinal Stresses Before Damage Initiation

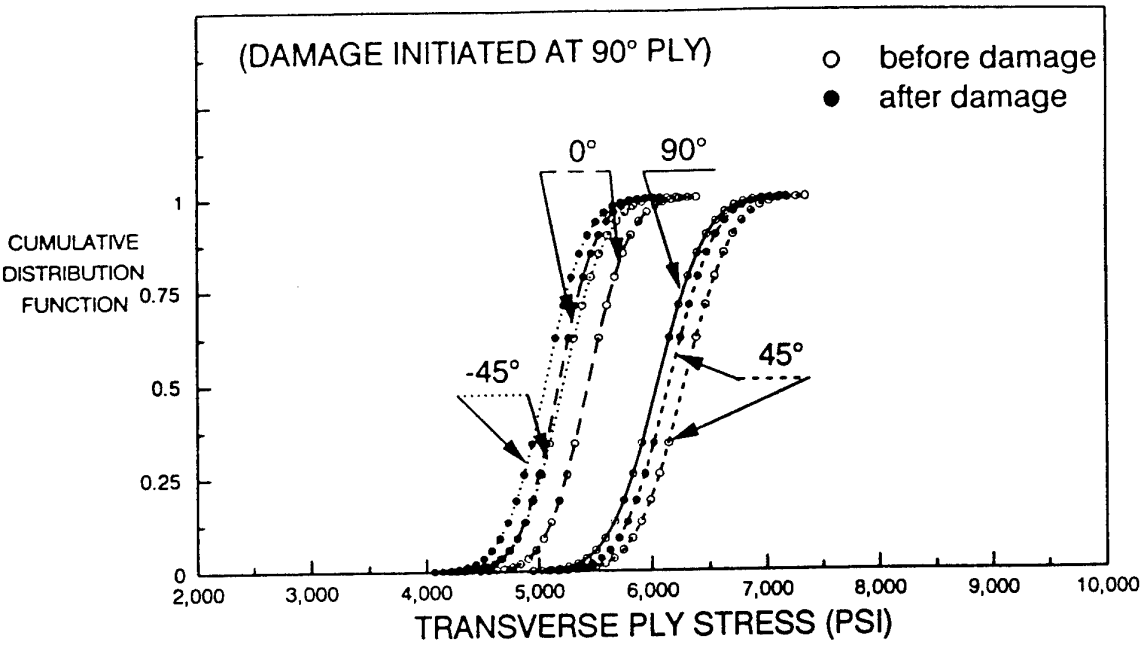


Figure 9 - Ply Transverse Stress Before and After Damage

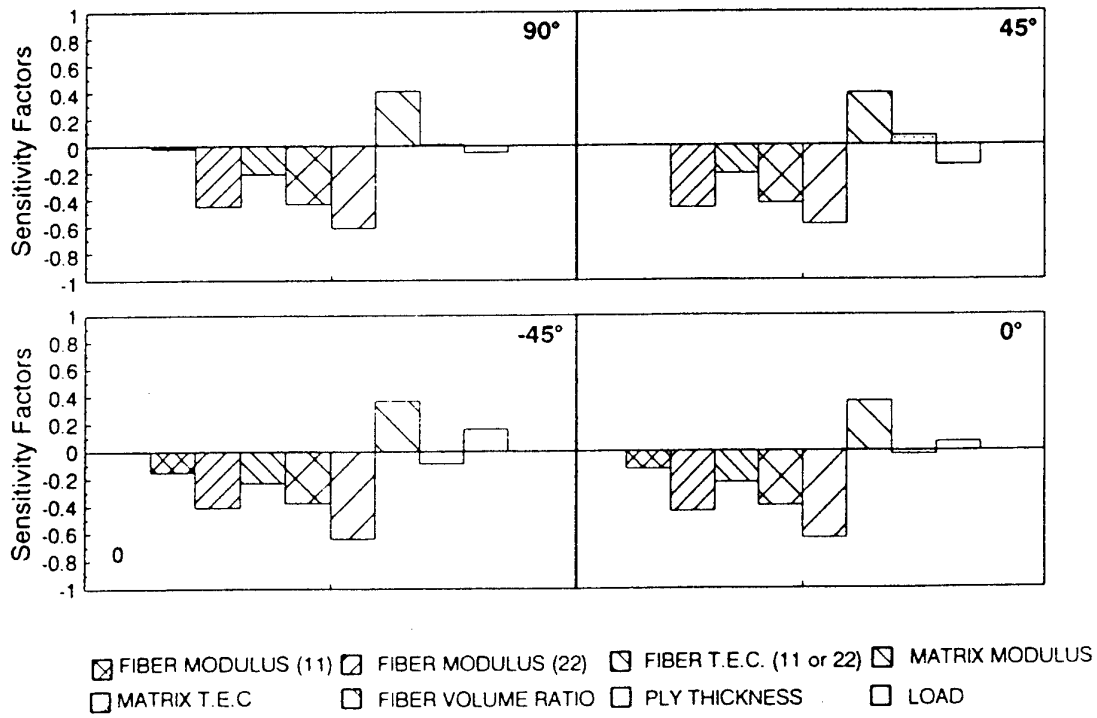


Figure 10 - Sensitivity Factors For 0.001 Cumulative Probability of Ply Transverse Stresses Before Damage Initiation

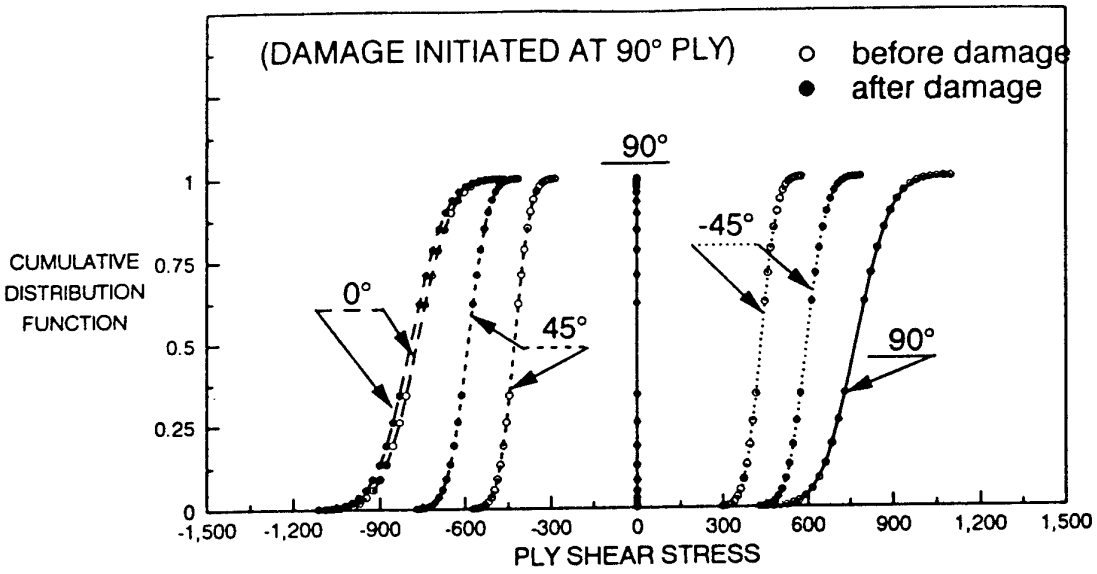


Figure 11 - Ply Shear Stress Before and After Damage

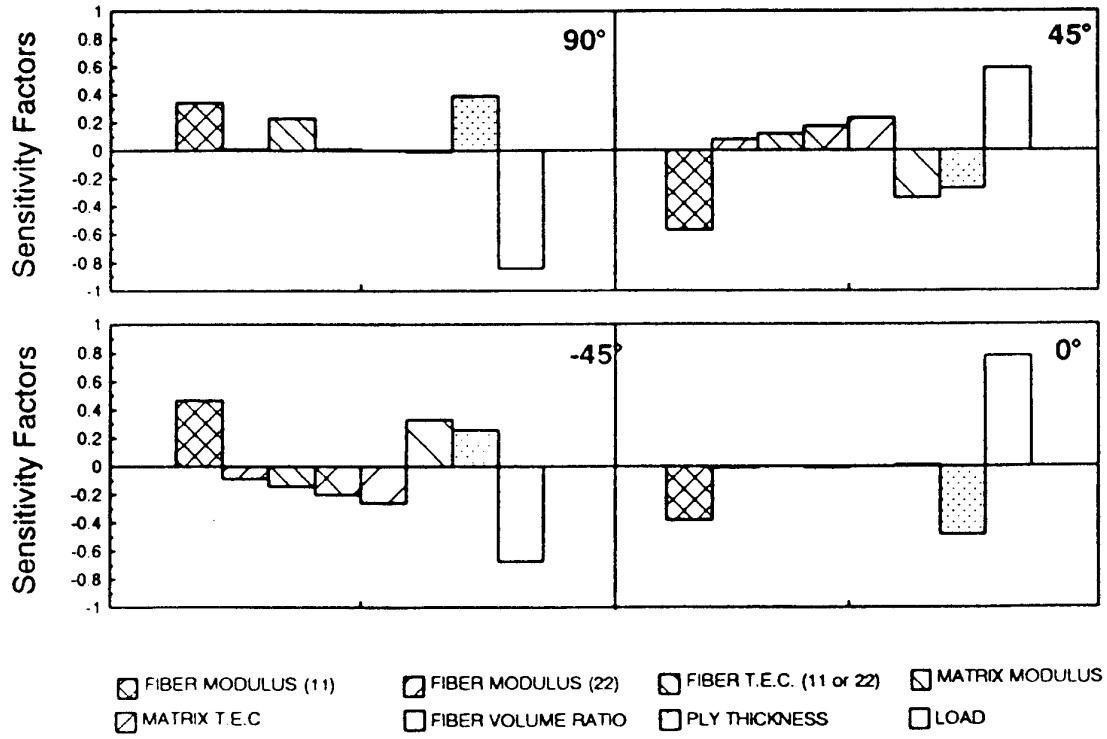


Figure 12 - Sensitivity Factors For 0.001 Cumulative Probability of Ply Shear Stresses Before Damage Initiation

REPORT DOCUMENTATION PAGE

1. Recipient's Reference	2. Originator's Reference	3. Further Reference	4. Security Classification of Document
	AGARD-CP-590	ISBN 92-836-1046-6	UNCLASSIFIED/ UNLIMITED

5. Originator Advisory Group for Aerospace Research and Development
North Atlantic Treaty Organization
7 rue Ancelle, 92200 Neuilly-sur-Seine, France

6. Title

Bolted/Bonded Joints in Polymeric Composites

7. Presented at/sponsored by

The 83rd Meeting of the AGARD Structures and Materials Panel, held in Florence, Italy, 2-3 September 1996

8. Author(s)/Editor(s)	9. Date
Multiple	January 1997
10. Author's/Editor's Address	**11. Pages**
Multiple	290

12. Distribution Statement There are no restrictions on the distribution of this document. Information about the availability of this and other AGARD unclassified publications is given on the back cover.

13. Keywords/Descriptors

Bolted joints	Joining
Bonded joints	Stress analysis
Composite structures	Failure
Composite materials	Laminates
Polymers	Strength
Airframes	Fatigue (materials)
Structural analysis	Maintenance
Structural design	Durability

14. Abstract

The objective of this AGARD Specialists' Meeting on Bolted/Bonded Joints in Polymeric Composites was to examine the state of the art in joining polymeric composites, to consider the relative merits of the various methods and to highlight gaps in the technology which should be addressed.

The papers presented cover a number of aspects concerning the application of adhesively bonded and mechanically fastened joints in the analysis, design, manufacturing, and repair of fibre-polymer composites. The focus is on aerospace rather than commercial products. The number of papers presented is 25, of which 8 cover the subject of Bolted Joints, 6 address Bonded Joints, 4 pertain to so-called Novel Joints, and 8 papers discuss Design Validation and Service Experience.

AGARD

NATO OTAN

7 RUE ANCELLE • 92200 NEUILLY-SUR-SEINE

FRANCE

Télécopie 0(1)55.61.22.99 • Télex 610 176

DIFFUSION DES PUBLICATIONS

AGARD NON CLASSIFIEES

Aucun stock de publications n'a existé à AGARD. A partir de 1993, AGARD détiendra un stock limité des publications associées aux cycles de conférences et cours spéciaux ainsi que les AGARDographies et les rapports des groupes de travail, organisés et publiés à partir de 1993 inclus. Les demandes de renseignements doivent être adressées à AGARD par lettre ou par fax à l'adresse indiquée ci-dessus. *Veuillez ne pas téléphoner.* La diffusion initiale de toutes les publications de l'AGARD est effectuée auprès des pays membres de l'OTAN par l'intermédiaire des centres de distribution nationaux indiqués ci-dessous. Des exemplaires supplémentaires peuvent parfois être obtenus auprès de ces centres (à l'exception des Etats-Unis). Si vous souhaitez recevoir toutes les publications de l'AGARD, ou simplement celles qui concernent certains Panels, vous pouvez demander à être inclu sur la liste d'envoi de l'un de ces centres. Les publications de l'AGARD sont en vente auprès des agences indiquées ci-dessous, sous forme de photocopie ou de microfiche.

CENTRES DE DIFFUSION NATIONAUX

ALLEMAGNE
Fachinformationszentrum Karlsruhe
D-76344 Eggenstein-Leopoldshafen 2

BELGIQUE
Coordonnateur AGARD-VSL
Etat-major de la Force aérienne
Quartier Reine Elisabeth
Rue d'Evere, 1140 Bruxelles

CANADA
Directeur - Gestion de l'information de recherche et de développement - DRDGI 3
Ministère de la Défense nationale
Ottawa, Ontario K1A 0K2

DANEMARK
Danish Defence Research Establishment
Ryvangs Allé 1
P.O. Box 2715
DK-2100 Copenhagen Ø

ESPAGNE
INTA (AGARD Publications)
Carretera de Torrejón a Ajalvir, Pk.4
28850 Torrejón de Ardoz - Madrid

ETATS-UNIS
NASA Goddard Space Flight Center
Code 230
Greenbelt, Maryland 20771

FRANCE
O.N.E.R.A. (Direction)
29, Avenue de la Division Leclerc
92322 Châtillon Cedex

GRECE
Hellenic Air Force
Air War College
Scientific and Technical Library
Dekelia Air Force Base
Dekelia, Athens TGA 1010

ISLANDE
Director of Aviation
c/o Flugrad
Reykjavik

ITALIE
Aeronautica Militare
Ufficio del Delegato Nazionale all'AGARD
Aeroporto Pratica di Mare
00040 Pomezia (Roma)

LUXEMBOURG
Voir Belgique

NORVEGE
Norwegian Defence Research Establishment
Attn: Biblioteket
P.O. Box 25
N-2007 Kjeller

PAYS-BAS
Netherlands Delegation to AGARD
National Aerospace Laboratory NLR
P.O. Box 90502
1006 BM Amsterdam

PORTUGAL
Estado Maior da Força Aérea
SDFA - Centro de Documentação
Alfragide
2700 Amadora

ROYAUME-UNI
Defence Research Information Centre
Kentigern House
65 Brown Street
Glasgow G2 8EX

TURQUIE
Millî Savunma Başkanliği (MSB)
ARGE Dairesi Başkanliği (MSB)
06650 Bakanliklar-Ankara

Le centre de distribution national des Etats-Unis ne détient PAS de stocks des publications de l'AGARD.
D'éventuelles demandes de photocopies doivent être formulées directement auprès du NASA Center for AeroSpace Information (CASI) à l'adresse ci-dessous. Toute notification de changement d'adresse doit être fait également auprès de CASI.

AGENCES DE VENTE

NASA Center for AeroSpace Information (CASI)
800 Elkridge Landing Road
Linthicum Heights, MD 21090-2934
Etats-Unis

The British Library
Document Supply Division
Boston Spa, Wetherby
West Yorkshire LS23 7BQ
Royaume-Uni

Les demandes de microfiches ou de photocopies de documents AGARD (y compris les demandes faites auprès du CASI) doivent comporter la dénomination AGARD, ainsi que le numéro de série d'AGARD (par exemple AGARD-AG-315). Des informations analogues, telles que le titre et la date de publication sont souhaitables. Veuiller noter qu'il y a lieu de spécifier AGARD-R-nnn et AGARD-AR-nnn lors de la commande des rapports AGARD et des rapports consultatifs AGARD respectivement. Des références bibliographiques complètes ainsi que des résumés des publications AGARD figurent dans les journaux suivants:

Scientific and Technical Aerospace Reports (STAR)
publié par la NASA Scientific and Technical Information Division
NASA Langley Research Center
Hampton, Virginia 23681-0001
Etats-Unis

Government Reports Announcements and Index (GRA&I)
publié par le National Technical Information Service
Springfield
Virginia 22161
Etats-Unis
(accessible également en mode interactif dans la base de données bibliographiques en ligne du NTIS, et sur CD-ROM)

Imprimé par le Groupe Communication Canada
45, boul. Sacré-Cœur, Hull (Québec), Canada K1A 0S7

AGARD

NATO OTAN

7 RUE ANCELLE • 92200 NEUILLY-SUR-SEINE

FRANCE

Telefax 0(1)55.61.22.99 • Telex 610 176

DISTRIBUTION OF UNCLASSIFIED

AGARD PUBLICATIONS

AGARD holds limited quantities of the publications that accompanied Lecture Series and Special Courses held in 1993 or later, and of AGARDographs and Working Group reports published from 1993 onward. For details, write or send a telefax to the address given above. *Please do not telephone.*

AGARD does not hold stocks of publications that accompanied earlier Lecture Series or Courses or of any other publications. Initial distribution of all AGARD publications is made to NATO nations through the National Distribution Centres listed below. Further copies are sometimes available from these centres (except in the United States). If you have a need to receive all AGARD publications, or just those relating to one or more specific AGARD Panels, they may be willing to include you (or your organisation) on their distribution list. AGARD publications may be purchased from the Sales Agencies listed below, in photocopy or microfiche form.

NATIONAL DISTRIBUTION CENTRES

BELGIUM
Coordonnateur AGARD — VSL
Etat-major de la Force aérienne
Quartier Reine Elisabeth
Rue d'Evere, 1140 Bruxelles

CANADA
Director Research & Development
Information Management - DRDIM 3
Dept of National Defence
Ottawa, Ontario K1A 0K2

DENMARK
Danish Defence Research Establishment
Ryvangs Allé 1
P.O. Box 2715
DK-2100 Copenhagen Ø

FRANCE
O.N.E.R.A. (Direction)
29 Avenue de la Division Leclerc
92322 Châtillon Cedex

GERMANY
Fachinformationszentrum Karlsruhe
D-76344 Eggenstein-Leopoldshafen 2

GREECE
Hellenic Air Force
Air War College
Scientific and Technical Library
Dekelia Air Force Base
Dekelia, Athens TGA 1010

ICELAND
Director of Aviation
c/o Flugrad
Reykjavik

ITALY
Aeronautica Militare
Ufficio del Delegato Nazionale all'AGARD
Aeroporto Pratica di Mare
00040 Pomezia (Roma)

LUXEMBOURG
See Belgium

NETHERLANDS
Netherlands Delegation to AGARD
National Aerospace Laboratory, NLR
P.O. Box 90502
1006 BM Amsterdam

NORWAY
Norwegian Defence Research Establishment
Attn: Biblioteket
P.O. Box 25
N-2007 Kjeller

PORTUGAL
Estado Maior da Força Aérea
SDFA - Centro de Documentação
Alfragide
2700 Amadora

SPAIN
INTA (AGARD Publications)
Carretera de Torrejón a Ajalvir, Pk.4
28850 Torrejón de Ardoz - Madrid

TURKEY
Millî Savunma Başkanliği (MSB)
ARGE Dairesi Başkanliği (MSB)
06650 Bakanliklar-Ankara

UNITED KINGDOM
Defence Research Information Centre
Kentigern House
65 Brown Street
Glasgow G2 8EX

UNITED STATES
NASA Goddard Space Flight Center
Code 230
Greenbelt, Maryland 20771

The United States National Distribution Centre does NOT hold stocks of AGARD publications.
Applications for copies should be made direct to the NASA Center for AeroSpace Information (CASI) at the address below.
Change of address requests should also go to CASI.

SALES AGENCIES

NASA Center for AeroSpace Information
(CASI)
800 Elkridge Landing Road
Linthicum Heights, MD 21090-2934
United States

The British Library
Document Supply Centre
Boston Spa, Wetherby
West Yorkshire LS23 7BQ
United Kingdom

Requests for microfiches or photocopies of AGARD documents (including requests to CASI) should include the word 'AGARD' and the AGARD serial number (for example AGARD-AG-315). Collateral information such as title and publication date is desirable. Note that AGARD Reports and Advisory Reports should be specified as AGARD-R-nnn and AGARD-AR-nnn, respectively. Full bibliographical references and abstracts of AGARD publications are given in the following journals:

Scientific and Technical Aerospace Reports (STAR)
published by NASA Scientific and Technical
Information Division
NASA Langley Research Center
Hampton, Virginia 23681-0001
United States

Government Reports Announcements and Index (GRA&I)
published by the National Technical Information Service
Springfield
Virginia 22161
United States
(also available online in the NTIS Bibliographic
Database or on CD-ROM)



Printed by Canada Communication Group
45 Sacré-Cœur Blvd., Hull (Québec), Canada K1A 0S7

ISBN 92-836-1046-6